GREENHOUSE CLIMATE – INSIGHTS FROM EARLY AND MIDDLE EOCENE STRATIGRAPHIC AND PALAEOCLIMATIC RECONSTRUCTIONS OF THE ROCKALL TROUGH, NE ATLANTIC

by

Ulrike Katharina Baranowski

A thesis submitted to the University of Birmingham for the degree of Doctor of Philosophy

School of Geography, Earth and Environmental Sciences

College of Life and Environmental Sciences

University of Birmingham

April 2020

ABSTRACT

The early Eocene climate optimum (EECO) was the time of peak Cenozoic warmth with ice free poles. The EECO is an essential time interval to study climate proxies, which provide the data to test climate models under conditions of extreme greenhouse gas forcing. The relatively scarce sea surface temperature (SST) proxy data from the Eocene indicate a puzzling reduced latitudinal temperature gradient, which is difficult to reproduce in climate models. Therefore, high quality Eocene SST data with good age control are required, especially within large geographical proxy data gaps. This study presents new temperature proxy data from mixed layer (*Acarinina bullbrooki*, pF-SSTs) and thermocline dwelling (*Subbotina eocaena,* pF-STT) planktic foraminiferal oxygen isotopes and from thaumarchaeotal membrane lipids (SST-H). This data is underlain by a new age model based on high-resolution bulk carbonate oxygen and carbon isotopes and nannofossil biostratigraphy from Site 16/28-sb01, NE (North East) Atlantic (palaeolatitude 49˚N). Carbon isotope excursions (CIE) P, R, S, T, U, V and W are detected within the EECO bulk isotope record of Site 16/28-sb01. Within this CIEs, elemental variability (XRF), foraminiferal abundance, temperatures and radiolarian abundance do not show a systematic response linked to the carbon cycle perturbations. Therefore, it is concluded that the main causes for variability at this shallow Site, is likely salinity variability coupled to an enhanced hydrologic cycle, sedimentary system ageing and subsidence. Site 16/28-sb01, subsided from ~300 to ~1000 m water depth from the early Eocene to the middle Eocene. In the EECO both SST-H and pF-SST agree on an average temperature of ~28˚C confirming a greatly reduced EECO latitudinal SST gradient (and pF-STT ~19˚C). In the middle Eocene the SST proxies show a pronounced offset, with SST-H implying ~28˚C and pF-SSTs ~17˚C (pF-TT ~15˚C). This SST offset in the middle Eocene is most likely caused by a combination of slight change of $\delta^{18}O_{SW}$ combined with either a slight winter bias of *A. bullbrooki*, a slightly deeper depth habitat of *A. bullbrooki* or a less stratified water column in the middle Eocene compared to the early Eocene. The unconformity between early and middle Eocene at Site 16/28-sb01 might be caused by a more erosional regime linked to Northern Component deep- Water onset around ~49 Ma.

*

For all my loved ones.

*

*

If one would knock against walls,

how long until they would break?

And how long – till flowers would grow in the small cracks?

Yet – nothing would be the same.

*

I. Acknowledgements

First, I would like thank my supervisor Tom Dunkley Jones for offering me to work on this project and for providing academic support throughout the journey of this thesis. Second, I would like to thank my supervisor Kirsty Edgar for coming into the project half way in providing enormous support especially for the planktic foraminiferal part of this thesis and beyond that. Stephen Jones from the University of Birmingham I would like to thank for background insight into seismic interpretations from nearby the study site. I would like to thank James Bendle and Marcelo De Lira Mota for helping with the pilot and resampling. Special thanks to the Petroleum infrastructure program Ireland (PIP) core store in Dublin for providing us with the sampling allowance and access to the sediment of Site 16/28-sb01. Hanna Gruszczynska with the help of David Naafs for running the GDGTs at the National Environmental Research Council (NERC) Life Science Mass Spectrometry Facility (LSMSF) under the lead of Ian Bull at the University of Bristol. Hilary Sloan under the lead of Melanie Leng for running the super low weights for carbon and oxygen planktic foraminiferal isotopes at the NERC Isotope Geoscience Facilities (NIGL) at the British Geological Survey (BGS) in Nottingham. Ian Boomer, Heiko Moossen and Dominica Nala for running lots of the endless bulk carbonate oxygen and carbon samples at the University of Birmingham. Emma Hanson and Emily Hollingworth for running all the X-ray fluorescence (XRF) samples at the University of Birmingham. Frederike Wittkopp, Heiko Moossen, Bethany Chamberlain and Kate Newton for teaching me how to extract GDGTs. Calian Hazell for producing calcareous nannofossil smear slides for Site 16/28-sb01 during his master thesis contributing thereby to the calcareous nannofossil age dates of this thesis. Further I would like to thank Emma Hanson, Witty De Souza, Sev Kender and his technician, Dominica Nala, Daisy Mortimer, Emily Hollingsworth and Ivan Nikiforov for processing lots of the resampled foraminiferal samples and for preparing lots of the XRF and bulk isotope samples. Thanks as well to Phil Sexton from the Open University in Milton Keynes, who took some time to look at the pilot foraminiferal samples and met with us at the very beginning of the project. I would like to thank Christopher Hollis, GNS Science (New Zealand), for answering my questions about “cenospheroid” radiolarian. Juan Castaneda for lending me his XRF book. Special thanks, to Gretchel Coldicott who

was always able with her kind nature to sort out any disasters with payments or bureaucracy with the University of Birmingham. I thank Lesley Ann Boyle for the quick processing and payment for the urgent laptop repair right at the end of my thesis. I thank the volcanology and igneous petrology experimental research (VIPER) lab at the University of Birmingham and Alan Hastie for providing a silent work space during the end of my thesis. I thank Sarah Greene for patiently listing to some of my random questions at the end of my thesis. One important thank you almost at the end, I thank the University of Birmingham and the NERC CDT for Oil and Gas, who provided funding for my PhD thesis and for the six-month training included within this PhD program. From the NERC CDT Oil and Gas team I would like to thank John Underhill, Anna Clark and Lorna Morrow all based at Heriot-Watt University of Edinburgh for excellent training provision and organization. Last but most importantly, I would like to thank my colleges at the University of Birmingham, my friends especially Anni, Betty, Rike, Heiko, Simiao, Gaël, Andy, Chris, Derren, Plamen, Alastair and Dan, my family and my partner, without all of you and the big and small supports each of you gave me this thesis would not be what it is now.

II. TABLE OF CONTENT

III. List of Figures

IV. List of Tables

1 INTRODUCTION

1.1 Rationale for the study of Eocene palaeoclimates of the NE Atlantic

A major challenge for the 21st century is understanding and predicting the development of future warm climate states in response to rising atmospheric carbon dioxide (CO_2) concentrations especially in excess of 500 ppm (parts per million) (IPCC, 2013). Atmospheric CO_2 concentrations were at least as high in the Eocene epoch (Pagani et al., 2005, Zhang et al., 2013, Anagnostou et al., 2016, Foster et al., 2017), as those predicted by the Intergovernmental Panel on Climate Change (IPCC, 2013) for the year 2100 under unabated emission scenarios (~800 to ~1100 ppm). Eocene climate reconstructions are therefore invaluable to test and verify climate model behaviour under greatly elevated atmospheric CO_2 concentrations, that can for example help to constrain uncertainty in future climate predictions (Hollis et al., 2019). Inter-comparison between proxy data and model simulations of past climates is key for a better understanding of the climate of the early Eocene (Lunt et al., 2012, Evans et al., 2018b), but also for understanding the potential dynamics of future high CO_2 climate states (Zachos et al., 2008, Meinshausen et al., 2011, IPCC, 2013, Hansen et al., 2013, Zeebe and Zachos, 2013, Anagnostou et al., 2016, Foster et al., 2018, Kiehl et al., 2018, Burke et al., 2018). In this instance, James Hutton's principle of uniformitarianism "the present is the key to the past", can be recast as "the past as the key to the future" (e.g., Doe, 1983).

The Eocene (~56 – 34 Ma) is the most prominent warm interval in the Cenozoic (Zachos et al., 1994), especially during the early Eocene Climate Optimum (EECO) 53 – 49 Ma (Westerhold et al., 2018a, Lauretano et al., 2018). During the Eocene the Earth was so warm that little or no ice is assumed to have been accumulated at the poles (Sluijs et al., 2006, Bijl et al., 2009, Cramer et al., 2011). The early Eocene warm climate state is also punctuated by short-lived transient negative carbon isotope excursions (CIEs), often referred to as "hyperthermals" (Cramer et al., 2003). Most of these CIEs are associated with additional short-term warming (Lauretano et al., 2018)

and are thought to be driven by orbital, predominantly eccentricity, variability (Lourens et al., 2005, Lauretano et al., 2018, Westerhold et al., 2018a).

Climate model simulations of Eocene warm climate states require high-quality proxy data for verification of model behaviour, of which planetary surface temperature estimates are the most important (Barron and Peterson, 1991, Lunt et al., 2012). In the oceans, the most commonly used proxies for reconstructing sea surface temperatures (SSTs) are the TEX_{86} (Tetra Ether index of tetraethers consisting of 86 carbon atoms)-index using the Glycerol Dialkyl Glycerol Tetraethers (GDGT) distribution of these organic membrane lipids (Schouten et al., 2002) and the oxygen isotopic ($\delta^{18}O$) and trace element compositions (Mg/Ca) of planktic foraminifera tests (Lunt et al., 2012, Hollis et al., 2019). There are, however, large geographic gaps in the availability of reliable SST proxy data, especially in the mid to high latitudes during conditions of early Eocene peak warmth (Lunt et al., 2012, Evans et al., 2018b) (Figure 1.1.). The scarce availability of marine proxy data for the early Eocene, a total of 16 EECO sites (Hollis et al., 2019), indicate a puzzling equator-to-pole surface temperature gradient — or meridional temperature gradient (MTG) — that was substantially smaller during this greenhouse period than in the modern Earth system (Shackleton and Boersma, 1981, Barrera and Huber, 1991, Zachos et al., 1994, Sluijs et al., 2006, Bijl et al., 2009, Huber and Caballero, 2011, Lunt et al., 2012, Hollis et al., 2012, Dunkley Jones et al., 2013, Evans et al., 2018b, Evans et al., 2018a, Hollis et al., 2019). If the marine proxy data are correct, this reduced latitudinal temperature gradient is still not adequately reproduced by climate models (Sloan and Rea, 1995, Sloan et al., 1995, Huber and Caballero, 2011, Lunt et al., 2012, Evans et al., 2018b, Vahlenkamp et al., 2018b) and results in a model to proxy data discrepancy (Figure 1.1.).

There is no agreement on the cause of this enigmatic discrepancy. Some argue that the warmer SSTs inferred from proxy data from the higher latitudes could partially be due to proxy uncertainties, especially where there are proxy-proxy mismatches such as between SST reconstructions from organic lipids (GDGTs) and foraminiferal oxygen isotopes in the Southern Ocean (Hollis et al., 2012, Lunt et al., 2012, Dunkley Jones et al., 2013, Hollis et al., 2019). Yet the discovery of terrestrial fossils of alligators, giant tortoise and subtropical to warm temperate swamp forests close to the poles, and

mangroves in northern Europe during the early Eocene, confirm the presence of very warm conditions and higher precipitation in high-latitude terrestrial environments (Markwick, 2007, Greenwood et al., 2010, Eberle and Greenwood, 2012, West et al., 2015). Further, pollen and spore analysis indicate high-latitude frost-free winters with a flora including *inter alia* palm trees (Arecaceae) in Antarctica (Pross et al., 2012, Huber and Sloan, 2001) and in the Arctic (Sluijs et al., 2009; and references therein). This additional terrestrial fossil data strongly supports assessments of the best available marine multi-proxy SST records (Hollis et al., 2012, Evans et al., 2018b, Hollis et al., 2019) that indicate a significantly reduced latitudinal temperature gradient during early Eocene peak warmth. Thus, the causes of climate model underperformance in simulating the early Eocene warm climate system should be carefully considered in evaluations of model predictions of future climates, especially the drivers of high-latitude warmth and the magnitude of polar amplification (IPCC, 2013, Zachos et al., 2008, Zeebe and Zachos, 2013, Zhu et al., 2019). Obviously, there can be no direct analogy between past deep-time climate states and future climates, when key boundary conditions are substantially different, including orbital configuration, sunspot activity, plate tectonic settings, greenhouse gas concentrations and rates of change, the positioning of oceanic gateways and the resultant atmospheric and oceanic circulation (see for example: Crowley, 1990, Zachos et al., 2008, IPCC, 2013, Zeebe et al., 2016). All of these boundary conditions potentially interact with positive and negative feedbacks, including strong biosphere and carbon cycle dynamics, and could result in long-term variations in equilibrium climate sensitivity (Farnsworth et al., 2019), defined as the response of global annual mean surface temperature to a doubling in CO_2, equivalent to a radiative forcing of 3.7 Wm^{-2} (Skinner, 2012, PALAEOSENS, 2012, Rohling et al., 2018). Further, the long-term Earth system equilibrium responses of ice-free climate states of the Eocene will not be analogous to the highly transient conditions of a future "high CO_2 glaciated world", even if greenhouse gas radiative forcings are similar (Zeebe et al., 2016, Farnsworth et al., 2019). Fundamentally, however, the only data we have to constrain the Earth's response to greatly elevated levels of CO_2 comes from deep-time palaeoclimates (IPCC, 2013).

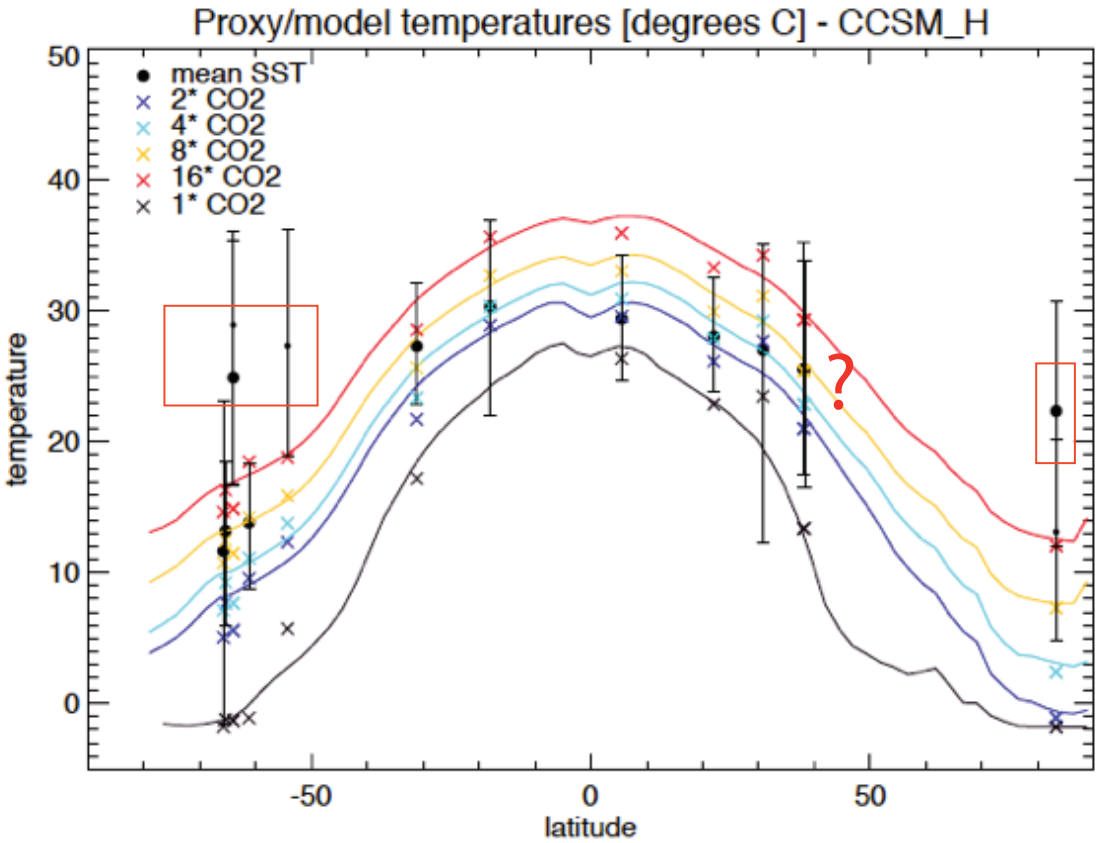

Figure 1.1. Comparison of climate model and proxy data reconstruction of early Eocene ocean surface temperatures across latitudes (after Lunt et al., 2012). The Core position of 16/28-sb01 is represented by a red question mark and lies within a proxy data gap. For proxy data sources see Lunt et al. (2012), data mean Eocene (large filled dots) and from the EECO (small filled dots) represent the mean proxy temperature, the error bars show the temperature range. Climate model results are a variation of the CCSM3 and CCSM_H model (Liu et al., 2009, Huber and Caballero, 2011), with modelled SST with different pCO_2 forcings (represented by x (modelled temperature at the same position as the proxy data) and lines (modelled zonal mean temperatures). For higher latitudes in the Southern and Northern Hemispheres there is a proxy to model data discrepancy (orange boxes), with proxy data indicating warmer temperatures than the models (Lunt et al., 2012).

1.2 Aims and Objectives

The overarching aim of this thesis is to achieve new palaeoclimatic understandings of the early and middle Eocene of the NE Atlantic Ocean by generating new sedimentological and geochemical records from marine sediment cores recovered at Site 16/28-sb01 from the Rockall Basin, to the West of Ireland (Figure 1.2.).

To date, there are very few sites with high-resolution and multi-proxy SST data covering the early Eocene (Cramer et al., 2003, Zachos et al., 2010, Littler et al., 2014), especially around the northern paleolatitude (~49˚N) of Site 16/28-sb01 (Lunt et al., 2012, Evans et al., 2018b) (Figure 1.1.) and even less SST reconstructions are available from the EECO. Site 16/28-sb01 is unique because it covers parts of the EECO, and

sediments are exceptional in the quality of their preservation of marine and terrestrial microfossils and organic biomarkers suitable for multi-proxy SST reconstructions. Thus, new records from this site will be a source of indispensable information for the palaeoclimate proxy and model research community.

1.2.1 Chapter 2: Stratigraphic and palaeoenvironmental reconstructions of Site 16/28-sb01 of the Rockall Basin, NE Atlantic

To put the new palaeoclimate data of this thesis into a global context it is key to have a reliable age model. Therefore, the main aim of this chapter is to develop a robust age model on the GTS2012 for Site 16/28-sb01. Specific objects are:

- To review published biostratigraphies and sedimentology of Site 16/28-sb01
- This reviews are than used to compare and develop a new calcareous nannofossil biostratigraphy, which will be aligned to the calcareous nannofossil scheme of Agnini et al. (2014)
- To improve this age alignment based on calcareous biostratigraphy a new high-resolution bulk carbon ($\delta^{13}C$) and oxygen ($\delta^{18}O$) isotope stratigraphy will be developed and correlated to the high-resolution target isotope curve of Sexton et al. (2011) and Kirtland Turner et al. (2014) from ODP Site 1258, Demerara rise, equatorial Atlantic.

The secondary aim of this chapter is to determine the early to middle Eocene palaeoenvironment of Site 16/28-sb01 and investigate possibly detected CIEs in detail. Following objectives are used to achieve this:

- Generate a high-resolution (~5 ka resolution) XRF (X-Ray Fluorescence) dataset to characterized the elemental distribution and possible changes within the bulk sediments of Site 16/28-sb01 and within the detected CIEs.
- Utilise the new high-resolution bulk $\delta^{13}C$ and $\delta^{18}O$ isotope data to study fine scale climate variability within the CIEs.
- Compare in Chapter 3 and 4 as well the absolute foraminiferal genera abundance, coarse fraction (> 63 µm) percentage and cenospehroid radiolarian presence and absence and variability within the reconstructed SSTs with the found CIEs.

1.2.2 Chapter 3: Early and middle Eocene palaeo-climate and -ecology from well-preserved planktic foraminifera in the Rockall Basin

SST reconstructed from glassy (well-preserved) foraminifera are rare for the early Eocene, in fact by following the EECO definition of Westerhold et al. (2018b) (53-49 Ma), just two marine sites provide glassy planktic foraminiferal $\delta^{18}O$ records so far: one around ~53.2 Ma (Tanzania Drilling Project (TDP) Site 3) and one ~48.5 Ma from Hampden Beach, New Zealand (Hollis et al., 2019). Thus, the aim of this chapter is to provide another glassy foraminiferal SST record within the EECO and the middle Eocene of Site 16/28-sb01. Following objectives are used:

- First of all, to reconstruct the palaeoecology of planktic foraminifera in two time slices from the early and middle Eocene in order to A) identify which foraminiferal species lived in which water depth and B) to identify the best possible planktic foraminiferal species to measure for a long-term stable oxygen isotope ($\delta^{18}O$) record.
- Secondly to generate a long-term stable oxygen isotope ($\delta^{18}O$) record from glassy preserved planktic foraminifera in the surface and thermocline ocean to reconstruct SST and thermocline ocean temperature.
- Thirdly to use the abundance of planktic foraminifera to identify possible changes in the local depositional environment and possible climate and oceanographic implications.

1.2.3 Chapter 4: Early and middle Eocene SST record based on TEX_{86} for Site 16/28-sb01.

So far ten marine records provide SSTs based on the organic membrane lipids (GDGTs) of Thaumarchaeota within the EECO (Hollis et al., 2019) indicating the presence of a reduced latitudinal temperature gradient. Often each SST approach has its very own caveats and uncertainties so using a multi-proxy approach has the power to reduce and help constraint the uncertainty of SST reconstructions at specific sites. The aim of this chapter is to provide an additional SST proxy based on GDGTs of Site 16/28-sb01. Objectives used therefore are:

- To extract the organics of the 16/28-sb01 samples at the same depth as the foraminiferal SST reconstructions

- To measure and integrate the different GDGTs and use them to reconstruct SSTs.
- To test if there is unusual GDGT distribution or if different calibrations do change the SST reconstructions
- To compare with the foraminiferal based SSTs reconstructions of the previous Chapter.
- To conclude if both SST proxies fit within the bigger Eocene picture of reduced latitudinal SST gradient, as postulated by previous proxy studies (Hollis et al., 2012, Evans et al., 2018b, Hollis et al., 2019)

Within the remaining sections of this Introduction (Chapter 1) a brief introduction to the general climate and ocean circulation of the Eocene will be given, to set the scene for data and interpretations presented in this thesis.

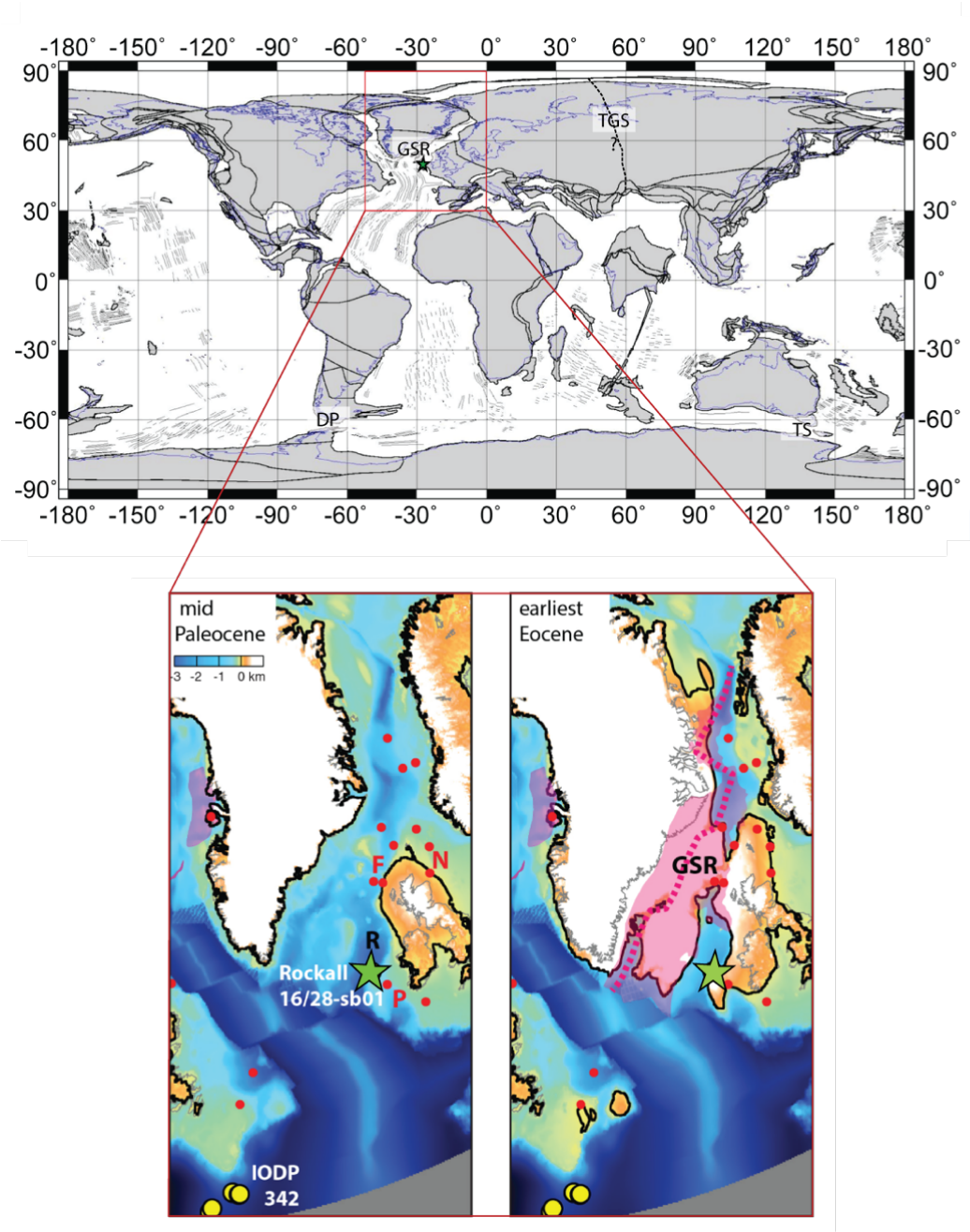

Figure 1.2. Early Paleogene paleogeographies to highlight the study Site 16/28-sb01 (green star). The top map shows a palaeogeography reconstruction from the early Eocene (50 Ma) generated by using the website: http://www.odsn.de/odsn/services/paleomap/paleomap.html. The plates are moved relative to a Magnetic Reference Frame with an equidistant cylindrical map projection. Showing the approximate palaeolocation of Site 16/28-sb01 with a green star. Important gateways during this time are shown including the: GSR = Greenland Scotland Ridge; TGS = Turgay Strait; DP= Drake Passage and TS= Tasman Strait. The modern shore line is indicated with a blue line and the palaeoplate boundaries are in black. Within the global overview map (top) the magnetic lineations are given with black lines within the ocean basins to indicate the mid ocean ridge spreading. The bottom map shows the influence of the North Atlantic Igneous Province (NAIP) on the uplift of the GSR relative to the study Site location (indicated with the green star) from the mid Paleocene to the earliest Eocene, obtained from co-supervisor Stephan Jones (pers. comm.) and after Maclennan and Jones (2006). The map uses seismic reflector data constraints for the palaeogeography which are indicated with red dots. The important basins are indicated with R=Rockall Trough, F=Faroe-Shetland Basin, N=North Sea and P=Porcupine Basin. The yellow dots indicate site locations of the IODP Expedition 342 on the Newfoundland Ridge.

1.3 Eocene climate evolution, stratigraphy and its recurrent CIEs

The Eocene (56.0 – 33.9 Ma) consists of three intervals and four stages, the early Eocene, consisting of the Ypresian (56.0 – 47.8 Ma), the middle Eocene, consisting of the Lutetian (47.8 – 41.2 Ma) and the Bartonian (41.2 – 37.8 Ma) and the late Eocene, consisting of the Priabonian (37.8 – 33.9 Ma) (Aubry et al., 2007, Vandenberghe et al., 2012) (Figure 1.3.). The Eocene is the warmest interval of the Cenozoic (Zachos et al., 2008), with polar regions more than 20˚C warmer than the modern (Bijl et al., 2009, Sluijs et al., 2006, Lunt et al., 2012, Hollis et al., 2019). Under these conditions of warmth, the poles are presumed to have been ice-free: the Eocene had "greenhouse" climate conditions, with no dynamic ice-albedo effect. The base of the Eocene is identified by the most extreme CIE of the Cenozoic (Aubry et al., 2007, Vandenberghe et al., 2012), associated with the onset of the so called Paleocene Eocene Thermal Maximum (PETM) (Kennett and Stott, 1991, Vandenberghe et al., 2012), which occurred around ~56 Ma (Kennett and Stott, 1991, Zachos et al., 1993, Westerhold et al., 2017).

The general early Paleogene climate evolution was a long-term warming trend, starting in the mid to late Paleocene (Zachos et al., 2008, Cramer et al., 2009). This trend culminated in the early Eocene Climate Optimum (EECO) 53 – 49 Ma (Westerhold et al., 2018a). The EECO is the zenith of persistent warmth during the Cenozoic (Zachos et al., 2001, Nicolo et al., 2007, Zachos et al., 2008, Bijl et al., 2009, Westerhold and Röhl, 2009, Stap et al., 2010b, Huber and Caballero, 2011, Hollis et al., 2012, Pross et al., 2012, Inglis et al., 2015, Westerhold et al., 2018a). After the EECO the climate of the Earth cooled, through the middle-to-late Eocene (Zachos et al., 1994, Barrett, 1996, Zachos et al., 1996, Coxall et al., 2005, Katz et al., 2008), but the drivers of this long-term trend are still poorly constrained. The two primary candidates are ocean circulation changes, such as the onset of Antarctic Circumpolar Current (ACC) with progressive Southern Ocean gateway opening (Kennett, 1977, Kennett and Exon, 2004, Stickley et al., 2004, Bijl et al., 2013) and/or declining atmospheric greenhouse gas concentrations (Huber et al., 2004, Pagani et al., 2005, Zhang et al., 2013, Inglis et al., 2015, Anagnostou et al., 2016, Cramwinckel et al.,

2018). This cooling trend culminated in the Eocene/Oligocene transition and the establishment of a “one-cold” pole glaciated climate state (Pälike et al., 2006).

Superimposed on this long-term, post-EECO, cooling trend are shorter climate reversals, including at ~40 Ma, in the early Bartonian, a warming event lasting ~500 ka, known as the Middle Eocene Climate Optimum (MECO) (Bohaty and Zachos, 2003, Bohaty et al., 2009). The cause of the MECO (Bohaty and Zachos, 2003) is proposed to be an increase of atmospheric CO_2 (Bijl et al., 2010) correlated with the early stages of the Himalayan orogeny (collision of Asia and India) and/or enhanced ridge volcanism (Bohaty and Zachos, 2003). This highlights the importance of potential tectonic controls on the evolution of Eocene climate, as the major continents continue to move towards their modern configuration, including the opening of the North Atlantic (e.g., Hallam, 1971, Saunders et al., 1997) and the early stages of the formation of the Himalaya orogeny (Rowley, 1996). In the context of this project, as well as records of early Eocene peak warmth, the Rockall cores also provide comparative North Atlantic proxy data between the EECO and cooler, later middle Eocene climates, before the MECO warm reversal. These data will thus help to quantify the magnitude of high mid-latitude cooling associated with this long-term climate evolution.

The peak warmth of the Eocene, the EECO, is a key focus of this study due to the sparse availability of palaeoclimate proxy data within this time interval, and its importance as an “end-member” warm climate state for the Cenozoic. It is also of interest for short-term (~40 – 60 ka) climate transients, in the form of reoccurring CIEs of magnitude ~1 ‰, that occur repeatedly every ~100 to ~400 ka throughout the warming trend of the late Paleocene to the middle Eocene (Cramer et al., 2003, Sexton et al., 2011, Kirtland Turner et al., 2014, Lauretano et al., 2015, Lauretano et al., 2016). An alphabetic numbering system for these CIEs (A – L) was introduced by Cramer et al. (2003) and expanded by Lauretano et al. (2016) (M – W). An alternative nomenclature for the CIEs based on magnetostratigraphy was developed by Sexton et al. (2011) and Kirtland Turner et al. (2014). An overview figure of all identified late Paleocene to early Eocene CIEs, with the different nomenclatures is shown in Figure 1.4. (taken from Westerhold et al., 2018a). These CIEs are useful for the stratigraphic correlation of high-resolution isotopic records (Cramer et al., 2003), as the CIEs are a

global phenomenon and are assumed to be synchronous between ocean basins (Coccioni et al., 2012, Lauretano et al., 2015, Abels et al., 2016, Luciani et al., 2017a, Westerhold et al., 2018a, Galeotti et al., 2019). The potential mechanism and drivers of CIEs are discussed further in Section 1.4 below.

The exact definition of the start and end, and hence duration, of the warm EECO varies from 53 – 51 Ma (Zachos et al., 2008) to 52 – 50 Ma (Vandenberghe et al., 2012) or, in more recent publications, 53 – 49 Ma (Slotnick et al., 2012, Slotnick et al., 2015, Lauretano et al., 2015, Luciani et al., 2016). A recent suggestion for defining the timing of the EECO is given in Galeotti et al. (2017), who proposed defining the EECO as the interval which is highly sensitive to eccentricity and is located during magnetochron C23n (51.8 – 50.6 Ma), comprising CIEs: N, O, P and Q. Westerhold et al. (2018a) prefer the earlier, longer duration definitions, and propose a start at the J CIE (53.26 Ma) through to 49.14 Ma (on the GTS2012 timescale). In this thesis this most recent definition of the EECO from Westerhold et al. (2018a) is followed. Throughout this thesis the GTS2012 timescale will be used for consistency with recently published plankton biostratigraphic schemes (Agnini et al., 2014), and for inter-comparison between sites within the DeepMIP database as recommended in Hollis et al. (2019).

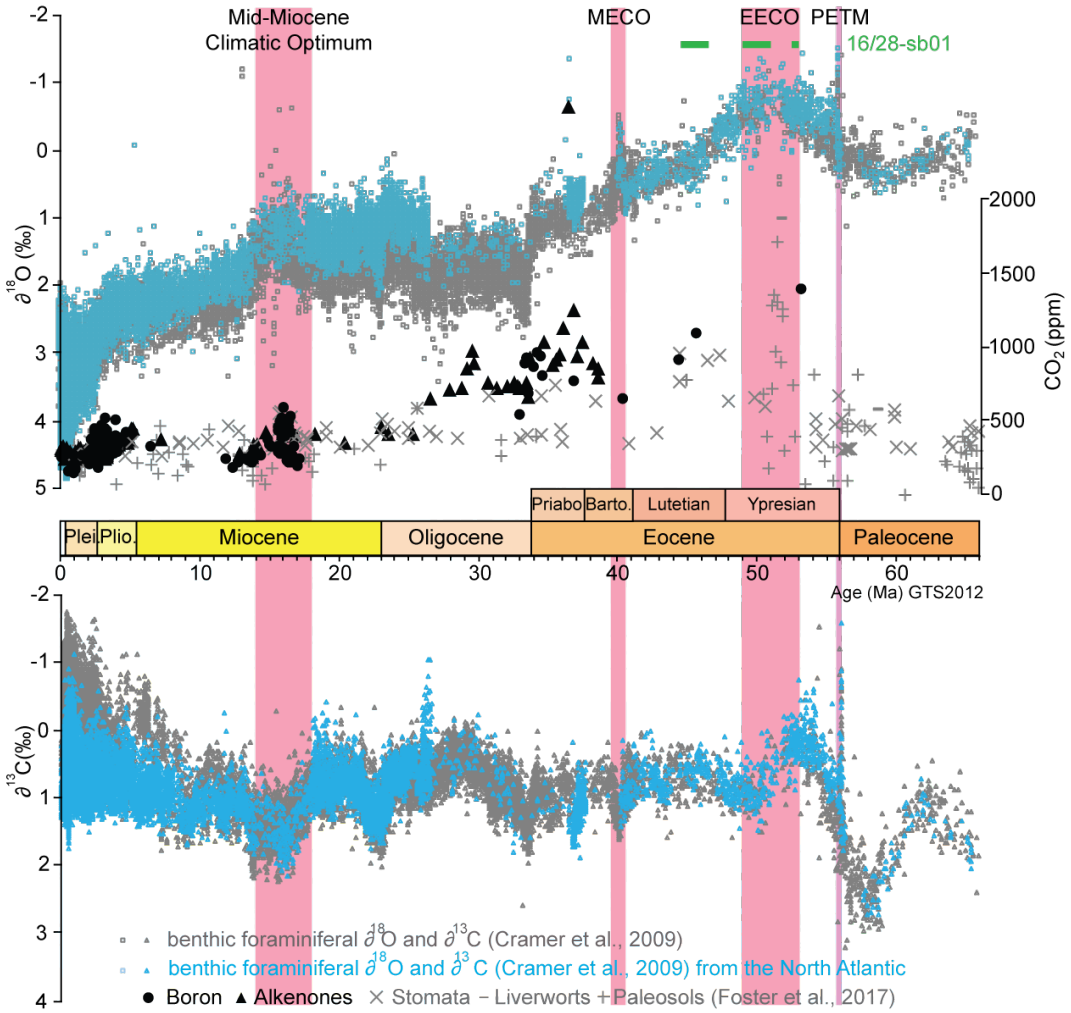

Figure 1.3. An overview of general Cenozoic climate trends and its climate optima is given together with atmospheric CO_2 reconstructions. Therefore, the global marine isotope compilation of Cramer et al. (2009) consistent for benthic foraminiferal $\delta^{13}C$ and $\delta^{18}O$ values (grey triangle and square) and Foster et al. (2017) data compilation for CO_2 values (black and light black symbols) is used. As the Site 16/28-sb01 is located in the North Atlantic the North Atlantic isotope data are highlighted (blue square and triangle). The 16/28-sb01 core recovery (green bars) and major warming events within the Cenozoic (pink bars) are also indicated: Mid-Miocene Climatic Optimum; MECO= Middle Eocene Climatic Optimum; EECO= early Eocene Climatic Optimum and PETM= Paleocene Eocene Thermal Maximum).

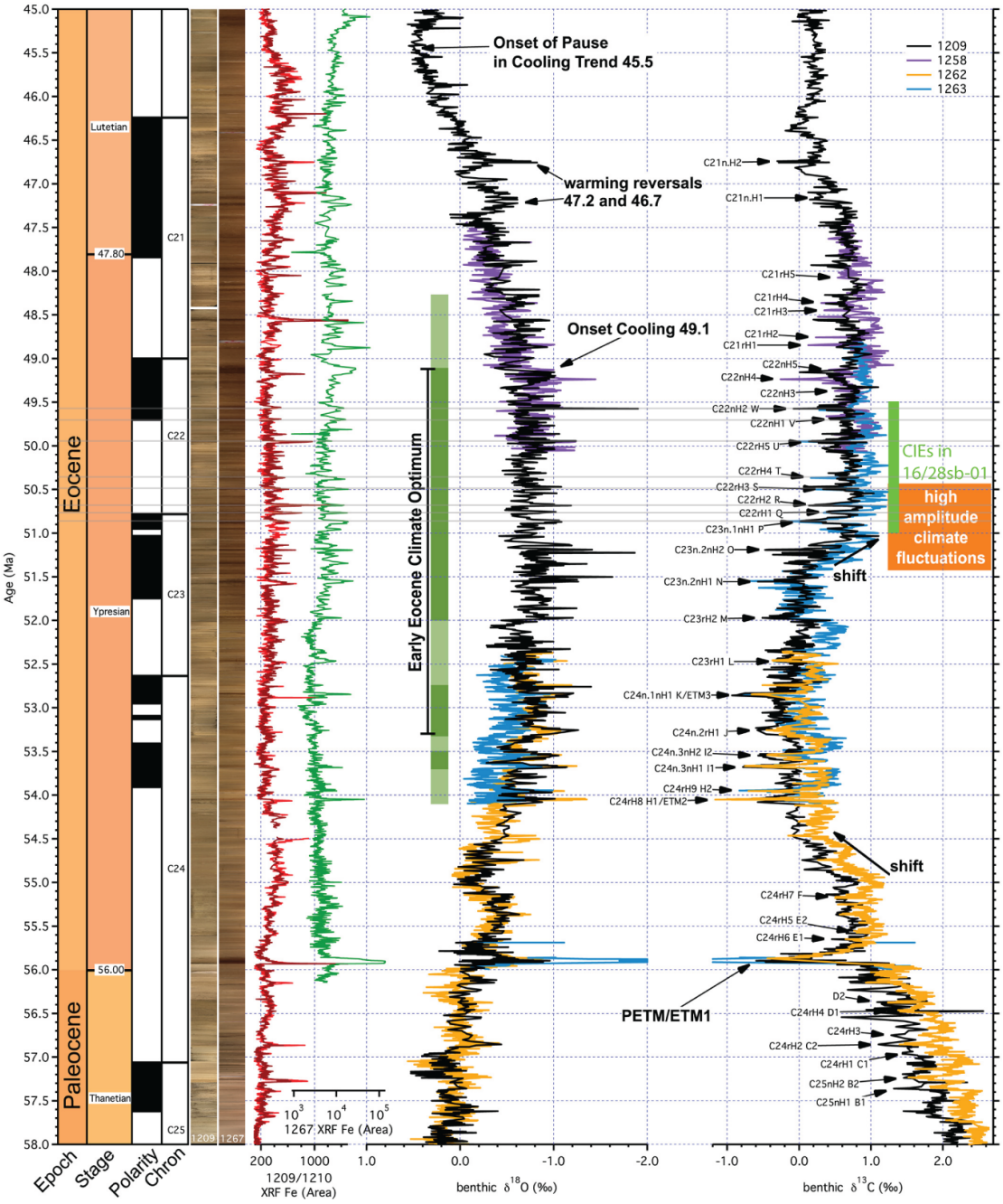

Figure 1.4. A recent compilation of the late Paleocene to middle Eocene transient CIEs and their nomenclature from Westerhold et al. (2018a) and references therein. The CIEs are typically associated with peaks in sedimentary iron content in open marine settings. In 16/28-sb01, a part of the EECO interval was recovered (indicated in green) and the CIEs within the carbonate bulk isotope data will be used for the age alignment and are presented in Chapter 2. ODP Site 1209 is in the North Pacific, Site 1258 in the equatorial Atlantic, Sites 1262 and 1263 are in the South Atlantic.

1.4 Understanding the Eocene CIEs and hyperthermals

The late Paleocene to early Eocene CIEs are thought to be triggered by pulses of greenhouse gas release from a ^{13}C-depleted carbon source, very likely linked to orbital forcing, in particular eccentricity maxima (Cramer et al., 2003, Lourens et al., 2005, Westerhold et al., 2007, Nicolo et al., 2007, Zachos et al., 2010, Hilgen et al., 2010, Galeotti et al., 2010, Sexton et al., 2011, Kirtland Turner et al., 2014, Littler et al., 2014, Lauretano et al., 2015, Lauretano et al., 2016, Laurin et al., 2016, Galeotti et al., 2017, Westerhold et al., 2017, Westerhold et al., 2018a, Barnet et al., 2019). These CIEs have been observed in both benthic foraminiferal (Sexton et al., 2011, Westerhold et al., 2017) and bulk carbonate isotope records (Cramer et al., 2003, Kirtland Turner et al., 2014), often paired with negative $\delta^{18}O$ excursions.

Within the CIEs, a sub-set of larger CIE magnitude events, associated with independent evidence for substantial global warming, are known as “hyperthermals”. These more prominent events were discovered first, and are better studied than the smaller CIEs. Many of these hyperthermals are named outside of the alphabetic system: the PETM (alternative name: Eocene Thermal Maximum 1 (ETM-1)), ETM-2 (alias H1, associated with the Elmo-clay-layer) (Lourens et al., 2005, Stap et al., 2009, Stap et al., 2010b) and ETM-3 (alias K (Cramer et al., 2003) or X (Röhl et al., 2005)) event. Although there are still uncertainties in the late Paleocene to early Eocene timescale, as discussed in Westerhold et al. (2008) and Westerhold et al. (2017), the most pronounced CIE, the PETM is placed at ~56 Ma, followed by the ETM-2 at ~53.7 Ma (Lourens et al., 2005, Stap et al., 2009, Stap et al., 2010b) and the ETM-3 at ~52 Ma (Röhl et al., 2005, Westerhold and Röhl, 2009). The CIEs associated with these “hyperthermals” are also observed in planktic foraminifera carbon and oxygen isotope records (Thomas et al., 1999, Stap et al., 2010a) and in terrestrial $\delta^{13}C$ records from carbonate nodules (Abels et al., 2012, Abels et al., 2016) or diffuse organic matter (e.g., Manners et al., 2013).

Although it is still debated whether the most frequently investigated CIE, the PETM, is orbitally driven (Cramer et al., 2003, Lourens et al., 2005, Westerhold et al., 2018b), the extensive studies of the PETM are informative about both carbon cycle dynamics and the behaviour of the early Paleogene Earth System to transient warming events.

The PETM is associated with a negative CIE of ~4 ‰ and a negative excursion of >1 ‰ in planktic and benthic foraminifera $\delta^{18}O$, consistent with a warming of ~5˚C or more (Stott et al., 1990, Zachos et al., 2001, Zachos et al., 2007, Dunkley Jones et al., 2010, Hollis et al., 2012, Dunkley Jones et al., 2013). The causes of this ~220 ka (Röhl et al., 2000) or more recently ~200 ka (Westerhold et al., 2018b) long "hyperthermal" are still under debate. Hypotheses include sub-seafloor methane hydrate dissociation (Dickens et al., 1995, Dickens et al., 1997, Katz et al., 2001, Kennett et al., 2003, Maclennan and Jones, 2006, Lunt et al., 2010, Dickens, 2011), the seasonal thawing of permafrost (DeConto et al., 2012), volcanic CO_2 and thermogenic methane release from the North Atlantic Igneous Province (NAIP) (Svensen et al., 2004, Schmitz et al., 2004, Maclennan and Jones, 2006, Storey et al., 2007, Wieczorek et al., 2013, Rampino, 2013, Frieling et al., 2016, Gutjahr et al., 2017, Jones et al., 2019), combustion or oxidation of buried terrestrial organic carbon (Kurtz et al., 2003, Higgins and Schrag, 2006, Zachos et al., 2010), a comet impact (Kent et al., 2003, Cramer and Kent, 2005, Schaller et al., 2016, Kent et al., 2017, Schaller and Fung, 2018) and explosive volcanism in the Caribbean (Bralower et al., 1997). Of these carbon sources, igneous activity and comet impacts are events that are highly unlikely to be able to provide the ^{13}C-depleted carbon at semi-regular intervals for all the repeated CIE events from the late Paleocene through to the early Eocene, especially when these events exhibit some degree of orbital forcing. The similar scaling of CIE magnitudes in marine and terrestrial records for PETM, ETM-2 and ETM-3, has been used to suggest that these events share a similar source of ^{13}C-depleted carbon (Abels et al., 2012). Likewise, the relationship of CIEs to the coupled oxygen isotope excursions recorded in benthic foraminifera, suggests an additional contribution from a more ^{13}C-depleted (e.g. CH_4) source during the PETM, ETM2, ETM3, P, S, T and C21nH1 — compared to all the other transient CIEs (Westerhold et al., 2018a). One of the most recent studies from Kocken et al. (2019) uses the LOSCAR (Long-term Ocean-atmosphere-Sediment CArbon cycle Reservoir model) to support the hypotheses of organic carbon burial and oxidation in the ocean as a possibility for triggering orbital-forced disturbances in the carbon cycle. However the exact cause and source/s of this repeated transient CIEs remains a conundrum.

In pelagic sediments recovered from open marine settings, the CIEs are usually accompanied by peaks in the abundance of iron associated with carbonate dissolution (Zachos et al., 2005, Lourens et al., 2005, Zachos et al., 2010, Sexton et al., 2011). Deep-ocean carbonate dissolution, and shoaling of the CCD (Carbonate Compensation Depth), is pronounced in the larger "hyperthermals", including the PETM (Thomas, 1998, Thomas et al., 1999, Zachos et al., 2005, Zachos et al., 2007, Zeebe and Zachos, 2007), ETM-2 (Lourens et al., 2005, Stap et al., 2009) and ETM-3 (Stap et al., 2009, Agnini et al., 2009, Leon-Rodriguez and Dickens, 2010), but is also observed in several of the smaller CIEs (Galeotti et al., 2017, Westerhold et al., 2018a). As well as deep ocean carbonate dissolution, new planktic foraminiferal boron (B/Ca and δ^{11}B) data show that the PETM, and hence potentially other CIEs as well, is associated with some degree of surface ocean acidification (Penman et al., 2014, Babila et al., 2016, Gutjahr et al., 2017, Babila et al., 2018, Harper et al., 2019). Both the short-term deep ocean carbonate dissolution during the "hyperthermals", and potential surface ocean acidification, are consistent with rapidly increased atmospheric greenhouse gas concentrations, the absorption of a large proportion of this CO_2 by the ocean, and the resultant disturbance in oceanic carbonate system equilibrium (Panchuk et al., 2008, Zeebe et al., 2009, Cui et al., 2011, Hönisch et al., 2012). Over time, this short-term carbonate system disequilibrium — with a shallowing of the CCD — is assumed to be counter balanced by increased silicate weathering, driven by warming and an accelerated hydrological cycle (Walker et al., 1981, Hönisch et al., 2012, Zeebe and Zachos, 2013), and enhanced rates of organic carbon burial (Bowen and Zachos, 2010). In the early Eocene, enhanced marine silicate deposition is found to take place within the Atlantic and is suggested to be linked to the CIEs (Penman et al., 2019).

The warmer climate of the early Eocene is associated with an intensified hydrological cycle compared to modern, especially during its CIEs, leading to enhanced fresh water and terrigenous influx into the oceans (Kaiho et al., 1996, Slotnick et al., 2012). In many locations there is evidence that this enhanced freshwater influx increased water column stratification in restricted ocean basins and shallow marine environments (Barron et al., 1989, Slotnick et al., 2012, Slotnick et al., 2015, Carmichael et al., 2016, Carmichael et al., 2017), and in extreme cases led to bottom water anoxia (Carmichael et al., 2017), for example in the Arctic Ocean during ETM-2 (Sluijs et al., 2009).

Modelled early Eocene precipitation distributions show enhanced moisture transport to the higher latitudes and poles relative to the modern, driven by the warmer background climate state and a substantially reduced latitudinal temperature gradient (Barron et al., 1989, Speelman et al., 2010, Carmichael et al., 2016, Carmichael et al., 2017). Proxy evidence to support these models results include the abundant occurrence of the freshwater fern *Azolla* within the Arctic basin from around ~50 Ma (Brinkhuis et al., 2006). Recently it was suggested that the *Azolla* event was restricted to the Arctic Eurasian basin, with increased terrestrial run off, driven by enhanced hydrological cycle into the Arctic Amerasian basin (Neville et al., 2019). Clay enrichment within upper slope marine sediments during the early Eocene CIEs in higher latitude locations has also been linked to increased terrestrial runoff (Slotnick et al., 2012, Slotnick et al., 2015).

The larger hyperthermals, especially the PETM, are associated with faunal and floral changes, including extinctions in marine and terrestrial environments (Wing, 1998, Thomas and Shackleton, 1996, Thomas, 1998, Crouch et al., 2001, Gingerich, 2003, Wing et al., 2005, Gibbs et al., 2006), such as the biggest benthic foraminiferal extinction interval in the Cenozoic associated with the PETM (e.g., Thomas, 1990, Thomas, 1998, Thomas, 2007, Alegret et al., 2005). There are fewer biotic records from the smaller CIEs but some work has been carried out on benthic (Thomas, 1998, Arreguín-Rodríguez et al., 2016, Arreguín-Rodríguez et al., 2018) and planktic foraminifera (Luciani et al., 2016, Luciani et al., 2017a, Luciani et al., 2017b). Of the surviving benthic foraminifera taxa of the PETM, one of the most common, *Nuttallides truempyi,* shows declines in abundance during the PETM and the ETM3, whereas ETM2 is linked with increased abundances (Arreguín-Rodríguez et al., 2016). This complex pattern is likely the result of competing influences — e.g. circulation, oxygenation, productivity, temperature, carbonate chemistry — that may vary between the CIEs.

In the realm of planktic foraminifera, of early to middle Eocene assemblages three genera are very typically studied. Two of these are mixed-layer (surface) dwellers — *Morozovella* and *Acarinina* — and one is a thermocline dweller — *Subbotina* (Pearson et al., 2006, and references therein). *Acarinina* tend to dominate mixed-layer assemblages from the J event, which marks the onset of the EECO (Luciani et al.,

2017b), whereas *Morozovella* abundances decline and do not recover to pre-EECO abundance (Luciani et al., 2016). The abundance of thermocline-dwelling *Subbotina* remains broadly stable through the Eocene, with only a decline towards the peak EECO followed with a swift recovery even before the EECO ends (Luciani et al., 2016). As for the benthic foraminifera, there are no consistent patterns in planktic foraminifera assemblage changes between the each of these CIEs, implying a complex interaction between environmental change and biotic responses in the surface oceans (Luciani et al., 2017a).

1.5 Ocean circulation in the Eocene with a focus on the Atlantic

Deep-water formation is one of the main drivers of global oceanic circulation that distributes heat, salinity and nutrients across the ocean basins (Broecker and Peng, 1982). Today deep-water formation is bipolar, with primary sources in the Northern Atlantic (North Atlantic Deep Water (NADW)) and in the Southern Ocean (Antarctic bottom water (AABW)). Within the North Atlantic, there are two dominant regions of deep-water formation: the Norwegian Sea, which exports deeper and colder water via two different pathways into the bottom layer of the NADW, and the Labrador Sea, which exports the slightly warmer top layer of NADW (Broecker and Peng, 1982, Dickson and Brown, 1994). Although knowledge of Eocene global circulation is limited, a short overview is provided here of the first order, large-scale circulation patterns and then focus on the Northern Atlantic regional context for the study site.

Reconstruction of past circulation patterns relies on the characterisation of deep-water properties from sedimentological or geochemical proxies, such as temperature ($\delta^{18}O$) and water-mass chemistry, including the isotopic composition of dissolved inorganic carbon (DIC) and dissolved neodymium (ε_{Nd}). To reconstruct global patterns, this proxy data is required from multiple sites across all ocean basins, with $\delta^{13}C$ of DIC ($\delta^{13}C_{DIC}$) estimated from benthic foraminiferal test carbonate (Sexton et al., 2006a, Cramer et al., 2009) and seawater ε_{Nd} from fossil fish teeth/remains (Scher and Martin, 2004, Thomas, 2004, Via and Thomas, 2006). For the early Eocene, benthic foraminiferal $\delta^{13}C$ records provide some of the best data to reconstruct patterns of global deep water circulation (Sexton et al., 2006a, Cramer et al., 2009; Figure 1.3.;

Figure 1.5.), with newly formed deep water possessing more positive $\delta^{13}C_{DIC}$ values than older water masses. As water masses age they collect more nutrients and ^{12}C — from the oxidation of ^{12}C-rich organic matter — leading to more negative $\delta^{13}C$ signatures (Kroopnick, 1985). Within an extensive compilation of early Eocene benthic foraminiferal isotopes (Cramer et al., 2009) and already in an earlier study on benthic foraminiferal isotopes (Sexton et al., 2006a) values of carbon and oxygen isotopes are found to be similar (<0.5 ‰ inter-basinal isotopic difference) across the South Atlantic, Southern Ocean, Pacific and Indian Oceans (Sexton et al., 2006a, Cramer et al., 2009). This apparent isotopic homogeneity between the basins (Figure 1.3.) is consistent with limited water mass aging due to either: (1) a single Southern Ocean deep-water source combined with a reduced biological pump or (2) multiple sites of deep-water formation with relatively short deep-ocean circulation pathways (Sexton et al., 2006a). In the second case, however, the multiple source regions are very likely to introduce more heterogeneity in-between the ocean basins (Sexton et al., 2006a). From 50 Ma and into the middle Eocene there is a divergence of benthic foraminiferal $\delta^{13}C$ signatures between ocean basins — with more positive $\delta^{13}C$ values from 50 – 48 Ma in the Southern Indian Ocean compared to the more homogeneous tropical Atlantic, Pacific Ocean and Southern Ocean and then from 48 – 44 Ma the most positive $\delta^{13}C$ values occur in the Indian and Southern Ocean compared to less positive values in the tropical Atlantic, with the lowest recorded values in the Pacific (Sexton et al., 2006a). This pattern is interpreted to represent a dominant Southern Ocean deep water source close to the Indian Ocean in the early to middle Eocene, but might have switched to multiple sites of deep water formation during intervals when there is increased isotopic heterogeneity (Sexton et al., 2006a). In the compilation of Cramer et al. (2009) there is increasing heterogeneity in $\delta^{13}C$ signatures between the ocean basins starting from ~46 Ma, with most positive $\delta^{13}C$ values in the Pacific and Southern Ocean, which is interpreted as enhanced wind induced water mass mixing and the gradual establishment of the proto-ACC, linked to the opening of the shallow Drake Passage

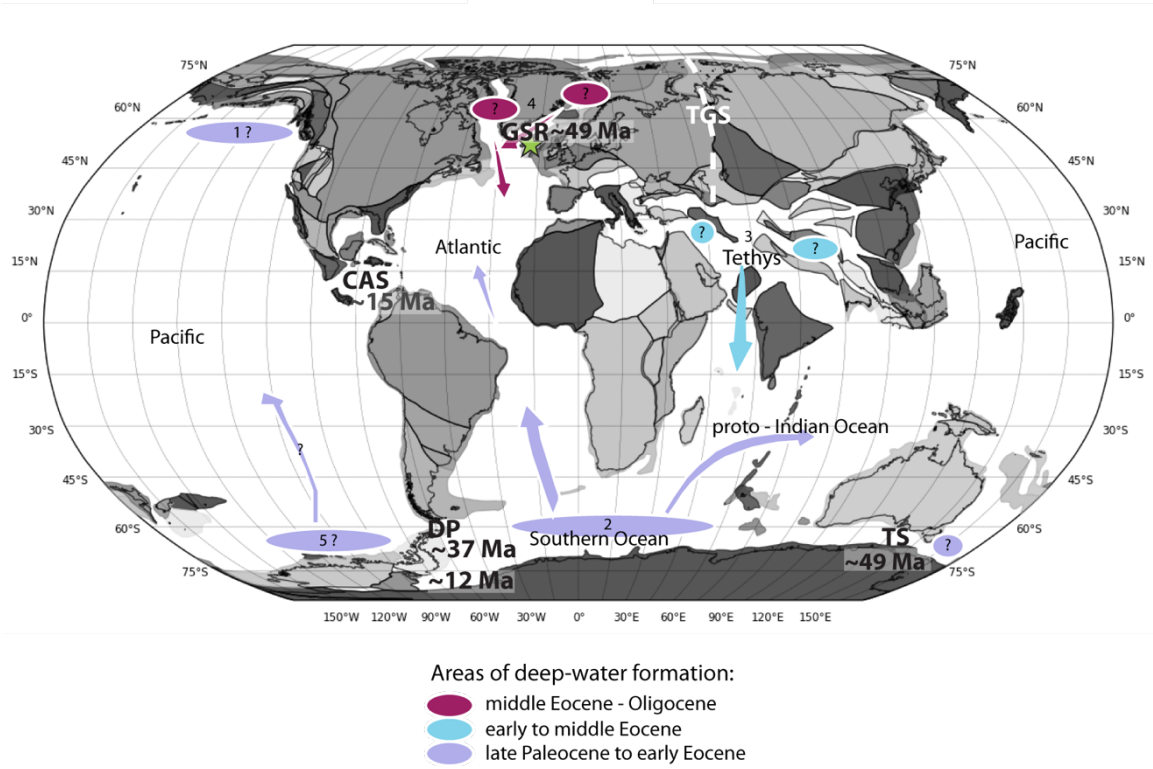

Figure 1.5. Summary of early Paleogene areas of deep-water formation and proposed flow paths. This palaeomap was reconstructed for ~50 Ma on the website https://portal.gplates.org/portal/paleomapmaker/ using Robinsons projections and the Paleomap model. The palaeolocation of Site 16/28-sb01 is given with a green star; deep-water formation sites are given in purple, blue and aubergine. Abbreviations mean: GSR=Greenland Scotland Ridge, TGS=Turgay Strait, DP=Drake Passage, TS=Tasman Strait and CAS= Central America Seaway. The numbers below the gateways in black imply their inferred opening times for the DP ~37 Ma (Scher and Martin, 2004), ~12 Ma (Dalziel et al., 2013); for the TS ~49 Ma (Bijl et al., 2013); GSR ~49 Ma (Hohbein et al., 2012) and in grey their closure times CAS ~15 Ma (Montes et al., 2012, Montes et al., 2015). Different possible deep water formation sites: 1) North Pacific: Paleocene (Barron and Peterson, 1991), ~PETM (Tripati and Elderfield, 2005, Lunt et al., 2010) ~65 – 40 Ma (Thomas, 2004); 2) Southern Ocean: late Paleocene (Barron and Peterson, 1991, Mountain and Miller, 1992, Bice and Marotzke, 2002, Thomas et al., 2003, Tripati and Elderfield, 2005, Nunes and Norris, 2006), early Eocene (Pak and Miller, 1992, Ramsay et al., 1994, Thomas et al., 2003, Tripati and Elderfield, 2005, Nunes and Norris, 2006, Sexton et al., 2006a), middle Eocene (Ramsay et al., 1994, Scher and Martin, 2004, Sexton et al., 2006a); 3) Tethys: late Paleocene (O'Connell et al., 1996), PETM (Kaiho et al., 1996, Lunt et al., 2010), early Eocene (Barron and Peterson, 1991, Pak and Miller, 1992, Mountain and Miller, 1992, Huber and Sloan, 2001), middle Eocene (Barron and Peterson, 1991, Scher and Martin, 2004); 4) Northern seas: ~PETM (Bice and Marotzke, 2002, Nunes and Norris, 2006, Lunt et al., 2010), ~50 Ma (Huber and Sloan, 2001); 5) Southern Pacific: PETM (Lunt et al., 2010).

and the Tasman gateway, between Australia and Antarctica from ~49 Ma (Bijl et al., 2013).

These inter-basinal homogeneous $\delta^{13}C$ gradients are consistent with model simulations of a much weaker overturning circulation during Eocene greenhouse conditions compared to the modern (Huber and Sloan, 2001, Sexton et al., 2006a, Winguth et al., 2010, Lunt et al., 2010) with a predominantly Southern Ocean deep water source, inferred from hiatus data, Nd isotopes, a seismic unconformity on the Bermuda Rise, benthic foraminiferal carbon isotope and benthic foraminiferal assemblage data (Mountain and Miller, 1992, Pak and Miller, 1992, Ramsay et al., 1994, Thomas et al., 2003, Nunes and Norris, 2006). This weaker ocean circulation may be causatively linked to an accelerated hydrological cycle and increased freshwater delivery to the polar regions, resulting in reduced ocean salinity and enhanced density stratification of the water column, causing a slow-down of high-latitude deep water production (Barron et al., 1989, Kaiho et al., 1996, Bice and Marotzke, 2002, Brinkhuis et al., 2006, Lunt et al., 2010). Within this broad picture, there is some evidence for transient or small-scale deep-water formation in other regions (Figure 1.5.). For example, Pacific ε_{Nd} and benthic foraminiferal $\delta^{13}C$ values indicate a component of deep-water formation in the Northern Pacific (~65 – 40 Ma) (Thomas, 2004, Tripati and Elderfield, 2005) (Figure 1.5.). Modelling studies also show that a switch from southern to northern high-latitude deep water formation is possible during the PETM with a strongly intensified hydrological cycle, but only if North Atlantic to Arctic Ocean gateways are closed (Bice and Marotzke, 2002). This finding is supported by inter-basinal carbon isotope gradients that suggest a switch from southern to northern hemisphere deep-water formation for ~40 ka at the onset of the PETM (Nunes and Norris, 2006). More recent modelling studies also identify the potential for Tethyan saline intermediate water formation in the winter months, causing enhanced warming of equatorial Atlantic intermediate waters, during the PETM (Lunt et al., 2010). Other publications also suggest some component of lower latitude or eastern Tethys deep water formation during the late Paleocene to middle Eocene using General Circulation Models, benthic foraminiferal carbon isotopes (comparison Atlantic, Pacific and Southern Ocean), seismic and sedimentary interpretation on the Bermuda Rise (western North Atlantic) and Nd isotopes from Maud Rise (Southern Ocean) (Barron

and Peterson, 1991, Pak and Miller, 1992, O'Connell et al., 1996, Mountain and Miller, 1992, Scher and Martin, 2004).

For this study the key feature of global deep-water evolution is the progressive transition from a late Paleocene to an early Eocene system, dominated by weak ventilation from regions of the Southern Ocean, towards a more modern pattern with strong ventilation and deep-water production from both the North Atlantic and Southern Ocean (Cramer et al., 2009, Vahlenkamp et al., 2018a, Vahlenkamp et al., 2018b). In this, the study site is well placed, near potential deep-water source regions in the Greenland and Norwegian Seas, to trace changes in water mass properties between the early and middle Eocene. These patterns of northern hemisphere water mass properties are intimately related to the degree of connection between the restricted and fresh Arctic Ocean basin and the global oceans (Gleason et al., 2009). During the late Paleocene to early Eocene, the Turgay Strait connected the Arctic Ocean to the Tethys, but the degree of connection is still very uncertain, with very little data available (Iakovleva et al., 2001, Iakovleva and Heilmann-Clausen, 2007, Marramà et al., 2019). The presence of Tethyan dinoflagellates in the Arctic from the late Paleocene to early Eocene is evidence for some connection but this may not have been deep (Iakovleva and Heilmann-Clausen, 2007). Strontium and neodymium isotope data from the Lomonosov ridge, in the central Arctic Ocean provides some indication of the degree of connectivity between the Arctic and other ocean basins (Gleason et al., 2009). More radiogenic strontium in the Arctic compared to the other Eocene oceans (Gleason et al., 2009) is consistent with a low salinity and stratified Arctic Ocean coincident with the "*Azolla*" event (Brinkhuis et al., 2006). Early Eocene Arctic ε_{Nd} values do not conclusively identify regional connectivity to other ocean basins, but most closely match the North Atlantic with a possible contribution of the Pacific and the Tethys (Gleason et al., 2009). Together, these indicate a largely isolated Arctic Ocean basin during the early Eocene, with limited shallow water connectivity via the Fram, proto-Berling and Turgay Strait (Gleason et al., 2009).

Modelling studies have shown that the main driver of the development of Northern Component Water (NCW) — antecedent of the modern NADW — in the early to middle Eocene is the tectonic deepening of the Greenland Scotland Ridge (GSR) (Vahlenkamp et al., 2018b). The GSR separated cool surface Arctic waters in the

Norwegian sea from warmer surface North Atlantic waters. The height of the GSR during the early Paleogene was closely linked to the development of the NAIP and the Icelandic mantle plume, with regional thermal anomalies leading to uplift close to the Paleocene-Eocene boundary, followed by progressive cooling and subsidence through the early to middle Eocene (see Figure 1.2.) (Maclennan and Jones, 2006, Parnell-Turner et al., 2014). This regional subsidence in the early Eocene (Maclennan and Jones, 2006) would have been accelerated by the full development of an extensional regime associated with sea floor spreading in the northeast Atlantic (e.g., Hallam, 1971, Saunders et al., 1997). The timing of the development of a connection through the GSR occurs close to the onset of the Northern Component Water (NCW) deep-water formation, inferred from the onset of major drift sedimentation on the Newfoundland Ridge close to the early-middle Eocene boundary (Norris et al., 2014, Boyle et al., 2017, Vahlenkamp et al., 2018a). Based on the palaeo water depth of Newfoundland drifts (~3000 m) Vahlenkamp et al. (2018a) argue that the main deep-water source for middle Eocene NCW comes from the Norwegian rather than the Labrador Sea, with the GSR low enough to allow significant water exchange. Vahlenkamp et al. (2018b) test this hypothesis with the Earth System model COSMOS, find that GSR subsidence of 200 to 500 m below sea level would have been enough to trigger the formation of NCW. At the southwest margin of the Faroe-Shetland Basin, northeast Atlantic, the base of the contourite Judd Fall Drift, dated at ~49.5 Ma, is also strong evidence for NCW initiation by the start of the middle Eocene (Hohbein et al., 2012). The far-field transit and impact of NCW onset is, however, less certain, with a distinct North Atlantic ε_{Nd} signal only apparent in the South Atlantic from the earliest Oligocene (Via and Thomas, 2006).

Overall, the onset of NCW is part of a wider switch through the early to middle Eocene, from a relative weak Southern Ocean deep water source in the late Paleocene to early Eocene towards bipolar, Southern Ocean and North Atlantic (NCW), deep-water formation in the middle Eocene (Boyle et al., 2017, Vahlenkamp et al., 2018a). This may be linked to the first stages of the onset of a proto-ACC onset and represent the first steps on the transition to the modern icehouse world (Cramer et al. 2009). Although the overall trends of this developing circulation are clear, there is uncertainty in linking tectonic reconstructions of gateway development with the

paleoceanographic records of circulation. There are key questions of the timing of gateway deepening, but also how gateway depth controls circulation. For example, although ACC spin-up is linked to the opening of the Tasmanian gateway around ~49 Ma (Bijl et al., 2013), ε_{Nd} data indicate that the Drake Passage is not open to substantial deep water flow before the late Eocene ~37 Ma (Scher and Martin, 2004), whilst evidence from bathymetric surveys and the dating and compositional analysis of lavas suggest this region was blocked by an emerged arc barrier, even up until ~12 Ma (Dalziel et al., 2013). This highlights the complexity of interpreting water mass mixing proxies, including ε_{Nd}, which will be influenced by Pacific – Atlantic water mass exchange through both the Central American Seaway (CAS) and the shallow Drake Passage during the middle Eocene (Scher and Martin, 2004). A recent study dates the onset of the proto-ACC to be at 36 Ma (Sarkar et al., 2019).

This thesis seeks to address the question of timing and nature of intermediate water circulation changes in the northeast Atlantic using sedimentological and stable isotopic data. In particular it will be focused on the major changes within the circulation system around ~50 – 49 Ma as seen in benthic foraminiferal isotope compilations (Sexton et al., 2006a), in a global-ocean-wide erosive unconformity at ~48 – 49 Ma (Norris et al., 2001) and the onset of drift sedimentation at the southwest margin of the Faroe-Shetland Basin, all indicating NCW onset at this time (Hohbein et al., 2012). This is also the "*Azolla*" interval of reduced salinity in the Arctic Ocean, from ~49 – 48.3 Ma (Brinkhuis et al., 2006, Gleason et al., 2009). These changes in deep-water formation are not only important for an understanding of past physical oceanography but may also contribute to climate cooling through enhanced upwelling, biological productivity and carbon burial leading to the long-term decline in atmospheric CO_2 and the "descent into the icehouse" world (Anagnostou et al., 2016).

2 STRATIGRAPHIC AND PALAEOENVIRONMENTAL RECONSTRUCTIONS OF SITE 16/28-SB01 OF THE ROCKALL BASIN, NE ATLANTIC

2.1 Rationale

The overall aim of this PhD thesis is to generate early Eocene palaeoclimate proxy data from a globally important sequence of sediments recovered from the Rockall Basin, NE Atlantic. The sediments of 16/28-sb01 yield exceptionally preserved and diverse organic biomarkers and calcareous microfossils and are therefore optimal for the generation of multiple SST proxies at this northern latitude (see Chapter 3 and 4). To usefully deploy the geochemical analyses from these sediments for the purposes of palaeoclimate studies, however, two key supporting components are required: first, a reliable age model for the recovered core successions; and second, an understanding of the broad palaeoenvironment and palaeogeography of the study location at the time of deposition. In this Chapter, these two key components will be provided for the marine sediments from Site 16/28-sb01, based on: A) a review of the regional tectonic understanding of the Rockall Basin (Section 2.2); B) a review of existing sedimentological and biostratigraphic data (Section 2.3); C) a refined biostratigraphic framework, based on calcareous nannoplankton (Section 2.5.1); and, D) chemostratigraphic data from X-ray fluorescence (XRF) (Section 2.5.2) and new high-resolution bulk isotopic data (Section 2.5.3).

2.2 Tectonic evolution of the Rockall Basin

A primary objective of this study is to gather and present sedimentological and palaeontological evidence for changes in water depth and regional geography, including distance to shoreline, during the time of deposition of Site 16/28-sb01. This objective requires an understanding of the regional tectonic evolution of the Rockall Basin, which is summarised below.

The Rockall Basin is located in the northeast Atlantic (Figure 2.1.), and today it is an approximately ~250 km wide and ~3000 m deep marine basin, orientated in a NE to SW direction. The basin, at the north western tip of the Eurasian continental plate,

has a complex rifting history (Shannon et al., 1995) as one of the failed proto-North Atlantic rift arms. Rifting only reached the stage of oceanic crust development in the southernmost part of the basin, and is for the most part underlain by stretched continental crust thinning towards the south (Shannon et al., 1999, Roberts et al., 1999, Klingelhöfer et al., 2005). To the southeast the Rockall Basin is boarded by the United Kingdom (U.K.) and the Irish continental shelf, and to the northwest by the Rockall Bank, which is also called the Rockall Plateau (Figure 2.1.).

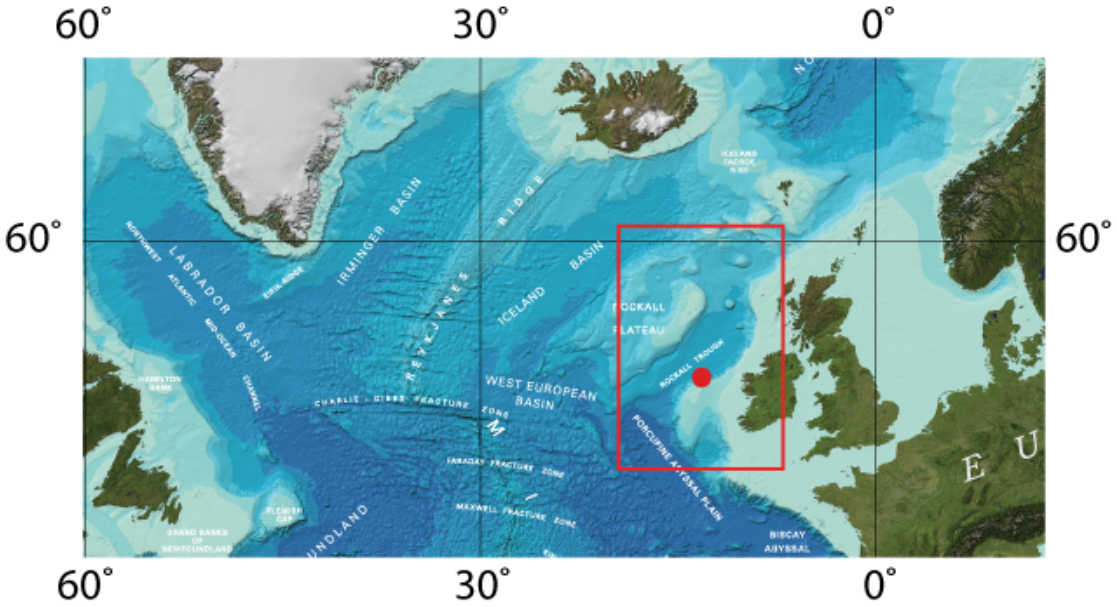

Figure 2.1. A map of the recent northern Atlantic showing the Rockall Basin (red box) and the Site 16/28-sb01 position (red dot). The map is reproduced from GEBCO (General Bathymetric Chart of the Oceans) world map 2014, https://www.gebco.net/data_and_products/printable_maps/gebco_world_map/.

The Precambrian crystalline basement of the Rockall Basin was assembled during the Palaeozoic Caledonian orogeny, and consists of terranes from Laurentia, Baltica and Eastern Avalonia (Chambers et al., 2005, Woodcock and Strachan, 2009, and references therein). The Northern Rockall Basin is underlain by basement from Laurentia and Baltica, which collided during the subduction of the Northern Iapetus Ocean ~460 Ma. These merged continents then collided with Eastern Avalonia around 430 to 400 Ma, with the subduction of the southern Iapetus and the Tornquist Sea, which forms the basement of the southernmost Southern Rockall Basin (Roberts et al., 1999, Woodcock and Strachan, 2009, Hitchen et al., 2013, and references therein). In the early Permian, the Variscan orogeny to the south of the Rockall area, marks the

assembly of the supercontinent Pangaea (Roberts et al., 1999, Woodcock and Strachan, 2009, and references therein). The major ~NE-SW tectonic trends from the Caledonian and ~E-W trends from the Variscan orogeny dominate the structural features that are reactivated in the complex rifting of the Rockall Basin (Musgrove and Mitchener, 1996, Doré et al., 1997, Roberts et al., 1999, Doré et al., 1999, Naylor and Shannon, 2005).

In the Late Triassic to Early Jurassic Pangaean breakup lead to extensional stresses and the development of two rift systems in the vicinity of the Rockall Basin: 1) the Arctic Rift, north of the Rockall Basin, which prograded southwards; and, 2) the Atlantic Rift, south of the Rockall area, which prograded northwards (Roberts et al., 1999, Shannon et al., 1999). In the Rockall Basin, this Permo-Triassic extensional regime led to the formation of terrestrial half-graben basins — including *inter alia* the Porcupine, Slyne, Erris, Donegal and Hebrides Basins — oriented ~NE-SW along inherited Caledonian weaknesses (Shannon, 1991, Corfield et al., 1999, Roberts et al., 1999, Doré et al., 1999, Thomson and McWilliam, 2001, Naylor and Shannon, 2005). Some of these basins must have acted as sediment sinks before their development into half grabens, maybe as continental sag basins, as some of them are found to contain terrestrial sediments dating back to the Carboniferous (Naylor et al., 1999, Thomson and McWilliam, 2001).

In the Early Jurassic the Atlantic rift propagated north, with the opening of the central North Atlantic (Pitman et al., 1971, Vogt et al., 1971, Knott et al., 1993), whereas the Arctic rift was again active in the Middle Jurassic with extension in the North and Norwegian Seas (Knott et al., 1993), leading to first shallow marine transgression, from the north, into the Permo-Triassic half graben basins of the Rockall Basin (Trueblood and Morton, 1991, Dancer et al., 1999). In the Late Jurassic to Early Cretaceous a complete marine connection between the Arctic and the Atlantic rifts developed (Smythe, 1989, Roberts et al., 1999, Shannon et al., 1999). Whilst Arctic rifting slowed in the Cretaceous, the Atlantic rifting continued to open the Rockall Basin until ~mid-Cretaceous times (Musgrove and Mitchener, 1996, Roberts et al., 1999, Doré et al., 1999, Walsh et al., 1999), with a switch of the rift axis from the eastern edge to the centre of the Rockall Basin (e.g., Naylor et al., 1999, Shannon et al., 1999). In the mid-Cretaceous times Proto-North Atlantic rift progradation ceased completely in the

Rockall area, with major rift continuation from the late Paleocene within the Labrador Sea (Smythe, 1989, Knott et al., 1993, Chalmers et al., 1993, Musgrove and Mitchener, 1996, Saunders et al., 1997, Roberts et al., 1999, Doré et al., 1999, Nielsen et al., 2002, Chauvet et al., 2019). The Reykjanes spreading between East Greenland and NW Europe established around 55 Ma linked to the large-scale volcanism associated with the NAIP (North Atlantic Igneous Province) and Iceland mantle plume (Smythe, 1989, Knott et al., 1993, Saunders et al., 1997, Doré et al., 1999, Skogseid et al., 2000). Therefore, the Rockall Basin spreading was gradually abandoned with the Labrador spreading onset, followed by major and then only Reykjanes ridge spreading (Roberts et al., 1999, Skogseid et al., 2000, Nielsen et al., 2002). The NW-SE Wyville Thomson Ridge Anticline, that forms the northern gateway between the Rockall Basin and the Faroe-Shetland Channel, also originates from the late Paleocene onwards, due to basin-wide compression from ridge push and the distant Alpine and Pyrenean Orogenies (Johnson et al., 2005, Tuitt et al., 2010). The Wyville Thomson Ridge is found to experience major episodes of growth in the early to middle Eocene, late Eocene and Miocene, and might have influenced the oceanography and deep water circulation of the Rockall Basin (Johnson et al., 2005, Tuitt et al., 2010).

In the mid to late Paleocene the NE Atlantic, including the Rockall Basin, was heavily impacted by magmatic and tectonic activity associated with a major pulse of the Iceland mantle hotspot, including basin-wide volcanic intrusions and kilometre-scale uplift (Roberts et al., 1999, Maclennan and Jones, 2006). By the early Eocene, a reduction in NAIP volcanic activity coupled with rapid thermal subsidence led to major relative sea level rise and the creation of accommodation space in the Rockall Basin (Thomson and McWilliam, 2001, Jones et al., 2002). The complexity of thermal subsidence histories of passive margins, including the North Atlantic, are still being explored, and might involve more active tectonics than previously assumed. An exact subsidence history determination for any area relies on detailed and well-dated sedimentary records, which in the Rockall Basin includes the Eocene succession studied herein (Jones et al., 2001, Stoker et al., 2010, Stoker et al., 2012).

In the Rockall Basin, the early to middle Eocene rate of basin subsidence was high enough to partly outpace sediment supply, leading to basin-wide sediment starvation, especially in the deeper or more isolated parts of the basin, with sediment-trapping

in the Permo-Triassic half grabens proximal to the shoreline (Shannon et al., 1994, Shannon et al., 1995, Naylor and Shannon, 2005). Sediment starved regions are typically represented by low energy marine sediment deposition (Shannon et al., 1995). At the same time as this thermal subsidence, the creation of oceanic crust to the west of the Rockall Basin is thought to create a compressional regime (Doré et al., 1999) and the uplift of Rockall Basin margins, Porcupine High and Irish mainland (Jones et al., 2001, Allen et al., 2002, Naylor and Shannon, 2005). The uplift of these sediment source areas may have contributed to the onset of prograding sedimentary systems in the Rockall area, in regions where subsidence did not outpace siliciclastic sedimentation, for example on the east coast of the northern Rockall Basin, on the east side of the northern tip of the Rockall Bank and within the Porcupine Basin (Shannon et al., 1995, McInroy et al., 2006, Stoker et al., 2012). Progradational wedges on Rockall Bank are thought to be Ypresian in age (Shannon et al., 1995, McInroy et al., 2006, Stoker et al., 2012). The combination of rapid Eocene subsidence and sediment starvation in distal Rockall Basin environments, led to slope failure and slumping (Musgrove and Mitchener, 1996, Thomson and McWilliam, 2001). The end of these prograding sedimentary systems on Rockall Bank is concomitant with a direction change in the plate motion of Greenland relative to North America and Eurasia around 49 Ma, coupled with a significant sea floor spreading slow down (Gaina et al., 2009) and a further increase in the regional compressional regime (Stoker et al., 2012, Doré et al., 1999). Similar prograding systems are well-known in the North Sea and the Faroe-Shetland Basins sourced from the denudation of the NAIP-uplifted British landmasses (Jones and Milton, 1994, White and Lovell, 1997). The next subsidence episode in the Rockall Basin spans the latest Eocene to early Oligocene connected with deeper marine deposits and is represented by the bottom current erosion caused C30 seismic unconformity (Stoker et al., 2001, McDonnell and Shannon, 2001).

2.3 Recovery and Lithology of Site 16/28-sb01

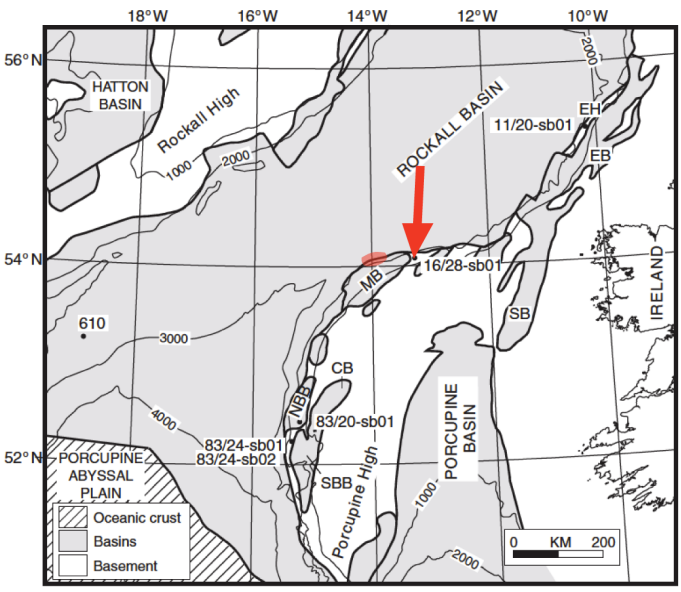

Figure 2.2. The offshore Irish Rockall Trough with its west coast (Irish coast) bound Permo-Triassic basins. The location of Site 16/28-sb01 is indicated by the red arrow. It is located within the Irish-continental shelf of the Rockall Trough. The red oval marks the location of the Drol Igneous Centre. This map is taken from Haughton et al. (2005). Haughton et al. (2005) used MB - Macdara Basin; CB - Cilian Basin; EB - Erris High; SB - Slyne Basin; NBB - North Brona Basin; SBB - South Brona Basin. The Fastnet Basin just east of 16/28-sb01 is covered by the label for 16/28-sb01.

Site 16/28-sb01 (54°01'19.989'' N and 13°30'51.575'' W) was drilled by the MV Bucentaur during a collaborative project between the British Geological Survey (BGS) and the Rockall Studies Group (RSG) in 1999. This activity was undertaken within the framework of the Irish PIP (Petroleum Infrastructure Program Ireland), with the cores recovered during this cruise now stored at the PIP core store in Dublin. With a focus on improving the background stratigraphy and geological data of the Rockall Basin for the purposes of hydrocarbon exploration, boreholes were numbered according to exploration licence block numbers, with 16/28-sb01 located in block 16/28 (Stroker, 1999). Borehole 16/28-sb01 is located on the northern margin of the Porcupine High (Figure 2.2.), at a recent water depth of ~1465 m (Skinner and Tulloch, 1999, Stroker, 1999). To the northwest water depths increase into the main Rockall Basin, whilst the small Macdara Basin lies to the southwest of the drill site and the small Fastnet Basin to the NE (Figure 2.2.). The drill-site 16/28-sb01 is located on a sea bed terrace in-between these two basins (Haughton et al., 2002). The cored intervals from 16/28-sb01 are the most continuous of any site of the MV Bucentaur cruise (Haughton et al., 2002) and penetrated to 148.25 m below sea bed (Stroker, 1999). All the drill-sites of the MV Bucentaur cruise were selected to penetrate relatively deep-time successions — back to the Late Cretaceous and early Paleogene, with relatively shallow drilling (< 200 m) (Haughton et al., 2005). The Eocene palaeoposition of Site 16/28-sb01 was estimated as 48.8˚N

and 18.3˚W using the GPlates software with plate rotation poles of Boyden et al. (2011) (Figure 1.2.).

Millenia Ltd. biostratigraphic consultants were contracted by the RSG to provide initial shipboard biostratigraphy, and provided planktic foraminiferal biozonations against both “in-house” and the standard Berggren et al. (1995) zonations (Table 1 in Appendix 1) (Jacovides, 1999). This was followed by a Millenia Ltd. in-house report with nannofossil zonation (Zucchi, 2000), that is not publicly available. Further biostratigraphical investigations included calcareous nannofossils — using a modified zonation scheme after Martini (1971) — and marine and terrestrial palynomorphs (Table 2 in Appendix 1) (Harrington et al., 2000). The work of all these biostratigraphic reports was re-evaluated in Jacovides (2000) and set into a broader basin-wide context (Table 3 in Appendix 1). For Site 16/28-sb01, Jacovides (2000) assigns the oldest sediments above the basalt (Figure 2.3.) to be of Paleocene age but with no nannofossil zone determination possible. These are overlain by a thick (~130 m) Eocene succession, assigned to nannofossil Zones NP12 (intra) (early Eocene) and NP15 (middle Eocene). Overlying the Eocene succession are Quaternary sediments, heavily disturbed by drilling, assigned to nannofossil Zone NN19b (Pleistocene). A comparison of these biostratigraphic studies is shown in Figure 2.4.. Within this thesis the nannofossil biostratigraphy of the Eocene succession is re-evaluated by Dr Tom Dunkley Jones, in light of the new Paleogene zonation scheme of Agnini et al. (2014).

The first sedimentological investigations on the Site 16/28-sb01 were carried out by Haughton et al. (2002). Later Haughton et al. (2005) presented all the primary results from the previous sedimentology, biostratigraphy (Jacovides, 1999, Harrington et al., 2000, Jacovides, 2000), seismic and thermal history (Green, 2001) and set them into a basin wide interpretation. A brief summary of the core lithologies, from oldest to youngest, following Haughton et al. (2002) and reference therein, is provided below and summarized in Figure 2.3..

Basaltic rock (148.25 – 147.30 m) is recovered at the base of the core and is interpreted to be an extrusive basaltic lava flow (Green, 2001). Apatite fission track data from sediments above the basalt show no indications of thermal heating, which would support the interpretation of a basaltic lava flow (Green, 2001). Geochemical elemental measurements from Haughton et al. (2002) indicate an Icelandic-type

source for the basalt, as defined by Fitton et al. (1997), which was moderately enriched in mantle (relative to mid ocean ridge basalt (MORB)), but with no evidence of crustal contaminations (Haughton et al., 2002). The basalt was interpreted by this geochemical signature to be derived from the Drol Igneous Centre, situated on the north western side of the Macdara Basin (Figure 2.2.) (Haughton et al., 2005). However, the top basalt - sediment contact is not recovered in the core, leaving some uncertainty in the above interpretation of basalt emplacement (Figure 2.3.). Based on stratigraphic relationships the basalt is assumed to be Cretaceous in age (Haughton et al., 2002).

Above the basalt, Upper Cretaceous sediments are recovered: a calcareous sandstone (147.30 – 147.06 m) and a calcareous limestone (146.00 – 145.95 m). The thin calcareous sandstone is described as homogeneous, well sorted and coarse grained (Haughton et al., 2002). No fragments of the underlying basalt were observed, supporting the extrusive interpretation (Haughton et al., 2005). The sand often contains rounded fragments of fossil algae, echinoderms and bryozoans (Haughton et al., 2002). The biostratigraphy of Harrington et al. (2000) assigns this unit an age of Maastrichtian or older and it is interpreted to represent deposition on a high-energy shallow open marine shelf, proximal to the sediment source area, which was comprised of quarzitic and granitic bedrock (Haughton et al., 2002). The overlying calcareous limestone is finer grained and classified as a bioclastic packstone (Haughton et al., 2002). Fossils described include echinoderms, algae, molluscs and foraminifera (Haughton et al., 2002). The fining up of grain size between these two lithologies is interpreted to reflect falling energy, potentially caused by a rise of local relative sea levels (Haughton et al., 2002).

After a significant unconformity, with all of the Paleocene missing, lower Eocene sediments are recovered: bryozoan lime- and mudstone (145.95 – 138.00 m) and “smectitic clays” (138.00 – 88.58 m) (Haughton et al., 2002). At the base, the lower Eocene succession is rather heterogeneous interbedded with calcareous lime-, silt- and mudstones leading into the more homogenous clay-prone section above 138 m (Haughton et al., 2002). Fossil contents across this transition are described as developing from assemblages dominated by bryozoan fragments with minor foraminiferal content, into sediments with common planktonic foraminifera

(Haughton et al., 2002). The general transition to more uniformly fine-grained, clay-rich sediments is interpreted to represent a regional relative sea level rise, from an outer shelf heterogeneous section (bryozoan lime- and mudstone) to a low and stable-energy bathyal slope, with homogeneous smectitic clay deposition out of suspension settling (Haughton et al., 2002).

At 88.58 m, a distinct shear zone — including several glauconite smeared shear planes — is recovered within the cores, which corresponds with the lower to middle Eocene transition (Haughton et al., 2002). This shear plane is interpreted as a slope re-configuration event, causing instability and sliding (Haughton et al., 2002). Above the shear zone a middle Eocene calcareous sandstone (88.58 – 40.77 m) is recovered (Haughton et al., 2002). It is described as very fine to fine grained calcareous sand, which, at the base, is more heterogeneous with interlayered clay-rich units (Haughton et al., 2002). The nannofossil abundance within this lithology indicates normal fully marine conditions (Harrington et al., 2000).

Haughton et al. (2002) describe an unconformity on top of 40.77 m followed by caved poorly recovered pebbles (35.00 – 33.08 m). Above this, Haughton et al. (2002) describe a middle Eocene section (25.70 – 25.00 m), which is described as more muddy than the earlier middle Eocene sandstone section. The youngest recovered sediments are Quaternary sand- and gravel-prone deposits (14.50 – 12.78 m) that show extensive coring-related deformation. These are interpreted as glacial derived deposits with sand sourced from a proximal slope (Haughton et al., 2002). Fossil content in this unit is still dominated by planktonic foraminifera (Haughton et al., 2002).

Haughton et al. (2005) merge seismic data with their sedimentologic description and find four different seismic entities: The Upper Cretaceous sediments referred to as entity C, the lower Eocene section as B2, the middle Eocene as B1 and the Quaternary Section as entity A.

The majority of sediments recovered from 16/28-sb01 — about 100 of the recovered 148 core meters — are certainly Eocene in age (Haughton et al., 2002, Haughton et al., 2005, Jacovides, 1999, Jacovides, 2000, Zucchi, 2000, Harrington et al., 2000). This project is focused on the sediments from 40.82 – 145.99 m, more specifically on their microfossil content, their elemental and their organic components. For ease of reference the Eocene succession is divided into three units from oldest to youngest

Unit 1 (U1), consisting of the bryozoan lime- and mudstones; Unit 2 (U2), consisting of the lower Eocene clays; and Unit 3 (U3), consisting of the middle Eocene calcareous sands (Figure 2.3.). The exact boundaries of these units are discussed further in Section 2.5.2 on the basis of XRF elemental data.

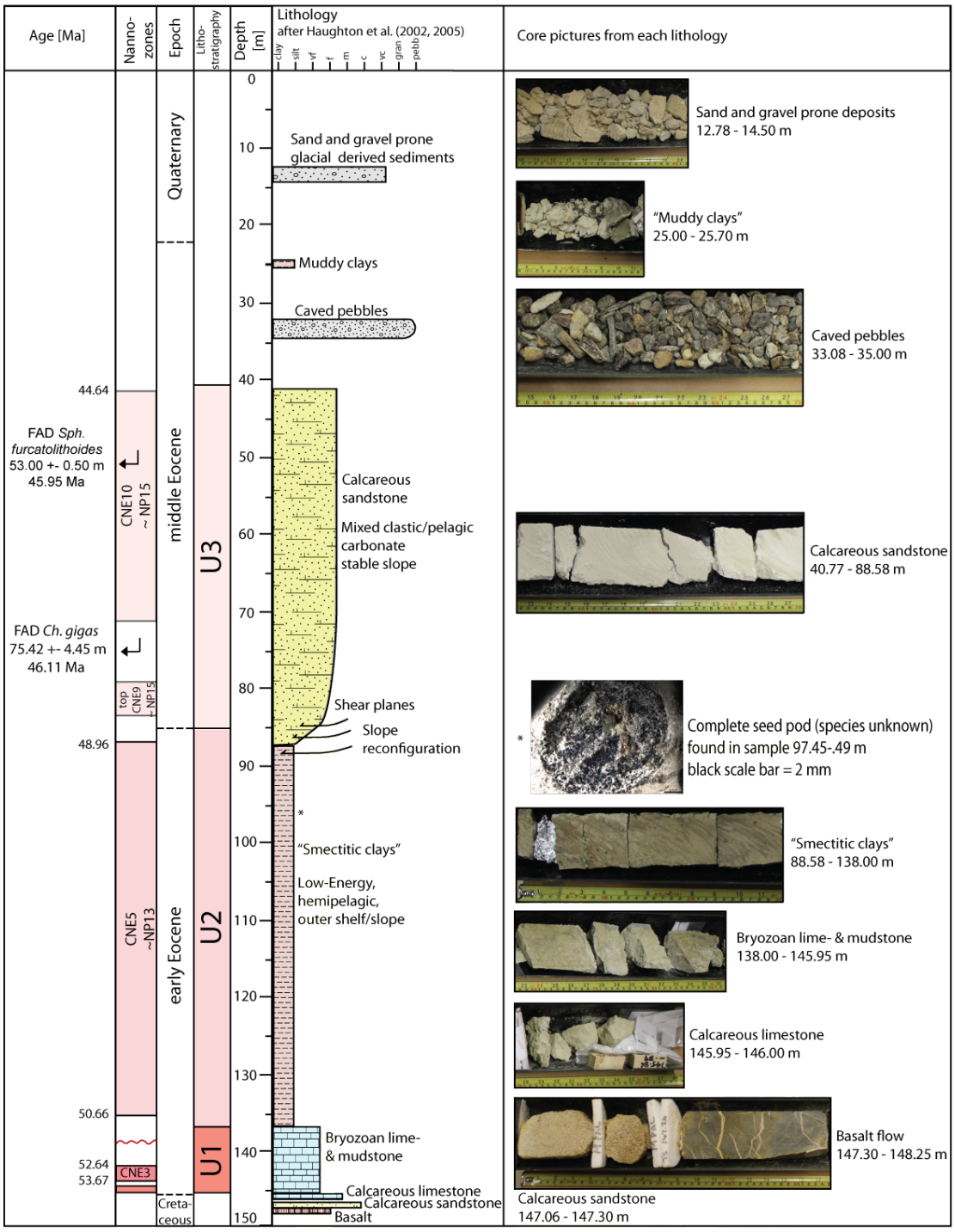

Figure 2.3. Stratigraphic summary of Site 16/28-sb01 its different sedimentological units and the new age constraints given by calcareous nannofossil biostratigraphy (see Section 1.6.1). For each Unit an exemplary picture is provided and named. At 97.45 – .49 m a complete seed pod (species unassigned) was found. All pictures of the whole core section can be found in Appendix 2.

2.4 Methods

All core sections of Site 16/28-sb01 were photographed before sampling and are available in Appendix 2. A total of 983 thumbnail-sized samples have been taken at the PIP core store in Dublin in 2015, with the aim of investigating a high-resolution bulk stable isotope stratigraphy and to analyse for different elemental distributions using XRF. For bulk stable oxygen and carbon isotope analysis and XRF analyses all samples were homogenised with a mortar and pestle. One to three grams of each sample was saved for future high-resolution nannofossil analyses and the rest of the bulk sample was halved, with one half each for XRF analysis and bulk carbonate carbon and oxygen stable isotope analysis.

Due to limitations on available sample mass in some cases, and prioritisation of stable isotope analyses, a total of 849 XRF analyses were undertaken on wax pressed pellets, each of which included between 0.005 to 0.591 g (on average 0.502 g) of the homogenised bulk sediment and Spectro Blend 44 µm wax. Exact sample and wax weights for each pellet are given in Appendix 1 Table 4. Wax pellets were analysed on a S8 TIGER Wavelength Dispersive X-Ray fluorescence (WDXRF) device coupled with QUANT-EXPRESS^{TM} with an automated calibration from Bruker and were run at the University of Birmingham. All samples were analysed with a seven-minute run to achieve full detection using an eight-mm mask and thirteen mm pressed pellets. The results of the detected elements are given in weight percent of the element (wt.%).

Bulk carbonate stable isotope analyses used the other half of the homogenized bulk sediment, all 983 samples and an additional 66 reruns were performed at the University of Birmingham. Guided by calculated $CaCO_3$ wt.% inferred from the Ca wt.% from XRF analyses and pilot measurements of bulk carbonate stable isotopes — sample weights between 120 and 6589 µg were used — with the aim of analysing ~100 µg of calcium carbonate within each sample. Every sample was placed in a 4 ml glass vial sealed by a lid with a pierceable septum. The vials were heated to 90˚C and the headspace of the vials was replaced by pure helium using the Isoprime Multiflow preparation system, which comprises an automated needle injection system. In a second step 200 µl of phosphoric acid was manually injected into each sample and left for a minimum of one hour. In a last step, the headspace gas was sampled and injected

into the continuous-flow Isoprime mass spectrometer. A duplicate was measured from each sample and a mean value was calculated for $\delta^{13}C$ and $\delta^{18}O$. Results were calibrated using the International Atomic Energy Agency (IAEA) standards NBS 18 and NBS-19 and are given in per mill (‰) relative to the Vienna Pee Dee Belemnite (VPDB) standard. Usually an external precision better than 0.1 ‰ is achieved for both $\delta^{13}C$ and $\delta^{18}O$. All following isotope data in this thesis are reported relative to the VPDB standard.

Calcareous nannofossil biostratigraphy was conducted by Tom Dunkley Jones at the University of Birmingham, using 24 standard smear slides (Bown and Young, 1998) and polarizing optical transmission microscopy. Samples were examined so as to pin-point biostratigraphic biohorizons to the nearest available sample. Calcareous nannofossil zones and bioevent ages are reported using the zonation scheme of Agnini et al. (2014) and the Geological Time Scale 2012 (GTS 2012) (Vandenberghe et al., 2012).

2.5 Results

2.5.1 Nannofossil age constrains

A comparison of the new biostratigraphy with the one from Jacovides (2000) is shown (Figure 2.4). In detail, the basal sample examined for calcareous nannofossils, at a depth of 145.20 m, has a low abundance of nannofossils, dominated by *Toweius pertusus* and other small *Toweius* placoliths, which are clear evidence for an early Paleocene to early Eocene depositional age. Preservation of these specimens is generally good where found. There is a high abundance of abiogenic calcite within the mineral component of this sample but no Cretaceous taxa were observed. Above this, at 144.70 m, nannofossils are common with very good preservation. They show a typical early Eocene assemblage, dominated by *Toweius* placoliths and with the characteristic marker *Tribrachiatus orthostylus* consistently present between depths of 144.70 to 143.90 m. Although discoasters are frequently observed within the assemblage, *Discoaster lodoensis* is absent. On this basis, this basal section (144.70 to 143.90 m) is assigned to nannofossil zone CNE3, with an age range of 53.67 to 52.64 Ma.

At a depth of 137.20 m there is a distinct assemblage shift, with the appearance of common reticulofenestrid placoliths, which now dominate the placolith component, although *Toweius* species are still present. *D. lodoensis* is also observed frequently and *T. orthostylus* is absent. This evidence, together with the absence of the '5-rayed' *Discoaster sublodoensis* indicates an age of CNE5. This suggests a minor unconformity within the core gap between 143.90 and 137.20 m, with CNE4 missing, or not recovered during drilling. The remainder of the Unit 2 clay succession, between 137.20 to 87.90 m, has a consistently abundant and very well-preserved early Eocene nannofossil assemblage, consistent with zone CNE5 (50.66 to 48.96 Ma). *D. lodoensis* is present to the top of this interval, and the '5-rayed' *D. sublodoensis* form is still absent.

Calcareous nannofossil preservation in samples from 83.90 m upwards is more variable than the lower Eocene succession (Unit 2), although nannofossils are consistently common to abundant. Preservation ranges from moderate to very good in places. The assemblage within the sample from 83.90 m is notable for abundant and large reticulofenestra, *Coccolithus* and *Chiasmolithus* placoliths, as well as *Helicosphaera* and *Pontosphaera* muroliths. Discoaster assemblages are dominated by multi-rayed forms (*Discoaster. saipanensis* and *Discoaster barbadiensis*) but also now with a component of free-rayed discoasters (*Discoaster tanii*). Within this assemblage *Discoaster lodoensis* and the '5-rayed' *Discoaster sublodoensis* are both absent. Although no *Nannotetrina* specimens have been observed — most likely due to the mid-latitude and continental margin palaeoenvironment of this site — the absence of *D. sublodoensis* and the presence of rare *Sphenolithus spiniger* indicates a middle Eocene, CNE9-equivalent, age for this sample. Samples between 83.90 and 79.86 m recover a similar assemblage to that at 83.90 m.

At 70.97 m the distinct large *Chiasmolithus* species *Chiasmolithus gigas* appears and remains consistently present up to the top of this middle Eocene succession (41.00 m). The calibrated age of the base of *Ch. gigas*, which defines the base of Nannofossil Zone CNE10, is 46.11 Ma. We constrain this biohorizon to be at a depth of 75.42 m ± 4.45 m. Within the interval 70.97 to 41.00 m *Sphenolithus cuniculus* is not observed, and we assign this whole interval to CNE10 (46.11 to 44.64 Ma). Although sphenoliths are relatively rare, *Sphenolithus furcatolithoides* is observed towards the top of this

interval, it comes in between sample 53.50 to 52.50 m and above. On this basis, the base of *Sph. furcatolithoides* is constrained to be 53.00 m ± 0.5 m. This has a calibrated age of 45.95 Ma (Agnini et al., 2014) taken from the sub-tropical ODP 1051 (Blake Nose). Given the higher latitude location of this site, and the observed stratigraphic separation of the base of *Ch. gigas* (46.11 Ma at 75.42 m) and *Sph. furcatolithoides* (45.95 Ma at 53.00 ± 0.5 m) in this succession, it is suspected that the first occurrence of *Sph. furcatolithoides* might be somewhat diachronous, with a later appearance in the Rockall Basin compared to ODP Site 1051.

This biostratigraphy could not be refined by using planktonic foraminifera due to the absence of the marker species of Wade et al. (2011), a problem already noted in high-latitude environments (Jenkins, 1985). Planktonic foraminifera abundances and diversity are also low at Site 16/28-sb01, making age assignments trickier. Further results relating to planktic foraminifera of Site 16/28-sb01 are presented in Chapter 3.

Table 2.1. Summary of the calcareous nannofossil biostratigraphic constraints (by Dr Tom Dunkley Jones)

Nannofossil Zone (Agnini et al., 2014)	Depth [m]	Age [Ma]
CNE10 approx.: NP15	Top 41.00 m 53.00 ± 0.5 m Bottom: 75.42 m ± 4.5 m	Older than 44.64 Ma 45.95 Ma 46.11 Ma
CNE9 approx.: NP15	Top 79.86 Bottom: 83.90	
CNE5 approx.: NP13	Top 87.90 m Bottom 137.20	Older than 48.96 Ma Younger than 50.66 Ma
CNE3	Top: 143.90 Bottom: 144.70	Older than 52.64 Ma Younger than 53.67 Ma
	145.20 m	No cretaceous species found

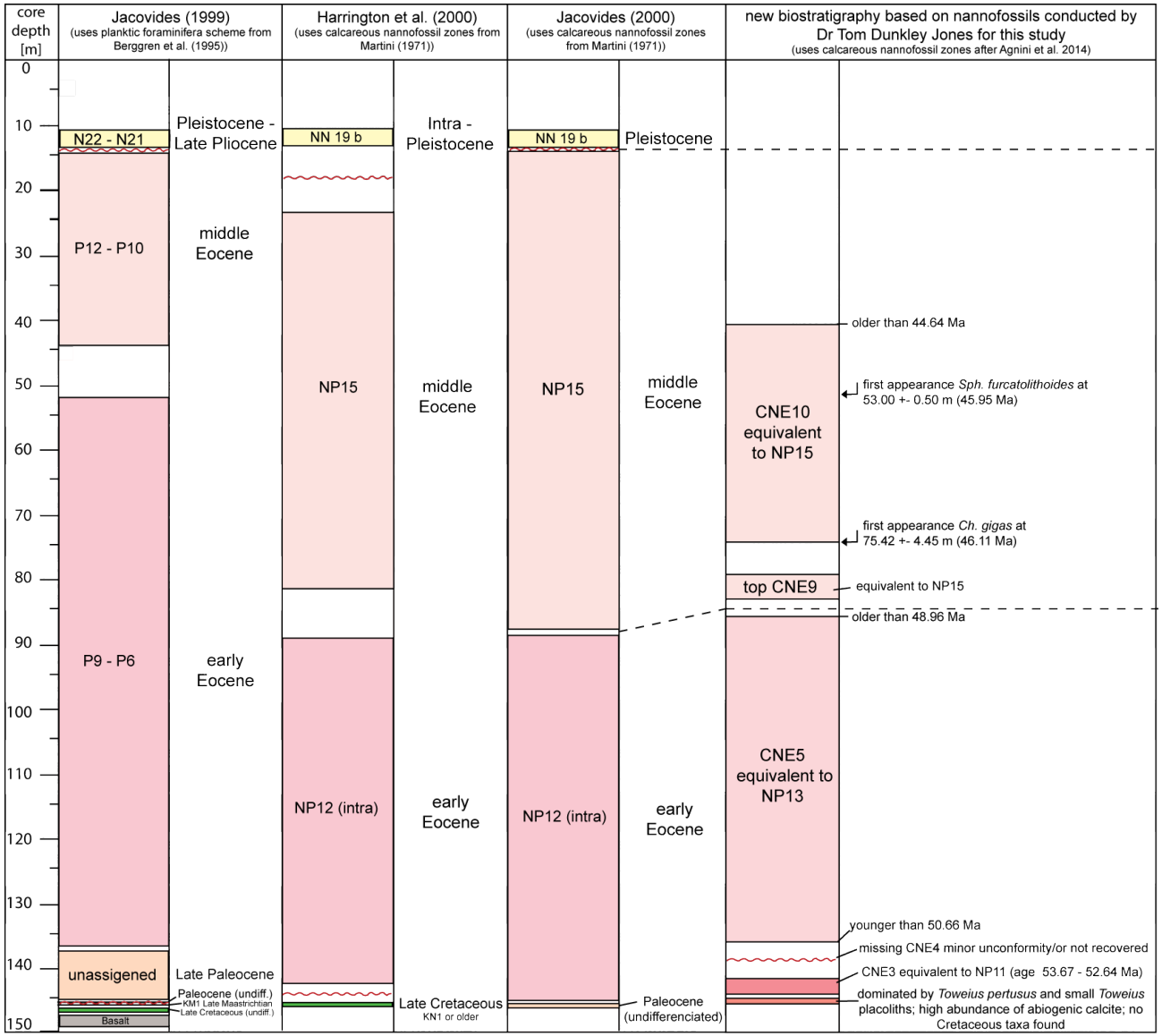

Figure 2.4. Comparison of the different biostratigraphic approaches for Site 16/28-sb01 from (Jacovides, 1999, Harrington et al., 2000, Jacovides, 2000) and the new one of this study. Red wavy lines indicate unconformities. Refinement include the identification of CNE3 (~NP11); a reassignment of the major part of the early Eocene succession to CNE5 (~NP13); and a new age constraint at 75.42 m ± 4.45 m to 46.11 Ma, representing the zonal boundary between CNE9 and CNE10.

2.5.2 XRF results

XRF data from a total of 849 samples provide a record of bulk sediment elemental concentrations throughout the Eocene of Site 16/28-sb01. Detected elements are Aluminium (Al), Barium (Ba), Calcium (Ca), Iron (Fe), Potassium (K), Magnesium (Mg), Manganese (Mn), Phosphorus (P), Rubidium (Rb), Silicon (Si), Sulfur (S), Strontium (Sr), Titanium (Ti) and Zirconium (Zr). All the results are given in wt.% in Appendix 1, Table 4. Overall, 5 elements have average abundance above 1 wt.%, which are, ordered in decreasing mean abundance: Ca, Si, Fe, Al and K. Nine elements have average abundances below 1 wt.%, which are, ordered in decreasing mean abundance: Ti, Mg, S, Ba, P, Sr, Mn, Zr and Rb. In Figure 2.5. all the elements detected, except Zr — due to its abundance close to the lower detection limit and general variability below 0.1 wt.% — are shown against core depth and biostratigraphy. In this section the overall major changes in sediment composition, as determined by the XRF results, are first summarized using a multivariate analysis in order to refine the existing lithostratigraphy of the core. Using this framework there then follows a more detailed discussion of some of the major patterns of change within elements or element ratios that are useful for palaeoenvironmental reconstruction.

2.5.2.1 Sediment composition and lithostratigraphy of Site 16/28-sb01

In order to determine any coupled, general patterns of variation a multivariate Principal Component Analysis (PCA) is undertaken on all the XRF data. This can be used to simplify the description of the XRF data by reducing its dimensionality but maintain a representation of its variability, that is achieved by summarising the variables of the input dataset to a set of new variables called the principal components (PCs). If this statistical analysis is useful, the majority of variability in the original dataset should be represented by first (PC1), second (PC2) and third (PC3) principal components. The different loadings of each variable express how strongly each of the input variables are linked to the different PCs. The eigenvalue for each PC reflects the percentage of variance it represents.

Prior to employing the PCA on the dataset it was simplified, such that elements with low abundance and the ones not showing significant variability — comprising Ba, P, Rb and Zr — were excluded. Afterwards the data were rescaled to ensure a sum to a

total of 100 %. All zeros values (non-detects) were replaced with very low but non-zero values (0.01) following Martín-Fernández and Thió-Henestrosa (2006) prior to an Additive Log Ratio (ALR) transform of the data following Weltje and Tjallingii (2008). This transform makes non-normal and constrained relative abundance compositional data suitable for standard multivariate analyses by moving them from a simplex space (restricted space, in this study case values from 1 – 100) into an Euclidean space structure (unlimited space) (Pawlowsky-Glahn and Egozcue, 2006, Weltje and Tjallingii, 2008, and references therein). It also requires a reduction of the dataset by one degree of freedom; this is achieved by normalising all data to a common and consistently occurring element prior to taking the natural logarithm (Pawlowsky-Glahn and Egozcue, 2006). To test the effects of this normalisation on the final PCA analysis, this normalisation was undertaken twice, first with a dataset normalised to Ca (PCA^{Ca}) and a second to Si (PCA^{Si}). The PCA was run using the software PAlaeontological STatistics (PAST) (Hammer et al., 2001). In both analyses of this dataset (PCA^{Ca} and PCA^{Si}) the majority of variation is represented by PC1 and PC2. For PCA^{Ca} the $PC1^{Ca}$ has an eigenvalue of 84.8 % and $PC2^{Ca}$ of 8.6 %; together explaining 93.3 % of the variance. For PCA^{Si} the $PC1^{Si}$ eigenvalue is 51.4 % and for $PC2^{Si}$ 26.8 %; together explaining 78 % of the variance. Both PC1s and PC2s are shown (Figure 2.6.) and their loadings (Figure 2.7.). Major changes in bulk sediment chemistry, including $PC1^{Ca}$ and $PC1^{Si}$ are clearly visible between the lithostratigraphic units (ordered from oldest to youngest) U1, U2 and U3. Whereas the PC2s in both analyses show considerably variation within lithostratigraphic units, tending to switch between end-members in a kind of bimodal distribution, mainly influenced by the elements ordered by decreased loading influence inferred from the loadings on $PC2^{Ca}$ Mn, S, Si, Al, K, Ti and Fe.

As $PC1^{Ca}$ and $PC1^{Si}$ describes the majority of variance they are used, together with the elemental distribution (XRF data) and the sedimentological definitions from Haughton et al. (2002) (Section 2.3), to define three lithostratigraphic units. The changes in bulk sediment composition that characterise the lithostratgraphic units are most apparent in the elements Ca, Si, Fe, Al, K and Ti, but is also seen in Mg, S and Sr. The most pronounced of these changes is seen between the lower and middle Eocene (Figure 2.5.), and is clearly reflected in the PC1s (Figure 2.6.). Distinctively different values are

obtained in the XRF data and PCAs from 87.50 m and below, which is slightly above the 88.58 m indicated from the sedimentological report (Haughton et al., 2002, Haughton et al., 2005). On this basis, the top of U2 is here defined as being at 87.50 m. Between 87.50 and 83.96 m there is a core and sample gap, with the next available sample above the top of U2 is sample 83.96 m clearly indicating a distinct compositional change to those distinctive of lithostratigraphic unit U3. Due to the core gap, it is unclear where to locate the boundary of U2 and U3, but here the report of Haughton et al. (2002) is followed and in this study it is this boundary is placed at the topmost observation of U2 lithologies at 87.50 m.

The top of U3 is defined to be the top of the investigated interval at 40 m. This study did not focus on or collect data above that depth, where there is little sediment recovered and what is available appears to be substantial disturbed by drilling and/or is caved from the borehole walls (Section 2.3).

The change between lithostratigraphic U2 and U1 is more difficult to define due to U1s more variable character. On scatter plots of PC1 and PC2, samples of U1 plot within the middle of the data point-cloud of U2 and U3 (Figure 2.7.). Based on the XRF values and the PCA^{Ca}, there is a change in the natural compositional variability between 137.99 and 144.30 m. Again, there is no data between these depths because of a core and sample gap. In the original sedimentology, a lithostratigraphic boundary was placed between these two data points at 138 m, which is followed in this study, with the base of U2 and top of U1 placed at 138 m. The base of U1 at 145.95 m also follows the sedimentology (Haughton et al., 2005), which is also the bottom sample analysed for bulk isotopes and by XRF. In summary, U1: extends from 145.95 to 138 .00 m (comprising 39 bulk samples), U2: 138.00 – 87.50 m (673 bulk samples) and U3 87.50 – 40.00 m (269 bulk samples). The clear definition of these units, based on new high-resolution (~every 10 cm) data of sediment composition, provides the lithostratigraphic context for the description of the data within this study, and will be used throughout the thesis. There is a good separation of the units visible on the PC1 against PC2 plots confirming the validity and the differing character of the three lithological units (Figure 2.7.).

2.5.2.2 Sediment composition and palaeoenvironmental reconstruction

The elemental composition of marine sediments reflects their particular depositional environment, especially the balance between, and nature of biogenic components and detrital sediments. Processes that contribute to their final composition include biogenic productivity — whether biogenic carbonate or opal — water depth of deposition, ocean circulation, local climate, terrestrial influx, type and direction of sediment transport, sediment source area and rock-type, sedimentation rate and degree of oxygenation (Calvert and Pedersen, 2007). After deposition, compositions may also be altered by diagenesis and associated geochemical reactions (Calvert and Pedersen, 2007).

At Site 16/28-sb01 clear variations in the concentrations Ca, Si, Fe, Al, K and Ti can be seen between the three lithostratigraphic units (Table 2.2.). In contrast, the concentrations of Mg, S, Ba, P, Sr, Mn, Zr and Rb remain almost constant, with slight variations around a mean value (Table 2.2.). Rb, which in general is most common in clays where it often substitutes for K, is only detected once in U3, which is consistent with the carbonate-dominated nature of this unit compared to the clays in U2 and 1 (Rothwell, 2015).

As identified within the PCA analysis above, all lithostratigraphic units — U1, U2 and U3 — have distinct sediment compositions, although the largest change in composition is clearly seen between the lower Eocene U2 and the middle Eocene U3. The concentrations of elemental tracers of siliciclastic deposits are all higher within U2 compared to U3, with mean value differences of 7.6 wt.% (Si), 3.43 wt.% (Al), 1.01 wt.% (K), 0.50 wt.% (Ti) and 3.7 wt.% (Fe). Si can have a biogenic source in marine settings (radiolaria and diatoms) additional to terrigenous sediment from continental runoff. The reverse is true for Ca concentrations, which have a mean value higher in U3 relative to U2 by 24.46 wt.%. In U1 the average concentrations of Ca, Si, Al, K, Ti, Rb, Fe, Mg and S are in-between the average concentrations of U2 and U3. Average concentrations of Ba, P, Sr and Mn are slightly higher, and Zr and Rb are slightly lower in U1 compared U2 and 3. Higher concentrations of the elements Al, Ti, K, Rb and Fe are generally used as indicator of increased terrestrial influx (Plank and Langmuir, 1998, Calvert and Pedersen, 2007). Normalisations of key elements against Al such as Si/Al, Ti/Al and Zr/Al — are used in many studies for an indication of grain size, with

higher values indicating coarser grains and lower values finer grains (Calvert and Pedersen, 2007, Rothwell, 2015). In this study, lower values of Si/Al and Ti/Al ratios in U2 compared with U1 and U3, are consistent with the dominance of clay in this unit and therefore smaller grain sizes. The Al within this ratio is a tracer of clay (Calvert and Pedersen, 2007, Rothwell, 2015), and therefore higher ratios in U3 are consistent with less clay and a coarser grain fraction. Zr/Al is not shown due to the low concentration of Zr, but data is available in Appendix 1, Table 4. Within U2, concentrations of Al, Ti, K, Rb and Fe, which are commonly derived from a continental source, are all elevated.

The XRF results presented here — the first detailed quantitative analysis of sediment character through this succession — confirm the sedimentological observations and lithostratigraphic divisions of Haughton et al. (2005). In terms of palaeoenvironments, the XRF data is consistent with the deposition of U2 in a more proximal upper slope environment, closer to land with a shallower water depth and more terrestrial influx then U3. This elevated terrestrial clay input could be explained by the peak warmth of the early Eocene climate, linked to enhanced chemical weathering due to the accelerated hydrological cycle (Barron et al., 1989). The higher Ca concentration combined with less terrestrial influx in the middle Eocene U3 compared to U2 supports the deeper water succession interpretation of Haughton et al. (2005). The grain size of U3 is clearly coarser than that of U2 (see Chapter 3 for greatly increased >63 μm residue weights in U3 compared to U2), which is best explained by the onset of increased bottom current strength during the middle Eocene and an increased component of sand-sized biogenic carbonate (foraminifera) (Introduction, Section 1.4). If this is the case, it is difficult to distinguish whether the loss of fine-grained clays within U3 sediments was due to a reduced input from surrounding landmasses (possibly caused by the deepening in the succession), from winnowing of clays by increased current velocities, or some combination of the two. Normalisation of the terrestrial elements against each other (Figure 2.6.), shows slight variations in-between U3 and U2 and might indicate some provenance change of the siliclastic material. These changes are, however, so subtle that generally comparable hinterland source areas and weathering conditions can be assumed through early and middle Eocene.

Redox-sensitive elements Fe, Mn and S (Rothwell, 2015) are normalized against Al and each other (Figure 2.6.). These show only slight variations between the units, indicative of no major change in the redox chemistry of the sediments, or bottom water oxygenation, through time. There is a subtle increase in Fe/Al and Mn/Fe ratios between U2 and U3, which might be related to increased early diagenetic precipitation of iron-manganese oxyhydroxides within this coarser-grained, more carbonate rich and potentially better ventilated middle Eocene deeper water depositional system (Rothwell, 2015). Despite its generally very low abundance, within the PCA, Mn is shown to have the most significant loading on both $PC2^{Ca}$ and $PC2^{Si}$. A close examination of the data suggests that this is due to high-frequency variations between samples with Mn absent, or below XRF detection limits, and samples with detectable Mn. This variation may be random due to the stochastic sampling of slightly larger carbonate particles on which Mn oxides may preferentially nucleate (Pedersen and Price, 1982, Boyle, 1983).

The concentrations of Ba are normalized against both Al and Ti, on the basis that increased Ba accumulation relative to the siliciclastic component is thought to be driven by increased rates of export productivity (Calvert and Pedersen, 2007, Rothwell, 2015, and references therein). Although the wt.% of Al, Ti and Ba all decline between U2 and U3, the Ba/Al and Ba/Ti both show a slight, but consistent increase in U3. This suggests slightly increased generation of biogenic Ba associated with increased export productivity in the middle Eocene but may be associated with the increased water depths rather than a substantial change in primary production. General outliers are 91.95 and 96.64 m in all elements, but most clearly seen in P (Figure 2.5.); an outlier at 107.53 m in Fe and Mn only; and, an outlier at 79.91 m in Rb with lower concentrations in Ti, Si and Ca (Figure 2.5.).

Table 2.2. The average concentrations of each element [wt.%] in each unit and the differences of the average values of U2 and U3 are presented in the table below.

	Ca	Si	Fe	Al	K	Ti	Mg	S	Ba	P	Sr	Mn	Zr	Rb
U3 (middle Eocene) average [wt.%]	28.91	11.22	3.32	1.77	1.17	0.42	0.41	0.13	0.16	0.08	0.11	0.07	0.03	0.020
U2 (lower Eocene) average [wt.%]	4.44	18.82	7.02	5.20	2.18	0.93	0.66	0.38	0.23	0.15	0.09	0.06	0.04	0.024
Average differences in-between U3 and U2	24.46	-7.60	-3.70	-3.43	-1.01	-0.50	-0.25	-0.25	-0.07	-0.07	0.02	0.003	-0.01	-0.004
U1 (lower Eocene) average [wt.%]	15.94	15.29	5.01	3.03	1.71	0.44	0.62	0.27	0.27	0.15	0.14	0.09	0.02	0.01

Figure 2.5. (on p.45): The elemental distribution throughout Site 16/28-sb01, measured by XRF, shown against the lithostratigraphic units and the biostratigraphy. Variations in the concentration of Ca, Si, Al, K, Ti, Rb and Fe can be seen between the units, whereas the concentrations of Mn, Sr, Mg, Ba and P remain broadly constant. Increased concentrations of Si, Al, K, Ti, Rb and Fe within U2 are taken to indicate increased terrestrial influx and a more proximal location relative to the palaeo shoreline than U3. Increased Ca in U2 is consistent with higher biogenic carbonate contents in U3 compared to U1 and U2.

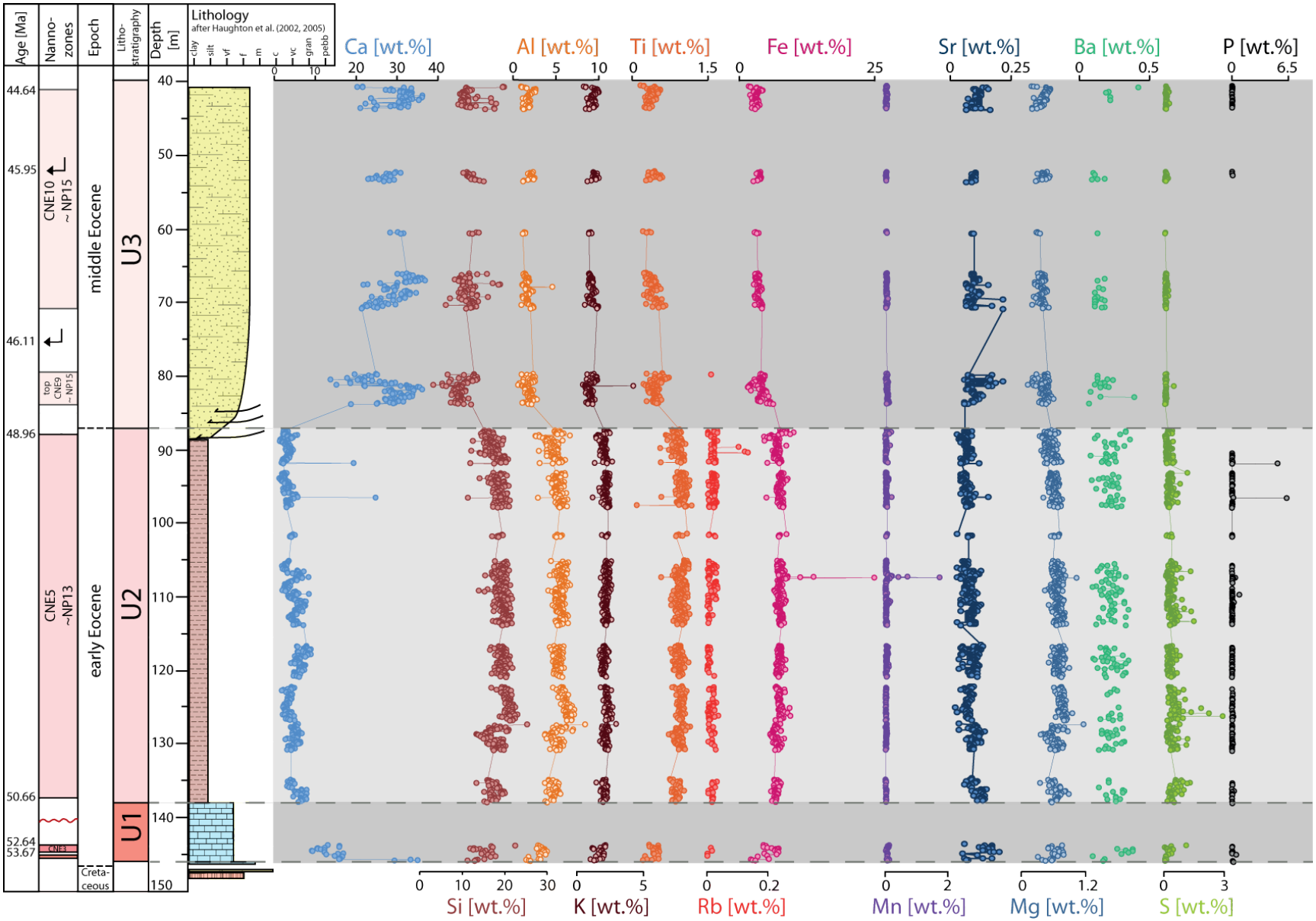
Age [Ma]
Nanno-zones
Epoch
Litho-stratigraphy
Depth [m]
Lithology
after Haughton et al. (2002, 2005)
clay
silt
vf
f
m
c
vc
gran
pebb
44.64
45.95
46.11
48.96
50.66
52.64
53.67
CNE10 ~ NP15
top CNE9 ~ NP15
CNE5 ~NP13
CNE3
middle Eocene
early Eocene
Creta-ceous
U3
U2
U1
40
50
60
70
80
90
100
110
120
130
140
150
Ca [wt.%]
Al [wt.%]
Ti [wt.%]
Fe [wt.%]
Sr [wt.%]
Ba [wt.%]
P [wt.%]
Si [wt.%]
K [wt.%]
Rb [wt.%]
Mn [wt.%]
Mg [wt.%]
S [wt.%]

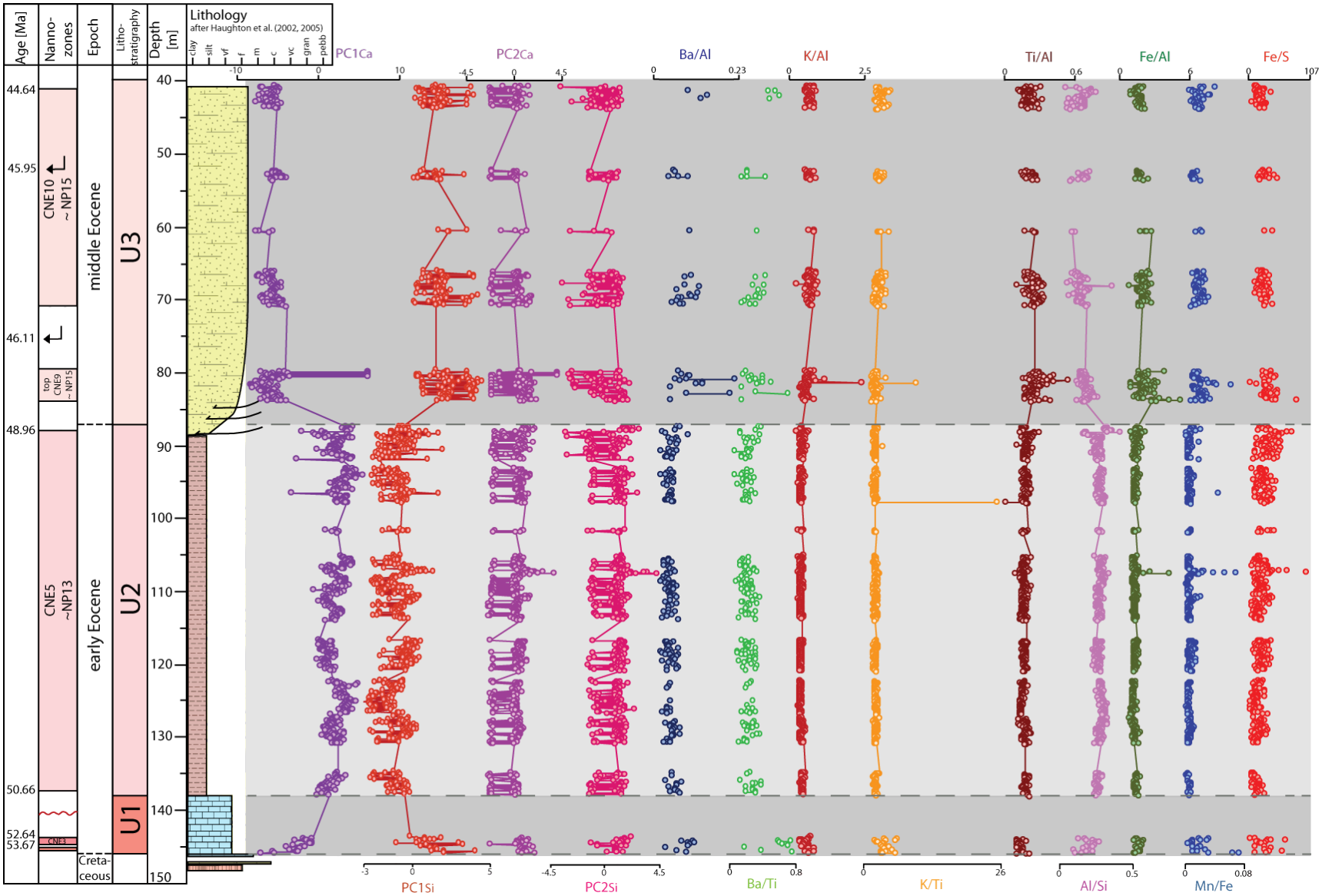
Age [Ma]
Nanno-zones
Epoch
Litho-stratigraphy
Depth [m]
Lithology
after Haughton et al. (2002, 2005)
clay
silt
vf
f
m
c
vc
gran
pebb
PC1Ca
PC2Ca
Ba/Al
K/Al
Ti/Al
Fe/Al
Fe/S
44.64
45.95
46.11
48.96
50.66
52.64
53.67
CNE10 ~ NP15
top CNE9 ~ NP15
CNE5 ~NP13
CNE4
middle Eocene
early Eocene
Creta-ceous
U3
U2
U1
40
50
60
70
80
90
100
110
120
130
140
150
PC1Si
PC2Si
Ba/Ti
K/Ti
Al/Si
Mn/Fe

Figure 2.6. (on p. 46): The PC1s and PC2s of the PCA normalized against Ca and Si are shown, and used to confirm the definitions of the lithostratigraphic Units 1, 2 and 3. PCA was undertaken using the software PAST (Hammer et al., 2001) Normalizations of Ba against terrestrial influx elements Al and Ti are shown as potential proxy for palaeoproductivity. All the terrestrial influx elements are shown normalized against each other to determine any major sediment provenance changes, but only show minor variations between units. Redox sensitive elements Mn, Fe and S are also shown.

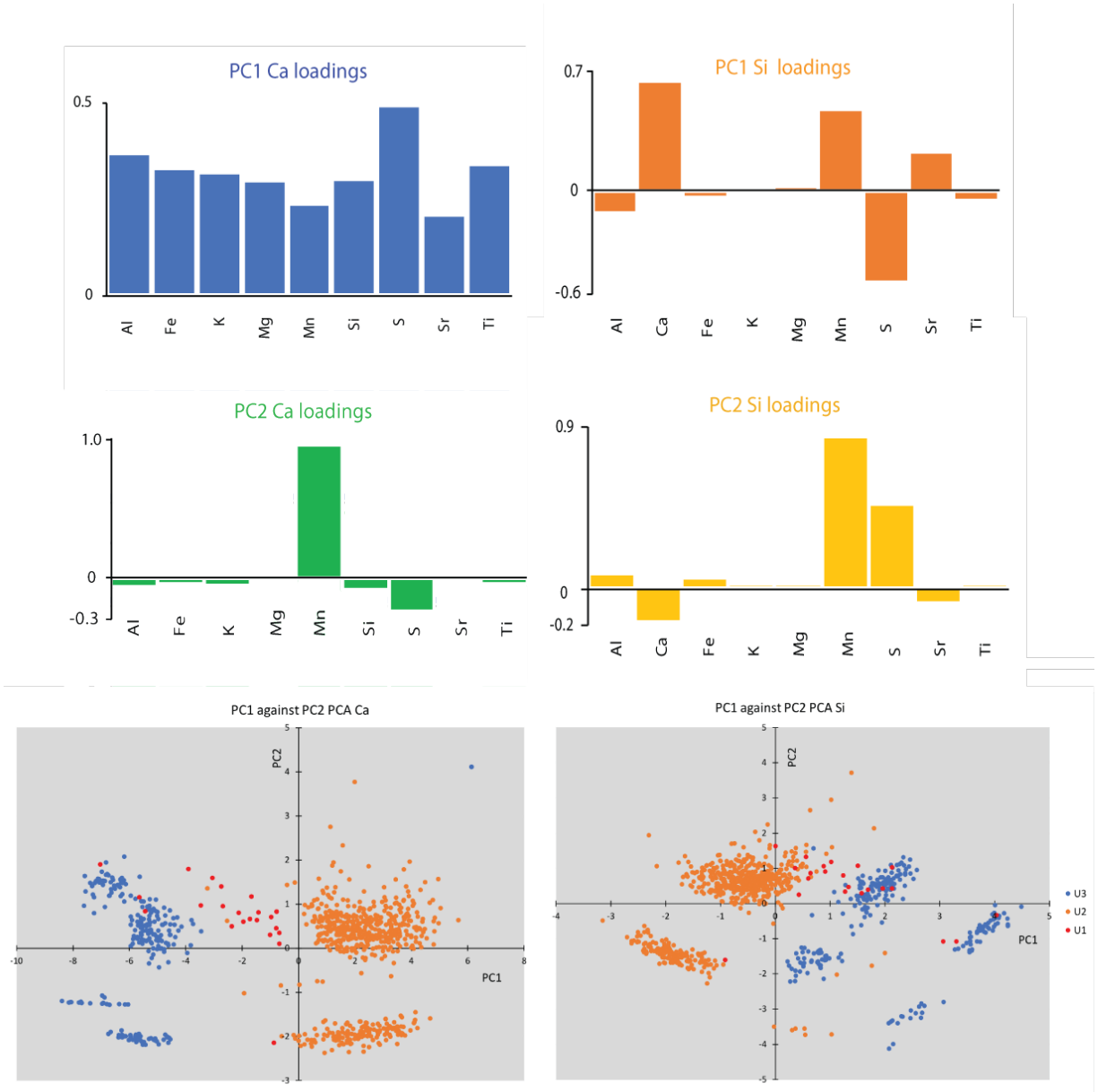

Figure 2.7. Multivariate PCA analysis of the XRF values, used to reduce the dimensionality of the XRF data. The top shows the different loadings resulting from normalisation against Ca and Si for PC1 and PC2. In the bottom two x-y plots PC1 is plotted against PC2 for both normalizations — the three different lithological units or highlighted 1 (red), 2 (orange) and 3 (blue).

2.5.3 Bulk isotopes

Results of 983 bulk carbonate stable isotope analyses are shown (Figure 2.8.) and are given in Appendix 3. Similar to the XRF results there are distinct shifts in the bulk carbon isotope ($\delta^{13}C$) and bulk oxygen isotopes ($\delta^{18}O$) values between the three lithological units (Table 2.3.).

Carbon isotope values are on average lowest in U1 (average -0.14 ‰), most positive in the lower Eocene U2 (average 1.34 ‰), before shifting back to slightly lower values in U3 (average 0.88 ‰). Oxygen bulk isotopes are on average -1.56 ‰ in U1 and shift to -2.63 ‰ in the lower Eocene U2 — these then shift to the most positive average values (~0.05 ‰) recorded within the middle Eocene U3. There are also significant differences in estimates of wt.% $CaCO_3$ between units, as derived from both bulk isotopes and XRF measurements, with lowest $CaCO_3$ content within lower Eocene U2 and highest in the middle Eocene U3 and intermediate within lower Eocene U1. It is assumed that the $CaCO_3$ derived from XRF are higher due to incomplete reaction of $CaCO_3$ during isotope analysis or due to Ca source from lithic material — e.g. feldspars (plagioclase) or clinopyroxenes — in the sediments besides $CaCO_3$. The middle Eocene U3 has ~7 times the amount of $CaCO_3$ than the clay-rich lower Eocene U2. There are two outliers (91.95 m and 96.64 m) in Unit 2, which display anomalous values in all three parameters: calcium carbonate content (anomalous high), $\delta^{13}C$ (anomalous low) and $\delta^{18}O$ (anomalous high) (Figure 2.8.). Furthermore, this corresponds to outliers in Si (anomalous low), Al (anomalous low), K (anomalous low), Ti (anomalous low), Fe (anomalous low), Sr (anomalous high), P (anomalous high) in the XRF results and $PC1_{Ca}$ and $PC1_{Si}$ (Section 2.5.2.2). It is likely that these two samples include some component of diagenetic or authigenic carbonate and are therefore excluded from further analysis.

To test the homogeneity of samples with respect to their isotopic composition, four replicates have been run on one middle Eocene (U3; 68.43 m) and one lower Eocene (U2; 113.28 m) sample. The standard deviation of these analyses is 0.037 for $\delta^{13}C$ and 0.101 for $\delta^{18}O$ for the U3 sample, and 0.035 for $\delta^{13}C$ and 0.103 for $\delta^{18}O$ for the sample from U2. These results are better than the external precision of the instrument indicating a very good homogeneity of isotopic composition within the samples.

Table 2.3. Calculated averages for each stratigraphic unit.

	Depth [m]	$\delta^{13}C$ ‰ VPDB (average)	$\delta^{18}O$ ‰ VPDB (average)	Carbonate % from bulk isotopes (average)	$CaCO_3$ % from XRF (average)
U3	40 – 87.49	0.88	0.05	47.2	72.3
U2	87.50 – 138	1.34	-2.63	6.0	11.1
U1	138 – 145.95	-0.14	-1.56	21.7	39.9

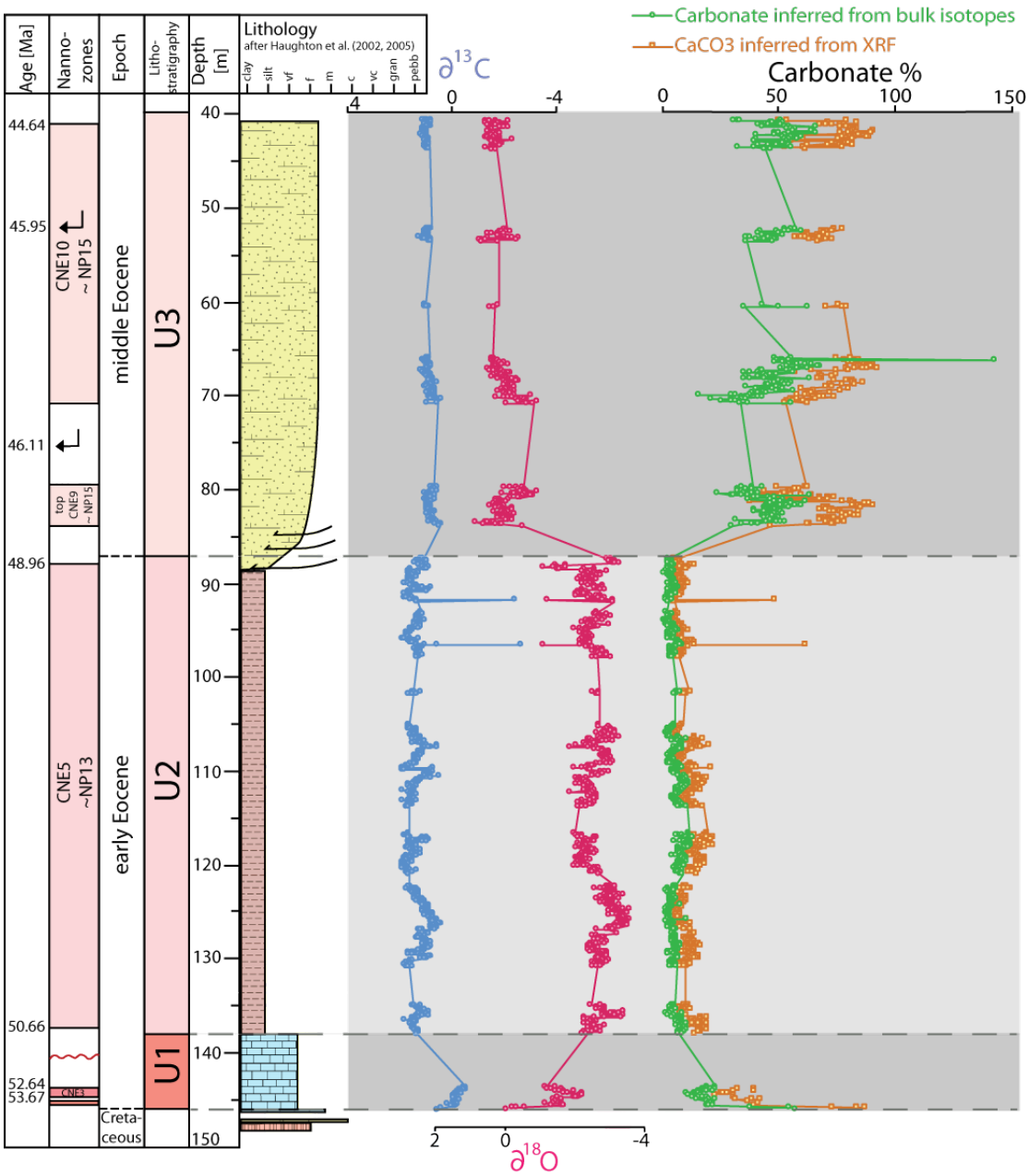

Figure 2.8. Lithostratigraphy compared with the bulk carbonate carbon and oxygen isotopes. Also shown is the weight percent carbonate content inferred from both XRF and isotope analyses.

2.6 Age model refinement

The first indications for the new age model of this study were inferred from the existing biostratigraphies (Section 2.3) and were refined by the new calcareous nannofossil biostratigraphy (Section 2.5.1). An initial age estimation for the succession is based on linear interpolation between these biostratigraphic age constraints (Table 2.4.).

Table 2.4. Biostratigraphic age constrains used to construct an initial age estimation. "Tie-points" are based on specific biostratigraphic events identified in Section 2.5.1 and "estimation" points are not linked to a biostratigraphic event but are constructed by using the bottom and top of the total range of the biozone.

Depth [m]	Biostratigraphic constraint/ tie points	Uncertainty	Age [Ma]
41	estimation 1	older than	44.64
53	tie point	± 0.5 m	45.95
75.42	tie point	± 4.5 m	46.11
87.9	estimation 3	older than	48.96
138	estimation 4	younger than	50.66
143.9	estimation 5	older than	52.64
144.7	estimation 6	younger than	53.67

As noted in the Introduction Section 1.2 and 1.3 the early Eocene is marked by a series of notable negative carbon isotope excursions (CIEs), recorded within high-resolution $\delta^{13}C$ records (Kirtland Turner et al., 2014, Sexton et al., 2011). The distribution of CIEs provides a series of useful stratigraphic markers within the early Eocene (Sexton et al., 2011, Kirtland Turner et al., 2014, Lauretano et al., 2016), and where CIEs are detected within the new high-resolution bulk isotope record of Site 16/28-sb01, they were used to fine-tune the age estimation within the framework of the biostratigraphic age constraints of Table 2.4. CIEs within Site 16/28-sb01 record are tied to the stable isotope datasets of Sexton et al. (2011) (benthic foraminifera, ODP Site 1258, Demerara rise, equatorial Atlantic), Kirtland Turner et al. (2014) (bulk isotopes from ODP Site 1258) and Lauretano et al. (2016) (benthic foraminiferal $\delta^{13}C$ isotopes, ODP Site 1263, Walvis Ridge, South East Atlantic). These records are used for tuning the Rockall record, because they are all Atlantic single site records, with prominent early Eocene CIEs. The age model of this study is adjusted to GTS2012 which is most widely

used in Eocene records (Hollis et al., 2019). As the astronomical tuning for this interval is still ongoing and is frequently slightly changed (Lauretano et al., 2016, Westerhold et al., 2017) the tuning to GTS2012 is seen as the most parsimonious and conservative approach, which can be translated, once the early Eocene timescale is more settled.

Within the Site 16/28-sb01 isotope record, there is no sign of the CIEs, associated with the PETM, ETM2 and ETM3 events. This is consistent with the biostratigraphic constraints on the ages of the recovered sediments. Instead, tie points are based on correlations to more subtle fluctuations in the bulk (Kirtland Turner et al., 2014) and benthic foraminiferal (Sexton et al., 2011) stable isotope records from ODP Site 1258 — the combination of which is referred to from here on as the KT/S target curve. The computer program AnalySeries 2.0 (Paillard et al., 1996) is used to match the high-resolution isotope data from this study to the KT/S target curve. The suitability of the KT/S target curve as a recorder of globally recognisable climate and/or carbon cycle perturbations, was supported in Lauretano et al. (2016) which compared the KT/S target curve with the high-resolution benthic foraminiferal $\delta^{13}C$ record from Walvis Ridge ODP Site 1263 in the South Atlantic and found the same series of CIEs (Lauretano et al., 2016). In this thesis the KT/S target curve is used for alignment to Site 16/28-sb01 instead of Lauretano et al. (2016) because it is A) geographically closer to Site 16/28-sb01, B) consists in the part of Kirtland Turner et al. (2014) of bulk carbonate measurements consistent to the bulk carbonate data of Site 16/28-sb01 and C) provides additional $\delta^{18}O$ data whereas Lauretano et al. (2016) only reports benthic foraminiferal $\delta^{13}C$.

The CIEs of the KT/S target curve were named following the nomenclature of Cramer et al. (2003), as indicated in Figure 5 of Lauretano et al. (2016) and redrawn for this study in Figure 2.9. Offsets between the Lauretano et al. (2016) age model and that of Kirtland Turner et al. (2014) are discussed in Lauretano et al. (2016). The alignment of the record of Kirtland Turner et al. (2014) by Lauretano et al. (2016) to the nomenclature of Cramer et al. (2003) is used within this study and is extended to the whole KT/S target curve (Figure 2.9.) to name as well the CIEs in Sexton et al. (2011) data. The CIEs are potential stratigraphic markers that are likely to be present in $\delta^{13}C$ records derived from both surface (bulk) and deep water (benthic foraminifera)

carbonates, and from sites that are geographically widespread as previously discussed (Introduction Section 1.2 and 1.3).

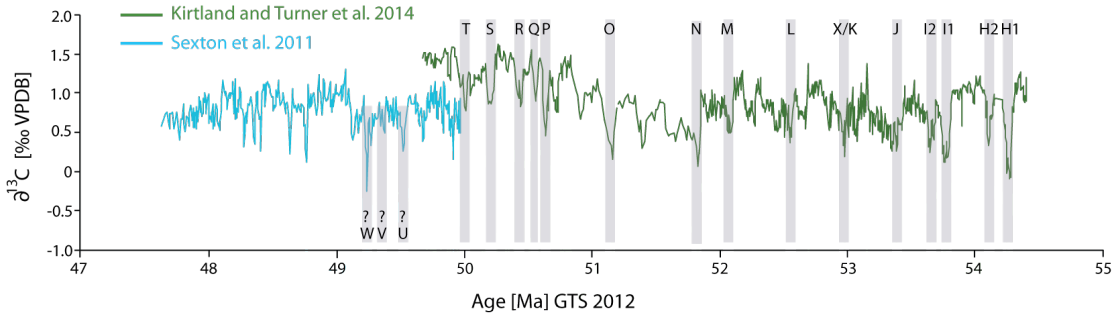

Figure 2.9. Early Eocene CIEs are globally distributed and can be used as stratigraphic markers. The $\delta^{13}C$ record of Sexton et al. (2011) (turquoise) and Kirtland and Turner et al. (2014) (green) are displayed with the matching CIEs as suggested on Figure 5 in Lauretano et al. (2016). In this thesis the U, V and W events are found to be present within the Sexton et al. (2011) record, by comparing it with the CIEs indicated in Lauretano et al. (2016), but there is some uncertainty here if they are correctly identified, indicated with the question mark.

Biostratigraphic tie-points provide initial constraints on Site 16/28-sb01 match to the KT/S target curve, and this is then improved by identifying best-fit tie-points between the $\delta^{13}C$ record of 16/28-sb01 and that of KT/S. The resultant tied records are then cross-checked with the $\delta^{18}O$ isotope records from both 16/28-sb01 and KT/S, to identify erroneous ties based on a significant mismatch in $\delta^{18}O$. The resulting improved age model for 16/28-sb01 is based on the best constraints possible, but is still subject to uncertainty, both in the identification of tie points, and the assumption of linear sedimentation rates between tie points. However, there is confidence in the identification of the series of P, R, S, T in 16/28-sb01, and likely U, V and W, as they are within the biostratigraphic age constraints and the magnitude and pattern of the CIE recorded in both the KT/S and ODP 1263 records (Lauretano et al., 2016) are similar to those recorded in 16/28-sb01 (Figure 2.10.).

The tie points between Site 16/28-sb01 and KT/S $\delta^{13}C$ records are given in Table 2.5. Unit 2 is the thickest of the three lithological units, and has the most complete core recovery and resultant bulk isotope record. As a result, this is the interval in which the best isotopic ties to the KT/S record can be achieved, and is the best starting point for relating the stratigraphy of Site 16/28-sb01 to global records. The biostratigraphic age window for Unit 2 — between 48.96 to 50.66 Ma — includes the P to W CIEs (Figure 2.11.). The first constraint on the age of U2 is based on the recovery pattern after the

W CIE in the KT/S target curve. This recovery is a rapid and > 1 ‰ increase in benthic foraminiferal $\delta^{13}C$ at ODP Site 1258 (Sexton et al., 2011) located at the younger end of

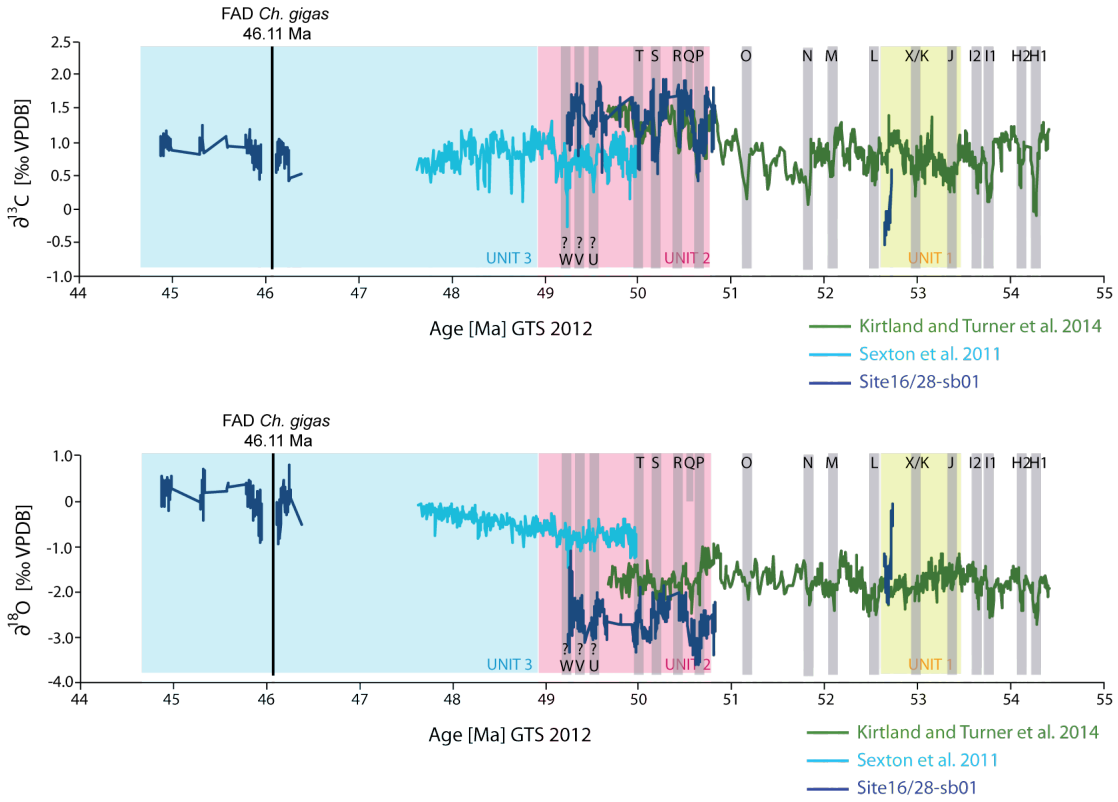

Figure 2.10. Schematics of fine-tuning the age estimation for Site 16/28-sb01 based on biostratigraphic constraints (Unit 1, 2 and 3) and CIEs for the early Eocene. Bulk carbon $\delta^{13}C$ and $\delta^{18}O$ isotope records from the Rockall Site 16/28-sb01 (dark blue) with the new age model developed from $\delta^{13}C$ ties to the KT/S target curve (turquoise and green). The biostratigraphic limits for each interval are shown with background shading: Unit1 (yellow) is older than 52.64 and younger than 53.64 Ma; Unit 2 (red) is older than 48.96 and younger than 50.66 Ma; and Unit 3 (blue) is older than 44.64 and younger than 48.96 Ma. The black line in U3 indicates the first appearance datum (FAD) of *Ch. gigas,* which has a calibrated age of 46.11 Ma. Key carbon cycle perturbations are highlighted and named following the nomenclature of Cramer et al. (2003) as applied in Lauretano et al. (2016).

this age window. This is not detected in the 16/28-sb01 record. The most similar familiar feature at the youngest end of the 16/28-sb01 U2 record is the negative $\delta^{13}C$ excursion identified as the V event, which looks most similar to the W event of the KT/S target curve (Figure 2.11.). Shifting this up to correlate with the V event, however, is favoured because it results in a more stable sedimentation rate rather than assuming V in the 16/28-sb01 record would be the W event in the KT/S target curve. If V of 16/28-sb01 would be the W event of the KT/S it would result in very high sedimentation rates in-between T and U. At the base of U2, the oldest significant point is the P event (50.64 Ma). To tie the record older than the P event it is matched with the distribution pattern of the smaller excursions and two significant points are used

to tie it in, as given in Table 2.5. and shown in Figure 2.11., this is done to achieve most stable sedimentation rates. It however shifts the basal boundary of Unit 2 slightly older (to 50.82 Ma) than suggested by the biostratigraphy (50.66 Ma). This is a minor mismatch (161 ka) that is within the likely error on the calibration of the biostratigraphic constraint, the top of *Tribrachiatus orthuostylus* (Agnini et al., 2014). Alignment to P as the basal CIE results in the difficulty of defining the Q event of the KT/S target curve — if R would be aligned to it — sedimentation rates would be markedly higher. Additionally, one of the most characteristic shaped CIEs in global records is the T CIE, with it's typical "funnel-like" shape, appears to be well developed in the 16/28-sb01 record. If interpreted to be aligned to T as it is presented here and according alignment it might be that the Q event in the 16/28-sb01 record is in a core gap or poorly expressed. Many different CIE alignments were tried within the biostratigraphic constraints, from which the presented one is the most parsimonious approach, in terms of the match to the KT/S target curve and the most stable sedimentation rates. Overall the new age model results in average sedimentation rates of 3.8 cm/ka within U2.

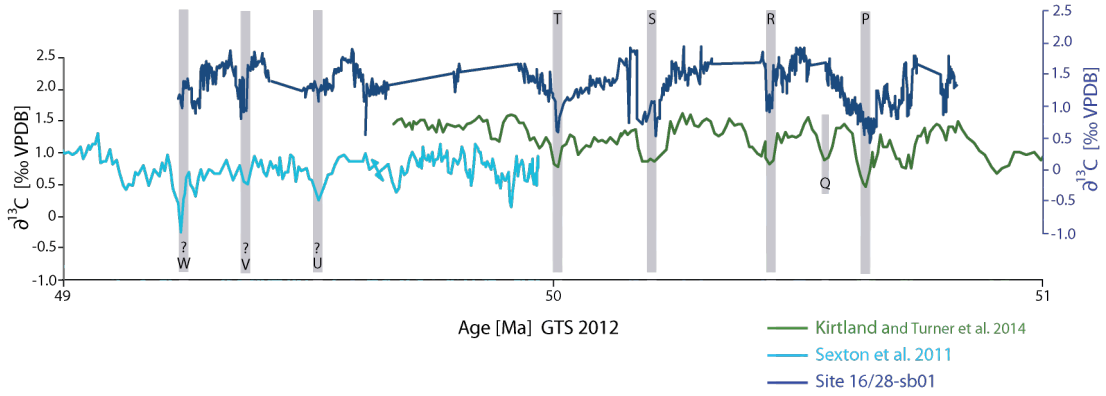

Figure 2.11. Final age alignment of the KT/S target curve to Site 16/28-sb01 in the lower Eocene Unit 2. CIEs P, R, S, T, U, V and W are detected — with CIE Q missing.

The biostratigraphic age constraints for Unit 3 suggest that it is older than 44.64 and younger than 48.96 Ma. Within this, the recognition of the first appearance datum (FAD) of *Chiasmolithus gigas* at 75.42 m is seen as most reliable age control point within this section. Further ties based on $\delta^{13}C$ records were not possible due to the relatively short interval of U3 and less complete core recovery, as well as the absence of a comparable target curve to the KT/S record covering the age of U3. Instead, the

age model for U3 was established using the biostratigraphic age of FAD of *Ch. gigas* and then assuming a slightly lower sedimentation rate (~2.8 cm/ka) than that determined for U2 (~3.8 cm/ka). This assumption is based on the relatively high clay input into U2 coupled with the higher "terrestrial element" inputs inferred from the XRF analysis interpreted as higher sedimentation rates than within U1 and U3, which have less clay and less of the "terrestrial input" elements (Section 2.5.2). The lower sedimentation rate estimate of 2.8 cm/ka was thus applied to both U1 and U3. In this analysis, the FAD *Sphenolithus furcatolithoides* at 45.95 Ma (53.00 m) was not used, in combination with the FAD *Ch. gigas* to estimate sedimentation rates. *S. furcatolithoides* is a tropical species, with an age calibration taken from sub-tropical ODP Site 1051 (Agnini et al., 2014), where it is closely coupled to the FAD of *Ch. gigas*. Given that Site 16/28-sb01 is in the high mid-latitudes, it is likely that there is more of a temporal offset between these two events. If the ODP 1051 calibration were applied to 16/28-sb01, they generate what appears to be unrealistically high sedimentation rates for U3 of 14 cm/ka.

As with U3, given the limited stratigraphic thickness of Unit 1 and the relatively wide biostratigraphic age constraints, the age model for U1 was based on a sedimentation rate estimate derived from U2. Like U3, U1 also has a lower clay content than U2, and it is assumed that this is the result of lower siliclastic input to the system and a lower sedimentation rate of 2.8 cm/ka is assumed for this U1. This sedimentation rate is applied across the recovered core interval of U1, which is lined up using the biostratigraphic constraint for the top of this interval, to give an age of 52.64 Ma at 143.74 m. In this case we assume that the top of U1 is at this age constraint (143.74 m is at 52.64 Ma) and the rest of the recovered cored interval is assigned ages older than this based on the assumed linearly applied sedimentation rate. Clearly this is subject to significant uncertainty, with the recovered record potentially representing any of the interval within the yellow shaded area (Figure 2.10.).

To show the uncertainty within the age estimation the sedimentation rates are plotted against age (Figure 2.12.) and age against depth (Figure 2.13.). They are highest at the onset (oldest) part of U2. Two unconformities or episodes of no deposition where found in between 50.82 – 52.71 Ma and 46.38 – 49.31 Ma.

Table 2.5. New depth to age tie-points from correlations to the Kirtland Turner et al. (2014) and Sexton et al. (2011) target isotope record for the lower Eocene Unit 2. The point named "significant point" and "end of record U2" are used to deal with the oldest bit of U2 older than the P event and is aligned to smaller changes it the KT/S target curve.

Core depth [m]	Age [Ma]	Carbon isotope event
87.51	49.23	W
90.89	49.37	V
94.01	49.52	U
107.43	50.01	T
110.58	50.21	S
117.36	50.44	R
130.02	50.73	P
136.00	50.80	Significant point
137.89	50.82	End of record U2

Table 2.6. New depth age correlation points for Unit 1 and 3, with a steady sedimentation rate estimation applied to derive age estimates for these Units.

Core depth [m]	Age [Ma]	Sedimentation rate
75.42	46.11	2.8 cm/ka
143.74	52.64	2.8 cm/ka

Figure 2.12. (top of p.57) Plotting sedimentation rates against age can help to highlight uncertainty in the age model as well as changes within the accumulation patterns of the sediments. On average 3.8 cm/ka sedimentation rates are found for U2 and the inferred 2.8 cm/ka for U1 and U3 for the final age model of this thesis.

Figure 2.13. (bottom of p.57) Plotting age against depth is a useful way of looking at the depositional history of a sedimentary record, it highlights sedimentation rate changes and "sedimentation gaps". Site 16/28-sb01 sedimentation rates are shown and two intervals of no deposition, no core recovery or erosion are found within the final age estimation.

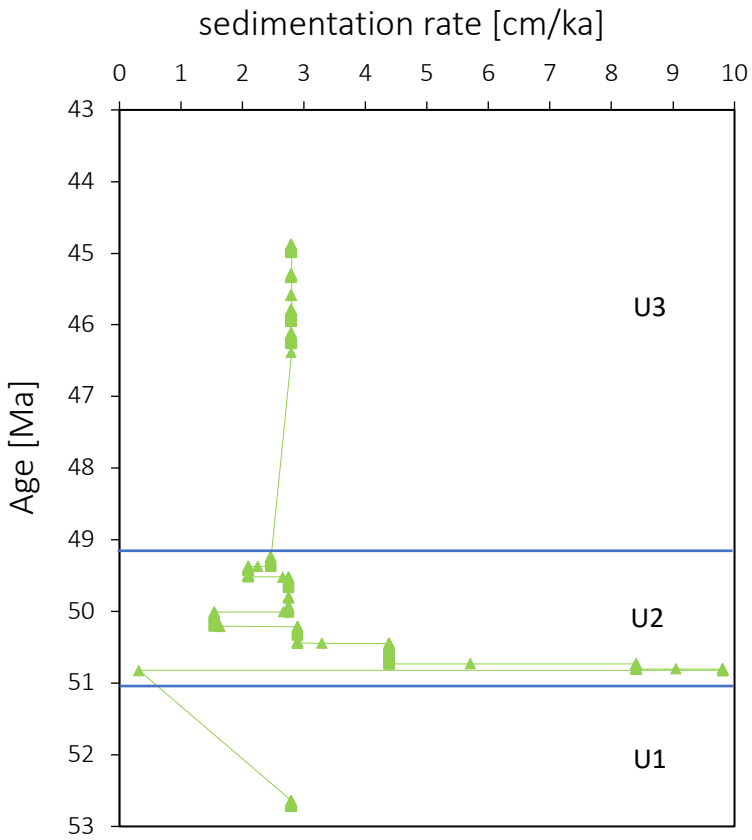
sedimentation rate [cm/ka]
0
1
2
3
4
5
6
7
8
9
10
43
44
45
46
47
48
49
50
51
52
53
Age [Ma]
U3
U2
U1

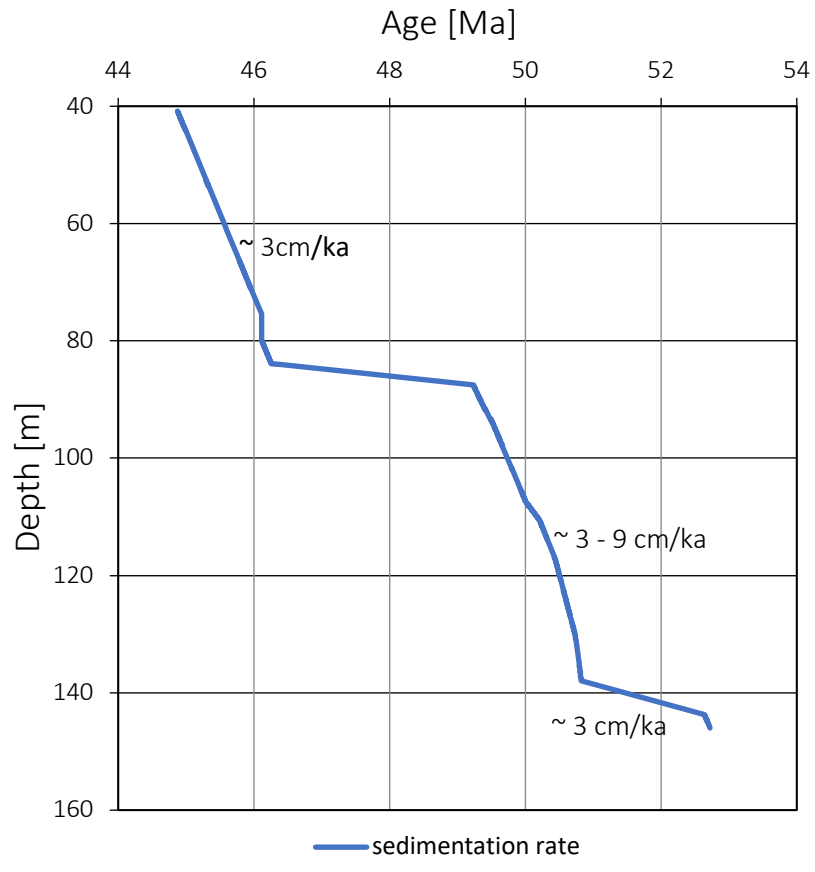
Age [Ma]
44
46
48
50
52
54
40
60
80
100
120
140
160
Depth [m]
~ 3cm/ka
~ 3 - 9 cm/ka
~ 3 cm/ka
sedimentation rate

As a broad cross-check for the developed bio- and chemostratigraphic age model for Site 16/28-sb01, the bulk records of this core are compared to the benthic foraminiferal stable isotope compilation of Cramer et al. (2009) (Figure 2.14.). Although a direct correlation between these bulk carbonate (from a shallow site and ~surface water) and benthic foraminiferal (deep water) records should not necessarily be expected, they should both carry a signal of the long-term secular evolution of both global climate and the exogenic carbon cycle. In this, there is a good correlation between the two records, especially in $\delta^{13}C$, where both show the distinct positive shift in $\delta^{13}C$ through the early Eocene, when $\delta^{18}O$ remains on a negative trend. This is followed by a return to more negative $\delta^{13}C$ values through the earliest part of the middle Eocene. The $\delta^{18}O$ record almost mirrors these trends in $\delta^{13}C$ through this interval, with a slight negative trend in benthic foraminiferal records through the early Eocene, whilst there is a strong negative shift in 16/28-sb01 bulk carbonate $\delta^{18}O$ between Unit 1 and 2. Through the earliest middle Eocene, both $\delta^{18}O$ records shift to more positive values, with a stronger shift in the bulk records. In both records the EECO interval — as recovered in Unit 2 — represents the point of peak separation between $\delta^{18}O$ and $\delta^{13}C$. The enhanced response in 16/28-sb01 bulk $\delta^{18}O$ to EECO warming most likely reflects an amplification of regional NE Atlantic surface ocean warming relative to Southern Ocean locations of deep-water formation (see Introduction Section 1.4). It could also be exaggerated by local $\delta^{18}O$ vital effects within the coccolithophore algae, the dominant contributors to carbonate contents in 16/28-sb01.

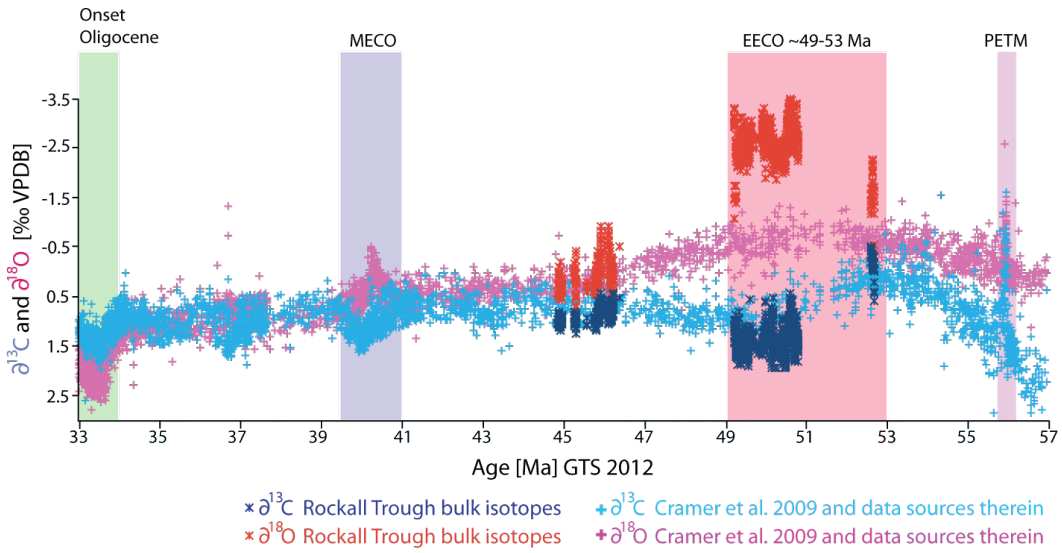

Figure 2.14. The bulk isotope data from Site 16/28-sb01 [red asterisks $\delta^{18}O$ and blue asterisks $\delta^{13}C$] are shown with our new age model tuned to GTS 2012 against the global record of benthic foraminiferal isotopes from Cramer et al. (2009) $\delta^{13}C$ [light blue crosses] and $\delta^{18}O$ [pink crosses]and data sources therein.

2.7 Discussion and summary

The stratigraphic data presented in this chapter are the indispensable foundation of this thesis, and for future research on the 16/28-sb01 record. This Chapter sets the study site into a global context by providing the best possible age constraints for this succession, in particular across the EECO, which is sparsely studied (Hollis et al., 2019). The refined sedimentology of the succession, based on elemental, stable isotopic and micropalaeontological analyses, increase confidence in determining palaeoenvironmental and depositional regimes and their relationship to the wider tectonic evolution of the Rockall Basin. In this discussion, the new data is integrated with the previous publications on the core and interpretations from unpublished seismic-data made by Stephen Jones from the University of Birmingham in the adjacent Porcupine Basin region, to provide facies and palaeoenvironmental models for each of the three key stratigraphic units (U1, U2, U3).

2.7.1 Lower Eocene (Unit 1) summary and interpretation

At the base of Site 16/28-sb01 basaltic igneous rocks are recovered (148.25 – 147.30 m), they are interpreted to be extrusive lavas obtained from the adjacent Drol Igneous Centre (Green, 2001, Haughton et al., 2005). The basalt flow is overlain by Upper Cretaceous sediments (147.30 – 145.95 m), an older calcareous sandstone and a

younger calcareous limestone (Haughton et al., 2002, Harrington et al., 2000). Based on the age of these sediments and the extensional regime in the region during the Late Cretaceous (Hallam, 1971, Saunders et al., 1997), the basalt unit is inferred to be Late Cretaceous in age or older although the contact is not recovered (Haughton et al., 2002). The Upper Cretaceous sediments were previously interpreted to be from a slightly deepening succession — as indicated by a fining upwards trend — on a high-energy shallow open marine shelf (Haughton et al., 2002). It is typical for regions on the flanks of the Porcupine High, the Slyne and Erris Basin to have a thin or absent Cretaceous succession (Naylor and Shannon, 2005), probably caused by a transient ~450 m uplift in the Early Cretaceous times of the Porcupine High and Basin followed by ~250 m subsidence (Jones et al., 2001). These Upper Cretaceous sediments were probably accumulated during this Cretaceous subsidence and are overlain by a lower Eocene bryozoan lime- and mudstone (145.95 – 138.00 m), section U1, which, in this study, is dated to be from calcareous nannofossil Zone CNE3 (~53.67 – 52.64 Ma) (Agnini et al., 2014). As the recovered sediments are placed at the top of zone CNE3 their maximum age uncertainty would be smaller than + 1 Ma, inferred from the maximum length of CNE3.

Peak Cenozoic uplift at the centre of the NAIP occurs in the latest Paleocene ~55 Ma (Maclennan and Jones, 2006). Peak uplift in the Rockall Basin, which is offset to the south east from the centre of the NAIP, might be slightly after this, but would still have occurred within ~1 Ma of peak uplift at the centre of the province, with an estimated uplift of ~400 m of the Porcupine flanks at the Paleocene to Eocene boundary (Jones et al., 2001). It is thus likely that the unconformity, non-deposition and potential erosion between the Upper Cretaceous and lower Eocene sediments in 16/28-sb01 was caused by NAIP-associated regional uplift (Jones et al., 2001, Maclennan and Jones, 2006) and sediment starvation (Shannon et al., 1995). There is full break-up between North America and Eurasia in the early Eocene (Pitman and Talwani, 1972) with the main spreading axis switching to the Labrador Sea and eventually to the Reykjanes ridge — away from the too rigid Rockall Basin spreading axis (Smythe, 1989, Knott et al., 1993, Musgrove and Mitchener, 1996, Roberts et al., 1999). This process is associated with the onset of subsidence across the NW European continental margin, including the Rockall Basin, and fits with the deposition of the lower Eocene

outer shelf sediments of U1. The palaeodepth of ~250 m determined from planktic foraminifera percent (% P) in this study (Chapter 3, Section 3.3.2, Appendix 6) indicates a rather proximate location to the continent, which might indicate, based solely on water depth, inner shelf rather than an outer shelf position as suggested in Haughton et al. (2002). However, one has to keep in mind that the Site location is on the Porcupine High so probably at this time as well separated from the Irish continental margin by the Porcupine and Slyne Basin. So evidently the application of estimating palaeowater depth from % P is a simplification as would be any other palaeo-waterdepth estimation based on planktic and benthic foraminifera as it is an approximation which can be complicated by basin structure due to influencing primary productivity, salinity, bottom water oxygenation and sedimentation rates. Theoretically, however, if there would have not been a significant change in the primary production, sedimentation rate, salinity and bottom water oxygenation the water depth should be as well recorded by the percentage of planktic to benthic foraminifera in this outer Rockall Basin setting of Site 16/28-sb01 as at any other Site. In Figure 2.12 and 2.13 the sedimentation rates for Site 16/28-sb01 are shown as they are high and very variable there is a higher uncertainty on the palaeodepth estimate from % P, further in Chapter 3, Section 3.3.2, appendix 6 it is shown that very low abundances of both planktic and benthic foraminifera are available, which support the high sedimentation rates inferred from the new age model of this thesis and indicates that palaeodepth estimations from foraminifera are complicated at Site 16/28-sb01 and have to be looked at as guideline for relatively shallower or deeper water here at Site 16/28-sb01 rather than absolute water depth values.

The overall offset between $\delta^{18}O$ and $\delta^{13}C$ within the bulk carbonate stable isotopes of U1 are comparable to those of the global benthic compilation (Cramer et al., 2009) for the earliest Eocene. Absolute values of bulk $\delta^{18}O$ are ~0.5 ‰ lower than the global benthic foraminifera stack (Cramer et al., 2009), which is consistent with slightly cooler SSTs at the higher latitude (Southern Ocean) regions of deep-water formation as to be expected to be represented by the benthic foraminiferal isotopes (Introduction; Section 1.4.), than warmer surface waters in the Rockall Basin — possibly coupled with lower salinity in the restricted Rockall Basin. The $\delta^{13}C$ values are comparable to the ones from Cramer et al. (2009). Compared to the tropical bulk

carbonate record of Kirtland Turner et al. (2014) 16/28-sb01 $\delta^{13}C$ values are ~0.5 ‰ lower and the bulk $\delta^{18}O$ values are slightly more positive, consistent with more nutrient replete but slightly cooler surface water conditions at the Rockall Basin.

2.7.2 Lower Eocene Unit 2

2.7.2.1 Overall character of Unit 2

The second lower Eocene Unit (U2), the "smectitic clay" (138.00 – 87.50 m) (Haughton et al., 2002), is finer grained and more homogeneous than U1 and is the most completely recovered unit of Site 16/28-sb01. Haughton et al. (2002) interpret the palaeoenvironment of U2 as a low- and stable-energy bathyal slope setting where the clays are deposited via suspension settling, implying a significant sea level rise between U1 and U2. The whole of U2 is assigned to calcareous nannofossil zone CNE5, with the improved isotopic stratigraphy providing age constraints of 50.65 Ma (137.99 m) and 48.86 Ma (87.50 m) for the bottom and top of this succession.

Bulk sediment chemistry determined in this study demonstrates a clear difference in composition between U1 and U2. In its mean values, U2 is relative to U1 lower in Ca (-11.50 wt.%), and hence estimated calcium carbonate content, as well as Sr (-0.05 wt.%); whilst it has higher average values of Si (+3.53 wt.%), Al (+2.17 wt.%), K (+0.47 wt.%), Ti (+0.49 wt.%) and Fe (+2.01 wt.%). In bulk carbonate isotopes there is a positive shift of ~1.5 ‰ in $\delta^{13}C$ and a negative shift of ~1.1 ‰ in $\delta^{18}O$ values between U1 and U2. These clear differences in the chemistry and isotopic composition of U1 and U2 sediments, are clear evidence for a stratigraphic break between these two lower Eocene units, and strongly supports the earlier lithologic differentiation of Haughton et al. (2002). The biostratigraphic and age model constraints presented here indicate that this is an unconformity with ~1.9 Ma missing between U1 and U2. The Icelandic mantle plume, which sits underneath the NAIP is responsible for NAIP associated uplift, is observed to continue to "pulse" with a ~3 Ma period through the Eocene (Parnell-Turner et al., 2014), and this gap matches with the next pulse of the NAIP at ~52 Ma (Parnell-Turner et al., 2014) and might have caused this Eocene hiatus or erosion between U1 and U2 at Site 16/28-sb01.

Comparison of the 16/28-sb01 bulk carbonate stable isotope data to global records (Cramer et al., 2009) provides further confidence in the age model for U1 and U2. There is a ~1.5 ‰ positive shift in $\delta^{13}C$ and a ~1.1 ‰ negative shift in $\delta^{18}O$ between the lower Eocene U1 and mid-EECO U2 of 16/28-sb01, compared to ~0.9 ‰ positive shift in in $\delta^{13}C$ and a ~0.2 ‰ negative shift in $\delta^{18}O$ of the global benthic foraminiferal isotope compilation (Cramer et al., 2009). During the interval represented by U2, 16/28-sb01 bulk carbonate $\delta^{18}O$ is more negative than in the KT/S target curve, indicating warmer or lower salinity within the Rockall Basin relative to tropical ODP Site 1258, whilst $\delta^{13}C$ is comparable to the KT/S curve. The larger magnitude changes in 16/28-sb01 bulk carbonate oxygen isotope records relative to the benthic compilations, and absolute values more negative than ODP Site 1258, are likely due to a combination of pronounced EECO warming in the shallow water Rockall area, vital effects within the nannofossil carbonate and/or local salinity effects within the Rockall Basin. Similar $\delta^{13}C$ values to the KT/S target curve suggest improved exchange of open ocean Atlantic water masses into its northern-most basins, which is in concordance with the subsiding Site 16/28-sb01.

Foraminiferal % P (Van der Zwaan et al., 1990) suggest an average palaeowater depth of ~330 m during the deposition of U2, which is ~80 m deeper than U1 (~250m). That is in concordance with Haughton et al. (2002) who interpret a significant deepening in the depositional environment between U1 and U2.

Stephen Jones of the University of Birmingham has unpublished data, which shows the development of a deltaic system in the Porcupine Basin during the early Eocene, similar to the prograding wedges on the east coast of the northern Rockall Basin, east side of the northern Rockall Bank and within the Porcupine Basin (Section 2.2) (Shannon et al., 1995, McInroy et al., 2006, Stoker et al., 2012). The unpublished seismic data show a deltaic channel network developing from around 52.5 Ma (Jones and Mudge, pers. comm.), maybe linked to slight uplift due to the ~52 Ma pulse from the NAIP (Parnell-Turner et al., 2014), such a prograding system could also supply the relatively homogenous “smectitic clays” of U2, dated to start around 50.65 Ma. The interpretation of U2 as part of a distal prograding system would be consistent with the elevated input of terrestrial “markers” (Si, Al, K, Ti and Fe) in bulk sediment XRF analysis and the input of macroscopic plant material to the core site (Figure 2.3.). The

age offset of ~2 Ma could mean that all the terrestrial derived sediment before 50.65 Ma is trapped in the Porcupine Basin, whilst the area west of the Porcupine High (around Site 16/28-sb01) is sediment starved and/or subjected to regional uplift (Naylor and Shannon, 2005, Parnell-Turner et al., 2014), coupled with non-deposition or an erosional regime at Site 16/28-sb01. However, at 50.65 Ma this potential uplift might have stopped and the Porcupine flanks might have subsided to allow sufficient accommodation space for the clay rich deposition of U2. Potentially the accommodation space could have been saturated in the Porcupine Basin allowing the end of sediment starvation at Site 16/28-sb01. There are two possible depositional regimes: A) U2 was deposited as outermost/most distal deposit of a deltaic system or B) U2 was deposited as suspension settling, which was previously suggested by Haughton et al. (2002).

The development of the Porcupine delta system is associated with the relaxation phase and regional subsidence after the main uplift phase of the NAIP (Jones and Mudge, pers. comm. and Jones et al. (2001)). The progradation of the early Eocene delta system within a context of increasing accommodation space implies a large terrestrial sediment input into the system. Increased terrestrial sediment supply is consistent with conditions of EECO peak-warmth, enhanced hydrological cycling, erosion and weathering (Barron et al., 1989, Speelman et al., 2010, Bornemann et al., 2014, Carmichael et al., 2017). The palaeolatitude of ~49˚N is within the enhanced precipitation area modelled for the early to middle Eocene by Speelman et al. (2010), which could explain the lower $\delta^{18}O$ values of Site 16/28-sb01 compared to the tropics as indication with localised lower salinity. The increased sediment supply during the EECO interval caused by this enhance hydrologic cycle, could also explain the transition to the more homogeneous fine-grained clay succession of U2 in addition to the change in estimated water depth between U1 and U2. The average sedimentation rate of U2 is reconstructed to be 3.8 cm/ka (see Figure 2.12.). This interpreted increased sedimentation rates in U2 are also consistent with low concentrations of foraminifera tests, which are less than the statistically significant 300 specimens per sample (Imbrie and Kipp, 1971) (see Chapter 3). Whether U2 was part of a distal progradational wedge or mainly reflects the deposition of lots of terrestrial material out of suspension in sea water, possibly derived from the progradational sediment

systems in its vicinity, cannot be concluded within this study, detailed clay particle analysis, sediment provenance analysis and seismic interpretation in proximity to 16/28-sb01 would be necessary.

It is intriguing to note that the progradational system on Rockall Bank ceased around 49 Ma which matches the end of U2 in the 16/28-sb01 sediment succession at 48.86 Ma. Forty-nine million years seems to be a key date for the Eocene: it is as well-known as a global ocean wide unconformity (Norris et al., 2001), it is dated as the time of northern component water (NCW) onset in the Faroe Shetland Basin (Hohbein et al., 2012), the end of the "*Azolla*" interval in the Arctic (Brinkhuis et al., 2006, Gleason et al., 2009) and a direction change of the plate motion of Greenland relative to North America and Eurasia, linked to a sea floor spreading slow down (Gaina et al., 2009), the end of the EECO (Westerhold et al., 2018a) and is one of the proposed dates for the opening of the shallow Tasman Gateway (Bijl et al., 2013). It is clear that all these dates are subject to their very own uncertainties, however, the concentration of these events around 49 Ma, is a strong indication for its significance as major time of global change: tectonically, oceanographically and within the early Eocene climate. Possibly NCW onset could have caused a more erosive regime in the Rockall Basin and a cessation of the depositional regime of U2.

2.7.2.2 High-frequency isotopic and elemental variations in Unit 2

A key component of this study was the correlation of distinct CIEs, recorded in U2, to similar CIEs recorded in the open-ocean (Kirtland Turner et al., 2014, Sexton et al., 2011). First of all, these CIEs, which are superimposed on the general EECO warming trend, are detectable in multiple records, and within the orbital stratigraphies for these sites are synchronous in timing (Kirtland Turner et al., 2014, Lauretano et al., 2016, Galeotti et al., 2019). Although there is no independent orbital tuning of the 16/28-sb01 record, bulk carbonate $\delta^{13}C$ values within the lower Eocene Unit 2 show very similar variability — in magnitude and shape — as the CIEs of the KT/S target curve and the detailed benthic foraminiferal isotopic records from Walvis Ridge (Lauretano et al., 2016).

Although there has been some uncertainty as to whether CIEs P to W have a strong global expression, the new 16/28-sb01 record supports their global ubiquity and use as stratigraphic markers, with clear correlations possible to the composite bulk carbonate and benthic foraminiferal KT/S target curve (Kirtland Turner et al., 2014, Sexton et al., 2011) and the benthic foraminiferal records from ODP Site 1263 (Lauretano et al., 2016).

The upper slope location of 16/28-sb01, which is relatively proximal to the coast compared to the open ocean Atlantic reference successions (Sexton et al., 2011, Kirtland Turner et al., 2014, Lauretano et al., 2016), opens up the potential for the 16/28-sb01 record to be used to infer the impact of environmental change associated with the EECO CIEs on terrestrial and continental marginal sedimentary systems and, to investigate if the CIEs are linked to hydroclimate. If these CIEs are genuine "hyperthermals", with a climatically significant warming, they could provide key information on the scaling of the hydroclimate perturbations and sedimentary responses to a range of forcings and background climate states across the early Eocene.

To determine if there is a consistent signal in the elemental variation throughout the lower Eocene Unit 2, these CIEs are compared with $PC1^{Si}$, $PC2^{Si}$ and the Calcium, Silicate, Aluminium and Iron XRF results (Figure 2.15.). None of the elemental variations show a consistent correlation to the identified CIEs, although there are indications that several of the CIEs are associated with clear excursions in particular elements. For example, Ca concentrations are slightly enhanced in CIEs R, S, T, V and W, as is Fe in CIEs P, S, T, U and W. As the response of bulk sediment chemistry is not reproduced consistently across all CIEs it suggests a long-term control in the system properties, which evolves through time. This could be a long-term evolution of the sedimentary system, such as the position of delta front of channel distribution systems relative to the core location, or a long-term change in the responsiveness of the terrestrial catchments to precipitation anomalies, as would be expected with catchment ageing through an interval of intense weathering and erosion (Armitage et al., 2011).

To understand the changing nature of the response to CIE events, two events are discussed in more detail below. The P event is the only CIE event in 16/28-sb01 to

show the characteristic paired negative excursions in $\delta^{13}C$ (~1 ‰) and $\delta^{18}O$ (~1 ‰). This typically paired excursions in oxygen and carbon isotopes are recorded in other high-resolution records for all the CIEs recovered at Site 16/28-sb01 coupled with a peak in iron (e.g., Westerhold et al., 2018a, see Figure 1.4.). This iron peak in the deep sea is mostly interpreted as dissolution event there (e.g., Westerhold et al., 2018a). The only CIE not coupled with a pronounced negative $\delta^{18}O$ excursion, but still with an iron peak, in the Westerhold et al. (2018a) compilation, seems to be the T CIE, Figure 1.4. The P event is the largest negative CIE after a rather positive trend in $\delta^{13}C$ following the N CIE in the reference records from the Atlantic (Kirtland Turner et al., 2014) as well as in records from Italy and the Pacific (Galeotti et al., 2017, Westerhold et al., 2018a). The magnitude of the negative $\delta^{13}C$ excursion of the P event reaches from ~0.6 – ~1.3 ‰ in these global records, compared to ~1 ‰ in 16/28-sb01. Associated with this event in 16/28-sb01 are increases in markers for terrigenous sediment input — Si, Al and Fe content — and a minimum in Ca. The minimum in Ca, assumed to be dominantly biogenic pelagic calcium carbonate, is consistent with dilution due to enhanced siliciclastic influx, but could also contain a component of reduced pelagic carbonate production. Coupled reductions in carbonate productivity and increased siliciclastic input would be consistent with higher rates of freshwater and sediment outflow from an adjacent delta system. A transient drop in surface water salinity could contribute to the negative peak in $\delta^{18}O$, although this might solely represent sea surface warming. Direct estimates of SSTs through the CIEs, foraminiferal abundance and the branched and isoprenoid tetraether (BIT) index (Hopmans et al., 2004) (Chapter 3 and 4) help to indicate possible salinity bias on temperature signals within these $\delta^{18}O$ records (see Chapter 3, Section 3.4.3, C) salinity and Chapter 4, Section 4.4.1, Figure 4.4.2). The coupled changes in bulk carbonate isotopes and bulk sediment chemistry across the P event could represent a coherent response of a siliciclastic-dominated upper slope setting, near to a major terrestrial sediment source, to transient global warming (Dunkley Jones et al., 2018). Coupled negative excursions in $\delta^{13}C$ and $\delta^{18}O$ are assumed to be the characteristic signal of the oxidation of carbon from global reservoirs and associated greenhouse-gas forced warming (e.g., Zachos et al., 2010, Kocken et al., 2019), whilst the local declines in

carbonate content and increase in terrigenous sediment flux to continental margins are indicative of an enhanced hydrological cycle and increased catchment erosion (Speelman et al., 2010, Carmichael et al., 2017).

The next significant CIE in the 16/28-sb01 record is the R event, during which both $\delta^{18}O$ and $\delta^{13}C$ show slightly negative excursions of ~0.5 and ~1 ‰ respectively, but these are slightly smaller than the P event excursion in 16/28-sb01. In the $\delta^{13}C$ of the KT/S record, the R CIE has a magnitude of ~0.5 ‰, and is 1 ‰ in Lauretano et al. (2016). Concentrations of the elements Si, Fe at 16/28-sb01 do increase at the R event but not to the extent expected based on responses through the P event CIE. For comparison, the percentage Si increases relative to initial conditions, and normalised to the magnitude of the CIE of each event, are ~8.4 wt.% per ~1 ‰ CIE for the P event and ~2.2 wt.% per ~1 ‰ at the R event. In contrast to the P event, carbonate content has recovered by the onset of the R event, and actually peaks during the event. This might either indicate a slow relative sea level rise at the palaeoposition of Site 16/28-sb01 — consistent with continued early Eocene regional subsidence — which takes the palaeolocation of Site 16/28-sb01 further from the delta front and associated freshwater influence and hence into more oceanic conditions favourable to pelagic carbonate producers. Or the same process may reduce sediment input and the dilution of carbonate. Either way, it is clear that in this case, the CIE perturbation during R actually enhances carbonate content, must likely be relative water depth increase and increased primary carbonate production. Similar patterns for the Si, Al and Fe can be seen for the S and T event.

Only Fe shows consistent, although small peaks within almost all CIEs (P, S, T, U, W), this could represent higher aeolian dust input, although this is unlikely based on dust sources in Eocene climate simulations (Herold et al., 2014). In the basal P event this is coupled with an increase in sulphur concentrations and would suggest the increased presence of pyrite in this layer related to either increased organic carbon content, reduced pore water oxygenation or reduced sea floor oxygenation at this time. The sulphur concentration is well aligned with aluminium concentration through U2 and can therewith be explained as well with higher terrestrial influx. In the T events, Fe is not coupled to S, but with an increase in both Mn and the dominance of calcium carbonate indicators. In this interval, an increase in Fe is most likely a result of

increased component of iron-manganese oxy-hydroxides precipitating on the increase component of calcium carbonate grains. Within the iron peaks of the S and W event both a slight increase in sulphur and manganese can be seen, which is interpreted as a mixture of above outlined processes coupled with an increased Ca concentration. Whereas the U event again is not coupled with S and has lower Ca concentrations but a peak in iron and manganese. Here it is suggested that all these intervals observed variations in iron concentrations are mostly driven by early diagenetic, redox-controlled remobilization and precipitation of iron-rich phases.

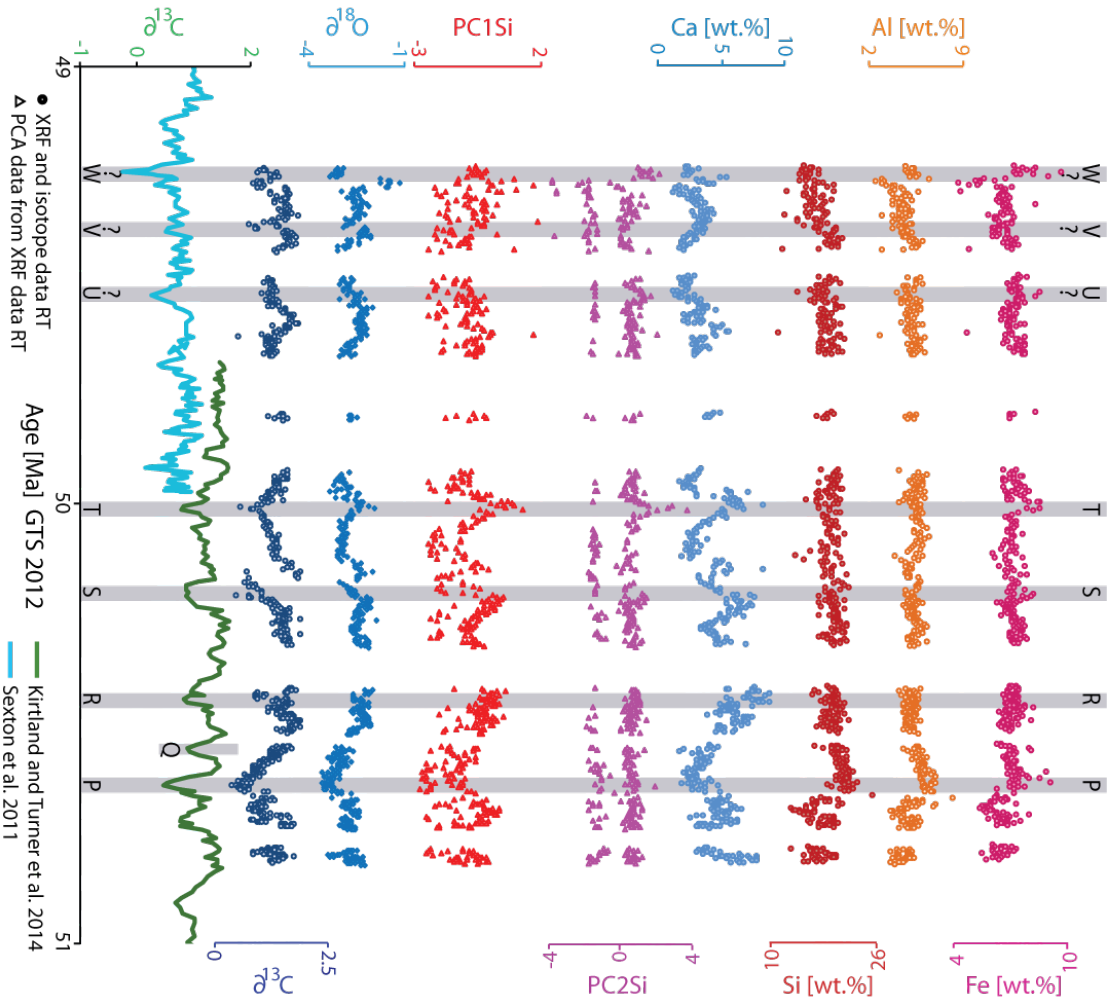

Figure 2.15. It is focused on the lower Eocene sediment Unit 2 (138.00 – 87.50 m), described as the "smectitic clay" unit (Haughton et al., 2002), the most complete section of the core. The target stable isotope curves to refine the age model of this study (Kirtland Turner et al., 2014, Sexton et al., 2011) is shown in the continues green and turquoise lines to the left [‰ VPDB]. These target curves are compared to the data of Site 16/28-sb01, first from right the bulk carbonate stable isotopes $\delta^{13}C$ and $\delta^{18}O$ [‰ VPDB]; the $PC1^{si}$; $PC2^{Si}$; Ca; Si; Al and Fe. The inferred "hyperthermals" are highlighted in grey.

In the S event $\delta^{18}O$ is still negative but in T the $\delta^{18}O$ shows a positive trend. The succession of R to T is interpreted as a transitional stage were the terrestrial influx

from a drowning continental margin decreases and this might be accompanied by changes in the water circulation at Site 16/28-sb01. With regional subsidence, in these warming events more saline oceanic waters from the Atlantic might penetrate northwards into the Rockall Basin, with strongest effects at the T event, changing the $\delta^{18}O$ to more positive values, weakening the $\delta^{18}O$ signal in the S and R event (Lunt et al., 2012).

Table 2.7. shows a summary of the identified CIEs in the 16/28-sb01 record, including the length of perturbations — based on the assumed linear sedimentation rates between tie points — and the magnitude of each CIE. In general CIEs last ~50 to ~200 ka years, which are comparable durations to other global CIE records (Introduction 1.2), e.g. Sexton et al. (2011), and typically consist of ~1 per mill negative shift in $\delta^{13}C$, in accordance with the definition of the CIEs (Cramer et al., 2003).

Table 2.7. This table shows the approximate duration of the transient CIEs of Site 16/28-sb01 based on this studies age model and their carbon excursions. The durations of the CIE perturbations are estimated by using the last point before the isotope curve starts to drop as onset and the point at which the carbon isotopes are recovered to pre-CIE values as end of the CIEs. The maximum excursions of the CIEs are estimated by using the onset value (before it starts to drop) till the most negative point of each CIE. The isotope excursions for $\delta^{18}O$ within the CIEs are estimated using the onset value (at onset time as defined in this table) minus the oxygen isotope value at the same depth as the lowest $\delta^{13}C$ used to define the CIE extent, same is applied for elemental data variation in the CIEs.

Transient CIE event of Site 16/28-sb01	onset of CIE [ka]	end of CIE [ka]	duration [ka]	isotopes onset $\delta^{13}C$ [per mil]	isotopes most negative $\delta^{13}C$ [per mil]	Maximum CIE excursion $\delta^{13}C$ [per mil]
P	50736.75	50563.67	~173	1.78	0.51	~1.4
R	50511.73	50427.03	~85	1.91	0.98	~1.0
S	50251.51	50170.92	~81	1.69	0.52	~1.2
T	50148.32	49942	~206	1.75	0.59	~1.2
U?	49570.39	49404.21	~166	1.82	1.18	~0.7
V?	49389.89	49339.07	~51	1.85	0.93	~0.9
W?	49286.68	49234.69	~52	1.65	0.88	~0.8

Transient CIE event of Site 16/28-sb01	Isotope excursion $\delta^{18}O$ for CIE [per mil]	Ca [wt.%] variation for CIE	Fe [wt.%] variation for CIE	Si [wt.%] variation for CIE	Al [wt.%] variation for CIE	S [wt.%] variation for CIE
P	~0.8	~-0.9	~-2.2	~0.4	~-0.6	~-2.54
R	~0.1	~-3.8	~-0.1	~-0.2	~0.1	~0.08
S	~0.2	~0.4	~-0.3	~-0.1	~0.4	~-0.09
T	~-0.5	~-2.2	~-4.5	~2.0	~-0.2	~-0.06
U?	~0.1	~0.9	~0.2	~4.5	~0.7	~-0.07
V?	~0.5	~-1.4	~-0.3	~0.9	~-0.4	~-0.01
W?	~-0.8	~-0.4	~0.6	~0.1	~1.5	~-0.1

2.7.3 Middle Eocene Unit 3:

The middle Eocene Unit 3 (87.50 – 40.00 m) is described as calcareous sandstone (Haughton et al., 2002). Biostratigraphic data place this succession in the middle Eocene (CNE 9 and CNE 10), with the top sample 40.82 m with an age of 44.87 Ma and the bottom sample 83.96 m with an age of 46.38 Ma. The close spacing of the FAD of *Sphenolithus furcatotithoides* and *Chiasmolithus gigas* within Unit 3, relative to their assigned ages (Agnini et al., 2014), is likely due to diachroneity in the FAD of *Sph. furcatotithoides*, with an earlier appearance in the sub-tropics, where this bioevent is calibrated, than in the higher latitudes (16/28-sb01). XRF elemental data show, on average, an increase in Ca (24.91 wt.%) and a drop in all terrestrial influx indicators Si (7.60 wt.%), Fe (3.70 wt.%), Al (3.43 wt.%), K (1.01 wt.%) in U3 relative to U2. Whilst bulk isotopes show a drop of 0.46 ‰ in mean $\delta^{13}C$ and a positive increase of 2.68 ‰ in mean $\delta^{18}O$ from U2 to U3; changes which are similar to the global benthic isotope record of Cramer et al. (2009). The persistent subsidence following the relaxation of the NAIP mantle plume in the Rockall and Porcupine areas through the early Eocene slowly drowns the Porcupine deltaic network at around ~49 Ma (Stephen Jones pers. comm.). The loss of fine-grained clastic sedimentation from terrestrial hinterlands and drowning of the deltaic system could explain the shift to more pelagic open-ocean type calcareous ooze sedimentation after 49 Ma at Site 16/28-sb01. The transition from U2 to U3 is also associated with increased water depth, as estimated by P %, from ~300 m to nearly ~1000 m (Van der Zwaan et al., 1990). Again, this deepening is consistent with a marked relative transgression and shoreline retreat, driven by regional subsidence. The age of the U2 to U3 unconformity, starting at ~49 Ma, correlates with well-known changes in other records and is correlated to major circulation change (see Introduction, Section 1.4 and Chapter 2, Section 2.7.2). On the seismic line crossing the 16/28-sb01 borehole, Haughton et al. (2005) interpret the U2 to U3 boundary to be partially faulted due to slumping that is typical for the steep sediment starved Rockall Basin margins. This slumping could also have been triggered by NCW onset and more erosive circulation compared to sluggish circulation in a rather small and restricted early Eocene basin.

2.8 Conclusion

The review of the Rockall Basin's regional tectonic, existing biostratigraphic and sedimentologic publications of Site 16/28-sb01 combined with the new data presented in this thesis chapter, namely the new biostratigraphy based on calcareous nannofossils, high-resolution XRF data and bulk carbonate $\delta^{13}C$ and $\delta^{18}O$ data, were used to establish a new age model for shallow marine Site 16/28-sb01 and a palaeoenvironmental reconstruction. This makes it possible to place Site 16/28-sb01 into a global stratigraphic framework and allows detailed comparisons with other successions, especially those that recover early Eocene CIEs (Galeotti et al., 2010, Kirtland Turner et al., 2014, Lauretano et al., 2015, Lauretano et al., 2016, Galeotti et al., 2017, Lauretano et al., 2018, Galeotti et al., 2019). The clear deepening of the depositional environment, through the early to middle Eocene, recorded in the sedimentary character and microfossil content of Site 16/28-sb01 fits well within the basin-wide subsidence records, driven by the waning of the NAIP activity. This evidence includes the period of erosion or non-deposition between the Upper Cretaceous and lower Eocene successions, which correlates with the time of maximum NAIP uplift (Maclennan and Jones, 2006). Following this, full breakup, the establishment of a passive margin to the west of Rockall and the end of NAIP activity, causes regional subsidence throughout the Eocene as represented in the transition from the inner shelf sediments of Unit 1, to the upper slope, ~300m water depth, environments of Unit 2 and the open ocean, bathyal deposition in ~1000 m water depth of Unit 3.

The key interval of Site 16/28-sb01, and the best recovered part of 16/28-sb01, is the lower Eocene U2, which includes CIEs P to W and the later part of the EECO. This succession is one of the rare marginal marine section in the Northern Hemisphere to contain such a detailed sediment, elemental and isotopic record of multiple EECO CIEs. These CIEs allowed within this thesis to refine the biostratigraphic age model and will allow in the following Chapter 3 and 4 to place the SST proxy estimates from $\delta^{18}O$ and GDGTs into a temporal framework and therefore into a global context. Their accompanying elemental distributions indicate perturbations in the sedimentation which are not repeated across all the CIEs, which indicate a system control rather than

a CIE control on the elemental distribution. Elemental abundances clearly respond across the late EECO CIEs, but their character changes through time due to the background evolution and subsidence of the system.

3 EARLY AND MIDDLE EOCENE PALAEO-CLIMATE AND -ECOLOGY FROM WELL-PRESERVED PLANKTIC FORAMINIFERA IN THE ROCKALL BASIN

3.1 Introduction

Past greenhouse climates, like the warm, high-CO_2 early Eocene, particularly the early Eocene Climate Optimum (EECO) ~53 – 49 Ma, are especially interesting and useful to study in order to understand warm (e.g. future) climate system behaviour (Pagani et al., 2005, Lunt et al., 2012, Zhang et al., 2013, IPCC, 2013, Anagnostou et al., 2016, Foster et al., 2017, Westerhold et al., 2018a, Lauretano et al., 2018, Hollis et al., 2019). However, as outlined in Section 1.1., EECO climate model predictions of sea surface temperatures (SSTs) are divergent from the few proxy-based SSTs estimates at mid to high latitudes (Huber and Caballero, 2011, Lunt et al., 2012, Evans et al., 2018b, Hollis et al., 2019). Specifically, the available SST proxy reconstructions imply a ~32±10 % reduction of the latitudinal temperature gradient in the early Eocene (Evans et al., 2018b) compared to the present day (Crowley and Zachos, 2000). This reduced latitudinal temperature gradient largely reflects substantial polar amplification in the proxy reconstructions, resulting in significantly higher high latitudinal temperatures reconstructions from proxies compared to model simulations (Huber and Caballero, 2011, Lunt et al., 2012, Evans et al., 2018b, Hollis et al., 2019). Of fundamental interest for the palaeo-climate research community is therefore, to obtain more high-quality, multi-proxy SST records, especially from the EECO, that fill the proxy data gaps outlined in Lunt et al. (2012) and Hollis et al. (2019) in order to fully evaluate existing discrepancy between model and proxy data, as well as between SST estimates from different proxies.

Over half a century ago, the ratio of stable oxygen isotopes ($\delta^{18}O$) in the calcium carbonate ($CaCO_3$) shells of marine organisms was recognized as preserving a record of past marine water temperatures, in organisms that precipitate their calcium carbonate shells more or less in equilibrium with contemporaneous sea water (Urey, 1947, McCrea, 1950, Urey et al., 1951, Epstein et al., 1951, Epstein et al., 1953, Emiliani, 1955). Oxygen isotope ratios from planktic foraminifera are thus one of the

most established tools we have to estimate SSTs (Epstein et al., 1953, Emiliani, 1955). $\delta^{18}O$ values are measured in conjunction with carbon isotopes ($\delta^{13}C$) which reflect the isotopic composition of dissolved inorganic carbon (DIC) in the sea water from which foraminiferal tests precipitate. Together, the $\delta^{18}O$ and $\delta^{13}C$ compositions of planktic foraminifera can be used to reconstruct water column structure and the intensity of the oceanic biological pump (Shackleton et al., 1973, Kroopnick, 1985, Spero and Williams, 1988, Sigman and Haug, 2003, John et al., 2013).

Planktic foraminifera are unicellular zooplanktic organisms, present since the Toarcian (Hart et al., 2003), which precipitate calcium carbonate (low magnesium calcite (e.g., Erez, 2003)) "tests" (shells) more or less in equilibrium with sea water (Epstein et al., 1953, Erez and Luz, 1983). The relatively high preservation potential of their tests and their ubiquitous occurrence in the marine fossil record make foraminiferal tests an excellent target for measuring $\delta^{18}O$ and $\delta^{13}C$ values (see Pearson, 2012, Schiebel et al., 2018, for reviews). Planktic foraminiferal $\delta^{18}O$ values are lowest in tests that have calcified in warmer and/or near-surface waters, becoming higher in $\delta^{18}O$ in foraminifera living in colder and/or deeper waters (Emiliani, 1954), (Figure 3.1.). Planktic foraminiferal $\delta^{13}C$ values are higher in surface waters — which are ^{12}C depleted due to photosynthetic fractionation — and relatively lower in deeper sub-surface waters because of the oxidation and decomposition of sinking ^{12}C-rich organic matter, together with little or no photosynthetic activity (Shackleton et al., 1973, Kroopnick, 1985, Spero and Williams, 1988, Sigman and Haug, 2003), (Figure 3.1.). The stable carbon isotope gradient in the water column reflects the biological pump intensity, which is dependent on the rates of photosynthetic fixation, organic carbon export and remineralization (Volk and Hoffert, 1985, Sigman and Haug, 2003, John et al., 2013). This carbon isotope gradient between surface and deep waters was likely steeper and larger in the early and middle Eocene tropical oceans compared to the present-day, perhaps indicating an enhanced biological pump and a much shallower remineralization depth of the organic matter due to warmer surface and sub-surface waters (John et al., 2013, John et al., 2014). Further the carbon isotope gradient is also controlled by ocean circulation, advection and mixing, the general deep-water circulation is assumed to be much weaker in the early Eocene than today, see Section

1.5, p. 18 - 24. However, in a recent paper by Gaskell and Hull (2019) it is argued that the large Eocene $\delta^{13}C_{DIC}$ gradients — inferred from surface to deep dwelling planktic foraminiferal $\delta^{13}C$ — were not as steep as previously suggested. They argue that the high $\delta^{13}C$ values in the surface dwelling extinct muricate planktic foraminiferal group (*Morozovella* and *Acarinina*), could also be explained by a very different arrangement of their algal photosymbionts.

Nowadays it is well known that $\delta^{18}O$ and $\delta^{13}C$ values recorded in foraminiferal tests can be biased from an accurate representation of calcification temperature or seawater $\delta^{13}C_{DIC}$ by a range of biological, physical and post-mortem factors — contributing to uncertainty in past SST reconstructions (e.g., Pearson, 2012, Edgar et al., 2015, Schiebel and Hemleben, 2017), (Figure 3.1.). These factors include: A) uncertainties in reconstructing the $\delta^{18}O$ of past seawater ($\delta^{18}O_{SW}$) and past ocean salinity, B) ocean pH, C) seasonality D) vital effects, E) water depth-related isotope variability and F) diagenesis and dissolution of foraminiferal tests. Below a brief summary of these caveats is provided:

A) Past $\delta^{18}O_{SW}$ and ocean salinity

An estimation of $\delta^{18}O_{SW}$ is needed to determine the SSTs from planktic foraminiferal $\delta^{18}O$ (Section 3.2, equation 1). Ocean $\delta^{18}O_{SW}$ is a function of global ice volume over long timescales and is modified by the hydrological cycle (local and global evaporation vs. precipitation) related to the site location and ocean circulation, and so difficult to reconstruct and subject to substantial uncertainty (Zachos et al., 1994, LeGrande and Schmidt, 2006, Rohling, 2013, Hollis et al., 2019). In an ice-free world such as the early and middle Eocene, palaeo-$\delta^{18}O_{SW}$ can be estimated based on the contribution from modern ice sheets to modern $\delta^{18}O_{SW}$ (see Section 3.2 for more detail) (Cramer et al., 2011). An alternative means of determining palaeo-$\delta^{18}O_{SW}$ is to use an independent temperature proxy, e.g., Mg/Ca or TEX_{86} in conjunction with measured foraminiferal $\delta^{18}O$ values (Elderfield and Ganssen, 2000, Wuchter et al., 2004, Pearson, 2012, Elling et al., 2015).

Epstein et al. (1951) found that $\delta^{18}O$ varies roughly linearly with salinity in surface waters. Lower salinity waters would therefore result in lower $\delta^{18}O_{SW}$ values — due to a depletion of the heavier oxygen isotope relative to standard mean ocean water —

and therefore reconstructed SSTs are too warm and vice versa for higher salinity surface waters. There are multiple means of correcting for salinity effects on $\delta^{18}O_{SW}$ in the past. If the palaeolatitude of the site is known then modern $\delta^{18}O_{SW}$-latitude relationships can be applied (Zachos et al., 1994, LeGrande and Schmidt, 2006) or modelled $\delta^{18}O_{SW}$ values can be used (Tindall et al., 2010, Roberts et al., 2011). However, model outputs are palaeo-climate model specific and not recommended for standard usage in correcting SSTs (Hollis et al., 2019). This approach would also bias independent model-proxy comparison.

B) Ocean pH:

Decreasing ocean pH corresponds to decreases in the concentration of the carbonate ion [CO_3^{2-}], and increases of both the bicarbonate ion [HCO_3^-] and carbon dioxide in seawater [CO_2 (aq.)] (Spero et al., 1997, Zeebe, 2001, Zeebe, 1999). This decrease in the [CO_3^{2-}] and pH is linked with higher $\delta^{18}O$ values (reflecting colder than actual SSTs) in planktic foraminifera (Spero et al., 1997, Zeebe, 2001) and lower $\delta^{13}C$ values (Spero et al., 1997, Bemis et al., 2000). Theoretically $\delta^{18}O$ changes with a slope of -1.42 ‰ per pH unit this is found by studying recent species *Orbulina universa* (Spero et al., 1997, Zeebe, 1999, Zeebe, 2001). In the Eocene, average sea surface pH was ~7.7 (Zeebe, 2012), slightly lower than today (~8.2) (Marion et al., 2011, Zeebe, 2012). This would artificially bias measured foraminiferal $\delta^{18}O$ values ~0.71 ‰ higher, and result in SST reconstructions ~0.8˚C too cold (Zeebe, 2001). The pH effect may be exacerbated if samples are from close to the oxygen minimum zone, or during transient carbon cycle perturbations. One way to improve the accuracy of SST reconstructions is to also measure pH, e.g. the boron stable isotope ratio ($\delta^{11}B$) in planktic foraminifera alongside $\delta^{18}O$ and $\delta^{13}C$ values.

C) Seasonality:

Seasonality, especially in mid to high latitudes with strong seasonality, can influence the reconstructed temperatures from planktic foraminifera tests, e.g., if one species predominantly lives and thus, calcifies during the summer, whereas another predominately lives during the winter (Tolderlund and Bé, 1971, Erez and Honjo, 1981, Fraile et al., 2009, Jonkers and Kučera, 2015, Kretschmer et al., 2018, Davies et al., 2019). Therefore recorded SSTs might be biased towards foraminifera 'growing'

season (Davies et al., 2019) or the season with highest primary production (Sluijs et al., 2006). It has been proposed that seasonality could influence the isotope values measured in mixed layer planktic foraminifera more than their living water depth (Pearson et al., 1993). Thus, if few individuals are averaged then there might be a stronger bias towards one of the seasons (Ganssen et al., 2011). However, a reduced Eocene latitudinal temperature gradient relative to today also implies a weaker latitudinal seasonal bias (e.g., Andreasson and Schmitz, 2000, Archibald et al., 2010, Huber and Caballero, 2011). To combat the seasonality effect, any single analysis should comprise a large number of specimens to ensure a good average of the species temperature range or lots of individual specimens (>25 or more) should be analysed to try to capture the seasonal temperature range of each species (Spero and Williams, 1989, Ganssen et al., 2011).

D) Vital effects:

"Vital effects" includes all the biological effects affecting the biomineralization process, that may act to shift the foraminiferal test isotopic ratio away from isotopic equilibrium with sea water — calcification and growth rate ("kinetic" effects), and respiration and photosynthesis ("metabolic" effects) (Urey et al., 1951, Weiner and Dove, 2003). First, foraminifera regulate and modify their own calcifying microenvironment by vacuolizing seawater and transporting it to the from the environment isolated site of calcium carbonate precipitation, formed by extruded cell material in the shape of the new last chamber in front of the former last chamber of the foraminiferal test (Erez, 2003, De Nooijer et al., 2014, for review). This type of biomineralization is referred to as "extracellular biologically controlled" (Lowenstam, 1981, Mann, 1983, Weiner and Dove, 2003, Erez, 2003). Biomineralization is prone to fractionation during the transport of ions along chemical gradients from the seawater to the transport vacuole and then to the precipitation site, for example, pH increases within transport vacuoles and thereby increasing [CO_3^{2-}] leading to lower $\delta^{18}O$ values (Zeebe et al., 1999, Erez, 2003, Bentov et al., 2009, De Nooijer et al., 2009). Kinetic effects are also more pronounced with rapid crystal precipitation from the internal carbon pool. Faster precipitation occurs with, e.g. higher pH or light levels and early in the foraminifera life stage, leading to lower calcite $\delta^{18}O$ and $\delta^{13}C$ values relative to ambient seawater and strong co-variation of the two ratios (McConnaughey, 1989,

Norris, 1998, Erez, 2003, for review). However to date, the exact biomineralization process of foraminifera is only partly understood (De Nooijer et al., 2014, for a review), therefore it is difficult to account for all the vital effects, e.g. (Spero and Williams, 1989, Spero et al., 1991).

Photosymbiotic algae (dinoflagellates or chrysophytes), hosted by more than a quarter of extant taxa, can also alter the foraminifera calcifying microenvironment through the preferential uptake of ^{12}C by these symbionts during photosynthesis (Hemleben et al., 1989). Hence, if dinoflagellate photosymbiont activity is enhanced (e.g., during high light conditions or in large individuals with more photosymbionts) this results in higher $\delta^{13}C$ test values relative to isotopic equilibrium (Erez, 1978, Kahn, 1979, Erez and Honjo, 1981, Spero and Williams, 1988, Spero et al., 1991, D'Hondt and Zachos, 1993, Spero and Lea, 1993, Spero and Lea, 1996, Bemis et al., 2000).

The effects of respiration are most pronounced in faster growing, smaller foraminifera (< 150 µm), which incorporate proportionally more respired CO_2 (enriched in ^{12}C and ^{16}O) into their tests than larger (generally "older") individuals, leading to increasing $\delta^{13}C$ and $\delta^{18}O$ with increasing test size (Berger et al., 1978, Kahn and Williams, 1981, Oppo and Fairbanks, 1989, Birch et al., 2012, Spero and Williams, 1988, Spero and Lea, 1993, Bornemann and Norris, 2007).

Due to the combined influence of kinetic and metabolic effects, it is recommended to measure foraminifera from larger size fractions (Kahn, 1979), >150 µm (Birch et al., 2012), above ~212 µm (John et al., 2013) or greater than 250 µm (Birch et al., 2013) where offsets from isotopic equilibrium are minimised. Above ~350 µm photosynthetic symbiont effects are more pronounced (Birch et al., 2013), so size fractions between 212 – 350 µm are ideal. Due to the ontogenetic changes a limited size fraction, with maximum range ~50 µm, is recommended, and should be morphospecies specific (Birch et al., 2012, Birch et al., 2013, John et al., 2013).

During gametogenesis some species of planktic foraminifera precipitate gametogenetic calcite, which differs in isotopic composition to the primary test. However, it is unclear how pronounced the influence on the isotopic ratios is and the percentage of gametogenetic calcite compared to ontogenetic calcite might be negligible (Bé, 1980, Norris, 1998, short review, Hamilton et al., 2008).

E) Water depth-related isotope variability:

Depth habitats of planktic foraminifera have been recognized for over half a century by the differences in the $\delta^{18}O$ and $\delta^{13}C$ values between species (Emiliani, 1954). As their long discussed participation in diurnal vertical migration was just recently rejected, relatively stable vertical depth habitats have been confirmed in extant planktic foraminifera (Meilland et al., 2019). Extant planktic foraminiferal species living in the upper water column, are known as mixed layer inhabitants, below this are the thermocline species and below that the so-called deep-dwelling, sub-thermocline species (e.g., Rebotim et al., 2017, Meilland et al., 2019). The $\delta^{18}O$ and $\delta^{13}C$ dependency on depth habitat in planktic foraminifera makes it feasible to use fossil multi-species analysis to reconstruct their relative depth habitats and past vertical water column structures (Savin and Douglas, 1973, Berger et al., 1978, Erez and Honjo, 1981, Pearson et al., 1993, John et al., 2013).

F) Diagenesis:

Diagenesis of planktic foraminifera tests affects their $\delta^{18}O$ and $\delta^{13}C$ values through recrystallisation of the test, development of infill and overgrowth (Pearson et al., 2001, Wilson et al., 2002, Sexton et al., 2006c, Pearson et al., 2007, Edgar et al., 2015). This is because secondary diagenetic calcite is precipitated in equilibrium with bottom waters at the sediment-water interface or from pore fluids within the sediment column, shifting the $\delta^{18}O$ of planktic foraminifera tests towards higher values (Schrag et al., 1995, Pearson et al., 2001, Sexton et al., 2006c, Pearson and Burgess, 2008, Edgar et al., 2015). In the past, SSTs inferred for the Eocene and the Cretaceous from recrystallized planktic foraminiferal $\delta^{18}O$ led to SST reconstructions that were too low in the low latitudes relative to modern and model outputs — the “cool tropics paradox” (Shackleton and Boersma, 1981, Bralower et al., 1995, D'Hondt and Arthur, 1996, Pearson et al., 2001). More accurate SST reconstructions are achieved by targeting “glassy” (i.e., not recrystallized) foraminifera (Pearson et al., 2001, Sexton et al., 2006c).

To identify if foraminiferal specimens have been diagenetically altered, light and scanning electron microscopy (SEM) are used (Sexton et al., 2006c, Pearson and Burgess, 2008). Foraminiferal tests, which are recrystallised and/or overgrown appear opaque under the binocular light microscope and are described as “frosty” (Sexton et

al., 2006c). Test opacity is caused by microscale diagenetic changes to the original radial calcite orientation, which is initially perpendicular to the test outline, and an increase in crystal size (e.g., Erez, 2003), this can be observed under SEM (Pearson et al., 2001, Sexton et al., 2006c, Pearson and Burgess, 2008). For detailed SEMs comparing frosty vs. glassy preservation see Sexton et al. (2006c) and Pearson and Burgess (2008). Sites hosting planktic foraminifera with a "glassy" style preservation are rare in the Eocene and often associated with clay-rich hemipelagic sediments (Pearson et al., 2001). For the EECO (53 – 49 Ma), "glassy" planktic foraminifera stable isotope data are only available for four sites globally (Hollis et al., 2019). Two sections are on land: Tumey Gulch (pre-EECO?, ~53.79 Ma) and Lodo Gulch, USA (EECO, 49.11 – 53.76 Ma) both from a palaeo-shelf setting and probably not completely glassy in the EECO (John et al., 2008) and two marine sections: Tanzania Drilling Project (TDP) Site 3 (pre-EECO?, ~53.2 Ma, 500 m water depth) (Pearson et al., 2007, Anagnostou et al., 2016) and Hampden Beach, New Zealand (EECO, ~48.5 Ma, shelf setting) (Hollis et al., 2012).

Early and middle Eocene planktic foraminiferal ecology is relatively well known and encompasses similar ecological niches to modern planktic foraminiferal species (Pearson et al., 2006, and references therein). Eocene stable isotope studies typically focus on three genera: mixed layer dwellers *Acarinina* and *Morozovella* and intermediate dweller *Subbotina* (Pearson et al., 2006, and references therein), (Chapter 1, Section 1.3). At the J event (defining the onset of the EECO at 53 Ma), the dominance of mixed layer species in assemblages permanently shifts from the genus *Morozovella* towards *Acarinina* (Luciani et al., 2016, Luciani et al., 2017b). Furthermore, superimposed on background assemblage changes during the Eocene, it is found that planktic foraminiferal ecology is not static in space or time, for example *Hantkenina* shift from a deep to mixed layer depth habitat through their evolution (Coxall et al., 2000). Whereas *Morozovella* and *Acarinina* lost their algal photosymbionts temporarily at the EECO onset (only shortly after the J event) (Luciani et al., 2017b) and *Morozovelloides crassatus* lost its symbionts before its extinction in the middle Eocene (Wade et al., 2008).

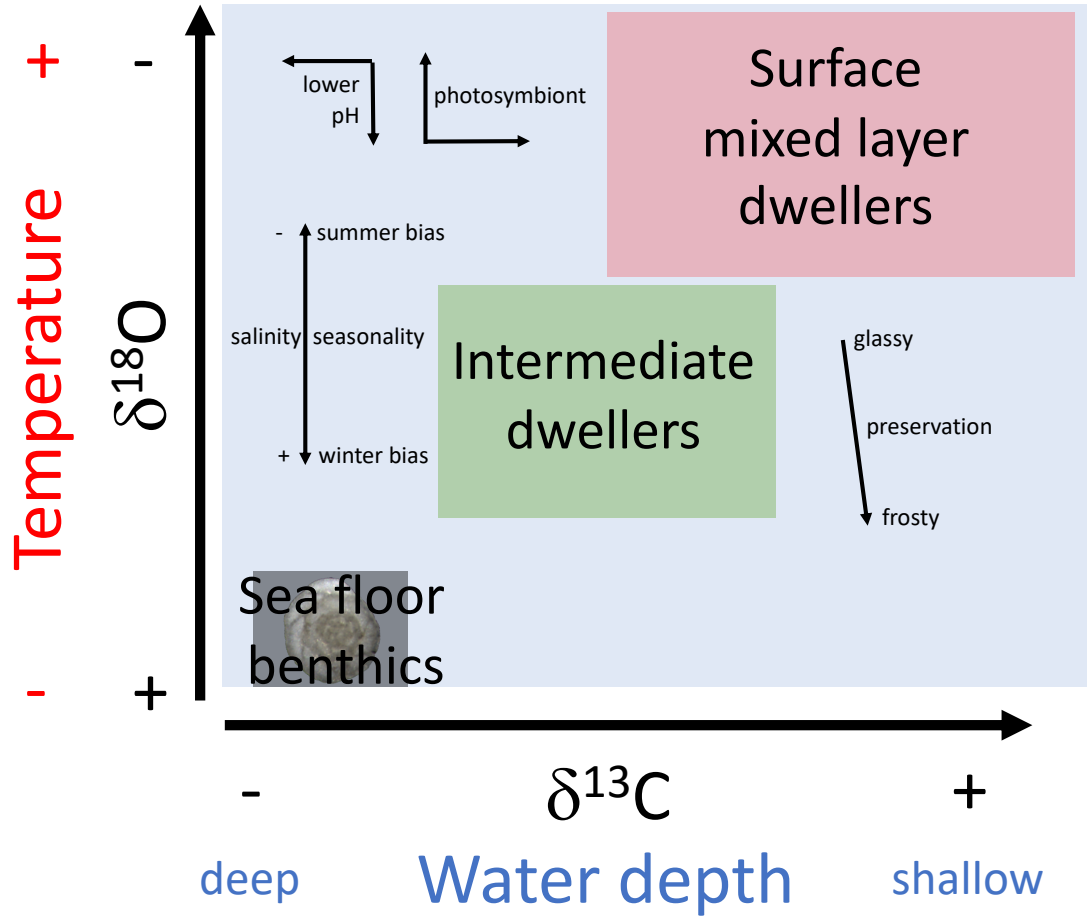

Figure 3.1. Vertical depth habitats of planktic foraminifera can be reconstructed by measuring their $\delta^{18}O$ and $\delta^{13}C$ values. Potential biasing factors that can influence foraminiferal isotope values like pH, salinity, seasonality, photosymbiosis and diagenesis are also shown along with an indication of the direction that they shift isotopic values in.

Sediments cored at Rockall Basin Site 16/28-sb01 in the Northeast Atlantic Ocean, which form the basis for this thesis, fall within the mid-latitude SST proxy data gap identified by Lunt et al. (2012) and Hollis et al. (2019) (Figure 1.1.). Because the preservation of planktic foraminifera and organic components is exceptional at Site 16/28-sb01, these sediments open up the unique possibility of generating multiple independent SST proxies (e.g., Markwick, 2007), combating the inherent uncertainties involved in each (see Hollis et al., 2019 for further discussion). Therefore, the overall goal of this Chapter is to reconstruct SSTs from planktic foraminiferal oxygen isotopes and then in Chapter 4, analyse Glycerol dialkyl glycerol tetraethers (GDGTs) to reconstruct SSTs for comparison with the new $\delta^{18}O$-based SST estimates. Thus, here high-quality, size-specific multi-species planktic foraminifera $\delta^{18}O$ and $\delta^{13}C$ measurements from the Rockall Basin Site 16/28-sb01 (palaeolatitude 49˚N) between

~44 and 53 Ma (see Chapter 2, Section 2.6) is presented. First, size-specific, multi-species planktic foraminiferal isotope depth transects for two discrete timeslices in the early and middle Eocene (~46.6 and ~50.5 Ma, respectively) are utilised in order to; (1) evaluate the relative depth habitat of each species through time, (2) evaluate the presence or absence of dinoflagellate photosymbionts in each species, and (3) compare these interpretations to published species depth habitats, to develop a robust ecological concept and constrain "vital effects". Second, these multi-species timeslices are used to identify the planktic foraminiferal species and size fraction most suitable for generating a long term early to middle Eocene SST record at Site 16/28-sb01.

3.2 Material and Methods

Before the start of this PhD project, 99 pilot samples were taken from the Petroleum Infrastructure Program Ireland (PIP) core store in Dublin, by Dr James Bendle, University of Birmingham. These pilot samples were supplemented by 238 higher-resolution samples (~20 cc each) collected during this PhD project by Dr Tom Dunkley Jones, Dr Kirsty Edgar, Dr Marcelo De Lira Mota and myself. Samples from the second sample batch were taken adjacent to the pilot samples. The pilot samples were halved; one half was used for foraminifera sample processing and the other half was used to extract and measure GDGTs (see Chapter 4). The halves of the pilot samples used for foraminiferal analysis were weighed, freeze-dried and weighed prior to wash down, (Appendix 005). The additional higher-resolution samples were weighed to obtain the "wet" bulk weight and then dried in the oven below 40˚C (for approximately one week, until no further weight loss was recorded) and then weighed again (to obtain the dry bulk sediment weight) prior to being washed down, (Appendix 005). All samples were then soaked in deionized water for 20 – 120 mins and occasionally agitated to bring the sediment particles into dispersion, prior to being washed down over a 63 µm sieve. Pilot samples were washed down with tap-water with a final rinse of deionized water, additional samples were washed down using deionized water whilst collecting the fine fraction (<63 µm), then washed down with tap water as well and again a final rinse of deionized water was applied before adding

to the drying oven. Washing with deionized water in the second sample batch was key to reduce possible contamination of the fine fraction (<63 µm) used for extracting GDGTs in this thesis and for future organic chemistry work. In addition, to the first wash down over a 63 µm mesh sized sieve, a second wash down with a prior Calgon step was necessary to remove the clay component of the samples. The sodium ions in the Calgon, attach to the clinging clay particles, resulting in a negative charge of the clay and therefore the particles repel each other and disperse and break down in an aqueous wash down. The use of Calgon was essential for the early Eocene samples. The samples were heated in glass beakers with 100 – 200 ml of an oversaturated Calgon solution (15 g of Calgon per 1 l of water) and kept at the boiling point for 1 to 2 minutes before being washed down over the 63 µm sieve for a second time. Sometimes the Calgon treatment was repeated, due to the very high clay content of the early Eocene samples, before adding the sample to the drying oven. The dry coarse fraction (>63 µm) sediment weight was then recorded, see Appendix 005. Within the second batch of samples the first three litres of the sediment fine fraction (< 63 µm), was retained in large glass beakers and left to settle out (maximum seven days). Glass beakers were thoroughly cleaned before use, using a DECON/LIPSOL detergent and by soaking for 24 h within a DECON/LIPSOL solution (14 l tap water with 5 % DECON/LIPSOL detergent) and then rinsed with water before used to minimise any contamination of the fine fraction. After settling out of the fine fraction, the supernatant water was siphoned off and the fine fraction was dried in the drying oven below 40˚C. This generally took one to two weeks. Once dry, the fine fraction was wrapped in furnaced aluminium foil (foil was furnaced for 8h at 450˚C) to reduce any organic contamination and stored in a Ziploc bag. The fine fraction (< 63 µm) of the pilot samples was not retained.

To reconstruct the character of the palaeowater column and SSTs through the early and middle Eocene from the stable isotopes values of planktic foraminifera, ideally a species that is present throughout the entire record is needed. Hence, all pilot samples from the early Eocene and two samples from the middle Eocene were counted at the genus level, following the morphospecies concept of Pearson et al. (2006). Benthic foraminifera were picked and counted but not identified and it was recorded if cenospheroid radiolaria were present or absent, see Appendix 006. The % P from the

pilot data counts were used to calculate the palaeowater depth after Van der Zwaan et al. (1990), (Appendix 006), uncertainties with the usage of % P at Site 16/28-sb01 palaeolocation and with variable sedimentation rates is discussed in Chapter 2, section 2.7.1, p.61.

Planktic foraminiferal genus level counts were used to select diverse assemblages to produce two water depth transects, one for the early and one for the middle Eocene. These transects are used to identify and constrain the relative depth habitat and ecology of species and their relative stability through time. Ultimately three samples with rich assemblages were selected to produce the two depth transects. The early Eocene timeslice comprising individuals from two samples, due to the low absolute abundance of planktic foraminifera in the early Eocene: 119.38 – 119.40 m and 119.80 – 119.82 m and one sample was used from the middle Eocene timeslice: 83.90 – 83.92 m. In the early Eocene, planktic foraminiferal assemblages were less diverse and individuals were smaller than in the middle Eocene. All species with sufficient mass for stable isotope analysis (6 – 148 µg) within a series of narrow sieve size windows (~50 µm) were analysed. Size fractions used were: >355 µm; 300 – 355 µm; 250 – 300 µm; 212 – 250 µm; 180 – 212 µm; 150 – 180 µm; 125 – 150 µm. As outlined in Section 3.1, planktic foraminifera < 125 µm are: A) assumed to incorporate more metabolic CO_2 and have therefore a stronger vital effect, and B) very difficult to differentiate using binocular microscopy, and are thereby excluded from analysis here.

Prior to analysing the foraminiferal specimens for stable isotopes, all of them were imaged using a Leica microscope and *Image Pro Premier* software, the images are given in electronic Appendix 004. Measured foraminiferal specimens were cleaned prior to isotope analysis, initially with deionized water and a paint brush and subsequently by ultrasonicating them for 1 – 3 seconds in deionized water. Because of breakage and therefore specimen loss, not all specimens in the depth transects were cleaned using ultrasonication. All data, cleaning procedures and a qualitative assessment of preservation state of each foraminiferal isotope sample are given in Appendix 007. For all specimens, a qualitative assessment of preservation state has been carried out and can be found in Appendix 007.

In total 63 isotope samples, weighing between 19 – 148 µg, were run for stable isotopes in the middle Eocene sample, of which one sample failed (Appendix 007).

This comprised 20 planktic and one benthic foraminifera across multiple size fractions; ten in >355 μm, ten in 300 – 355 μm, 12 in 250 – 300 μm, 11 in 212 – 250 μm, ten in 180 – 212 μm, nine in 150 – 180 μm and one in 125 – 150 μm (Appendix 007). Isotope values have an average standard deviation 1σ of 0.02 for δ^{13}C ‰ VPDB (Vienna Pee Dee Belemnite) and 0.04 for δ^{18}O ‰ VPDB.

In the early Eocene depth transect, a total of 18 isotope samples, including six planktic and one benthic foraminiferal species, were run for stable isotopes (each weighing 6 – 44 μg), of which one failed (Appendix 007). Stable isotope values have an average standard deviation 1σ of 0.03 for δ^{13}C ‰ VPDB and 0.03 for δ^{18}O ‰ VPDB.

To generate a surface-thermocline record covering the whole Eocene at 16/28-sb01, *Acarinina bullbrooki* and *Subbotina eocaena* were picked from the 250 – 300 μm sieve size fraction. A total of 82 samples were run, of which six failed, resulting in 26 measurements from *A. bullbrooki* and 53 for *S. eocaena*. Weights from 5 – 305 μg were run; all results are given in Appendix 007.

Stable isotope (δ^{18}O and δ^{13}C) measurements of all the foraminiferal samples were conducted at the BGS (British Geological Survey) in Keyworth, U.K. by Hilary Sloane in the stable isotope facility, part of the National Environment Research Council (NERC) Isotope Geoscience Facilities (NIGL), under the lead of Prof Melanie Leng. All foraminiferal samples weighing between 10 – 300 μg, exact weights per foraminiferal sample are given in Appendix 007, were analysed using an IsoPrime dual inlet mass spectrometer plus Multiprep device. Each sample is loaded into a glass vial and sealed with a septum. The automated system evacuates the vials and injects anhydrous phosphoric acid to the carbonate at 90˚C. The acid reacts with carbonate and creates CO_2, which is collected for 15 minutes, cryogenically cleaned and transferred to the mass spectrometer. Isotope values (δ^{13}C and δ^{18}O) are reported as per mill (‰) deviations of the isotopic ratios (^{13}C/^{12}C, ^{18}O/^{16}O) calculated to the VPDB standard using a within-run laboratory standard (KCM) calibrated against NBS-19. The calcite-acid fractionation factor applied to the gas values is 1.00798. Due to the long run time of 21 hours a drift correction is applied across the run, calculated by using the standards interspersed amongst the samples. The Craig correction is applied to account for δ^{17}O (Craig, 1957). The average analytical reproducibility of the standard

calcite (KCM) is 0.05 ‰ for $\delta^{13}C$ and $\delta^{18}O$ for samples above 20 µg and 0.1 ‰ for those below 20 µg.

As palaeotemperatures in extinct planktic foraminifera species are reconstructed, following the recommendation of Pearson (2012) the Kim and O'Neil (1997) reformulated by Bemis et al. (1998) formula, calibrated on synthetic inorganic calcite, is used (see Equation 1). This equation is suitable for the warm Eocene as it is calibrated on synthetic calcite precipitated from water temperatures between 10 - 40˚C, as other calibrations are only tested for temperatures below 30˚C (e.g., Pearson, 2012). Equation 1 is calibrated on synthetic calcite and it is therefore best suited for asymbiotic and benthic species. For symbiotic species the SSTs using the Kim and O'Neil (1997) reformulated by Bemis et al. (1998) formula might result in temperature slightly biased to warmer values (e.g., Hollis et al., 2019) of around ~1.5˚C (Spero and Williams, 1988, Pearson, 2012). Through Bayesian calibration modelling and the use of modern mixed layer dwelling foraminiferal species from a global core top sample dataset the maximum uncertainty of SST calculations from foraminiferal calcite has been estimated to be $\pm$2.8˚C (Malevich et al., 2019), however in an ice-free world uncertainty is given with the estimation of local variation in $\delta^{18}O_{SW}$. The $\delta^{18}O_{SW}$ value for an ice free ocean from Cramer et al. (2011) is applied in this study as -0.89 ‰ ± 0.02 ‰ VSMOW (Vienna Standard Mean Ocean Water). They calculated this value by using the modern $\delta^{18}O_{SW}$ for all sea water masses and assuming a melting of all the ice masses in Antarctic and Greenland using the average ice $\delta^{18}O$ values from L'Homme et al. (2005). VSMOW is converted into VPDB by subtracting 0.27 ‰ (Pearson, 2012), resulting in $\delta^{18}O_{SW}$ = -1.16 ‰ VPDB. All values in this chapter are given in ‰ VPDB, if not stated otherwise. A latitudinal correction of 0.12 ‰ is subtracted from all $\delta^{18}O$ measurements (Zachos et al., 1994) for a paleolatitude for the 16/28-sb01 core of 49˚N. Calculations of this bulk Eocene $\delta^{18}O_{SW}$ by Cramer et al. (2011) are found to be reasonable for the tropics and are found to be no more than 2-3 ‰ more negative for the NE European continental margin (precisely for the Hampshire, Belgium and Paris Basin) possibly influenced by local freshening, by measuring coupled Mg/Ca and clumped isotopes Δ_{47} on large benthic foraminifera (Evans et al., 2018b). Due to the fact that at the Site 16/28-sb01 of this study no paired

Mg/Ca and clumped isotopes are available a more accurate estimation of $\delta^{18}O_{SW}$ cannot be given at this point. By assuming a reasonable salinity variability of +2, +1, -1, -2 ‰ around bulk Eocene $\delta^{18}O_{SW}$ resulting temperatures would be biased by around +9, +4, -6, -11 ˚C, respectively using Equation 1.

$$T(^{\circ}C) = 16.1 - 4.64\ (\delta^{18}O_{cc} - \delta^{18}O_{SW}) + 0.09\ (\delta^{18}O_{cc} - \delta^{18}O_{SW})^2 \quad \text{(Equation 1)}$$

$\delta^{18}O_{CC}$ is the $\delta^{18}O$ of the measured calcium carbonate of the planktic foraminifera in ‰ VPDB

$\delta^{18}O_{SW}$ is the $\delta^{18}O$ value of the seawater (converted from VSMOW into VPDB by subtracting 0.27 ‰).

16.1; -4.64 and +0.09 are experimental variables, with 16.1 being the temperature when $\delta^{18}O_{CC}=\delta^{18}O_{SW}$; -4.64 is the slope of the equation and +0.09 is the correction of the slope away from being completely linear.

For the calculation of the bottom water temperature two benthic foraminiferal isotope measurements from *N. truempyi* have been translated into temperature using Equation 1. However, no latitudinal correction factor for salinity is applied. To align *N. truempyi* to *Cibicidoides* spp. which is thought to precipitate its tests closest to equilibrium with sea water, Equation 2 was used (Katz et al., 2003). The isotope values plotted in all following figures of this chapter are the original measured values of *N. truempyi* and not the corrected values.

$$\delta^{18}O_{Cibicidoides} = ((\delta^{18}O_{N.truempyi} + 0.10)/0.89) \quad \text{(Equation 2)}$$

3.3 Results

3.3.1 Coarse fraction (>63 µm) and foraminiferal content compared to the lithological changes of Site 16/28-sb01

The dry coarse fraction (>63 µm) in weight percent [wt.%], foraminifera concentrations and Ca content from XRF data are shown (Figure 3.2.) corresponds to the different lithological units (Unit 1, 2 and 3) as defined in Chapter 2 (raw data in Appendix 005; average values see Table 3.1.). The early Eocene (Units 1 and 2; 145.95 – 87.50 m) contain low numbers of planktic foraminifera, low coarse fraction

percentages and low bulk sediment Ca percentages relative to the middle Eocene (Unit 3, 87.50 – 40.00 m).

The coarse fraction (>63 µm) record shows little relationship to the CIEs, with three exceptions: there are peaks in the amount of coarse fraction coincident with the T event, slightly "elevated" values in the V? event and shortly before the W? event, that also coincide with Ca peaks in the XRF data (Figure 3.3 and 2.15.) and higher bulk $\delta^{18}O$ values. However, the T event differs from the other CIEs in U2 due to a pronounced shift to higher $\delta^{18}O$ values in contrast to a shift to lower $\delta^{18}O$ values in the other CIEs. The planktic foraminiferal assemblage changes from very low (around 13 foraminiferal species) to medium (around 25 foraminiferal species) diversity between the early and middle Eocene. The absolute abundance of planktic and benthic foraminifera in U2 generally correlates with coarse fraction, the Ca from the XRF results (Figure 3.3. and 2.15.)

Table 3.1 Overview over the general findings in Chapter 3 related to the lithological units.

Lithological units	Core depth [m]	Sediment > 63µm [wt.%]	Planktic foraminifera [per g sediment]	Benthic foraminifera [per g sediment]	P %	Palaeowater depth [m]	Average SSTs from *A. bullbrooki* [℃]	Average Ts from *S. eocaena* [℃]	Bottom water Ts from *N. truempyi* [℃]
U3	87.50 – 40.00	36	64	5	93	981	16.98	15.19	11.28
U2	138.00 – 87.50	1	4	1	54	334	26.67	18.76	14.02
U1	145.95 – 138.00	12	7	2	38	253	26.04	19.12	

and the abundance of the dominant planktic foraminifera genus *Subbotina.* The exception to this is the T CIE where there is no significant increase in foraminifera with elevated coarse fraction and elevated Ca. Foraminiferal abundance correlates with bulk $\delta^{18}O$, with lower bulk $\delta^{18}O$ values corresponding to lower foraminiferal abundance and vice versa, except in the T event, where no increase in foraminifera is

seen. *Subbotina* dominate the assemblage in U2, followed by *Acarinina* and rare *Pseudohastigerina, Morozovella* and *Globoturborotalita*. *Subbotina* are found in all investigated samples in U2, but there are three intervals in which *Acarinina, Morozovella*, and *Pseudohastigerina* are absent (indicated by blue arrows in Figure 3.3.): across the P event, between the S and T CIE and at the start of the U to just before the V CIE (including a core gap), and coincide with decreased Ca in the sediment (Figure 2.15.). The gap shortly after the R CIE and the gap in the approximate middle of the age interval in-between T and U CIEs, coincides with a core gap. In general, there is no consistent trend in foraminiferal abundance across CIEs, with the exception of *Acarinina*, which increases in abundance before P, R, before and after the S and before the U CIEs and are present throughout the T CIE, these *Acarinina* and *Subbotina* peaks correspond to abundance maxima in benthic and planktic foraminifera.

3.3.2 Palaeowater depth reconstruction for Site 16/28-sb01

The percentage of planktic foraminifera (P %) in 16/28-sb01, calculated after Van der Zwaan et al. (1990), (Appendix 006), increases up-core — U1: 38 %, for U2: 54 % and for U3: 93 %. Resulting palaeowater depth estimates suggest a progressive increase in water depth through the succession from ~253 m in U1, ~334 m in U2 to ~981 m in U3 (Figure 3.2.). Note that the very low abundance of planktic foraminifera per gram sediment (e.g., Imbrie and Kipp, 1971), might impact the robustness of palaeowater depth calculations in U2 in particular. Possible uncertainties of this palaeowater depth estimates are discussed in Chapter 2, Section 2.7.1, p. 61: uncertainties arise due to the outer position of Site 16/28-sb01 in the Rockall Trough, which might have had influence on productivity and sedimentation rates. Low accumulation rates and high sedimentation rates can alter the palaeowater depth estimates as well as changes in salinity. Therefore, palaeowater depth reconstructions should only be seen as a guidance for shallowing versus deeping at Site 16/28-sb01.

3.3.3 Preservation of foraminiferal tests

The preservation of all specimens for stable isotope analyses was recorded and analysed (Appendices 004 and 007) to differentiate between glassy, glassy with minor

diagenetic overprint (glassy to frosty) and frosty preservation (Pearson et al., 2001, Sexton et al., 2006c). In general, foraminifera tests are very well preserved throughout the study interval. This is particularly true in U2 where there are abundant glassy foraminifera (Figure 3.4. and Figure 3.5.). The internal test wall was examined in these well-preserved specimens with SEM — the original bilamellar wall structure can be seen in Figure 3.4. and 3.5., including the position of the organic membrane, which crosses the pores. There is visual evidence for slight secondary overgrowth on the inside of the *Subbotina* sp. in Figure 3.4., indicated by slightly rounded, coarser calcite crystals. No secondary crystals can be seen in the SEM of *A. boudreauxi* Figure 3.5. In general, only the best-preserved specimens were used for isotope analysis, but due to the low foraminifera abundance, slightly less well-preserved specimen — defined as glassy to frosty — were used where necessary (see Appendix 007 for details).

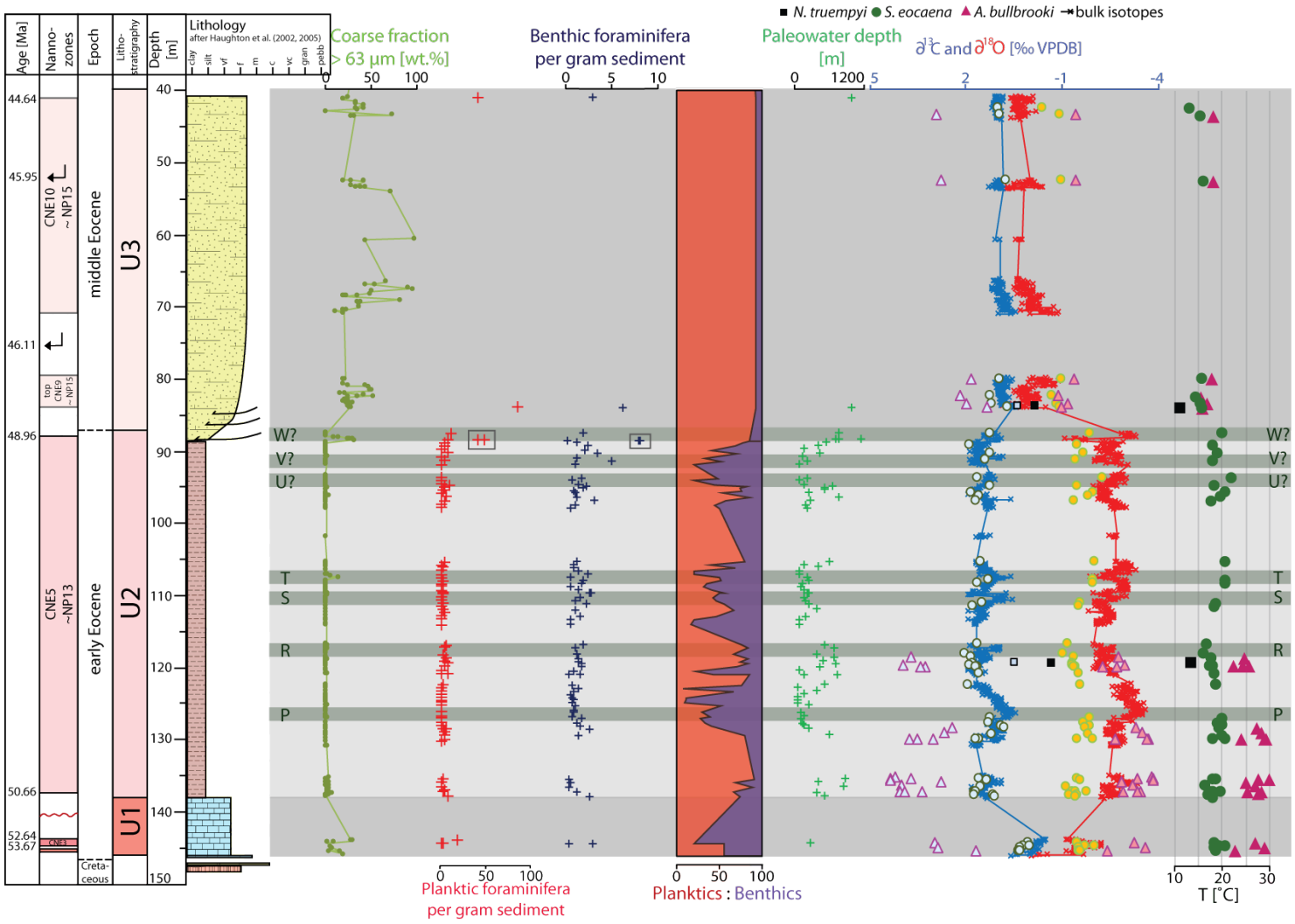

Figure 3.2. Foraminiferal abundances compared with lithology and the new carbon and oxygen isotope record. The different lithological Units 1, 2 and 3, as defined in the previous Chapter are shown against core depth [m] and from left to right against: the coarse fraction >63µm [wt.%] of the foraminiferal sample [light green]; planktic foraminifera per gram sediment (red crosses); benthic foraminifera (blue crosses). Black rectangles mark high abundances of planktic and benthic foraminifera in the early Eocene, excluded in Figure 3.3. Then planktic : benthic foraminifera percentage follow; palaeowater depth after Van der Zwaan et al. (1990) (green crosses), the $\delta^{18}O$ of bulk sediment (red line); *S. eocaena* (green circle, orange fill); *A. bullbrooki* (pink triangle, pink fill) and *N. truempyi* (no correction factor applied – solid black squares); the $\delta^{13}C$ of bulk sediment (blue line); *S. eocaena* (green circles, blue fill) and *A. bullbrooki* (pink triangle, blue fill) and *N. truempyi* (black squares with blue fill); and finally the reconstructed SSTs from planktic foraminifera $\delta^{18}O$ values (*S. eocaena*, green circles; *A. bullbrooki*, pink triangles). In U2 the interpreted CIEs P-W are shown

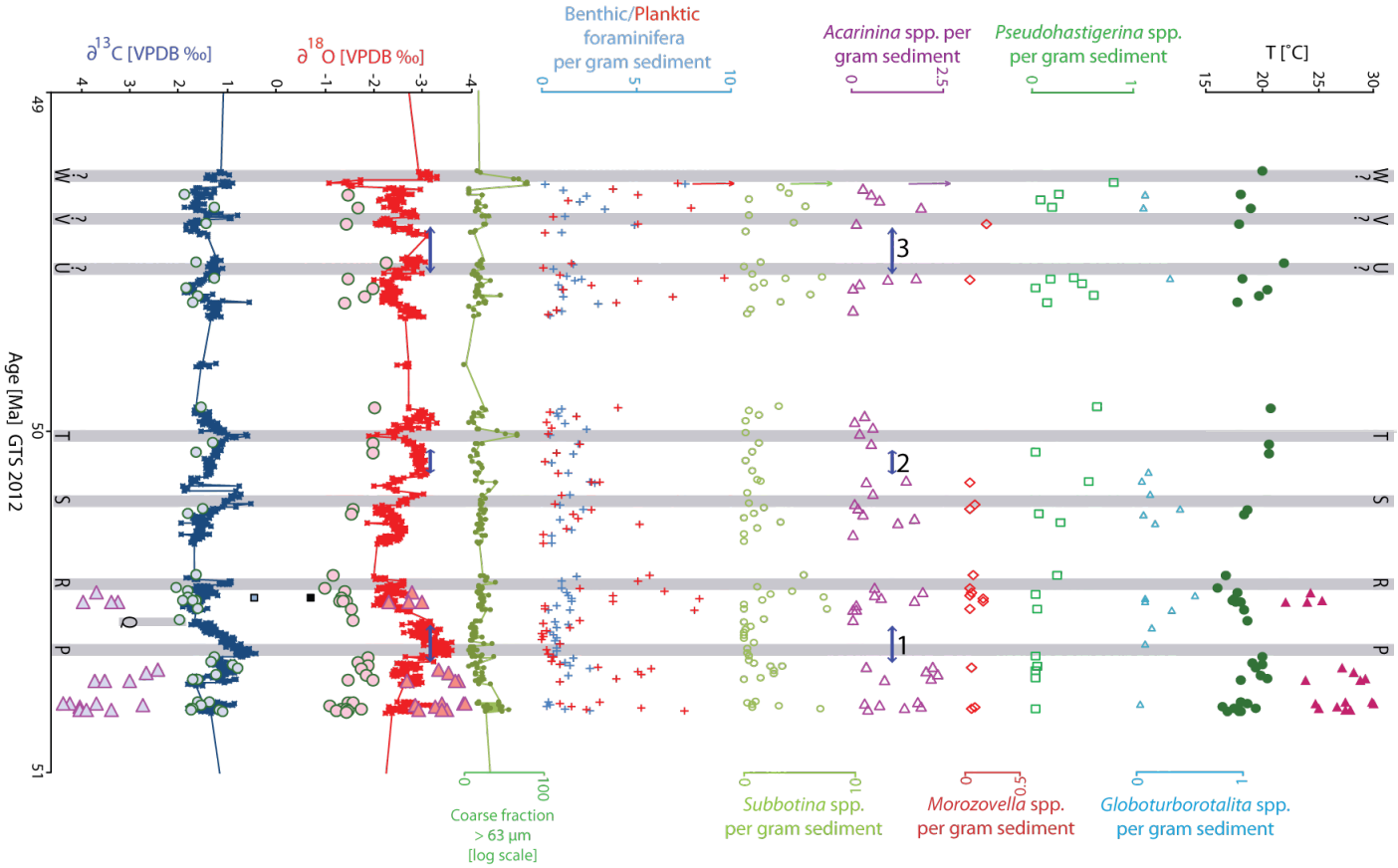

Figure 3.3. Close-up of Unit 2 plotted against age. Grey horizontal bars indicate the interpreted CIEs. From left to right: $\delta^{13}C$: (*A. bullbrooki*, (pink triangles with blue centre); *S. eocaena* (green circles with blue centre), bulk isotopes (blue line) and *N. truempyi* (black square with blue fill)); $\delta^{18}O$ (*A. bullbrooki* (pink triangle with red centre), *S. eocaena* (green circles with red centre), bulk isotopes (red line) and *N. truempyi* (black squares)); coarse fraction > 63µm (green line); benthic (blue crosses) and planktic foraminifera (red crosses) per gram sediment – the red, green and purple arrows indicated data points with planktic abundances of 42 and 49 per gram sediment before the W CIE; points excluded from the plot to showcase small scale variability within U2 (in *Acarinina* spp. 20, in *Subbotina* spp. 21, in *Morozovella* 4 specimen/gram are recorded at this point), not shown here. Concentrations of *Subbotina* spp.; *Acarinina* spp.; *Morozovella* spp.; *Pseudohastigerina* spp. and *Globoturborotalita* spp. per gram sediment. Far right, reconstructed ocean temperatures (T) from *S. eocaena* (filled green dots) and *A. bullbrooki* (filled pink triangle). Intervals where *Acarinina* are absent highlight by double-headed blue arrows labelled 1 -3.

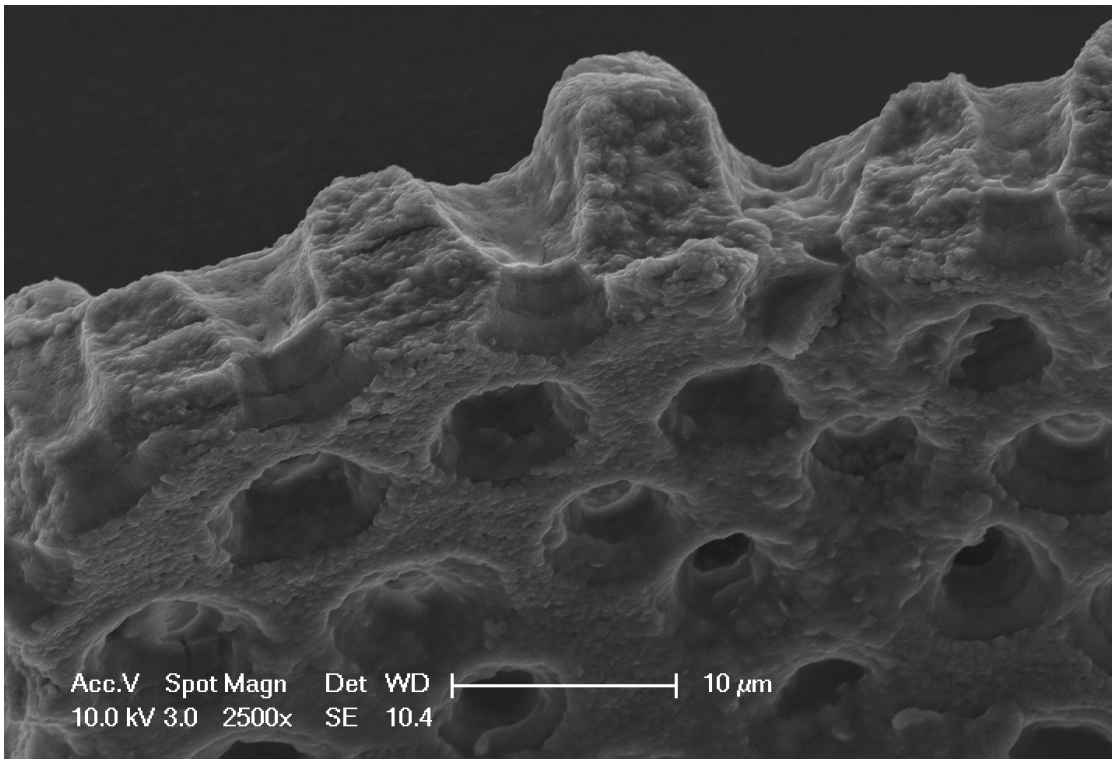

Figure 3.4. SEM image of glassy *Subbotina* sp. From Sample 16/28-sb01 122.36 – .38 m shows the bilamellar wall structure preserved. There might be some overgrowth on the inside. Image taken by Kirsty Edgar

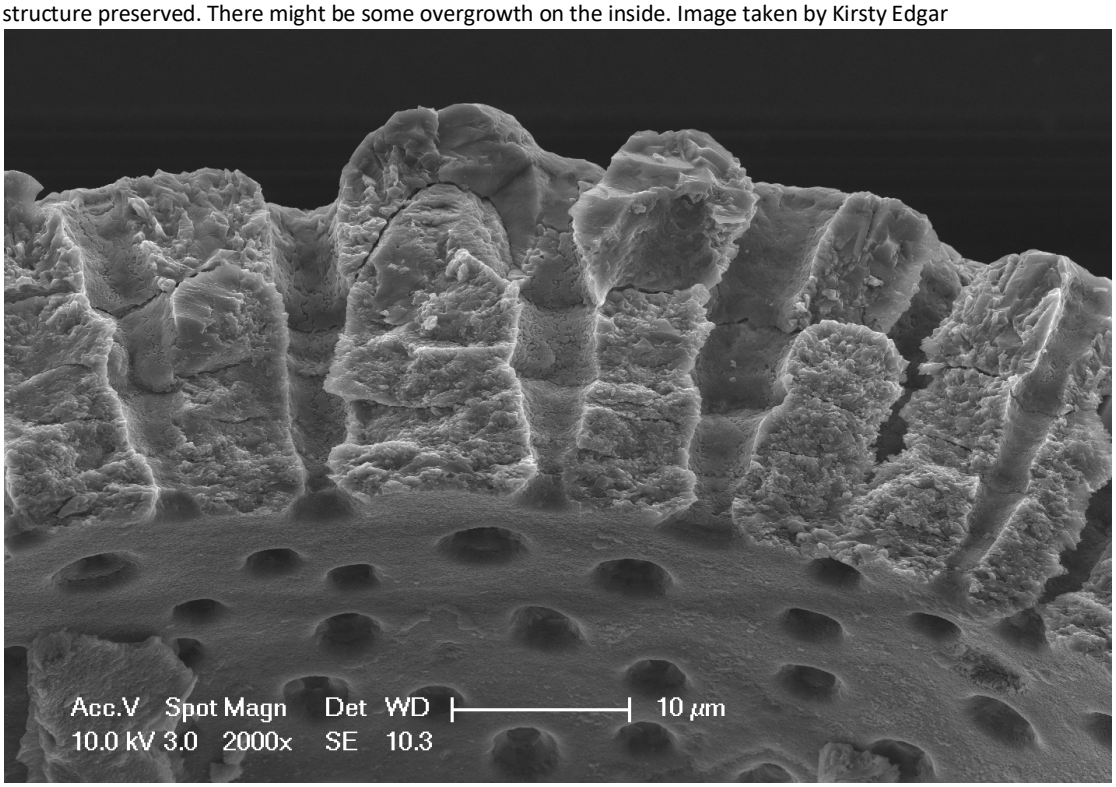

Figure 3.5. SEM image of glassy *Acarinina boudreauxi*, from Sample 16/28-sb01 122.36 – .38 m (from the early Eocene U2). Image taken by Kirsty Edgar.

3.3.4 Stable isotope data

3.3.4.1 Carbon and oxygen isotope based foraminiferal ecology

Multi-species water column profiles were generated for ~46.4 Ma (83.90 – .92 m) in the middle Eocene and ~50.5 Ma (119.38 – .40m; 119.80 – .82 m) in the early Eocene (Figure 3.6.). The assemblage changes from very low species diversity in the early Eocene to medium diversity in the middle Eocene, so five species can be measured in both timeslices (Figure 3.7. – 3.9.). In both timeslices, *Acarinina* and *Morozovella* consistently show the lowest $\delta^{18}O$ values and highest $\delta^{13}C$ values compared to the other genera (Figure 3.6.). *Subbotina* occupy an intermediate $\delta^{18}O$ and $\delta^{13}C$ space between *Acarinina* and *Morozovella,* and benthic foraminifera. *Catapsydrax unicavus, Globoturborotalita bassriverensis* and *Guembelitroide nuttalli* are found in a similar isotope space as *Subbotina* in the middle Eocene. The benthic species *N. truempyi* has the highest $\delta^{18}O$ values in both depth transects, it has the lowest $\delta^{13}C$ value in the early Eocene but not in the middle Eocene, where *Pseudohastigerina* spp. show the lowest $\delta^{13}C$ but sits close to *Subbotina* spp. in $\delta^{18}O$ space.

Each species with more than one measured value is plotted against their size fraction for both $\delta^{13}C$ and $\delta^{18}O$ (Figure 3.7. – 3.9.). *Acarinina* and *Morozovella* show a general trend towards higher $\delta^{13}C$ with increased body size in both depth timeslices (Figure 3.7.) with the exception of *A. cuneicamerata*. *Subbotina* spp. (Figure 3.8.) show comparatively little difference in $\delta^{13}C$ with increased body size. *Pseudohastigerina* spp. show a tendency towards lower $\delta^{13}C$ with increasing size fraction (Figure 3.9.). The $\delta^{18}O$ values of all measured species show no consistent relationship with increasing size fraction.

To reconstruct the water column character through the early-middle Eocene at higher-resolution, *Subbotina eocaena* (thermocline dweller) and *Acarinina bullbrooki* (surface dweller) were ultimately selected to be picked throughout the record because of their relative abundance in the larger size fractions and distinctive morphology.

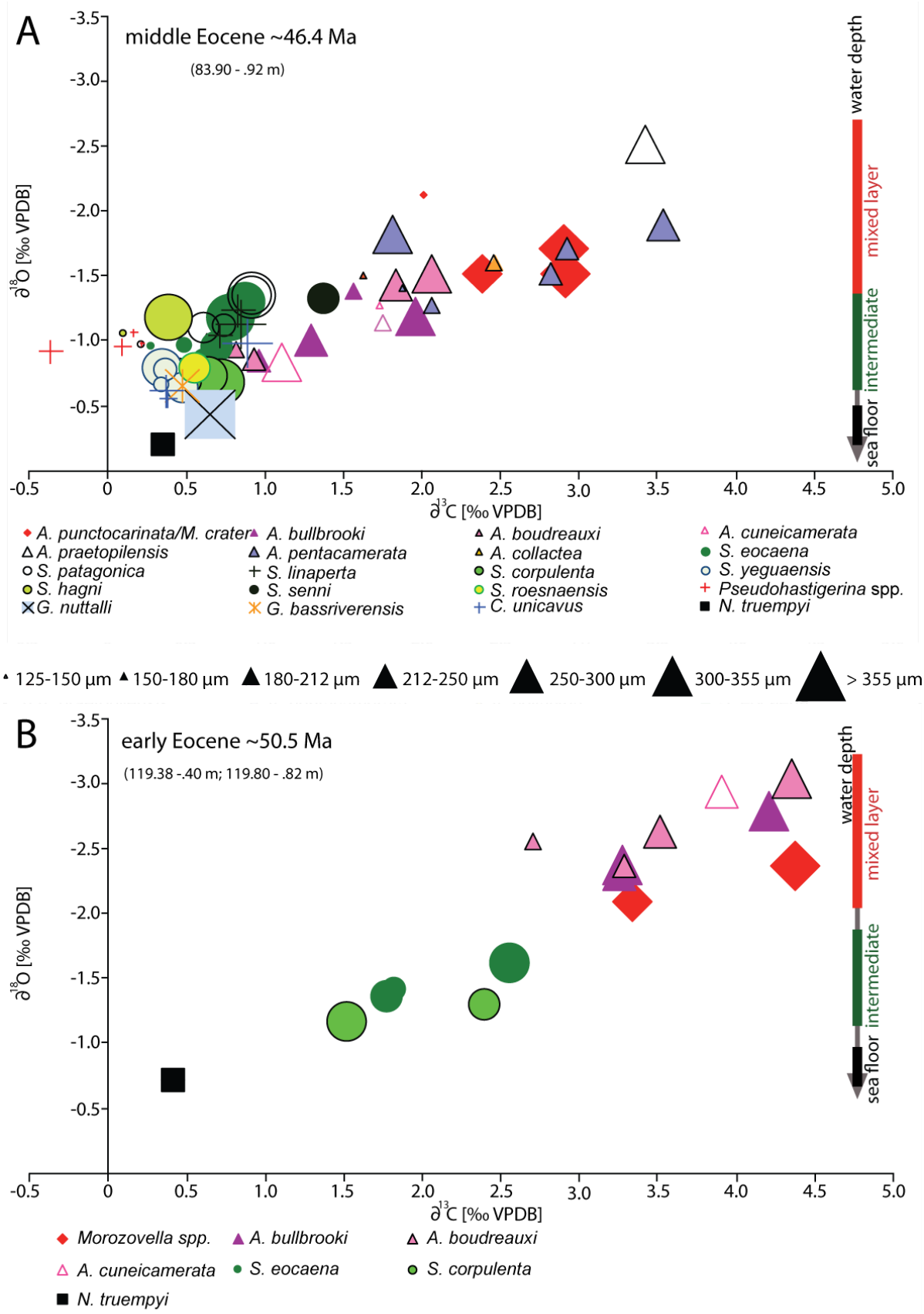

Figure 3.6. Size-specific $\delta^{18}O$ and $\delta^{13}C$ values of multiple foraminiferal species in the early and middle Eocene at Site 16/28-sb01. All results are plotted using the lower value of each size fraction, e.g. in the size fraction 200-250 µm it would be plotted against 200 µm. An interpretation of the relative water depth is shown on the right-hand side of the figure.

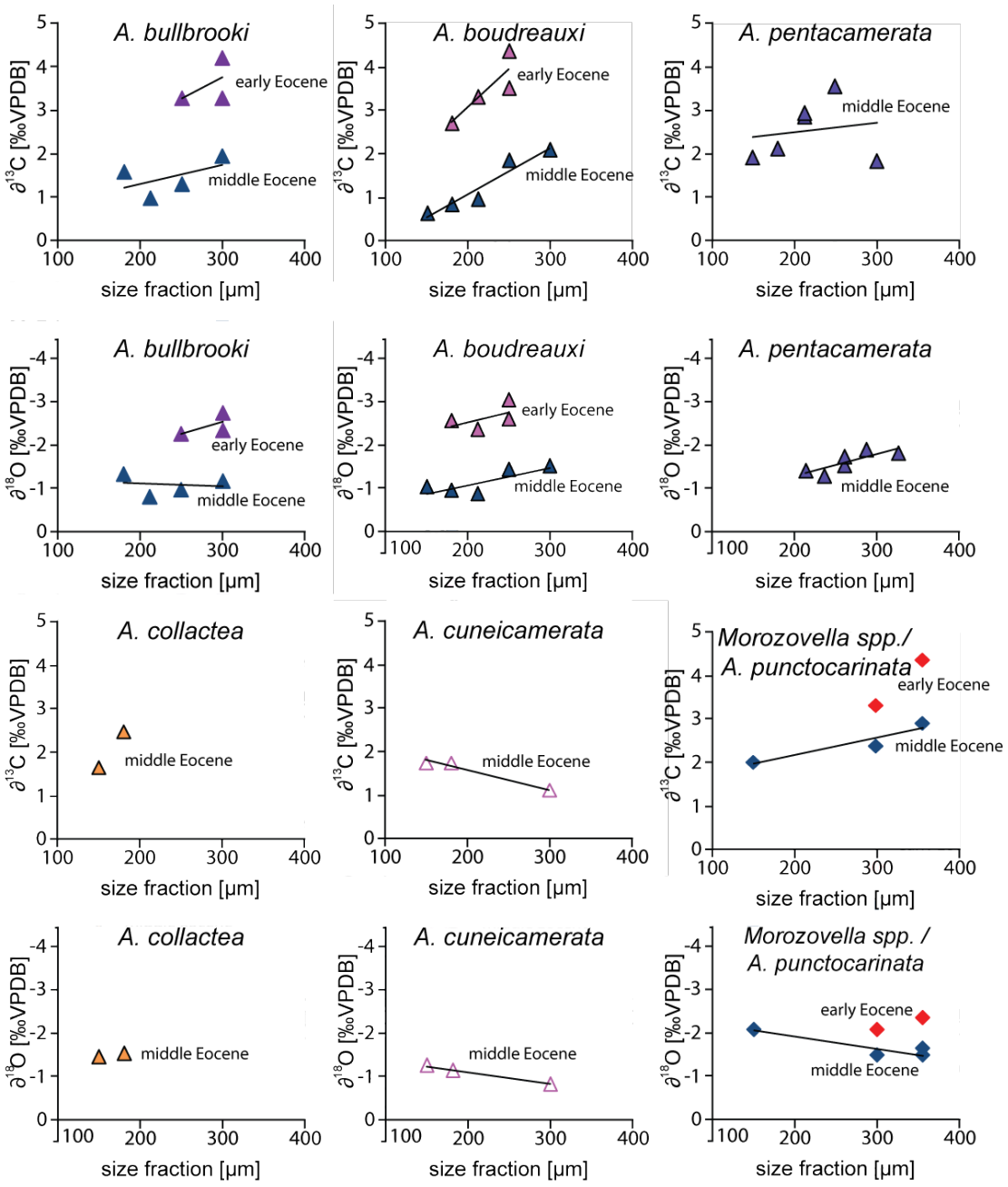

Figure 3.7. Size-specific trends in *Morozovella* and *Acarinina* $\delta^{13}C$ and $\delta^{18}O$ in the early and middle Eocene at Site 16/28-sb01. Same symbols and colours per species as in Figure 3.6., where data are available from both timeslices, the middle Eocene values are plotted in dark blue All results are plotted using the lower value of each size fraction, e.g. in the size fraction 200-250 µm it would be plotted against 200 µm.

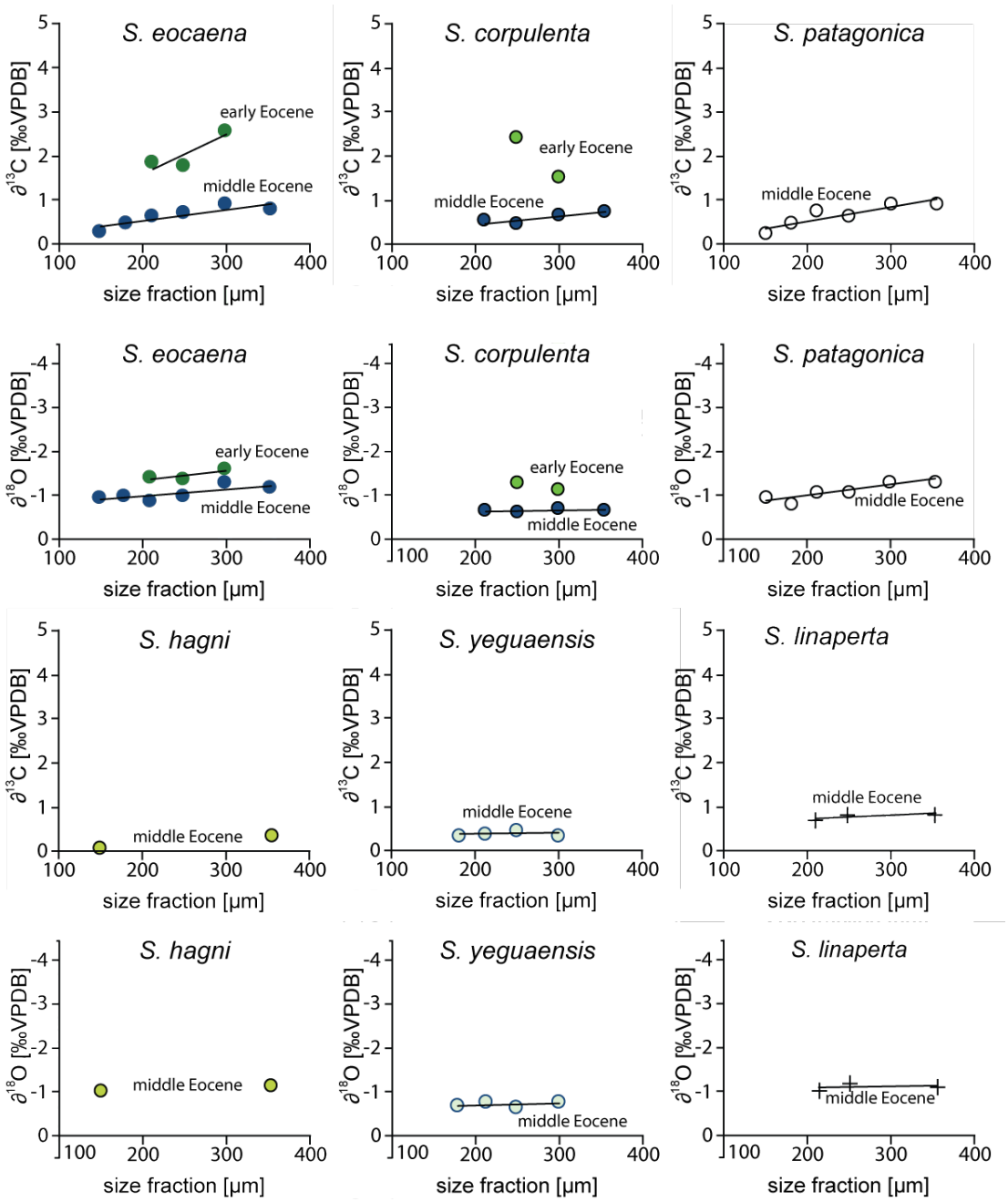

Figure 3.8. Size-specific trends in *Subbotina* $\delta^{13}C$ and $\delta^{18}O$ values in the early and middle Eocene at Site 16/28-sb01. Same symbols and colours per species as in Figure 3.6., where data are available from both timeslices, the middle Eocene values are plotted in dark blue. Otherwise the same symbols and colours are used as in Figure 3.6.. All results are plotted using the lower value of each size fraction, e.g. in the size fraction 200 – 250 µm it would be plotted against 200 µm.

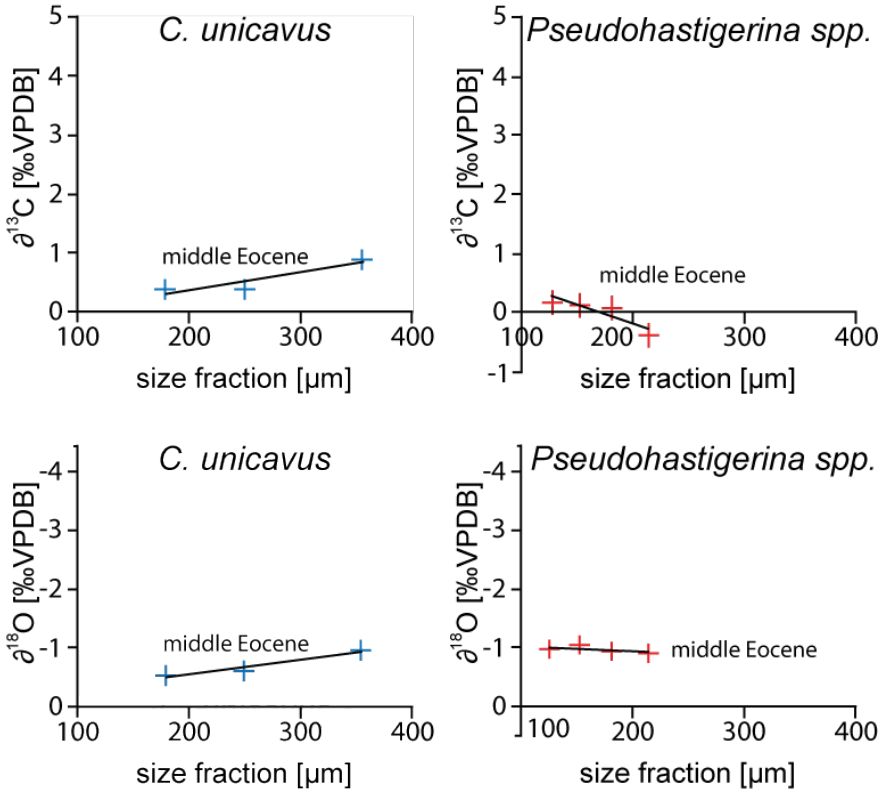

Figure 3.9. Size-specific trends in *Catapsydrax* and *Pseudohastigerina* $\delta^{13}C$ and $\delta^{18}O$ in the early and middle Eocene at Site 16/28-sb01. Same symbols and colours per species as in Figure 3.6., where data are available from both timeslices, the middle Eocene values are plotted in dark blue. Otherwise the same symbols and colours are used as in Figure 3.6. All results are plotted using the lower value of each size fraction, e.g. in the size fraction 200 – 250 µm it would be plotted against 200 µm.

3.3.4.2 Early to middle Eocene evolution of water column gradients

At Site 16/28-sb01, *A. bullbrooki, S. eocaena* and bulk $\delta^{18}O$ and $\delta^{13}C$ values generally follow the trends of the global benthic isotope compilation of Cramer et al. (2009) with some offsets in absolute values between the different records (Figure 3.10.). The $\delta^{13}C$ from *S. eocaena* are very similar in terms of trends to the bulk isotopes as well as the global compilation of benthic foraminiferal values (Cramer et al., 2009). Whereas the $\delta^{18}O$ of *S. eocaena* is about ~1 ‰ lower than the global compilation (Cramer et al., 2009) in all units, but similar to the bulk isotopes in U1, ~1 ‰ higher than the bulk isotopes in the U2 and ~1‰ lower than the bulk isotopes in U3. The $\delta^{13}C$ of *A. bullbrooki* is ~3 ‰ higher in U1 and U2 and ~2 ‰ higher in the U3 compared to the global compilation (Cramer et al., 2009), the bulk isotopes and the $\delta^{13}C$ of *S. eocaena*. *A. bullbrooki* $\delta^{18}O$ is in U1 and U2 are on average ~2 ‰ lower and about ~1 ‰ lower in U3 compared to the global compilation (Cramer et al., 2009). Thus, the relationship between *Acarinina,* bulk and *Subbotina* $\delta^{18}O$ varies down-core. In U1, $\delta^{18}O$ of *A.*

bullbrooki is ~2 ‰ lower than in the bulk and *S. eocaena* records, in U2 it is similar to the bulk $\delta^{18}O$ but ~1.5 ‰ lower than $\delta^{18}O$ of *S. eocaena* and in U3 the $\delta^{18}O$ of *A. bullbrooki* and *S. eocaena* are similar with slightly lower compared to the $\delta^{18}O$ of bulk isotopes and the global compilation.

Estimated ocean temperatures decrease from the early to middle Eocene. Calculated *A. bullbrooki* SSTs in U1 are ~26.0˚C, in U2: ~26.7˚C and in U3: ~17.0˚C. Temperature estimates from *S. eocaena* in U1 are ~19.1˚C, in U2 18.8˚C and in U3: 15.2˚C. Bottom water temperatures are ~14˚C for U2 and ~11˚C for U3. The average temperature difference between *S. eocaena* and *A. bullbrooki* is ~7 – 8˚C in U1 and U2, but only ~2˚C in U3. The surface-bottom water temperature also decreases from ~13˚C to ~6˚C between U2 and U3. The average difference between *S. eocaena* and bottom waters over the same time interval is ~4 – 5˚C.

Within the inferred CIEs, bulk $\delta^{18}O$ values decrease in the P, R, S, V and W events, increase within the T event and show no clear trend during the U event (Figure 3.3.). There are few foraminiferal isotope data that fall within the CIEs but the U and V CIEs show slightly lower $\delta^{18}O$ in *S. eocaena*.

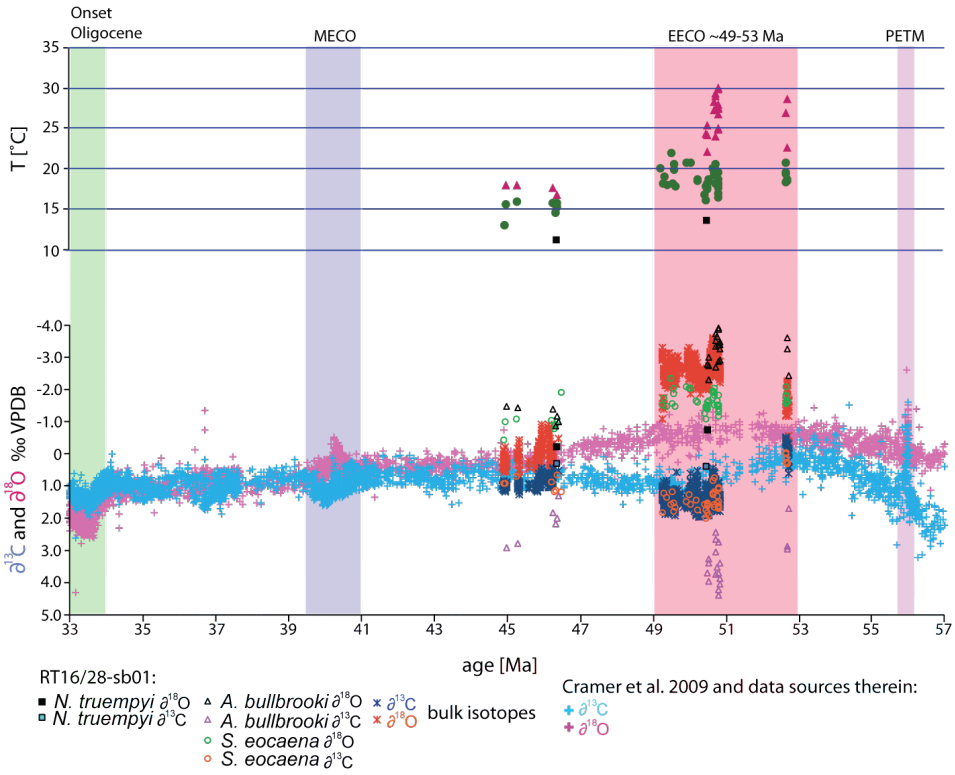

Figure 3.10.The long term trend of benthic isotope data from Cramer et al. (2009) compared to the data from Site 16/28-sb01 and calculated temperatures (T). The main climate events are indicated by coloured vertical bars: PETM (Paleocene-Eocene-Thermal-Maximum, dark pink), EECO (early Eocene climatic optimum; pink), MECO (mid-Eocene climatic optimum; purple) and the onset of the Oligocene (green).

3.4 Discussion and Interpretation

3.4.1 Foraminiferal abundance and diversity in lithologic Unit 1 - 3 of Site 16/28-sb01

Planktic foraminifera per gram of sediment are on average in U1: 7, in U2: 4 and in U3: 64, whereas benthic foraminifera per gram of sediment are in all units very low and are on average in U1: 2, in U2: 1 and U3: 5. Both the accumulation rate and the absolute abundance of both planktic and benthic foraminifera is very low in all Eocene lithological Units of Site 16/28-sb01 compared to standard open ocean calcareous ooze sites (e.g., Boscolo Galazzo et al., 2014, Jehle et al., 2019). The low numbers of benthic foraminifera are likely due to elevated sedimentation rates, reconstructed to be 3 – 9 cm/ka for Site 16/28-sb01 (see Chapter 2, Section 2.6), or might be associated with some degree of basin restriction (see Chapter 2, Section 2.2). The lower abundance and diversity of planktic foraminifera (and coarse fraction) in the early Eocene (U1 and U2) compared to the middle Eocene are likely related to the early Eocene palaeoenvironment including: A) relatively shallow water depth at the site, B) sediment dilution by input of higher terrestrial fine fraction to the system i.e., by clay particles from the nearby delta system, as indicated by the dominance of "terrestrial influx elements" in the XRF data (Figure 2.5.), C) potential lowered salinity through basin restriction and an enhanced hydrological cycle, D) water column stratification, and E) restricted circulation with the open North Atlantic. Planktic foraminiferal abundances and diversity in the middle Eocene are higher than in the early Eocene. However, they do not reach fully open marine abundances and diversity at Site 16/28-sb01 (e.g., Kucera, 2007) which could be up to a maximum diversity of ~60 species in the middle Eocene and ~45 in the early Eocene (Berggren et al., 1995, Stewart and Pearson, 2000, Sexton et al., 2006b). This low to medium diversity at Site 16/28-sb01 could be influenced by its mid to high latitude position — but latitude alone cannot account for this lower diversity when combined with the very low total foraminiferal abundances. It is more likely that the low number of benthic and planktic foraminifera is linked to the relatively high influx of terrestrial sediment or different (i.e., non-favourable) sea water chemistry, e.g. lower surface salinity would lead to lower planktic foraminiferal abundances and/or lower bottom water oxygenation would lead to lower benthic foraminiferal abundances. The high abundance of fine fraction,

especially in U1 (fine fraction <63 µm: ~88 wt.%) and U2 (~99 wt.%), and relative high sedimentation rates (3 – 9 cm/ka) are consistent with the relatively quick burial of marine fossils in clay-rich sediments, protecting them against diagenetic alteration and favouring the glassy style preservation found at Site 16/28-sb01 (Figure 3.5., Appendix 004 and 007).

3.4.2 Isotope-based ecology of planktic foraminifera

Within this study, based on the lowest $\delta^{18}O$ and amongst the highest $\delta^{13}C$ values in the assemblage, and a positive $\delta^{13}C$ - test size trend (e.g., Ezard et al., 2015), *Acarinina bullbrooki, A. boudreauxi, A. cuneicamerata, A. praetopilensis, A. pentacamerata, A. punctocarinata/M. crater, A. collactea* and *Morozovella* spp. are interpreted to be mixed layer dwellers and possess algal photosymbionts, (Figure 3.6., Figure 3.7.). This is consistent with the findings of Luciani et al. (2017b), whom find a short-term symbiont bleaching event at the onset of the EECO but not within the EECO. Notably the more robust *Acarinina — A. bullbrooki, A. boudreauxi* and *A. collactea,* sit slightly deeper in the mixed layer relative to the other inferred surface-dwelling taxa, (Figure 3.6.), which is also found in other studies (Pearson et al., 2001, Sexton et al., 2006c, John et al., 2013, Anagnostou et al., 2016). A possible explanation could be that they precipitated gametogenetic calcite slightly deeper in the water column towards the end of their life cycle, based on analogy to recent species (Bé, 1980, Norris, 1998, short review, Hamilton et al., 2008, Figure 3.6.) or that they inhabited a slightly deeper depth habitat. *Acarinina pentacamerata* and *A. cuneicamerata* show a decrease in $\delta^{13}C$ at sizes greater than 300 µm, as observed in "death assemblages" of recent planktic foraminifera, which plateau in $\delta^{13}C$ values at their maximum possible test size (Ezard et al., 2015). In the case of *A. cuneicamerata* slightly higher $\delta^{18}O$ and lower $\delta^{13}C$ at sizes greater than 300 µm could be explained by a depth habitat change or some seasonal bias. The following are interpreted as occupying an intermediate or thermocline habitat and lacking photosymbionts, based on relatively high $\delta^{18}O$ and low $\delta^{13}C$ values, and lack of distinctive size-$\delta^{13}C$ trends are: *Subbotina senni, S. patagonica, S. hagni, S. linaperta, S. corpulenta, S. roesnaensis, S. yeguaensis, S. eocaena, Guembelitroides nuttalli, Globoturborotalita bassriverensis, Catapsydrax*

unicavus and *Pseudohastigerina* spp, (Figure 3.6., 3.8. and 3.9.). Generally, the planktic foraminiferal ecologies recognised at Site 16/28-sb01 are consistent with the results of previous publications (Poore and Matthews, 1984, Shackleton et al., 1985, Boersma et al., 1987, Stott et al., 1990, Pearson et al., 1993, D'Hondt et al., 1994, Quillévéré et al., 2001, Pearson et al., 2001, Sexton et al., 2006c, Birch et al., 2012, John et al., 2013, Bornemann et al., 2014, Edgar et al., 2015, Anagnostou et al., 2016, Luciani et al., 2017b). A notable exception to this is *Globoturborotalita bassriverensis,* which is recorded as a surface dweller in the late middle Eocene, with a possible winter preference, and therefore higher $\delta^{18}O$ values than other surface dwelling taxa but only slightly lower $\delta^{13}C$ values (Sexton et al., 2006b). At Site 16/28-sb01, *G. bassriverensis* appears to occupy a deeper water habitat (Figure 3.6.) in the middle Eocene. Thus, this might represent a change in depth habitat through time as seen in multiple other Eocene groups (e.g., Coxall et al., 2000) or difficulties in the taxonomy of *G. bassriverensis.* It is morphologically very similar to *S. yeguaensis,* both have similar stable isotopic composition in this study and the picked specimens may have been a slightly different morphotype of *S. yeguaensis* (Figure 3.11., 3.12.).

The data presented herein support the hypothesis that the ecology of *Pseudohastigerina* spp. is not static through time or space. Boersma et al. (1987) interpret *Pseudohastigerina* spp. as occupying the surface layer within the late Eocene but in the middle Eocene they have much higher $\delta^{18}O$ values, indicating a much deeper (intermediate) depth habitat below *Catapsydrax* and *Hantkeninina.* Whereas, Pearson et al. (2001) and John et al. (2013) find *Pseudohastigerina micra* (including *P.* cf. *acutimarginata*)*, P. pseudowilsoni* and *P. inaequispira* had very low $\delta^{18}O$, as low as their surface dwellers or slightly higher values, and $\delta^{13}C$ values almost as low or slightly lower than their benthic $\delta^{13}C$ measurements in the same timeslice, in the middle and late Eocene. Pearson et al. (2006) note that *Pseudohastigerina* spp. were likely adapted to upwelling regions with lots of nutrients which is consistent with the variable depth habitat observed for upwelling species today (Kucera, 2007). The decreasing $\delta^{13}C$ values with increasing test size of *Pseudohastigerina* spp. at Site 16/28-sb01 in the middle Eocene might indicate metabolic and kinetic effects within

the small test sizes of this rather minute species, or it might indicate some kind of seasonal upwelling regime (e.g., Birch et al., 2013).

Figure 3.11. Determined in this study as *Globoturborotalita bassriverensis* and measured for isotopes within the middle Eocene depth transect (83.90 – .92 m) size fraction 250 – 300 µm from Site 16/28-sb01, for more detail and spiral side see electronic Appendix 004.

Figure 3.12. *Subbotina yeguaensis* measured for the middle Eocene depth transect (83.90 – .92 m) size fraction 250 – 300 µm from Site 16/28-sb01, see electronic Appendix 004.

3.4.3 Foraminiferal abundances and the early Eocene CIEs

In Chapter 2, an age model for the early Eocene was developed using high-resolution bulk carbonate carbon and oxygen isotope records, where the $\delta^{13}C$ values could be aligned to the KT/S (Kirtland Turner/Sexton) target curve, consisting of bulk (Kirtland Turner et al., 2014) and benthic foraminiferal stable isotope records from equatorial Atlantic ODP Site 1258 (Sexton et al., 2011), (Figure 2.10.). However, it was more difficult to align the bulk carbonate $\delta^{18}O$ values of Site 16/28-sb01 to the KT/S target curve (Figure 2.10.). In certain intervals, Site 16/28-sb01 has lower $\delta^{18}O$ values (indicating warmer or lower salinity conditions) than the KT/S target curve and than bulk carbonate $\delta^{18}O$ records from the Tethys or Southern Atlantic (Coccioni et al., 2012, Luciani et al., 2017a). Within the CIEs of Site 16/28-sb01 the excursions of bulk carbonate $\delta^{18}O$ do not always match the KT/S target curve in trend and magnitude. For example, although the negative CIEs generally show more negative $\delta^{18}O$ values, at the T event there is a clear positive excursion in bulk carbonate $\delta^{18}O$. This inverse pattern is in contrast to matching negative excursions in both $\delta^{18}O$ and $\delta^{13}C$ across the T event in other records, from the Tethys, Atlantic and Pacific (e.g., Sexton et al., 2011, Coccioni et al., 2012, Littler et al., 2014, Kirtland Turner et al., 2014, Lauretano et al., 2015, Luciani et al., 2017a, Westerhold et al., 2018a, Lauretano et al., 2018, Barnet et al., 2019). Therefore, here it is explored if there is a correlation between the new data of this Chapter and the bulk $\delta^{18}O$ values of Site 16/28-sb01 which could explain the mismatches to the $\delta^{18}O$ KT/S target curve. And in fact, this studies data show that the absolute abundances of planktic foraminifera and XRF-Ca values (Figure 2.15.) in the early Eocene U2 (Figure 3.3.) broadly follow the bulk carbonate $\delta^{18}O$ record, with lower $\delta^{18}O$ values, coinciding with lower foraminiferal abundances and lower XRF-Ca values. An exception to the above correlation can be seen just a little younger than the T event, where lower $\delta^{18}O$ values are coupled with slightly higher abundances of planktic foraminifera, dominated by the thermocline dwellers *Subbotina* spp. (Figure 3.3.) and within the T event where higher $\delta^{18}O$ values correlate with a peak in XRF-Ca but no significant increase in foraminiferal abundance. There are also gaps in the appearance of the surface-dwelling taxa *Acarinina* and *Morozovella* (labelled 1, 2 and 3 and indicated with blue arrows, Figure 3.3.) coincident with low abundances of

Subbotina spp. and lower bulk $\delta^{18}O$ values. In the big picture of the bulk $\delta^{18}O$ of Site 16/28-sb01 not consistently matching with the $\delta^{18}O$ of the KT/S target curve — the apparent correlations of low Ca and low planktic foraminiferal abundance with low bulk carbonate $\delta^{18}Os$ might be explained by localized factors: A) elevated surface water temperature, B) increased nutrients, C) reduced salinity or D) preservation.

A) Elevated water temperature

Acarinina and *Morozovella* dominate Eocene assemblages (Luciani et al., 2016, Luciani et al., 2017a, Luciani et al., 2017b). *Acarinina* are a relatively cosmopolitan group whereas *Morozovella* are more commonly found in (sub)tropical (low latitude) environments (Pearson et al., 2006). At Site 16/28-sb01 *Acarinina* are more abundant with only rare *Morozovella* consistent with the site's mid-high latitude position. The occasional appearance of *Morozovella* might be explained by Site 16/28-sb01 in the early Eocene being just at the northern ecological limit of *Morozovella,* with their intermittent occurrences at this mid-to high latitude site correlated with intervals of peak early Eocene warming.

As discussed above, lower abundance or absence of planktic foraminifera generally occur at times with more negative bulk carbonate $\delta^{18}O$ values. If this was a pure warming signal, it would imply that thermal stress was a potential cause of foraminiferal exclusion. This is, however, extremely unlikely as the only studies with any indication of thermal stress causing exclusion of marine zooplankton, are at tropical locations during the Paleocene-Eocene Thermal Maximum, with SSTs of >35˚C (Aze et al., 2014, Frieling et al., 2017, Frieling et al., 2018). At Site 16/28-sb01 reconstructed SSTs are <30˚C, thus it is highly unlikely that the water temperature exceeded species tolerance at this mid-high latitude site and if anything abundance of these taxa, especially *Morozovella,* should have been favoured by warming (Aze et al., 2014, Pearson et al., 2006) but they are not.

B) Nutrient availability

Acarinina and *Morozovella* are oligotrophic (low nutrient) favouring taxa (Pearson et al., 2006) and *Subbotina* favour more nutrient rich (meso- to eutrophic environments)

(e.g., Olsson et al., 2006, Pearson et al., 2006, Luciani et al., 2010). Thus, changes in nutrient availability in surface waters may have impacted the abundance of these taxa — in particular elevated nutrient availability in the water column may have heavily impacted both *Acarinina* and *Morozovella* which are sensitive to nutrient changes and occupy similar ecological niches (e.g., Luciani et al., 2010). Within Site 16/28-sb01, assemblages are dominated by *Subbotina* with subordinate *Acarinina,* and very rare *Morozovella* linked to low total foraminiferal abundances.

Luciani et al. (2017b) find evidence for elevated radiolaria abundances, indicating increased eutrophication within the surface waters of the mid-latitudinal western Atlantic (ODP Site 1051) at the onset of the EECO coinciding with a shift from *Morozovella* to *Acarinina* dominated assemblages, which they attribute to an enhanced hydrological cycle rather than increased upwelling. At Site 16/28-sb01, transient appearances of "cenospheroid" radiolaria occur as shown in Figure 3.13., which could indicate episodes of higher nutrient influx into the Rockall Basin. However, the radiolaria pulses do not systematically correlate with the surface-dweller gaps (1 – 3 on Figure 3.3.), and therefore the surface dweller gaps and the total abundance variation of planktic foraminifera may not be explained by nutrients alone.

Enhanced nutrients in sea water is coupled with enhanced primary production and should lead to more ^{12}C export to the seafloor, higher $\delta^{13}C$ values in the surface waters and lower $\delta^{13}C$ values at the sea floor. This pattern is not seen in Site 16/28-sb01 record neither in the surface dweller gaps nor during the "cenospheroid" radiolaria occurrences. In the broader comparison with the $\delta^{18}O$ of the KT/S target curve, the "cenospheroid" radiolaria occurrences seem to be mainly linked to lower $\delta^{18}O$ values than the KT/S target curve, with the exception shortly before and during the R event. This supports that their occurrence is related to something other than nutrients in the Rockall Basin.

C) Salinity

The Rockall Basin is a marginal basin with uncertainty as to the extent of connectivity to the open marine North Atlantic in the south (see Chapter 2, Section 2.2 and e.g.,

Brinkhuis et al. (2006)) and of surface water exchange over the GSR to the North (e.g., Andreasson et al., 1996). Restricted connectivity, and an enhanced early Eocene hydrological cycle (Barron et al., 1989, Speelman et al., 2010, Greenwood et al., 2010, Carmichael et al., 2016, Carmichael et al., 2017, Luciani et al., 2017b, Inglis et al., 2020) could have made the basin susceptible to periods of intensified water column stratification, lower surface salinities and increased nutrient influx into the basin, as well as conditions generally more favourable to *Subbotina*.

Lower surface ocean salinities, and enhanced water column stratification exacerbated by high water temperatures, would also contribute to lowered bulk carbonate $\delta^{18}O$ values. Lowered salinity is thus the most likely explanation of lower planktic foraminifera abundances, especially mixed-layer dwelling planktic foraminifera, at times of lower bulk carbonate $\delta^{18}O$ and for lower bulk $\delta^{18}O$ than the KT/S target curve. Modern salinity ranges for planktic foraminifera differ from species to species with ranges around 27 – 45 psu for *Globigerinella siphonifera* and 22 – 49 psu for more salinity tolerant species *Globigerinoides ruber* (Bijma et al., 1990, Schiebel and Hemleben, 2017, for review). Generally planktic foraminiferal species seem to have smaller test sizes if salinity is lower or higher than normal marine (33 – 37 ‰) (Bijma et al., 1990, Schiebel and Hemleben, 2017, for review). Therefore, potential surface water freshening in the early Eocene Rockall Basin could have led to diminished planktic foraminiferal abundances and sizes.

This hypothesis is consistent with foraminifera gaps 1 and 3 (Figure 3.3., 3.13.) coinciding with elevated "terrestrial influx" elements (Si, Al and Fe) (Figure 2.15.), indicative of increased freshwater runoff and lowered surface water salinities possibly not suitable for the surface-dwelling species *Acarinina* and *Morozovella*. Gap 2 shows lower "terrestrial influx" elements, but is still a time of lower bulk carbonate $\delta^{18}O$ values, consistent with regional surface water freshening.

Conversely the higher bulk carbonate $\delta^{18}O$ values could reflect intervals with a stronger connectivity with open North Atlantic waters and a more saline water tongue, as discussed in Chapter 2, Section 2.7.2.2, travelling into this southern Rockall Basin bringing with it the surface dwellers *Acarinina* and *Morozovella*. The peak of bulk carbonate $\delta^{18}O$ just before the W? CIE, coinciding with the highest planktic and

benthic foraminiferal abundances of the whole U2 succession, at ~49.2 Ma might reflect the strongest connectivity with the North Atlantic during the whole U2, it is coupled with high Ca and low terrestrial influx elements (Si, Al and Fe). This short-term stronger connectivities could have been driven by a varied strength of the precipitation cell over the Rockall Trough allowing this switch from lower to higher saline surface waters.

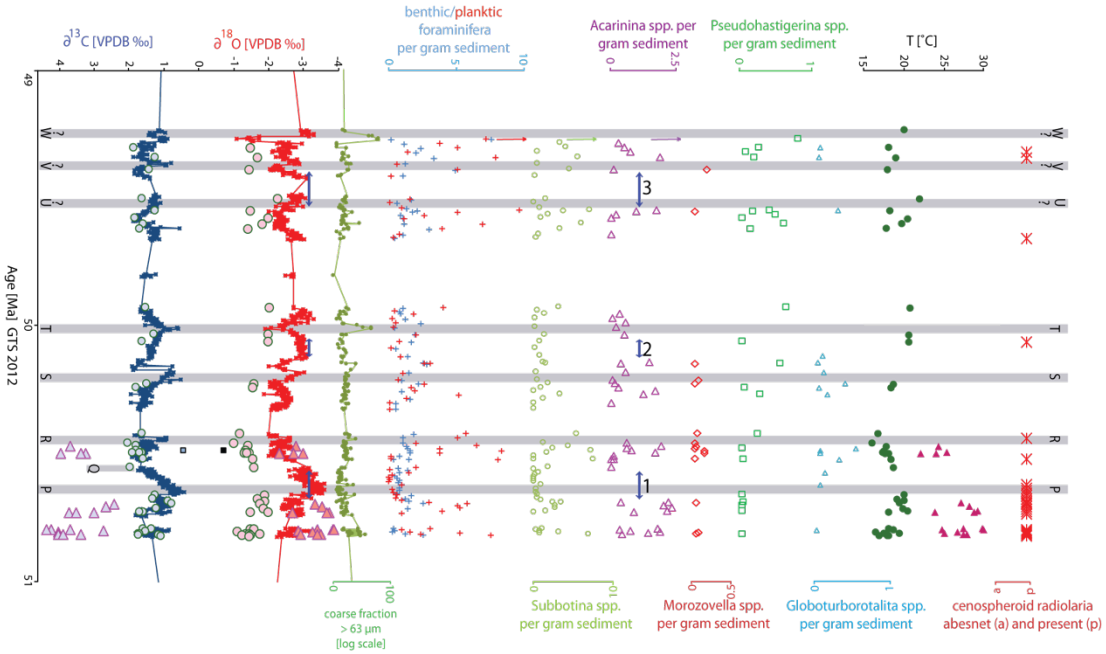

Figure 3.13. Modified Figure 3.3. showing additionally the presence and absence of "cenospheroid" radiolaria to test if they can shed light on possible higher nutrient influx into the Rockall Basin at Site 16/28-sb01.

An alternative source of low salinity waters could be surface water from the north, with episodic influence of lower salinity and higher nutrient content waters from the Arctic rift (e.g., Willard et al., 2019) with brackish waters in the Arctic ~24 ‰ (Waddell and Moore, 2008, Greenwood et al., 2010) and reduced salinity in the Norway-Greenland Basin ~25 ‰ (Andreasson et al., 1996). These could have flowed over the GSR into the surface Rockall Basin and be dependent on subsidence history and relative sea level stand.

The scenario of southern sourced more saline surface water influx into the Rockall Basin appears likely if compared with modern circulation patterns, where the main surface influx to the northeast Atlantic is driven by the Gulf Stream from the south. In Paleogene configurations, the intensity of this influx is linked with the GSR gateway

opening, which causes a spin-up of whole ocean circulation (Vahlenkamp et al., 2018a, Vahlenkamp et al., 2018b). At Site 16/28-sb01, this spin-up might be detected shortly before the W? CIE by the higher $\delta^{18}O$ values coupled with higher foraminiferal abundances (as discussed above) and the unconformity between U2 and U3 which occurs shortly afterwards, which is assumed to be caused by slope failure (Haughton et al., 2005). If these brief higher $\delta^{18}O$ peaks in U2 would reflect intervals of stronger connectivity with the North Atlantic it could indicate short term influx of proto gulf stream driven influx into the Rockall Trough which might was not continuous during the Eocene greenhouse climate with a stronger precipitation control, which cannot be excluded nor proven within this thesis. Slope failure on the very steep flanks of the Porcupine Basin might be caused by the stronger circulation system established through sufficient gateway opening, and could have been some time after the U2 to U3 transition. Before intensified circulation, a lower salinity surface water outflow from the Arctic might have played a role counteracting Northern Atlantic water influx into the Rockall Basin or periods with higher precipitation and river run off, which cannot be excluded nor proven within this thesis.

In their model, Tindall et al. (2010) find higher $\delta^{18}O_{sw}$ values (~0.8 ‰) at Site 16/28-sb01, due to limited palaeogeographic flow in-between the North Atlantic and Arctic Oceans, indicating higher salinity in the Rockall Basin. Thus, if bulk carbonate $\delta^{18}O$ values from Site 16/28-sb01 indicate salinity as well as temperature, they might shed light on how much the circulation and hydrological cycle changed within this key position in the North Atlantic, close to the opening of the GSR (Hohbein et al., 2012). Specifically, they might indicate that the modelled salinities of Tindall et al. (2010) are too high for this area, most likely due to uncertainties in the global model representation of local fresh water runoff and uncertainties of surface water connectivity to the lower salinity waters of the North. However, more study sites are necessary to complete the picture and to determine if the depth of the GSR (open versus closed) has an influence on salinity and $\delta^{18}O_{SW}$ in the Rockall Basin.

D) Preservation

Another way of explaining the sporadic occurrence of *Acarinina* and *Subbotina* is through the dissolution of carbonate. However, Petrizzo (2007) find in the PETM that *Subbotina* are most susceptible to dissolution, which are the most abundant in 16/28-sb01 and most consistently present through the cores, making dissolution an unlikely explanation of the *Acarinina* and *Morozovella* gaps in this record.

Therefore, in addition to the discussion in Section 2.7.2.2, the expression of the CIEs within shallow marine Site 16/28-sb01 in the Rockall Basin is complex. It appears most likely the bulk carbonate $\delta^{18}O$ is affected by a combination of temperature, water column stratification, the degree of connectivity with the open Atlantic and lowered salinities during intermittent intervals of higher precipitation. Transient increases in runoff are also coupled with evidence for increased input of terrestrial sediment, and likely increased nutrient supply to the basin and some eutrophication of the water column.

An exemption to the above established pattern is the T event where higher $\delta^{18}O$ values, implying increased salinities, are associated with the re-occurrence of *Acarinina* and a high in bulk sediment Ca content, although there is not an increase in absolute planktic foraminiferal abundance. The T event is further linked to higher Fe values and slightly higher Mn values, interpreted in Chapter 2 as indicating different redox conditions during early diagenesis compared to the rest of the U2. The coarse fraction increase consists mainly of red sediment particles instead of foraminifera and is distinct to the rest of the U2 16/28-sb01 record. A possible explanation for the coarse fraction peak during the T event could be an increased bottom water current — winnowing out the fine fraction — possibly changing bottom water oxygenation, which would be consistent with a regional opening and deepening of the Rockall Basin. It is however difficult to imagine that this would only occur during the T event. The exact reasons for the anomaly in the T event are therefore complex and difficult to pin point.

3.4.4 Benthic isotopes and their implication(s)

Absolute $\delta^{18}O$ values from benthic foraminifera at Site 16/28-sb01 are consistent with the global benthic temperature compilation of Cramwinckel et al. (2018), which reconstructs bottom water temperatures of ~12 – 16˚C for peak-EECO and ~7 – 12˚C for the middle Eocene. Although the magnitude of bottom water cooling from early to middle Eocene is smaller at Site 16/28-sb01 (~3˚C) than seen in the global compilation. The two benthic $\delta^{13}C$ isotope measurements from the depth profiles of this study, fit within the range of $\delta^{13}C$ benthic foraminiferal isotope data from Cramer et al. (2009), but do not show a significant change in absolute values between the early and middle Eocene, and are at the more negative end of the data cloud for benthic foraminiferal $\delta^{13}C$ of Cramer et al. (2009), consistent with the North Atlantic and the more shallow water depth of Site 16/28-sb01, especially during the early Eocene. This could support that the North Atlantic and the Rockall Basin was influenced by old intermediate/bottom waters in the early and middle Eocene, as water is most positive in $\delta^{13}C$ when newly formed and then acquires more negative values whilst it travels through the deeper water layers of the ocean (see Introduction, Section 1.4 for details). Another possibility would be that the relatively low benthic $\delta^{13}C$ in the Rockall Basin is a localized signal reflecting high primary productivity and nutrient export to the sea floor combined with the more shallow depositional depth at Site 16/28-sb01. Published studies propose the onset of NCW (Northern Component Water) around 49 Ma (Hohbein et al., 2012, see Introduction, section 1.4) — this might significantly change the deep-water regime to the west of the Rockall Basin into the Iceland Basin but this is not reflected by changing benthic $\delta^{13}C$ at Site 16/28-sb01. The sedimentology of 16/28-sbo01, however, does show the onset of an erosional regime within the Rockall Basin recorded at 49 Ma — at the U2/3 break — but could have happened later and eroded down but no later than ~ 46.23 Ma (onset of U3) and changes to more coarse-grained carbonate oozes in the middle Eocene (Figure 3.2.). Both of these observations are consistent with deep water current intensification in the Rockall Basin with the onset of NCW formation and the shift of Rockall Basin salinity towards normal sea water (Vahlenkamp et al., 2018a, Vahlenkamp et al., 2018b), indicating that the $\delta^{13}C$ of benthic foraminifera is reflecting

localized signals rather than deep water circulation, which is consistent with the shallow water depth at Site 16/28-sb01 especially during U2. However more benthic isotope data are needed to complete the picture.

The $\delta^{13}C$ difference between *N. truempyi* and *A. boudreauxi* (300 – 355 µm) is ~4 ‰ for the early Eocene and ~2 ‰ for the middle Eocene (~3 ‰ in the middle Eocene if the topmost surface dweller is selected instead), (Figure 3.6.). In general, all foraminiferal species in the early Eocene have higher $\delta^{13}C$ values than in the middle Eocene, by ~1 – 2 ‰. The higher $\delta^{13}C$ values in the early Eocene could be caused by a steeper water column gradient of $\delta^{13}C_{DIC}$, as previously proposed (John et al., 2013, John et al., 2014). To investigate the $\delta^{13}C_{DIC}$ gradients a schematic approximation is shown in Figure 3.14., the water depth at which foraminifera precipitate their tests is approximated by comparing it to water depth per genus at Tanzanian sites (John et al., 2013). Water depth estimates are obviously subject to a range of uncertainties so given values are a guideline only. The early Eocene depth transects at Site 16/28-sb01 has more positive $\delta^{13}C$ values in the surface ocean than in the middle Eocene (Figure 3.6., Figure 3.14.) and the majority of time slices from the Eocene of the Tanzanian sites of John et al. (2013). This might imply higher removal of ^{12}C in the surface waters in the early Eocene at Site 16/28-sb01, for example by higher photosynthetic activity caused by higher primary production. In the thermocline of the early Eocene at Site 16/28-sb01, $\delta^{13}C$ values reduce to ~2.5 ‰ and 1.5 ‰ in the middle Eocene.

The $\delta^{18}O$ difference between *N. truempyi* and *A. boudreauxi* (300 – 355 µm) is ~2.33 ‰ for the early Eocene and ~1.33 ‰ for the middle Eocene. The $\delta^{18}O$ difference between *N. truempyi* and the shallowest dweller in the early and middle Eocene is ~2.33 ‰, (Figure 3.6.). This indicates that the same $\delta^{18}O$ (temperature) range was inhabited by the foraminifera in the early and middle Eocene and obviously is influenced by the deepening in the succession from the early and middle Eocene.

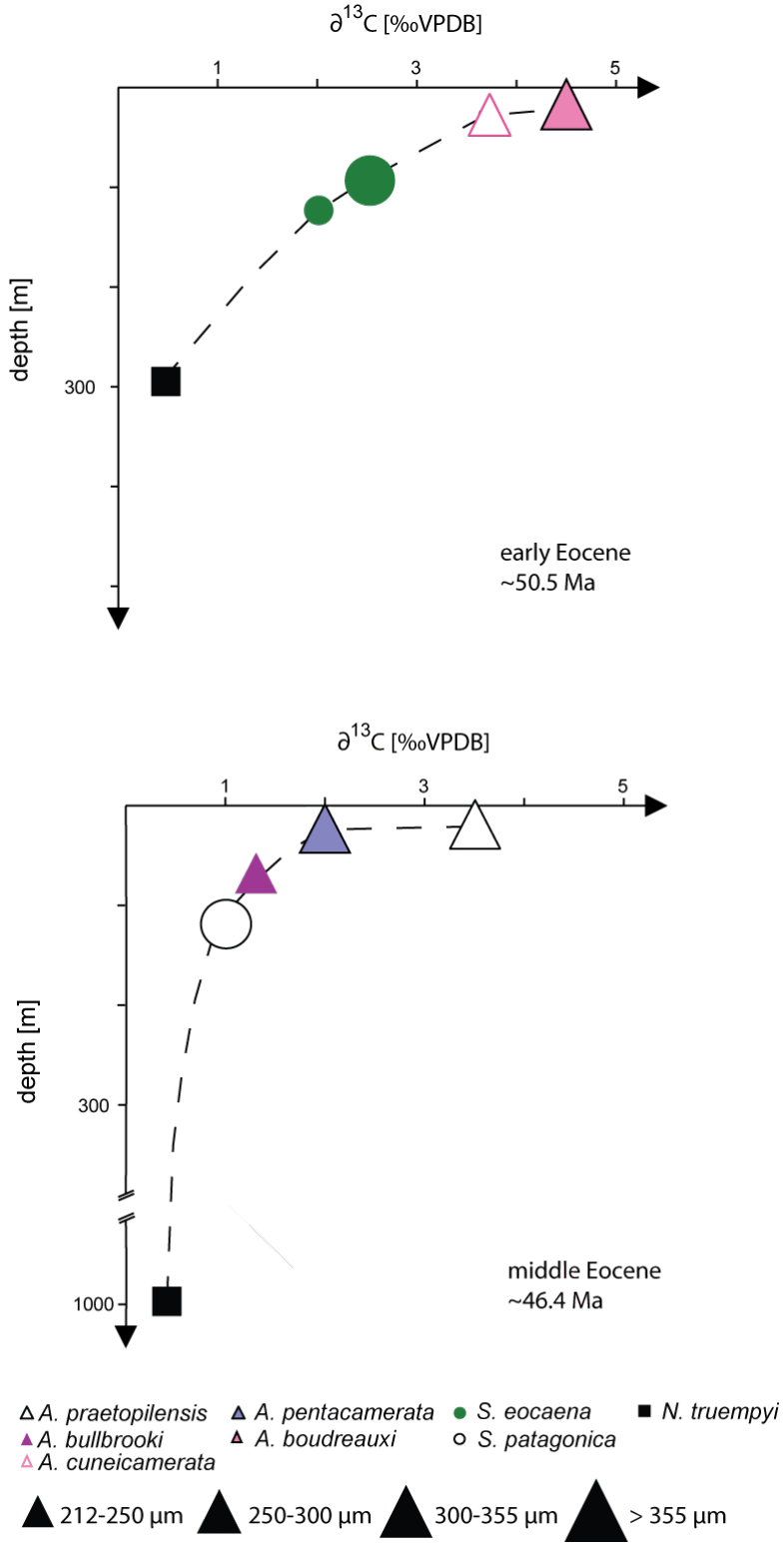

Figure 3.14. Theoretical approach of showing an approximation of the $\delta^{13}C_{DIC}$ gradients in the early and middle Eocene of Site 16/28-sb01. The depth of the thermocline dwellers is difficult to estimate and might have been much deeper than displayed here. Here the reconstructed palaeo water depth from this thesis is used as total depth of water column and then the planktic genus depth assignments based on comparison with Tanzanian $\delta^{13}C$ DIC gradients reconstructed depth habitats from John et al. (2013).

3.4.5 Local and global SST reconstructions

In the early Eocene, *A. bullbrooki* (250 – 300 µm) show an average SST for ~26.6˚C, with a total range of ~22 – 30˚C. In the middle Eocene, *A. bullbrooki* gives an average SST of ~17˚C, with a total range of ~15 – 18˚C. This implies local SST cooling of ~10˚C between ~51 to ~45 Ma. This shift is significantly larger than the global mean average cooling of 3˚C over the same time interval, from ~29˚C at ~51 Ma to ~26˚C in the middle Eocene (Cramwinckel et al., 2018), and is consistent with site specific records indicating larger cooling signals at higher latitudes (Hollis et al., 2012, Inglis et al., 2015, Hollis et al., 2019). $\mathrm{TEX}_{86}^{\mathrm{H}}$-based SST estimates from the equatorial Atlantic Site 959 (Cramwinckel et al., 2018), are ~34˚C for the EECO and ~32˚C at around 46 Ma in the middle Eocene, implying a ~2˚C cooling. Within a recent compilation of TEX_{86} SSTs, Inglis et al. (2015) estimate a high latitude (>55˚) cooling of ~7˚C from ~51 – ~46 Ma, and ~2.5 ˚C of cooling for tropical latitudes (similar to Cramwinckel et al. (2018)). In the Southern high latitudes (~46˚S) at the New Zealand mid-Waipara-River section a cooling of ~8˚C is found with SSTs reconstructed from *Morozovella* from 50 Ma (~28˚C) to 46 Ma (20˚C) (Hollis et al., 2012, Hollis et al., 2019, Crouch et al., 2020). They attribute their large shift in SSTs recorded from planktic foraminifera to preservation issues, with their Mg/Ca SSTs indicating a cooling of 5˚C from 30˚C at 50 Ma to 25˚C at 46 Ma. Interestingly the $\mathrm{TEX}_{86}^{\mathrm{H}}$ from the same site implies only ~2˚C cooling from ~32˚C at 50 Ma to 30˚C at 46 Ma (Crouch et al., 2020). At North Atlantic, Bay of Biscay DSDP Site 401 Bornemann et al. (2016) find that surface dwellers record similar δ^{18}O values from 50 – 46 Ma giving SSTs of ~19˚C indicating no significant cooling between EECO and the middle Eocene. They interpret this lack of cooling a result of the muted North Atlantic sea surface temperature response to the EECO. Subsurface dwellers at Site 401 also show little changes in δ^{18}O values giving temperatures of ~16˚C for both the early and middle Eocene, whereas benthic foraminifera indicate a ~5˚C cooling. However, the early Eocene planktic foraminifera at Site 401 might also be biased to colder temperatures by diagenesis, especially in the mixed layer, for example *Acarinina* test wall cross section (Bornemann et al., 2016, p.133) does not show the clear lamellar wall structure expected of very well preserved foraminifera (e.g., Pearson et al., 2001).

Reconstructions of early Eocene North Atlantic seasonality are on the order of ~4˚C (Andreasson and Schmitz, 2000), with summer SSTs ~26˚C and winter SSTs ~22˚C, similar to the range of reconstructed temperatures from *A. bullbrooki* at Site 16/28-sb01. However, *A. bullbrooki* at Site 16/28-sb01 might be slightly biased to higher temperatures by lower salinities, as discussed in Section 3.4.3, part C, theoretical bias of slight changes of $\delta^{18}O_{SW}$ is given on p.86. The fact that *Acarininas* only occur in U2 when bulk $\delta^{18}O$ values are closer to the KT/S target curve (and thereby closer to normal Atlantic salinity) might imply that the bias is actually not very high. But without a further proxy like Mg/Ca or clumped isotopes the exact salinity cannot be estimated for Site 16/28-sb01.

The $\delta^{18}O$-derived SSTs of ~27˚C in the early and ~17˚C in the middle Eocene, as well as surface water-cooling of ~10˚C, at Site 16/28-sb01, are large in comparison to published records (Hollis et al., 2012, Inglis et al., 2015, Bornemann et al., 2016, Cramwinckel et al., 2018, Hollis et al., 2019, Crouch et al., 2020). Potential reasons for this are discussed below. Possible explanations include: A) that the preservation of foraminiferal calcite in the Rockall Basin is better than at other sites estimating SSTs from foraminifera $\delta^{18}O$ (e.g. DSDP Site 401 (Bornemann et al., 2016)), B) the Rockall Basin surface waters had lower salinities during the early Eocene, and thus records too warm SSTs, exaggerating apparent cooling (see Section 3.4.3,C), C) U1 and U2 are deposited at shallow (~300 m) water depths beneath a highly stratified water column, which might be locally warmer than more open marine settings like DSDP Site 401, and D) diagenetic differences in foraminiferal calcite preservation between the early and middle Eocene at Site 16/28-sb01, specifically more chemically altered specimens in the middle Eocene.

First, to test if differences in diagenesis caused the large cooling signal at Site 16/28-sb01, the metadata recorded on foraminiferal preservation and test weight based on sample analyses for stable isotopes were considered. In the middle Eocene, a low surface-deep $\delta^{18}O$ gradient with higher weights per measured planktic foraminifera (per specimen: *A. bullbrooki* U3: ~13 µg; U2: ~10 µg and U1: ~14 µg; *S. eocaena:* U3: 16 µg; U2: 7 µg and U1: 18 µg) could hypothetically indicate infilling and overgrowth, biasing $\delta^{18}O$ values towards bottom water temperatures (BWT). However visual

preservation (Appendix 004 and 007) is recorded as similar between the early and middle Eocene. In general *A. bullbrooki* are less well preserved than *S. eocaena*. If infilling and/or overgrowth is the cause of the slightly higher test weight in the middle Eocene, it should have resulted in artificially lower temperatures especially for *A. bullbrooki* in the middle Eocene, and an overly large temperature shift between the early and middle Eocene. However, the test weight difference is ~3 µg or ~30 % in *A. bullbrooki* between the early and middle Eocene and the overgrowth or infilling consisted often of pyrite. If the weight difference was caused by diagenetic carbonate it might have contributed to the big SST shift, but this should have resulted in an even stronger temperature shift of the thermocline dwelling *Subbotinas,* which show an increase of ~9 µg from early to middle Eocene. *Subbotinas* are more susceptible to dissolution (as outline in section 3.4.3., D) preservation p. 109 onwards) and therefore should display a temperature shift as big as or bigger than *Acarinina* which is not the case. So preservation is ruled out to be the major factor of the 10˚C SST shift of *A. bullbrooki* from early to middle Eocene.

On a global scale, the early Eocene data of Site 16/28-sb01 are consistent with proxy compilations that indicate a reduced latitudinal SST gradient and high levels of CO_2 forcing (Lunt et al., 2012, Hollis et al., 2019), (Figure 3.15., Figure 3.16.). Within the most recent compilation of carbonate proxy based SST estimates from Hollis et al. (2019), (Figure 3.16.), Site 16/28-sb01 is the northern most record available for the EECO. The surface dwelling *A. bullbrooki* record gives similar values to Sites at similar latitudes and confirms reduced latitudinal gradients implied by other proxy records in the early Eocene (Hollis et al., 2019). The subsurface temperature record from *S. eocaena* gives similar values to recrystallized mixed-layer $\delta^{18}O$ SST from nearby sites, supporting the interpretation that these other sites have a diagenetic cool-bias (see unfilled boxes for recrystallized temperature estimates in Figure 3.16. (e.g., Site Lodo G, DSDP 401, DSDP 577).

Over the early-middle Eocene, the thermocline dweller *S. eocaena* indicates thermocline sea water cooling of ~3.6˚C from ~18.8˚C, to ~15.2˚C and is consistently slightly warmer than the benthic *N. truempyi,* which gives bottom water temperatures of ~14.0˚C and ~11.3˚C, and a cooling of ~2.8˚C. Considering the surface to bottom water temperature gradient, the water column in the early Eocene Rockall Basin at

Site 16/28-sb01 was more stratified (gradient ~13˚C) than in the middle Eocene (gradient ~6˚C). From the mixed layer to the thermocline the gradient was ~7˚C in the early Eocene, and ~2˚C in the middle Eocene. The difference in-between subsurface to bottom water in the early Eocene is ~5˚C and in the middle Eocene ~4˚C and therefore changes are only minor in the subsurface stratification.

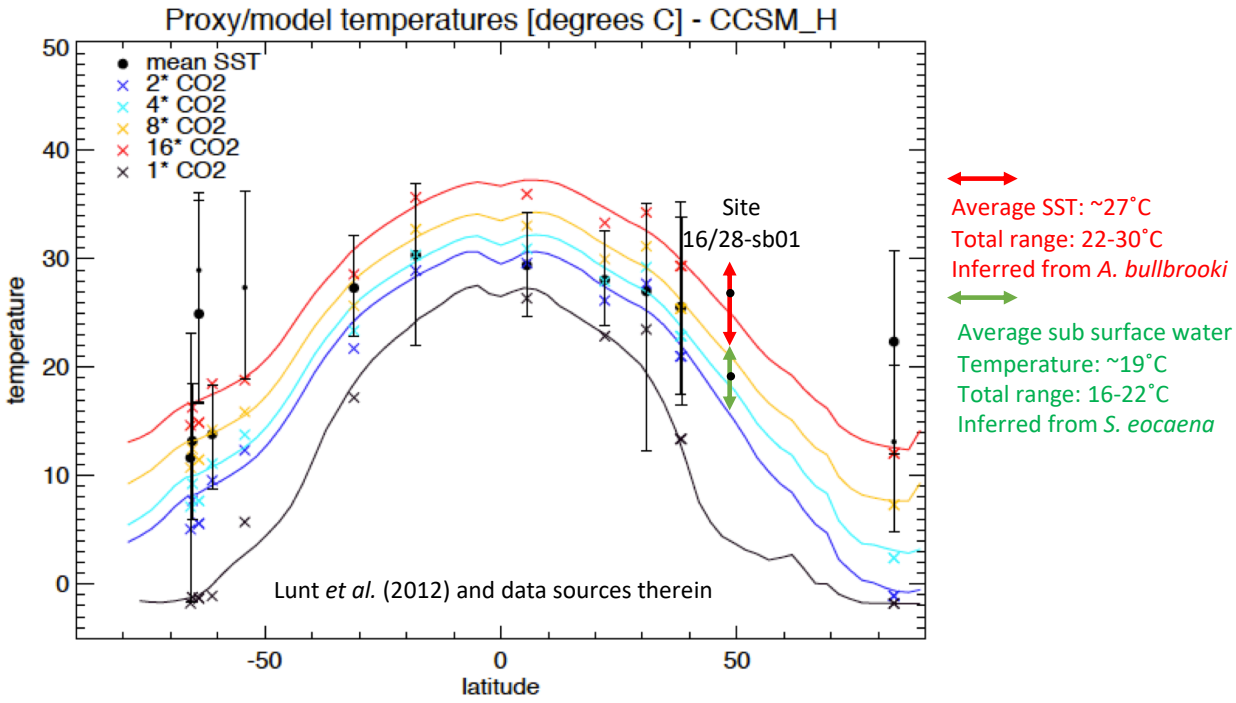

Figure 3.15. Figure modified after Lunt et al. (2012) showing modeled SST with different pCO_2 forcings (Lunt et al., 2012), [represented by lines (represent zonal mean) and x (modelled temperature at the same location as the proxy data] compared to available proxy data for the mean Eocene (big filled dots) and the EECO (Early Eocene Climate Optimum; represented by small filled dots). For the northern and southern latitudes, the proxy data show much warmer temperatures as recovered in the model data. Which would imply a reduced T-gradient between the poles to the equator. At Site 16/28-sb01 from the EECO surface temperatures are inferred from *A. bullbrooki* and represented in red double arrow — with an average of ~27˚C and the subsurface temperatures inferred from *S. eocaena* are displayed with a green double arrow with an average of ~19˚C.

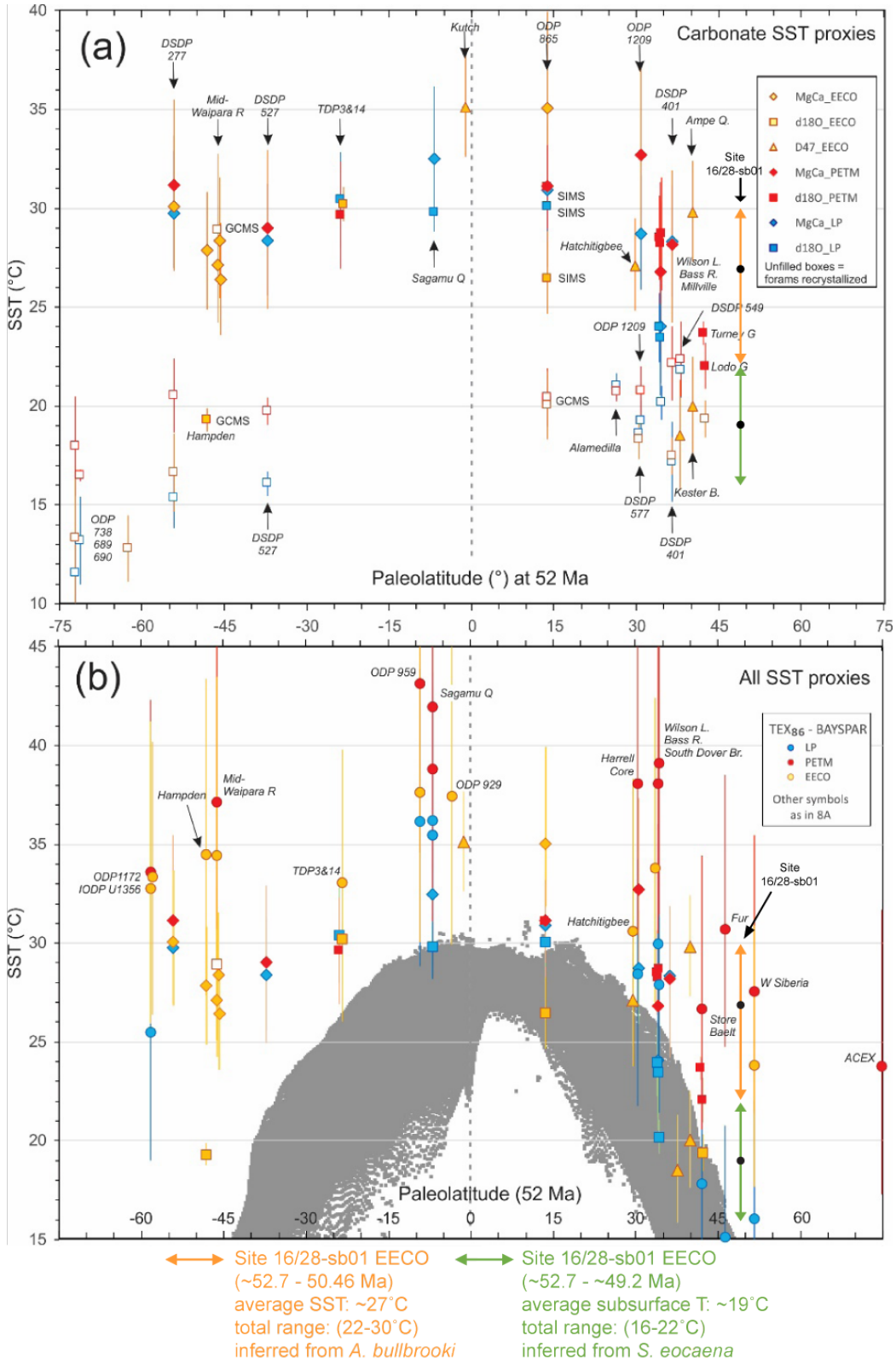

Figure 3.16. Modified after the proxy compilation from (Hollis et al., 2019, and references therein). With the surface and subsurface data from Site 16/28-sb01 integrated, indicated with for surface dwellers orange double arrow, and subsurface dweller green double arrow, the mean EECO temperature for each is indicated by a black dot on each double arrow. The grey data cloud represents the modern SST latitudinal temperature gradient, derived from the European Centre for Medium-Range Weather Forecasts (2017), ERA5 Reanalysis Monthly Means data.

3.5 Conclusions

To address SST proxy gaps in the northern hemisphere and test the inferred reduced temperature gradient in the EECO, Site 16/28-sb01 from the Rockall Basin in the North Atlantic (49˚N) is used to generate new foraminiferal species-specific stable isotope records. In general, planktic foraminiferal ecology from Site 16/28-sb01 is comparable to other Eocene ecologic studies, with *Acarinina* and *Morozovella* occupying the mixed layer and *Subbotina, Guembelitroides, Globoturborotalita, Catapsydrax* and *Pseudohastigerina* an intermediate habitat. Evidence is found in this study that the depth habitat of *Pseudohastigerina* is possibly not static through the Eocene as found in previous studies. One noticeable exception found in this thesis is *Globoturbortalita bassriverensis*, which either has a deeper water depth habitat in the middle Eocene at Site 16/28-sb01 than other studies, or is possibly a morphotype of *Subbotina* at Site 16/28-sb01.

The $\delta^{18}O$ data from mixed-layer planktic foraminifera at Site 16/28-sb01 are consistent with a reduced global SST gradient during the EECO, with average SSTs around ~27˚C and a 10˚C cooling to the middle Eocene, the thermocline dwellers indicate a ~4˚C cooling and the benthic foraminifera indicate a ~3˚C cooling. These temperatures are comparable to estimated temperatures and temperature shifts from other records. However, they might be slightly biased to higher temperatures in the early Eocene by restricted Rockall Basin circulation, leading to periods with lower salinities and elevated nutrients, interlinked with variability in hydrological cycle intensities. The reconstructed early Eocene CIEs show no systematic patterns with foraminiferal abundances or species, foraminiferal $\delta^{18}O$ values and “cenospheroid” radiolarian abundances confirming the complex nature of this lesser known carbon-cycle perturbations as postulated from the XRF data in Chapter 2 at Site 16/28-sb01.

4 EARLY AND MIDDLE EOCENE SST RECORD BASED ON TEX_{86} FOR SITE 16/28-SB01

4.1 Introduction

In addition to $\delta^{18}O$, one commonly used SST palaeoproxy in the Eocene is the relative distribution of the isoprenoid Glycerol dialkyl glycerol tetraether (GDGT) lipids, using the tetraether index of tetraethers consisting of 86 carbons (TEX_{86}) relationship to infer SSTs (Schouten et al., 2002, Schouten et al., 2013, Inglis et al., 2015, Cramwinckel et al., 2018). The isoprenoid GDGTs (isoGDGTs) are specialized membrane lipids forming a monolayered cell membrane (opposed to the more generally found bilayered cell membranes), composed of isoprenoids ether-bound to glycerol (opposed to the fatty acids ester-bound to glycerol found in bilayered membranes) and are found in several groups of prokaryotic Archaea (e.g., Schouten et al., 2013, for review). Non-extremophile sourced isoGDGTs, which are found predominantly in lakes and the sea (Karner et al., 2001, Pester et al., 2011), are derived from the Archaea phylum: Thaumarchaeota (formerly part of the Crenarchaeota phylum) (Brochier-Armanet et al., 2008, Spang et al., 2010, Pester et al., 2011). Within the isoGDGT, crenarcheol contains one additional cyclohexane ring (Sinninghe Damsté et al., 2002), (Figure 4.1.). The other isoGDGTs have variable numbers of cyclopentane rings (De Rosa and Gambacorta, 1988), with the number of these rings providing a naming convention (see Figure 4.1., for more detail and exemptions, from Schouten et al. (2013)).

In addition to isoGDGTs, branched GDGTs (brGDGTs) are commonly detected in terrestrial and shallow marine sediments, (Figure 4.1.) (Sinninghe Damsté et al., 2000, Weijers et al., 2006a). These brGDGTs are also ether bound (Sinninghe Damsté et al., 2000), but unlike the isoGDGTs the isoprenoid alkyl units consist of branched carbon chains, which are typically synthesized by bacteria (Weijers et al., 2006a), (Figure 4.1.). The brGDGTs have cyclopentane moieties with a stereochemistry in the opposite direction to isoGDGTs, again a typical signature of bacterial production (Weijers et al., 2006a), and are thought to be sourced from anaerobic bacteria (Weijers et al., 2006a), likely from the phylum Acidobacteria (Sinninghe Damsté et al., 2011). BrGDGTs are

predominantly found in terrestrial environments (soils and peats) (Weijers et al., 2006a, Weijers et al., 2007), but can be transported by rivers to shallow marine sites (e.g., Zell et al., 2014).

Molecular modelling indicates that increasing numbers of cyclopentane moieties in a cell membrane increase its negative charge, the degree of membrane packing and the stability of the membrane (Gabriel and Chong, 2000). Today it is quite well established that the cyclopentane rings in the membranes containing GDGTs increase with increased environmental stress, mainly correlated with increasing growth temperature and with decreasing pH (De Rosa et al., 1980, Gliozzi et al., 1983, De Rosa and Gambacorta, 1988, Uda et al., 2001, Schouten et al., 2002, Uda et al., 2004, Wuchter et al., 2004, Pearson et al., 2008, Boyd et al., 2011, Kaur et al., 2015). This is the basis of using relative isoGDGTs distribution, in the mesophilic environment of the oceans and lakes, to reconstruct SSTs, and a good correlation between GDGTs abundances and SST has been shown in core-top and mesocosm studies (e.g., Schouten et al., 2002, Wuchter et al., 2004, Schouten et al., 2007) with much less influence from pH in the marine realm compared to extremophile habitats (Schouten et al., 2002, Schouten et al., 2013, for review).

The correlation of relative GDGTs abundances with SST uses the TEX_{86} index (Schouten et al., 2002):

$$\mathrm{TEX}_{86} = \frac{([\mathrm{isoGDGT-2}]+[\mathrm{isoGDGT-3}]+[\mathrm{cren.isomer}])}{([\mathrm{isoGDGT-1}]+[\mathrm{isoGDGT-2}]+[\mathrm{isoGDGT-3}]+[\mathrm{cren.isomer}])} \quad (1)$$

Several calibrations of TEX based-SST have been proposed: the first one was a linear calibration based on modern marine sediment core tops (Schouten et al., 2002), which was updated with an enhanced global core top dataset within which a linear relationship held only between 5 to 30˚C (Kim et al., 2008). Revised calibrations of the proxy were then proposed, with $\mathrm{TEX}_{86}^{\mathrm{L}}$ index recommended for the polar ocean and SSTs below 15˚C, whilst $\mathrm{TEX}_{86}^{\mathrm{H}}$ was recommended for SST greater than 15˚C (Kim et al., 2010). Whilst the Kim et al. (2010) $\mathrm{TEX}_{86}^{\mathrm{H}}$ change TEX_{86} by taking the base 10 logarithm Liu et al. (2009) use the reciprocal value ($1/TEX_{86}$) prior to their temperature calculation, both is done to flatten the calibration slope in each calibration. An alternative approach has used inter-comparisons between multiproxy SST records from the Eocene to develop a “palaeo-calibration” called $pTEX_{86}$ (Hollis et al., 2012).

One caveat of using $\mathrm{TEX}_{86}^{\mathrm{H}}$ and $\mathrm{TEX}_{86}^{\mathrm{L}}$ in ancient sediments is that, although calibrated to SSTs, the dominant depth habitat of Thaumarchaeota is relatively poorly known and could have changed through time and with environmental change, introducing potential bias in SST calculations, although this is found to be a minor issue in shallow marine sites (Taylor et al., 2013). The other downside of the most commonly used $\mathrm{TEX}_{86}^{\mathrm{H}}$ (Kim et al., 2010) is that it does not consider abnormal modern core-top values obtained in the restricted basin of the modern Red Sea, which are assumed to be caused by endemic Thaumarchaeota, and are likely important for constraining GDGT production in warmer times, like the Eocene, with potential higher evaporation (e.g., Kim et al., 2008, Trommer et al., 2009, Inglis et al., 2015). Liu et al. (2009) had included the Red Sea dataset, however this enhances their calibration error to +-3.7˚C compared to $\pm$2.5˚C for the $\mathrm{TEX}_{86}^{\mathrm{H}}$ calibration (Kim et al., 2010). A newer approach includes the Red Sea data into the calibration data set and uses linear Bayesian analysis (BAYSPAR), to determine best-fit calibration parameters based on either geographic proximity or similarity of TEX_{86} values (Tierney and Tingley, 2014, Tierney and Tingley, 2015). Work continues on GDGT-based SST calibrations but for the purpose of this thesis, and to provide cross-comparison to existing studies (e.g., Inglis et al., 2015, Cramwinckel et al., 2018), in this thesis the most commonly used proxy form, $\mathrm{TEX}_{86}^{\mathrm{H}}$ is applied and is compared to BAYSPAR and the 1/TEX86 .

The benefits of isoGDGTs as SST proxy are that it is thought to be independent of marine salinity changes (Wuchter et al., 2004, Elling et al., 2015). Therefore, the TEX reconstructed SSTs might be used to reconstruct an independent estimate of $\delta^{18}O_{SW}$ to estimate any potential salinity influence on planktic foraminiferal derived $\delta^{18}O$ SSTs (Hollis et al., 2019). TEX_{86} can however be biased by seasonality (e.g., Herfort et al., 2006), sediment maturity (Schouten et al., 2004) and by changes in the dominant depth habitat of the Thaumarchaeota (e.g., Taylor et al., 2013), as well as the uncertainty in the contribution of terrestrial produced isoGDGTs (see BIT index next paragraph), see Schouten et al. (2013), for review.

Additional to SST reconstructions, GDGTs are used in shallow marine environments as proxies to trace the influx of riverine terrestrial organic matter (Hopmans et al., 2004, Peterse et al., 2009), soil pH and annual mean air temperature (MAT) (Weijers et al.,

2007, Peterse et al., 2012, De Jonge et al., 2014). The branched and isoprenoid tetraether (BIT) index (Hopmans et al., 2004) measures how much terrestrial organic material was supplied relatively to the marine site. The BIT is based on the predominant occurrence of brGDGTs in soils and peats and crenarchaeol dominantly in the marine environments (Hopmans et al., 2004, Schouten et al., 2013, for review). The BIT index is therefore theoretically found to be close to 1 in soils and peats, indicating lack of crenarchaeol, and close to 0 in open marine settings, indicating lack of brGDGTs and variable in the coastal areas (Hopmans et al., 2004). A study suggested that GDGT-based SST might be biased by the input of terrestrial material if the BIT index is higher than ~0.3, due the production of crenarchaeol in soils, which, with a substantial soil-derived contribution in a marine environment could bias reconstructed SSTs (Weijers et al., 2006b).

There is uncertainty connected to each sea surface temperature (SST) proxy, as was discussed in detail in the previous Chapter for planktic foraminiferal $\delta^{18}O$. The motivation of this Chapter is to present an additional SST proxy — based on TEX_{86} index within Rockall Basin Site 16/28-sb01 sediments — that is completely independent to the planktic foraminiferal $\delta^{18}O$ SSTs. Through the comparison between TEX_{86} and planktic foraminifera $\delta^{18}O$ SST estimates the aim is to improve the robustness of SST reconstructions from the early and middle Eocene of the Rockall Basin.

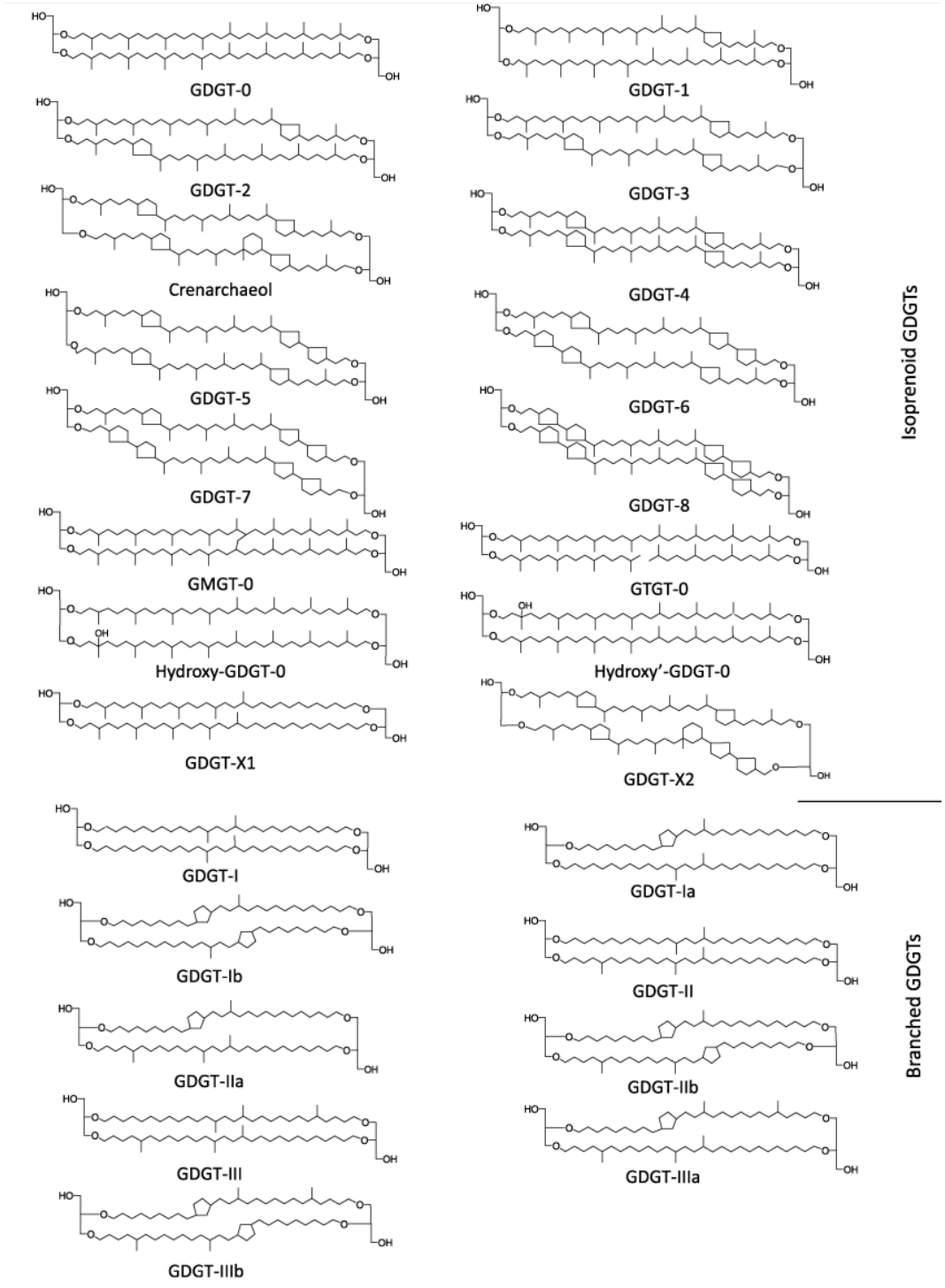

Figure 4.1. The variable stereochemical structure of the isoprenoids and branched Glycerol dialkyl glycerol tetraethers (GDGTs) taken from *Schouten et al. (2013)*.

4.2 Methods GDGT and TEX analysis

To reconstruct SST from GDGTs it was necessary to extract all the organic components from the marine sediment samples. In this study, these extractions were undertaken on 97 of the original 99 pilot sediment samples halves from Site 16/28-sb01, of which one half was used for the foraminiferal analysis (previous Chapter, Section 3.2). For these samples, all the available bulk material was used (15.9 – 5.1 g) to extract the organics, (Appendix 008, Table 3). A second sample batch was also extracted from the collected fine fraction (< 63 μm) of samples that were washed with deionized water (see Section 3.2). Eleven of the total of 238 fine fraction residues were used in this study to extract organics, the fine fraction of the remaining 227 being kept in storage for future studies. For both the fine fraction residues and the whole sediment halves the same method for extracting the organics was followed. The 97 pilot samples were extracted into four fractions N1 to N4 by Bethany Chamberlain, a technician, under the supervision of Dr. Heiko Moossen at the University of Birmingham prior to and at the beginning of this project, with the further 11 fine fraction samples were extracted as part of this study. For all samples ultrasonic extraction coupled with silica gel column chromatography was used (e.g., Schouten et al., 2013, for review). All freeze dried 108 samples were homogenized and the sample dry weights are given in Appendix 008, Table 3. To extract the organic components four steps of solvent dichlormethane (DCM):methanol (MeOH) (3:1,v/v) extraction coupled with ultrasonication was used. In the first step 20 ml DCM:MeOH (3:1,v/v) was added to the homogenized sediment in a 30 ml test tube and brought into solution by vortexing followed by 20 minutes of ultrasonication. To get optimal extraction this solution was kept for 1 h at 40˚C and was added to the centrifuge (1000 reps/min) for 3 min. The supernatant was pipetted off and kept in a 100 ml test tube. This step was repeated for three times with 10 ml DCM:MeOH (3:1,v/v). The collected supernatant with all the organic components still contained the added DCM and MeOH, which needed removing before analysis. This was achieved using a Buechi Sycore (Polyvap) connected to a Buechi Vaccum pump V-700, set to 40˚C, 250 rpm and a pressure of 850 mbar for DCM and 200 mbar for MeOH. The remaining extracted organic compounds were then transferred into a small screw top glass container using DCM

and MeOH, followed by nitrogen drying. The dry weight of this total lipid extract (TLE) was recorded, (Appendix 008, Table 3), which varied from 0.001 – 0.1 g. The TLE was further separated by silica gel column chromatography into four fractions N1 – N4. Silica columns were cleaned prior by use with 3 ml of Hexane. To split the TLE into four fractions N1 – N4: 4 ml hexane [N1; aliphatic fraction]; 2 ml 2:1 hexane:DCM [N2, aromatic fraction]; 4 ml DCM [N3; aldehydes and ketones] and 5 ml MeOH [N4; polar fraction containing GDGTs] were used and collected separately, followed by nitrogen drying. Afterwards each fraction was transferred using hexane for N1 and N2 and DCM for N3 and N4. To store these fractions, they were dried after this step, N1 to N3 were kept for future studies. N4, the polar fraction that contains the GDGTs, was use in this study. In a last step, after redissolution in 500 µl 99:1 hexane:isopropanol (IPA), all of the 108 N4 fractions were filtered through 0.45 µm; 4 mm diameter polytetrafluorethylene (PTFE) filters to remove the coarsest particles, and then dried and stored in 200 µl insets in the fridge.

All 108 N4 fractions were sent to the National Environmental Research Council (NERC) Life Science Mass Spectrometry Facility (LSMSF) in Bristol to analyse the relative GDGT abundances, following Hopmans et al. (2016). Samples were run over the period February to April 2017 by their technician Hanna Gruszczynska with the help of Dr David Naafs under the lead of Dr Ian Bull. The analysis was undertaken using high performance liquid chromatography-atmospheric pressure chemical ionisation - mass spectrometry (HPLC-APCI-MS), using a HPLC-APCI ThermoScientific TSQ Quantum Access triple quadruple MS connected to an Acela pump and Acela autosampler. All 108 samples were re-dissolve in 100 µl HPLC grade hexane:IPA (99:1 vol/vol, Rathburn) prior to analysis and then singly injected. Where a repeat was necessary only 80 µl was used, due to the low amounts of organics in the samples of Site 16/28-sb01, especially in U3. 80 µl is the minimum for the autosampler needle to inject the 15 µl needed for analysis.

Normal phase separation was achieved by using two silica columns (Aquity UPLC BEH HILIC columns, length 150 mm x ID 2.1 mm; particle size: 1.7 µm; pore size: 130 Å, Waters) coupled with a guard cartridge and maintained at 20˚C, after Hopmans et al. (2016). The HPLC pump was run at a constant flow rate of 200 µl/min, with a maximum back pressure of 300 bar. The two silica columns are coupled to enhance the run

length of the chromatography and therefore obtain better separation of all the previously very closely eluting GDGT peaks especially important for crenarchaeol and its isomere (Hopmans et al., 2016). These two silica columns are the stationary phase, with mobile phases of A) hexane and B) hexane:IPA (90:10 vol/vol, Rathburn). A 15 µL aliquot of each sample was injected via the autosampler and the separation was performed by applying a gradient elution: which means that the proportions of the mobile phases change over the run. Within the total runtime the system runs for 25 minutes isocratic with 82 % A and 18 % B, for the next 25 minutes it changes with a linear gradient to 65 % A and 35 % B and then for 30 minutes it changes with a linear gradient gradually to 0 % A and 100 % B. At the end of each run, the system re-equilibrates to starting conditions of 82 % A and 18 % B for ten minutes. Prior to the next injection, the whole system is cleaned, by running a wash for 45 minutes consisting of an injection of 25 µl hexane:IPA (99:1 vol/vol, Rathburn), which also rinses the autosampler needle.

After passing the columns the most non-polar of the analysed component will elute first and the most polar (in this case the branched GDGTs elute later) components will elute last. A nitrogen nebulizer was used (vaporizer temperature was set to 300˚C) and one of the quadruple analysers was used for detection. The machine was set to SIMQ1MS, which means selected ion monitoring (SIM) within a positive ion mode and was used to monitor abundance of the $[M+H]^+$ ion (protonated molecular ion) of the different GDGTs instead of full-scan acquisition in order to improve the signal-to-noise ratio and therefore yield higher sensitivity and reproducibility. The machine was only looking for certain mass/charge (m/z) ranges to detect compounds. SIM parameters were set to detect the protonated molecules of isoprenoid and branched GDGTs (using m/z 653 to 1302), with a dwell time, which is the time the MS spends on scanning one ion, of 0.234 s per ion.

Table 4.1. Summarized are the mass/charge ranges used to detect the different GDGTs in the selected ion monitoring.

	m/z values
Isoprenoid GDGTs	1302, 1300, 1298, 1296, 1294, 1292
Branched GDGTs	1050, 1048, 1046, 1036, 1034, 1032, 1022, 1020, 1018, 744, 653

GDGT peaks were integrated manually using Xcalibur software (Version 2.0; ThermoScientific) within this study, (Appendix 008). From the 108 samples data of 78 samples could be obtained. No internal standard — for the quantification of absolute amounts of GDGTs in the sample — was used. External standards — one marine and one peat — were run in a sequence for every 7 samples and integrated in the same way as the unknowns. In-house generated standard solutions were measured daily to assess system performance. Analytical precision (standard deviation, σ) is based on repeat analyses of in-house standards following the same analytical sequence as the samples and measured over the same period.

In this thesis $\mathrm{TEX}_{86}^{\mathrm{H}}$ (Kim et al., 2010) is used with a calibration error of ±2.5˚C, as it is the most commonly and widely used method for temperatures above 15˚C and thereby easiest to compare to other publications. The log of the original TEX_{86}, equation 1 (Schouten et al., 2002) is used in Kim et al. (2010) for $\mathrm{TEX}_{86}^{\mathrm{H}}$ (equation 1 and 2) to calculate their SST-H (equation 3). For comparison the calibration of Liu et al. (2009)(equation 3.1) and BAYSPAR (Tierney and Tingley, 2014, Tierney and Tingley, 2015) are used additionally to give SSTs. To reconstruct BAYSPAR temperatures, the "deep-time" of the matlab script (from: https://figshare.com/collections/A_TEX86_surface_sediment_database_and_extended_Bayesian_calibration/1348830) is used, which searches for similar TEX_{86} values rather than closest geographic location, the 5th, 50th (mean temperature estimate) and 95th percentile is given in Appendix 008, Table 4. All the peak integration data for each GDGT is available in Appendix 008, allowing for the calculation of all existing GDGT-based SSTs as required, as recommended for publication in Hollis et al. (2019).

$$\mathrm{TEX}_{86}^{\mathrm{H}} = \log\left(\mathrm{TEX}_{86}\right) \qquad (2)$$

$$\mathrm{SST} - \mathrm{H} = 68.4 * \mathrm{TEX}_{86}^{\mathrm{H}} + 38.6 \qquad (3)$$

$$\mathrm{SST} - \frac{1}{\mathrm{TEX86}} = 50.475 - 16.332 * \left(\frac{1}{\mathrm{TEX}_{86}}\right) \quad (3.1)$$

The BIT index is calculated following equation 4 (Hopmans et al., 2004).

$$\mathrm{BIT\ index} = \frac{([\mathrm{brGDGT-1}]+[\mathrm{brGDGT-2}]+[\mathrm{brGDGT-3}])}{([\mathrm{Crenarchaeol}]+[\mathrm{brGDGT-1}]+[\mathrm{brGDGT-2}]+[\mathrm{brGDGT-3}])} \qquad (4)$$

For a quality check of the GDGT distribution within the discussion of this Chapter it is tested for typical Red Sea distribution using the $\%GTGT_{RS}$, equation 5 (Inglis et al.,

2015), values of greater than 30 are indicative of atypical and possibly Red Sea type distributions.

$$\%GDGT_{RS} = \left(\frac{[Crenarchaeol']}{([GDGT-0]+[Crenarchaeol'])}\right) * 100 \qquad (5)$$

Further the Methane index (MI) (Zhang et al., 2011), equation 6, is used to evaluate if there was a influence of higher methanotrophic Euryarchaota in the sediments, which indicate higher abundances of GDGT-1, -2 and -3 over crenarchaeol.

$$MI = \frac{([GDGT-1]+[GDGT-2]+[GDGT-3])}{([GDGT-1]+[GDGT-2]+[GDGT-3]+[Crenarchaeol]+Crenarchaeol'])} \qquad (6)$$

All calculated SSTs from for $\mathrm{SST-H}$, SSTs from 1/TEX86 are given in Appendix 008, Table 4, as well as the BIT, $\%GDGT_{RS}$ and MI.

4.3 Results

4.3.1 TEX_{86}, BIT and SST reconstruction

The new results for TEX_{86}, SST-H and the BIT index are shown in Figure 4.2.1., and an average for each lithological unit of Site 16/28-sb01 is given in Table 4.2.1. The mean TEX_{86} value across all samples is ~0.71, with a minimum of 0.61 and a maximum of 0.83. The mean BIT index value is ~0.36 with a minimum of 0.17 and a maximum of 0.49. Within U1 only one BIT value could be calculated and within U3 no BIT index could be established as brGDGT were not detected or the peaks were too small to identify and integrate. The isoGDGTs in the middle Eocene U3 result in weak peaks and are also difficult to integrate; they failed in the first run and the diluted second run recorded even weaker signals. In the resulting data there is little variation in TEX_{86} values between the different lithological Units of Site 16/28-sb01. Reconstructed SST-H for the whole section are on average ~29˚C, with 1˚C difference in U1 and U2 (Table 4.2.1) and a standard deviation of ~1.4˚C. BAYSPAR results in ~29˚C To see if initial sample dry weight or the TLE biases BIT or TEX_{86} the ratio of TLE/dry weight is shown (Figure 4.2.1). No correlation can be seen within X-Y plots of the different components and no systematic correlation can be seen within Figure 4.2.1, with the conclusion that the main variability is caused by a primary signal of GDGT abundances within the sediments. It was postulated by Weijers et al. (2006b) that high BIT above 0.3 could bias SST-H towards terrestrial temperatures. Therefore Figure 4.3. shows a X-Y-plot

for BIT versus SST-H no systematic correlation can be seen. Therefore, no systematic bias from terrestrial input within the lower Eocene samples can be assumed. To see if the different extraction methods did have an influence on the data the fine fraction derived values are highlighted within Figure 4.2.1, they show similar values to their closest neighbour data within SST-H, BIT and TEX_{86} and it is therefore concluded that both extraction methods produce comparable results.

Table 4.2.1 Average values of the TEX_{86}, SST-H, BIT and TLE are given for the different lithological units.

Lithological units	Core depth [m]	TEX_{86}	SST-H [℃]	BIT	TLE [g]
U3	87.50 – 40.00	0.69	~28		~0.006
U2	138.00 – 87.50	0.72	~29	~0.36	~0.009
U1	145.95 – 138.00	0.73	~30	~0.16	~0.008

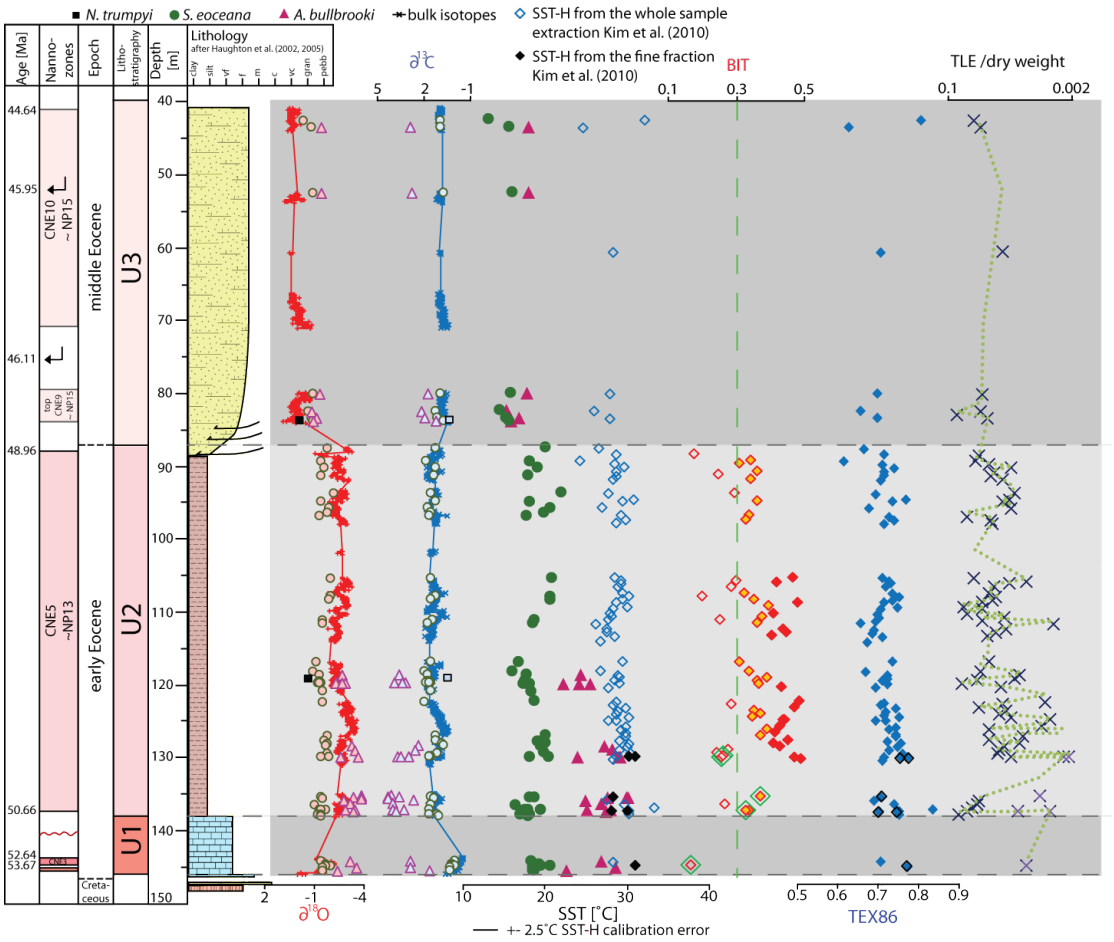

Figure 4.2.1 The lithological Units of Site 16/28-sb01 are shown with core depth and the results of the isotope results of the previous Chapters against the new results of SST-H (blue diamonds without fill; black diamonds with fill (from fine fraction)), BIT (red surrounded diamonds, green surrounded diamonds (from fine fraction), BIT below 0.3 red unfilled diamonds, BIT >0.3-<0.4 red and orange filled diamonds, >0.4 red diamonds), TEX_{86} (blue filled diamonds, black unfilled diamonds (from fine fraction)) and TLE divided by total samples dry weight (black x, purple x (from fine fraction), green dotted line moving average). The green dashed line within the BIT index shows the 0.3 limit given by Weijers et al. (2006b) over which they assume TEX_{86} reconstructed SST might be biased by soil derived isoGDGTs.

4.3.2 Different calibrations for SSTs reconstructed from GDGTs

In Table 4.2.2 the average values of SST-H (Kim et al., 2010), SST-BAYSPAR (Tierney and Tingley, 2014, Tierney and Tingley, 2015) and SST-1/TEX86 (Liu et al., 2009) are given for the different lithologic Units, in Appendix 008, Table 4 all calculated SST values for all three calibrations are given. On average the calibrations have a standard deviation of maximum 1.1 in Unit 1 and below one in Unit 2 and 3. In Figure 4.2.2 all three SST calibrations are shown against core depth and the ± 2.5˚C calibration uncertainty of SST-H and besides two values all values of SST-BAYSPAR (Tierney and

Tingley, 2014, Tierney and Tingley, 2015) and SST-1/TEX86 (Liu et al., 2009) fall within this calibration uncertainty of SST-H and therewith it is concluded that for this dataset SST-H is a reasonable calibration to be used.

Table 4.2.2 Average values for SST-H (Kim et al., 2010), SST-BAYSPAR (Tierney and Tingley, 2014, Tierney and Tingley, 2015), SST-1/TEX86 (Liu et al., 2009), MI (Zhang et al., 2011) and %GDGT-RS (Inglis et al., 2015) are given for the different lithological units.

Lithological units	Core depth [m]	SST-H [℃]	BAYSPAR [℃]	1/TEX86 -SST [℃]	MI	%GDGT-RS
U3	87.50 – 40.00	~28	~28	~27	~0.2	~15
U2	138.00 – 87.50	~29	~29	~28	~0.3	~18
U1	145.95 – 138.00	~30	~31	~28	~0.3	~17
	40.00 – 145.95	~29	~29	~28		

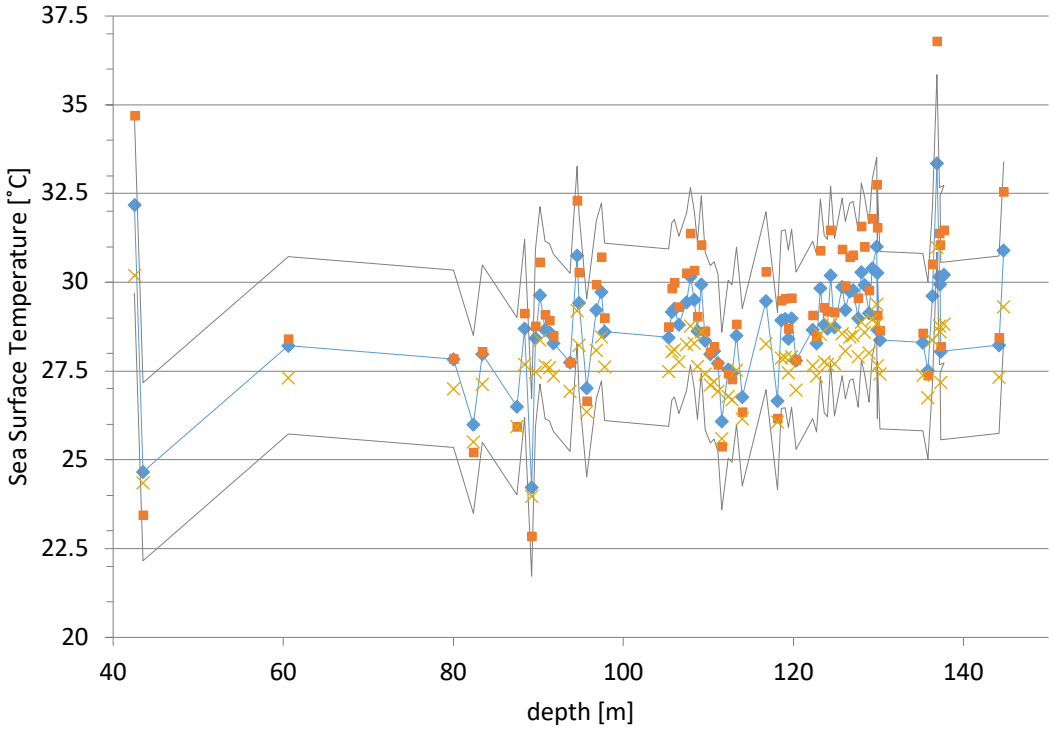

Figure 4.2.2 To highlight the calibration uncertainty in the SST-H calibration (Kim et al., 2010), which is shown with blue diamonds its uncertainty frame of ±2.5˚C (Kim et al., 2010) is given by the grey thin lines. Additionally, the calculated SSTs of BAYSPAR (orange squares) (Tierney and Tingley, 2014, Tierney and Tingley, 2015) and the SST-1/TEX86 (yellow X) (Liu et al., 2009) are shown.

4.3.3 TEX_{86}, BIT and SST-H within the CIEs of lithological Unit 2

In order to help disentangle the complex nature of the CIEs in Site 16/28-sb01, TEX_{86}, SST-H and BIT are plotted through lithologic Unit 2 alone (Figure 4.4.). SST-H reconstructions for U2 only show slight variations (standard deviation: 1.3˚C) around ~29˚C with a total range of ~24 to ~33˚C. Although the BIT index is more variable, there is no systematic correlation to the CIEs. The TLE divided by initial dry weight shows some similar fluctuations to the BIT index, but this is not consistent through the whole U2, and as crossplot of the BIT index versus dry weight or TLE show no trend, it is reasonable to conclude that there is no systematic correlation between these two variables.

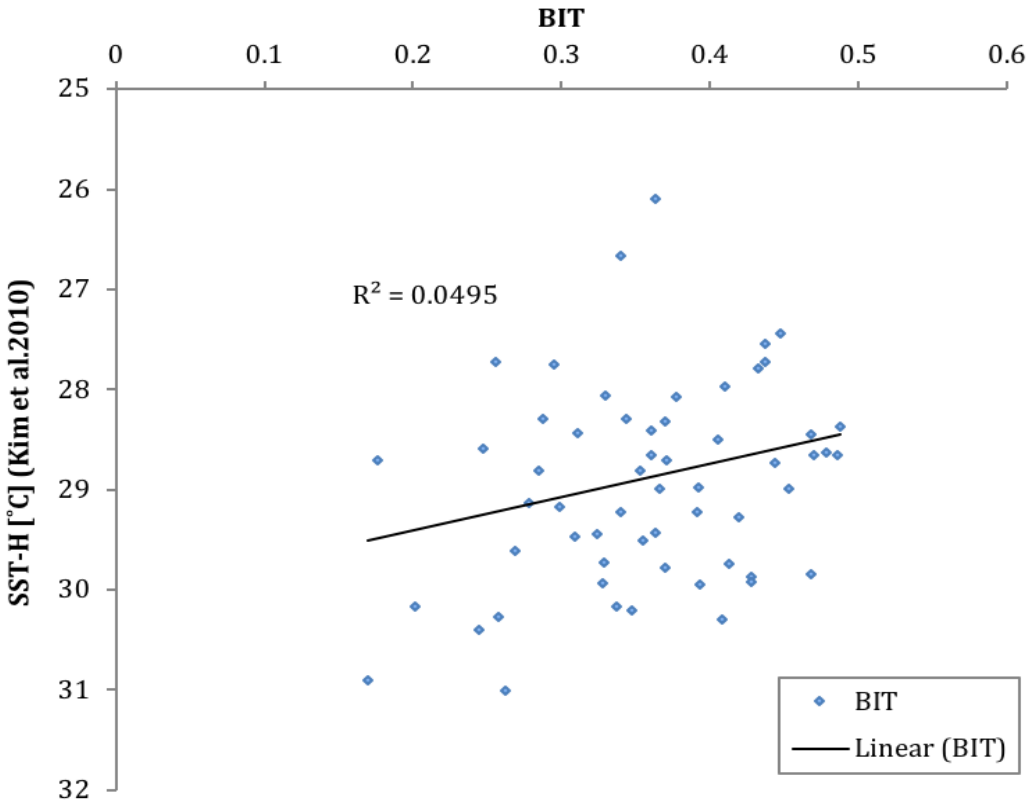

Figure 4.3. To test for terrestrial influx BIT is plotted versus SST-H, no correlation is found between BIT and SST-H.

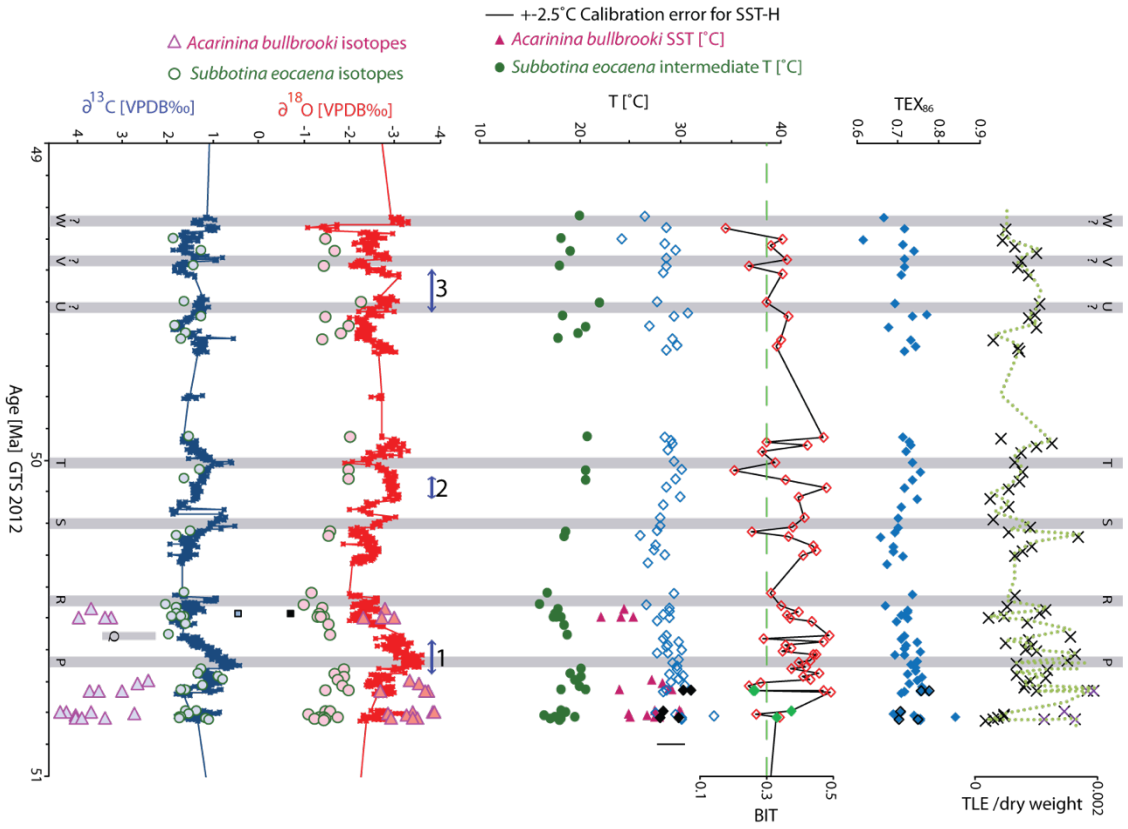

Figure 4.4.1. The CIEs of early Eocene lithologic Unit 2 of Site 16/28-sb01 are shown with age and the isotope results of the previous Chapters as well as the new results of SST-H (blue diamonds without fill; black diamonds with fill from fine fraction), BIT (red unfilled diamonds, green filled diamonds from fine fraction), TEX_{86} (blue filled diamonds, black unfilled diamonds from fine fraction) and TLE divided by total samples dry weight (black crosses, purple crosses from fine fraction; green dotted line moving average). The green dashed line within the BIT index shows the 0.3 limit given by Weijers et al. (2006b) over which they assume TEX_{86} reconstructed SST could be biased by soil derived isoGDGTs. Blue double-arrows labelled 1, 2 and 3 represent the interpreted surface dweller gaps of planktic foraminifera from Chapter 3.

4.4 Discussion

4.4.1 General trends in TEX_{86}, SST-H and BIT

Examining the variation in BIT across the different units, the absence of brGDGTs within U3 (middle Eocene) is in accordance with a palaeoenvironmental interpretation of a deeper-water, more open-ocean, depositional regime with less terrestrial influx during the middle Eocene. The higher BIT values within U2 indicate the stronger

terrestrial influx within the early Eocene, as already established in Chapter 2 and as discussed in Chapter 3.

There is no systematic correlation of BIT, SST-H and TEX_{86} with the interpreted CIEs within the early Eocene Unit 2, (Figure 4.4.1.). The BIT index should reflect riverine terrestrial material influx (Hopmans et al., 2004, Peterse et al., 2009), and higher BIT values are found during surface dweller gap 1 and 2, from Chapter 3. In the lithologic unit U2 the lows in the BIT index are generally accompanied by the occurrence of *Acarinina* spp.*,* and supports the discussion in Chapter 3 that links these periods with less terrestrial influx and better connectivity with the open North Atlantic (Figure 4.4.1, 4.4.2. and Figure 3.3.). From 51 Ma until the U CIE the Ca from the XRF seems qualitatively (by looking at Figure 4.4.1., 4.4.2. and Figure 2.15.) inversely correlated with the BIT index, this confirms that Ca production — mostly from marine production — in the early Eocene U2 is, for the most part, in anti-phase with riverine influx. At the younger end of the U2 this correlation weakens, and this could be explained by a fading of the hydrological dominance on the depositional regime at the end of the EECO, which is consistent with the subsiding regime at Site 16/28-sb01 through the Eocene succession, see Chapter 2.

4.4.2 SST proxy comparison from Site 16/28-sb01

In the early Eocene GDGT derived temperatures (SST-H) do on average imply SSTs which are ~2˚C warmer than SSTs derived from $\delta^{18}O$ of *Acarinina bullbrooki* (pF-SSTs (±2.8˚C (Malevich et al., 2019)), which is within the calibration error of TEX_{86}^{H} (±2.5˚C (Kim et al., 2010)), implying a good match of the two SST proxies, (Figure 4.5. and Figure 4.6.). On average for the early Eocene U2 SST-H imply ~29˚C, BAYSPAR-SSTs ~29˚C and 1/TEX86-SSTs imply ~28˚C compared to ~27˚C from pF-SSTs. Within the middle Eocene SST-H and BAYSPAR-SST are on average ~11˚C (10˚C for 1/TEX86-SST) warmer than the pF-SSTs and represent a major mismatch of the two proxies in this interval. This mismatch in the middle Eocene might be explained by A) diagenesis in planktic foraminifera, B) different distribution of GDGTs within a greenhouse world like the Eocene, C) less well detectable GDGTs within U3 and might be flawed by isoGDGTs peaks at the detection limit, D) different surface water sources in the different seasons, E) there are significant changes in surface ocean $\delta^{18}O_{SW}$ between

the early and middle Eocene caused by regional salinity changes or F) the water column stratification changes.

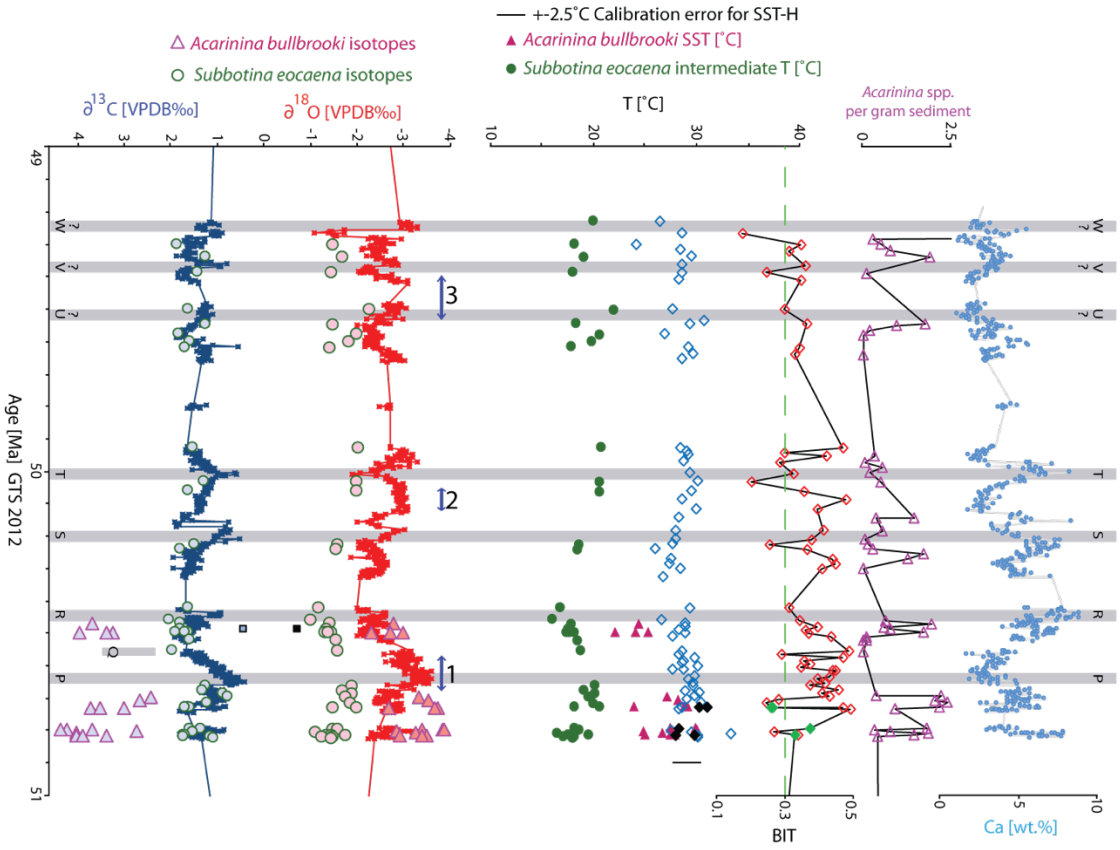

Figure 4.4.2. The CIEs of early Eocene lithologic Unit 2 of Site 16/28-sb01 are shown with age and the isotope results of the previous Chapters as well as the new results of SST-H (blue diamonds without fill; black diamonds with fill from fine fraction), BIT (red unfilled diamonds, green filled diamonds from fine fraction), *Acarinina* spp. abundance (pink triangles) and Ca (blue dots). The green dashed line within the BIT index shows the 0.3 limit given by Weijers et al. (2006b) over which they assume TEX_{86} reconstructed SST could be biased by soil derived isoGDGTs. Blue double-arrows labelled 1, 2 and 3 represent the interpreted surface dweller gaps of planktic foraminifera from Chapter 3.

A) Diagenesis in planktic foraminifera could have biased planktic foraminifera in the middle Eocene U3 towards bottom water temperatures. The reduction in the temperature gradient from *A. bullbrooki* to subsurface dweller *S. eocaena* could point towards a preservation issue. The reduction in this gradient is not matched by a similar reduction in *Subbotina* to benthic gradient, which would be expected if planktic foraminifera where undergoing overgrowth or recrystallisation which resets the whole assemblage towards benthic values. There is a slightly higher weight per specimen of *A. bullbrooki* and *S. eoceana*

in the middle Eocene, but this could be caused by primary calcification or slight dissolution in the more organic rich early Eocene sediments, as well as representing slight overgrowth in middle Eocene sediments. The visual preservation within the middle Eocene is recorded to be still very good and is unlikely to account for the whole cooling offset in-between SST-H and pF-SST. As already discussed in detail discussed in Chapter 3, Section 3.4.3.2. foraminiferal preservation is an unlikely cause for the proxy mismatch.

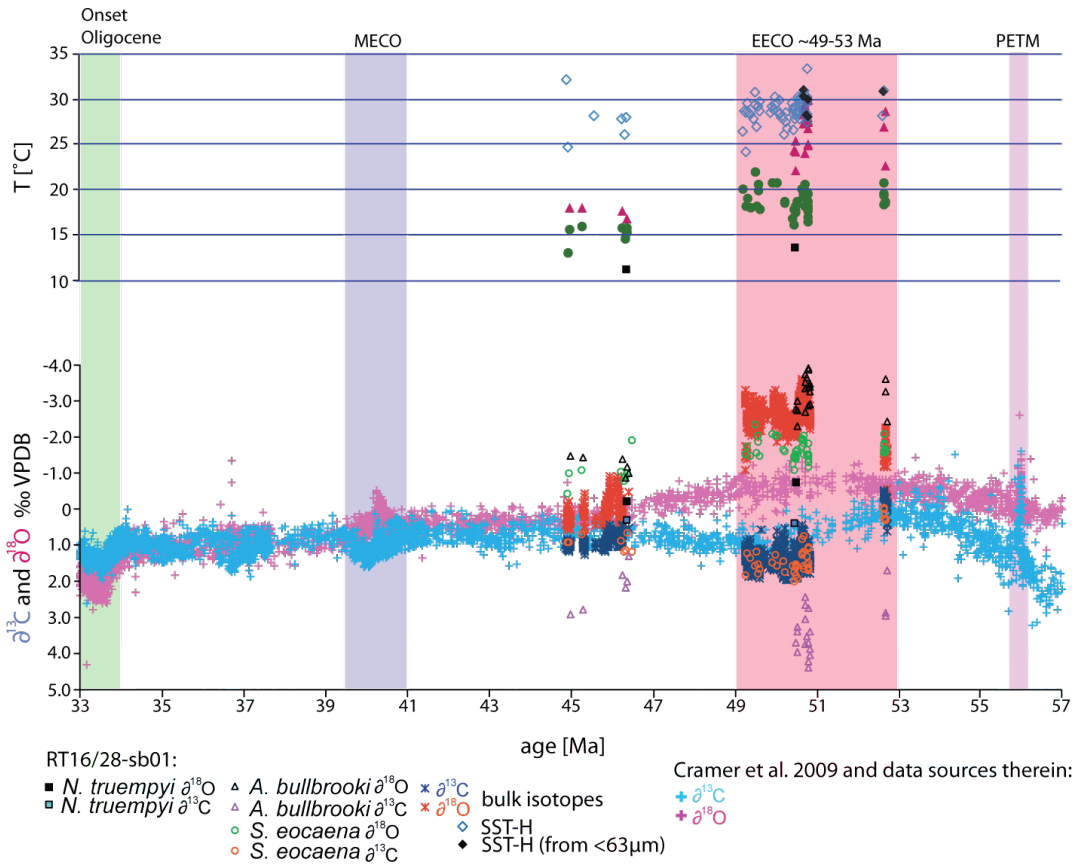

Figure 4.5. Compares the two different SST proxies with each other and them with the global benthic foraminiferal record against time.

B) In the Eocene, southern mid- to high-latitude and low-latitude sites are found to have distributions of isoGDGT typical of the modern Red Sea (Inglis et al., 2015, Crouch et al., 2020). These Red Sea type distributions are identified by having $\%GDGT_{RS}$ greater than 30, indicative of atypical GDGT-0 and crenarchaeol' distributions (Trommer et al., 2009, Inglis et al., 2015). At Site 16/28-sb01 there are only 2 samples with $\%GDGT_{RS}$ (Inglis et al., 2015) above 30, with average values of ~17 across the whole section (average ~15 in the middle and ~17 within the early Eocene). There is thus no evidence for a strong

bias from atypical Red Sea-type GDGT distributions at Site 16/28-sb01. Further, the MI index (Zhang et al., 2011), can be used to trace an enhanced influence of methane oxidation within sediments, with values above 0.3 in modern samples, as well as the impact of methane hydrates when values exceed 0.5. At Site 16/28-sb01 the MI is on average ~0.28 (total range 0.14 to 0.43). Site 16/28-sb01 has 29 samples which are slightly above 0.3 but none higher than 0.5, which indicates methane oxidation within a normal marine range, but with some values at the upper limit, which is consistent with the idea that there were periods with more nutrients within the shallow Rockall Basin, especially during U2 (see discussion in Chapter 3). On average the MI is ~0.23 in the middle Eocene compared to ~0.29 in the early Eocene of Site 16/28-sb01, consistent with this interpretation — that more nutrients in the early Eocene water column can locally produce lower oxygen conditions and enhanced anaerobic methane oxygenation.

To test if there is any bias by deeper dwelling Thaumarchaeota on SST-H a ratio of ([isoGDGT-2]/[isoGDGT-3]) was calculated (Taylor et al., 2013). Average values of this index are ~3.8 in the early Eocene and ~4.3 in the middle Eocene, which are consistent with modern production on shelf to upper slope environments (~1000 m), and supports the water depth reconstructions from Chapter 3 based on foraminifera. All three screening indices — %$GDGT_{RS}$, MI and (GDGT-2/GDGT-3) — are within "normal" tolerance for almost all samples and cannot explain the offset of SST-H to pF-SST in the middle Eocene.

C) In general, the TLE is relatively low in the middle Eocene (Table 4.2.1). All the middle Eocene samples of U3 had a standard fail in the first run and had to be rerun, but the resulting peaks were so small that it was very difficult to impossible to integrate them. So, high SSTs in the middle Eocene might be a result of low polar fraction concentrations and it is unclear if the signal detected in U3 is reflective of the contained isoGDGTs, and how this low concentration influenced reconstructed SSTs.

D) Another more speculative explanation of divergent SST records from both proxies in the middle Eocene Rockall Basin, could be caused by circulation. Two different surface water sources could be responsible. After the assumed

opening of the Greenland Scotland Ridge (GSR), one surface water source could be from the north bringing colder and more nutrient rich waters (e.g., Brinkhuis et al., 2006), in which the mixed layer planktic foraminifera might have preferably dwelled, possibly with a predominant winter influx into the Rockall Basin. And one with warmer surface waters sourced from the south, like an intermittent proto-golf-stream bringing in warm surface waters from the tropics (e.g., Pearson et al., 2007, Cramwinckel et al., 2018) in which the Thaumarchaeota dwelled, possibly with a predominant summer influx. Some evidence for influx of northern sourced water masses is given in the supplement of Brinkhuis et al. (2006) where they find *"Azolla"* remains within the Rockall Basin during the middle Eocene. Following this speculative assumption — SST-H would represent values biased to summer SSTs (e.g., Bijl et al., 2009) and lower latitudes, whereas the pF-SST would be biased towards winter SSTs and higher latitudes, thereby causing the proxy offset. However, the difference of 11˚C seems to be too big for estimated seasonality at Site 16/28-sb01 (e.g., Andreasson et al., 1996) and surface ocean water circulation in the past is difficult to constrain — therefore it might be unlikely that different surface water sources caused the middle Eocene proxy offset in the Rockall Basin, but without further Eocene SST proxy records from the Rockall Basin it cannot be excluded as an explanation.

E) Intervals of lower salinities in the early Eocene were discussed in Chapter 3 indicated by deviation of the bulk $\delta^{18}O$ value of Site 16/28-sb01 from the KT/S target curve as well as by comparison with the bulk $\delta^{13}C$ and surface-dwelling foraminiferal abundances. The uncertainty of estimating correct $\delta^{18}O_{SW}$ values in the geological past is difficult. The good match of SST-H and pF-SST in the early Eocene could imply that the value of -1.28 ‰ VPDB (including latitudinal correction of 0.12) for $\delta^{18}O_{SW}$ is a good approximation for the early Eocene surface waters at Site 16/28-sb01 with its lower salinities. The deviation of both proxies in the middle Eocene could be caused by the more open marine deeper depositional regime with normal salinities leading to a relatively higher $\delta^{18}O_{SW}$ value. If $\delta^{18}O_{SW}$ were theoretically aligned to be consistent with SST-H

this would result in average theoretical $\delta^{18}O_{SW}$ values of ~0.7 ‰ VPDB (including latitudinal correction of 0.12) for the middle Eocene based on Chapter 3, equation 1. Approximately 2 ‰ heavier than assumed in this thesis, this would be the same offset as between on average *A. bullbrooki* $\delta^{18}O$ values from U2 and U3. Therefore, the offset of SST-H to pF-SSTs in the middle Eocene might be solely related to surface salinity differences between the early and middle Eocene. Simulations of Eocene $\delta^{18}O_{SW}$ show large gradients of more than 2 ‰ in surface waters of this region of the northeast Atlantic (Tindall et al., 2010). Calculations of Eocene $\delta^{18}O_{SW}$ by Cramer et al. (2011) are found to be reasonable for the tropics and are found to be no more than 2-3 ‰ more negative for the NE European continental margin (precisely for the Hampshire, Belgium and Paris Basin) possibly influenced by local freshening there, by measuring coupled Mg/Ca and clumped isotopes Δ_{47} on large benthic foraminifera (Evans et al., 2018b). So, a local difference of 2 ‰ is generally possible. With major changes in gateway configuration between early and middle Eocene, as well as climate, it is very likely that these surface water gradients in $\delta^{18}O_{SW}$ also moved substantially and could explain the larger changes in mixed layer dwelling foraminiferal $\delta^{18}O$. These considerations suggest large changes in salinity as a potential driver of the early to middle Eocene SST offsets at Site 16/28-sb01. If the offset in *A. bullbrooki* is mainly caused by surface salinity changes, this would indicate that the signal from SST-H indicating almost no surface water cooling from early to middle Eocene would be the "real" SST signal. Additionally, surface water salinity should have less influence on *Subbotina* which shows a reduced change in $\delta^{18}O$ between the early and middle Eocene data (on average ~0.8 ‰ difference between U2 and U3). It is likely that surface salinity changes could thus provide an explanation for the SST proxy offsets. However, without further proxy data from Mg/Ca or clumped isotopes from planktic foraminifera it is not possible to conclude if salinity was the major driver for the middle Eocene proxy mismatch.

F) If in the middle Eocene Site 16/28-sb01 was substantially subsided (~1000m water depth) compared with the early Eocene (~300 m water depth) a difference in the water column stratification could have caused the difference in the pF-SST between early Eocene and middle Eocene. In Figure 3.6. the two depth transects for all planktic foraminiferal species are shown and it is important to point out that *Acarinina bullbrooki* sits in and intermediate isotope space and not as in the early Eocene at the lowest end of the $\delta^{18}O$ and highest end of $\delta^{13}C$ values relatively speaking. This could be explained either by a lower water column stratification, *A. bullbrooki* with a tendency to live preferable in the colder winter season or *A. bullbrooki* change their depth habitat to a deeper depth in the middle Eocene.

A similar, although less pronounced, mismatch between planktic foraminifera $\delta^{18}O$ SSTs and TEX_{86}^{H} was found in the middle Eocene of southern high latitude of New Zealand succession (Hollis et al., 2012, Hollis et al., 2019, Crouch et al., 2020), which is interpreted as a preservation issue of their planktic foraminifera in the middle Eocene. In summary, the discrepancy between the SST-H and the pF-SSTs in U3 could be influenced by a preservation issue in U3 within the planktic foraminifera biasing them towards bottom water (benthic foraminifera in the middle Eocene indicate ~11˚C), but as *S. eocaena* is not as biased as *A. bullbrooki* and the visual preservation is recorded to be similar in both Units this seems unlikely. Further it could be a preservation issue within the GDGTs resulting from the low total organics preserved, which might be below the interpretational limits, and cannot be ruled out at this point. However, if both signals SST-H and pF-SST represent a real signal an explanation could be different surface water influxes from the north and south for which there is little other supporting evidence. Another explanation for the middle Eocene proxy offset at Site 16/28-sb01 would be salinity changes from lower surface salinity waters in the early Eocene to higher or normal salinity waters in the middle Eocene with surface water $\delta^{18}O_{SW}$ offset of ~2 ‰ VPDB, implying small (1 – 4˚C) cooling from early to middle Eocene, as recorded in SST-H: ~1˚C; in *S. eocaena* ~4˚C and in the benthic foraminifera ~3˚C. Or that *Acarinina bullbrooki* records slightly cooler values than surface dwelling

values due to a less stratified water column in the middle Eocene, a winter preference or a slightly deeper depth habitat. But to date with no further measurements on foraminiferal Mg/Ca and clumped isotopes a final explanation for the enigmatic proxy offset cannot be given.

The SST-H matching with pF-SST in the early Eocene increase the certainty of the SST reconstructions for the early Eocene implying values around ~29˚C inferred from TEX_{86} and ~27˚C from *A. bullbrooki.* The low 1˚C difference between the early and middle Eocene at Site 16/28-sb01 inferred from TEX_{86} is slightly lower than low tropical cooling inferred from TEX_{86} and well-preserved planktic foraminifera (Pearson et al., 2007, Cramwinckel et al., 2018) and southern high latitudinal ~2˚C cooling inferred from TEX_{86} (Crouch et al., 2020). However the general higher latitude data compilation of ~4˚C cooling in Inglis et al. (2015), inferred from TEX_{86} is slightly higher. So, compared with other TEX_{86} data the SST data at Site16/28-sb01 seems to give reasonable cooling values of (1 – 4˚C), as well if compared with the global temperature gradients for early and middle Eocene from Bijl et al. (2009), based on TEX_{86}.

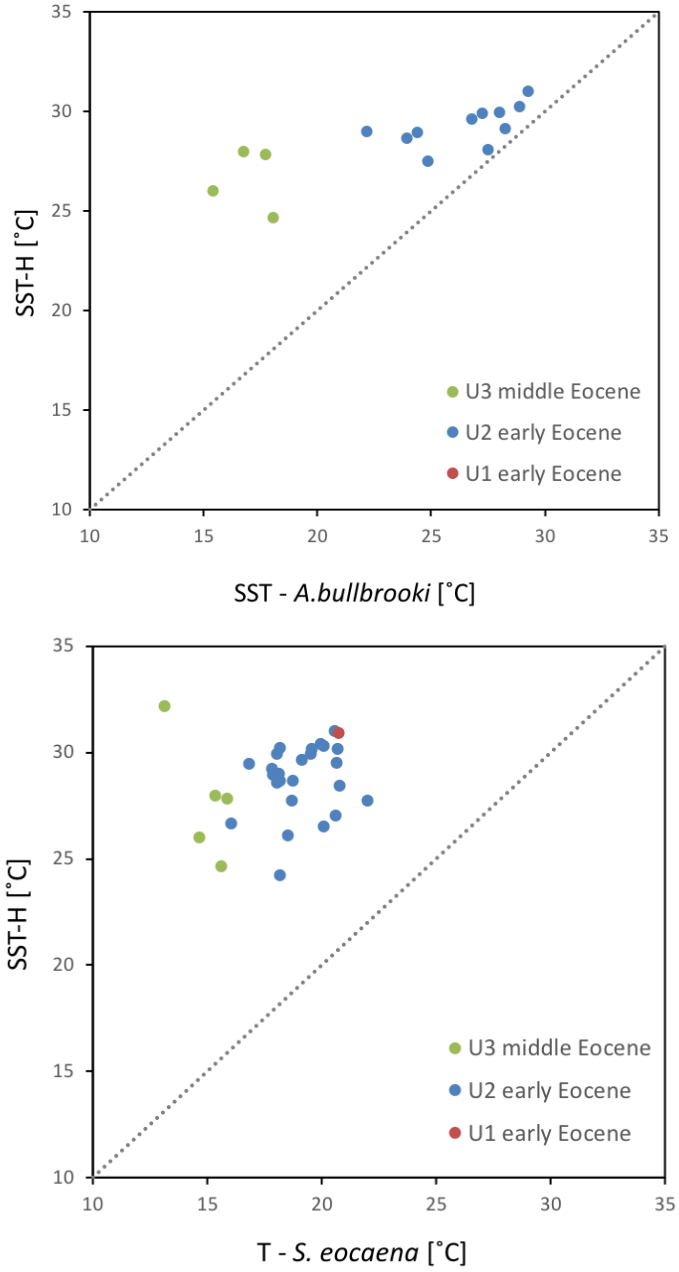

Figure 4.6. Crossplots of both proxies with each other, the top showing SST-H versus SST from A. bullbrooki and bottom showing SST-H versus intermediate dweller S. eocaena. Emphasizing the difference in-between the different lithologic Units.

4.5 Conclusion

The reconstructed SST-H for Site 16/28-sb01 of ~29˚C for the early Eocene with a ~1˚C cooling to the middle Eocene ~28˚C fits well within the early Eocene proxy compilation of Hollis et al. (2019), (Figure 4.6.). SST-H strengthens confidence in the SST reconstructed from *A. bullbrooki* in the early Eocene of ~27˚C. Both proxies

support the reduced latitudinal gradient within the early Eocene at Site 16/28-sb01 of a palaeolatitude of 49˚N. The cooling of 10˚C towards the middle Eocene reconstructed from foraminiferal $\delta^{18}O$ cannot be found within the SST-H and herewith there is uncertainty why the proxies disagree, it is either a result of *A. bullbrooki* preservation, which did not impact *S. eoceana*, preservation or abundance of GDGTs within a more carbonate rich depositional regime with slower sedimentation rates. Another explanation could be that the different proxies reflect different surface water sources one from the north (cooler water SST *A. bullbrooki*) and one from the south (intermittent proto gulf stream warmer SST-H) combined with an enhanced seasonality signal, however with data from one site such a hypothesis is highly speculative. MI and $\%GDGT_{RS}$ do not show significant differences from a normal marine distribution of GDGTs. However elevated BIT and slightly elevated MI values within U2 confirm the higher terrestrial and possibly higher primary productivity, possibly interlinked with an on and off stronger connectivity with the North Atlantic or a stronger hydrological control on Site 16/28-sb01. This could support that the SST proxy offset in the middle Eocene of Site 16/28-sb01 is caused by increased $\delta^{18}O_{SW}$ values of approximately 2 ‰ VPDB in the middle Eocene, which is in agreement with higher modelled Eocene $\delta^{18}O_{SW}$ values and that the lower $\delta^{18}O_{SW}$ values for the early Eocene reflect a lower salinity regime at Site 16/28-sb01. One explanation could be a difference in the water column stratification combined with a slightly cooler winter biased or deeper water habitat of *A. bullbrooki* in the middle Eocene. But to date with no further measurements on foraminiferal Mg/Ca and clumped isotopes a final explanation for the enigmatic proxy offset cannot be given. It is likely that a combination of the three main factors might explain the enigmatic proxy offset in the middle Eocene: 1) GDGTs at the detection limit might change TEX_{86} values and thereby SST-H, 2) salinity changes from a shallow Site 16/28-sb01 in the early Eocene to a deeper Site 16/28-sb01 in the middle Eocene and/or 3) a difference in the palaeo water column structure with a less stratified water column in the relatively deeper water middle Eocene succession compared to early Eocene, or a slightly winter bias of *A. bullbrooki* and/or a slight depth habitat change of *A. bullbrooki* in the middle Eocene.

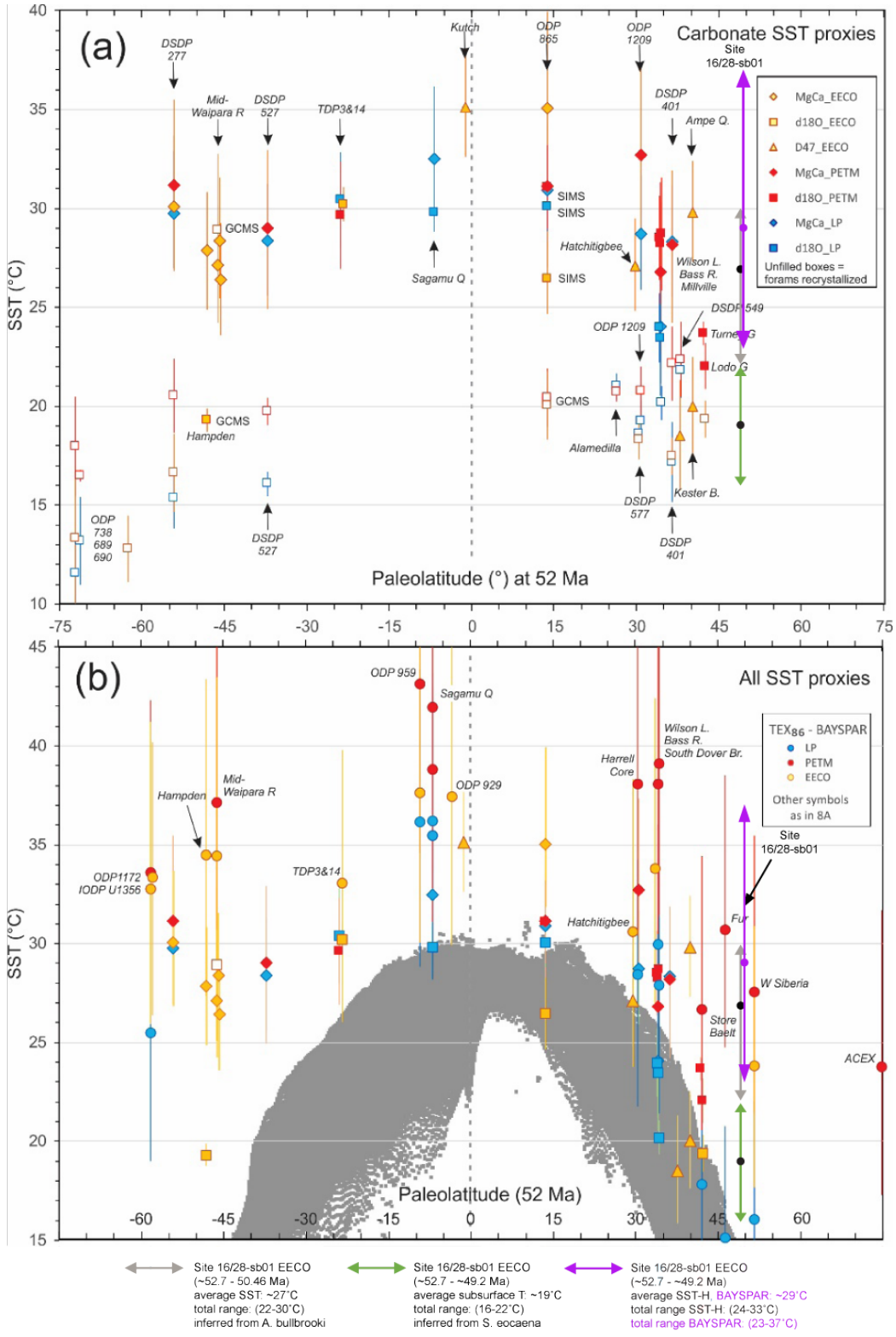

Figure 4.7. Taken from the proxy compilation of Hollis et al. (2019, and references therein). With the surface, subsurface planktic foraminiferal SST and SST-H reconstructions from Site 16/28-sb01 integrated, indicated for surface dwellers grey double arrow, subsurface dweller green double arrow and SST-BAYSPAR blue purple double arrow. All averages on each double arrow are indicated with a dot.

5 FINAL CONCLUSIONS

In times of climate change detailed knowledge of the complex climate interactions during past greenhouse states is indispensable to help us as a climate research community and as society to understand the climate system of a future warmer world. Site 16/28-sb01 in the Northern Atlantic is in an excellent location to gain new insight into the greenhouse climate of the early to middle Eocene from a palaeolatitude of ~49˚N, as it fills in a geographical data gap in existing sea surface water temperature (SST) reconstructions. The two SST proxies presented in this thesis are based on: A) planktic foraminiferal oxygen isotopes (pF-SST); and B) thaumarchaeotal Glycerol dialkyl glycerol tetraether lipids (SST-H). Estimated SSTs are on average ~27˚C (pF-SST) to ~29˚C (SST-H) in the early Eocene and ~17˚C (pF-SST) to 28˚C (SST-H) in the middle Eocene. The temperature proxy records are offset by 2˚C within the early Eocene, which is within the calibration error (±2.5˚C) of SST-H and within the calibration error of pF-SST (±2.8˚C), and 11˚C in the middle Eocene. The minor offset between pF-SST and SST-H within the early Eocene, and offsets with intermediate and deep δ^{18}O-derived temperatures, provides confidence that SST records from this interval are representative of actual temperature regimes at this time. The larger offset in SST reconstructions within the middle Eocene implies either that the two proxies: A) record different temperature signals; or, B) that one or both proxies are biased or not suitable to record SSTs correctly in the middle Eocene of Site 16/28-sb01. Cooling from the early to middle Eocene is well known from the global benthic foraminiferal δ^{18}O stack, assumed to reflect SST cooling in the deep-water source regions of the high southern latitudes, and is of ~5˚C compared to the ~10˚C observed from pF-SSTs at Site 16/28-sb01. The SST-H implies almost no cooling which is a similar signal as temperature records from equatorial and tropical sites, and is a more similar trend to *Subbotina eocaena* temperatures which also show limited cooling (cooling of ~4˚C), as well as benthic isotopes from *Nuttallides truempyi* which indicate ~3˚C cooling. With some degree of Greenland Scotland Ridge (GSR) gateway opening in the middle Eocene, this might imply that SST-H reflects stronger circulation from the lower latitudes, whereas the pF-SSTs might record higher northern latitude water

temperatures. This pattern might be supported by seasonality-enhanced circulation processes, with pF-SSTs possibly reflecting winter circulation and SST-H recording summer circulation patterns. Weights of planktic foraminifera are, however, higher in the middle Eocene and might be biased by a diagenetic calcite overprint towards bottom water temperatures. However, the similar magnitude of cooling in *Subbotina eoceana* and *Nuttallides truempyi,* which show similar preservation are a strong implication that preservation is not the explanation. Conversely, middle Eocene samples have low total organics preserved and the peak heights of GDGTs are very low, which might not be high enough to reproduce accurate SST-H reconstructions. Another way to explain the proxy offset in the middle Eocene are sea surface salinity differences, with lower surface salinities in the early Eocene and normal surface salinities within the middle Eocene, which would, with the same $\delta^{18}O_{SW}$ assumption, lead to the bias in *A. bullbrooki* SSTs and would not reflected as much cooling in the subsurface dweller *S. eoceana*, as found at Site 16/28-sb01. It indicates approximated changes of 2 per mill heavier $\delta^{18}O_{SW}$ in middle Eocene compared to the early Eocene at Site 16/28-sb01. Or in the middle Eocene *A. bullbrooki* might record cooler values due to a slight winter bias, a slight deeper depth habitat or a less stratified water column. To finalize if salinity played a role in the proxy mismatch between early and middle Eocene planktic foraminiferal Mg/Ca and clumped isotope measurements would be needed and without that this question cannot be finalized within this thesis.

Site 16/28-sb01s, palaeoclimate reconstructions are underlain by a new age model and palaeoenvironmental reconstructions based on microfossil, calcareous nannofossils, high-resolution X-ray fluorescence (XRF) and bulk carbonate carbon and oxygen isotopes. These data can be used to divide the Eocene sediments recovered at Site 16/28-sb01, consisting of ~100 core meters, into three lithologic Units, two from the early Eocene: U1 (145.95 – 138.00 m) ~52.71 – ~52.64 Ma (sedimentation rate ~3 cm/ka), U2 (138.00 – 87.50 m) ~50.82 – ~49.23 Ma (sedimentation rates of ~4 cm/ka) and one for the middle Eocene U3 (87.50 – 40.00 m) ~46.23 – ~44.87 Ma (sedimentation rate 3 cm/ka). Within the early Eocene U2: carbon isotope excursions (CIEs): P, R, S, T, U, V and W are detected. Early Eocene clay-rich lithologic U1 and U2 are reconstructed to be deposited on the flanks of the Porcupine High with shallow water depth of ~300 m influenced by a high degree of terrestrial influx. The middle

Eocene lithologic U3 is a carbonate ooze deposited after early to middle Eocene subsidence, at ~1000 m water depth with fading terrestrial influx.

All detected CIEs in U2 are evaluated in detail for elemental distribution (XRF), foraminiferal abundance, with regards to foraminiferal $\delta^{18}O$ and $\delta^{13}C$, temperature and BIT index. In general, no common trends in all above named parameters are found between the different CIEs, which is probably an expression of subsidence history of the site coupled with an accelerated hydrological cycle, resulting in different sedimentological and geochemical patterns in each of the CIEs found in the early Eocene Climate Optimum (EECO). The decoupled bulk carbonate $\delta^{13}C$ and $\delta^{18}O$ values during intervals of the early Eocene CIEs, together with low benthic and planktic foraminiferal absolute abundances and intermittent occurrence of the surface-dwelling genera *Morozovella* and *Acarinina* supports the interpretation that the Rockall Basin was influenced by periods of lower salinities. Such lowered salinities would be similar to the regional regime of the Arctic, northern seas and North Sea, implying more restricted basin conditions than the open North Atlantic and South Atlantic sites or the influx of lower salinity surface water from the North. As basin subsidence increases, bulk carbonate $\delta^{18}O$ values might also be offset to positive values during periods of stronger connectivity with the North Atlantic bringing in higher salinities surface waters and the surface dwelling planktic foraminiferal genera *Acarinina* and *Morozovella*. And could as well be linked to episodes of an enhanced hydrological cycle resulting in episodic lower salinites.

Site 16/28-sb01 provides the palaeoclimate research community with good SST data from two proxies for the early Eocene, but opens up the questions about the nature of local environmental responses to early Eocene CIEs. The new records indicate that the expression of this orbital driven phenomena in sedimentary successions are manifold and difficult to narrow down, therefore future detailed high-resolution studies of the late Paleocene to middle Eocene CIEs will be needed to shed more light on the complex interactions of the climate system components. Transient climate perturbations of the past, such as these Eocene CIEs, have the potential to inform our understanding of future responses to the unprecedented Anthropocene CO_2 rise. The complex responses to the Eocene CIEs documented here show the importance of latitudinal position, ocean basin configuration and the global precipitation cell

distribution on controlling the intensity of the hydrological cycle responses to warming. To understand the late Paleocene to middle Eocene CIEs a global comparison of many different records will be needed for each timeslice to disentangle the most important latitudinal variations. That each of these transient climate events does cause significant changes to the local climate, oceanographic and biological system is not in doubt, and emphasizes how important it is to take precautions for future climate change, especially when response to climate perturbations are complex and will likely remain difficult to predict exactly within the next decades and centuries.

6 REFERENCES

ABELS, H. A., CLYDE, W. C., GINGERICH, P. D., HILGEN, F. J., FRICKE, H. C., BOWEN, G. J. & LOURENS, L. J. 2012. Terrestrial carbon isotope excursions and biotic change during Palaeogene hyperthermals. *Nature Geoscience,* 5, 326-329.

ABELS, H. A., LAURETANO, V., VAN YPEREN, A. E., HOPMAN, T., ZACHOS, J. C., LOURENS, L. J., GINGERICH, P. D. & BOWEN, G. J. 2016. Environmental impact and magnitude of paleosol carbonate carbon isotope excursions marking five early Eocene hyperthermals in the Bighorn Basin, Wyoming. *Climate of the Past,* 12, 1151-1163.

AGNINI, C., MACRÌ, P., BACKMAN, J., BRINKHUIS, H., FORNACIARI, E., GIUSBERTI, L., LUCIANI, V., RIO, D., SLUIJS, A. & SPERANZA, F. 2009. An early Eocene carbon cycle perturbation at~ 52.5 Ma in the Southern Alps: chronology and biotic response. *Paleoceanography,* 24, PA2209. http://doi.org/10.1029/2008PA001649.

AGNINI, C., FORNACIARI, E., RAFFI, I., CATANZARITI, R., PÄLIKE, H., BACKMAN, J. & RIO, D. 2014. Biozonation and biochronology of Paleogene calcareous nannofossils from low and middle latitudes. *Newsletters on Stratigraphy,* 47, 131-181.

ALEGRET, L., ORTIZ, S., ARENILLAS, I. & MOLINA, E. 2005. Palaeoenvironmental turnover across the Palaeocene/Eocene boundary at the Stratotype section in Dababiya (Egypt) based on benthic foraminifera. *Terra Nova,* 17, 526-536.

ALLEN, P. A., BENNETT, S. D., CUNNINGHAM, M. J., CARTER, A., GALLAGHER, K., LAZZARETTI, E., GALEWSKY, J., DENSMORE, A. L., PHILLIPS, W. A. & NAYLOR, D. 2002. The post-Variscan thermal and denudational history of Ireland. *Geological Society, London, Special Publications,* 196, 371-399.

ANAGNOSTOU, E., JOHN, E. H., EDGAR, K. M., FOSTER, G. L., RIDGWELL, A., INGLIS, G. N., PANCOST, R. D., LUNT, D. J. & PEARSON, P. N. 2016. Changing atmospheric CO2 concentration was the primary driver of early Cenozoic climate. *Nature,* 533, 380-384.

ANDREASSON, F., SCHMITZ, B. & SPIEGLER, D. 1996. Oxygen isotopic composition of early Eocene fishapatite from hole 913 B, ODP Leg 151: An indicator of the early Norwegian-Greenland Sea paleosalinity. *Proceedings of the Ocean Drilling Program: Scientific Results,* 151, 583-591.

ANDREASSON, F. P. & SCHMITZ, B. 2000. Temperature seasonality in the early middle Eocene North Atlantic region: Evidence from stable isotope profiles of marine gastropod shells. *Geological Society of America Bulletin,* 112, 628-640.

ARCHIBALD, S. B., BOSSERT, W. H., GREENWOOD, D. R. & FARRELL, B. D. 2010. Seasonality, the latitudinal gradient of diversity, and Eocene insects. *Paleobiology,* 36, 374-398.

ARMITAGE, J. J., DULLER, R. A., WHITTAKER, A. C. & ALLEN, P. A. 2011. Transformation of tectonic and climatic signals from source to sedimentary archive. *Nature Geoscience,* 4, 231.

ARREGUÍN-RODRÍGUEZ, G. J., THOMAS, E., D'HAENENS, S., SPEIJER, R. P. & ALEGRET, L. 2018. Early Eocene deep-sea benthic foraminiferal faunas: Recovery from

the Paleocene Eocene Thermal Maximum extinction in a greenhouse world. *PLoS ONE,* 13, e0193167. https://doi.org/10.1371/journal.pone.0193167.

ARREGUÍN-RODRÍGUEZ, G. J., ALEGRET, L. & THOMAS, E. 2016. Late Paleocene-middle Eocene benthic foraminifera on a Pacific seamount (Allison Guyot, ODP Site 865): Greenhouse climate and superimposed hyperthermal events. *Paleoceanography,* 31, 346-364.

AUBRY, M.-P., OUDA, K., DUPUIS, C., BERGGREN, W. A., VAN COUVERING, J. A., ALI, J., BRINKHUIS, H., GINGERICH, P., HEILMANN-CLAUSEN, C. & HOOKER, J. 2007. The Global Standard Stratotype-section and Point (GSSP) for the base of the Eocene Series in the Dababiya section (Egypt). *Episodes,* 30, 271-286.

AZE, T., PEARSON, P. N., DICKSON, A. J., BADGER, M. P., BOWN, P., PANCOST, R. D., GIBBS, S. J., HUBER, B. T., LENG, M. & COE, A. 2014. Extreme warming of tropical waters during the Paleocene–Eocene Thermal Maximum. *Geology,* 42, 739-742.

BABILA, T. L., ROSENTHAL, Y., WRIGHT, J. D. & MILLER, K. G. 2016. A continental shelf perspective of ocean acidification and temperature evolution during the Paleocene-Eocene Thermal Maximum. *Geology,* 44, 275-278.

BABILA, T. L., PENMAN, D. E., HÖNISCH, B., KELLY, D. C., BRALOWER, T. J., ROSENTHAL, Y. & ZACHOS, J. C. 2018. Capturing the global signature of surface ocean acidification during the Palaeocene–Eocene Thermal Maximum. *Phil. Trans. R. Soc. A,* 376, 20170072. http://dx.doi.org/10.1098/rsta.2017.0072.

BARNET, J., LITTLER, K., WESTERHOLD, T., KROON, D., LENG, M., BAILEY, I., RÖHL, U. & ZACHOS, J. 2019. A High-Fidelity Benthic Stable Isotope Record of Late Cretaceous–Early Eocene Climate Change and Carbon-Cycling. *Paleoceanography and Paleoclimatology,* 34, 672-691.

BARRERA, E. & HUBER, B. T. 1991. Paleogene and early Neogene oceanography of the southern Indian Ocean: Leg 119 foraminifer stable isotope results. *Proc. ODP, Sci. Results,* 119, 693-717.

BARRETT, P. J. 1996. Antarctic palaeoenvironments through Cenozoic times. *Terra Antarctica,* 3, 103-119.

BARRON, E. J., HAY, W. W. & THOMPSON, S. 1989. The hydrologic cycle: a major variable during Earth history. *Global and Planetary Change,* 1, 157-174.

BARRON, E. J. & PETERSON, W. H. 1991. The Cenozoic ocean circulation based on ocean General Circulation Model results. *Palaeogeography, Palaeoclimatology, Palaeoecology,* 83, 1-28.

BÉ, A. 1980. Gametogenic calcification in a spinose planktonic foraminifer, Globigerinoides sacculifer (Brady). *Marine Micropaleontology,* 5, 283-310.

BEMIS, B. E., SPERO, H. J., BIJMA, J. & LEA, D. W. 1998. Reevaluation of the oxygen isotopic composition of planktonic foraminifera: Experimental results and revised paleotemperature equations. *Paleoceanography,* 13, 150-160.

BEMIS, B. E., SPERO, H. J., LEA, D. W. & BIJMA, J. 2000. Temperature influence on the carbon isotopic composition of Globigerina bulloides and Orbulina universa (planktonic foraminifera). *Marine Micropaleontology,* 38, 213-228.

BENTOV, S., BROWNLEE, C. & EREZ, J. 2009. The role of seawater endocytosis in the biomineralization process in calcareous foraminifera. *Proceedings of the National Academy of Sciences,* 106, 21500-21504.

BERGER, W. H., KILLINGLEY, J. & VINCENT, E. 1978. Stable isotopes in deep-sea carbonates-box core ERDC-92, west equatorial Pacific. *Oceanologica Acta,* 1, 203-216.

BERGGREN, W. A., KENT, D. V., SWISHER III, C. C. & AUBRY, M.-P. 1995. A revised Cenozoic geochronology and chronostratigraphy. *Geochronology Time Scale and Global Stratigraphic Correlation, SEPM Special Publication,* 54, 129-212.

BICE, K. L. & MAROTZKE, J. 2002. Could changing ocean circulation have destabilized methane hydrate at the Paleocene/Eocene boundary? *Paleoceanography,* 17, 1018. https://doi.org/10.1029/2001PA000678.

BIJL, P. K., SCHOUTEN, S., SLUIJS, A., REICHART, G.-J., ZACHOS, J. C. & BRINKHUIS, H. 2009. Early Palaeogene temperature evolution of the southwest Pacific Ocean. *Nature,* 461, 776-779.

BIJL, P. K., HOUBEN, A. J., SCHOUTEN, S., BOHATY, S. M., SLUIJS, A., REICHART, G.-J., SINNINGHE DAMSTÉ, J. S. & BRINKHUIS, H. 2010. Transient Middle Eocene atmospheric CO2 and temperature variations. *Science,* 330, 819-821.

BIJL, P. K., BENDLE, J. A., BOHATY, S. M., PROSS, J., SCHOUTEN, S., TAUXE, L., STICKLEY, C. E., MCKAY, R. M., RÖHL, U. & OLNEY, M. 2013. Eocene cooling linked to early flow across the Tasmanian Gateway. *Proceedings of the National Academy of Sciences,* 110, 9645-9650.

BIJMA, J., FABER, W. W. & HEMLEBEN, C. 1990. Temperature and salinity limits for growth and survival of some planktonic foraminifers in laboratory cultures. *The Journal of Foraminiferal Research,* 20, 95-116.

BIRCH, H., COXALL, H. K., PEARSON, P. N., KROON, D. & O'REGAN, M. 2013. Planktonic foraminifera stable isotopes and water column structure: Disentangling ecological signals. *Marine Micropaleontology,* 101, 127-145.

BIRCH, H. S., COXALL, H. K. & PEARSON, P. N. 2012. Evolutionary ecology of Early Paleocene planktonic foraminifera: size, depth habitat and symbiosis. *Paleobiology,* 38, 374-390.

BOERSMA, A., SILVA, I. P. & SHACKLETON, N. 1987. Atlantic Eocene planktonic foraminiferal paleohydrographic indicators and stable isotope paleoceanography. *Paleoceanography and Paleoclimatology,* 2, 287-331.

BOHATY, S. M. & ZACHOS, J. C. 2003. Significant Southern Ocean warming event in the late middle Eocene. *Geology,* 31, 1017-1020.

BOHATY, S. M., ZACHOS, J. C., FLORINDO, F. & DELANEY, M. L. 2009. Coupled greenhouse warming and deep-sea acidification in the middle Eocene. *Paleoceanography,* 24, PA2207. https://doi.org/10.1029/2001PA000678.

BORNEMANN, A. & NORRIS, R. D. 2007. Size-related stable isotope changes in Late Cretaceous planktic foraminifera: implications for paleoecology and photosymbiosis. *Marine Micropaleontology,* 65, 32-42.

BORNEMANN, A., NORRIS, R. D., LYMAN, J. A., D'HAENENS, S., GROENEVELD, J., RÖHL, U., FARLEY, K. A. & SPEIJER, R. P. 2014. Persistent environmental change after the Paleocene–Eocene Thermal Maximum in the eastern North Atlantic. *Earth and Planetary Science Letters,* 394, 70-81.

BORNEMANN, A., D'HAENENS, S., NORRIS, R. D. & SPEIJER, R. P. 2016. The demise of the early Eocene greenhouse–Decoupled deep and surface water cooling in the eastern North Atlantic. *Global and planetary change,* 145, 130-140.

BOSCOLO GALAZZO, F., THOMAS, E., PAGANI, M., WARREN, C., LUCIANI, V. & GIUSBERTI, L. 2014. The middle Eocene climatic optimum (MECO): A multiproxy record of paleoceanographic changes in the southeast Atlantic (ODP Site 1263, Walvis Ridge). *Paleoceanography,* 29, 1143-1161.

BOWEN, G. J. & ZACHOS, J. C. 2010. Rapid carbon sequestration at the termination of the Palaeocene–Eocene Thermal Maximum. *Nature Geoscience,* 3, 866-869.

BOWN, P. R. & YOUNG, J. R. 1998. Techniques. *In:* BOWN, P. R. (ed.) *Calcareous Nannofossil Biostratigraphy.* London: Chapman and Hall; Kluwer Academic.

BOYD, E. S., PEARSON, A., PI, Y., LI, W.-J., ZHANG, Y. G., HE, L., ZHANG, C. L. & GEESEY, G. G. 2011. Temperature and pH controls on glycerol dibiphytanyl glycerol tetraether lipid composition in the hyperthermophilic crenarchaeon Acidilobus sulfurireducens. *Extremophiles,* 15, 59-65.

BOYDEN, J. A., MÜLLER, R. D., GURNIS, M., TORSVIK, T. H., CLARK, J. A., TURNER, M., IVEY-LAW, H., WATSON, R. J. & CANNON, J. S. 2011. Next-generation plate-tectonic reconstructions using GPlates. *In:* KELLER, G. R. & BARU, C. (eds.) *Geoinformatics: Cyberinfrastructure for the Solid Earth Sciences.* Cambridge: Camrbide University Press.

BOYLE, E. A. 1983. Manganese carbonate overgrowths on foraminifera tests. *Geochimica et Cosmochimica Acta,* 47, 1815-1819.

BOYLE, P. R., ROMANS, B. W., TUCHOLKE, B. E., NORRIS, R. D., SWIFT, S. A. & SEXTON, P. F. 2017. Cenozoic North Atlantic deep circulation history recorded in contourite drifts, offshore Newfoundland, Canada. *Marine Geology,* 385, 185-203.

BRALOWER, T., THOMAS, D., ZACHOS, J., HIRSCHMANN, M., ROHL, U., SIGURDSSON, H., THOMAS, E. & WHITNEY, D. 1997. High-resolution records of the late Paleocene thermal maximum and circum-Caribbean volcanism: Is there a causal link? *Geology,* 25, 963-966.

BRALOWER, T. J., ZACHOS, J. C., THOMAS, E., PARROW, M., PAULL, C. K., KELLY, D. C., SILVA, I. P., SLITER, W. V. & LOHMANN, K. C. 1995. Late Paleocene to Eocene paleoceanography of the equatorial Pacific Ocean: stable isotopes recorded at ocean drilling program site 865, Allison Guyot. *Paleoceanography,* 10, 841-865.

BRINKHUIS, H., SCHOUTEN, S., COLLINSON, M. E., SLUIJS, A., SINNINGHE DAMSTÉ, J. S., DICKENS, G. R., HUBER, M., CRONIN, T. M., ONODERA, J. & TAKAHASHI, K. 2006. Episodic fresh surface waters in the Eocene Arctic Ocean. *Nature,* 441, 606-609.

BROCHIER-ARMANET, C., BOUSSAU, B., GRIBALDO, S. & FORTERRE, P. 2008. Mesophilic Crenarchaeota: proposal for a third archaeal phylum, the Thaumarchaeota. *Nature Reviews Microbiology,* 6, 245-252.

BROECKER, W. S. & PENG, T.-H. 1982. *Tracers in the Sea,* Lamont-Doherty Geological Observatory, Columbia University, Palisades, New York 10964, Eldigo Press.

BURKE, K., WILLIAMS, J., CHANDLER, M., HAYWOOD, A., LUNT, D. & OTTO-BLIESNER, B. 2018. Pliocene and Eocene provide best analogs for near-future climates. *Proceedings of the National Academy of Sciences,* 115, 13288-13293.

CALVERT, S. & PEDERSEN, T. 2007. Chapter fourteen elemental proxies for palaeoclimatic and palaeoceanographic variability in marine sediments: interpretation and application. *Developments in Marine Geology,* 1, 567-644.

CARMICHAEL, M. J., LUNT, D. J., HUBER, M., HEINEMANN, M., KIEHL, J., LEGRANDE, A., LOPTSON, C. A., ROBERTS, C. D., SAGOO, N. & SHIELDS, C. 2016. A model–model and data–model comparison for the early Eocene hydrological cycle. *Climate of the Past,* 12, 455-481.

CARMICHAEL, M. J., INGLIS, G. N., BADGER, M. P., NAAFS, B. D. A., BEHROOZ, L., REMMELZWAAL, S., MONTEIRO, F. M., ROHRSSEN, M., FARNSWORTH, A. & BUSS, H. L. 2017. Hydrological and associated biogeochemical consequences of rapid global warming during the Paleocene-Eocene Thermal Maximum. *Global and Planetary Change,* 157, 114-138.

CHALMERS, J., PULVERTAFT, T., CHRISTIANSEN, F., LARSEN, H., LAURSEN, K. & OTTESEN, T. 1993. The southern West Greenland continental margin: rifting history, basin development, and petroleum potential. *Geological Society of London, Petroleum Geology Conference series,* 4, 915-931.

CHAMBERS, L., DARBYSHIRE, F., NOBLE, S. & RITCHIE, D. 2005. NW UK continental margin: chronology and isotope geochemistry. *BGS Commissioned Report.* Keyworth, Nottingham British Geological Survey.

CHAUVET, F., GEOFFROY, L., GUILLOU, H., MAURY, R. C., LE GALL, B., AGRANIER, A. & VIANA, A. 2019. Eocene continental breakup in Baffin Bay. *Tectonophysics,* 757, 170-186.

COCCIONI, R., BANCALA, G., CATANZARIT, R., FORNACIARI, E., FRONTALINI, F., GIUSBERTI, L., JOVANE, L., LUCIANI, V., SAVIAN, J. & SPROVIERI, M. 2012. An integrated stratigraphic record of the Palaeocene–lower Eocene at Gubbio (Italy): new insights into the early Palaeogene hyperthermals and carbon isotope excursions. *Terra Nova,* 24, 380-386.

CORFIELD, S., MURPHY, N. & PARKER, S. 1999. The structural and stratigraphic framework of the Irish Rockall Trough. *In:* FLEET, A. J. & BOLDY, S. A. R. (eds.) *Petroleum Geology of Northwest Europe: Proceedings of the 5th Conference.* London: Geological Society

COXALL, H. K., PEARSON, P. N., SHACKLETON, N. J. & HALL, M. A. 2000. Hantkeninid depth adaptation: an evolving life strategy in a changing ocean. *Geology,* 28, 87-90.

COXALL, H. K., WILSON, P. A., PÄLIKE, H., LEAR, C. H. & BACKMAN, J. 2005. Rapid stepwise onset of Antarctic glaciation and deeper calcite compensation in the Pacific Ocean. *Nature,* 433, 53-57.

CRAIG, H. 1957. Isotopic standards for carbon and oxygen and correction factors for mass-spectrometric analysis of carbon dioxide. *Geochimica et cosmochimica acta,* 12, 133-149.

CRAMER, B., TOGGWEILER, J., WRIGHT, J., KATZ, M. & MILLER, K. 2009. Ocean overturning since the Late Cretaceous: Inferences from a new benthic foraminiferal isotope compilation. *Paleoceanography,* 24, PA4216. http://doi.org/10.1029/2008PA001683.

CRAMER, B., MILLER, K., BARRETT, P. & WRIGHT, J. 2011. Late Cretaceous–Neogene trends in deep ocean temperature and continental ice volume: Reconciling records of benthic foraminiferal geochemistry (δ18O and Mg/Ca) with sea level history. *Journal of Geophysical Research: Oceans,* 116, C12023. http://doi.org/10.1029/2011JC007255.

CRAMER, B. S., WRIGHT, J. D., KENT, D. V. & AUBRY, M. P. 2003. Orbital climate forcing of δ13C excursions in the late Paleocene–early Eocene (chrons C24n–C25n). *Paleoceanography,* 18, 1097. http://doi.org/10.1029/2003PA000909.

CRAMER, B. S. & KENT, D. V. 2005. Bolide summer: The Paleocene/Eocene thermal maximum as a response to an extraterrestrial trigger. *Palaeogeography, Palaeoclimatology, Palaeoecology,* 224, 144-166.

CRAMWINCKEL, M. J., HUBER, M., KOCKEN, I. J., AGNINI, C., BIJL, P. K., BOHATY, S. M., FRIELING, J., GOLDNER, A., HILGEN, F. J. & KIP, E. L. 2018. Synchronous tropical and polar temperature evolution in the Eocene. *Nature,* 559, 382-386.

CROUCH, E., SHEPHERD, C., MORGANS, H., NAAFS, B., DALLANAVE, E., PHILLIPS, A., HOLLIS, C. & PANCOST, R. 2020. Climatic and environmental changes across the Early Eocene Climatic Optimum at mid-Waipara River, Canterbury Basin, New Zealand. *Earth-Science Reviews*, 102961. https://doi.org/10.1016/j.earscirev.2019.102961.

CROUCH, E. M., HEILMANN-CLAUSEN, C., BRINKHUIS, H., MORGANS, H. E., ROGERS, K. M., EGGER, H. & SCHMITZ, B. 2001. Global dinoflagellate event associated with the late Paleocene thermal maximum. *Geology,* 29, 315-318.

CROWLEY, T. J. 1990. Are there any satisfactory geologic analogs for a future greenhouse warming? *Journal of Climate,* 3, 1282-1292.

CROWLEY, T. J. & ZACHOS, J. C. 2000. Comparison of zonal temperature profiles for past warm time periods. *In:* HUBER, B. T., KENNETH, G. M. & SCOTT, L. W. (eds.) *Warm Climates in Earth History.* Cambridge: Cambridge University Press.

CUI, Y., KUMP, L. R., RIDGWELL, A. J., CHARLES, A. J., JUNIUM, C. K., DIEFENDORF, A. F., FREEMAN, K. H., URBAN, N. M. & HARDING, I. C. 2011. Slow release of fossil carbon during the Palaeocene–Eocene Thermal Maximum. *Nature Geoscience,* 4, 481-485.

D'HONDT, S. & ZACHOS, J. C. 1993. On stable isotopic variation and earliest Paleocene planktonic foraminifera. *Paleoceanography,* 8, 527-547.

D'HONDT, S., ZACHOS, J. C. & SCHULTZ, G. 1994. Stable isotopic signals and photosymbiosis in late Paleocene planktic foraminifera. *Paleobiology,* 20, 391-406.

D'HONDT, S. & ARTHUR, M. A. 1996. Late Cretaceous oceans and the cool tropic paradox. *Science,* 271, 1838-1841.

DALZIEL, I., LAWVER, L. A., PEARCE, J. A., BARKER, P., HASTIE, A., BARFOD, D., SCHENKE, H.-W. & DAVIS, M. B. 2013. A potential barrier to deep Antarctic circumpolar flow until the late Miocene? *Geology,* 41, 947-950.

DANCER, P., ALGAR, S. & WILSON, I. 1999. Structural evolution of the Slyne Trough. *In:* FLEET, A. J. & BOLDY, S. A. R. (eds.) *Petroleum Geology of Northwest Europe: Proceedings of the 5th Conference.* Geological Society of London.

DAVIES, A., HUNTER, S. J., GRÉSELLE, B., HAYWOOD, A. M. & ROBSON, C. 2019. Evidence for seasonality in early Eocene high latitude sea-surface temperatures. *Earth and Planetary Science Letters,* 519, 274-283.

DE JONGE, C., HOPMANS, E. C., ZELL, C. I., KIM, J.-H., SCHOUTEN, S. & SINNINGHE DAMSTÉ, J. S. 2014. Occurrence and abundance of 6-methyl branched glycerol dialkyl glycerol tetraethers in soils: Implications for palaeoclimate reconstruction. *Geochimica et Cosmochimica Acta,* 141, 97-112.

DE NOOIJER, L. J., TOYOFUKU, T. & KITAZATO, H. 2009. Foraminifera promote calcification by elevating their intracellular pH. *Proceedings of the National Academy of Sciences,* 106, 15374-15378.

DE NOOIJER, L. J., SPERO, H., EREZ, J., BIJMA, J. & REICHART, G.-J. 2014. Biomineralization in perforate foraminifera. *Earth-Science Reviews,* 135, 48-58.

DE ROSA, M., ESPOSITO, E., GAMBACORTA, A., NICOLAUS, B. & BU'LOCK, J. D. 1980. Effects of temperature on ether lipid composition of Caldariella acidophila. *Phytochemistry,* 19, 827-831.

DE ROSA, M. & GAMBACORTA, A. 1988. The lipids of archaebacteria. *Progress in lipid research,* 27, 153-175.

DECONTO, R. M., GALEOTTI, S., PAGANI, M., TRACY, D., SCHAEFER, K., ZHANG, T., POLLARD, D. & BEERLING, D. J. 2012. Past extreme warming events linked to massive carbon release from thawing permafrost. *Nature,* 484, 87-91.

DICKENS, G. R., O'NEIL, J. R., REA, D. K. & OWEN, R. M. 1995. Dissociation of oceanic methane hydrate as a cause of the carbon isotope excursion at the end of the Paleocene. *Paleoceanography,* 10, 965-971.

DICKENS, G. R., CASTILLO, M. M. & WALKER, J. C. 1997. A blast of gas in the latest Paleocene: Simulating first-order effects of massive dissociation of oceanic methane hydrate. *Geology,* 25, 259-262.

DICKENS, G. R. 2011. Down the rabbit hole: Toward appropriate discussion of methane release from gas hydrate systems during the Paleocene-Eocene thermal maximum and other past hyperthermal events. *Climate of the Past,* 7, 831-846.

DICKSON, R. R. & BROWN, J. 1994. The production of North Atlantic Deep Water: sources, rates, and pathways. *Journal of Geophysical Research: Oceans,* 99, 12319-12341.

DOE, B. R. 1983. The past is the key to the future. *Geochimica et Cosmochimica Acta,* 47, 1341-1354.

DORÉ, A., LUNDIN, E., FICHLER, C. & OLESEN, O. 1997. Patterns of basement structure and reactivation along the NE Atlantic margin. *Journal of the Geological Society,* 154, 85-92.

DORÉ, A., LUNDIN, E., JENSEN, L., BIRKELAND, Ø., ELIASSEN, P. & FICHLER, C. 1999. Principal tectonic events in the evolution of the northwest European Atlantic margin. *In:* FLEET, A. J. & BOLDY, S. A. R. (eds.) *Petroleum Geology of Northwest Europe: Proceedings of the 5th Conference.* Geological Society of London.

DUNKLEY JONES, T., LUNT, D., MASLIN, M., SCHMIDT, D. & VALDES, P. 2010. A Palaeogene perspective on climate sensitivity and methane hydrate instability. *Philosophical Transactions of the Royal Society of London A: Mathematical, Physical and Engineering Sciences,* 368, 2395-2415.

DUNKLEY JONES, T., LUNT, D. J., SCHMIDT, D. N., RIDGWELL, A., SLUIJS, A., VALDES, P. J. & MASLIN, M. 2013. Climate model and proxy data constraints on ocean warming across the Paleocene–Eocene Thermal Maximum. *Earth-Science Reviews,* 125, 123-145.

DUNKLEY JONES, T., MANNERS, H. R., HOGGETT, M., KIRTLAND TURNER, S., WESTERHOLD, T., LENG, M. J., PANCOST, R. D., RIDGWELL, A., ALEGRET, L. & DULLER, R. 2018. Dynamics of sediment flux to a bathyal continental margin

section through the Paleocene–Eocene Thermal Maximum. *Climate of the Past,* 14, 1035-1049.
EBERLE, J. J. & GREENWOOD, D. R. 2012. Life at the top of the greenhouse Eocene world—A review of the Eocene flora and vertebrate fauna from Canada's High Arctic. *Bulletin,* 124, 3-23.
EDGAR, K. M., ANAGNOSTOU, E., PEARSON, P. N. & FOSTER, G. L. 2015. Assessing the impact of diagenesis on δ11B, δ13C, δ18O, Sr/Ca and B/Ca values in fossil planktic foraminiferal calcite. *Geochimica et Cosmochimica Acta,* 166, 189-209.
ELDERFIELD, H. & GANSSEN, G. 2000. Past temperature and δ 18 O of surface ocean waters inferred from foraminiferal Mg/Ca ratios. *Nature,* 405, 442-445.
ELLING, F. J., KÖNNEKE, M., MUSSMAN, M., GREVE, A. & HINRICHS, K.-U. 2015. Influence of temperature, pH, and salinity on membrane lipid composition and TEX86 of marine planktonic thaumarchaeal isolates. *Geochimica et Cosmochimica Acta,* 171, 238-255.
EMILIANI, C. 1954. Depth habitats of some species of pelagic foraminifera as indicated by oxygen isotope ratios. *American Journal of Science,* 252, 149-158.
EMILIANI, C. 1955. Pleistocene temperatures. *The Journal of Geology,* 63, 538-578.
EPSTEIN, S., BUCHSBAUM, R., LOWENSTAM, H. & UREY, H. C. 1951. Carbonate-water isotopic temperature scale. *Geological Society of America Bulletin,* 62, 417-426.
EPSTEIN, S., BUCHSBAUM, R., LOWENSTAM, H. A. & UREY, H. C. 1953. Revised carbonate-water isotopic temperature scale. *Geological Society of America Bulletin,* 64, 1315-1326.
EREZ, J. 1978. Vital effect on stable-isotope composition seen in foraminifera and coral skeletons. *Nature,* 273, 199-202.
EREZ, J. & HONJO, S. 1981. Comparison of isotopic composition of planktonic foraminifera in plankton tows, sediment traps and sediments. *Palaeogeography, Palaeoclimatology, Palaeoecology,* 33, 129-156.
EREZ, J. & LUZ, B. 1983. Experimental paleotemperature equation for planktonic foraminifera. *Geochimica et Cosmochimica Acta,* 47, 1025-1031.
EREZ, J. 2003. The source of ions for biomineralization in foraminifera and their implications for paleoceanographic proxies. *Reviews in mineralogy and geochemistry,* 54, 115-149.
EVANS, D., BADGER, M. P., FOSTER, G. L., HENEHAN, M. J., LEAR, C. H. & ZACHOS, J. C. 2018a. No substantial long-term bias in the Cenozoic benthic foraminifera oxygen-isotope record. *Nature Communications,* 9, 1-3. http://doi.org/10.1038/s41467-018-05303-4.
EVANS, D., SAGOO, N., RENEMA, W., COTTON, L. J., MÜLLER, W., TODD, J. A., SARASWATI, P. K., STASSEN, P., ZIEGLER, M. & PEARSON, P. N. 2018b. Eocene greenhouse climate revealed by coupled clumped isotope-Mg/Ca thermometry. *Proceedings of the National Academy of Sciences,* 115, 1174-1179.
EZARD, T. H., EDGAR, K. M. & HULL, P. M. 2015. Environmental and biological controls on size-specific δ13C and δ18O in recent planktonic foraminifera. *Paleoceanography,* 30, 151-173.
FARNSWORTH, A., LUNT, D., O'BRIEN, C., FOSTER, G., INGLIS, G., MARKWICK, P., PANCOST, R. & ROBINSON, S. 2019. Climate Sensitivity on Geological

Timescales Controlled by Nonlinear Feedbacks and Ocean Circulation. *Geophysical Research Letters,* 46, 9880-9889.

FITTON, J., SAUNDERS, A., NORRY, M., HARDARSON, B. & TAYLOR, R. 1997. Thermal and chemical structure of the Iceland plume. *Earth and Planetary Science Letters,* 153, 197-208.

FOSTER, G. L., ROYER, D. L. & LUNT, D. J. 2017. Future climate forcing potentially without precedent in the last 420 million years. *Nature Communications,* 8, 14845. http://doi.org/10.1038/ncomms14845

FOSTER, G. L., HULL, P., LUNT, D. J. & ZACHOS, J. C. 2018. Placing our current 'hyperthermal'in the context of rapid climate change in our geological past. *Phil. Trans. R. Soc. A,* 376, 20170086. http://dx.doi.org/10.1098/rsta.2017.0086.

FRAILE, I., MULITZA, S. & SCHULZ, M. 2009. Modeling planktonic foraminiferal seasonality: Implications for sea-surface temperature reconstructions. *Marine Micropaleontology,* 72, 1-9.

FRIELING, J., SVENSEN, H. H., PLANKE, S., CRAMWINCKEL, M. J., SELNES, H. & SLUIJS, A. 2016. Thermogenic methane release as a cause for the long duration of the PETM. *Proceedings of the National Academy of Sciences,* 113, 12059-12064.

FRIELING, J., GEBHARDT, H., HUBER, M., ADEKEYE, O. A., AKANDE, S. O., REICHART, G.-J., MIDDELBURG, J. J., SCHOUTEN, S. & SLUIJS, A. 2017. Extreme warmth and heat-stressed plankton in the tropics during the Paleocene-Eocene Thermal Maximum. *Science advances,* 3, e1600891. http://doi.org/10.1126/sciadv.1600891.

FRIELING, J., REICHART, G.-J., MIDDELBURG, J. J., RÖHL, U., WESTERHOLD, T., BOHATY, S. M. & SLUIJS, A. 2018. Tropical Atlantic climate and ecosystem regime shifts during the Paleocene–Eocene Thermal Maximum. *Climate of the Past,* 14, 39-55.

GABRIEL, J. L. & CHONG, P. L. G. 2000. Molecular modeling of archaebacterial bipolar tetraether lipid membranes. *Chemistry and Physics of Lipids,* 105, 193-200.

GAINA, C., GERNIGON, L. & BALL, P. 2009. Palaeocene–Recent plate boundaries in the NE Atlantic and the formation of the Jan Mayen microcontinent. *Journal of the Geological Society,* 166, 601-616.

GALEOTTI, S., KRISHNAN, S., PAGANI, M., LANCI, L., GAUDIO, A., ZACHOS, J. C., MONECHI, S., MORELLI, G. & LOURENS, L. 2010. Orbital chronology of Early Eocene hyperthermals from the Contessa Road section, central Italy. *Earth and Planetary Science Letters,* 290, 192-200.

GALEOTTI, S., MORETTI, M., SABATINO, N., SPROVIERI, M., CECCATELLI, M., FRANCESCONE, F., LANCI, L., LAURETANO, V. & MONECHI, S. 2017. Cyclochronology of the Early Eocene carbon isotope record from a composite Contessa Road-Bottaccione section (Gubbio, central Italy). *Newsletters on Stratigraphy,* 50, 231-244.

GALEOTTI, S., SPROVIERI, M., RIO, D., MORETTI, M., FRANCESCONE, F., SABATINO, N., FORNACIARI, E., GIUSBERTI, L. & LANCI, L. 2019. Stratigraphy of early to middle Eocene hyperthermals from Possagno (Southern Alps, Italy) and comparison with global carbon isotope records. *Palaeogeography, Palaeoclimatology, Palaeoecology,* 527, 39-52.

GANSSEN, G., PEETERS, F., METCALFE, B., ANAND, P., JUNG, S., KROON, D. & BRUMMER, G.-J. 2011. Quantifying sea surface temperature ranges of the Arabian Sea for the past 20 000 years. *Climate of the Past,* 7, 1337-1349.

GASKELL, D. E. & HULL, P. M. 2019. Symbiont arrangement and metabolism can explain high δ13C in Eocene planktonic foraminifera. *Geology,* 47, 1156-1160.

GIBBS, S. J., BOWN, P. R., SESSA, J. A., BRALOWER, T. J. & WILSON, P. A. 2006. Nannoplankton extinction and origination across the Paleocene-Eocene Thermal Maximum. *Science,* 314, 1770-1773.

GINGERICH, P. D. 2003. Mammalian responses to climate change at the Paleocene-Eocene boundary: Polecat Bench record in the northern Bighorn Basin, Wyoming. *Special Papers-Geological Society of America,* 369, 463-478.

GLEASON, J., THOMAS, D., MOORE, T., BLUM, J., OWEN, R. & HALEY, B. 2009. Early to middle Eocene history of the Arctic Ocean from Nd-Sr isotopes in fossil fish debris, Lomonosov Ridge. *Paleoceanography and Paleoclimatology,* 24, PA2215. http://doi.org/10.1029/2008PA001685.

GLIOZZI, A., PAOLI, G., DE ROSA, M. & GAMBACORTA, A. 1983. Effect of isoprenoid cyclization on the transition temperature of lipids in thermophilic archaebacteria. *Biochimica et Biophysica Acta (BBA)-Biomembranes,* 735, 234-242.

GREEN, P. F. 2001. Thermal history reconstruction in Irish Rockall Trough boreholes 16/28-sb01, 83/20-sb01, 83/24-sb02 using AFTA, VR and fluid inclusion data. Technical report by Geotrack, Report.

GREENWOOD, D. R., BASINGER, J. F. & SMITH, R. Y. 2010. How wet was the Arctic Eocene rain forest? Estimates of precipitation from Paleogene Arctic macrofloras. *Geology,* 38, 15-18.

GUTJAHR, M., RIDGWELL, A., SEXTON, P. F., ANAGNOSTOU, E., PEARSON, P. N., PÄLIKE, H., NORRIS, R. D., THOMAS, E. & FOSTER, G. L. 2017. Very large release of mostly volcanic carbon during the Palaeocene–Eocene Thermal Maximum. *Nature,* 548, 573-577.

HALLAM, A. 1971. Mesozoic geology and the opening of the North Atlantic. *The Journal of Geology,* 79, 129-157.

HAMILTON, C. P., SPERO, H. J., BIJMA, J. & LEA, D. W. 2008. Geochemical investigation of gametogenic calcite addition in the planktonic foraminifera Orbulina universa. *Marine Micropaleontology,* 68, 256-267.

HAMMER, Ø., HARPER, D. & RYAN, P. 2001. PAST-Palaeontological statistics. *Palaeontologia electronica,* 4, 1-9.

HANSEN, J., SATO, M., RUSSELL, G. & KHARECHA, P. 2013. Climate sensitivity, sea level and atmospheric carbon dioxide. *Phil. Trans. R. Soc. A,* 371, 20120294. http://dx.doi.org/10.1098/rsta.2012.0294.

HARPER, D., HÖNISCH, B., ZEEBE, R., SHAFFER, G., HAYNES, L., THOMAS, E. & ZACHOS, J. 2019. The magnitude of surface ocean acidification and carbon release during Eocene Thermal Maximum 2 (ETM-2) and the Paleocene–Eocene Thermal Maximum (PETM). *Paleoceanography and Paleoclimatology,* 35, e2019PA003699. https://doi.org/10.1029/2019PA003699.

HARRINGTON, G., HIGGS, K. & ZUCCHI, D. 2000. Biostratigraphic report on shallow borehole cores: 11/20-sb01, 16/28-sb01, 82/20-sb1, 83/24-sb01 and 83/24-sb02. *RSG Report, Project 97/34.*

HART, M., HYLTON, M., OXFORD, M., PRICE, G., HUDSON, W. & SMART, C. 2003. The search for the origin of the planktic Foraminifera. *Journal of the Geological Society,* 160, 341-343.

HAUGHTON, P., PRAEG, D., TYRRELL, S., MORRISSEY, T., GERAGHTY, D. & AMY, L. 2002. Integrated sedimentological report on shallow borehole cores: 11/20 - sb01 16/28 - sb01 83/20 - sb01 83/24 - sb01 83/24 - sb02. *Rockall Studies Group Technical Report* RSG Project 97/28.

HAUGHTON, P., PRAEG, D., SHANNON, P., HARRINGTON, G., HIGGS, K., AMY, L., TYRRELL, S. & MORRISSEY, T. 2005. First results from shallow stratigraphic boreholes on the eastern flank of the Rockall Basin, offshore western Ireland. *In:* DORÉ, A. G. & VINING, B. A. (eds.) *Petroleum Geology: North West Europe and Global Persepctives - Proceedings of the 6th Petroleum Geology Conference.* Geological Society of London.

HEMLEBEN, C., SPINDLER, M. & ANDERSON, O. R. 1989. *Modern planktonic foraminifera*, Springer Science & Business Media.

HERFORT, L., SCHOUTEN, S., BOON, J. P. & SINNINGHE DAMSTÉ, J. S. 2006. Application of the TEX86 temperature proxy to the southern North Sea. *Organic Geochemistry,* 37, 1715-1726.

HEROLD, N., BUZAN, J., SETON, M., GOLDNER, A., GREEN, J., MÜLLER, R., MARKWICK, P. & HUBER, M. 2014. A suite of early Eocene (~ 55 Ma) climate model boundary conditions. *Geoscientific Model Development,* 7, 2077-2090.

HIGGINS, J. A. & SCHRAG, D. P. 2006. Beyond methane: towards a theory for the Paleocene–Eocene thermal maximum. *Earth and Planetary Science Letters,* 245, 523-537.

HILGEN, F. J., KUIPER, K. F. & LOURENS, L. J. 2010. Evaluation of the astronomical time scale for the Paleocene and earliest Eocene. *Earth and Planetary Science Letters,* 300, 139-151.

HITCHEN, K., JOHNSON, H. & GATLIFF, R. 2013. *Geology of the Rockall Basin and adjacent areas*, British Geological Survey.

HOHBEIN, M. W., SEXTON, P. F. & CARTWRIGHT, J. A. 2012. Onset of North Atlantic Deep Water production coincident with inception of the Cenozoic global cooling trend. *Geology,* 40, 255-258.

HOLLIS, C. J., TAYLOR, K. W., HANDLEY, L., PANCOST, R. D., HUBER, M., CREECH, J. B., HINES, B. R., CROUCH, E. M., MORGANS, H. E. & CRAMPTON, J. S. 2012. Early Paleogene temperature history of the Southwest Pacific Ocean: Reconciling proxies and models. *Earth and Planetary Science letters,* 349, 53-66.

HOLLIS, C. J., DUNKLEY JONES, T., ANAGNOSTOU, E., BIJL, P. K., CRAMWINCKEL, M., CUI, Y., DICKENS, G. R., EDGAR, K. M., ELEY, Y., EVANS, D., FOSTER, G. L., FRIELING, J., INGLIS, G. N., KENNEDEY, E., KOZDON, R., LAURETANO, V., LEAR, H., LITTLER, K., MECKLER, N., NAAFS, B. D. A., PÄLIKE, H., PANCOST, R. D., PEARSON, P. N., ROYER, D. L., SALZMANN, U., SCHUBERT, B., SEEBECK, H., SLUIJS, A., SPEIJER, R., STRASSEN, P., TIERNEY, J., TRIPATI, A., WADE, B., WESTERHOLD, T., WITKOWSKI, C., ZACHOS, J., ZHANG, Y. G., HUBER, M. & LUNT, D. J. 2019. The DeepMIP contribution to PMIP4: methodologies for selection, compilation and analysis of latest Paleocene and early Eocene climate proxy data, incorporating version 0.1 of the DeepMIP database. *Geoscientific Model Development,* 12, 3149-3206.

HÖNISCH, B., RIDGWELL, A., SCHMIDT, D. N., THOMAS, E., GIBBS, S. J., SLUIJS, A., ZEEBE, R., KUMP, L., MARTINDALE, R. C. & GREENE, S. E. 2012. The geological record of ocean acidification. *science,* 335, 1058-1063.

HOPMANS, E. C., WEIJERS, J. W., SCHEFUS, E., HERFORT, L., SINNINGHE DAMSTÉ, J. S. & SCHOUTEN, S. 2004. A novel proxy for terrestrial organic matter in sediments based on branched and isoprenoid tetraether lipids. *Earth and Planetary Science Letters,* 224, 107-116.

HOPMANS, E. C., SCHOUTEN, S. & SINNINGHE DAMSTÉ, J. S. 2016. The effect of improved chromatography on GDGT-based palaeoproxies. *Organic Geochemistry,* 93, 1-6.

HUBER, M. & SLOAN, L. C. 2001. Heat transport, deep waters, and thermal gradients: Coupled simulation of an Eocene greenhouse climate. *Geophysical Research Letters,* 28, 3481-3484.

HUBER, M., BRINKHUIS, H., STICKLEY, C. E., DÖÖS, K., SLUIJS, A., WARNAAR, J., SCHELLENBERG, S. A. & WILLIAMS, G. L. 2004. Eocene circulation of the Southern Ocean: was Antarctica kept warm by subtropical waters? *Paleoceanography,* 19, PA4026. http://doi.org/10.1029/2004PA001014.

HUBER, M. & CABALLERO, R. 2011. The early Eocene equable climate problem revisited. *Climate of the Past,* 7, 603-633.

IAKOVLEVA, A. I., BRINKHUIS, H. & CAVAGNETTO, C. 2001. Late Palaeocene–Early Eocene dinoflagellate cysts from the Turgay Strait, Kazakhstan; correlations across ancient seaways. *Palaeogeography, Palaeoclimatology, Palaeoecology,* 172, 243-268.

IAKOVLEVA, A. I. & HEILMANN-CLAUSEN, C. 2007. Wilsonidium pechoricum new species—A new dinoflagellate species with unusual asymmetry from the Paleocene/Eocene transition. *Journal of Paleontology,* 81, 1020-1030.

IMBRIE, J. & KIPP, N. G. 1971. A new micropaleontological method for quantitative paleoclimatology: application to a late Pleistocene Caribbean core. *In:* F, F. R. & K, T. K. (eds.) *The late Cenozoic glacial ages.* New Haven: Yale University Press.

INGLIS, G. N., FARNSWORTH, A., LUNT, D., FOSTER, G. L., HOLLIS, C. J., PAGANI, M., JARDINE, P. E., PEARSON, P. N., MARKWICK, P. & GALSWORTHY, A. M. 2015. Descent toward the Icehouse: Eocene sea surface cooling inferred from GDGT distributions. *Paleoceanography,* 30, 1000-1020.

INGLIS, G. N., CARMICHAEL, M. J., FARNSWORTH, A., LUNT, D. J. & PANCOST, R. D. 2020. A long-term, high-latitude record of Eocene hydrological change in the Greenland region. *Palaeogeography, Palaeoclimatology, Palaeoecology,* 537, 109378. https://doi.org/10.1016/j.palaeo.2019.109378.

IPCC 2013. Climate Change 2013: The Physical Science Basis. Contribution of Working Group I to the Fifth Assessment Report of the Intergovernmental Panel on Climate Change. *In:* STOCKER, T. F., QIN, D., PLATTNER, G.-K., TIGNOR, M., ALLEN, S. K., BOSCHUNG, J., NAUELS, A., XIA, Y., BEX, V. & MIDGLEY, P. M. (eds.) *Cambridge University Press.* Cambridge, United Kingdom and New York, NY, USA, 1535 pp.

JACOVIDES, J. 1999. Onsite biostratigraphic analyses of five boreholes from the Irish Rockall Trough. *Technical report by Millenia Ltd. Stratigraphic Consultants.*

JACOVIDES, J. 2000. Biostratigraphic review of the Tertiary sequence from: UK Rockall Trough well 132/15-1, Erris Trough well 12/13-1, and the shallow boreholes 11/20-Sb01, 16/28-Sb01, 83/20-Sb01, 83/24-Sb01 and 83/24-Sb-02, Irish Rockall Trough. *RSG Tertiary Biostratigraphy Review,* Project No: 441/00.

JEHLE, S., BORNEMANN, A., LÄGEL, A. F., DEPREZ, A. & SPEIJER, R. P. 2019. Paleoceanographic changes across the Latest Danian Event in the South Atlantic Ocean and planktic foraminiferal response. *Palaeogeography, Palaeoclimatology, Palaeoecology,* 525, 1-13.

JENKINS, D. 1985. Southern mid-latitude Paleocene to Holocene planktic foraminifera. *In:* BOLLI, H. M., SAUNDERS, J. B. & PERCH-NIELSEN, K. (eds.) *Plankton stratigraphy.* Cambridge: Cambridge University Press.

JOHN, C. M., BOHATY, S. M., ZACHOS, J. C., SLUIJS, A., GIBBS, S., BRINKHUIS, H. & BRALOWER, T. J. 2008. North American continental margin records of the Paleocene-Eocene thermal maximum: Implications for global carbon and hydrological cycling. *Paleoceanography,* 23, PA2217. http://doi.org/10.1029/2007PA001465.

JOHN, E. H., PEARSON, P. N., COXALL, H. K., BIRCH, H., WADE, B. S. & FOSTER, G. L. 2013. Warm ocean processes and carbon cycling in the Eocene. *Phil. Trans. R. Soc. A,* 371, 20130099. http://dx.doi.org/10.1098/rsta.2013.0099.

JOHN, E. H., WILSON, J. D., PEARSON, P. N. & RIDGWELL, A. 2014. Temperature-dependent remineralization and carbon cycling in the warm Eocene oceans. *Palaeogeography, Palaeoclimatology, Palaeoecology,* 413, 158-166.

JOHNSON, H., RITCHIE, J., HITCHEN, K., MCINROY, D. & KIMBELL, G. 2005. Aspects of the Cenozoic deformational history of the Northeast Faroe–Shetland Basin, Wyville–Thomson Ridge and Hatton Bank areas. *In:* DORÉ, A. G. & VINING, B. A. (eds.) *Petroleum Geology: North-West Europe and Global Perspectives - Proceedings of the 6th Petroleum Geology Conference.* Geological Society of London.

JONES, R. W. & MILTON, N. J. 1994. Sequence development during uplift: Palaeogene stratigraphy and relative sea-level history of the Outer Moray Firth, UK North Sea. *Marine and Petroleum Geology,* 11, 157-165.

JONES, S. M., WHITE, N. & LOVELL, B. 2001. Cenozoic and Cretaceous transient uplift in the Porcupine Basin and its relationship to a mantle plume. *Geological Society, London, Special Publications,* 188, 345-360.

JONES, S. M., WHITE, N., CLARKE, B. J., ROWLEY, E. & GALLAGHER, K. 2002. Present and past influence of the Iceland Plume on sedimentation. *Geological Society, London, Special Publications,* 196, 13-25.

JONES, S. M., HOGGETT, M., GREENE, S. E. & JONES, T. D. 2019. Large Igneous Province thermogenic greenhouse gas flux could have initiated Paleocene-Eocene Thermal Maximum climate change. *Nature Communications,* 10, 1-16.

JONKERS, L. & KUČERA, M. 2015. Global analysis of seasonality in the shell flux of extant planktonic Foraminifera. *Biogeosciences,* 12, 2207-2226.

KAHN, M. 1979. Non-equilibrium oxygen and carbon isotopic fractionation in tests of living planktonic foraminifera. *Oceanologica Acta,* 2, 195-208.

KAHN, M. I. & WILLIAMS, D. F. 1981. Oxygen and carbon isotopic composition of living planktonic foraminifera from the northeast Pacific Ocean. *Palaeogeography, Palaeoclimatology, Palaeoecology,* 33, 47-69.

KAIHO, K., ARINOBU, T., ISHIWATARI, R., MORGANS, H. E., OKADA, H., TAKEDA, N., TAZAKI, K., ZHOU, G., KAJIWARA, Y. & MATSUMOTO, R. 1996. Latest Paleocene benthic foraminiferal extinction and environmental changes at Tawanui, New Zealand. *Paleoceanography,* 11, 447-465.

KARNER, M. B., DELONG, E. F. & KARL, D. M. 2001. Archaeal dominance in the mesopelagic zone of the Pacific Ocean. *Nature,* 409, 507-510.

KATZ, M. E., CRAMER, B. S., MOUNTAIN, G. S., KATZ, S. & MILLER, K. G. 2001. Uncorking the bottle: What triggered the Paleocene/Eocene thermal maximum methane release? *Paleoceanography,* 16, 549-562.

KATZ, M. E., KATZ, D. R., WRIGHT, J. D., MILLER, K. G., PAK, D. K., SHACKLETON, N. J. & THOMAS, E. 2003. Early Cenozoic benthic foraminiferal isotopes: Species reliability and interspecies correction factors. *Paleoceanography and Paleoclimatology,* 18, 1024. http://doi.org/10.1029/2002PA000798.

KATZ, M. E., MILLER, K. G., WRIGHT, J. D., WADE, B. S., BROWNING, J. V., CRAMER, B. S. & ROSENTHAL, Y. 2008. Stepwise transition from the Eocene greenhouse to the Oligocene icehouse. *Nature Geoscience,* 1, 329.

KAUR, G., MOUNTAIN, B. W., STOTT, M. B., HOPMANS, E. C. & PANCOST, R. D. 2015. Temperature and pH control on lipid composition of silica sinters from diverse hot springs in the Taupo Volcanic Zone, New Zealand. *Extremophiles,* 19, 327-344.

KENNETT, J. & STOTT, L. 1991. Abrupt deep sea warming, paleoceanographic changes and benthic extinctions at the end of the Paleocene. *Nature,* 353, 225-229.

KENNETT, J. P. 1977. Cenozoic evolution of Antarctic glaciation, the circum-Antarctic Ocean, and their impact on global paleoceanography. *Journal of Geophysical Research,* 82, 3843-3860.

KENNETT, J. P., CANNARIATO, K. G., HENDY, I. L. & BEHL, R. J. 2003. *Methane Hydrates in Quaternary Climate Change: The Clathrate Gun Hypothesi,* Washington, DC, American Geophysical Union.

KENNETT, J. P. & EXON, N. F. 2004. Paleoceanographic evolution of the Tasmanian Seaway and its climatic implications. *The Cenozoic Southern Ocean: Tectonics, Sedimentation, and Climate Change Between Australia and Antarctica*, 345-367.

KENT, D. V., CRAMER, B. S., LANCI, L., WANG, D., WRIGHT, J. D. & VAN DER VOO, R. 2003. A case for a comet impact trigger for the Paleocene/Eocene thermal maximum and carbon isotope excursion. *Earth and Planetary Science Letters,* 211, 13-26.

KENT, D. V., LANCI, L., WANG, H. & WRIGHT, J. D. 2017. Enhanced magnetization of the Marlboro Clay as a product of soil pyrogenesis at the Paleocene–Eocene boundary? *Earth and Planetary Science Letters,* 473, 303-312.

KIEHL, J. T., SHIELDS, C. A., SNYDER, M. A., ZACHOS, J. C. & ROTHSTEIN, M. 2018. Greenhouse- and orbital-forced climate extremes during the early Eocene. *Phil. Trans. R. Soc. A,* 376, 20170085. http://dx.doi.org/10.1098/rsta.2017.0085.

KIM, J.-H., SCHOUTEN, S., HOPMANS, E. C., DONNER, B. & SINNINGHE DAMSTÉ, J. S. 2008. Global sediment core-top calibration of the TEX86 paleothermometer in the ocean. *Geochimica et Cosmochimica Acta,* 72, 1154-1173.

KIM, J.-H., VAN DER MEER, J., SCHOUTEN, S., HELMKE, P., WILLMOTT, V., SANGIORGI, F., KOÇ, N., HOPMANS, E. C. & SINNINGHE DAMSTÉ, J. S. 2010. New indices and calibrations derived from the distribution of crenarchaeal isoprenoid tetraether lipids: Implications for past sea surface temperature reconstructions. *Geochimica et Cosmochimica Acta,* 74, 4639-4654.

KIM, S.-T. & O'NEIL, J. R. 1997. Equilibrium and nonequilibrium oxygen isotope effects in synthetic carbonates. *Geochimica et Cosmochimica Acta,* 61, 3461-3475.

KIRTLAND TURNER, S., SEXTON, P. F., CHARLES, C. D. & NORRIS, R. D. 2014. Persistence of carbon release events through the peak of early Eocene global warmth. *Nature Geoscience,* 7, 748-751.

KLINGELHÖFER, F., EDWARDS, R., HOBBS, R. & ENGLAND, R. W. 2005. Crustal structure of the NE Rockall Trough from wide-angle seismic data modeling. *Journal of Geophysical Research: Solid Earth* 110, B11105. http://doi.org/10.1029/2005JB003763.

KNOTT, S., BURCHELL, M., JOLLEY, E. & FRASER, A. 1993. Mesozoic to Cenozoic plate reconstructions of the North Atlantic and hydrocarbon plays of the Atlantic margins. *In:* PARKER, J. R. (ed.) *Petroleum Geology of Northwest Europe: Proceedings of the 4th Conference.* London: Geological Society of London.

KOCKEN, I. J., CRAMWINCKEL, M. J., ZEEBE, R. E., MIDDELBURG, J. J. & SLUIJS, A. 2019. The 405 kyr and 2.4 Myr eccentricity components in Cenozoic carbon isotope records. *Climate of the Past,* 15, 91-104.

KRETSCHMER, K., JONKERS, L., KUCERA, M. & SCHULZ, M. 2018. Modeling seasonal and vertical habitats of planktonic foraminifera on a global scale. *Biogeosciences,* 15, 4405-4429.

KROOPNICK, P. 1985. The distribution of 13C of ΣCO2 in the world oceans. *Deep Sea Research Part A. Oceanographic Research Papers,* 32, 57-84.

KUCERA, M. 2007. Chapter six planktonic foraminifera as tracers of past oceanic environments. *Developments in marine geology,* 1, 213-262.

KURTZ, A., KUMP, L., ARTHUR, M., ZACHOS, J. & PAYTAN, A. 2003. Early Cenozoic decoupling of the global carbon and sulfur cycles. *Paleoceanography,* 18, 1090. http://doi.org/10.1029/2003PA000908.

L'HOMME, N., CLARKE, G. K. & RITZ, C. 2005. Global budget of water isotopes inferred from polar ice sheets. *Geophysical Research Letters,* 32, L20502. http://doi.org/10.1029/2005GL023774.

LAURETANO, V., LITTLER, K., POLLING, M., ZACHOS, J. & LOURENS, L. 2015. Frequency, magnitude and character of hyperthermal events at the onset of the Early Eocene Climatic Optimum. *Climate of the Past,* 11, 1313-1324.

LAURETANO, V., HILGEN, F., ZACHOS, J. & LOURENS, L. 2016. Astronomically tuned age model for the early Eocene carbon isotope events: A new high-resolution δ13 Cbenthic record of ODP Site 1263 between~ 49 and~ 54 Ma. *Newsletters on Stratigraphy,* 49, 383-400.

LAURETANO, V., ZACHOS, J. C. & LOURENS, L. J. 2018. Orbitally Paced Carbon and Deep-Sea Temperature Changes at the Peak of the Early Eocene Climatic Optimum. *Paleoceanography and Paleoclimatology,* 33, 1050-1065.

LAURIN, J., MEYERS, S. R., GALEOTTI, S. & LANCI, L. 2016. Frequency modulation reveals the phasing of orbital eccentricity during Cretaceous Oceanic Anoxic

Event II and the Eocene hyperthermals. *Earth and Planetary Science Letters,* 442, 143-156.

LEGRANDE, A. N. & SCHMIDT, G. A. 2006. Global gridded data set of the oxygen isotopic composition in seawater. *Geophysical Research Letters,* 33, L12603. http://doi.org/10.1029/2006GL026011.

LEON-RODRIGUEZ, L. & DICKENS, G. R. 2010. Constraints on ocean acidification associated with rapid and massive carbon injections: The early Paleogene record at ocean drilling program site 1215, equatorial Pacific Ocean. *Palaeogeography, Palaeoclimatology, Palaeoecology,* 298, 409-420.

LITTLER, K., RÖHL, U., WESTERHOLD, T. & ZACHOS, J. C. 2014. A high-resolution benthic stable-isotope record for the South Atlantic: Implications for orbital-scale changes in Late Paleocene–Early Eocene climate and carbon cycling. *Earth and Planetary Science Letters,* 401, 18-30.

LIU, Z., PAGANI, M., ZINNIKER, D., DECONTO, R., HUBER, M., BRINKHUIS, H., SHAH, S. R., LECKIE, R. M. & PEARSON, A. 2009. Global cooling during the Eocene-Oligocene climate transition. *Science,* 323, 1187-1190.

LOURENS, L. J., SLUIJS, A., KROON, D., ZACHOS, J. C., THOMAS, E., RÖHL, U., BOWLES, J. & RAFFI, I. 2005. Astronomical pacing of late Palaeocene to early Eocene global warming events. *Nature,* 435, 1083-1087.

LOWENSTAM, H. A. 1981. Minerals formed by organisms. *Science,* 211, 1126-1131.

LUCIANI, V., GIUSBERTI, L., AGNINI, C., FORNACIARI, E., RIO, D., SPOFFORTH, D. J. & PÄLIKE, H. 2010. Ecological and evolutionary response of Tethyan planktonic foraminifera to the middle Eocene climatic optimum (MECO) from the Alano section (NE Italy). *Palaeogeography, Palaeoclimatology, Palaeoecology,* 292, 82-95.

LUCIANI, V., DICKENS, G. R., BACKMAN, J., FORNACIARI, E., GIUSBERTI, L., AGNINI, C. & D'ONOFRIO, R. 2016. Major perturbations in the global carbon cycle and photosymbiont-bearing planktic foraminifera during the early Eocene. *Climate of the Past,* 12, 981-1007. http://doi.org/10.5194/cp-12-981-2016.

LUCIANI, V., D'ONOFRIO, R., DICKENS, G. R. & WADE, B. S. 2017a. Planktic foraminiferal response to early Eocene carbon cycle perturbations in the southeast Atlantic Ocean (ODP Site 1263). *Global and Planetary Change,* 158, 119-133.

LUCIANI, V., D'ONOFRIO, R., DICKENS, G. R. & WADE, B. S. 2017b. Did Photosymbiont Bleaching Lead to the Demise of Planktic Foraminifer Morozovella at the Early Eocene Climatic Optimum? *Paleoceanography,* 32, 1115-1136.

LUNT, D. J., VALDES, P. J., JONES, T. D., RIDGWELL, A., HAYWOOD, A. M., SCHMIDT, D. N., MARSH, R. & MASLIN, M. 2010. CO2-driven ocean circulation changes as an amplifier of Paleocene-Eocene thermal maximum hydrate destabilization. *Geology,* 38, 875-878.

LUNT, D. J., DUNKLEY JONES, T., HEINEMANN, M., HUBER, M., LEGRANDE, A., WINGUTH, A., LOPTSON, C., MAROTZKE, J., ROBERTS, C. & TINDALL, J. 2012. A model–data comparison for a multi-model ensemble of early Eocene atmosphere–ocean simulations: EoMIP. *Climate of the Past,* 8, 1717-1736.

MACLENNAN, J. & JONES, S. M. 2006. Regional uplift, gas hydrate dissociation and the origins of the Paleocene–Eocene Thermal Maximum. *Earth and Planetary Science Letters,* 245, 65-80.

MALEVICH, S. B., VETTER, L. & TIERNEY, J. E. 2019. Global Core Top Calibration of δ 18O in Planktic Foraminifera to Sea Surface Temperature. *Paleoceanography and Paleoclimatology,* 34, 1292-1315.

MANN, S. 1983. Mineralization in biological systems. *In:* CONNETT, P. H., FOLLMANN, H., LAMMERS, M., MANN, S., ODOM, J. D. & WETTERHAHN, K. E. (eds.) *Inorganic Elements in Biochemistry.* Springer-Verlag Berlin Heidelberg GmbH.

MANNERS, H. R., GRIMES, S. T., SUTTON, P. A., DOMINGO, L., LENG, M. J., TWITCHETT, R. J., HART, M. B., JONES, T. D., PANCOST, R. D. & DULLER, R. 2013. Magnitude and profile of organic carbon isotope records from the Paleocene–Eocene Thermal Maximum: Evidence from northern Spain. *Earth and Planetary Science Letters,* 376, 220-230.

MARION, G., MILLERO, F. J., CAMÕES, M., SPITZER, P., FEISTEL, R. & CHEN, C.-T. 2011. pH of seawater. *Marine Chemistry,* 126, 89-96.

MARKWICK, P. 2007. The palaeogeographic and palaeoclimatic significance of climate proxies for data-model comparisons. *In:* WILLIAMS, M., HAYWOOD, A. M., GREGORY, F. J. & SCHMIDT, D. N. (eds.) *Deep-time perspectives on climate change: marrying the signal from computer models and biological proxies.* London: The Geological Society for The Micropalaeontological Society.

MARRAMÀ, G., CARNEVALE, G., SMIRNOV, P. V., TRUBIN, Y. S. & KRIWET, J. 2019. First report of Eocene gadiform fishes from the Trans-Urals (Sverdlovsk and Tyumen regions, Russia). *Journal of Paleontology,* 93, 1001-1009.

MARTÍN-FERNÁNDEZ, J. & THIÓ-HENESTROSA, S. 2006. Rounded zeros: some practical aspects for compositional data. *Geological Society, London, Special Publications,* 264, 191-201.

MARTINI, E. 1971. Standard Tertiary and Quaternary calcareous nannoplankton zonation. Proceedings II Planktonic Conference, 1971 1971 Roma. 739-785.

MCCONNAUGHEY, T. 1989. 13C and 18O isotopic disequilibrium in biological carbonates: II. In vitro simulation of kinetic isotope effects. *Geochimica et Cosmochimica Acta,* 53, 163-171.

MCCREA, J. M. 1950. On the isotopic chemistry of carbonates and a paleotemperature scale. *The Journal of Chemical Physics,* 18, 849-857.

MCDONNELL, A. & SHANNON, P. 2001. Comparative Tertiary stratigraphic evolution of the Porcupine and Rockall basins. *Geological Society, London, Special Publications,* 188, 323-344.

MCINROY, D., HITCHEN, K. & STOKER, M. 2006. Potential Eocene and Oligocene stratigraphic traps of the Rockall Plateau, NE Atlantic margin. *Geological Society, London, Special Publications,* 254, 247-266.

MEILLAND, J., SICCHA, M., WEINKAUF, M. F., JONKERS, L., MORARD, R., BARANOWSKI, U., BAUMEISTER, A., BERTLICH, J., BRUMMER, G.-J., DEBRAY, P., FRITZ-ENDRES, T., GROENEVELD, J., MARGERL, L., MUNZ, P., RILLO, M. C., SCHMIDT, C., TAKAGI, H., THEARA, G. & KUCERA, M. 2019. Highly replicated sampling reveals no diurnal vertical migration but stable species-specific vertical habitats in planktonic foraminifera. *Journal of Plankton Research,* 41, 127-141.

MEINSHAUSEN, M., SMITH, S. J., CALVIN, K., DANIEL, J. S., KAINUMA, M., LAMARQUE, J.-F., MATSUMOTO, K., MONTZKA, S., RAPER, S. & RIAHI, K. 2011. The RCP greenhouse gas concentrations and their extensions from 1765 to 2300. *Climatic change,* 109, 213-241.

MONTES, C., CARDONA, A., MCFADDEN, R., MORÓN, S., SILVA, C., RESTREPO-MORENO, S., RAMÍREZ, D., HOYOS, N., WILSON, J. & FARRIS, D. 2012. Evidence for middle Eocene and younger land emergence in central Panama: implications for Isthmus closure. *Bulletin,* 124, 780-799.

MONTES, C., CARDONA, A., JARAMILLO, C., PARDO, A., SILVA, J., VALENCIA, V., AYALA, C., PÉREZ-ANGEL, L., RODRIGUEZ-PARRA, L. & RAMIREZ, V. 2015. Middle Miocene closure of the Central American seaway. *Science,* 348, 226-229.

MOUNTAIN, G. S. & MILLER, K. G. 1992. Seismic and geologic evidence for early Paleogene deepwater circulation in the western North Atlantic. *Paleoceanography,* 7, 423-439.

MUSGROVE, F. & MITCHENER, B. 1996. Analysis of the pre-Tertiary rifting history of the Rockall Trough. *Petroleum Geoscience,* 2, 353-360.

NAYLOR, D., SHANNON, P. & MURPHY, N. 1999. Irish Rockall Basin region - a standard structural nomenclature system. *Special Publication 1/99.* Dublin: Petroleum Affairs Division, Department of the Marine and Natural Resources.

NAYLOR, D. & SHANNON, P. 2005. The structural framework of the Irish Atlantic Margin. *In:* DORÉ, A. G. & VINING, B. A. (eds.) *Petroleum Geology: North-West Europe Global Perspectives - Proceedings of the 6th Petroleum Geology Conference.* London: Geological Society.

NEVILLE, L. A., GRASBY, S. E. & MCNEIL, D. H. 2019. Limited freshwater cap in the Eocene Arctic Ocean. *Scientific reports,* 9, 4226. https://doi.org/10.1038/s41598-019-40591-w

NICOLO, M. J., DICKENS, G. R., HOLLIS, C. J. & ZACHOS, J. C. 2007. Multiple early Eocene hyperthermals: Their sedimentary expression on the New Zealand continental margin and in the deep sea. *Geology,* 35, 699-702.

NIELSEN, T. K., LARSEN, H. C. & HOPPER, J. R. 2002. Contrasting rifted margin styles south of Greenland: implications for mantle plume dynamics. *Earth and Planetary Science Letters,* 200, 271-286.

NORRIS, R., KLAUS, A. & KROON, D. 2001. Mid-Eocene deep water, the late Palaeocene thermal maximum and continental slope mass wasting during the Cretaceous-Palaeogene impact. *Geological Society, London, Special Publications,* 183, 23-48.

NORRIS, R., WILSON, P., BLUM, P., FEHR, A., AGNINI, C., BORNEMANN, A., BOULILA, S., BOWN, P., COURNEDE, C., FRIEDRICH, O., GOSH, A., HOLLIS, C. J., HULL, P., JO, K., JUNIUM, C. K., KANEKO, M., LIEBRAND, D., LIPPERT, P., LIU, Z., MATSUI, H., MORIYA, K., NISHI, H., OPDYKE, B., PENMAN, D., ROMANS, B., SCHER, H., SEXTON, P., TAKAGI, H., TURNER, S., WHITESIDE, J., YAMAGUCHI, T. & YAMAMOTO, Y. 2014. Expedition 342 summary. *In:* NORRIS, R., WILSON, P., BLUM, P. & SCIENTISTS, A. T. E. (eds.) *Proc. IODP, 342.* College Station, TX (Integrated OCean Drilling Progam).

NORRIS, R. D. 1998. Recognition and macroevolutionary significance of photosymbiosis in molluscs, corals, and foraminifera. *The Paleontological Society Papers,* 4, 68-100.

NUNES, F. & NORRIS, R. D. 2006. Abrupt reversal in ocean overturning during the Palaeocene/Eocene warm period. *Nature,* 439, 60-63.

O'CONNELL, S., CHANDLER, M. A. & RUEDY, R. 1996. Implications for the creation of warm saline deep water: Late Paleocene reconstructions and global climate model simulations. *Geological Society of America Bulletin,* 108, 270-284.

OLSSON, R. K., HEMLEBEN, C., HUBER, B. T. & BERGGREN, W. A. 2006. Taxonomy, biostratigraphy, and phylogeny of Eocene Globigerina, Globoturborotalita, Subbotina, and Turborotalita. *Atlas of Eocene Planktonic Foraminifera. Cushman Foundation Special Publication,* 41, 111-168.

OPPO, D. W. & FAIRBANKS, R. G. 1989. Carbon isotope composition of tropical surface water during the past 22,000 years. *Paleoceanography,* 4, 333-351.

PAGANI, M., ZACHOS, J. C., FREEMAN, K. H., TIPPLE, B. & BOHATY, S. 2005. Marked decline in atmospheric carbon dioxide concentrations during the Paleogene. *Science,* 309, 600-603.

PAILLARD, D., LABEYRIE, L. & YIOU, P. 1996. Macintosh program performs time-series analysis. *Eos, Transactions American Geophysical Union,* 77, 379-379.

PAK, D. K. & MILLER, K. G. 1992. Paleocene to Eocene benthic foraminiferal isotopes and assemblages: Implications for deepwater circulation. *Paleoceanography and Paleoclimatology,* 7, 405-422.

PALAEOSENS 2012. Making sense of palaeoclimate sensitivity. *Nature,* 491, 683-691.

PÄLIKE, H., NORRIS, R. D., HERRLE, J. O., WILSON, P. A., COXALL, H. K., LEAR, C. H., SHACKLETON, N. J., TRIPATI, A. K. & WADE, B. S. 2006. The heartbeat of the Oligocene climate system. *science,* 314, 1894-1898.

PANCHUK, K., RIDGWELL, A. & KUMP, L. 2008. Sedimentary response to Paleocene-Eocene Thermal Maximum carbon release: A model-data comparison. *Geology,* 36, 315-318.

PARNELL-TURNER, R., WHITE, N., HENSTOCK, T., MURTON, B., MACLENNAN, J. & JONES, S. M. 2014. A continuous 55-million-year record of transient mantle plume activity beneath Iceland. *Nature Geoscience,* 7, 914-919.

PAWLOWSKY-GLAHN, V. & EGOZCUE, J. J. 2006. Compositional data and their analysis: an introduction. *Geological Society, London, Special Publications,* 264, 1-10.

PEARSON, A., PI, Y., ZHAO, W., LI, W., LI, Y., INSKEEP, W., PEREVALOVA, A., ROMANEK, C., LI, S. & ZHANG, C. L. 2008. Factors controlling the distribution of archaeal tetraethers in terrestrial hot springs. *Appl. Environ. Microbiol.,* 74, 3523-3532.

PEARSON, P., SHACKLETON, N. & HALL, M. 1993. Stable isotope paleoecology of middle Eocene planktonic foraminifera and multi-species isotope stratigraphy, DSDP Site 523, South Atlantic. *The Journal of Foraminiferal Research,* 23, 123-140.

PEARSON, P., OLSSON, R., HUBER, B., HEMLEBEN, C. & BERGGREN, W. 2006. *Atlas of Eocene Planktonic Foraminifera*.

PEARSON, P. N., DITCHFIELD, P. W., SINGANO, J., HARCOURT-BROWN, K. G., NICHOLAS, C. J., OLSSON, R. K., SHACKLETON, N. J. & HALL, M. A. 2001. Warm tropical sea surface temperatures in the Late Cretaceous and Eocene epochs. *Nature,* 413, 481-487.

PEARSON, P. N., VAN DONGEN, B. E., NICHOLAS, C. J., PANCOST, R. D., SCHOUTEN, S., SINGANO, J. M. & WADE, B. S. 2007. Stable warm tropical climate through the Eocene Epoch. *Geology,* 35, 211-214.

PEARSON, P. N. & BURGESS, C. E. 2008. Foraminifer test preservation and diagenesis: comparison of high latitude Eocene sites. *Geological Society, London, Special Publications,* 303, 59-72.

PEARSON, P. N. 2012. Oxygen isotopes in foraminifera: Overview and historical review. *Paleontological Society Papers,* 18, 1-38.

PEDERSEN, T. & PRICE, N. 1982. The geochemistry of manganese carbonate in Panama Basin sediments. *Geochimica et Cosmochimica Acta,* 46, 59-68.

PENMAN, D. E., HÖNISCH, B., ZEEBE, R. E., THOMAS, E. & ZACHOS, J. C. 2014. Rapid and sustained surface ocean acidification during the Paleocene-Eocene Thermal Maximum. *Paleoceanography,* 29, 357-369.

PENMAN, D. E., KELLER, A., D'HAENENS, S., KIRTLAND TURNER, S. & HULL, P. M. 2019. Atlantic Deep-Sea Cherts Associated With Eocene Hyperthermal Events. *Paleoceanography and Paleoclimatology,* 34, 287-299.

PESTER, M., SCHLEPER, C. & WAGNER, M. 2011. The Thaumarchaeota: an emerging view of their phylogeny and ecophysiology. *Current opinion in Microbiology,* 14, 300-306.

PETERSE, F., KIM, J.-H., SCHOUTEN, S., KRISTENSEN, D. K., KOÇ, N. & SINNINGHE DAMSTÉ, J. S. 2009. Constraints on the application of the MBT/CBT palaeothermometer at high latitude environments (Svalbard, Norway). *Organic Geochemistry,* 40, 692-699.

PETERSE, F., VAN DER MEER, J., SCHOUTEN, S., WEIJERS, J. W., FIERER, N., JACKSON, R. B., KIM, J.-H. & SINNINGHE DAMSTÉ, J. S. 2012. Revised calibration of the MBT–CBT paleotemperature proxy based on branched tetraether membrane lipids in surface soils. *Geochimica et Cosmochimica Acta,* 96, 215-229.

PETRIZZO, M. R. 2007. The onset of the Paleocene–Eocene Thermal Maximum (PETM) at Sites 1209 and 1210 (Shatsky Rise, Pacific Ocean) as recorded by planktonic foraminifera. *Marine Micropaleontology,* 63, 187-200.

PITMAN, W., TALWANI, M. & HEIRTZLER, J. 1971. Age of the North Atlantic Ocean from magnetic anomalies. *Earth and Planetary Science Letters,* 11, 195-200.

PITMAN, W. C. & TALWANI, M. 1972. Sea-floor spreading in the North Atlantic. *Geological Society of America Bulletin,* 83, 619-646.

PLANK, T. & LANGMUIR, C. H. 1998. The chemical composition of subducting sediment and its consequences for the crust and mantle. *Chemical geology,* 145, 325-394.

POORE, R. & MATTHEWS, R. 1984. Oxygen isotope ranking of late Eocene and Oligocene planktonic foraminifers: implications for Oligocene sea-surface temperatures and global ice-volume. *Marine Micropaleontology,* 9, 111-134.

PROSS, J., CONTRERAS, L., BIJL, P. K., GREENWOOD, D. R., BOHATY, S. M., SCHOUTEN, S., BENDLE, J. A., RÖHL, U., TAUXE, L. & RAINE, J. I. 2012. Persistent near-tropical warmth on the Antarctic continent during the early Eocene epoch. *Nature,* 488, 73-77.

QUILLÉVÉRÉ, F., NORRIS, R. D., MOUSSA, I. & BERGGREN, W. A. 2001. Role of photosymbiosis and biogeography in the diversification of early Paleogene acarininids (planktonic foraminifera). *Paleobiology,* 27, 311-326.

RAMPINO, M. R. 2013. Peraluminous igneous rocks as an indicator of thermogenic methane release from the North Atlantic Volcanic Province at the time of the

Paleocene–Eocene Thermal Maximum (PETM). *Bulletin of volcanology,* 75, 678. http://doi.org/10.1007/s00445-012-0678-x.

RAMSAY, A. T., SYKES, T. J. & KIDD, R. B. 1994. Waxing (and Waning) lyrical on hiatuses: Eocene-Quaternary Indian Ocean hiatuses as proxy indicators of water mass production. *Paleoceanography,* 9, 857-877.

REBOTIM, A., VOELKER, A. H., JONKERS, L., WANIEK, J. J., MEGGERS, H., SCHIEBEL, R., FRAILE, I., SCHULZ, M. & KUCERA, M. 2017. Factors controlling the depth habitat of planktonic foraminifera in the subtropical eastern North Atlantic. *Biogeosciences,* 14, 827-859.

ROBERTS, C. D., LEGRANDE, A. N. & TRIPATI, A. K. 2011. Sensitivity of seawater oxygen isotopes to climatic and tectonic boundary conditions in an early Paleogene simulation with GISS ModelE-R. *Paleoceanography,* 26, PA4203. http://doi.org/10.1029/2010PA002025.

ROBERTS, D., THOMPSON, M., MITCHENER, B., HOSSACK, J., CARMICHAEL, S. & BJØRNSETH, H.-M. 1999. Palaeozoic to Tertiary rift and basin dynamics: mid-Norway to the Bay of Biscay – a new context for hydrocarbon prospectivity in the deep water frontier. *In:* FLEET, A. J. & BOLDY, S. A. R. (eds.) *Petroleum Geology of Northwest Europe: Proceedings of the 5th Conference.* London: Geological Society

RÖHL, U., BRALOWER, T., NORRIS, R. & WEFER, G. 2000. New chronology for the late Paleocene thermal maximum and its environmental implications. *Geology,* 28, 927-930.

RÖHL, U., WESTERHOLD, T., MONECHI, S., THOMAS, E., ZACHOS, J. C. & DONNER, B. The Third and Final Early Eocene Thermal Maximum: Characteristics, Timing and Mechanisms of the 'X'Event. GSA Annual Meeting, 2005.

ROHLING, E. J. 2013. Oxygen isotope composition of seawater. *The Encyclopedia of Quaternary Science. Amsterdam: Elsevier,* 2, 915-922.

ROHLING, E. J., MARINO, G., FOSTER, G. L., GOODWIN, P. A., VON DER HEYDT, A. S. & KÖHLER, P. 2018. Comparing climate sensitivity, past and present. *Annual review of marine science,* 10, 261-288.

ROTHWELL, R. G. 2015. Twenty years of XRF core scanning marine sediments: What do geochemical proxies tell us? *Micro-XRF Studies of Sediment Cores.* Springer.

ROWLEY, D. B. 1996. Age of initiation of collision between India and Asia: A review of stratigraphic data. *Earth and Planetary Science Letters,* 145, 1-13.

SARKAR, S., BASAK, C., FRANK, M., BERNDT, C., HUUSE, M., BADHANI, S. & BIALAS, J. 2019. Late Eocene onset of the Proto-Antarctic Circumpolar Current. *Scientific Reports,* 9, 10125. https://doi.org/10.1038/s41598-019-46253-1.

SAUNDERS, A., FITTON, J., KERR, A., NORRY, M. & KENT, R. 1997. The north Atlantic igneous province. *Large igneous provinces: Continental, oceanic, and planetary flood volcanism,* 100, 45-93.

SAVIN, S. M. & DOUGLAS, R. G. 1973. Stable isotope and magnesium geochemistry of recent planktonic foraminifera from the South Pacific. *Geological Society of America Bulletin,* 84, 2327-2342.

SCHALLER, M. F., FUNG, M. K., WRIGHT, J. D., KATZ, M. E. & KENT, D. V. 2016. Impact ejecta at the Paleocene-Eocene boundary. *Science,* 354, 225-229.

SCHALLER, M. F. & FUNG, M. K. 2018. The extraterrestrial impact evidence at the Palaeocene–Eocene boundary and sequence of environmental change on the continental shelf. *Phil. Trans. R. Soc. A,* 376, 20170081.

SCHER, H. D. & MARTIN, E. E. 2004. Circulation in the Southern Ocean during the Paleogene inferred from neodymium isotopes. *Earth and Planetary Science Letters,* 228, 391-405.

SCHIEBEL, R. & HEMLEBEN, C. 2017. *Planktic foraminifers in the modern ocean*, Springer.

SCHIEBEL, R., SMART, S. M., JENTZEN, A., JONKERS, L., MORARD, R., MEILLAND, J., MICHEL, E., COXALL, H. K., HULL, P. M. & DE GARIDEL-THORON, T. 2018. Advances in planktonic foraminifer research: New perspectives for paleoceanography. *Revue de Micropaléontologie,* 61, 113-138.

SCHMITZ, B., PEUCKER-EHRENBRINK, B., HEILMANN-CLAUSEN, C., ÅBERG, G., ASARO, F. & LEE, C.-T. A. 2004. Basaltic explosive volcanism, but no comet impact, at the Paleocene–Eocene boundary: high-resolution chemical and isotopic records from Egypt, Spain and Denmark. *Earth and Planetary Science Letters,* 225, 1-17.

SCHOUTEN, S., HOPMANS, E. C., SCHEFUS, E. & SINNINGHE DAMSTÉ, J. S. 2002. Distributional variations in marine crenarchaeotal membrane lipids: a new tool for reconstructing ancient sea water temperatures? *Earth and Planetary Science Letters,* 204, 265-274.

SCHOUTEN, S., HOPMANS, E. C. & SINNINGHE DAMSTÉ, J. S. 2004. The effect of maturity and depositional redox conditions on archaeal tetraether lipid palaeothermometry. *Organic Geochemistry,* 35, 567-571.

SCHOUTEN, S., FORSTER, A., PANOTO, F. E. & SINNINGHE DAMSTÉ, J. S. 2007. Towards calibration of the TEX86 palaeothermometer for tropical sea surface temperatures in ancient greenhouse worlds. *Organic Geochemistry,* 38, 1537-1546.

SCHOUTEN, S., HOPMANS, E. C. & SINNINGHE DAMSTÉ, J. S. 2013. The organic geochemistry of glycerol dialkyl glycerol tetraether lipids: A review. *Organic Geochemistry,* 54, 19-61.

SCHRAG, D. P., DEPAOLO, D. J. & RICHTER, F. M. 1995. Reconstructing past sea surface temperatures: Correcting for diagenesis of bulk marine carbonate. *Geochimica et Cosmochimica Acta,* 59, 2265-2278.

SEXTON, P. F., WILSON, P. A. & NORRIS, R. D. 2006a. Testing the Cenozoic multisite composite δ18O and δ13C curves: New monospecific Eocene records from a single locality, Demerara Rise (Ocean Drilling Program Leg 207). *Paleoceanography,* 21, PA2019. http://doi.org/1029/2005PA001253.

SEXTON, P. F., WILSON, P. A. & PEARSON, P. N. 2006b. Palaeoecology of late middle Eocene planktic foraminifera and evolutionary implications. *Marine Micropaleontology,* 60, 1-16.

SEXTON, P. F., WILSON, P. A. & PEARSON, P. N. 2006c. Microstructural and geochemical perspectives on planktic foraminiferal preservation:“Glassy” versus “Frosty”. *Geochemistry, Geophysics, Geosystems,* 7, Q12P19. http://doi.org/10.1029/2006GC001291.

SEXTON, P. F., NORRIS, R. D., WILSON, P. A., PÄLIKE, H., WESTERHOLD, T., RÖHL, U., BOLTON, C. T. & GIBBS, S. 2011. Eocene global warming events driven by ventilation of oceanic dissolved organic carbon. *Nature,* 471, 349-352.

SHACKLETON, N., WISEMAN, J. & BUCKLEY, H. 1973. Non-equilibrium isotopic fractionation between seawater and planktonic foraminiferal tests. *Nature,* 242, 177-179.

SHACKLETON, N. & BOERSMA, A. 1981. The climate of the Eocene ocean. *Journal of the Geological Society,* 138, 153-157.

SHACKLETON, N., CORFIELD, R. & HALL, M. 1985. Stable isotope data and the ontogeny of Paleocene planktonic foraminifera. *The Journal of Foraminiferal Research,* 15, 321-336.

SHANNON, P. 1991. The development of Irish offshore sedimentary basins. *Journal of the Geological Society,* 148, 181-189.

SHANNON, P., JACOB, A., MAKRIS, J., O'REILLY, B., HAUSER, F. & VOGT, U. 1994. Basin evolution in the Rockall region, North Atlantic. *First break,* 12, 515-522.

SHANNON, P., JACOB, A., MAKRIS, J., O'REILLY, B., HAUSER, F. & VOGT, U. 1995. Basin development and petroleum prospectivity of the Rockall and Hatton region. *Geological Society, London, Special Publications,* 93, 435-457.

SHANNON, P., JACOB, A., O'REILLY, B., HAUSER, F., READMAN, P. & MAKRIS, J. 1999. Structural setting, geological development and basin modelling in the Rockall Trough. *In:* FLEET, A. J. & BOLDY, S. A. R. (eds.) *Petoleum Geology of Northwest Europe: Proceedings of the 5th Conference.* London: Geological Society.

SIGMAN, D. M. & HAUG, G. 2003. *The biological pump in the past*, Elservier.

SINNINGHE DAMSTÉ, J., HOPMANS, E., PANCOST, R., SCHOUTEN, S. & GEENEVASEN, J. 2000. Newly discovered non-isoprenoid dialkyl diglycerol tetraether lipids in sediments. *Chemical Communications*, 1683-1684. http://doi.org/10.1039/b004517i.

SINNINGHE DAMSTÉ, J., HOPMANS, E., SCHOUTEN, S., VAN DUIN, A. & GEENEVASEN, J. 2002. Crenarchaeol: The characteristic core glycerol dibiphytanyl glycerol tetraether membrane lipid of cosmopolitan pelagic crenarchaeota. *Journal of Lipid Research,* 43, 1641-1651.

SINNINGHE DAMSTÉ, J., RIJPSTRA, W., HOPMANS, E., WEIJERS, J., FOESEL, B., OVERMANN, J. & DEDYSH, S. 2011. 13, 16-Dimethyl octacosanedioic acid (iso-diabolic acid), a common membrane-spanning lipid of Acidobacteria subdivisions 1 and 3. *Applied and Environmental Microbiology,* 77, 4147-4154.

SKINNER, A. & TULLOCH, G. 1999. Rockall Studies Group, RSG Project 97/50, Shallow Coring Programme in the Irish Rockall Trough. Operation Report. *Marine Reports Series,* BGS Technical Report WB/99/17C.

SKINNER, L. 2012. A long view on climate sensitivity. *Science,* 337, 917-919.

SKOGSEID, J., PLANKE, S., FALEIDE, J. I., PEDERSEN, T., ELDHOLM, O. & NEVERDAL, F. 2000. NE Atlantic continental rifting and volcanic margin formation. *Geological Society, London, Special Publications,* 167, 295-326.

SLOAN, L. C. & REA, D. 1995. Atmospheric carbon dioxide and early Eocene climate: A general circulation modeling sensitivity study. *Palaeogeography, Palaeoclimatology, Palaeoecology,* 119, 275-292.

SLOAN, L. C., WALKER, J. C. & MOORE, T. 1995. Possible role of oceanic heat transport in early Eocene climate. *Paleoceanography and Paleoclimatology,* 10, 347-356.

SLOTNICK, B., DICKENS, G., HOLLIS, C., CRAMPTON, J., PERCY STRONG, C. & PHILLIPS, A. 2015. The onset of the early Eocene climatic optimum at branch stream, Clarence River valley, New Zealand. *New Zealand Journal of Geology and Geophysics,* 58, 262-280.

SLOTNICK, B. S., DICKENS, G. R., NICOLO, M. J., HOLLIS, C. J., CRAMPTON, J. S., ZACHOS, J. C. & SLUIJS, A. 2012. Large-amplitude variations in carbon cycling and terrestrial weathering during the latest Paleocene and earliest Eocene: The record at Mead Stream, New Zealand. *The journal of geology,* 120, 487-505.

SLUIJS, A., SCHOUTEN, S., PAGANI, M., WOLTERING, M., BRINKHUIS, H., SINNINGHE DAMSTÉ, J. S., DICKENS, G. R., HUBER, M., REICHART, G.-J. & STEIN, R. 2006. Subtropical Arctic Ocean temperatures during the Palaeocene/Eocene thermal maximum. *Nature,* 441, 610-613.

SLUIJS, A., SCHOUTEN, S., DONDERS, T. H., SCHOON, P. L., RÖHL, U., REICHART, G.-J., SANGIORGI, F., KIM, J.-H., SINNINGHE DAMSTÉ, J. S. & BRINKHUIS, H. 2009. Warm and wet conditions in the Arctic region during Eocene Thermal Maximum 2. *Nature Geoscience,* 2, 777-780.

SMYTHE, D. K. 1989. Rockall Trough—Cretaceous or Late Palaeozoic? *Scottish Journal of Geology,* 25, 5-43.

SPANG, A., HATZENPICHLER, R., BROCHIER-ARMANET, C., RATTEI, T., TISCHLER, P., SPIECK, E., STREIT, W., STAHL, D. A., WAGNER, M. & SCHLEPER, C. 2010. Distinct gene set in two different lineages of ammonia-oxidizing archaea supports the phylum Thaumarchaeota. *Trends in Microbiology,* 18, 331-340.

SPEELMAN, E. N., SEWALL, J. O., NOONE, D., HUBER, M., VON DER HEYDT, A., SINNINGHE DAMSTÉ, J. S. & REICHART, G.-J. 2010. Modeling the influence of a reduced equator-to-pole sea surface temperature gradient on the distribution of water isotopes in the Early/Middle Eocene. *Earth and Planetary Science Letters,* 298, 57-65.

SPERO, H. & WILLIAMS, D. 1989. Opening the carbon isotope “vital effect” black box 1. Seasonal temperatures in the euphotic zone. *Paleoceanography,* 4, 593-601.

SPERO, H. J. & WILLIAMS, D. F. 1988. Extracting environmental information from planktonic foraminiferal δ13C data. *Nature,* 335, 717-719.

SPERO, H. J., LERCHE, I. & WILLIAMS, D. F. 1991. Opening the carbon isotope" vital effect" black box, 2, quantitative model for interpreting foraminiferal carbon isotope data. *Paleoceanography,* 6, 639-655.

SPERO, H. J. & LEA, D. W. 1993. Intraspecific stable isotope variability in the planktic foraminiferaGlobigerinoides sacculifer: Results from laboratory experiments. *Marine Micropaleontology,* 22, 221-234.

SPERO, H. J. & LEA, D. W. 1996. Experimental determination of stable isotope variability in Globigerina bulloides: implications for paleoceanographic reconstructions. *Marine Micropaleontology,* 28, 231-246.

SPERO, H. J., BIJMA, J., LEA, D. W. & BEMIS, B. E. 1997. Effect of seawater carbonate concentration on foraminiferal carbon and oxygen isotopes. *Nature,* 390, 497-500.

STAP, L., SLUIJS, A., THOMAS, E. & LOURENS, L. 2009. Patterns and magnitude of deep sea carbonate dissolution during Eocene Thermal Maximum 2 and H2, Walvis Ridge, southeastern Atlantic Ocean. *Paleoceanography,* 24, PA1211. http://doi.org/10.1029/2008PA001655.

STAP, L., LOURENS, L., VAN DIJK, A., SCHOUTEN, S. & THOMAS, E. 2010a. Coherent pattern and timing of the carbon isotope excursion and warming during Eocene Thermal Maximum 2 as recorded in planktic and benthic foraminifera. *Geochemistry, Geophysics, Geosystems,* 11, Q11011. http://doi.org/10.1029/2010GC003097.

STAP, L., LOURENS, L. J., THOMAS, E., SLUIJS, A., BOHATY, S. & ZACHOS, J. C. 2010b. High-resolution deep-sea carbon and oxygen isotope records of Eocene Thermal Maximum 2 and H2. *Geology,* 38, 607-610.

STEWART, D. & PEARSON, P. 2000. A Database of Planktonic Foraminiferal Ranges.

STICKLEY, C. E., BRINKHUIS, H., SCHELLENBERG, S. A., SLUIJS, A., RÖHL, U., FULLER, M., GRAUERT, M., HUBER, M., WARNAAR, J. & WILLIAMS, G. L. 2004. Timing and nature of the deepening of the Tasmanian Gateway. *Paleoceanography,* 19, PA4027. http://doi.org/10.1029/2004PA001022.

STOKER, M., VAN WEERING, T. C. & SVAERDBORG, T. 2001. A mid-to late Cenozoic tectonostratigraphic framework for the Rockall Trough. *Geological Society, London, Special Publications,* 188, 411-438.

STOKER, M. S., HOLFORD, S. P., HILLIS, R. R., GREEN, P. F. & DUDDY, I. R. 2010. Cenozoic post-rift sedimentation off northwest Britain: Recording the detritus of episodic uplift on a passive continental margin. *Geology,* 38, 595-598.

STOKER, M. S., KIMBELL, G. S., MCINROY, D. B. & MORTON, A. C. 2012. Eocene post-rift tectonostratigraphy of the Rockall Plateau, Atlantic margin of NW Britain: Linking early spreading tectonics and passive margin response. *Marine and Petroleum Geology,* 30, 98-125.

STOREY, M., DUNCAN, R. A. & SWISHER, C. C. 2007. Paleocene-Eocene thermal maximum and the opening of the northeast Atlantic. *Science,* 316, 587-589.

STOTT, L. D., KENNETT, J. P., SHACKLETON, N. J. & CORFIELD, R. M. 1990. 48. The evolution of Antarctic surface waters during the Paleogene: inferences from the stable isotopic composition of planktonic foraminifers, ODP leg 1131. *In:* BARKER, P. F. & KENNETT, J. P. (eds.) *Proceedings of the Ocean Drilling Program, Scientific Results.*

STROKER, M. 1999. Irish Rockall shallow drilling 1999 Stratigraphic summary. *British Geological survey,* Technical Report WB/99/22C, 1-71.

SVENSEN, H., PLANKE, S., MALTHE-SØRENSSEN, A., JAMTVEIT, B., MYKLEBUST, R., EIDEM, T. R. & REY, S. S. 2004. Release of methane from a volcanic basin as a mechanism for initial Eocene global warming. *Nature,* 429, 542-545.

TAYLOR, K. W., HUBER, M., HOLLIS, C. J., HERNANDEZ-SANCHEZ, M. T. & PANCOST, R. D. 2013. Re-evaluating modern and Palaeogene GDGT distributions: Implications for SST reconstructions. *Global and Planetary Change,* 108, 158-174.

THOMAS, D. J., BRALOWER, T. J. & ZACHOS, J. C. 1999. New evidence for subtropical warming during the late Paleocene thermal maximum: Stable isotopes from Deep Sea Drilling Project Site 527, Walvis Ridge. *Paleoceanography,* 14, 561-570.

THOMAS, D. J., BRALOWER, T. J. & JONES, C. E. 2003. Neodymium isotopic reconstruction of late Paleocene–early Eocene thermohaline circulation. *Earth and Planetary Science Letters,* 209, 309-322.

THOMAS, D. J. 2004. Evidence for deep-water production in the North Pacific Ocean during the early Cenozoic warm interval. *Nature,* 430, 65-68.

THOMAS, E. 1990. Late Cretaceous through Neogene deep-sea benthic foraminifers (Maud Rise, Weddell Sea, Antarctica). *In:* BARKER, P. F. & KENNETT, J. P. (eds.) *Proceedings of the Ocean Drilling Program, Scientific Results.* College Station, TX (Ocean Drilling Program).

THOMAS, E. & SHACKLETON, N. J. 1996. The Paleocene-Eocene benthic foraminiferal extinction and stable isotope anomalies. *Geological Society, London, Special Publications,* 101, 401-441.

THOMAS, E. 1998. Biogeography of the Late Paleocene Benthic Foraminiferal Extinction. *In:* AUBRY, M.-P., SPENCER, L. & BERGGREN, W. A. (eds.) *Late Paleocene-Early Eocene Climatic and Biotic Events in the Marine and Terrestrial Records.* New York: Columbia University Press.

THOMAS, E. 2007. Cenozoic mass extinctions in the deep sea: What disturbs the largest habitat on Earth? *Division III Faculty Publications,* Paper 97, 1-23. http://doi.org/10.1130/2007.2424(01).

THOMSON, A. & MCWILLIAM, A. 2001. The structural style and evolution of the Bróna Basin. *Geological Society, London, Special Publications,* 188, 401-410.

TIERNEY, J. E. & TINGLEY, M. P. 2014. A Bayesian, spatially-varying calibration model for the TEX86 proxy. *Geochimica et Cosmochimica Acta,* 127, 83-106.

TIERNEY, J. E. & TINGLEY, M. P. 2015. A TEX 86 surface sediment database and extended Bayesian calibration. *Scientific data,* 2, 150029. http://doi.org/10.1038/sdata.2015.29.

TINDALL, J., FLECKER, R., VALDES, P., SCHMIDT, D. N., MARKWICK, P. & HARRIS, J. 2010. Modelling the oxygen isotope distribution of ancient seawater using a coupled ocean–atmosphere GCM: implications for reconstructing early Eocene climate. *Earth and Planetary Science Letters,* 292, 265-273.

TOLDERLUND, D. S. & BÉ, A. W. 1971. Seasonal distribution of planktonic foraminifera in the western North Atlantic. *Micropaleontology,* 17, 297-329.

TRIPATI, A. & ELDERFIELD, H. 2005. Deep-sea temperature and circulation changes at the Paleocene-Eocene thermal maximum. *Science,* 308, 1894-1898.

TROMMER, G., SICCHA, M., VAN DER MEER, M. T., SCHOUTEN, S., SINNINGHE DAMSTÉ, J. S., SCHULZ, H., HEMLEBEN, C. & KUCERA, M. 2009. Distribution of Crenarchaeota tetraether membrane lipids in surface sediments from the Red Sea. *Organic Geochemistry,* 40, 724-731.

TRUEBLOOD, S. & MORTON, N. 1991. Comparative sequence stratigraphy and structural styles of the Slyne Trough and Hebrides Basin. *Journal of the Geological Society,* 148, 197-201.

TUITT, A., UNDERHILL, J. R., RITCHIE, J., JOHNSON, H. & HITCHEN, K. 2010. Timing, controls and consequences of compression in the Rockall-Faroe area of the NE Atlantic Margin. *In:* VINING, B. A. & PICKERING, S. C. (eds.) *Petoleum Geology: From Mature Basins to New Frontiers - Proceedings of the 7th Petroleum Geology Conference.* Geological Society of London.

UDA, I., SUGAI, A., ITOH, Y. H. & ITOH, T. 2001. Variation in molecular species of polar lipids from Thermoplasma acidophilum depends on growth temperature. *Lipids,* 36, 103-105.

UDA, I., SUGAI, A., ITOH, Y. H. & ITOH, T. 2004. Variation in molecular species of core lipids from the order Thermoplasmales strains depends on the growth temperature. *Journal of Oleo Science,* 53, 399-404.

UREY, H. C. 1947. The thermodynamic properties of isotopic substances. *Journal of the Chemical Society (Resumed)*, 562-581.

UREY, H. C., LOWENSTAM, H. A., EPSTEIN, S. & MCKINNEY, C. R. 1951. Measurement of paleotemperatures and temperatures of the Upper Cretaceous of England, Denmark, and the southeastern United States. *Geological Society of America Bulletin,* 62, 399-416.

VAHLENKAMP, M., NIEZGODZKI, I., DE VLEESCHOUWER, D., BICKERT, T., HARPER, D., TURNER, S. K., LOHMANN, G., SEXTON, P., ZACHOS, J. & PÄLIKE, H. 2018a. Astronomically paced changes in deep-water circulation in the western North Atlantic during the middle Eocene. *Earth and Planetary Science Letters,* 484, 329-340.

VAHLENKAMP, M., NIEZGODZKI, I., DE VLEESCHOUWER, D., LOHMANN, G., BICKERT, T. & PÄLIKE, H. 2018b. Ocean and climate response to North Atlantic seaway changes at the onset of long-term Eocene cooling. *Earth and Planetary Science Letters,* 498, 185-195.

VAN DER ZWAAN, G., JORISSEN, F. & DE STIGTER, H. 1990. The depth dependency of planktonic/benthic foraminiferal ratios: constraints and applications. *Marine Geology,* 95, 1-16.

VANDENBERGHE, N., HILGEN, F., SPEIJER, R., OGG, J., GRADSTEIN, F., HAMMER, O., HOLLIS, C. & HOOKER, J. 2012. The Paleogene Period. *In:* GRADSTEIN, F., OGG, J., SCHMITZ, M. & OGG, G. (eds.) *The Geologic Time Scale 2012.* Elsevier.

VIA, R. K. & THOMAS, D. J. 2006. Evolution of Atlantic thermohaline circulation: Early Oligocene onset of deep-water production in the North Atlantic. *Geology,* 34, 441-444.

VOGT, P., JOHNSON, G., HOLCOMBE, T., GILG, J. & AVERY, O. 1971. Episodes of sea-floor spreading recorded by the North Atlantic basement. *Tectonophysics,* 12, 211-234.

VOLK, T. & HOFFERT, M. I. 1985. Ocean carbon pumps: Analysis of relative strengths and efficiencies in ocean-driven atmospheric CO2 changes. *The carbon cycle and atmospheric CO2: natural variations Archean to present,* 32, 99-110.

WADDELL, L. M. & MOORE, T. C. 2008. Salinity of the Eocene Arctic Ocean from oxygen isotope analysis of fish bone carbonate. *Paleoceanography,* 23, PA1S12. http://doi.org/10.1029/2007PA001451.

WADE, B. S., AL-SABOUNI, N., HEMLEBEN, C. & KROON, D. 2008. Symbiont bleaching in fossil planktonic foraminifera. *Evolutionary Ecology,* 22, 253-265.

WADE, B. S., PEARSON, P. N., BERGGREN, W. A. & PÄLIKE, H. 2011. Review and revision of Cenozoic tropical planktonic foraminiferal biostratigraphy and calibration to the geomagnetic polarity and astronomical time scale. *Earth-Science Reviews,* 104, 111-142.

WALKER, J. C., HAYS, P. & KASTING, J. F. 1981. A negative feedback mechanism for the long-term stabilization of Earth's surface temperature. *Journal of Geophysical Research: Oceans,* 86, 9776-9782.

WALSH, A., KNAG, G., MORRIS, M., QUINQUIS, H., TRICKER, P., BIRD, C. & BOWER, S. 1999. Petroleum geology of the Irish Rockall Trough – a frontier challenge. *In:*

FLEET, A. J. & BOLDY, S. A. R. (eds.) *Petroleum Geology of Northwest Europe: Proceedings of the 5th Conference.* London: Geological Society.

WEIJERS, J. W., SCHOUTEN, S., HOPMANS, E. C., GEENEVASEN, J. A., DAVID, O. R., COLEMAN, J. M., PANCOST, R. D. & SINNINGHE DAMSTÉ, J. S. 2006a. Membrane lipids of mesophilic anaerobic bacteria thriving in peats have typical archaeal traits. *Environmental Microbiology,* 8, 648-657.

WEIJERS, J. W., SCHOUTEN, S., SPAARGAREN, O. C. & SINNINGHE DAMSTÉ, J. S. 2006b. Occurrence and distribution of tetraether membrane lipids in soils: Implications for the use of the TEX86 proxy and the BIT index. *Organic Geochemistry,* 37, 1680-1693.

WEIJERS, J. W., SCHOUTEN, S., VAN DEN DONKER, J. C., HOPMANS, E. C. & SINNINGHE DAMSTÉ, J. S. 2007. Environmental controls on bacterial tetraether membrane lipid distribution in soils. *Geochimica et Cosmochimica Acta,* 71, 703-713.

WEINER, S. & DOVE, P. M. 2003. An overview of biomineralization processes and the problem of the vital effect. *Reviews in mineralogy and geochemistry,* 54, 1-29.

WELTJE, G. J. & TJALLINGII, R. 2008. Calibration of XRF core scanners for quantitative geochemical logging of sediment cores: theory and application. *Earth and Planetary Science Letters,* 274, 423-438.

WEST, C. K., GREENWOOD, D. R. & BASINGER, J. F. 2015. Was the Arctic Eocene 'rainforest'monsoonal? Estimates of seasonal precipitation from early Eocene megafloras from Ellesmere Island, Nunavut. *Earth and Planetary Science Letters,* 427, 18-30.

WESTERHOLD, T., RÖHL, U., LASKAR, J., RAFFI, I., BOWLES, J., LOURENS, L. J. & ZACHOS, J. C. 2007. On the duration of magnetochrons C24r and C25n and the timing of early Eocene global warming events: Implications from the Ocean Drilling Program Leg 208 Walvis Ridge depth transect. *Paleoceanography,* 22, PA2201. http://doi.org/10.1029/2006PA001322.

WESTERHOLD, T., RÖHL, U., RAFFI, I., FORNACIARI, E., MONECHI, S., REALE, V., BOWLES, J. & EVANS, H. F. 2008. Astronomical calibration of the Paleocene time. *Palaeogeography, Palaeoclimatology, Palaeoecology,* 257, 377-403.

WESTERHOLD, T. & RÖHL, U. 2009. High resolution cyclostratigraphy of the early Eocene–new insights into the origin of the Cenozoic cooling trend. *Climate of the Past,* 5, 309-327.

WESTERHOLD, T., RÖHL, U., FREDERICHS, T., AGNINI, C., RAFFI, I., ZACHOS, J. C. & WILKENS, R. H. 2017. Astronomical calibration of the Ypresian time scale: Implications for seafloor spreading rates and the chaotic behaviour of the solar system. *Climate of the Past,* 13, 1129-1152.

WESTERHOLD, T., RÖHL, U., DONNER, B. & ZACHOS, J. 2018a. Global Extent of Early Eocene Hyperthermal Events–a new Pacific Benthic Foraminiferal Isotope Record from Shatsky Rise (ODP Site 1209). *Paleoceanography and Paleoclimatology,* 33, 626-642. https://doi.org/10.1029/2017PA003306.

WESTERHOLD, T., RÖHL, U., WILKENS, R. H., GINGERICH, P. D., CLYDE, W. C., WING, S. L., BOWEN, G. J. & KRAUS, M. J. 2018b. Synchronizing early Eocene deep-sea and continental records – cyclostratigraphic age models for the Bighorn Basin Coring Project drill cores. *Climate of the Past,* 14, 303-319. https://doi.org/10.5194/cp-14-303-2018.

WHITE, N. & LOVELL, B. 1997. Measuring the pulse of a plume with the sedimentary record. *Nature,* 387, 888.

WIECZOREK, R., FANTLE, M. S., KUMP, L. R. & RAVIZZA, G. 2013. Geochemical evidence for volcanic activity prior to and enhanced terrestrial weathering during the Paleocene Eocene Thermal Maximum. *Geochimica et Cosmochimica Acta,* 119, 391-410.

WILLARD, D. A., DONDERS, T. H., REICHGELT, T., GREENWOOD, D. R., SANGIORGI, F., PETERSE, F., NIEROP, K. G., FRIELING, J., SCHOUTEN, S. & SLUIJS, A. 2019. Arctic vegetation, temperature, and hydrology during Early Eocene transient global warming events. *Global and planetary change,* 178, 139-152.

WILSON, P. A., NORRIS, R. D. & COOPER, M. J. 2002. Testing the Cretaceous greenhouse hypothesis using glassy foraminiferal calcite from the core of the Turonian tropics on Demerara Rise. *Geology,* 30, 607-610.

WING, S. L. 1998. Late Paleocene – early Eocene floral and climatic change in the Bighorn Basin, Wyoming. *In:* AUBRY, M., LUCAS, S. & BERGGREN, W. (eds.) *Late Paleocene-Early Eocene Biotic and Climatic Events.* New York: Columbia University Press.

WING, S. L., HARRINGTON, G. J., SMITH, F. A., BLOCH, J. I., BOYER, D. M. & FREEMAN, K. H. 2005. Transient floral change and rapid global warming at the Paleocene-Eocene boundary. *Science,* 310, 993-996.

WINGUTH, A., SHELLITO, C., SHIELDS, C. & WINGUTH, C. 2010. Climate response at the Paleocene–Eocene thermal maximum to greenhouse gas forcing—a model study with CCSM3. *Journal of Climate,* 23, 2562-2584.

WOODCOCK, N. H. & STRACHAN, R. A. 2009. *Geological history of Britain and Ireland*, John Wiley & Sons.

WUCHTER, C., SCHOUTEN, S., COOLEN, M. J. & SINNINGHE DAMSTÉ, J. S. 2004. Temperature-dependent variation in the distribution of tetraether membrane lipids of marine Crenarchaeota: Implications for TEX86 paleothermometry. *Paleoceanography,* 19, PA4028. http://doi.org/10.1029/2004PA001041.

ZACHOS, J., PAGANI, M., SLOAN, L., THOMAS, E. & BILLUPS, K. 2001. Trends, rhythms, and aberrations in global climate 65 Ma to present. *Science,* 292, 686-693.

ZACHOS, J. C., LOHMANN, K. C., WALKER, J. C. & WISE, S. W. 1993. Abrupt climate change and transient climates during the Paleogene: A marine perspective. *The Journal of Geology,* 101, 191-213.

ZACHOS, J. C., STOTT, L. D. & LOHMANN, K. C. 1994. Evolution of early Cenozoic marine temperatures. *Paleoceanography,* 9, 353-387.

ZACHOS, J. C., QUINN, T. M. & SALAMY, K. A. 1996. High-resolution (104 years) deep-sea foraminiferal stable isotope records of the Eocene-Oligocene climate transition. *Paleoceanography,* 11, 251-266.

ZACHOS, J. C., RÖHL, U., SCHELLENBERG, S. A., SLUIJS, A., HODELL, D. A., KELLY, D. C., THOMAS, E., NICOLO, M., RAFFI, I. & LOURENS, L. J. 2005. Rapid acidification of the ocean during the Paleocene-Eocene thermal maximum. *Science,* 308, 1611-1615.

ZACHOS, J. C., BOHATY, S. M., JOHN, C. M., MCCARREN, H., KELLY, D. C. & NIELSEN, T. 2007. The Palaeocene–Eocene carbon isotope excursion: constraints from individual shell planktonic foraminifer records. *Philosophical Transactions of*

the Royal Society of London A: Mathematical, Physical and Engineering Sciences, 365, 1829-1842.

ZACHOS, J. C., DICKENS, G. R. & ZEEBE, R. E. 2008. An early Cenozoic perspective on greenhouse warming and carbon-cycle dynamics. *Nature,* 451, 279-283.

ZACHOS, J. C., MCCARREN, H., MURPHY, B., RÖHL, U. & WESTERHOLD, T. 2010. Tempo and scale of late Paleocene and early Eocene carbon isotope cycles: Implications for the origin of hyperthermals. *Earth and Planetary Science Letters,* 299, 242-249.

ZEEBE, R. E. 1999. An explanation of the effect of seawater carbonate concentration on foraminiferal oxygen isotopes. *Geochimica et Cosmochimica Acta,* 63, 2001-2007.

ZEEBE, R. E., BIJMA, J. & WOLF-GLADROW, D. A. 1999. A diffusion-reaction model of carbon isotope fractionation in foraminifera. *Marine Chemistry,* 64, 199-227.

ZEEBE, R. E. 2001. Seawater pH and isotopic paleotemperatures of Cretaceous oceans. *Palaeogeography, palaeoclimatology, palaeoecology,* 170, 49-57.

ZEEBE, R. E. & ZACHOS, J. C. 2007. Reversed deep-sea carbonate ion basin gradient during Paleocene-Eocene thermal maximum. *Paleoceanography,* 22, PA3201. http://doi.org/10.1029/2006PA001395.

ZEEBE, R. E., ZACHOS, J. C. & DICKENS, G. R. 2009. Carbon dioxide forcing alone insufficient to explain Palaeocene–Eocene Thermal Maximum warming. *Nature Geoscience,* 2, 576-580.

ZEEBE, R. E. 2012. History of seawater carbonate chemistry, atmospheric CO2, and ocean acidification. *Annual Review of Earth and Planetary Sciences,* 40, 141-165.

ZEEBE, R. E. & ZACHOS, J. C. 2013. Long-term legacy of massive carbon input to the Earth system: Anthropocene versus Eocene. *Phil. Trans. R. Soc. A,* 371, 20120006. http://dx.doi.org/10.1098/rsta.2012.0006.

ZEEBE, R. E., RIDGWELL, A. & ZACHOS, J. C. 2016. Anthropogenic carbon release rate unprecedented during the past 66 million years. *Nature Geoscience,* 9, 325-329.

ZELL, C., KIM, J.-H., BALSINHA, M., DORHOUT, D., FERNANDES, C., BAAS, M. & SINNINGHE DAMSTÉ, J. S. 2014. Transport of branched tetraether lipids from the Tagus River basin to the coastal ocean of the Portuguese margin: consequences for the interpretation of the MBT'/CBT paleothermometer. *Biogeosciences,* 11, 5637-5655.

ZHANG, Y. G., ZHANG, C. L., LIU, X.-L., LI, L., HINRICHS, K.-U. & NOAKES, J. E. 2011. Methane Index: a tetraether archaeal lipid biomarker indicator for detecting the instability of marine gas hydrates. *Earth and Planetary Science Letters,* 307, 525-534.

ZHANG, Y. G., PAGANI, M., LIU, Z., BOHATY, S. M. & DECONTO, R. 2013. A 40-million-year history of atmospheric CO2. *Philosophical Transactions of the Royal Society A: Mathematical, Physical and Engineering Sciences,* 371, 20130096. http://dx.doi.org/10.1098/rsta.2013.0096.

ZHU, J., POULSEN, C. J. & TIERNEY, J. E. 2019. Simulation of Eocene extreme warmth and high climate sensitivity through cloud feedbacks. *Science advances,* 5, eaax1874. http://doi.org/10.1126/sciadv.aax1874.

ZUCCHI, D. 2000. Nannofossil analysis of five boreholes from the Irish Rockall Trough. *Rockall Studies Group Project 97/34,* Millenia Ltd. Project no 417/00.

Appendix 1: Previously published biostratigraphies summarized

Table 1 - Shipboard biostratigraphy by Jacovides, (1999)

Initial biostratigraphy of 16/28-sb01 (Jacovides, 1999) based on microfossil assemblage and planktonic foraminiferal zones				
Core depth [m]	Planktonic foraminifera zones after (Berggren et al., 1995)	Age	Assignment of top of interval based on:	lithology
12.78 -13.80	N22-21	Pleistocene-Late Pliocene	The presence of *G. truncatulinoides*	Foraminiferal sand, light olive brown-yellowish brown (slope)
UNCONFORMITY				
14.50 – 44.00	P12 – P10	Middle Eocene	*Hantkenina dutemplei* Comment: this is not a species I can find in the Eocene planktic foraminifera Atlas - it is assumed that there might be a typo and it is supposed to be *Hantkenina dumblei* (occurring in the middle Eocene E9 – mid E13) (Pearson et al., 2006)	Clay, greenish grey massive, glauconite with abundant sponge spicules (slope)
53.99 – 137.92	P9 – P6	Early Eocene	Presence of *A. soldadoensis* and *M. subbotinae*	Clay, dark greenish grey, massive (slope)
138.00 – 145.66	unassigned	Late Palaeocene	By influx of large specimen of cenospherid radiolaria	Clay, dark greenish grey, massive (slope)
145.95	unassigned	Palaeocene (undiff.)	The influx of superabundant bryozoan dabris	Mudstone, green grey (shelf)
UNCONFORMITY				
146	KM1	Late Maastrichtian	Diagnostic late Cretaceous planktic foraminifera	Siltstone, white, calcareous (shelf)
UNCONFORMITY				
147.17 – 147.23	Unassigned	Late Cretaceous (undiff.)	Influx sparse microfauna dominated by *Bairida* spp.	Sandstone, dark yellow, brown (shelf)
147.30/ 149.5?	n.a.	Basalt sample not analysed		

Table 2 - Further biostratigraphy by Harrington et al. (2000)

Further/palynological biostratigraphy of 16/28-sb01 (Harrington et al., 2000) based on nannofossil; dinocysts and palynomorphs						
Core depth [m]	Assigned zones (Nannofossil zones modified after (Martini, 1971)	Age	Core depth [m]	Palynology zones after Bujak et al. 1980 Powell 1992 Heilmann-Clausen 1988 Costa and Manum 1988	Core depth [m]	Bioevent
13.00	NN 19b	Intra-Pleistocene			13	Superabundant *Gephyrocapsa* spp. (small) no Pliocene markers
UNCONFORMITY						
24.70 - 81.60	NP15	Middle Eocene	25.60 – 81.87	Indeterminable (Bujak et al. 1980)	24.70	FDO of *R. gladius*
					34.00	FDO *C. gigas*
89.25 - 143.50	NP12 (intra)	Early Eocene	82.72 – 88.88	Indeterminable (Bujak et al. 1980)	88.55	FDO *E. ursulae*
					88.88	FDO *C. coleothrypta*
					89.25	Occurrence of *C. barbatus*
			89.51 – 137.93	B1 – LC3 (Bujak et al. 1980) Ccl/Pla (Powell 1992) *C. coleothrypta/ A diktyoplokus* Zones (Heilmann-Clausen 1988) D8-basal D9 (Costa and Manum 1988)	90.90	FDO of abundant *E. ursulae*
					93.40	FDO *C. depressum*
					94.13	FDO abundant *P. echinatum*
					106.80	FDO *H. septate*
					112.98	FDO *D. varielongitudum*
					113.48	FDO *D. condylos*
					118.19	LDO *C. ?insolitum*
					124.94	Abundant *Nypa*
					130.00	FDO *D. simile*
	Latest NP11 – earliest NP12	Early Eocene	143.56 – 145.78	?Dva (Powell 1992) *D. varielongitudum* (Heilmann-Clausen 1988) Lower D8 (Costa and Manum 1988)		
UNCONFORMITY						
146.00	KN1 or older	Late Cretaceous			146	FDO *E. turriseiffelii, G. obliquum,* and *P. cretaceus*

Table 1 - Reviewed biostratigraphy by Jacovides (2000)

Reviewed biostratigraphy from (Jacovides, 2000)						
Core depth [m]	Nannofossil zone modified after Martini, 1971	age	planktonic foraminifera	Top defined by nannofossils	palynozones	Palaeo-environment
12.78 – 13.80	NN 19 b	Pleistocene	Top defined *G. truncatulinoides*	Superabundant *Gephyrocapsa spp.* (small)		Marine, slope/bathyal
Stratigraphic break						
14.50 – 88.55	NP 15	Middle Eocene	Top defined by presence of abundant *H. dutemplei*	Lower intervals defined by different species	25.60 – 81.87 m barren of palynomorphs; 82.72 m sample yield rare palynological assemblage 83.96 m barren of palynomorphs	Marine, slope/bathyal with good oxygenated water masses
89.25 – 145.78	NP 12 (intra)	Early Eocene	92 m faunal break: -decline numbers and diversity of planktonic foraminifera; greater diversity of calcareous benthic foraminifera; dominance of dwarf species of calcareous benthic and planktonic foraminifera	Occurrence of *C. barbatus*		Marine, slope/bathyal, probably restricted water circulation
145.95	Undifferenciated Defined by superabundant bryozoan debris	Palaeocene (undifferenciated) *needs confirmation by using nannofossils	Abundant benthic foraminfera: *Cibicidoides*; poorly preserved *Globigerina* spp.			Marine, shelf

XRF data and weights for press pellets

Table 4: Shows the results from the XRF on the high-resolution bulk sediment samples. Results are discussed in Chapter 2 of this thesis. Additionally, the weight which was used to produce the wax pellet and the amount of wax used for each sample. And detected elements: Aluminium (Al), Barium (Ba), Calcium (Ca), Iron (Fe), Potassium (K), Magnesium (Mg), Manganese (Mn), Phosphorus (P), Rubidium (Rb), Silicon (Si), Strontium (Sr), Titanium (Ti) and Zirconium (Zr). Data presented as elemental weight percent [wt.%].

core section	sample ID	top bulk sample depth (m)	sample spacing	sediment description any abnormalities, colour, drilling mud, rind removed?	grinded ID of student who was working on it: EM=Emma; IV=Ivan; BGS=British Geological Survey; DN=Dominika; UL=Ulrike; EH=Emily	weight of sample taken for XRF [g]	weight of wax added to sample for XRF pellet [g]	Al [wt.%]	Ba [wt.%]	Ca [wt.%]	Fe [wt.%]	K [wt.%]	Mg [wt.%]	Mn [wt.%]	P [wt.%]	Rb [wt.%]	Si [wt.%]	S [wt.%]	Sr [wt.%]	Ti [wt.%]	Zr [wt.%]
6/69	Ub001	40.82	0.05	brown, core mud removed	DN	0.50	0.10	0.89	n/a	21.66	1.45	0.54	0.20	0.06	0.07	n/a	19.86	0.12	0.14	0.17	n/a
6/69	Ub002	40.87	0.05	brown, core mud removed	DN	0.52	0.10	1.02	n/a	20.34	1.78	0.73	0.24	n/a	n/a	n/a	20.13	n/a	0.15	0.24	n/a
6/69	Ub003	40.92	0.05	brown, core mud removed	DN	0.45	0.11	1.00	0.42	21.65	1.80	0.70	0.30	0.04	n/a	n/a	19.79	0.13	0.16	0.23	0.02
6/69	Ub004	40.97	0.05	brown, core mud removed	DN	0.51	0.12	1.41	n/a	31.79	2.94	1.18	0.47	0.08	0.10	n/a	11.12	n/a	0.10	0.45	0.01
6/69	Ub005	41.02	0.05	light brown	DN	n/a	n/a	n/a	n/a	n/a	n/a	n/a	n/a	n/a	n/a	n/a	n/a	n/a	n/a	n/a	n/a
6/69	Ub006	41.07	0.05	light brown	DN	0.53	0.11	1.57	n/a	33.61	2.91	1.35	0.48	0.07	0.06	n/a	11.04	0.17	0.11	0.43	0.01
6/69	Ub007	41.12	0.05	light brown	DN	n/a	n/a	n/a	n/a	n/a	n/a	n/a	n/a	n/a	n/a	n/a	n/a	n/a	n/a	n/a	n/a
6/69	Ub008	41.17	0.05	light brown	DN	0.45	0.11	2.61	n/a	28.71	3.58	1.53	0.55	n/a	0.11	n/a	11.62	0.20	0.12	0.48	0.01
6/69	Ub009	41.22	0.05	light brown	DN	0.51	0.11	2.38	n/a	28.71	3.51	1.58	0.51	0.04	n/a	n/a	11.58	0.15	0.11	0.37	n/a
6/69	Ub010	41.27	0.05	light brown	DN	0.51	0.11	2.50	n/a	27.35	3.70	1.57	0.55	n/a	0.08	n/a	12.44	0.14	0.12	0.30	0.01
6/69	Ub011	41.32	0.05	light brown	DN	0.45	0.11	2.46	n/a	28.33	3.42	1.37	0.47	n/a	n/a	n/a	11.13	0.12	0.12	0.50	0.01
6/69	Ub012	41.37	0.05	light brown	DN	0.50	0.10	2.60	n/a	29.20	4.03	1.64	0.54	n/a	0.09	n/a	12.01	0.15	0.12	0.56	n/a

6/69	Ub013	41.42	0.05	light brown	DN	0.50	0.11	2.31	n/a	30.87	3.84	1.45	0.53	0.03	n/a	n/a	11.04	0.19	0.12	0.35	0.01
6/69	Ub014	41.47	0.05	light brown	DN	0.51	0.10	2.35	n/a	31.50	2.35	1.48	0.53	n/a	0.05	n/a	11.22	0.12	0.13	0.56	n/a
6/69	Ub015	41.52	0.05	light brown, core mud removed	DN	0.50	0.10	2.30	0.21	32.65	3.29	1.52	0.49	0.04	n/a	n/a	10.62	0.12	0.12	0.37	0.01
6/69	Ub016	41.57	0.01	light brown, core mud removed	DN	0.51	0.13	2.40	n/a	32.70	2.40	1.35	0.44	0.05	n/a	n/a	10.20	0.15	0.12	0.53	n/a
6/69	Ub017	41.58	0.01	light brown	DN	0.53	0.11	2.57	n/a	30.85	3.30	1.53	0.46	n/a	n/a	n/a	10.32	0.17	0.12	0.36	0.01
7/69	Ub018	41.59	0.05	light brown	DN	0.53	0.10	1.90	n/a	31.76	3.17	1.69	0.46	0.05	0.07	n/a	10.79	0.26	0.12	0.35	n/a
7/69	Ub019	41.64	0.05	light brown, core mud removed	DN	0.50	0.11	2.08	0.19	33.75	3.01	1.61	0.44	n/a	n/a	n/a	10.11	0.15	0.12	0.39	n/a
7/69	Ub020	41.69	0.05	light brown, core mud removed	DN	0.48	0.11	2.14	n/a	32.47	3.04	1.46	0.51	n/a	n/a	n/a	10.50	0.22	0.13	0.51	n/a
7/69	Ub021	41.74	0.05	light brown	DN	0.51	0.11	2.17	n/a	33.64	3.12	1.34	0.50	0.07	n/a	n/a	10.21	0.08	0.12	0.35	0.01
7/69	Ub022	41.79	0.05	light brown	DN	n/a	n/a	n/a	n/a	n/a	n/a	n/a	n/a	n/a	n/a	n/a	n/a	n/a	n/a	n/a	n/a
7/69	Ub023	41.84	0.05	light brown, core mud removed	DN	0.52	0.11	1.97	n/a	33.60	2.83	1.26	0.47	0.05	n/a	n/a	9.60	0.13	0.12	0.36	n/a
7/69	Ub024	41.89	0.05	light brown	DN	0.52	0.11	2.00	n/a	32.53	3.02	1.43	0.41	0.05	n/a	n/a	9.97	n/a	0.13	0.52	n/a
7/69	Ub025	41.94	0.05	light brown	DN	0.52	0.11	1.98	n/a	32.87	2.83	1.25	0.41	n/a	0.07	n/a	10.42	0.11	0.11	0.37	n/a
7/69	Ub026	41.99	0.05	light brown, core mud removed	DN	0.51	0.12	1.73	n/a	33.42	1.73	1.30	0.41	0.06	0.05	n/a	10.93	0.11	0.11	0.34	0.01
7/69	Ub027	42.04	0.05	light brown	DN	0.51	0.11	1.73	n/a	36.32	2.66	1.11	0.48	0.09	n/a	n/a	10.64	n/a	0.12	0.41	0.01
7/69	Ub028	42.09	0.1	light brown, core mud removed	DN	n/a	n/a	n/a	n/a	n/a	n/a	n/a	n/a	n/a	n/a	n/a	n/a	n/a	n/a	n/a	n/a
7/69	Ub028.5	42.14	0.1	light brown	DN	0.50	0.14	1.74	n/a	30.78	2.90	1.17	0.40	0.06	n/a	n/a	11.43	0.12	0.11	0.31	n/a
7/69	Ub029	42.19	0.05	light brown, core mud removed	DN	0.50	0.10	1.69	n/a	32.23	2.74	1.10	0.41	0.07	n/a	n/a	13.75	0.18	0.11	0.36	0.01
7/69	Ub030	42.24	0.05	light brown	DN	0.51	0.10	1.52	0.22	33.78	2.87	1.20	0.38	0.07	n/a	n/a	11.54	0.14	0.12	0.36	n/a
7/69	Ub031	42.29	0.13	light brown	DN	0.52	0.11	1.62	n/a	36.24	2.78	1.17	0.38	n/a	0.07	n/a	10.35	0.14	0.12	0.38	n/a
8/69	Ub032	42.42	0.05	light brown, secondary minerals removed	DN	0.51	0.11	1.08	n/a	23.73	2.04	0.80	0.24	n/a	n/a	n/a	16.97	0.14	0.08	0.26	0.02

8/69	Ub033	42.47	0.05	light brown	DN	0.52	0.11	1.53	n/a	31.40	2.62	1.11	0.40	0.05	0.09	n/a	13.33	0.14	0.11	0.31	n/a
8/69	Ub034	42.52	0.05	light brown	DN	0.51	0.11	1.44	n/a	33.83	2.83	1.05	0.45	0.07	n/a	n/a	11.30	0.12	0.12	0.48	0.02
8/69	Ub035	42.57	0.05	light brown, core mud removed	DN	0.49	0.11	1.80	n/a	35.55	3.02	1.22	0.36	n/a	n/a	n/a	10.05	0.13	0.12	0.35	0.01
8/69	Ub036	42.62	0.05	light brown	DN	0.50	0.10	1.77	n/a	33.13	2.98	1.36	0.47	0.05	n/a	n/a	11.60	0.12	0.11	0.47	0.02
8/69	Ub037	42.67	0.05	light brown, core mud removed	DN	0.52	0.10	1.72	0.22	35.46	3.13	1.11	0.49	0.08	n/a	n/a	9.85	0.12	0.12	0.44	0.02
8/69	Ub038	42.72	0.05	light brown, core mud removed	DN	0.51	0.13	1.97	n/a	32.53	3.23	1.32	0.47	0.04	n/a	n/a	11.53	0.17	0.12	0.48	n/a
8/69	Ub039	42.77	0.05	light brown, secondary minerals removed	DN	0.51	0.11	1.97	n/a	31.25	2.95	1.42	0.43	n/a	0.10	n/a	11.66	0.14	0.11	0.41	n/a
8/69	Ub040	42.82	0.05	light brown, core mud removed	EH	0.51	0.12	1.73	n/a	31.89	3.06	1.02	0.44	0.04	0.10	n/a	10.10	n/a	0.11	0.29	0.01
8/69	Ub041	42.87	0.05	light brown, core mud removed	DN	0.52	0.12	1.67	n/a	32.74	2.95	1.05	0.44	n/a	0.11	n/a	10.57	n/a	0.11	0.42	n/a
8/69	Ub042	42.92	0.05	light brown	EH	0.51	0.12	1.84	n/a	30.58	3.27	1.41	0.36	0.03	n/a	n/a	10.34	0.16	0.11	0.35	n/a
8/69	Ub043	42.97	0.05	light brown, core mud removed	DN	0.52	0.10	1.48	n/a	24.47	2.12	0.90	0.30	0.04	0.07	n/a	17.14	0.16	0.09	0.28	0.02
8/69	Ub044	43.02	0.13	light brown	EH	0.52	0.11	1.76	n/a	31.92	2.93	1.20	0.34	n/a	n/a	n/a	9.97	0.11	0.12	0.35	n/a
8/69	Ub045	43.15	0.1	light brown, secondary minerals removde	DN	0.51	0.10	1.11	n/a	22.36	2.08	0.94	0.28	0.03	n/a	n/a	18.21	0.28	0.07	0.32	0.04
8/69	Ub046	43.25	0.01	light brown, mould and core mud removed	DN	n/a	n/a	n/a	n/a	n/a	n/a	n/a	n/a	n/a	n/a	n/a	n/a	n/a	n/a	n/a	n/a
9/69	Ub047	43.26	0.05	light brown	EH	0.51	0.10	1.58	n/a	32.98	3.18	1.28	0.38	0.05	0.07	n/a	9.20	0.10	0.12	0.37	0.01
9/69	Ub048	43.31	0.05	light brown	EH	0.52	0.12	1.86	n/a	31.78	3.11	1.33	0.38	0.07	0.07	n/a	10.73	0.11	0.12	0.37	n/a
9/69	Ub049	43.36	0.05	light brown, core mud removed	EH	0.50	0.11	1.89	n/a	32.18	3.45	1.49	0.43	n/a	0.07	n/a	10.64	0.12	0.12	0.30	n/a
9/69	Ub050	43.41	0.05	light brown	EH	0.51	0.13	1.77	n/a	29.48	2.87	1.24	0.39	0.05	n/a	n/a	10.03	0.13	0.10	0.35	0.03
9/69	Ub051	43.46	0.05	light brown	EH	0.50	0.14	1.39	n/a	25.18	2.49	1.16	0.29	0.05	0.06	n/a	13.38	0.16	0.09	0.32	0.03

9/69	Ub052	43.51	0.05	light brown, core mud removed, **red/orange layer and cone**	EH	0.51	0.12	1.97	n/a	28.52	3.09	1.37	0.38	0.06	0.08	n/a	12.16	n/a	0.10	0.29	0.04
9/69	Ub053	43.56	0.05	light brown	EH	0.52	0.12	1.68	n/a	32.82	3.08	1.28	0.40	0.05	0.07	n/a	11.01	0.11	0.13	0.36	0.01
9/69	Ub054	43.61	0.05	light brown	EH	0.50	0.11	1.68	n/a	30.61	2.93	1.35	0.35	0.07	0.07	n/a	11.34	0.13	0.10	0.33	0.02
9/69	Ub055	43.66	0.1	light brown	EH	0.51	0.10	1.86	n/a	31.05	2.99	1.29	0.37	n/a	0.07	n/a	12.07	0.10	0.11	0.40	n/a
9/69	Ub056	43.76	0.1	light brown, blue spots core mud removed and smudges	EH	0.51	0.13	1.07	n/a	21.09	2.02	0.80	0.21	0.03	0.07	n/a	17.72	0.10	0.17	0.25	n/a
9/69	Ub057	43.86	0.05	light brown, core mud removed	EH	0.51	0.10	1.34	n/a	24.50	2.60	0.70	0.30	0.06	n/a	n/a	17.83	0.09	0.07	0.28	0.07
9/69	Ub058	43.91	0.09	light brown, core mud removed, red patches	EH	0.51	0.10	1.18	n/a	24.76	2.63	0.98	0.21	0.05	n/a	n/a	15.59	0.13	0.07	0.35	0.04
9/69	Ub059	44.00	8.44	light brown	EH	n/a	n/a	n/a	n/a	n/a	n/a	n/a	n/a	n/a	n/a	n/a	n/a	n/a	n/a	n/a	n/a
10/69	Ub060	52.44	0.05	light brown	EH	0.51	0.11	2.31	n/a	29.77	3.62	1.26	0.49	n/a	0.06	n/a	11.25	0.10	0.11	0.45	0.01
10/69	Ub061	52.49	0.05	light brown	EH	n/a	n/a	n/a	n/a	n/a	n/a	n/a	n/a	n/a	n/a	n/a	n/a	n/a	n/a	n/a	n/a
10/69	Ub062	52.54	0.05	light brown	EH	0.51	0.10	1.92	0.10	30.97	3.19	1.35	0.40	0.06	n/a	n/a	10.42	0.12	0.11	0.43	0.01
10/69	Ub063	52.59	0.05	light brown	EH	0.51	0.11	2.12	n/a	29.47	3.34	1.29	0.44	n/a	n/a	n/a	11.58	0.13	0.11	0.33	0.01
10/69	Ub064	52.64	0.05	light brown	EH	0.51	0.11	2.18	n/a	27.54	3.45	1.57	0.41	0.04	n/a	n/a	11.57	0.12	0.10	0.40	0.03
10/69	Ub065	52.69	0.05	light brown	EH	0.52	0.11	1.69	n/a	28.25	2.91	1.39	0.31	0.04	0.07	n/a	12.75	0.13	0.09	0.41	0.05
10/69	Ub066	52.74	0.05	light brown	EH	n/a	n/a	n/a	n/a	n/a	n/a	n/a	n/a	n/a	n/a	n/a	n/a	n/a	n/a	n/a	n/a
10/69	Ub067	52.79	0.05	light brown, core mud removed	EH	0.51	0.10	1.97	0.11	28.22	3.58	1.33	0.43	0.05	n/a	n/a	11.87	0.17	0.10	0.48	0.02
10/69	Ub068	52.84	0.05	light brown, core mud removed	EH	n/a	n/a	n/a	n/a	n/a	n/a	n/a	n/a	n/a	n/a	n/a	n/a	n/a	n/a	n/a	n/a
10/69	Ub069	52.89	0.05	light brown, core mud removed	EH	n/a	n/a	n/a	n/a	n/a	n/a	n/a	n/a	n/a	n/a	n/a	n/a	n/a	n/a	n/a	n/a
10/69	Ub070	52.94	0.05	light brown, core mud removed	EH	0.50	0.12	1.92	n/a	25.12	3.57	1.33	0.44	0.05	0.12	n/a	11.30	n/a	0.09	0.51	0.05
10/69	Ub071	52.99	0.05	light brown	EH	0.51	0.10	2.11	n/a	27.88	3.53	1.59	0.42	0.04	n/a	n/a	11.50	0.12	0.10	0.57	0.03

10/69	Ub072	53.04	0.05	light brown	EH	0.49	0.11	1.96	n/a	28.51	3.56	1.23	0.54	0.03	n/a	n/a	11.57	0.10	0.11	0.32	0.01
10/69	Ub073	53.09	0.05	light brown, core mud removed	EH	0.50	0.10	2.02	n/a	26.84	3.46	1.36	0.47	0.05	n/a	n/a	11.75	0.09	0.09	0.46	0.03
10/69	Ub074	53.14	0.1	light brown, core mud removed	EH	0.50	0.13	1.95	n/a	24.80	3.49	1.39	0.45	n/a	n/a	n/a	11.92	0.11	0.09	0.54	0.02
10/69	Ub074.5	53.19	0.09	light brown, core mud removed	EH	0.49	0.10	2.37	n/a	25.24	3.75	1.50	0.46	0.04	n/a	n/a	12.49	0.08	0.09	0.53	0.04
10/69	Ub075	53.24	0.04	light brown, core mud removed	EH	0.49	0.10	2.50	n/a	24.65	3.64	1.69	0.38	0.05	n/a	n/a	12.84	0.11	0.10	0.46	0.06
10/69	Ub076	53.28	0.02	light brown, core mud removed	EH	0.50	0.10	2.33	n/a	27.23	3.50	1.40	0.52	n/a	n/a	n/a	12.45	0.14	0.10	0.52	0.02
11/69	Ub077	53.30	0.05	light brown	DN	0.49	0.11	2.16	n/a	23.39	3.59	1.51	0.40	0.04	n/a	n/a	12.90	0.22	0.09	0.60	0.04
11/69	Ub078	53.35	0.05	light brown	DN	0.51	0.11	2.00	0.18	23.94	3.69	1.49	0.46	0.06	n/a	n/a	12.83	0.14	0.09	0.40	0.05
11/69	Ub079	53.40	0.05	light brown	DN	0.50	0.12	2.05	0.13	23.00	3.65	1.39	0.46	n/a	n/a	n/a	12.31	0.16	0.09	0.56	0.05
11/69	Ub080	53.45	0.05	light brown	DN	0.51	0.10	2.38	0.09	25.67	3.43	1.47	0.47	0.04	n/a	n/a	13.48	0.09	0.09	0.55	0.05
11/69	Ub081	53.50	0.05	light brown	DN	0.50	0.11	1.70	n/a	29.41	3.04	1.16	0.40	n/a	n/a	n/a	13.17	0.16	0.11	0.34	0.02
11/69	Ub082	53.55	0.05	cream core mud removed	DN	n/a	n/a	n/a	n/a	n/a	n/a	n/a	n/a	n/a	n/a	n/a	n/a	n/a	n/a	n/a	n/a
11/69	Ub083	53.60	0.1	cream	DN	0.47	0.13	1.22	n/a	28.24	3.07	1.11	0.31	0.04	n/a	n/a	14.31	0.06	0.09	0.36	0.01
11/69	Ub084	53.70	0.05	light brown	DN	0.46	0.12	1.14	n/a	26.91	2.31	0.83	0.28	0.05	n/a	n/a	15.30	0.11	0.07	0.28	0.02
11/69	Ub085	53.75	6.86	light brown (**harder from her upwards** no hammer used)	DN	n/a	n/a	n/a	n/a	n/a	n/a	n/a	n/a	n/a	n/a	n/a	n/a	n/a	n/a	n/a	n/a
12a/69	Ub086	60.61	0.05	light brown	DN	0.48	0.15	1.26	n/a	30.28	2.70	1.08	0.31	0.06	n/a	n/a	13.51	n/a	0.09	0.22	n/a
12a/69	Ub087	60.66	0.09	light brown	DN	0.45	0.12	1.40	n/a	28.40	2.55	0.95	0.29	0.04	n/a	n/a	14.09	0.09	0.09	0.34	0.03
12a/69	Ub088	60.75	0.05	light brown, core mud removed	DN	0.49	0.10	1.38	0.13	31.69	3.30	1.15	0.32	n/a	n/a	n/a	11.85	n/a	0.10	0.38	n/a
12a/69	Ub089	60.80	5.41	light brown	DN	0.50	0.12	1.08	n/a	31.05	2.94	0.94	0.36	0.07	n/a	n/a	12.57	0.07	0.10	0.29	0.01
12b/69	Ub090	66.21	0.05	light brown	DN	0.51	0.11	1.29	n/a	32.49	3.14	0.97	0.37	n/a	n/a	n/a	11.76	0.12	0.10	0.28	0.01
12b/69	Ub091	66.26	0.05	light brown	DN	0.53	0.10	1.39	n/a	30.20	2.73	0.93	0.32	0.07	n/a	n/a	16.06	0.15	0.09	0.25	0.01
12b/69	Ub092	66.31	0.05	light brown, core mud	DN	0.43	0.12	1.16	n/a	31.40	2.64	1.02	0.41	0.05	n/a	n/a	13.72	0.11	0.09	0.24	n/a

				removed																
12b/69	Ub093	66.36	0.05	light brown, core mud removed	DN	n/a	n/a	n/a	n/a	n/a	n/a	n/a	n/a	n/a	n/a	n/a	n/a	n/a	n/a	n/a
12b/69	Ub094	66.41	0.05	light brown	DN	0.43	0.11	1.36	n/a	33.31	3.22	1.06	0.38	0.04	n/a	n/a	9.98	0.10	0.10	0.34	0.01
12b/69	Ub095	66.46	0.05	light brown, core mud removed	DN	0.50	0.10	1.47	n/a	34.00	3.47	1.01	0.45	0.06	n/a	n/a	11.69	0.15	0.10	0.36	0.02
12b/69	Ub096	66.51	0.11	light brown	DN	n/a	n/a	n/a	n/a	n/a	n/a	n/a	n/a	n/a	n/a	n/a	n/a	n/a	n/a	n/a	n/a
13/69	Ub097	66.62	0.05	light brown	DN	0.51	0.12	1.26	n/a	32.95	3.35	1.11	0.42	0.06	n/a	n/a	11.19	n/a	0.10	0.33	0.01
13/69	Ub098	66.67	0.05	light brown	DN	n/a	n/a	n/a	n/a	n/a	n/a	n/a	n/a	n/a	n/a	n/a	n/a	n/a	n/a	n/a	n/a
13/69	Ub099	66.72	0.05	light brown	DN	0.50	0.11	1.45	n/a	32.13	2.89	1.09	0.33	n/a	n/a	n/a	12.01	0.11	0.10	0.37	n/a
13/69	Ub100	66.77	0.05	light brown, core mud removed	DN	0.54	0.10	1.78	n/a	35.37	2.65	1.07	0.43	0.05	n/a	n/a	11.93	0.10	0.12	0.38	n/a
13/69	Ub101	66.82	0.05	light brown, core mud removed	DN	0.51	0.13	1.47	n/a	36.23	2.74	1.12	0.45	0.07	n/a	n/a	9.52	n/a	0.11	0.27	n/a
13/69	Ub102	66.87	0.05	light brown, core mud removed	DN	0.51	0.11	1.59	n/a	35.10	3.17	1.22	0.42	0.06	n/a	n/a	10.80	0.14	0.11	0.45	n/a
13/69	Ub103	66.92	0.05	light brown, core mud removed	DN	0.50	0.11	1.77	0.18	36.54	2.90	1.12	0.39	n/a	n/a	n/a	9.54	0.08	0.11	0.41	n/a
13/69	Ub104	66.97	0.05	light brown	DN	0.47	0.10	1.69	n/a	35.33	3.09	0.95	0.40	0.08	n/a	n/a	9.22	n/a	0.12	0.40	n/a
13/69	Ub105	67.02	0.1	light brown	DN	0.51	0.13	1.47	n/a	35.95	2.80	1.05	0.42	n/a	n/a	n/a	8.39	0.10	0.11	0.29	n/a
13/69	Ub106	67.12	0.05	light brown	DN	0.50	0.10	1.47	n/a	34.48	3.23	1.22	0.46	0.07	n/a	n/a	9.38	0.12	0.10	0.37	0.01
13/69	Ub107	67.17	0.05	light brown, core mud removed	DN	0.49	0.10	1.61	0.13	37.00	3.13	1.02	0.44	0.08	n/a	n/a	9.48	0.11	0.11	0.40	n/a
13/69	Ub108	67.22	0.05	light brown	DN	0.50	0.12	1.89	n/a	35.36	2.82	1.19	0.43	0.08	n/a	n/a	9.30	0.13	0.11	0.40	0.01
13/69	Ub109	67.27	0.05	light brown	DN	0.50	0.10	1.76	n/a	34.61	3.44	1.06	0.44	0.07	n/a	n/a	10.32	0.14	0.10	0.34	0.01
13/69	Ub110	67.32	0.05	light brown, core mud removed	DN	0.50	0.10	1.45	n/a	33.31	3.23	1.11	0.40	n/a	n/a	n/a	10.40	0.17	0.11	0.44	0.02
13/69	Ub111	67.37	0.05	light brown	DN	0.48	0.10	1.70	n/a	32.01	2.86	1.26	0.32	0.08	n/a	n/a	11.35	0.12	0.10	0.34	n/a
13/69	Ub112	67.42	0.05	light brown	DN	0.50	0.10	1.65	n/a	32.37	3.17	1.07	0.26	0.08	n/a	n/a	11.54	0.10	0.10	0.48	n/a

13/69	Ub113	67.47	0.05	light brown **soft to grind down upwards**	DN	0.50	0.10	1.68	n/a	30.20	3.32	1.21	0.34	0.07	n/a	n/a	11.96	0.10	0.10	0.45	0.01
13/69	Ub114	67.52	0.05	light brown, core mud removed	DN	0.50	0.10	1.30	n/a	25.95	2.68	0.93	0.31	0.04	n/a	n/a	17.40	0.08	0.07	0.38	0.03
13/69	Ub115	67.57	0.06	light brown	DN	n/a	n/a	n/a	n/a	n/a	n/a	n/a	n/a	n/a	n/a	n/a	n/a	n/a	n/a	n/a	n/a
14/69	Ub116	67.63	0.05	light brown	DN	n/a	n/a	n/a	n/a	n/a	n/a	n/a	n/a	n/a	n/a	n/a	n/a	n/a	n/a	n/a	n/a
14/69	Ub117	67.68	0.05	light brown, core mud removed	DN	0.50	0.12	1.11	n/a	22.86	2.52	0.90	0.26	0.06	n/a	n/a	19.17	0.20	0.07	0.36	0.02
14/69	Ub118	67.73	0.05	light brown, core mud removed **hard to grind upwards**	EH	0.50	0.11	1.03	n/a	21.83	2.39	0.98	0.27	n/a	n/a	n/a	18.76	n/a	0.16	0.27	0.02
14/69	Ub119	67.78	0.05	light brown, core mud removed	DN	n/a	n/a	n/a	n/a	n/a	n/a	n/a	n/a	n/a	n/a	n/a	n/a	n/a	n/a	n/a	n/a
14/69	Ub120	67.83	0.05	light brown	EH	0.46	0.12	1.13	n/a	29.94	3.05	0.91	0.32	0.06	n/a	n/a	10.23	0.16	0.09	0.34	0.02
14/69	Ub121	67.88	0.05	light brown, core mud removed	DN	0.43	0.11	1.55	n/a	29.99	3.34	1.04	0.38	n/a	n/a	n/a	10.43	0.19	0.09	0.38	0.02
14/69	Ub122	67.93	0.05	light brown	EH	n/a	n/a	n/a	n/a	n/a	n/a	n/a	n/a	n/a	n/a	n/a	n/a	n/a	n/a	n/a	n/a
14/69	Ub123	67.98	0.05	light brown	EH	0.50	0.13	1.46	n/a	27.12	3.45	1.22	0.32	0.05	n/a	n/a	13.25	0.11	0.08	0.49	0.04
14/69	Ub124	68.03	0.05	light brown	DN	0.50	0.10	4.57	n/a	29.96	3.64	1.16	0.41	0.05	n/a	n/a	12.76	0.10	0.09	0.52	0.02
14/69	Ub125	68.08	0.05	light brown	DN	0.49	0.10	1.55	n/a	29.46	3.79	1.27	0.42	0.05	n/a	n/a	12.72	0.14	0.09	0.53	0.02
14/69	Ub126	68.13	0.05	light brown	EH	0.49	0.12	1.68	0.14	29.26	3.28	1.01	0.37	n/a	n/a	n/a	12.02	0.18	0.09	0.47	0.02
14/69	Ub127	68.18	0.05	light brown	DN	n/a	n/a	n/a	n/a	n/a	n/a	n/a	n/a	n/a	n/a	n/a	n/a	n/a	n/a	n/a	n/a
14/69	Ub128	68.23	0.05	light brown	EH	0.49	0.14	1.51	n/a	27.78	3.49	1.24	0.38	0.06	n/a	n/a	10.90	0.13	0.08	0.49	0.04
14/69	Ub129	68.28	0.05	light brown	EH	n/a	n/a	n/a	n/a	n/a	n/a	n/a	n/a	n/a	n/a	n/a	n/a	n/a	n/a	n/a	n/a
14/69	Ub130	68.33	0.05	light brown	DN	0.43	0.13	1.40	0.17	27.76	3.10	1.25	0.39	0.06	n/a	n/a	9.76	0.09	0.09	0.40	0.04
14/69	Ub131	68.38	0.05	light brown	EH	0.50	0.12	1.96	n/a	27.35	3.89	1.22	0.47	0.06	n/a	n/a	11.84	0.17	0.09	0.49	0.04
14/69	Ub132	68.43	0.01	light brown, core mud removed	EH	0.50	0.10	1.93	n/a	26.90	3.83	1.19	0.47	n/a	n/a	n/a	12.70	0.12	0.09	0.57	0.03
15/69	Ub133	68.44	0.05	light brown	DN	n/a	n/a	n/a	n/a	n/a	n/a	n/a	n/a	n/a	n/a	n/a	n/a	n/a	n/a	n/a	n/a
15/69	Ub134	68.49	0.05	light brown	DN	0.53	0.11	1.93	n/a	29.60	3.41	1.43	0.42	0.05	n/a	n/a	11.29	0.13	0.11	0.40	0.02

15/69	Ub135	68.54	0.1	light brown	EH	0.53	0.10	1.91	n/a	32.39	3.45	1.36	0.49	n/a	n/a	n/a	10.71	0.24	0.12	0.39	0.01
15/69	Ub136	68.64	0.05	light brown	DN	0.51	0.10	2.31	n/a	31.86	3.52	1.21	0.43	0.06	n/a	n/a	10.83	0.13	0.12	0.49	0.02
15/69	Ub137	68.69	0.05	light brown	DN	0.50	0.11	2.14	n/a	32.77	3.15	1.51	0.49	0.05	n/a	n/a	10.76	0.13	0.13	0.41	0.02
15/69	Ub138	68.74	0.05	light brown	EH	n/a	n/a	n/a	n/a	n/a	n/a	n/a	n/a	n/a	n/a	n/a	n/a	n/a	n/a	n/a	n/a
15/69	Ub139	68.79	0.05	light brown, core mud removed	DN	0.50	0.10	1.80	0.11	33.27	3.04	1.31	0.43	0.08	n/a	n/a	9.34	0.08	0.13	0.31	0.01
15/69	Ub140	68.84	0.05	light brown	DN	0.52	0.11	1.79	n/a	34.77	3.00	1.28	0.45	0.05	n/a	n/a	9.82	0.16	0.12	0.38	n/a
15/69	Ub141	68.89	0.05	light brown	EH	0.50	0.10	1.87	n/a	33.02	3.05	1.36	0.41	0.07	n/a	n/a	10.79	0.12	0.12	0.38	0.01
15/69	Ub142	68.94	0.05	light brown	DN	n/a	n/a	n/a	n/a	n/a	n/a	n/a	n/a	n/a	n/a	n/a	n/a	n/a	n/a	n/a	n/a
15/69	Ub143	68.99	0.05	light brown	DN	0.50	0.10	1.49	n/a	31.15	3.12	1.22	0.37	0.06	n/a	n/a	12.48	0.15	0.09	0.37	0.01
15/69	Ub144	69.04	0.05	light brown	DN	0.50	0.10	1.84	n/a	33.26	3.19	1.21	0.39	0.05	n/a	n/a	10.42	0.09	0.12	0.36	n/a
15/69	Ub145	69.09	0.05	light brown, core mud removed	DN	0.50	0.12	1.48	n/a	29.17	2.91	1.15	0.34	0.08	n/a	n/a	13.70	0.10	0.09	0.39	0.02
15/69	Ub146	69.14	0.1	light brown, core mud removed	DN	n/a	n/a	n/a	n/a	n/a	n/a	n/a	n/a	n/a	n/a	n/a	n/a	n/a	n/a	n/a	n/a
15/69	Ub147	69.24	0.04	light brown	DN	0.51	0.10	1.33	n/a	29.30	3.21	1.06	0.32	n/a	n/a	n/a	13.63	0.08	0.10	0.24	0.01
16/69	Ub148	69.28	0.1	light brown	EH	0.44	0.17	1.05	n/a	28.14	2.53	0.79	0.30	0.06	n/a	n/a	10.70	0.23	0.08	0.35	0.02
16/69	Ub149	69.38	0.05	light brown (hard hammer used)	EH	0.50	0.11	1.09	0.13	23.91	2.60	1.02	0.24	n/a	n/a	n/a	16.29	0.12	0.08	0.30	0.03
16/69	Ub150	69.43	0.05	light brown	EH	n/a	n/a	n/a	n/a	n/a	n/a	n/a	n/a	n/a	n/a	n/a	n/a	n/a	n/a	n/a	n/a
16/69	Ub151	69.48	0.05	light brown, core mud removed	DN	n/a	n/a	n/a	n/a	n/a	n/a	n/a	n/a	n/a	n/a	n/a	n/a	n/a	n/a	n/a	n/a
16/69	Ub152	69.53	0.05	light brown, core mud removed	EH	0.50	0.10	1.60	n/a	32.09	2.99	0.93	0.35	0.07	n/a	n/a	9.47	0.10	0.11	0.36	0.02
16/69	Ub153	69.58	0.05	light brown	EH	0.41	0.21	1.13	0.11	26.11	2.69	0.92	0.28	0.07	n/a	n/a	7.25	n/a	0.22	0.32	n/a
16/69	Ub154	69.63	0.05	light brown, core mud removed	DN	n/a	n/a	n/a	n/a	n/a	n/a	n/a	n/a	n/a	n/a	n/a	n/a	n/a	n/a	n/a	n/a
16/69	Ub155	69.68	0.05	light brown, core mud removed	DN	0.51	0.10	1.62	0.16	30.79	3.04	0.87	0.42	0.10	n/a	n/a	11.64	n/a	0.10	0.48	0.01
16/69	Ub156	69.73	0.05	light brown, core mud removed	DN	0.50	0.10	1.50	n/a	30.68	3.10	0.94	0.36	0.08	n/a	n/a	10.05	n/a	0.10	0.37	0.04

16/69	Ub157	69.78	0.05	light brown	EH	n/a	n/a	n/a	n/a	n/a	n/a	n/a	n/a	n/a	n/a	n/a	n/a	n/a	n/a	n/a	n/a
16/69	Ub158	69.83	0.05	light brown, core mud removed	DN	0.50	0.10	1.74	n/a	29.14	3.43	1.02	0.42	0.09	n/a	n/a	11.44	0.10	0.10	0.59	0.02
16/69	Ub159	69.88	0.05	light brown, core mud removed	EH	0.50	0.11	1.61	0.18	25.77	3.28	1.30	0.36	0.07	n/a	n/a	12.50	n/a	0.09	0.47	0.03
16/69	Ub160	69.93	0.05	light brown, core mud removed	EH	0.51	0.10	1.61	0.12	25.80	3.53	1.22	0.40	0.08	n/a	n/a	11.02	0.11	0.08	0.49	0.05
16/69	Ub161	69.98	0.05	light brown	DN	0.50	0.10	1.66	0.11	25.04	3.51	1.30	0.40	0.06	n/a	n/a	13.90	n/a	0.07	0.44	0.04
16/69	Ub162	70.03	0.05	light brown, core mud removed	EH	0.50	0.10	1.59	n/a	25.29	3.67	1.19	0.35	n/a	n/a	n/a	12.66	n/a	0.09	0.48	0.06
16/69	Ub163	70.08	0.04	light brown	DN	n/a	n/a	n/a	n/a	n/a	n/a	n/a	n/a	n/a	n/a	n/a	n/a	n/a	n/a	n/a	n/a
17/69	Ub164	70.12	0.05	light brown	DN	0.51	0.11	1.62	n/a	24.78	3.52	1.26	0.44	0.07	n/a	n/a	13.08	0.15	0.08	0.49	0.05
17/69	Ub165	70.17	0.05	light brown	EH	0.50	0.11	1.54	n/a	23.35	3.72	1.25	0.32	0.05	n/a	n/a	12.99	0.12	0.07	0.47	0.06
17/69	Ub166	70.22	0.05	light brown	EH	0.50	0.10	1.55	n/a	27.22	3.44	1.02	0.39	0.07	n/a	n/a	12.31	0.14	0.09	0.52	0.07
17/69	Ub167	70.27	0.05	light brown, core mud removed	DN	n/a	n/a	n/a	n/a	n/a	n/a	n/a	n/a	n/a	n/a	n/a	n/a	n/a	n/a	n/a	n/a
17/69	Ub168	70.32	0.05	light brown	EH	0.52	0.10	1.64	n/a	26.30	3.85	1.24	0.36	0.08	n/a	n/a	12.71	n/a	0.08	0.50	0.07
17/69	Ub169	70.37	0.05	light brown	DN	0.50	0.10	1.82	0.11	28.01	3.76	1.16	0.43	0.09	n/a	n/a	12.01	n/a	0.09	0.58	0.02
17/69	Ub170	70.42	0.05	light brown, core mud removed	EH	0.40	0.20	1.84	n/a	29.73	3.12	1.26	0.46	0.09	n/a	n/a	11.81	n/a	0.09	0.45	0.02
17/69	Ub171	70.47	0.05	light brown	DN	0.50	0.10	0.93	n/a	22.46	2.58	0.63	0.21	n/a	n/a	n/a	6.23	0.08	0.18	0.28	n/a
17/69	Ub172	70.52	0.05	light brown	EH	0.50	0.10	2.15	n/a	23.27	3.97	1.43	0.40	n/a	n/a	n/a	12.99	0.13	0.07	0.55	0.05
17/69	Ub173	70.57	0.05	light brown, core mud removed	DN	n/a	n/a	n/a	n/a	n/a	n/a	n/a	n/a	n/a	n/a	n/a	n/a	n/a	n/a	n/a	n/a
17/69	Ub174	70.62	0.05	light brown	EH	0.51	0.10	2.10	n/a	26.56	3.55	1.45	0.41	0.07	n/a	n/a	12.03	0.12	0.10	0.51	0.04
17/69	Ub175	70.67	0.05	light brown	DN	0.51	0.10	2.32	0.11	22.74	3.82	1.66	0.41	n/a	n/a	n/a	13.47	0.12	0.09	0.66	0.06
17/69	Ub176	70.72	0.05	light brown	DN	n/a	n/a	n/a	n/a	n/a	n/a	n/a	n/a	n/a	n/a	n/a	n/a	n/a	n/a	n/a	n/a
17/69	Ub177	70.77	0.05	light brown	DN	0.52	0.11	2.30	0.18	24.42	3.78	1.66	0.43	0.04	n/a	n/a	12.58	0.09	0.11	0.54	0.04
17/69	Ub178	70.82	0.05	light brown	EH	0.44	0.14	2.38	0.16	21.64	3.92	1.55	0.49	n/a	n/a	n/a	12.27	n/a	0.10	0.62	0.05
17/69	Ub179	70.87	0.05	light brown, core mud	DN	0.50	0.09	2.29	n/a	25.26	3.84	1.61	0.52	0.06	n/a	n/a	12.14	n/a	0.11	0.41	0.02

				removed																
17/69	Ub180	70.92	0.05	light brown	DN	n/a	n/a	n/a	n/a	n/a	n/a	n/a	n/a	n/a	n/a	n/a	n/a	n/a	n/a	n/a
17/69	Ub181	70.97	8.89	light brown, core mud removed	DN	0.49	0.11	2.01	n/a	21.42	3.90	1.55	0.41	0.04	n/a	n/a	11.06	0.13	0.22	0.53	n/a
18/69	Ub182	79.86	0.05	light brown	EH	0.41	0.19	2.31	n/a	24.94	3.70	1.32	0.50	0.07	n/a	n/a	12.95	0.15	0.08	0.60	0.05
18/69	Ub183	79.91	0.05	light brown, core mud removed	EH	0.53	0.10	0.96	n/a	19.70	3.62	0.81	0.29	0.05	n/a	0.02	6.67	0.09	0.18	0.29	n/a
18/69	Ub184	79.96	0.05	light brown	EH	0.53	0.10	1.58	n/a	25.20	3.97	1.12	0.44	n/a	n/a	n/a	10.55	n/a	0.08	0.46	0.05
18/69	Ub185	80.01	0.05	light brown, core mud removed	EH	n/a	n/a	n/a	n/a	n/a	n/a	n/a	n/a	n/a	n/a	n/a	n/a	n/a	n/a	n/a	n/a
18/69	Ub186	80.06	0.1	light brown, **reddish patches**	EH	0.52	0.11	2.00	0.13	23.18	4.43	1.23	0.46	0.09	n/a	n/a	12.90	n/a	0.09	0.61	0.05
18/69	Ub187	80.16	0.05	light brown	EH	n/a	n/a	n/a	n/a	n/a	n/a	n/a	n/a	n/a	n/a	n/a	n/a	n/a	n/a	n/a	n/a
18/69	Ub188	80.21	0.05	light brown, core mud removed	DN	0.50	0.10	2.26	n/a	23.88	4.42	1.43	0.46	n/a	n/a	n/a	12.62	n/a	0.09	0.56	0.06
18/69	Ub189	80.26	0.05	light brown	DN	0.51	0.11	2.53	n/a	22.20	4.14	1.54	0.51	0.07	n/a	n/a	13.66	0.13	0.09	0.55	0.04
18/69	Ub190	80.31	0.05	light brown	DN	n/a	n/a	n/a	n/a	n/a	n/a	n/a	n/a	n/a	n/a	n/a	n/a	n/a	n/a	n/a	n/a
18/69	Ub191	80.36	0.05	light brown	DN	0.51	0.11	2.31	n/a	22.13	3.73	1.51	0.44	n/a	n/a	n/a	13.00	n/a	0.09	0.65	0.05
18/69	Ub192	80.41	0.05	light brown	EH	0.40	0.20	1.36	n/a	17.84	3.41	1.00	0.22	0.04	n/a	n/a	9.34	n/a	0.17	0.45	n/a
18/69	Ub193	80.46	0.05	light brown	DN	0.51	0.14	1.72	0.13	20.84	3.63	1.19	0.32	n/a	n/a	n/a	11.72	0.09	0.16	0.73	0.02
18/69	Ub194	80.51	0.05	light brown	EH	n/a	n/a	n/a	n/a	n/a	n/a	n/a	n/a	n/a	n/a	n/a	n/a	n/a	n/a	n/a	n/a
18/69	Ub195	80.56	0.05	light brown, core mud removed	EH	0.50	0.11	2.22	0.20	21.55	3.86	1.34	0.43	n/a	n/a	n/a	13.75	0.08	0.06	0.70	0.07
18/69	Ub196	80.61	0.05	light brown, core mud removed	DN	0.37	0.23	1.15	n/a	13.78	2.51	0.77	0.25	0.03	n/a	n/a	7.44	n/a	0.17	0.46	n/a
18/69	Ub197	80.66	0.01	light brown, core mud removed	DN	0.51	0.13	1.92	n/a	21.29	4.04	1.28	0.50	n/a	n/a	n/a	12.70	0.10	0.08	0.66	0.07
19/69	Ub198	80.67	0.05	light brown, core mud removed **reddish patches**	EH	0.51	0.11	2.49	0.24	20.46	4.17	1.59	0.49	0.06	n/a	n/a	13.45	0.16	0.08	0.58	0.05
19/69	Ub199	80.72	0.05	light brown	EH	0.49	0.10	2.39	n/a	21.81	4.09	1.42	0.40	n/a	n/a	n/a	12.64	0.09	0.09	0.59	0.06

19/69	Ub200	80.77	0.05	light brown	DN	0.49	0.14	2.14	n/a	24.02	3.96	1.50	0.40	0.08	n/a	n/a	12.28	0.13	0.08	0.36	0.03
19/69	Ub201	80.82	0.05	light brown	EH	0.51	0.10	2.54	n/a	22.17	3.95	1.39	0.53	0.05	n/a	n/a	12.64	n/a	0.10	0.49	0.05
19/69	Ub202	80.87	0.05	light brown, core mud removed	DN	0.52	0.13	2.13	n/a	25.89	3.68	1.37	0.45	n/a	n/a	n/a	11.04	n/a	0.10	0.60	0.05
19/69	Ub203	80.92	0.05	light brown	EH	0.33	0.27	1.12	n/a	18.63	2.63	0.97	0.21	n/a	n/a	n/a	7.07	n/a	0.22	0.41	n/a
19/69	Ub204	80.97	0.05	light brown, core mud removed	DN	0.48	0.12	2.35	0.13	27.14	3.86	1.29	0.50	0.08	n/a	n/a	10.61	n/a	0.10	0.53	0.04
19/69	Ub205	81.02	0.05	light brown, **white clasts**	EH	0.50	0.11	1.94	0.17	29.70	3.62	1.34	0.43	0.11	n/a	n/a	10.85	0.13	0.09	0.59	0.01
19/69	Ub206	81.07	0.05	light brown, core mud removed	DN	0.51	0.10	2.06	0.18	28.74	3.50	1.16	0.46	0.08	n/a	n/a	11.41	n/a	0.09	0.54	0.01
19/69	Ub207	81.12	0.05	light brown, core mud removed	EH	0.37	0.30	0.68	0.15	18.68	2.07	0.80	0.22	0.05	n/a	n/a	5.37	n/a	0.19	0.37	n/a
19/69	Ub208	81.17	0.05	light brown, core mud removed	EH	0.50	0.10	1.79	n/a	28.78	3.60	1.06	0.37	n/a	n/a	n/a	10.39	0.10	0.09	0.58	0.04
19/69	Ub209	81.22	0.05	light brown	EH	n/a	n/a	n/a	n/a	n/a	n/a	n/a	n/a	n/a	n/a	n/a	n/a	n/a	n/a	n/a	n/a
19/69	Ub210	81.27	0.05	light brown, core mud removed	EH	0.50	0.13	1.55	0.11	27.25	3.84	0.89	0.39	n/a	n/a	n/a	9.01	n/a	0.08	0.43	0.04
19/69	Ub211	81.32	0.05	light brown	EH	0.43	0.16	0.54	n/a	15.25	1.73	0.48	0.13	n/a	n/a	n/a	3.24	n/a	0.15	0.23	n/a
19/69	Ub212	81.37	0.05	light brown	DN	0.52	0.11	1.82	n/a	32.46	3.97	0.97	0.51	0.09	n/a	n/a	9.56	n/a	0.09	0.46	0.01
19/69	Ub213	81.42	0.05	light brown	DN	0.31	0.31	0.97	n/a	22.05	2.73	0.64	0.24	0.09	n/a	n/a	5.53	n/a	0.18	0.30	n/a
19/69	Ub214	81.47	0.03	light brown	DN	0.50	0.11	1.73	n/a	30.97	1.73	4.29	0.50	0.07	n/a	n/a	10.13	n/a	0.08	0.43	0.01
19/69	Ub215	81.50	0.01	light brown	DN	0.31	0.30	1.08	n/a	22.22	3.10	0.70	0.28	0.07	n/a	n/a	6.34	n/a	0.16	0.27	n/a
20/69	Ub216	81.51	0.05	light brown	DN	0.51	0.11	1.45	0.19	32.70	1.45	0.79	0.51	0.06	n/a	n/a	9.33	0.51	n/a	0.37	0.01
20/69	Ub217	81.56	0.05	light brown	EH	0.50	0.11	1.31	n/a	33.19	3.94	0.91	0.49	n/a	n/a	n/a	9.52	0.14	0.09	0.32	0.01
20/69	Ub218	81.61	0.05	light brown, core mud removed	DN	0.51	0.10	1.61	0.21	35.19	1.61	0.86	0.51	0.07	n/a	n/a	9.25	0.12	0.09	0.50	0.01
20/69	Ub219	81.66	0.05	light brown, core mud removed	EH	0.50	0.10	1.30	0.15	35.70	1.30	0.82	0.51	n/a	n/a	n/a	9.96	n/a	0.09	0.43	0.02
20/69	Ub220	81.71	0.05	light brown, core mud removed	DN	0.51	0.11	1.40	n/a	32.78	1.40	0.84	0.48	0.09	n/a	n/a	9.24	n/a	0.08	0.33	0.03

20/69	Ub221	81.76	0.05	light brown, core mud removed	DN	0.51	0.12	1.31	n/a	34.11	3.76	0.69	0.40	n/a	n/a	n/a	8.44	n/a	0.08	0.48	n/a
20/69	Ub222	81.81	0.05	light brown, core mud removed	EH	0.50	0.11	1.36	n/a	33.02	3.61	0.78	0.44	0.08	n/a	n/a	8.32	n/a	0.07	0.37	0.02
20/69	Ub223	81.86	0.05	light brown	DN	0.51	0.12	1.69	n/a	33.47	3.85	0.72	0.37	n/a	n/a	n/a	9.55	0.13	0.08	0.39	0.01
20/69	Ub224	81.91	0.05	light brown, core mud removed	EH	0.50	0.10	1.42	n/a	33.88	3.32	0.75	0.39	n/a	n/a	n/a	9.03	n/a	0.08	0.44	0.02
20/69	Ub225	81.96	0.05	light brown, core mud removed	DN	0.51	0.10	1.35	n/a	36.27	4.10	0.88	0.44	0.05	n/a	n/a	8.09	n/a	0.08	0.41	0.01
20/69	Ub226	82.01	0.05	light brown, core mud removed	EH	0.51	0.10	2.17	n/a	28.74	3.97	1.14	0.46	0.05	n/a	n/a	10.57	0.12	0.08	0.54	0.01
20/69	Ub227	82.06	0.05	light brown	DN	0.50	0.10	2.34	n/a	27.99	4.42	1.16	0.50	0.09	n/a	n/a	10.92	n/a	0.09	0.51	0.01
20/69	Ub228	82.11	0.05	light brown, core mud removed	EH	0.50	0.10	1.84	n/a	34.19	1.84	1.11	0.41	n/a	n/a	n/a	8.44	n/a	0.10	0.32	n/a
20/69	Ub229	82.16	0.05	light brown, core mud removed	EH	0.50	0.10	1.94	n/a	28.65	4.09	0.76	0.46	0.07	n/a	n/a	10.61	0.10	0.09	0.47	0.05
20/69	Ub230	82.21	0.05	light brown, core mud removed	DN	0.50	0.11	2.09	n/a	27.12	4.68	1.26	0.48	0.06	n/a	n/a	10.90	n/a	0.09	0.40	0.01
20/69	Ub231	82.26	0.05	light brown, core mud removed	DN	0.51	0.11	1.83	0.08	28.41	4.19	1.08	0.44	0.07	n/a	n/a	9.36	n/a	0.10	0.51	0.02
20/69	Ub232	82.31	0.01	light brown, core mud removed	EH	0.51	0.10	2.00	n/a	29.32	4.42	0.91	0.46	0.06	n/a	n/a	9.61	n/a	0.09	0.40	0.01
21/69	Ub233	82.32	0.05	light brown, milk reddish patches, burrow	DN	0.52	0.10	1.86	n/a	29.27	4.39	0.88	0.48	n/a	n/a	n/a	8.95	0.12	0.09	0.46	n/a
21/69	Ub234	82.37	0.05	light brown	DN	0.51	0.11	1.77	n/a	29.10	4.76	1.03	0.53	0.07	n/a	n/a	10.12	n/a	0.09	0.33	0.02
21/69	Ub235	82.42	0.05	cream	EH	0.52	0.11	1.36	n/a	30.91	3.88	0.70	0.39~	0.08	n/a	n/a	7.76	n/a	0.10	0.40	0.03
21/69	Ub236	82.47	0.05	cream, core mud removed	DN	0.51	0.10	1.78	n/a	30.91	4.07	1.00	0.44	0.09	n/a	n/a	9.30	0.08	0.11	0.44	0.01
21/69	Ub237	82.52	0.05	cream core mud removed	EH	0.50	0.12	1.58	n/a	29.58	4.02	0.97	0.36	n/a	n/a	n/a	8.35	0.13	0.10	0.35	0.02
21/69	Ub238	82.57	0.05	cream core mud removed	DN	0.52	0.11	1.72	n/a	29.00	4.08	0.99	0.40	0.09	n/a	n/a	8.60	n/a	0.12	0.50	n/a

21/69	Ub239	82.62	0.05	cream	DN	0.50	0.10	2.15	n/a	33.92	3.82	0.99	0.54	0.11	n/a	n/a	9.76	n/a	0.13	0.44	n/a
21/69	Ub240	82.67	0.05	cream core mud removed	EH	0.50	0.11	1.63	n/a	32.72	3.53	0.88	0.42	0.09	n/a	n/a	7.63	n/a	0.12	0.42	n/a
21/69	Ub241	82.72	0.05	cream core mud removed	DN	0.50	0.11	2.11	n/a	31.38	4.10	0.98	0.46	n/a	n/a	n/a	9.08	0.14	0.13	0.45	n/a
21/69	Ub242	82.77	0.05	cream core mud removed	EH	0.51	0.12	1.97	n/a	31.26	4.26	1.09	0.47	0.09	n/a	n/a	9.23	0.13	0.12	0.47	n/a
21/69	Ub243	82.82	0.05	cream, core mud removed	DN	0.51	0.10	2.22	n/a	31.70	3.76	1.19	0.53	n/a	n/a	n/a	9.71	0.10	0.14	0.44	n/a
21/69	Ub244	82.87	0.05	cream	DN	0.50	0.11	1.79	n/a	33.80	3.90	1.12	0.49	0.10	n/a	n/a	9.13	0.08	0.11	0.45	n/a
21/69	Ub245	82.92	0.05	cream, core mud removed	DN	0.51	0.10	1.70	0.15	31.80	5.11	1.03	0.57	0.10	n/a	n/a	9.91	0.10	0.11	0.45	0.01
21/69	Ub246	82.97	0.08	cream	DN	0.51	0.11	1.89	0.39	33.16	3.58	1.15	0.45	0.11	n/a	n/a	9.81	0.10	0.11	0.54	0.01
21/69	Ub247	83.05	0.05	cream, core mud removed	DN	0.53	0.10	2.24	n/a	31.98	3.58	1.18	0.49	0.09	n/a	n/a	9.75	0.09	0.11	0.47	0.01
21/69	Ub248	83.10	0.05	cream	DN	0.50	0.10	2.20	n/a	30.99	3.72	1.18	0.44	n/a	n/a	n/a	9.08	0.13	0.11	0.55	0.01
21/69	Ub249	83.15	0.01	cream	DN	0.51	0.13	1.90	n/a	29.53	3.42	1.21	0.49	0.08	n/a	n/a	9.88	0.12	0.11	0.45	0.02
22/69	Ub250	83.16	0.05	cream	DN	0.53	0.12	2.56	n/a	28.43	3.84	1.18	0.54	0.09	n/a	n/a	11.64	0.16	0.12	0.47	0.01
22/69	Ub251	83.21	0.05	cream, core mud removed	DN	0.51	0.13	2.31	n/a	27.13	3.12	1.24	0.52	0.08	n/a	n/a	10.02	n/a	0.11	0.48	0.03
22/69	Ub252	83.26	0.05	cream	DN	0.50	0.11	2.52	n/a	29.88	3.94	1.16	0.61	0.08	n/a	n/a	10.31	n/a	0.11	0.47	0.01
22/69	Ub253	83.31	0.05	much lighter in colour	DN	0.51	0.10	2.76	n/a	28.99	3.29	1.22	0.46	0.07	n/a	n/a	10.38	0.11	0.11	0.48	0.01
22/69	Ub254	83.36	0.05	much lighter in colour	EH	0.51	0.11	2.01	n/a	27.32	3.30	1.39	0.49	0.09	n/a	n/a	9.80	n/a	0.11	0.48	0.04
22/69	Ub255	83.41	0.05	much lighter in colour	EH	0.51	0.15	1.94	n/a	28.60	3.28	1.08	0.44	0.09	n/a	n/a	8.63	0.11	0.10	0.42	0.02
22/69	Ub256	83.46	0.05	much lighter in colour	EH	0.50	0.11	2.32	n/a	30.44	3.56	1.20	0.41	0.08	n/a	n/a	9.61	n/a	0.11	0.58	n/a
22/69	Ub257	83.51	0.05	much lighter in colour	EH	0.51	0.11	1.92	n/a	30.40	3.15	0.93	0.37	0.10	n/a	n/a	9.09	0.10	0.09	0.44	0.03
22/69	Ub258	83.56	0.05	much lighter in colour	EH	0.51	0.11	1.72	n/a	30.49	3.34	1.11	0.42	0.12	n/a	n/a	9.05	0.10	0.09	0.41	0.02
22/69	Ub259	83.61	0.05	**much lighter in colour**	EH	0.50	0.10	1.79	n/a	31.66	3.66	0.96	0.42	0.10	n/a	n/a	9.08	0.12	0.10	0.50	0.01
22/69	Ub260	83.66	0.05	brown, core mud removed	EH	0.51	0.10	1.57	n/a	29.14	5.43	0.97	0.51	0.09	n/a	n/a	9.64	0.11	0.06	0.29	0.02

22/69	Ub261	83.71	0.05	brown, burrow	EH	0.50	0.10	1.17	n/a	28.37	4.92	0.73	0.34	0.08	n/a	n/a	7.41	n/a	0.06	0.42	0.04
22/69	Ub262	83.76	0.05	brown, core mud removed and burrow	EH	0.50	0.11	1.04	n/a	29.59	5.43	0.85	0.40	0.10	n/a	n/a	8.45	n/a	0.06	0.42	n/a
22/69	Ub263	83.81	0.05	brown	DN	0.50	0.10	1.76	n/a	25.35	5.25	0.95	0.39	0.14	n/a	n/a	9.13	n/a	0.07	0.45	0.04
22/69	Ub264	83.86	0.05	brown	EH	0.50	0.10	1.72	0.07	29.23	4.77	0.85	0.42	0.12	n/a	n/a	9.15	0.11	0.08	0.46	0.02
22/69	Ub265	83.91	0.05	brown **from here upwards sandy (easy to grind) lighter in colour**	DN	0.53	0.10	1.74	n/a	25.12	5.39	0.86	0.40	0.09	n/a	n/a	10.50	0.11	0.08	0.52	0.04
22/69	Ub266	83.96	3.54	brown, core mud removed	EH	0.51	0.11	2.14	n/a	18.81	5.98	1.23	0.47	0.06	n/a	n/a	12.26	0.07	0.06	0.49	0.06
23/69	Ub267	87.50	0.05	brown	DN	0.51	0.10	4.88	n/a	2.48	7.24	2.09	0.57	0.06	n/a	0.03	15.43	0.22	0.06	0.94	0.05
23/69	Ub268	87.55	0.05	brown	EH	0.52	0.10	5.43	n/a	2.31	8.43	2.24	0.58	0.10	n/a	0.03	16.53	0.43	0.06	0.80	0.05
23/69	Ub269	87.60	0.05	brown	EH	0.51	0.11	5.30	0.33	2.54	7.76	2.32	0.64	0.07	n/a	0.04	16.46	0.23	0.07	0.93	0.03
23/69	Ub270	87.65	0.05	brown, burrow, core mud removed	DN	0.50	0.10	4.83	n/a	3.34	8.27	2.15	0.51	0.11	n/a	n/a	15.57	0.29	0.09	0.80	0.02
23/69	Ub271	87.70	0.05	brown	DN	0.50	0.13	4.84	0.33	2.25	7.46	2.11	0.44	0.08	n/a	0.03	15.11	0.24	0.07	0.83	0.04
23/69	Ub272	87.75	0.05	brown	EH	0.51	0.10	5.53	n/a	2.86	7.99	2.45	0.52	0.07	n/a	0.01	17.49	0.38	0.08	0.86	0.02
23/69	Ub273	87.80	0.05	brown, secondary minerals, mould and core mud removed burrow present	DN	0.49	0.10	5.33	n/a	2.91	9.76	2.32	0.70	0.21	n/a	n/a	16.43	0.38	0.07	0.88	0.03
23/69	Ub274	87.85	0.05	brown, secondary minerals and core mud removed	EH	0.53	0.10	5.00	n/a	2.56	7.22	2.20	0.48	0.07	n/a	0.04	15.13	0.20	0.08	0.85	0.03
23/69	Ub275	87.90	0.05	brown, secondary minerals and core mud removed	DN	0.51	0.11	5.87	n/a	2.57	8.31	2.52	0.69	0.08	n/a	0.01	16.43	0.24	0.08	0.97	0.03
23/69	Ub276	87.95	0.05	brown, mould and core mud removed	EH	0.50	0.10	5.08	n/a	2.72	7.43	2.18	0.55	0.08	n/a	n/a	14.61	0.42	0.08	0.83	0.02
23/69	Ub277	88.00	0.05	brown, core mud removed	EH	0.55	0.10	5.68	n/a	2.15	7.58	2.24	0.64	0.05	n/a	n/a	17.62	0.24	0.07	0.94	0.04

23/69	Ub278	88.05	0.1	brown, secondary minerals removed **hard again to grind**	DN	0.50	0.10	5.17	0.29	2.48	9.10	2.04	0.64	0.14	n/a	0.01	15.57	0.22	0.03	0.88	0.05
23/69	Ub279	88.15	0.05	brown, **white clasts**	EH	0.53	0.10	2.99	n/a	5.61	5.61	1.61	0.46	n/a	n/a	0.02	15.76	n/a	0.09	0.89	0.07
23/69	Ub280	88.20	0.05	brown, core mud removed	DN	0.51	0.10	6.63	0.13	5.07	6.86~	1.76	0.42	n/a	n/a	0.02	16.13	0.14	0.07	0.90	0.07
23/69	Ub281	88.25	0.05	brown, core mud removed	EH	0.50	0.12	2.58	n/a	3.75	5.48	1.61	0.39	0.02	n/a	n/a	14.82	0.07	0.06	0.67	0.08
23/69	Ub282	88.30	0.05	brown	EH	0.51	0.13	2.64	n/a	3.10	5.20	1.71	0.35	n/a	n/a	n/a	15.62	n/a	0.05	0.69	0.09
23/69	Ub283	88.35	0.03	brown, core mud removed	DN	0.51	0.12	3.15	n/a	3.65	6.20	1.86	0.45	n/a	n/a	0.03	16.87	0.09	0.05	0.72	0.10
24/69	Ub284	88.38	0.1	brown	EH	0.50	0.10	3.07	n/a	3.27	4.29	1.48	0.40	n/a	n/a	0.02	17.65	0.08	0.05	0.81	0.12
24/69	Ub285	88.48	0.05	brown, core mud removed	DN	0.50	0.11	3.79	n/a	4.56	5.42	1.76	0.47~	0.04	n/a	n/a	18.21	0.09	0.07	0.88	0.09
24/69	Ub286	88.53	0.05	brown	EH	0.52	0.11	3.46	n/a	3.99	4.83	1.52	0.40	0.04	n/a	n/a	17.04	0.09	0.07	0.83	0.08
24/69	Ub287	88.58	0.05	brown 88.58 onwards is sandy(easy to grind) + lighter in colour	EH	0.51	0.10	3.99	0.11	4.20	5.27	1.50	0.48	0.04	n/a	n/a	19.94	n/a	0.07	0.74	0.07
24/69	Ub288	88.63	0.05	brown	DN	0.53	0.12	4.50	n/a	1.76	6.31	2.04	0.59	n/a	n/a	0.03	18.79	0.16	0.04	0.90	0.07
24/69	Ub289	88.68	0.05	brown core mud removed	EH	0.50	0.10	3.87	n/a	1.75	6.60	2.05	0.48	0.03	n/a	0.03	15.71	0.12	0.05	0.94	0.08
24/69	Ub290	88.73	0.05	brown, core mud removed	EH	0.50	0.12	3.99	0.36	2.32	7.16	1.99	0.54	0.02	n/a	0.03	16.82	n/a	0.06	0.97	0.04
24/69	Ub291	88.78	0.05	brown, core mud removed	DN	0.50	0.11	4.02	n/a	1.45	6.64	2.23	0.47	n/a	n/a	n/a	16.77	n/a	0.06	0.89	0.05
24/69	Ub292	88.83	0.05	brown, core mud removed	EH	0.52	0.11	4.69	n/a	3.28	6.83	2.10	0.49	n/a	n/a	n/a	16.94	n/a	0.08	0.90	0.03
24/69	Ub293	88.88	0.05	brown, core mud removed	DN	0.49	0.09	5.77	n/a	3.06	6.71	2.23	0.64	n/a	n/a	n/a	19.85	0.18	0.07	0.90	0.05
24/69	Ub294	88.93	0.05	brown	DN	0.30	0.29	3.72	n/a	1.88	4.35	1.72	0.45	n/a	n/a	0.04	12.70	n/a	0.06	0.70	n/a
24/69	Ub295	88.98	0.05	brown, core mud removed	EH	0.50	0.11	3.90	n/a	1.35	6.55	2.14	0.52	n/a	n/a	0.03	15.51	0.12	0.05	0.89	0.05
24/69	Ub296	89.03	0.05	brown, core mud removed	DN	0.51	0.11	4.92	n/a	2.68	6.75	2.18	0.54	0.06	n/a	0.03	17.13	0.47	0.08	0.99	0.06

24/69	Ub297	89.08	0.05	brown, core mud removed	EH	0.50	0.10	4.65	0.18	1.86	6.65	2.11	0.51	0.04	n/a	0.03	15.84	0.22	0.05	0.97	0.06
24/69	Ub298	89.13	0.05	brown	DN	0.50	0.10	5.15	n/a	2.76	6.91	2.02	0.60	n/a	n/a	n/a	18.24	0.21	0.06	0.96	0.05
24/69	Ub299	89.18	0.03	brown, core mud removed	EH	0.53	0.10	4.80	n/a	2.13	6.68	2.18	0.60	n/a	n/a	n/a	17.00	0.15	0.05	0.84	0.06
25/69	Ub300	89.21	0.05	brown, core mud removed	DN	0.51	0.11	4.16	0.25	2.79	6.45	1.97	0.45	0.04	n/a	0.03	15.32	0.21	0.07	0.86	0.03
25/69	Ub301	89.26	0.05	brown, secondary minerals removed	EH	0.49	0.10	4.14	0.23	3.36	7.05	2.09	0.44	0.03	n/a	0.03	16.06	0.26	0.07	0.94	0.04
25/69	Ub302	89.31	0.05	brown, core mud removed	DN	0.49	0.11	4.55	n/a	2.65	6.43	2.11	0.49	0.03	n/a	n/a	17.86	0.20	0.07	0.82	0.04
25/69	Ub303	89.36	0.05	brown	EH	0.52	0.10	3.88	n/a	3.60	6.37	2.06	0.44	0.04	n/a	0.03	16.67	0.13	0.07	0.86	0.06
25/69	Ub304	89.41	0.05	brown, mould removed	DN	0.50	0.11	5.27	0.24	2.57	6.75	1.85	0.69	0.04	n/a	0.03	19.60	0.17	n/a	1.04	0.08
25/69	Ub305	89.46	0.05	brown, mould removed	EH	0.50	0.10	4.69	n/a	2.99	6.87	2.16	0.55	n/a	n/a	0.02	18.53	0.14	0.06	1.06	0.06
25/69	Ub306	89.51	0.05	brown, mould and core mud removed	DN	0.50	0.12	4.35	n/a	2.77	6.55	1.93	0.45	0.06	n/a	0.03	16.86	0.15	0.07	0.99	0.04
25/69	Ub307	89.56	0.05	brown, mould removed **white crust**	EH	0.50	0.11	3.94	n/a	3.17	6.51	1.96	0.50	0.06	n/a	n/a	16.24	0.20	n/a	0.79	0.05
25/69	Ub308	89.61	0.05	brown, mould removed	DN	0.50	0.12	4.80	0.32	3.91	8.39	2.04	0.65	0.17	n/a	n/a	18.38	0.17	0.06	0.90	0.05
25/69	Ub309	89.66	0.05	brown, mould and secondary minerals removed	EH	0.50	0.12	4.61	n/a	3.07	6.83	2.17	0.57	0.06	n/a	0.03	16.77	0.12	0.07	0.91	0.05
25/69	Ub310	89.71	0.05	brown mould, core mud and secondary minerals removed	DN	0.51	0.10	5.02	n/a	3.30	7.02	2.04	0.60	0.04	n/a	n/a	17.79	0.29	0.07	0.94	0.05
25/69	Ub311	89.76	0.05	brown, mould removed	EH	0.52	0.10	4.42	0.19	3.11	6.67	2.13	0.51	0.04	n/a	0.11	16.64	0.12	0.08	0.92	0.05
25/69	Ub312	89.81	0.05	brown	EH	0.50	0.11	4.30	n/a	3.45	6.71	2.00	0.47	0.06	n/a	0.03	15.65	0.22	0.08	0.89	0.04
25/69	Ub313	89.86	0.05	brown, mould removed	DN	0.49	0.10	4.91	n/a	3.55	6.91	2.12	0.56	n/a	n/a	n/a	17.74	0.21	0.08	0.96	0.05
25/69	Ub314	89.91	0.05	brown	EH	0.49	0.10	4.58	0.27	3.98	6.75	1.92	0.45	0.05	n/a	0.03	16.89	0.17	0.08	0.87	0.05

25/69	Ub315	89.96	0.05	brown, core mud removed	DN	0.01	0.10	5.22	n/a	4.07	7.02	2.24	0.61	0.06	n/a	n/a	18.26	0.16	0.08	0.96	0.06
25/69	Ub316	90.01	0.05	brown, core mud and secondary minerals removed	DN	0.50	0.11	5.25	n/a	4.36	6.84	2.09	0.56	0.05	n/a	n/a	18.12	0.43	0.09	0.56	0.04
25/69	Ub317	90.06	0.01	brown, secondary minerals removed	DN	0.50	0.09	4.77	n/a	3.94	6.76	2.07	0.64	0.05	n/a	n/a	18.54	0.37	0.08	0.96	0.05
26/69	Ub318	90.07	0.05	brown	EH	0.52	0.09	4.32	n/a	2.77	7.19	2.23	0.59	n/a	n/a	0.02	16.47	0.32	0.07	0.91	0.06
26/69	Ub319	90.12	0.05	brown, core mud removed	DN	0.50	0.10	5.14	n/a	3.49	6.96	2.31	0.67	0.04	n/a	n/a	18.85	0.18	0.07	0.96	0.05
26/69	Ub320	90.17	0.05	brown, mould removed	EH	0.50	0.13	3.92	n/a	4.59	6.62	1.82	0.44	0.08	n/a	n/a	15.70	0.19	0.09	0.81	0.04
26/69	Ub321	90.22	0.05	brown, mould removed, **dark brown org. material**	DN	0.50	0.11	5.15	n/a	4.09	6.73	2.13	0.58	n/a	n/a	n/a	18.69	0.29	0.08	0.98	0.05
26/69	Ub322	90.27	0.05	brown, secondary minerals removed	EH	0.53	0.10	3.00	n/a	2.95	5.87	1.82	0.38	n/a	n/a	n/a	12.32	0.21	0.07	0.73	0.04
26/69	Ub323	90.32	0.05	brown, mould and secondary minerals removed	DN	0.50	0.10	4.76	n/a	3.57	7.26	2.21	0.60	0.03	n/a	n/a	18.26	0.19	0.08	0.89	n/a
26/69	Ub324	90.37	0.05	brown, mould removed	EH	0.51	0.09	4.38	n/a	3.99	6.32	1.93	0.47	0.03	n/a	0.13	15.85	0.13	0.09	0.88	0.03
26/69	Ub325	90.42	0.05	brown, mould and secondary minerals removed	DN	0.49	0.15	4.31	n/a	3.63	6.25	1.78	0.46	0.06	n/a	n/a	16.84	0.18	0.08	0.80	0.04
26/69	Ub326	90.47	0.05	brown mould removed	DN	0.51	0.11	4.61	n/a	3.77	6.28	2.15	0.52	n/a	n/a	0.03	17.32	0.11	0.08	0.83	0.05
26/69	Ub327	90.52	0.05	brown mould removed	EH	0.50	0.11	3.98	n/a	3.39	6.36	2.03	0.42	0.03	n/a	0.14	14.30	0.18	0.08	0.80	0.03
26/69	Ub328	90.57	0.05	brown, mould and core mud removed, **white bits in matris**	DN	0.51	0.13	4.59	n/a	4.14	7.17	2.21	0.57	n/a	0.06	0.03	17.87	0.24	0.08	0.93	0.05

26/69	Ub329	90.62	0.05	brown, mould and secondary minerals removed	EH	0.51	0.10	3.94	n/a	3.91	6.50	1.91	0.45	0.04	n/a	n/a	14.51	n/a	0.09	0.83	n/a
26/69	Ub330	90.67	0.05	brown, mould and core mud removed	DN	0.52	0.10	5.24	0.19	3.85	6.80	2.22	0.61	0.05	n/a	0.03	17.58	0.16	0.08	0.87	0.04
26/69	Ub331	90.72	0.05	brown, mould and secondary minerals removed	EH	0.52	0.10	5.10	n/a	3.61	6.91	2.13	0.53	0.04	n/a	0.02	17.33	0.19	0.07	0.94	n/a
26/69	Ub332	90.77	0.05	brown, mould removed	DN	0.50	0.10	4.84	0.25	3.25	7.12	2.20	0.59	0.04	n/a	n/a	18.97	0.13	0.09	0.92	0.04
26/69	Ub333	90.82	0.05	brown, mould and core mud removed	EH	0.50	0.10	4.39	0.20	3.69	6.49	2.02	0.49	0.04	0.07	n/a	15.51	0.16	0.10	0.86	0.03
26/69	Ub334	90.87	0.05	brown, mould removed	EH	0.51	0.10	4.37	n/a	3.29	6.65	2.07	0.65	0.03	0.08	0.03	17.95	0.22	0.07	0.92	0.07
26/69	Ub335	90.92	0.04	brown, secondary minerals removed	EH	0.51	0.10	4.48	0.08	3.61	6.09	1.78	0.51	n/a	n/a	n/a	16.92	0.47	0.08	1.03	0.05
26/69	Ub336	90.96	0.01	brown, core mud removed	EH	0.51	0.10	3.91	0.24	3.03	6.29	2.13	0.43	0.03	0.08	n/a	17.38	0.20	0.07	0.91	0.06
27/69	Ub337	90.97	0.04	brown, mould and secondary minerals removed	DN	0.51	0.10	4.87	n/a	3.34	6.43	2.16	0.69	n/a	n/a	0.02	20.25	0.24	0.07	0.98	0.06
27/69	Ub338	91.01	0.04	brown	EH	0.51	0.11	4.79	n/a	3.64	6.30	2.19	0.66	n/a	n/a	n/a	19.95	0.18	0.08	0.91	0.05
27/69	Ub339	91.05	0.04	brown	DN	0.52	0.10	5.07	0.21	3.78	6.95	2.21	0.68	n/a	0.07	0.02	20.23	0.16	0.07	0.85	0.07
27/69	Ub340	91.09	0.04	brown	EH	0.50	0.11	4.45	n/a	3.73	6.44	2.06	0.54	n/a	n/a	n/a	17.72	0.18	0.07	0.85	0.06
27/69	Ub341	91.13	0.05	brown, dark brown organic material, core mud removed	DN	0.53	0.11	5.27	n/a	3.19	6.89	2.23	0.63	n/a	n/a	n/a	20.04	0.15	0.07	0.94	0.08
27/69	Ub342	91.18	0.04	brown	EH	0.50	0.13	4.64	0.19	3.17	6.09	2.04	0.51	n/a	0.06	n/a	17.52	0.47	0.07	0.78	0.78
27/69	Ub343	91.22	0.04	brown, core mud removed	DN	0.50	0.10	5.02	0.25	3.68	6.87	2.29	0.60	n/a	n/a	n/a	19.40	0.13	0.09	1.01	0.06
27/69	Ub344	91.26	0.04	brown, mould removed	EH	0.50	0.10	4.85	n/a	2.65	6.28	2.03	0.47	n/a	n/a	0.03	18.46	n/a	0.07	1.02	0.06
27/69	Ub345	91.30	0.04	brown, core mud removed	DN	0.50	0.10	4.80	n/a	2.46	6.50	2.21	0.61	0.03	n/a	0.03	18.46	0.15	0.05	0.96	0.08

27/69	Ub346	91.34	0.05	brown mould, secondary minerals removed	EH	0.50	0.10	4.70	n/a	3.08	6.07	2.01	0.48	0.03	n/a	0.03	18.78	0.18	0.06	0.92	0.06
27/69	Ub347	91.39	0.04	brown, mould removed**, white elongated bits in matrix**	DN	0.50	0.11	4.84	n/a	2.29	6.38	2.22	0.57	0.03	n/a	0.02	19.45	0.18	0.05	1.01	0.07
27/69	Ub348	91.43	0.04	brown, mould removed	EH	0.51	0.10	5.53	n/a	2.10	7.35	2.35	0.72	n/a	n/a	0.02	21.06	0.20	0.07	0.99	0.06
27/69	Ub349	91.47	0.04	brown, mould removed	EH	0.50	0.10	5.36	n/a	3.04	7.01	2.33	0.61	0.04	n/a	n/a	19.28	0.31	0.07	1.00	0.05
27/69	Ub350	91.51	0.04	brown, mould and mud removed	DN	0.48	0.10	6.06	n/a	3.02	6.83	2.33	0.64	0.03	0.07	n/a	20.41	0.23	0.06	1.03	0.07
27/69	Ub351	91.55	0.05	brown, mould removed	EH	0.52	0.10	5.59	n/a	3.11	7.13	2.08	0.68	n/a	0.05	0.04	20.50	0.19	0.07	1.01	0.07
27/69	Ub352	91.60	0.04	brown, core mud removed	DN	0.51	0.10	5.21	0.17	1.96	7.14	2.33	0.60	0.03	n/a	n/a	19.27	0.19	0.05	1.02	0.07
27/69	Ub353	91.64	0.04	brown, mold removed	DN	0.52	0.12	5.50	n/a	2.10	6.97	2.06	0.58	0.04	n/a	0.03	19.85	0.19	0.06	0.98	0.06
27/69	Ub354	91.68	0.04	brown, mould removed	DN	0.52	0.12	5.42	n/a	2.21	6.74	2.37	0.65	0.03	n/a	0.03	18.57	0.13	0.06	0.96	0.07
27/69	Ub355	91.72	0.03	brown, mould removed	EH	0.52	0.12	5.62	n/a	2.00	7.25	2.35	0.70	0.03	n/a	0.02	19.55	0.24	0.05	0.97	0.07
28a/69	Ub356	91.75	0.05	brown, secondary minerals removed	DN	0.50	0.10	5.74	0.26	2.59	7.49	2.70	0.76	0.03	0.08	0.01	20.56	0.54	0.06	1.03	0.05
28a/69	Ub357	91.80	0.05	brown secondary minerals removed	EH	0.51	0.12	5.57	0.16	2.29	7.27	2.18	0.74	0.05	0.13	n/a	19.06	0.19	0.07	0.97	0.04
28a/69	Ub358	91.85	0.05	brown, core mud and mould removed	DN	0.51	0.11	5.65	0.20	2.18	6.92	2.00	0.67	0.06	n/a	0.04	20.53	0.21	0.06	0.90	0.07
28a/69	Ub359	91.90	0.05	brown, secondary minerals removed	EH	0.51	0.10	5.33	n/a	1.79	7.20	2.28	0.62	n/a	n/a	0.03	19.40	0.28	0.05	0.98	0.06
28a/69	Ub360	91.95	0.05	lighter brown, core mud removed	EH	0.52	0.12	3.07	n/a	19.47	4.89	1.37	0.45	0.10	5.27	n/a	12.08	0.48	0.13	0.57	0.02

28a/69	Ub361	92.00	1.27	brown white clast, secondary minerals removed	EH	0.51	0.12	4.62	0.21	2.18	7.12	2.31	0.49	n/a	0.06	n/a	17.76	0.16	0.05	0.97	0.05
28b/69	Ub362	93.27	0.05	brown, mould removed, orange burrow present	DN	0.50	0.10	5.04	n/a	2.47	7.45	2.15	0.55	0.03	0.07	n/a	17.55	1.18	0.07	0.90	0.04
28b/69	Ub363	93.32	0.05	brown, secondary minerals removed	EH	0.49	0.11	6.01	n/a	3.02	7.65	2.34	0.67	0.06	0.09	0.02	19.30	0.33	0.06	0.97	0.05
28b/69	Ub364	93.37	0.05	brown, core mud removed	DN	0.50	0.10	5.66	n/a	2.11	7.91	2.36	0.57	0.04	0.05	0.02	19.27	0.41	0.06	1.02	0.06
28b/69	Ub365	93.42	0.05	brown, mould removed	EH	0.50	0.11	5.64	n/a	1.87	7.50	2.51	0.64	0.04	n/a	0.03	20.14	0.35	0.05	1.04	0.06
28b/69	Ub366	93.47	0.05	brown, no mud removed	EH	0.51	0.11	5.60	n/a	2.35	7.27	2.16	0.55	n/a	0.05	0.03	19.54	0.37	0.07	0.97	0.06
28b/69	Ub367	93.52	0.05	brown, mould removed	DN	0.50	0.10	5.60	0.24	2.58	7.36	2.31	0.59	0.03	0.08	0.03	18.64	0.24	0.07	1.07	0.05
28b/69	Ub368	93.57	0.05	brown, mould removed, small borrow (orange)	EH	0.51	0.09	5.68	n/a	2.05	7.26	2.34	0.56	0.03	0.07	0.04	19.22	0.35	0.05	1.02	0.05
28b/69	Ub369	93.62	0.05	brown, core mud removed	DN	0.51	0.09	6.08	n/a	2.67	7.35	2.31	0.68	0.06	0.06	0.03	20.77	0.34	0.07	0.96	0.05
28b/69	Ub370	93.67	0.03	brown, core mud removed	DN	0.51	0.11	4.83	n/a	2.14	6.95	2.30	0.57	n/a	0.06	0.03	17.64	0.22	0.06	0.94	0.04
29/69	Ub371	93.70	0.05	brown, core mud removed	UL	0.52	0.10	4.66	n/a	1.96	7.00	2.15	0.63	0.04	0.08	0.04	17.19	0.28	0.07	1.00	0.03
29/69	Ub372	93.75	0.05	brown, mould removed	DN	0.50	0.10	5.06	n/a	2.47	7.23	2.36	0.61	n/a	n/a	0.03	17.85	0.35	0.07	0.99	0.05
29/69	Ub373	93.80	0.05	brown, mould removed	DN	0.50	0.10	4.90	n/a	2.35	7.49	2.27	0.59	0.07	n/a	0.02	17.76	0.34	0.06	0.96	0.04
29/69	Ub374	93.85	0.05	brown core mud removed	DN	0.51	0.09	5.43	0.28	2.54	7.60	2.37	0.67	0.06	n/a	n/a	18.51	0.28	0.07	1.00	0.04
29/69	Ub375	93.90	0.05	brown, mold removed	DN	0.51	0.12	5.52	n/a	2.48	7.04	2.48	0.61	n/a	0.06	0.03	18.28	0.33	0.07	0.94	0.04
29/69	Ub376	93.95	0.05	brown	DN	0.52	0.12	4.84	0.17	2.29	7.20	2.20	0.58	0.07	0.08	0.02	16.27	0.29	0.07	0.96	0.04

29/69	Ub377	94.00	0.05	brown, core mud removed, hardened clay minerals brown-rest in colour?	DN	0.50	0.13	4.14	0.20	1.23	7.17	2.02	0.52	0.04	n/a	0.03	14.30	0.46	0.05	0.86	0.07
29/69	Ub378	94.05	0.05	brown, mould removed	DN	0.50	0.11	4.93	n/a	1.62	7.45	2.24	0.56	0.05	0.07	0.03	16.87	0.35	0.06	0.87	0.06
29/69	Ub379	94.10	0.05	brown, mould removed	DN	0.52	0.11	4.98	0.14	1.94	8.64	2.42	0.70	0.12	n/a	0.03	18.79	0.40	0.06	0.87	0.06
29/69	Ub380	94.15	0.05	brown, core mud removed	DN	0.50	0.11	5.00	n/a	1.98	7.50	2.27	0.53	0.10	n/a	0.03	18.33	0.26	0.05	0.96	0.05
29/69	Ub381	94.20	0.05	brown, secondary minerals removed	DN	0.50	0.09	4.99	n/a	1.47	7.48	2.43	0.55	n/a	n/a	0.03	17.76	0.28	0.06	0.95	0.05
29/69	Ub382	94.25	0.05	brown, mould removed	DN	0.50	0.11	4.84	0.09	1.85	7.58	2.13	0.57	0.07	n/a	n/a	17.86	0.34	0.06	1.07	0.05
29/69	Ub383	94.30	0.05	brown, core mud removed	DN	0.50	0.09	5.17	0.23	2.96	8.42	2.23	0.68	0.12	0.08	0.03	18.63	0.21	0.06	1.03	0.06
29/69	Ub384	94.35	0.05	brown, mould removed	DN	0.53	0.11	4.58	n/a	2.51	7.76	2.40	0.58	0.10	0.06	0.03	17.80	0.27	0.05	0.93	0.06
29/69	Ub385	94.40	0.05	brown	DN	0.49	0.11	5.69	n/a	1.84	7.39	2.25	0.65	0.05	n/a	n/a	20.10	0.34	0.05	1.14	0.07
29/69	Ub386	94.45	0.05	brown, mould removed	DN	0.52	0.15	5.19	n/a	2.04	7.39	2.15	0.63	0.07	n/a	0.03	17.63	0.43	0.06	1.06	0.06
29/69	Ub387	94.50	0.02	brown, core mud removed	UL/DN	0.52	0.10	5.00	n/a	3.00	7.42	2.29	0.62	0.05	n/a	0.04	17.12	0.29	0.08	1.00	0.03
30/69	Ub388	94.52	0.05	brown	DN	0.51	0.10	5.95	n/a	3.50	7.69	2.29	0.64	0.09	n/a	0.01	20.02	0.27	0.07	1.01	0.05
30/69	Ub389	94.57	0.05	brown core mud removed	DN	0.50	0.10	4.57	n/a	2.56	7.33	2.19	0.50	0.03	n/a	n/a	16.42	0.24	0.07	0.96	0.03
30/69	Ub390	94.62	0.05	brown, secondary minerals removed	DN	0.51	0.13	5.04	n/a	2.53	7.44	2.39	0.66	0.05	n/a	0.03	18.33	0.28	0.06	0.96	0.05
30/69	Ub391	94.67	0.05	brown, secondary minerals removed	DN	0.51	0.11	5.65	0.27	3.12	7.80	2.30	0.67	n/a	n/a	0.03	18.89	0.33	0.07	0.88	0.04
30/69	Ub392	94.72	0.05	brown, secondary minerals removed	DN	0.51	0.12	4.50	0.24	2.51	6.92	2.21	0.55	0.04	n/a	n/a	17.10	0.27	0.07	0.93	0.03
30/69	Ub393	94.77	0.05	brown, burrow	DN	0.50	0.11	5.41	n/a	3.40	7.84	2.37	0.72	0.04	0.07	n/a	18.60	0.82	0.07	0.96	0.04

30/69	Ub394	94.82	0.05	brown	DN	0.52	0.10	5.38	0.19	3.46	7.23	2.28	0.61	0.06	n/a	n/a	20.24	0.25	0.08	1.07	0.04
30/69	Ub395	94.87	0.05	brown	DN	0.52	0.09	5.87	n/a	3.69	7.44	2.31	0.68	0.04	0.12	0.01	20.23	0.25	0.07	1.03	0.07
30/69	Ub396	94.92	0.05	brown, core mud reomoved	DN	0.52	0.11	5.89	0.23	3.68	7.16	2.52	0.64	0.05	n/a	0.03	20.76	0.25	0.07	1.04	0.05
30/69	Ub397	94.97	0.05	brown	DN	0.50	0.10	5.51	n/a	3.97	7.51	2.36	0.71	0.05	n/a	0.04	20.06	0.21	0.07	0.95	0.06
30/69	Ub398	95.02	0.05	brown, core mud removed	DN	0.52	0.11	5.78	0.22	4.09	7.41	2.35	0.70	0.06	0.07	0.01	21.20	0.15	0.08	1.03	0.05
30/69	Ub399	95.07	0.05	brown	DN	0.51	0.12	5.04	0.24	3.27	7.07	2.29	0.61	n/a	n/a	0.03	18.21	0.27	0.08	1.04	0.04
30/69	Ub400	95.12	0.05	brown, core mud removed	DN	0.50	0.13	5.92	n/a	3.73	7.09	2.37	0.70	0.05	n/a	n/a	20.24	0.16	0.08	1.01	0.05
30/69	Ub401	95.17	0.05	brown, core mud removed	DN	0.50	0.12	5.18	n/a	4.63	6.66	2.07	0.66	n/a	n/a	n/a	17.81	0.36	0.09	1.13	0.01
30/69	Ub402	95.22	0.05	brown some black bits in matrix	UL/DN	0.52	0.12	5.51	n/a	3.76	7.01	2.34	0.63	0.04	n/a	0.04	18.73	0.24	0.08	0.92	0.05
30/69	Ub403	95.27	0.03	brown, core mud removed	UL/DN	0.51	0.11	5.15	n/a	3.62	6.74	2.31	0.58	0.06	n/a	0.03	18.56	0.19	0.07	0.93	0.06
30/69	Ub404	95.30	0.02	brown, burrow, core mud removed	UL/DN	0.51	0.11	4.79	n/a	2.95	6.69	1.97	0.62	0.05	n/a	n/a	18.51	0.29	0.08	0.99	0.06
31/69	Ub405	95.32	0.05	brown no rind removed	BGS	0.52	0.12	5.60	0.28	3.26	6.83	2.22	0.51	n/a	n/a	0.03	19.48	0.35	0.06	0.98	0.06
31/69	Ub406	95.37	0.05	brown no rind removed	BGS	0.50	0.12	5.06	n/a	3.32	7.00	1.71	0.63	0.06	n/a	n/a	18.35	0.51	0.07	1.09	0.05
31/69	Ub407	95.42	0.05	brown no rind removed	BGS	0.51	0.10	4.83	0.12	2.15	7.35	2.28	0.57	n/a	n/a	0.03	18.84	0.39	0.06	1.05	0.07
31/69	Ub408	95.47	0.05	brown no rind removed	BGS	0.51	0.11	4.93	n/a	2.59	6.58	2.03	0.56	n/a	n/a	n/a	18.09	0.24	0.06	1.02	0.07
31/69	Ub409	95.52	0.05	brown no rind removed	BGS	n/a	n/a	n/a	n/a	n/a	n/a	n/a	n/a	n/a	n/a	n/a	n/a	n/a	n/a	n/a	n/a
31/69	Ub410	95.57	0.05	brown no rind removed	BGS	0.50	0.12	4.92	n/a	2.57	6.76	2.17	0.53	0.03	0.05	n/a	17.50	0.31	0.08	0.97	0.04
31/69	Ub411	95.62	0.05	brown no rind removed	BGS	0.51	0.10	5.03	n/a	3.50	7.28	2.21	0.60	n/a	n/a	0.03	18.89	0.38	0.06	0.90	0.06
31/69	Ub412	95.67	0.05	brown no rind removed	BGS	0.52	0.11	5.54	0.18	3.23	7.08	2.10	0.63	0.05	0.08	0.03	19.29	0.36	0.07	1.03	0.06
31/69	Ub413	95.72	0.05	brown no rind removed	BGS	n/a	n/a	n/a	n/a	n/a	n/a	n/a	n/a	n/a	n/a	n/a	n/a	n/a	n/a	n/a	n/a

31/69	Ub414	95.77	0.05	brown no rind removed	BGS	0.52	0.12	5.07	n/a	2.48	7.06	2.19	0.58	0.04	n/a	0.02	18.44	0.28	0.07	0.90	0.06
31/69	Ub415	95.82	0.05	brown no rind removed	BGS	0.50	0.13	4.93	n/a	2.18	6.61	1.77	0.54	0.04	n/a	0.03	18.37	0.22	0.07	0.86	0.05
31/69	Ub416	95.87	0.05	brown no rind removed	BGS	0.51	0.10	5.39	n/a	3.62	7.24	2.11	0.66	0.05	0.08	n/a	18.70	0.48	0.07	1.04	0.06
31/69	Ub417	95.92	0.05	brown no rind removed	BGS	0.50	0.13	4.53	n/a	3.43	6.88	2.03	0.53	0.04	n/a	0.03	17.46	0.19	0.07	1.06	0.05
31/69	Ub418	95.97	0.05	grey no rind removed	BGS	0.50	0.11	5.50	n/a	3.04	7.09	2.09	0.66	0.04	0.05	0.02	19.92	0.45	0.07	1.02	0.06
31/69	Ub419	96.02	0.05	brown no rind removed	BGS	0.50	0.09	6.20	n/a	3.54	7.87	2.34	0.67	0.05	n/a	0.01	20.85	0.17	0.07	1.07	0.06
31/69	Ub420	96.07	0.05	brown no rind removed	BGS	0.50	0.10	5.77	n/a	2.45	7.62	2.33	0.67	0.03	0.05	0.03	20.79	0.70	0.05	1.08	0.07
31/69	Ub421	96.12	0.02	brown no rind removed	BGS	n/a	n/a	n/a	n/a	n/a	n/a	n/a	n/a	n/a	n/a	n/a	n/a	n/a	n/a	n/a	n/a
32/69	Ub422	96.14	0.05	brown no rind removed	BGS	0.52	0.12	4.96	n/a	4.41	6.87	1.94	0.68	0.04	n/a	n/a	18.03	0.63	0.11	0.91	0.03
32/69	Ub423	96.19	0.05	brown no rind removed	BGS	0.51	0.14	5.38	n/a	5.27	7.00	2.13	0.66	0.05	0.08	0.01	19.85	0.47	0.07	0.99	0.06
32/69	Ub424	96.24	0.05	brown no rind removed	BGS	0.52	0.11	5.02	n/a	4.64	7.34	2.26	0.64	0.05	n/a	0.03	18.95	0.24	0.08	0.87	0.05
32/69	Ub425	96.29	0.05	brown no rind removed	BGS	0.50	0.10	5.48	0.27	5.00	6.90	2.17	0.70	0.07	0.07	n/a	19.27	0.62	0.09	1.00	0.04
32/69	Ub426	96.34	0.05	brown no rind removed	BGS	n/a	n/a	n/a	n/a	n/a	n/a	n/a	n/a	n/a	n/a	n/a	n/a	n/a	n/a	n/a	n/a
32/69	Ub427	96.39	0.05	brown no rind removed	BGS	0.50	0.10	5.46	n/a	4.57	7.01	2.13	0.69	0.06	n/a	0.03	19.40	0.21	0.08	1.09	0.04
32/69	Ub428	96.44	0.05	brown rind removed	BGS	n/a	n/a	n/a	n/a	n/a	n/a	n/a	n/a	n/a	n/a	n/a	n/a	n/a	n/a	n/a	n/a
32/69	Ub429	96.49	0.05	brown no rind removed	BGS	0.50	0.11	4.84	n/a	5.65	6.99	2.02	0.59	0.07	n/a	n/a	18.65	0.22	0.10	0.93	0.04
32/69	Ub430	96.54	0.05	brown no rind removed	BGS	0.50	0.10	4.92	0.22	5.60	7.05	2.14	0.62	0.07	n/a	n/a	18.04	0.18	0.10	1.05	0.05
32/69	Ub431	96.59	0.05	brown no rind removed	BGS	0.50	0.10	4.93	0.22	5.70	7.15	2.07	0.68	0.07	0.20	n/a	19.30	0.23	0.10	1.07	0.04
32/69	Ub432	96.64	0.05	brown no rind removed	BGS	0.52	0.11	2.88	n/a	24.85	4.73	1.22	0.42	0.22	6.32	n/a	11.50	0.37	0.16	0.58	0.02
32/69	Ub433	96.69	0.05	grey no rind removed	BGS	n/a	n/a	n/a	n/a	n/a	n/a	n/a	n/a	n/a	n/a	n/a	n/a	n/a	n/a	n/a	n/a

32/69	Ub434	96.74	0.05	brown no rind removed	BGS	0.50	0.10	5.68	n/a	4.49	7.19	2.10	0.72	0.08	n/a	n/a	20.75	0.19	0.08	1.05	0.05
32/69	Ub435	96.79	0.05	brown no rind removed	BGS	0.52	0.10	5.25	n/a	4.79	6.82	2.02	0.57	0.05	n/a	n/a	20.48	0.23	0.08	1.05	0.06
32/69	Ub436	96.84	0.05	brown no rind removed	BGS	n/a	n/a	n/a	n/a	n/a	n/a	n/a	n/a	n/a	n/a	n/a	n/a	n/a	n/a	n/a	n/a
32/69	Ub437	96.89	0.05	brown no rind removed	BGS	0.50	0.10	6.34	0.31	3.87	7.80	2.49	0.77	0.06	n/a	0.01	20.89	0.27	0.07	0.97	0.05
32/69	Ub438	96.94	0.05	brown no rind removed	BGS	n/a	n/a	n/a	n/a	n/a	n/a	n/a	n/a	n/a	n/a	n/a	n/a	n/a	n/a	n/a	n/a
32/69	Ub439	96.99	0.01	brown no rind removed	BGS	0.51	0.10	6.03	0.26	2.84	7.45	2.31	0.73	0.06	n/a	0.01	21.48	0.26	0.07	1.05	0.04
33/69	Ub440	97.00	0.04	brown no rind removed	BGS	0.51	0.10	5.61	n/a	3.52	6.82	2.22	0.67	n/a	n/a	0.03	17.98	0.30	0.08	0.99	0.03
33/69	Ub441	97.04	0.05	brown no rind removed	BGS	0.51	0.11	5.48	n/a	3.61	7.49	2.13	0.72	0.06	n/a	0.03	19.82	0.27	0.06	0.97	0.07
33/69	Ub442	97.09	0.05	brown no rind removed	BGS	0.50	0.10	5.76	0.21	3.29	7.36	2.39	0.64	0.06	n/a	0.03	19.35	0.45	0.07	0.99	0.05
33/69	Ub443	97.14	0.05	brown no rind removed	BGS	0.50	0.11	5.88	0.23	3.04	7.59	2.25	0.67	0.06	0.09	0.03	19.51	0.22	0.06	1.03	0.06
33/69	Ub444	97.19	0.05	brown no rind removed	BGS	0.50	0.10	5.38	n/a	3.26	6.88	2.10	0.57	0.05	n/a	n/a	18.39	0.50	0.07	1.03	0.05
33/69	Ub445	97.24	0.05	brown no rind removed	BGS	n/a	n/a	n/a	n/a	n/a	n/a	n/a	n/a	n/a	n/a	n/a	n/a	n/a	n/a	n/a	n/a
33/69	Ub446	97.29	0.05	brown no rind removed	BGS	0.51	0.10	4.94	n/a	3.05	7.81	1.88	0.60	0.05	n/a	0.04	18.39	0.71	0.06	0.90	0.06
33/69	Ub447	97.34	0.05	brown no rind removed	BGS	0.50	0.10	5.24	n/a	2.88	6.74	2.34	0.54	0.07	0.10	0.03	17.76	0.16	0.07	0.88	0.04
33/69	Ub448	97.39	0.05	brown no rind removed	BGS	0.51	0.09	5.35	0.23	3.21	7.78	2.47	0.59	0.05	n/a	0.03	19.96	0.40	0.07	0.96	0.03
33/69	Ub449	97.44	0.05	brown no rind removed	BGS	0.52	0.10	5.66	n/a	3.97	7.41	2.33	0.62	0.06	n/a	0.03	19.57	0.18	0.08	0.91	0.05
33/69	Ub450	97.49	0.05	brown no rind removed	BGS	0.51	0.11	5.89	n/a	3.18	7.48	2.17	0.70	0.06	0.10	0.03	20.57	0.19	0.07	0.90	0.05
33/69	Ub451	97.54	0.05	brown no rind removed	BGS	0.49	0.13	5.67	n/a	3.70	7.41	2.40	0.66	0.07	0.06	0.03	19.71	0.19	0.08	1.00	0.03
33/69	Ub452	97.59	0.05	brown no rind removed	BGS	0.49	0.11	5.19	0.16	4.15	7.07	2.05	0.64	0.04	n/a	n/a	17.50	0.28	0.09	0.93	0.03

33/69	Ub453	97.64	0.05	brown no rind removed	BGS	0.51	0.11	5.52	0.19	3.19	7.08	2.34	0.57	n/a	0.05	n/a	18.92	0.23	0.07	0.96	0.04
33/69	Ub454	97.69	0.05	brown no rind removed	BGS	0.51	0.11	5.85	0.23	3.46	7.57	2.40	0.75	0.07	n/a	0.01	19.14	0.25	0.09	1.02	0.04
33/69	Ub455	97.74	0.03	brown no rind removed	BGS	0.51	0.11	5.37	n/a	3.27	7.33	2.32	0.54	n/a	0.05	0.03	18.17	0.30	0.08	0.93	0.05
34/69	Ub456	97.77	0.05	brown no rind removed	BGS	0.50	0.10	5.69	0.30	3.00	7.53	2.44	0.73	0.03	0.09	n/a	20.60	0.22	0.07	0.10	0.05
34/69	Ub457	97.82	0.05	brown no rind removed	BGS	0.52	0.09	6.29	n/a	2.96	7.89	2.51	0.75	0.05	n/a	0.01	21.27	0.27	0.08	1.18	0.04
34/69	Ub458	97.87	0.05	brown no rind removed	BGS	0.53	0.11	5.32	n/a	3.14	7.25	2.24	0.62	0.06	n/a	0.03	17.52	0.30	0.08	1.08	0.04
34/69	Ub459	97.92	0.05	brown no rind removed	BGS	0.53	0.11	5.52	0.27	3.01	7.68	2.43	0.69	0.07	n/a	0.01	19.50	0.24	0.07	1.07	0.05
34/69	Ub460	97.97	3.66	brown no rind removed	BGS	0.51	0.10	5.43	n/a	3.01	7.80	2.35	0.69	0.08	0.05	0.03	18.61	0.28	0.07	1.05	0.03
34/69	Ub461	101.63	0.04	brown no rind removed	BGS	0.52	0.10	5.13	n/a	4.60	8.42	2.40	0.72	0.08	0.07	0.01	19.63	0.39	0.03	1.09	0.07
34/69	Ub462	101.67	0.06	brown no rind removed	BGS	n/a	n/a	n/a	n/a	n/a	n/a	n/a	n/a	n/a	n/a	n/a	n/a	n/a	n/a	n/a	n/a
34/69	Ub463	101.73	0.05	brown no rind removed	BGS	0.50	0.10	5.70	n/a	5.04	7.26	1.92	0.70	n/a	n/a	0.01	19.84	0.18	0.09	0.93	0.04
34/69	Ub464	101.78	0.05	brown no rind removed	BGS	0.50	0.10	5.28	n/a	4.09	7.02	2.31	0.62	0.07	0.05	0.03	18.85	0.21	0.09	0.91	0.04
34/69	Ub465	101.83	0.05	brown no rind removed	BGS	0.52	0.12	5.54	n/a	4.34	7.01	2.32	0.58	0.05	0.08	n/a	18.56	0.15	0.09	0.88	0.04
34/69	Ub466	101.88	0.05	brown no rind removed	BGS	0.51	0.12	4.89	n/a	3.84	6.98	2.20	0.56	n/a	0.06	n/a	17.28	0.30	0.08	0.97	0.06
34/69	Ub467	101.93	0.05	brown no rind removed	BGS	0.51	0.10	5.49	n/a	3.79	7.03	2.20	0.70	0.06	n/a	0.03	18.42	0.29	0.08	1.00	0.04
34/69	Ub468	101.98	3.25	brown no rind removed	BGS	0.51	0.10	5.05	n/a	4.15	7.04	2.27	0.63	0.04	n/a	n/a	18.77	0.42	0.08	0.87	0.06
35/69	Ub469	105.23	0.07	brown no rind removed	BGS	0.51	0.12	4.42	n/a	3.55	6.73	2.24	0.60	0.05	n/a	n/a	17.94	0.38	0.08	1.03	0.05
35/69	Ub470	105.30	0.11	brown no rind removed	BGS	0.52	0.10	5.79	n/a	3.40	7.41	2.63	0.69	0.04	n/a	0.01	20.63	0.39	0.06	1.09	0.07
35/69	Ub471	105.41	0.15	brown no rind removed	BGS	0.50	0.10	6.43	n/a	3.32	7.19	2.18	0.63	0.05	n/a	0.02	20.26	0.43	0.06	1.03	0.06
35/69	Ub472	105.56	0.05	brown rind	BGS	0.50	0.11	6.06	n/a	2.96	7.04	2.29	0.68	0.07	n/a	n/a	19.93	0.33	0.07	1.07	0.05

				removed																	
35/69	Ub473	105.61	0.05	brown no rind removed	BGS	0.52	0.10	6.17	0.25	3.12	7.31	2.39	0.58	0.04	n/a	0.02	19.99	0.59	0.06	1.04	0.05
35/69	Ub474	105.66	0.03	brown no rind removed	BGS	0.52	0.10	5.50	n/a	2.54	7.77	2.54	0.69	0.03	n/a	0.01	20.87	0.57	0.06	1.04	0.06
36/69	Ub475	105.69	0.1	brown no rind removed	BGS	0.51	0.09	5.89	n/a	2.83	7.56	2.52	0.77	0.05	n/a	n/a	20.90	0.44	0.06	1.12	0.07
36/69	Ub476	105.79	0.05	brown no rind removed	BGS	0.50	0.10	5.61	n/a	2.71	6.68	2.24	0.64	0.05	0.07	0.03	19.24	0.39	0.07	1.02	0.03
36/69	Ub477	105.84	0.05	brown no rind removed	BGS	0.49	0.11	5.50	0.20	2.55	7.00	2.32	0.64	0.05	n/a	0.03	18.83	0.23	0.07	1.12	0.05
36/69	Ub478	105.89	0.05	brown no rind removed	BGS	0.51	0.10	6.19	0.16	3.01	7.21	2.38	0.75	0.04	0.07	0.03	20.45	0.34	0.07	1.01	0.06
36/69	Ub479	105.94	0.05	brown no rind removed	BGS	0.53	0.12	5.23	n/a	1.87	6.68	2.13	0.63	n/a	n/a	0.03	19.40	0.33	0.06	1.10	0.05
36/69	Ub480	105.99	0.05	brown no rind removed	BGS	0.52	0.10	5.26	n/a	2.44	6.75	2.23	0.62	0.04	0.06	0.03	17.75	0.23	0.07	1.12	0.05
36/69	Ub481	106.04	0.05	brown no rind removed	BGS	0.51	0.12	6.10	n/a	2.34	7.52	2.08	0.62	0.04	n/a	0.04	20.03	0.49	0.06	1.01	0.05
36/69	Ub482	106.09	0.05	brown no rind removed	BGS	n/a	n/a	n/a	n/a	n/a	n/a	n/a	n/a	n/a	n/a	n/a	n/a	n/a	n/a	n/a	n/a
36/69	Ub483	106.14	0.05	brown no rind removed	BGS	0.52	0.10	5.73	n/a	2.50	7.31	2.33	0.69	0.03	n/a	0.03	19.65	0.37	0.06	0.88	0.06
36/69	Ub484	106.19	0.05	brown no rind removed	BGS	0.50	0.10	6.08	0.15	2.68	7.56	2.12	0.57	0.03	n/a	0.01	20.29	0.77	0.06	1.00	0.06
36/69	Ub485	106.24	0.05	brown no rind removed	BGS	0.51	0.10	5.74	0.26	2.30	7.34	2.40	0.69	0.05	n/a	n/a	20.00	0.48	0.05	1.07	0.07
36/69	Ub486	106.29	0.05	brown no rind removed	BGS	0.51	0.10	5.56	n/a	2.23	7.43	2.31	0.66	0.04	n/a	0.02	19.21	0.37	0.03	1.00	0.07
36/69	Ub487	106.34	0.05	brown no rind removed	BGS	0.49	0.12	5.46	n/a	2.07	6.74	2.21	0.62	0.03	n/a	0.03	19.67	0.26	0.05	1.04	0.06
36/69	Ub488	106.39	0.05	brown no rind removed	BGS	0.50	0.09	5.90	n/a	3.04	7.57	2.43	0.70	n/a	n/a	0.01	20.77	0.50	0.07	1.12	0.04
36/69	Ub489	106.44	0.05	brown no rind removed	BGS	0.52	0.10	5.54	n/a	2.58	7.84	2.46	0.73	0.04	n/a	0.02	19.88	0.66	0.05	1.01	0.06
36/69	Ub490	106.49	0.05	brown no rind removed	BGS	0.51	0.10	6.32	n/a	3.02	7.37	2.51	0.80	n/a	0.05	0.01	21.28	0.38	0.07	0.96	0.06
37/69	Ub491	106.54	0.05	brown no rind removed	BGS	0.53	0.13	5.57	n/a	5.63	7.53	2.16	0.58	0.03	n/a	n/a	18.60	0.46	0.10	0.85	0.03

37/69	Ub492	106.59	0.05	brown no rind removed	BGS	0.50	0.11	5.23	0.13	5.67	7.12	2.11	0.69	0.03	n/a	n/a	18.91	0.28	0.10	0.91	0.03
37/69	Ub493	106.64	0.05	brown no rind removed	BGS	0.51	0.10	4.82	n/a	5.84	8.12	2.02	0.60	0.05	n/a	0.01	17.76	1.35	0.09	0.84	0.04
37/69	Ub494	106.69	0.05	brown no rind removed	BGS	0.49	0.09	5.65	n/a	7.20	6.75	2.35	0.65	0.04	n/a	n/a	18.81	0.19	0.13	0.95	0.01
37/69	Ub495	106.74	0.05	brown no rind removed	BGS	0.50	0.09	5.01	0.20	5.84	6.95	2.21	0.69	0.04	n/a	n/a	17.21	0.20	0.10	1.01	0.03
37/69	Ub496	106.79	0.05	brown no rind removed	BGS	0.50	0.10	5.87	0.23	3.20	7.34	2.36	0.65	0.07	n/a	0.03	19.38	0.21	0.08	0.98	0.03
37/69	Ub497	106.84	0.05	brown no rind removed	BGS	0.52	0.09	6.20	n/a	3.26	7.80	2.51	0.73	0.07	0.06	0.01	19.94	0.25	0.07	1.01	0.05
37/69	Ub498	106.89	0.05	brown no rind removed	BGS	0.49	0.10	5.29	n/a	3.23	7.56	2.45	0.68	0.05	n/a	0.04	17.61	0.26	0.08	1.02	0.04
37/69	Ub499	106.94	0.05	brown no rind removed	BGS	0.52	0.11	4.91	0.21	4.50	6.92	2.28	0.59	0.05	n/a	n/a	17.86	0.27	0.10	1.03	0.03
37/69	Ub500	106.99	0.05	brown no rind removed	BGS	0.50	0.10	6.25	0.28	6.27	6.92	2.36	0.68	0.06	n/a	n/a	20.18	0.42	0.12	0.91	0.02
37/69	Ub501	107.04	0.05	brown no rind removed	BGS	0.52	0.11	5.52	n/a	5.86	7.01	2.24	0.74	0.05	n/a	n/a	19.26	0.26	0.10	0.94	0.03
37/69	Ub502	107.09	0.05	brown no rind removed	BGS	0.50	0.10	5.60	n/a	5.48	7.03	2.37	0.72	n/a	n/a	n/a	20.72	0.38	0.09	1.01	0.04
37/69	Ub503	107.14	0.05	brown no rind removed	BGS	0.50	0.11	4.61	n/a	6.53	7.15	2.23	0.65	0.11	n/a	n/a	17.20	0.13	0.11	0.99	0.02
37/69	Ub504	107.19	0.05	brown no rind removed	BGS	0.50	0.11	4.27	0.22	6.04	6.97	2.12	0.62	0.10	n/a	n/a	15.60	0.19	0.11	0.89	0.02
37/69	Ub505	107.24	0.05	brown no rind removed	BGS	0.49	0.10	5.57	0.28	6.50	7.84	2.17	0.83	0.11	n/a	0.01	20.18	0.24	0.05	0.92	0.06
37/69	Ub506	107.29	0.05	brown no rind removed	BGS	0.50	0.11	5.10	n/a	5.82	8.10	2.30	0.61	0.20	0.09	0.01	17.44	0.12	0.09	0.80	0.05
37/69	Ub507	107.34	0.05	brown no rind removed	BGS	0.51	0.11	5.75	n/a	6.63	8.63	2.18	0.76	0.23	0.18	0.02	19.91	0.20	0.05	0.87	0.06
37/69	Ub508	107.39	0.04	brown no rind removed	BGS	0.50	0.11	5.97	0.33	6.09	8.51	2.25	0.73	0.20	n/a	n/a	20.41	0.22	0.05	0.94	0.05
38/69	Ub509	107.43	0.05	brown no rind removed	BGS	0.50	0.10	5.24	n/a	8.39	13.44	2.03	0.74	0.73	0.41	0.01	18.61	0.34	0.05	0.92	0.02
38/69	Ub510	107.48	0.05	brown no rind removed	BGS	0.50	0.11	5.41	n/a	6.84	10.96	2.06	0.69	0.44	0.13	0.01	17.75	0.38	0.05	0.85	0.04

38/69	Ub511	107.53	0.05	brown no rind removed	BGS	0.50	0.14	5.94	n/a	6.44	24.66	1.84	1.04	1.75	0.19	0.01	17.67	0.24	0.03	0.58	0.02
38/69	Ub512	107.58	0.05	brown no rind removed	BGS	0.51	0.09	5.58	n/a	6.86	8.58	2.51	0.64	0.15	n/a	0.01	19.13	0.89	0.05	0.93	0.06
38/69	Ub513	107.63	0.05	brown no rind removed	BGS	0.50	0.10	5.88	n/a	5.22	7.90	2.36	0.73	0.14	0.08	n/a	19.30	0.46	0.09	0.89	0.03
38/69	Ub514	107.68	0.05	brown no rind removed	BGS	0.50	0.10	5.56	0.25	5.48	8.30	2.40	0.80	0.16	n/a	0.01	20.09	0.23	0.05	0.99	0.06
38/69	Ub515	107.73	0.05	brown no rind removed	BGS	0.52	0.10	6.05	n/a	5.32	7.51	2.19	0.76	0.08	n/a	0.01	20.83	0.22	0.09	0.87	0.03
38/69	Ub516	107.78	0.05	brown no rind removed	BGS	0.52	0.09	5.72	0.19	4.94	7.48	2.47	0.72	0.07	n/a	n/a	18.41	0.57	0.10	0.97	0.02
38/69	Ub517	107.83	0.05	brown no rind removed	BGS	0.51	0.10	5.32	0.19	5.25	7.17	2.23	0.70	0.06	n/a	n/a	18.31	0.28	0.09	0.89	0.03
38/69	Ub518	107.88	0.05	brown no rind removed	BGS	0.50	0.10	5.79	n/a	5.51	6.97	2.25	0.71	0.06	0.07	n/a	19.00	0.33	0.10	0.90	0.03
38/69	Ub519	107.93	0.05	brown no rind removed	BGS	0.52	0.10	5.57	n/a	4.46	6.75	2.23	0.69	0.06	n/a	n/a	18.94	0.35	0.10	1.03	0.02
38/69	Ub520	107.98	0.05	brown no rind removed	BGS	0.52	0.10	5.69	n/a	4.23	7.02	2.32	0.64	0.05	n/a	n/a	19.50	0.28	0.09	0.93	0.03
38/69	Ub521	108.03	0.05	brown no rind removed	BGS	0.52	0.10	6.02	n/a	3.93	7.11	2.09	0.74	0.03	n/a	0.04	20.30	0.45	0.08	1.01	0.05
38/69	Ub522	108.08	0.05	brown no rind removed	BGS	0.49	0.09	5.88	0.16	3.76	7.36	2.41	0.63	0.03	n/a	n/a	18.59	0.47	0.07	1.06	0.04
38/69	Ub523	108.13	0.05	brown no rind removed	BGS	0.50	0.10	6.10	n/a	4.13	7.22	2.28	0.69	0.07	0.10	0.03	19.96	0.47	0.09	1.04	0.04
38/69	Ub524	108.18	0.05	brown no rind removed	BGS	0.52	0.10	6.12	n/a	3.35	7.17	2.44	0.79	0.06	n/a	0.03	20.30	0.47	0.07	1.04	0.05
38/69	Ub525	108.23	0.05	brown no rind removed	BGS	0.50	0.10	6.46	0.21	3.46	7.34	2.50	0.71	n/a	n/a	n/a	20.63	0.33	0.08	0.90	0.05
38/69	Ub526	108.28	0.07	brown no rind removed	BGS	0.52	0.09	5.46	n/a	3.23	7.21	2.26	0.62	0.05	n/a	0.04	19.12	0.59	0.07	0.98	0.05
39/69	Ub527	108.35	0.05	brown no rind removed	BGS	0.52	0.10	5.47	n/a	2.97	6.94	2.38	0.72	0.04	n/a	0.03	19.17	0.36	0.08	0.93	0.04
39/69	Ub528	108.40	0.05	brown no rind removed	BGS	0.51	0.10	5.92	n/a	2.57	7.12	2.36	0.59	n/a	n/a	0.03	19.02	0.34	0.07	0.99	0.04
39/69	Ub529	108.45	0.05	brown no rind removed	BGS	0.51	0.10	5.87	n/a	3.24	6.90	2.42	0.56	n/a	n/a	n/a	19.01	0.29	0.09	0.98	0.03

39/69	Ub530	108.50	0.05	brown no rind removed	BGS	0.51	0.10	6.65	n/a	2.76	7.69	2.63	0.79	n/a	n/a	0.01	21.57	0.41	0.07	0.97	0.05
39/69	Ub531	108.55	0.05	brown no rind removed	BGS	0.50	0.10	5.91	0.24	2.84	7.21	2.44	0.67	n/a	n/a	0.04	19.67	0.36	0.08	1.08	0.04
39/69	Ub532	108.60	0.05	brown no rind removed	BGS	0.52	0.10	6.32	n/a	2.72	7.16	2.65	0.67	n/a	n/a	0.03	20.57	0.32	0.07	1.05	0.06
39/69	Ub533	108.65	0.05	brown no rind removed	BGS	0.51	0.10	5.65	0.12	3.95	7.19	2.28	0.70	0.03	n/a	0.03	19.48	0.49	0.08	0.96	0.04
39/69	Ub534	108.70	0.05	brown no rind removed	BGS	0.50	0.10	5.98	n/a	3.10	7.20	2.16	0.69	0.03	n/a	0.04	20.39	0.38	0.08	1.02	0.03
39/69	Ub535	108.75	0.05	brown no rind removed	BGS	0.50	0.11	5.87	0.09	2.83	6.85	2.43	0.61	n/a	n/a	0.03	19.93	0.22	0.07	1.08	0.04
39/69	Ub536	108.80	0.05	brown no rind removed	BGS	0.51	0.10	5.40	n/a	2.39	7.00	2.28	0.56	n/a	n/a	0.03	18.04	0.48	0.06	1.07	0.05
39/69	Ub537	108.85	0.05	brown no rind removed	BGS	0.50	0.12	6.12	n/a	2.81	7.12	2.32	0.68	n/a	n/a	0.03	20.43	0.39	0.07	1.07	0.04
39/69	Ub538	108.90	0.05	brown no rind removed	BGS	0.51	0.11	5.36	0.27	3.55	6.69	2.28	0.60	n/a	0.07	0.02	18.24	0.28	0.09	0.97	0.03
39/69	Ub539	108.95	0.05	brown no rind removed	BGS	0.51	0.10	5.08	0.17	2.73	7.17	2.43	0.59	0.03	n/a	n/a	18.79	0.40	0.07	0.90	0.03
39/69	Ub540	109.00	0.05	brown no rind removed	BGS	0.51	0.10	5.93	0.17	2.54	7.42	2.54	0.70	n/a	n/a	0.04	19.02	0.44	0.06	1.04	0.05
39/69	Ub541	109.05	0.05	brown no rind removed	BGS	0.50	0.12	4.96	n/a	2.34	6.60	2.04	0.51	n/a	n/a	n/a	16.19	0.30	0.07	0.91	0.04
39/69	Ub542	109.10	0.03	brown no rind removed	BGS	0.51	0.12	5.58	n/a	2.96	7.09	2.14	0.56	0.04	n/a	0.03	18.09	0.55	0.07	1.06	0.03
40/69	Ub543	109.13	0.05	brown no rind removed	BGS	0.52	0.10	5.60	n/a	3.27	7.22	2.53	0.73	0.04	n/a	n/a	19.01	0.41	0.09	0.95	0.04
40/69	Ub544	109.18	0.05	brown no rind removed	BGS	0.50	0.10	6.05	0.30	2.71	7.42	2.59	0.70	n/a	n/a	0.03	20.15	0.48	0.08	1.08	0.04
40/69	Ub545	109.23	0.05	brown no rind removed	BGS	0.51	0.17	4.10	0.15	1.96	6.16	2.02	0.45	0.03	n/a	n/a	14.12	0.22	0.06	0.98	0.06
40/69	Ub546	109.28	0.05	brown no rind removed	BGS	0.50	0.11	5.54	n/a	2.84	6.83	2.31	0.57	0.04	0.07	0.03	18.45	0.32	0.07	1.01	0.05
40/69	Ub547	109.33	0.05			0.51	0.10	5.80	n/a	2.69	7.69	2.44	0.78	n/a	0.09	0.02	20.90	0.27	0.06	0.97	0.05
40/69	Ub548	109.38	0.05	brown no rind removed	BGS	0.50	0.13	4.53	n/a	5.19	6.25	2.14	0.56	n/a	n/a	n/a	15.47	0.29	0.11	0.82	0.02
40/69	Ub549	109.43	0.05	brown no rind removed	BGS	0.52	0.11	4.89	0.29	4.77	6.76	2.01	0.60	0.04	n/a	n/a	17.93	0.26	0.09	1.02	0.04

40/69	Ub550	109.48	0.05	brown no rind removed	BGS	0.52	0.10	5.16	0.23	5.12	7.04	2.19	0.65	0.04	0.06	n/a	19.01	0.33	0.08	0.93	0.04
40/69	Ub551	109.53	0.05	brown no rind removed	BGS	0.52	0.11	5.27	n/a	4.67	7.05	2.47	0.66	0.03	n/a	n/a	21.21	0.24	0.09	0.97	0.05
40/69	Ub552	109.58	0.05	brown no rind removed	BGS	0.50	0.11	4.88	n/a	5.66	6.87	1.89	0.58	0.05	0.08	n/a	18.23	0.32	0.11	0.99	0.03
40/69	Ub553	109.63	0.05	brown no rind removed	BGS	0.51	0.10	5.24	n/a	4.60	6.49	2.14	0.63	0.03	0.06	n/a	19.79	0.32	0.09	0.97	0.04
40/69	Ub554	109.68	0.05	brown no rind removed	BGS	0.50	0.10	5.11	0.21	5.97	7.89	2.26	0.63	0.08	n/a	n/a	19.53	0.28	0.11	0.95	0.02
40/69	Ub555	109.73	0.05	brown no rind removed	BGS	0.50	0.10	4.98	0.26	8.49	7.18	2.10	0.68	n/a	0.89	n/a	19.44	0.20	0.06	0.89	0.06
40/69	Ub556	109.78	0.05	brown no rind removed	BGS	0.50	0.10	4.90	n/a	5.34	7.27	2.13	0.62	0.03	0.06	n/a	18.75	0.26	0.09	1.10	0.04
40/69	Ub557	109.83	0.05	brown no rind removed	BGS	0.51	0.10	5.04	0.16	5.49	6.75	2.36	0.68	n/a	0.06	n/a	19.58	0.29	0.10	0.96	0.03
40/69	Ub558	109.88	0.05	brown no rind removed	BGS	0.52	0.10	5.22	0.26	4.50	6.95	1.82	0.61	n/a	n/a	n/a	18.51	0.33	0.07	0.89	0.05
40/69	Ub559	109.93	0.05	brown no rind removed	BGS	0.50	0.10	5.85	n/a	3.43	7.56	2.19	0.66	n/a	0.11	0.01	21.74	0.30	0.07	0.96	0.04
40/69	Ub560	109.98	0.02	brown no rind removed	BGS	0.51	0.11	5.08	n/a	3.39	7.98	2.28	0.64	n/a	n/a	0.03	19.42	0.42	0.07	0.80	0.04
40/69	Ub561	110.00	0.14	brown no rind removed	BGS	0.49	0.10	4.99	0.20	4.38	6.78	2.10	0.59	n/a	n/a	0.03	18.34	0.24	0.08	0.91	0.05
41/69	Ub562	110.14	0.05	brown no rind removed	BGS	0.50	0.11	5.92	n/a	3.56	7.15	2.40	0.72	0.05	n/a	0.03	20.60	0.53	0.07	0.93	0.04
41/69	Ub563	110.19	0.05	brown no rind removed	BGS	0.51	0.10	5.81	n/a	4.45	7.41	2.19	0.71	n/a	0.06	n/a	20.04	0.50	0.10	1.05	0.03
41/69	Ub564	110.24	0.05	brown no rind removed	BGS	0.51	0.11	5.70	0.21	3.79	7.47	2.40	0.63	0.04	n/a	0.01	21.10	0.46	0.08	1.10	0.04
41/69	Ub565	110.29	0.05	brown no rind removed	BGS	0.52	0.10	5.85	n/a	4.36	7.50	2.40	0.75	0.04	n/a	n/a	21.36	0.28	0.09	1.05	0.05
41/69	Ub566	110.34	0.05	brown no rind removed	BGS	0.50	0.10	5.81	n/a	4.12	7.10	2.24	0.70	n/a	n/a	n/a	22.02	0.47	0.08	0.97	0.04
41/69	Ub567	110.39	0.05	brown no rind removed	BGS	0.50	0.10	4.89	n/a	5.12	7.05	2.06	0.66	0.04	0.08	0.04	18.73	0.25	0.09	0.94	0.03
41/69	Ub568	110.44	0.05	brown no rind removed	BGS	0.50	0.10	5.67	n/a	4.69	7.22	2.01	0.77	n/a	n/a	0.04	20.90	0.43	0.08	1.00	0.04

41/69	Ub569	110.49	0.05	brown no rind removed	BGS	0.52	0.10	5.31	0.22	4.89	7.87	2.11	0.68	0.06	0.08	n/a	19.53	0.92	0.07	0.97	0.04
41/69	Ub570	110.54	0.05	brown no rind removed	BGS	0.50	0.11	4.88	n/a	5.14	6.88	2.04	0.80	n/a	n/a	n/a	18.48	0.46	0.09	0.77	0.03
41/69	Ub571	110.59	0.05	brown no rind removed	BGS	0.51	0.10	5.00	n/a	6.11	7.14	2.29	0.80	0.04	0.10	0.02	19.93	0.34	0.10	1.03	0.03
41/69	Ub572	110.64	0.08	brown no rind removed	BGS	0.50	0.11	5.25	0.22	6.47	8.32	2.19	0.80	0.13	n/a	0.01	19.27	0.27	0.05	0.88	0.06
42/69	Ub573	110.72	0.05	brown no rind removed	BGS	0.52	0.10	5.35	n/a	7.42	7.29	2.34	0.70	0.11	0.21	0.01	17.77	0.23	0.05	0.86	0.06
42/69	Ub574	110.77	0.05	brown no rind removed	BGS	0.50	0.10	5.53	0.32	7.71	8.21	2.28	0.67	0.18	0.26	n/a	19.39	0.21	0.05	0.98	0.06
42/69	Ub575	110.82	0.05	brown no rind removed	BGS	n/a	n/a	n/a	n/a	n/a	n/a	n/a	n/a	n/a	n/a	n/a	n/a	n/a	n/a	n/a	n/a
42/69	Ub576	110.87	0.05	brown no rind removed	BGS	0.50	0.11	5.48	n/a	6.18	7.70	2.14	0.67	0.13	n/a	n/a	20.23	0.18	0.10	0.94	0.04
42/69	Ub577	110.92	0.05	brown no rind removed	BGS	0.50	0.10	4.98	n/a	5.62	7.09	2.16	0.68	0.06	n/a	n/a	19.34	0.20	0.08	1.01	0.03
42/69	Ub578	110.97	0.05	brown no rind removed	BGS	0.51	0.12	5.24	0.32	5.59	7.00	2.12	0.73	0.07	n/a	n/a	18.58	0.27	0.10	0.83	0.02
42/69	Ub579	111.02	0.05	brown no rind removed	BGS	0.51	0.10	5.80	0.25	6.80	8.00	2.23	0.71	0.14	0.05	0.01	19.09	0.22	0.05	0.87	0.06
42/69	Ub580	111.07	0.05	brown no rind removed	BGS	0.51	0.10	6.04	n/a	6.67	6.87	2.31	0.64	0.04	n/a	0.01	21.35	0.18	0.04	1.03	0.06
42/69	Ub581	111.12	0.05	brown no rind removed	BGS	0.51	0.10	5.78	n/a	6.38	7.21	1.91	0.77	0.07	0.11	n/a	20.33	0.21	0.11	0.91	0.02
42/69	Ub582	111.17	0.05	brown no rind removed	BGS	0.51	0.10	5.20	n/a	7.45	7.60	2.19	0.71	0.10	0.09	n/a	19.09	0.24	0.12	0.82	0.03
42/69	Ub583	111.22	0.05	brown no rind removed	BGS	0.51	0.09	4.60	n/a	5.60	6.35	2.02	0.52	0.05	0.06	n/a	17.49	0.17	0.10	0.91	0.04
42/69	Ub584	111.27	0.05	brown no rind removed	BGS	0.52	0.09	5.70	n/a	7.46	7.43	2.29	0.75	n/a	n/a	0.01	20.59	0.25	0.05	0.93	0.05
42/69	Ub585	111.32	0.05	brown no rind removed	BGS	0.52	0.13	5.29	0.23	7.61	6.59	1.97	0.70	0.08	n/a	n/a	19.63	0.62	0.13	0.78	0.01
42/69	Ub586	111.37	0.05	brown no rind removed	BGS	0.51	0.10	5.25	n/a	7.27	7.05	2.25	0.67	0.05	0.14	0.01	19.69	0.23	0.12	0.97	0.01
42/69	Ub587	111.42	0.05	brown no rind removed	BGS	0.52	0.10	5.45	n/a	6.55	7.28	2.25	0.68	0.06	0.07	n/a	19.70	0.21	0.12	1.07	0.04

42/69	Ub588	111.47	0.05	brown no rind removed	BGS	0.50	0.14	4.90	n/a	6.80	6.66	2.12	0.68	0.06	n/a	n/a	17.88	0.21	0.12	0.97	0.02
42/69	Ub589	111.52	0.02	brown no rind removed	BGS	0.50	0.10	5.17	n/a	5.88	6.92	2.23	0.71	0.05	0.05	n/a	19.51	0.27	0.10	0.94	0.03
43/69	Ub590	111.54	0.05	brown no rind removed	BGS	0.51	0.10	5.33	n/a	7.09	6.82	2.18	0.68	0.06	0.07	n/a	19.74	0.19	0.12	0.89	0.03
43/69	Ub591	111.59	0.05	brown no rind removed	BGS	0.50	0.10	5.47	0.17	6.34	7.13	2.24	0.70	0.06	0.05	n/a	20.08	0.49	0.11	0.95	0.02
43/69	Ub592	111.64	0.05	brown no rind removed	BGS	0.51	0.11	5.55	0.17	5.77	7.13	2.19	0.72	0.04	n/a	0.02	21.56	0.21	0.10	1.11	0.05
43/69	Ub593	111.69	0.05	brown no rind removed	BGS	0.50	0.10	5.06	n/a	6.56	7.11	2.12	0.76	n/a	0.07	n/a	19.86	1.02	0.11	1.01	0.03
43/69	Ub594	111.74	0.05	brown no rind removed	BGS	0.50	0.10	5.34	n/a	5.77	6.75	2.08	0.57	0.05	n/a	0.02	20.05	0.18	0.11	0.89	0.03
43/69	Ub595	111.79	0.05	brown no rind removed	BGS	0.51	0.11	5.44	n/a	6.51	6.86	2.12	0.68	0.05	0.05	n/a	19.80	0.25	0.11	0.97	0.04
43/69	Ub596	111.84	0.05	brown no rind removed	BGS	0.50	0.10	5.85	0.35	5.81	7.09	2.15	0.68	0.06	n/a	n/a	20.67	0.37	0.09	1.02	0.04
43/69	Ub597	111.89	0.05	brown no rind removed	BGS	0.51	0.10	5.44	n/a	4.99	7.25	2.32	0.71	n/a	0.07	n/a	20.47	0.60	0.10	0.91	0.02
43/69	Ub598	111.94	0.05	brown no rind removed	BGS	0.51	0.10	5.54	0.25	6.25	7.11	2.16	0.67	0.04	n/a	n/a	19.83	0.48	0.11	1.03	0.02
43/69	Ub599	111.99	0.05	brown no rind removed	BGS	0.50	0.11	5.43	0.22	5.02	7.00	2.27	0.64	0.05	n/a	n/a	19.19	0.43	0.09	0.86	0.03
43/69	Ub600	112.04	0.05	brown no rind removed	BGS	0.50	0.13	5.03	0.24	5.13	6.88	2.06	0.61	n/a	0.05	n/a	17.67	0.39	0.11	0.93	0.02
43/69	Ub601	112.09	0.05	brown no rind removed	BGS	0.51	0.11	5.10	n/a	6.95	7.27	2.10	0.62	n/a	n/a	n/a	20.46	1.37	0.04	0.98	0.06
43/69	Ub602	112.14	0.05	brown no rind removed	BGS	0.51	0.12	5.23	n/a	5.82	6.58	2.00	0.59	0.05	n/a	n/a	19.87	0.36	0.12	0.87	0.04
43/69	Ub603	112.19	0.05	brown no rind removed	BGS	0.49	0.11	5.53	n/a	5.36	7.35	2.19	0.70	0.05	n/a	n/a	20.42	0.54	0.10	0.99	0.05
43/69	Ub604	112.24	0.05	brown no rind removed	BGS	0.52	0.10	5.52	n/a	5.26	7.19	1.94	0.73	n/a	0.08	n/a	20.38	0.68	0.08	0.93	0.05
43/69	Ub605	112.29	0.05	brown no rind removed	BGS	0.51	0.10	5.86	0.23	5.54	7.22	2.33	0.82	0.06	n/a	n/a	20.62	0.39	0.10	0.98	0.04
43/69	Ub606	112.34	0.06	brown no rind removed	BGS	0.51	0.10	5.45	n/a	5.34	7.17	2.31	0.68	0.04	n/a	n/a	19.87	0.65	0.09	0.96	0.03

44/69	Ub607	112.40	0.05	brown no rind removed	BGS	0.50	0.11	5.72	n/a	4.74	7.11	2.26	0.67	0.04	n/a	n/a	20.72	0.41	0.09	1.07	0.03
44/69	Ub608	112.45	0.05	brown no rind removed	BGS	0.49	0.10	5.89	n/a	4.59	7.69	2.38	0.79	0.05	n/a	n/a	20.37	0.53	0.10	1.06	0.03
44/69	Ub609	112.50	0.05	brown no rind removed	BGS	0.51	0.10	5.70	n/a	5.46	7.49	2.22	0.66	0.04	0.05	n/a	19.98	0.52	0.09	0.90	0.03
44/69	Ub610	112.55	0.05	brown no rind removed	BGS	0.51	0.09	6.31	n/a	4.16	7.60	2.20	0.80	0.04	0.10	0.01	21.85	0.41	0.08	1.14	0.05
44/69	Ub611	112.60	0.05	brown no rind removed	BGS	0.52	0.10	5.62	0.21	4.44	7.19	2.10	0.75	0.04	n/a	0.03	20.44	0.27	0.08	1.01	0.03
44/69	Ub612	112.65	0.05	brown no rind removed	BGS	0.50	0.10	5.82	n/a	4.29	7.73	2.36	0.79	0.05	n/a	0.01	20.93	0.36	0.08	1.06	0.04
44/69	Ub613	112.70	0.05	brown no rind removed	BGS	0.50	0.10	6.41	n/a	3.87	7.32	2.41	0.71	0.04	n/a	n/a	21.82	0.38	0.08	0.99	0.04
44/69	Ub614	112.75	0.05	brown no rind removed	BGS	0.51	0.10	5.80	n/a	4.04	7.75	2.35	0.72	0.05	n/a	0.01	20.46	0.79	0.08	1.00	0.03
44/69	Ub615	112.80	0.05	brown no rind removed	BGS	0.50	0.10	6.10	n/a	4.25	7.47	2.31	0.72	0.03	0.05	n/a	20.37	0.48	0.08	1.06	0.05
44/69	Ub616	112.85	0.05	brown no rind removed	BGS	0.50	0.10	6.10	0.33	3.52	7.79	2.31	0.69	0.04	n/a	n/a	21.19	0.37	0.08	1.01	0.03
44/69	Ub617	112.90	0.05	brown no rind removed	BGS	0.52	0.10	5.88	n/a	3.49	7.26	2.27	0.81	0.04	n/a	n/a	19.70	0.26	0.08	1.01	0.04
44/69	Ub618	112.95	0.05	brown no rind removed	BGS	0.52	0.10	5.48	0.14	3.81	7.41	2.47	0.79	0.04	0.08	0.01	20.78	0.40	0.09	0.91	0.03
44/69	Ub619	113.00	0.05	brown no rind removed	BGS	0.51	0.10	5.45	n/a	4.58	7.42	2.24	0.76	0.04	n/a	n/a	20.36	0.47	0.09	1.01	0.02
44/69	Ub620	113.05	0.05	brown no rind removed	BGS	0.51	0.10	6.02	n/a	4.40	7.77	2.42	0.75	n/a	n/a	n/a	20.38	0.53	0.09	0.86	0.02
44/69	Ub621	113.10	0.05	brown no rind removed	BGS	0.50	0.09	5.96	n/a	4.11	7.61	2.34	0.79	n/a	n/a	0.01	20.03	0.39	0.08	1.08	0.04
44/69	Ub622	113.15	0.08	brown no rind removed	BGS	0.51	0.10	6.12	n/a	4.73	7.30	2.54	0.75	n/a	0.08	n/a	21.54	0.59	0.10	0.96	0.05
45/69	Ub623	113.23	0.05	brown no rind removed	BGS	0.49	0.10	5.81	0.23	4.22	7.55	2.65	0.69	0.05	n/a	0.01	21.22	0.59	0.08	0.97	0.04
45/69	Ub624	113.28	0.05	brown no rind removed	BGS	0.50	0.11	5.24	n/a	4.68	7.09	2.20	0.73	0.05	0.07	n/a	18.86	0.54	0.09	0.91	0.04
45/69	Ub625	113.33	0.05	brown no rind removed	BGS	0.52	0.12	4.93	n/a	4.77	7.01	2.32	0.63	n/a	n/a	n/a	18.42	0.61	0.09	0.93	0.02

45/69	Ub626	113.38	0.05	brown no rind removed	BGS	0.50	0.12	5.20	0.25	4.58	7.12	1.99	0.64	n/a	0.09	n/a	17.47	0.68	0.08	1.01	0.04
45/69	Ub627	113.43	0.05	brown no rind removed	BGS	0.51	0.10	5.27	0.25	5.58	7.57	2.37	0.70	n/a	n/a	n/a	19.01	1.51	0.09	0.83	0.03
45/69	Ub628	113.48	0.05	brown no rind removed	BGS	0.51	0.10	5.12	0.17	4.96	7.07	2.05	0.66	0.05	0.05	n/a	18.13	0.42	0.09	0.82	0.04
45/69	Ub629	113.53	0.05	brown no rind removed	BGS	0.50	0.10	5.07	n/a	5.51	7.39	2.29	0.67	0.05	n/a	n/a	19.60	0.56	0.10	1.04	0.02
45/69	Ub630	113.58	0.05	brown no rind removed	BGS	0.50	0.10	5.02	n/a	4.76	7.84	2.32	0.61	0.08	n/a	n/a	18.97	0.55	0.08	0.89	0.04
45/69	Ub631	113.63	0.05	brown no rind removed	BGS	0.51	0.11	5.58	n/a	4.77	7.62	2.18	0.78	0.03	n/a	n/a	21.41	0.50	0.09	0.98	0.02
45/69	Ub632	113.68	0.05	brown no rind removed	BGS	0.49	0.10	6.40	n/a	4.90	7.99	2.27	0.78	0.07	0.06	0.01	21.97	0.53	0.03	0.89	0.07
45/69	Ub633	113.73	0.1	brown no rind removed	BGS	0.50	0.11	5.61	n/a	5.96	7.17	2.26	0.66	0.04	0.06	n/a	19.77	0.55	0.10	1.04	0.02
	113.78?	113.78	0.1			0.49	0.10	5.77	n/a	5.47	7.11	2.25	0.85	0.06	n/a	n/a	20.98	0.47	0.11	0.92	0.03
45/69	Ub634	113.83	0.05	brown no rind removed	BGS	0.50	0.10	5.38	0.12	4.93	7.21	2.26	0.78	0.05	n/a	n/a	19.75	0.35	0.10	0.97	0.03
45/69	Ub635	113.88	0.05	brown no rind removed	BGS	0.50	0.10	5.24	n/a	5.14	7.31	2.14	0.72	0.05	n/a	n/a	20.72	0.31	0.10	1.01	0.03
45/69	Ub636	113.93	0.05	brown no rind removed	BGS	0.53	0.13	5.42	n/a	4.65	7.25	2.24	0.66	0.05	n/a	n/a	19.60	0.37	0.08	0.89	0.03
45/69	Ub637	113.98	2.8	brown no rind removed	BGS	0.50	0.10	5.18	0.33	7.11	7.46	2.25	0.67	0.08	n/a	n/a	19.73	0.32	0.05	1.00	0.07
46/69	Ub638	116.78	0.05	brown no rind removed	BGS	0.50	0.10	4.78	n/a	7.86	7.03	2.12	0.80	n/a	n/a	n/a	18.81	0.43	0.13	0.91	0.02
46/69	Ub639	116.83	0.05	brown no rind removed	BGS	0.51	0.10	5.88	n/a	5.54	7.39	2.03	0.72	0.06	n/a	n/a	19.80	0.32	0.10	0.96	0.02
46/69	Ub640	116.88	0.05	brown no rind removed	BGS	0.50	0.10	5.43	n/a	5.73	7.13	2.07	0.74	0.07	0.06	n/a	19.18	0.33	0.10	0.95	0.03
46/69	Ub641	116.93	0.05	brown no rind removed	BGS	0.50	0.10	4.27	n/a	7.68	6.99	2.10	0.59	0.08	n/a	0.01	17.05	0.17	0.14	0.86	0.00
46/69	Ub642	116.98	0.05	brown no rind removed	BGS	0.52	0.10	5.16	0.15	7.82	7.48	2.19	0.72	0.11	0.08	0.02	19.53	0.23	0.05	0.95	0.06
46/69	Ub643	117.03	0.05	brown no rind removed	BGS	0.50	0.10	5.62	0.19	8.07	7.33	2.20	0.65	0.10	0.07	0.01	20.17	0.25	0.05	0.88	0.06
46/69	Ub644	117.08	0.05	brown no rind removed	BGS	0.50	0.12	4.98	0.25	7.69	6.91	2.02	0.66	0.07	0.10	n/a	17.78	0.36	0.11	0.85	0.02

46/69	Ub645	117.13	0.05	brown no rind removed	BGS	0.51	0.10	5.09	n/a	7.22	7.50	2.25	0.77	0.09	n/a	0.01	20.06	0.21	0.05	0.96	0.07
46/69	Ub646	117.18	0.05	brown no rind removed	BGS	n/a	n/a	n/a	n/a	n/a	n/a	n/a	n/a	n/a	n/a	n/a	n/a	n/a	n/a	n/a	n/a
46/69	Ub647	117.23	0.05	brown no rind removed	BGS	0.50	0.10	5.76	n/a	8.97	7.34	2.23	0.83	0.07	n/a	0.01	20.64	0.29	0.06	0.95	0.06
46/69	Ub648	117.28	0.05	brown no rind removed	BGS	0.49	0.14	4.46	0.19	7.20	6.90	2.09	0.63	0.07	n/a	0.02	16.74	0.21	0.13	0.76	0.02
46/69	Ub649	117.33	0.05	brown no rind removed	BGS	0.50	0.10	5.41	n/a	8.64	7.15	2.34	0.77	0.08	0.07	0.01	19.79	0.21	0.06	0.90	0.06
46/69	Ub650	117.38	0.05	brown no rind removed	BGS	0.52	0.10	4.87	n/a	7.31	6.72	1.79	0.62	0.07	n/a	0.01	19.56	0.62	0.12	0.95	0.02
46/69	Ub651	117.43	0.05	brown no rind removed	BGS	0.50	0.09	5.33	0.19	7.03	7.00	2.13	0.73	0.06	n/a	n/a	20.26	0.21	0.12	0.90	0.03
46/69	Ub652	117.48	0.05	brown no rind removed	BGS	0.53	0.13	5.34	n/a	7.38	7.33	2.02	0.73	0.07	n/a	n/a	18.88	0.44	0.12	0.97	0.03
46/69	Ub653	117.53	0.05	brown no rind removed	BGS	0.50	0.11	5.23	0.21	6.93	7.08	2.03	0.78	0.06	0.08	n/a	19.80	0.45	0.12	0.85	0.02
46/69	Ub654	117.58	0.05	brown no rind removed	BGS	0.50	0.11	5.66	0.21	5.65	7.42	2.45	0.75	0.07	0.09	n/a	20.07	0.32	0.10	0.94	0.02
46/69	Ub655	117.63	0.04	brown no rind removed	BGS	0.50	0.10	5.29	n/a	5.89	7.21	2.38	0.72	0.08	0.07	n/a	18.62	0.35	0.12	0.87	0.02
47/69	Ub656	117.67	0.05	brown no rind removed	BGS	0.52	0.12	5.84	n/a	7.75	7.51	2.04	0.74	0.10	n/a	0.01	20.66	0.27	0.05	1.00	0.06
47/69	Ub657	117.72	0.05	brown no rind removed	BGS	0.50	0.10	4.89	n/a	7.66	7.34	1.95	0.77	0.08	n/a	n/a	19.77	0.30	0.12	0.91	0.01
47/69	Ub658	117.77	0.05	brown no rind removed	BGS	0.50	0.10	5.11	n/a	8.36	7.39	2.09	0.62	0.08	n/a	0.01	19.46	0.44	0.06	0.92	0.05
47/69	Ub659	117.82	0.05	brown no rind removed	BGS	0.52	0.09	4.98	0.20	8.12	6.78	2.16	0.73	0.07	n/a	n/a	19.43	0.28	0.12	0.79	n/a
47/69	Ub660	117.87	0.05	brown no rind removed	BGS	0.51	0.10	5.70	n/a	8.46	7.28	2.20	0.79	0.11	n/a	0.01	19.12	0.29	0.06	0.88	0.06
47/69	Ub661	117.92	0.05	brown no rind removed	BGS	0.51	0.11	5.70	n/a	8.94	7.34	2.10	0.70	0.11	n/a	0.02	20.31	0.28	0.05	0.85	0.06
47/69	Ub662	117.97	0.05	brown no rind removed	BGS	0.52	0.11	4.66	n/a	8.18	7.29	1.87	0.67	0.10	n/a	n/a	17.96	0.27	0.12	0.85	0.01
47/69	Ub663	118.02	0.3	brown no rind removed	BGS	0.52	0.10	4.90	0.31	8.16	7.31	1.95	0.75	0.07	0.09	n/a	20.85	0.67	0.05	0.96	0.07

47/69	Ub664	118.32	-0.25	brown no rind removed	BGS	0.48	0.14	4.73	0.16	6.38	6.85	2.09	0.67	0.08	n/a	n/a	19.51	0.24	0.09	0.93	0.04
47/69	Ub665	118.07	0.05	brown no rind removed	BGS	0.50	0.10	5.46	n/a	6.02	7.01	2.13	0.80	0.07	0.08	n/a	19.81	0.23	0.10	0.95	0.04
47/69	Ub666	118.12	0.05	brown no rind removed	BGS	0.50	0.10	4.64	0.19	5.77	7.46	1.74	0.56	0.05	0.06	n/a	18.58	0.81	0.09	0.85	0.03
47/69	Ub667	118.17	0.05	brown no rind removed	BGS	0.52	0.10	5.41	n/a	5.03	7.40	2.26	0.72	0.04	n/a	n/a	21.47	0.47	0.09	1.00	0.04
47/69	Ub668	118.22	0.05	brown no rind removed	BGS	0.50	0.13	5.38	0.19	6.50	7.00	2.11	0.71	0.07	0.07	n/a	19.78	0.19	0.11	0.88	0.02
47/69	Ub669	118.27	0.1	brown no rind removed	BGS	0.50	0.10	5.17	n/a	7.57	7.28	1.90	0.68	0.04	n/a	0.01	19.56	0.30	0.12	1.02	0.01
47/69	Ub670	118.37	0.05	brown no rind removed	BGS	0.50	0.10	5.26	n/a	6.22	6.97	2.19	0.71	0.04	n/a	n/a	19.43	0.33	0.12	0.96	0.02
47/69	Ub671	118.42	0.05	brown no rind removed	BGS	0.52	0.10	5.61	0.21	5.47	7.29	2.28	0.83	n/a	0.06	n/a	20.39	0.36	0.08	0.97	0.04
47/69	Ub672	118.47	0.05	brown no rind removed	BGS	0.53	0.10	5.80	0.10	5.80	7.46	2.28	0.79	0.06	0.08	n/a	21.09	0.29	0.09	0.94	0.04
47/69	Ub673	118.52	0.01	brown no rind removed	BGS	0.52	0.11	5.01	0.24	5.74	7.06	1.83	0.68	0.06	0.06	n/a	19.76	0.24	0.10	0.97	0.03
48/69	Ub674	118.53	0.05	brown no rind removed	BGS	0.50	0.10	5.31	n/a	6.07	7.78	2.32	0.71	0.05	n/a	n/a	19.45	0.41	0.11	0.99	0.03
48/69	Ub675	118.58	0.05	brown no rind removed	BGS	0.50	0.12	5.25	n/a	6.26	7.47	2.22	0.75	0.07	n/a	n/a	19.53	0.38	0.10	0.88	0.04
48/69	Ub676	118.63	0.05	brown no rind removed	BGS	0.48	0.09	5.59	0.11	5.45	7.83	2.32	0.82	0.05	n/a	0.01	21.21	0.46	0.04	1.05	0.07
48/69	Ub677	118.68	0.05	brown no rind removed	BGS	0.51	0.11	5.18	n/a	5.22	8.25	2.08	0.64	0.07	n/a	n/a	20.61	0.64	0.09	1.01	0.03
48/69	Ub678	118.73	0.05	brown no rind removed	BGS	0.51	0.09	5.58	0.35	5.72	7.50	1.97	0.79	0.05	n/a	n/a	20.76	0.37	0.11	1.04	0.03
48/69	Ub679	118.78	0.05	brown no rind removed	BGS	0.52	0.10	4.85	0.18	5.13	7.60	2.16	0.69	0.04	0.08	0.02	20.08	0.36	0.09	0.96	0.03
48/69	Ub680	118.83	0.05	brown no rind removed	BGS	0.53	0.11	5.41	0.17	5.55	6.99	2.43	0.71	0.04	0.05	n/a	20.12	0.20	0.11	1.05	0.01
48/69	Ub681	118.88	0.05	brown no rind removed	BGS	0.52	0.10	4.65	0.20	5.34	6.83	2.02	0.64	0.07	n/a	n/a	18.99	0.31	0.11	0.92	0.03
48/69	Ub682	118.93	0.05	brown no rind removed	BGS	0.50	0.11	5.12	n/a	4.77	7.73	2.09	0.74	0.06	n/a	n/a	19.19	0.39	0.10	0.81	0.02

48/69	Ub683	118.98	0.05	brown no rind removed	BGS	0.52	0.12	4.91	n/a	5.11	7.22	2.14	0.65	0.04	n/a	n/a	18.54	0.35	0.10	0.84	0.04
48/69	Ub684	119.03	0.05	brown no rind removed	BGS	0.51	0.10	5.06	n/a	6.35	6.77	2.15	0.52	0.06	n/a	0.02	18.40	0.29	0.11	0.92	0.04
48/69	Ub685	119.08	0.05	brown no rind removed	BGS	0.50	0.12	5.62	n/a	6.05	7.26	2.04	0.76	0.05	n/a	n/a	19.23	0.30	0.09	1.12	0.03
48/69	Ub686	119.13	0.05	brown no rind removed	BGS	0.51	0.09	5.41	0.33	4.09	7.53	1.91	0.65	n/a	0.07	0.01	20.45	0.45	0.09	1.00	0.04
48/69	Ub687	119.18	0.05	brown no rind removed	BGS	0.50	0.10	5.45	0.25	4.99	7.26	2.13	0.79	0.06	0.09	n/a	21.57	0.32	0.08	0.95	0.04
48/69	Ub688	119.23	0.05	brown no rind removed	BGS	0.51	0.09	4.99	n/a	6.34	6.51	2.00	0.66	0.07	n/a	n/a	18.46	0.35	0.11	0.87	0.03
48/69	Ub689	119.28	0.05	brown no rind removed	BGS	n/a	n/a	n/a	n/a	n/a	n/a	n/a	n/a	n/a	n/a	n/a	n/a	n/a	n/a	n/a	n/a
48/69	Ub690	119.33	0.03	brown no rind removed	BGS	0.51	0.11	5.44	0.27	7.08	7.59	1.99	0.71	0.12	n/a	n/a	18.96	0.19	0.11	0.88	0.02
49/69	Ub691	119.36	0.04	brown no rind removed	BGS	0.49	0.09	5.13	n/a	7.10	6.89	2.10	0.63	0.05	0.07	n/a	18.89	0.20	0.11	1.00	0.03
49/69	Ub692	119.40	0.05	brown no rind removed	BGS	0.53	0.10	5.22	n/a	7.58	7.04	2.15	0.72	n/a	0.05	0.01	20.37	0.21	0.05	0.98	0.06
49/69	Ub693	119.45	0.05	brown no rind removed	BGS	0.52	0.11	4.89	n/a	7.36	6.64	2.03	0.63	0.07	0.08	n/a	19.94	0.20	0.12	0.95	0.05
49/69	Ub694	119.50	0.05	brown no rind removed	BGS	0.51	0.10	5.02	n/a	6.90	7.02	2.23	0.69	0.05	0.07	n/a	20.34	0.32	0.12	0.85	0.04
49/69	Ub695	119.55	0.05	brown no rind removed	BGS	0.51	0.11	5.32	0.30	7.22	6.82	2.19	0.73	0.05	n/a	n/a	19.33	0.24	0.12	0.93	0.02
49/69	Ub696	119.60	0.05	brown no rind removed	BGS	0.51	0.10	5.17	n/a	6.95	6.83	2.02	0.67	0.06	n/a	0.01	18.85	0.32	0.12	0.88	0.03
49/69	Ub697	119.65	0.05	brown no rind removed	BGS	0.49	0.10	5.04	n/a	7.20	7.75	1.88	0.67	0.13	n/a	0.01	17.86	0.33	0.11	0.87	0.03
49/69	Ub698	119.70	0.05	brown no rind removed	BGS	0.50	0.10	5.45	0.23	6.11	7.37	1.92	0.64	0.05	n/a	n/a	19.12	0.35	0.10	0.93	0.03
49/69	Ub699	119.75	0.05	brown no rind removed	BGS	0.53	0.10	5.93	0.13	6.88	7.45	2.09	0.90	0.07	n/a	0.01	22.11	0.27	0.05	1.01	0.07
49/69	Ub700	119.80	0.05	brown no rind removed	BGS	0.52	0.11	5.61	0.27	6.37	7.09	2.18	0.78	0.07	n/a	n/a	20.72	0.24	0.10	1.04	0.03
49/69	Ub701	119.85	0.05	brown no rind removed	BGS	n/a	n/a	n/a	n/a	n/a	n/a	n/a	n/a	n/a	n/a	n/a	n/a	n/a	n/a	n/a	n/a

49/69	Ub702	119.90	0.05	brown no rind removed	BGS	0.51	0.11	4.91	0.18	6.98	6.83	2.00	0.65	0.05	0.05	0.01	18.64	0.37	0.11	0.90	0.03
49/69	Ub703	119.95	0.05	brown no rind removed	BGS	0.52	0.11	5.16	n/a	7.19	6.74	2.07	0.66	0.05	0.10	n/a	18.97	0.36	0.10	0.92	0.03
49/69	Ub704	120.00	0.05	brown no rind removed	BGS	0.53	0.10	5.08	n/a	6.04	8.20	2.02	0.80	0.06	0.09	0.01	19.65	0.44	0.04	0.86	0.07
49/69	Ub705	120.05	0.05	brown no rind removed	BGS	0.51	0.11	5.23	0.27	7.35	6.94	1.82	0.61	0.07	n/a	0.01	18.83	0.32	0.11	0.96	0.02
49/69	Ub706	120.10	0.05	brown no rind removed	BGS	0.53	0.12	4.78	n/a	6.02	6.59	2.04	0.68	0.06	n/a	n/a	20.18	0.18	0.10	0.82	0.03
49/69	Ub707	120.15	0.05	brown no rind removed	BGS	0.49	0.10	5.05	n/a	6.20	7.11	1.82	0.62	0.08	0.06	n/a	17.85	0.29	0.11	0.84	0.03
49/69	Ub708	120.20	0.05	brown no rind removed	BGS	0.52	0.10	4.77	n/a	6.77	6.73	2.06	0.68	n/a	n/a	n/a	20.30	0.21	0.12	0.94	0.05
50/69	Ub709	120.25	0.05	brown no rind removed	BGS	n/a	n/a	n/a	n/a	n/a	n/a	n/a	n/a	n/a	n/a	n/a	n/a	n/a	n/a	n/a	n/a
50/69	Ub710	120.30	0.05	brown no rind removed	BGS	n/a	n/a	n/a	n/a	n/a	n/a	n/a	n/a	n/a	n/a	n/a	n/a	n/a	n/a	n/a	n/a
50/69	Ub711	120.35	0.05	brown no rind removed	BGS	0.50	0.10	5.45	n/a	4.80	7.03	1.96	0.72	0.05	n/a	n/a	19.60	0.29	0.08	0.98	0.04
50/69	Ub712	120.40	0.05	brown no rind removed	BGS	0.50	0.10	5.50	0.33	5.01	6.96	2.08	0.71	0.03	n/a	0.01	20.14	0.27	0.09	0.97	0.04
50/69	Ub713	120.45	0.05	brown no rind removed	BGS	0.51	0.10	4.82	0.32	4.81	7.45	2.05	0.66	0.04	0.06	n/a	18.18	0.67	0.10	0.94	0.01
50/69	Ub714	120.50	0.05	brown no rind removed	BGS	0.49	0.14	4.74	n/a	5.09	6.45	1.91	0.61	n/a	n/a	n/a	17.19	0.22	0.10	0.96	0.03
50/69	Ub715	120.55	0.05	brown no rind removed	BGS	0.50	0.09	4.73	n/a	5.33	6.75	2.04	0.63	0.04	n/a	n/a	18.80	0.26	0.09	0.94	0.03
50/69	Ub716	120.60	0.05	brown no rind removed	BGS	0.53	0.10	5.02	0.18	4.97	7.13	2.10	0.69	n/a	n/a	n/a	19.33	0.38	0.10	0.98	0.03
50/69	Ub717	120.65	0.05	brown no rind removed	BGS	0.51	0.10	5.39	n/a	6.33	6.56	1.93	0.73	0.03	n/a	n/a	19.45	0.23	0.12	1.00	0.03
50/69	Ub718	120.70	0.05	brown no rind removed	BGS	0.52	0.10	5.52	n/a	4.95	6.63	2.05	0.72	0.04	0.06	n/a	20.79	0.22	0.10	1.00	0.04
50/69	Ub719	120.75	0.05	brown no rind removed	BGS	0.51	0.11	5.18	0.31	5.27	7.00	2.11	0.78	n/a	n/a	n/a	20.42	0.50	0.10	0.93	0.03
50/69	Ub720	120.80	0.05	brown no rind removed	BGS	n/a	n/a	n/a	n/a	n/a	n/a	n/a	n/a	n/a	n/a	n/a	n/a	n/a	n/a	n/a	n/a

50/69	Ub721	120.85	0.05	brown no rind removed	BGS	0.50	0.10	5.49	n/a	4.70	6.84	2.21	0.72	0.06	n/a	0.03	20.27	0.27	0.09	0.92	0.05
50/69	Ub722	120.90	0.05	brown no rind removed	BGS	0.51	0.09	5.40	n/a	5.48	7.11	2.19	0.73	0.08	0.05	n/a	19.27	0.44	0.09	0.96	0.02
50/69	Ub723	120.95	0.05	brown no rind removed	BGS	n/a	n/a	n/a	n/a	n/a	n/a	n/a	n/a	n/a	n/a	n/a	n/a	n/a	n/a	n/a	n/a
50/69	Ub724	121.00	1.28	brown no rind removed	BGS	0.50	0.10	5.75	0.19	6.07	6.98	2.25	0.76	0.06	n/a	n/a	20.57	0.39	0.11	0.93	0.02
51/69	Ub725	122.28	0.05	brown no rind removed	BGS	n/a	n/a	n/a	n/a	n/a	n/a	n/a	n/a	n/a	n/a	n/a	n/a	n/a	n/a	n/a	n/a
51/69	Ub726	122.33	0.05	brown no rind removed	BGS	0.52	0.12	5.64	n/a	4.23	6.53	2.18	0.76	n/a	n/a	n/a	19.57	0.25	0.10	0.99	0.03
51/69	Ub727	122.38	0.05	brown no rind removed	BGS	0.51	0.10	5.81	n/a	4.16	6.60	2.18	0.74	n/a	n/a	0.03	20.32	0.39	0.08	0.99	0.04
51/69	Ub728	122.43	0.05	brown no rind removed	BGS	0.50	0.11	4.63	n/a	4.38	6.38	1.82	0.62	n/a	n/a	n/a	17.08	0.30	0.09	0.83	0.04
51/69	Ub729	122.48	0.05	brown no rind removed	BGS	0.50	0.10	5.50	n/a	4.90	6.81	2.16	0.77	0.04	n/a	n/a	20.43	0.32	0.10	0.80	0.03
51/69	Ub730	122.53	0.05	brown no rind removed	BGS	0.51	0.09	5.80	n/a	4.32	6.63	2.36	0.74	0.06	0.06	n/a	19.42	0.30	0.09	0.95	0.03
51/69	Ub731	122.58	0.05	brown no rind removed	BGS	0.48	0.10	5.80	n/a	4.53	6.54	2.16	0.77	0.04	n/a	0.02	21.06	0.31	0.09	1.01	0.03
51/69	Ub732	122.63	0.05	brown no rind removed	BGS	0.52	0.10	5.77	0.25	3.27	7.03	2.39	0.69	n/a	n/a	0.03	20.53	0.55	0.07	0.89	0.04
51/69	Ub733	122.68	0.05	brown no rind removed	BGS	0.50	0.10	5.06	n/a	4.10	6.62	2.25	0.70	0.04	n/a	n/a	18.29	0.32	0.09	0.87	0.03
51/69	Ub734	122.73	0.05	brown no rind removed	BGS	0.48	0.10	5.81	n/a	2.18	8.03	2.35	0.71	0.06	n/a	0.01	21.04	0.99	0.06	0.93	0.04
51/69	Ub735	122.78	0.05	brown no rind removed	BGS	n/a	n/a	n/a	n/a	n/a	n/a	n/a	n/a	n/a	n/a	n/a	n/a	n/a	n/a	n/a	n/a
51/69	Ub736	122.83	0.05	brown no rind removed	BGS	0.51	0.09	6.06	0.27	1.84	7.27	2.63	0.80	0.03	n/a	0.03	21.75	0.30	0.05	1.03	0.06
51/69	Ub737	122.88	0.05	brown no rind removed	BGS	n/a	n/a	n/a	n/a	n/a	n/a	n/a	n/a	n/a	n/a	n/a	n/a	n/a	n/a	n/a	n/a
51/69	Ub738	122.93	0.05	brown no rind removed	BGS	n/a	n/a	n/a	n/a	n/a	n/a	n/a	n/a	n/a	n/a	n/a	n/a	n/a	n/a	n/a	n/a
51/69	Ub739	122.98	0.05	brown no rind removed	BGS	0.51	0.09	5.37	n/a	3.36	7.18	2.23	0.64	0.04	n/a	n/a	19.72	0.40	0.09	1.08	0.03

51/69	Ub740	123.03	0.05	brown no rind removed	BGS	0.51	0.10	5.56	n/a	3.51	7.09	2.31	0.77	0.04	n/a	n/a	20.39	0.35	0.07	0.94	0.04
51/69	Ub741	123.08	0.05	brown no rind removed	BGS	0.49	0.12	5.75	0.22	2.89	8.14	2.21	0.81	0.04	0.12	0.03	19.40	0.74	0.07	0.95	0.05
51/69	Ub742	123.13	0.03	brown no rind removed	BGS	n/a	n/a	n/a	n/a	n/a	n/a	n/a	n/a	n/a	n/a	n/a	n/a	n/a	n/a	n/a	n/a
52/69	Ub743	123.16	0.05	brown no rind removed	BGS	n/a	n/a	n/a	n/a	n/a	n/a	n/a	n/a	n/a	n/a	n/a	n/a	n/a	n/a	n/a	n/a
52/69	Ub744	123.21	0.05	brown no rind removed	BGS	n/a	n/a	n/a	n/a	n/a	n/a	n/a	n/a	n/a	n/a	n/a	n/a	n/a	n/a	n/a	n/a
52/69	Ub745	123.26	0.05	brown no rind removed	BGS	n/a	n/a	n/a	n/a	n/a	n/a	n/a	n/a	n/a	n/a	n/a	n/a	n/a	n/a	n/a	n/a
52/69	Ub746	123.31	0.05	brown no rind removed	BGS	0.50	0.10	6.16	n/a	3.49	7.33	2.18	0.68	0.03	n/a	0.03	20.61	0.57	0.08	1.05	0.03
52/69	Ub747	123.36	0.05	brown no rind removed	BGS	0.50	0.10	5.66	0.20	4.39	6.94	2.30	0.73	0.06	0.13	n/a	19.99	0.35	0.10	0.95	0.02
52/69	Ub748	123.41	0.05	brown no rind removed	BGS	0.50	0.10	6.43	n/a	3.86	7.24	2.31	0.80	0.03	n/a	n/a	21.91	0.53	0.08	1.00	0.04
52/69	Ub749	123.46	0.05	brown no rind removed	BGS	n/a	n/a	n/a	n/a	n/a	n/a	n/a	n/a	n/a	n/a	n/a	n/a	n/a	n/a	n/a	n/a
52/69	Ub750	123.51	0.05	brown no rind removed	BGS	0.51	0.10	5.94	n/a	4.01	7.07	2.36	0.81	0.04	n/a	n/a	20.27	0.35	0.09	0.88	0.03
52/69	Ub751	123.56	0.05	brown no rind removed	BGS	n/a	n/a	n/a	n/a	n/a	n/a	n/a	n/a	n/a	n/a	n/a	n/a	n/a	n/a	n/a	n/a
52/69	Ub752	123.61	0.05	brown no rind removed	BGS	n/a	n/a	n/a	n/a	n/a	n/a	n/a	n/a	n/a	n/a	n/a	n/a	n/a	n/a	n/a	n/a
52/69	Ub753	123.66	0.05	brown no rind removed	BGS	n/a	n/a	n/a	n/a	n/a	n/a	n/a	n/a	n/a	n/a	n/a	n/a	n/a	n/a	n/a	n/a
52/69	Ub754	123.71	0.05	brown no rind removed	BGS	0.49	0.09	5.26	n/a	3.49	6.83	2.22	0.74	n/a	n/a	n/a	21.03	0.24	0.08	1.03	0.05
52/69	Ub755	123.76	0.05	brown no rind removed	BGS	0.50	0.10	6.09	n/a	3.43	6.67	2.43	0.77	0.03	0.07	n/a	20.10	0.46	0.08	1.01	0.04
52/69	Ub756	123.81	0.05	brown no rind removed	BGS	0.50	0.11	5.78	n/a	3.21	6.78	2.31	0.74	0.06	0.10	n/a	20.65	0.24	0.08	0.99	0.03
52/69	Ub757	123.86	0.05	brown no rind removed	BGS	n/a	n/a	n/a	n/a	n/a	n/a	n/a	n/a	n/a	n/a	n/a	n/a	n/a	n/a	n/a	n/a
52/69	Ub758	123.91	0.05	brown no rind removed	BGS	n/a	n/a	n/a	n/a	n/a	n/a	n/a	n/a	n/a	n/a	n/a	n/a	n/a	n/a	n/a	n/a

52/69	Ub759	123.96	0.02	brown no rind removed	BGS	0.48	0.10	6.24	n/a	4.26	6.96	2.37	0.70	0.05	0.12	n/a	21.67	0.56	0.09	1.04	0.03
53/69	Ub760	123.98	0.05	brown no rind removed	BGS	0.50	0.10	6.04	n/a	3.53	6.95	2.25	0.76	0.03	0.10	0.03	20.95	0.44	0.08	0.95	0.04
53/69	Ub761	124.03	0.05	brown no rind removed	BGS	0.50	0.10	6.06	n/a	3.80	7.34	2.12	0.77	n/a	n/a	n/a	20.31	1.07	0.09	0.98	0.03
53/69	Ub762	124.08	0.05	brown no rind removed	BGS	n/a	n/a	n/a	n/a	n/a	n/a	n/a	n/a	n/a	n/a	n/a	n/a	n/a	n/a	n/a	n/a
53/69	Ub763	124.13	0.05	brown no rind removed	BGS	0.49	0.10	6.03	n/a	3.91	7.22	2.15	0.80	n/a	n/a	n/a	21.47	0.53	0.08	1.03	0.05
53/69	Ub764	124.18	0.05	brown no rind removed	BGS	0.50	0.09	5.93	n/a	3.13	6.89	2.03	0.84	n/a	n/a	n/a	21.31	0.41	0.07	0.99	0.04
53/69	Ub765	124.23	0.05	brown no rind removed	BGS	0.51	0.10	5.81	n/a	3.10	7.05	2.30	0.70	0.04	n/a	n/a	20.77	0.54	0.08	0.95	0.04
53/69	Ub766	124.28	0.05	brown no rind removed	BGS	n/a	n/a	n/a	n/a	n/a	n/a	n/a	n/a	n/a	n/a	n/a	n/a	n/a	n/a	n/a	n/a
53/69	Ub767	124.33	0.05	brown no rind removed	BGS	n/a	n/a	n/a	n/a	n/a	n/a	n/a	n/a	n/a	n/a	n/a	n/a	n/a	n/a	n/a	n/a
53/69	Ub768	124.38	0.05	brown no rind removed	BGS	n/a	n/a	n/a	n/a	n/a	n/a	n/a	n/a	n/a	n/a	n/a	n/a	n/a	n/a	n/a	n/a
53/69	Ub769	124.43	0.05	brown no rind removed	BGS	0.50	0.09	5.92	n/a	3.55	7.22	2.25	0.75	0.03	0.10	0.04	20.71	0.40	0.09	0.90	0.04
53/69	Ub770	124.48	0.05	brown no rind removed	BGS	0.50	0.10	6.29	n/a	3.52	7.02	2.37	0.75	n/a	n/a	0.04	21.42	0.24	0.08	0.94	0.04
53/69	Ub771	124.53	0.05	brown no rind removed	BGS	0.50	0.11	6.11	n/a	3.13	6.89	2.48	0.81	0.03	0.09	0.03	20.38	0.56	0.08	0.97	0.04
53/69	Ub772	124.58	0.05	brown no rind removed	BGS	0.50	0.10	6.35	n/a	3.71	7.13	2.43	0.79	n/a	n/a	0.01	21.78	0.69	0.08	1.00	0.04
53/69	Ub773	124.63	0.05	brown no rind removed	BGS	0.49	0.10	5.56	n/a	3.06	7.21	2.36	0.71	n/a	n/a	0.03	21.19	0.77	0.07	1.02	0.05
53/69	Ub774	124.68	0.05	brown no rind removed	BGS	0.52	0.10	6.60	n/a	2.49	6.99	2.30	0.74	n/a	n/a	0.03	22.30	0.43	0.07	1.00	0.05
53/69	Ub775	124.73	0.05	brown no rind removed	BGS	n/a	n/a	n/a	n/a	n/a	n/a	n/a	n/a	n/a	n/a	n/a	n/a	n/a	n/a	n/a	n/a
53/69	Ub776	124.78	0.02	brown no rind removed	BGS	0.49	0.10	6.30	n/a	2.87	6.92	2.34	0.82	0.04	0.07	n/a	21.51	0.47	0.08	0.89	0.04
54/69	Ub777	124.80	0.06	brown no rind removed	BGS	n/a	n/a	n/a	n/a	n/a	n/a	n/a	n/a	n/a	n/a	n/a	n/a	n/a	n/a	n/a	n/a

54/69	Ub778	124.86	0.05	brown no rind removed	BGS	n/a	n/a	n/a	n/a	n/a	n/a	n/a	n/a	n/a	n/a	n/a	n/a	n/a	n/a	n/a
54/69	Ub779	124.91	0.05	brown no rind removed	BGS	0.50	0.09	6.89	n/a	2.23	7.54	2.55	0.83	n/a	0.10	0.03	22.25	0.61	0.07	0.96	0.05
54/69	Ub780	124.96	0.05	brown no rind removed	BGS	n/a	n/a	n/a	n/a	n/a	n/a	n/a	n/a	n/a	n/a	n/a	n/a	n/a	n/a	n/a	n/a
54/69	Ub781	125.01	0.05	brown no rind removed	BGS	0.49	0.10	5.94	n/a	3.07	7.66	2.19	0.76	0.04	n/a	0.03	21.14	0.77	0.06	0.93	0.05
54/69	Ub782	125.06	0.05	brown no rind removed	BGS	0.50	0.10	6.23	n/a	2.25	7.31	2.49	0.74	0.04	0.05	0.02	22.78	0.52	0.07	0.99	0.04
54/69	Ub783	125.11	0.05	brown no rind removed	BGS	0.51	0.09	6.73	0.28	2.15	7.55	2.73	0.80	0.03	n/a	0.01	21.98	0.61	0.07	0.94	0.04
54/69	Ub784	125.16	0.05	brown no rind removed	BGS	n/a	n/a	n/a	n/a	n/a	n/a	n/a	n/a	n/a	n/a	n/a	n/a	n/a	n/a	n/a	n/a
54/69	Ub785	125.21	0.09	brown no rind removed	BGS	0.52	0.10	6.16	n/a	3.14	8.99	2.12	0.78	n/a	n/a	0.01	20.76	1.87	0.03	0.94	0.06
54/69	Ub786	125.30	0.05	brown no rind removed	BGS	n/a	n/a	n/a	n/a	n/a	n/a	n/a	n/a	n/a	n/a	n/a	n/a	n/a	n/a	n/a	n/a
54/69	Ub787	125.35	0.05	brown no rind removed	BGS	0.51	0.11	6.00	n/a	2.86	7.70	2.42	0.78	n/a	n/a	0.02	21.33	0.73	0.07	1.03	0.03
54/69	Ub788	125.40	0.05	brown no rind removed	BGS	0.50	0.09	7.16	n/a	2.48	7.75	2.47	0.83	n/a	n/a	0.01	22.10	0.68	0.06	0.96	0.05
54/69	Ub789	125.45	0.05	brown no rind removed	BGS	0.50	0.12	5.98	n/a	3.25	6.92	2.42	0.72	0.04	0.07	0.03	20.32	0.40	0.08	0.93	0.05
54/69	Ub790	125.50	0.05	brown no rind removed	BGS	0.52	0.10	6.03	n/a	2.65	7.11	2.56	0.70	0.04	n/a	0.02	20.33	0.54	0.06	0.95	0.05
54/69	Ub791	125.55	0.05	brown no rind removed	BGS	0.49	0.09	5.89	n/a	2.73	7.32	2.43	0.69	n/a	n/a	0.03	21.38	0.79	0.08	1.01	0.04
54/69	Ub792	125.60	0.05	brown no rind removed	BGS	n/a	n/a	n/a	n/a	n/a	n/a	n/a	n/a	n/a	n/a	n/a	n/a	n/a	n/a	n/a	n/a
54/69	Ub793	125.65	0.06	brown no rind removed	BGS	0.49	0.10	6.16	n/a	3.04	7.96	2.47	0.71	0.04	n/a	0.01	22.19	0.97	0.07	0.94	0.04
54/69	Ub794	125.71	0.01	brown no rind removed	BGS	n/a	n/a	n/a	n/a	n/a	n/a	n/a	n/a	n/a	n/a	n/a	n/a	n/a	n/a	n/a	n/a
55/69	Ub795	125.72	0.05	brown no rind removed	BGS	0.48	0.11	6.91	n/a	2.82	7.53	2.57	0.82	n/a	n/a	0.01	21.94	0.75	0.09	0.94	0.03
55/69	Ub796	125.76	0.05	brown no rind removed	BGS	0.49	0.10	6.12	n/a	4.28	8.09	2.06	0.71	0.04	0.14	0.01	20.19	1.37	0.07	0.92	0.04

55/69	Ub797	125.81	0.05	brown no rind removed	BGS	n/a	n/a	n/a	n/a	n/a	n/a	n/a	n/a	n/a	n/a	n/a	n/a	n/a	n/a	n/a	n/a
55/69	Ub798	125.86	0.05	brown no rind removed	BGS	n/a	n/a	n/a	n/a	n/a	n/a	n/a	n/a	n/a	n/a	n/a	n/a	n/a	n/a	n/a	n/a
55/69	Ub799	125.91	0.05	brown no rind removed	BGS	0.51	0.10	6.71	0.23	4.32	8.60	2.45	0.96	0.03	0.12	0.02	20.91	2.26	0.03	0.99	0.05
55/69	Ub800	125.96	0.05	brown no rind removed	BGS	0.49	0.09	6.82	n/a	3.28	7.17	2.47	0.85	0.04	n/a	0.01	22.19	0.41	0.07	0.96	0.04
55/69	Ub801	126.01	0.05	brown no rind removed	BGS	0.50	0.11	6.19	n/a	3.87	7.34	2.32	0.86	0.05	n/a	n/a	21.25	0.76	0.09	0.97	0.03
55/69	Ub802	126.06	0.05	brown no rind removed	BGS	0.46	0.10	7.13	n/a	3.05	7.11	2.71	0.77	0.04	n/a	0.01	23.30	0.31	0.07	1.05	0.05
55/69	Ub803	126.11	0.05	brown no rind removed	BGS	0.49	0.13	6.27	n/a	2.05	7.39	2.30	0.77	n/a	n/a	0.02	21.34	0.35	0.07	0.99	0.03
55/69	Ub804	126.16	0.05	brown no rind removed	BGS	0.47	0.09	6.80	0.29	2.57	7.49	2.51	0.82	0.05	n/a	0.01	22.65	0.67	0.07	1.01	0.04
55/69	Ub805	126.21	0.05	brown no rind removed	BGS	n/a	n/a	n/a	n/a	n/a	n/a	n/a	n/a	n/a	n/a	n/a	n/a	n/a	n/a	n/a	n/a
55/69	Ub806	126.26	0.05	brown no rind removed	BGS	0.51	0.12	6.32	n/a	3.54	7.09	2.24	0.80	0.05	0.20	0.04	21.49	0.59	0.08	0.90	0.04
55/69	Ub807	126.31	0.05	brown no rind removed	BGS	0.50	0.10	6.13	0.21	4.89	9.15	2.31	0.77	0.05	0.07	0.01	19.05	2.94	n/a	0.87	0.04
55/69	Ub808	126.36	0.05	brown no rind removed	BGS	n/a	n/a	n/a	n/a	n/a	n/a	n/a	n/a	n/a	n/a	n/a	n/a	n/a	n/a	n/a	n/a
55/69	Ub809	126.41	0.13	brown no rind removed	BGS	0.51	0.10	6.24	n/a	3.78	7.28	2.28	0.65	0.04	0.08	0.03	19.65	0.78	0.09	0.97	0.03
55/69	Ub810	126.54	0.05	brown no rind removed	BGS	n/a	n/a	n/a	n/a	n/a	n/a	n/a	n/a	n/a	n/a	n/a	n/a	n/a	n/a	n/a	n/a
56a/69	Ub811	126.59	0.05	brown no rind removed	BGS	0.51	0.11	6.38	0.21	2.81	7.86	2.67	0.79	n/a	n/a	0.01	22.71	0.97	0.07	0.96	0.04
56a/69	Ub812	126.64	0.05	brown no rind removed	BGS	0.47	0.10	6.52	0.29	3.30	7.52	2.51	0.87	n/a	n/a	0.01	20.83	0.61	0.08	0.90	0.03
56a/69	Ub813	126.69	0.05	brown no rind removed	BGS	0.51	0.10	6.62	0.15	2.80	7.52	2.67	0.83	n/a	n/a	0.02	22.10	0.71	0.08	1.00	0.04
56a/69	Ub814	126.74	0.04	brown no rind removed	BGS	0.50	0.10	6.86	n/a	3.37	7.03	2.45	0.81	0.06	0.10	0.02	22.16	0.38	0.08	0.98	0.03
56a/69	Ub815	126.78	0.07	brown no rind removed	BGS	n/a	n/a	n/a	n/a	n/a	n/a	n/a	n/a	n/a	n/a	n/a	n/a	n/a	n/a	n/a	n/a

56a/69	Ub816	126.85	0.04	brown no rind removed	BGS	0.50	0.10	6.82	0.24	3.82	7.28	2.37	0.85	0.05	n/a	0.01	22.13	0.29	0.08	0.94	0.04
56a/69	Ub817	126.89	0.03	brown no rind removed	BGS	0.52	0.09	6.26	n/a	4.99	6.39	2.21	0.81	0.03	n/a	n/a	21.50	0.19	0.09	0.94	0.03
56a/69	Ub818	126.92	0.05	brown no rind removed	BGS	n/a	n/a	n/a	n/a	n/a	n/a	n/a	n/a	n/a	n/a	n/a	n/a	n/a	n/a	n/a	n/a
56b/69	Ub819	126.97	0.43	brown no rind removed	BGS	n/a	n/a	n/a	n/a	n/a	n/a	n/a	n/a	n/a	n/a	n/a	n/a	n/a	n/a	n/a	n/a
57/69	Ub820	127.40	0.15	grey/ cream sediment	EM	0.48	0.90	8.41	n/a	5.82	7.27	3.00	1.17	0.07	0.06	0.01	25.59	0.80	0.04	1.02	0.02
57/69	Ub821	127.55	0.05	grey/cream sediment	EM	0.51	0.09	5.05	n/a	5.12	6.34	2.28	0.58	0.06	0.08	n/a	17.87	0.28	0.11	0.99	0.01
57/69	Ub822	127.60	0.05	grey/ cream sediment	EM	n/a	n/a	n/a	n/a	n/a	n/a	n/a	n/a	n/a	n/a	n/a	n/a	n/a	n/a	n/a	n/a
57/69	Ub823	127.65	0.05	grey/cream sediment	EM	n/a	n/a	n/a	n/a	n/a	n/a	n/a	n/a	n/a	n/a	n/a	n/a	n/a	n/a	n/a	n/a
57/69	Ub824	127.70	0.05	brown no rind removed	BGS	0.50	0.10	6.19	n/a	5.16	6.35	2.37	0.72	n/a	n/a	n/a	19.21	0.23	0.11	1.07	0.02
57/69	Ub825	127.75	0.05	grey/ cream sediment	EM	0.50	0.10	5.57	n/a	5.53	6.25	1.95	0.66	0.05	0.07	n/a	18.46	0.28	0.12	0.98	0.01
57/69	Ub826	127.80	0.05	brown no rind removed	BGS	0.49	0.11	6.12	n/a	4.01	6.82	2.32	0.81	0.05	n/a	0.03	20.48	0.34	0.09	1.15	0.02
57/69	Ub827	127.85	0.05	cream/ grey sediment	EM	0.50	0.10	4.64	n/a	4.61	6.22	2.27	0.60	0.02	n/a	n/a	16.53	0.29	0.12	0.97	0.01
57/69	Ub828	127.90	0.05	cream/ grey sediment	EM	0.50	0.09	5.57	n/a	4.94	6.67	2.17	0.58	0.05	0.06	n/a	19.12	0.51	0.10	1.10	0.01
57/69	Ub829	127.95	0.05	cream/ grey sediment	EM	0.48	0.09	5.41	0.31	4.30	6.88	2.35	0.61	0.07	0.07	n/a	17.31	0.42	0.10	1.00	0.01
57/69	Ub830	128.00	0.05	cream/ grey sediment	EM	0.47	0.09	5.12	n/a	4.82	6.85	1.92	0.60	n/a	n/a	n/a	17.33	0.64	0.09	0.87	0.02
57/69	Ub831	128.05	0.05	grey/ cream sediment	EM	0.50	0.10	5.77	n/a	5.20	6.55	2.25	0.70	0.05	n/a	n/a	18.48	0.40	0.10	0.93	0.02
57/69	Ub832	128.10	0.05	cream/ grey sediment/brown no rind removed	EM/BGS	0.52	0.09	7.01	n/a	4.77	6.71	2.43	0.79	n/a	n/a	0.01	21.21	0.33	0.08	0.93	0.03
57/69	Ub833	128.15	0.05			0.50	0.10	4.83	0.26	4.56	5.96	2.08	0.57	0.05	n/a	n/a	16.70	0.32	0.12	0.90	n/a
57/69	Ub834	128.20	0.05	grey/ cream sediment	EM	0.52	0.10	5.22	n/a	5.87	6.05	2.21	0.59	0.06	n/a	n/a	17.38	0.35	0.13	0.88	0.02
57/69	Ub835	128.25	0.05	grey/cream sediment	EM	0.50	0.09	5.31	0.16	4.73	6.27	2.29	0.69	n/a	n/a	n/a	16.94	0.28	0.09	0.94	0.02

57/69	Ub836	128.30	0.05	brown no rind removed	BGS	0.48	0.10	6.92	n/a	4.88	7.42	2.51	0.87	n/a	n/a	0.02	21.07	0.62	0.04	0.93	0.05
57/69	Ub837	128.35	0.11	brown no rind removed	BGS	0.48	0.09	5.67	n/a	4.69	7.35	2.43	0.88	0.07	n/a	n/a	20.66	0.71	0.10	1.06	0.02
58/69	Ub838	128.46	0.05	cream/ grey sediment	EM	0.51	0.09	4.50	0.20	4.96	6.00	2.20	0.57	0.05	0.06	0.03	15.76	0.29	0.11	0.92	n/a
58/69	Ub839	128.51	0.05	cream/ grey sediment	EM	0.50	0.10	5.00	n/a	6.19	5.81	2.28	0.57	0.07	0.07	n/a	16.91	0.24	0.12	0.85	0.02
58/69	Ub840	128.56	0.05	cream/ grey sediment	IV	0.49	0.09	4.42	0.22	6.48	5.95	2.13	0.57	0.06	0.12	0.03	15.80	0.18	0.15	0.91	0.00
58/69	Ub841	128.61	0.05	cream/grey sediment	IV	0.50	0.09	4.58	n/a	4.40	5.67	2.13	0.51	n/a	0.07	0.03	15.74	0.18	0.12	0.86	0.01
58/69	Ub842	128.66	0.05	cream/ grey sediment	IV	0.51	0.10	4.62	n/a	6.75	5.98	2.15	0.54	0.05	n/a	n/a	15.78	0.34	0.13	0.95	n/a
58/69	Ub843	128.71	0.05	cream/ grey sediment	IV	0.50	0.11	3.73	0.16	5.86	5.56	2.05	0.41	0.08	n/a	0.03	13.54	0.25	0.13	0.84	n/a
58/69	Ub844	128.76	0.05	cream/ grey sediment	IV	0.51	0.11	3.80	0.27	4.83	5.43	1.91	0.46	0.05	n/a	n/a	13.82	0.20	0.11	0.78	0.00
58/69	Ub845	128.81	0.05	cream/ grey sediment	IV	0.52	0.10	3.79	0.20	5.15	5.85	2.01	0.37	0.05	n/a	0.02	14.79	0.20	0.12	0.85	n/a
58/69	Ub846	128.86	0.05	cream/ grey sediment	IV	0.51	0.11	3.68	0.20	4.46	5.43	1.99	0.49	0.05	n/a	n/a	14.01	0.25	0.11	0.73	n/a
58/69	Ub847	128.91	0.05	cream/ grey sediment	EM	0.50	0.10	4.67	n/a	5.76	5.92	2.29	0.59	0.05	n/a	n/a	16.99	0.24	0.12	0.98	n/a
58/69	Ub848	128.96	0.05	cream/ grey **removed mud**	IV	0.50	0.10	4.49	0.24	5.50	5.81	2.10	0.53	0.07	0.07	n/a	15.35	0.20	0.12	0.83	0.01
58/69	Ub849	129.01	0.05	cream/ grey **removed mud**	IV	0.52	0.10	4.43	n/a	5.38	6.07	2.27	0.59	0.04	n/a	n/a	16.51	0.30	0.12	0.89	0.02
58/69	Ub850	129.06	0.05	cream/ grey sediment **removed mud**	IV	0.53	0.11	4.11	n/a	5.49	5.65	2.13	0.48	0.06	n/a	n/a	14.58	0.16	0.11	0.80	0.01
58/69	Ub851	129.11	0.05	light cream	IV	0.50	0.10	4.62	n/a	5.76	6.06	2.24	0.58	0.06	n/a	n/a	16.02	0.18	0.11	0.81	0.01
58/69	Ub852	129.16	0.05	light cream grey **removed mud**	IV	0.50	0.09	4.71	n/a	4.94	6.74	2.26	0.60	0.05	n/a	n/a	16.93	0.42	0.11	0.95	0.03
58/69	Ub853	129.21	0.05	cream/ grey sediment **drilling mud removed**	IV	0.52	0.12	4.33	n/a	4.64	5.82	2.09	0.51	0.04	n/a	n/a	15.82	0.19	0.10	0.90	0.03
58/69	Ub854	129.26	0.08	cream/ grey sediment	EM	0.50	0.10	4.42	0.21	5.57	6.39	2.03	0.57	0.04	0.06	n/a	15.96	0.40	0.12	0.95	n/a

59/69	Ub855	129.34	0.05	cream/ grey sediment bioturbated-copper	UL	0.51	0.11	3.89	n/a	3.12	6.69	2.10	0.46	0.04	0.09	n/a	15.25	0.74	0.08	0.92	0.04
59/69	Ub856	129.39	0.05	cream/ grey sediment	IV	0.48	0.10	5.32	n/a	3.75	8.01	2.34	0.69	n/a	n/a	n/a	19.37	1.19	0.08	0.99	0.03
59/69	Ub857	129.44	0.05	cream/ grey **removed drilling mud**	EM	0.50	0.11	5.75	n/a	4.46	6.96	2.19	0.69	0.05	n/a	n/a	19.94	0.23	0.09	1.01	0.02
59/69	Ub858	129.49	0.05	cream/ grey sediment	IV	0.51	0.10	4.50	n/a	2.71	7.43	2.30	0.57	n/a	n/a	0.02	18.12	0.57	0.07	0.99	0.04
59/69	Ub859	129.54	0.05	braun grey sediment **removed drilling mud**	IV	0.50	0.09	5.38	n/a	4.84	6.34	2.26	0.66	0.06	0.06	n/a	18.43	0.27	0.09	0.93	0.03
59/69	Ub860	129.59	0.05	cream/ grey sediment	EM	n/a	n/a	n/a	n/a	n/a	n/a	n/a	n/a	n/a	n/a	n/a	n/a	n/a	n/a	n/a	n/a
59/69	Ub861	129.64	0.05	cream/ grey sediment	IV	0.49	0.11	4.93	n/a	5.22	7.00	2.12	0.63	0.05	n/a	n/a	17.87	0.30	0.11	0.95	0.03
59/69	Ub862	129.69	0.05	cream/ grey sediment	EM	n/a	n/a	n/a	n/a	n/a	n/a	n/a	n/a	n/a	n/a	n/a	n/a	n/a	n/a	n/a	n/a
59/69	Ub863	129.74	0.05	cream/ grey **a lot of drilling mud removed**	EM	0.48	0.09	4.56	0.32	5.85	6.28	1.78	0.50	N/A	0.10	N/A	16.74	0.31	0.13	0.83	0.00
59/69	Ub864	129.79	0.05	cream/ grey **removed drilling mud**	EM	0.53	0.10	5.96	0.31	6.35	6.46	2.40	0.67	0.05	0.12	0.01	19.81	0.21	0.13	0.92	0.00
59/69	Ub865	129.84	0.05	cream/ grey **removed drilling mud**	EM	0.53	0.09	5.49	n/a	5.26	6.96	2.30	0.70	0.06	n/a	n/a	19.23	0.38	0.11	0.99	0.01
59/69	Ub866	129.89	0.05	cream/ grey removed **tiny bit of drilling mud**	IV	0.48	0.09	5.58	n/a	5.53	6.47	2.38	0.77	0.03	0.09	n/a	19.78	0.32	0.11	1.00	0.03
59/69	Ub867	129.94	0.05	cream grey sediment	EM	0.49	0.10	4.63	n/a	6.40	5.92	1.96	0.57	0.05	0.16	0.02	16.10	0.36	0.13	0.84	n/a
59/69	Ub868	129.99	0.05	cream grey sediment	IV	0.49	0.09	5.68	0.30	6.27	6.68	2.22	0.72	0.05	n/a	n/a	19.74	0.49	0.11	1.01	0.03
59/69	Ub869	130.04	0.05	cream/ grey sediment	IV	0.52	0.10	5.48	0.26	6.23	6.30	2.36	0.65	0.06	n/a	0.03	17.57	0.34	0.13	0.87	0.01
59/69	Ub870	130.09	0.13	cream/ grey sediment	EM	0.53	0.11	4.96	n/a	5.84	6.56	1.97	0.60	0.06	n/a	0.02	16.47	0.45	0.11	0.86	0.01

60/69	Ub871	130.22	0.05	cream grey sediment	IV	0.51	0.10	5.56	n/a	4.34	7.59	2.17	0.80	0.03	0.06	n/a	18.81	1.14	0.10	0.89	0.03
60/69	Ub872	130.27	0.05	grey/ cream sediment	IV	n/a	n/a	n/a	n/a	n/a	n/a	n/a	n/a	n/a	n/a	n/a	n/a	n/a	n/a	n/a	n/a
60/69	Ub873	130.32	0.05	grey/ cream sediment	IV	0.50	0.09	5.83	n/a	3.64	6.93	2.20	0.69	0.04	0.05	n/a	20.46	0.68	0.08	0.91	0.04
60/69	Ub874	130.37	0.05	grey/ cream sediment	IV	0.52	0.09	5.39	0.19	3.39	6.94	2.42	0.79	0.03	0.06	0.03	19.93	0.63	0.08	0.99	0.03
60/69	Ub875	130.42	0.05	grey/ cream sediment	IV	0.51	0.10	5.50	n/a	3.94	6.93	2.50	0.68	0.04	n/a	n/a	19.46	0.40	0.09	1.00	0.03
60/69	Ub876	130.47	0.05	grey/ cream sediment	IV	0.50	0.10	5.42	n/a	3.50	7.31	2.20	0.60	0.04	n/a	n/a	18.65	0.61	0.09	0.97	0.03
60/69	Ub877	130.52	0.05	grey/ cream sediment	IV	0.51	0.10	5.04	n/a	3.75	6.83	2.27	0.76	n/a	n/a	n/a	19.21	0.44	0.09	0.94	0.04
60/69	Ub878	130.57	0.05	grey/ cream sediment	IV	0.49	0.10	5.05	n/a	3.41	6.69	2.26	0.67	n/a	0.05	n/a	18.19	0.46	0.09	1.03	0.03
60/69	Ub879	130.62	0.05	grey/ cream sediment	IV	0.50	0.10	5.18	n/a	4.69	7.30	2.33	0.78	0.05	n/a	n/a	19.63	0.53	0.10	1.03	0.03
60/69	Ub880	130.67	0.05	grey/ cream --> **removed mud**	IV	0.51	0.10	4.82	0.21	3.99	6.59	2.34	0.55	0.04	n/a	n/a	17.47	0.39	0.09	0.95	0.03
60/69	Ub881	130.72	0.05	grey/ cream sediment	IV	0.49	0.09	5.21	0.18	5.07	6.88	2.27	0.62	0.05	n/a	n/a	18.02	0.72	0.10	0.97	0.01
60/69	Ub882	130.77	0.05	grey/	IV	0.50	0.12	4.31	n/a	4.42	6.84	2.17	0.55	n/a	0.06	n/a	17.82	0.68	0.10	0.93	0.02
60/69	Ub883	130.82	0.05	grey/ cream --> **removed mud**	IV	0.50	0.09	5.34	0.24	3.96	6.96	2.33	0.69	n/a	n/a	n/a	19.36	0.47	0.09	1.03	0.02
60/69	Ub884	130.87	0.05	grey/ cream	IV	0.49	0.10	5.43	0.14	3.13	6.93	2.26	0.66	n/a	n/a	0.04	20.04	0.42	0.09	1.05	0.03
60/69	Ub885	130.92	4.03	grey/ cream sediment --**>removed mud**	IV	0.50	0.10	5.04	n/a	4.14	6.34	2.40	0.64	0.03	0.06	n/a	17.63	0.35	0.10	0.92	0.03
61/69	Ub886	134.95	0.05	grey sediment	IV	0.51	0.11	4.14	n/a	4.00	6.16	2.22	0.51	0.03	n/a	n/a	16.15	0.60	0.09	0.75	0.03
61/69	Ub887	135.00	0.1	grey sediment	IV	0.48	0.10	4.65	0.21	3.88	6.74	2.01	0.63	n/a	n/a	n/a	16.65	0.89	0.08	0.81	0.02
61/69	Ub888	135.10	0.05	grey sediment	IV	0.48	0.10	4.12	n/a	4.57	6.26	2.04	0.57	0.05	n/a	n/a	16.39	0.66	0.09	0.77	0.02
61/69	Ub889	135.15	0.05	grey sediment	IV	n/a	n/a	n/a	n/a	n/a	n/a	n/a	n/a	n/a	n/a	n/a	n/a	n/a	n/a	n/a	n/a
61/69	Ub890	135.20	0.05	grey sediment red stain	IV	0.53	0.09	5.10	n/a	3.28	7.12	2.20	0.57	0.03	n/a	0.04	17.33	0.97	0.07	0.95	0.04
61/69	Ub891	135.25	0.05	grey sediment	IV	0.59	0.10	5.00	n/a	4.48	7.16	2.19	0.64	0.03	0.08	n/a	18.35	0.59	0.11	0.90	0.01
61/69	Ub892	135.30	0.05	grey sediment	IV	0.50	0.11	4.42	0.21	4.52	6.61	1.95	0.55	0.05	n/a	0.02	16.39	0.58	0.12	0.89	0.02

61/69	Ub893	135.35	0.05		IV	0.52	0.10	3.69	n/a	3.63	6.76	1.50	0.36	n/a	n/a	0.03	13.53	1.32	0.11	0.81	n/a
61/69	Ub894	135.40	0.05	grey sediment --> **removed mud**	IV	n/a	n/a	n/a	n/a	n/a	n/a	n/a	n/a	n/a	n/a	n/a	n/a	n/a	n/a	n/a	n/a
61/69	Ub895	135.45	0.05	grey sediment	IV	0.52	0.10	5.32	n/a	4.10	7.38	2.14	0.59	n/a	0.06	n/a	18.04	1.17	0.10	0.95	0.02
61/69	Ub896	135.50	0.12	grey sediment	IV	0.48	0.09	4.30	n/a	5.01	6.61	1.94	0.58	n/a	0.11	0.02	17.21	0.62	0.11	0.94	0.01
62/69	Ub897	135.62	0.05	grey sediment	EM	n/a	n/a	n/a	n/a	n/a	n/a	n/a	n/a	n/a	n/a	n/a	n/a	n/a	n/a	n/a	n/a
62/69	Ub898	135.67	0.05	grey sediment	EM	n/a	n/a	n/a	n/a	n/a	n/a	n/a	n/a	n/a	n/a	n/a	n/a	n/a	n/a	n/a	n/a
62/69	Ub899	135.72	0.05	grey/ cream sediment, red band and **mud removed**	EM	0.49	0.09	4.18	n/a	3.66	6.08	2.23	0.53	0.03	n/a	n/a	16.46	0.34	0.09	0.87	0.03
62/69	Ub900	135.77	0.05	grey/ cream sediment	EM	n/a	n/a	n/a	n/a	n/a	n/a	n/a	n/a	n/a	n/a	n/a	n/a	n/a	n/a	n/a	n/a
62/69	Ub901	135.82	0.05	grey/ cream sediment	EM	0.51	0.09	5.22	n/a	3.15	7.21	2.36	0.73	n/a	n/a	n/a	18.91	0.86	0.06	0.92	0.05
62/69	Ub902	135.87	0.05	grey/ cream sediment	EM	n/a	n/a	n/a	n/a	n/a	n/a	n/a	n/a	n/a	n/a	n/a	n/a	n/a	n/a	n/a	n/a
62/69	Ub903	135.92	0.05	grey/ cream sediment	EM	n/a	n/a	n/a	n/a	n/a	n/a	n/a	n/a	n/a	n/a	n/a	n/a	n/a	n/a	n/a	n/a
62/69	Ub904	135.97	0.05	grey/ cream sediment	EM	0.51	0.10	5.01	0.14	3.64	7.02	2.31	0.74	n/a	n/a	0.03	18.96	0.70	0.09	0.95	0.03
62/69	Ub905	136.02	0.05	grey sediment	EM	n/a	n/a	n/a	n/a	n/a	n/a	n/a	n/a	n/a	n/a	n/a	n/a	n/a	n/a	n/a	n/a
62/69	Ub906	136.07	0.05	grey/ cream sediment	EM	0.52	0.13	4.93	n/a	4.35	6.15	2.10	0.64	0.03	0.05	n/a	18.45	0.30	0.09	0.95	0.01
62/69	Ub907	136.12	0.1	grey sediment	EM	n/a	n/a	n/a	n/a	n/a	n/a	n/a	n/a	n/a	n/a	n/a	n/a	n/a	n/a	n/a	n/a
62/69	Ub908	136.22	0.05	grey/ cream sediment	EM	n/a	n/a	n/a	n/a	n/a	n/a	n/a	n/a	n/a	n/a	n/a	n/a	n/a	n/a	n/a	n/a
62/69	Ub909	136.27	0.05	grey/ cream sediment	EM	0.47	0.10	4.38	n/a	6.65	6.29	1.85	0.62	0.04	n/a	0.02	17.23	0.58	0.14	0.80	0.00
62/69	Ub910	136.32	0.03	grey/ cream sediment	EM	0.53	0.11	4.12	0.31	7.92	6.51	1.99	0.65	0.06	0.29	0.02	16.81	1.01	0.15	0.79	n/a
63/69	Ub911	136.35	0.05	grey/ green sediment	IV	n/a	n/a	n/a	n/a	n/a	n/a	n/a	n/a	n/a	n/a	n/a	n/a	n/a	n/a	n/a	n/a
63/69	Ub912	136.40	0.05	grey/ cream sediment	EM	n/a	n/a	n/a	n/a	n/a	n/a	n/a	n/a	n/a	n/a	n/a	n/a	n/a	n/a	n/a	n/a
63/69	Ub913	136.45	0.05	grey sediment	IV	0.52	0.09	5.11	0.32	6.68	6.61	1.99	0.83	0.06	0.07	0.01	19.67	0.45	0.13	0.99	0.00

63/69	Ub914	136.50	0.05	grey sediment --> **removed mud**	IV	0.54	0.09	5.33	n/a	4.97	6.97	2.32	0.82	0.05	n/a	n/a	20.11	0.70	0.09	1.03	0.02
63/69	Ub915	136.55	0.05	grey sediment --> **removed mud**	IV	0.53	0.15	3.87	0.24	5.63	5.56	1.80	0.51	n/a	n/a	n/a	15.36	0.26	0.14	0.83	n/a
63/69	Ub916	136.60	0.05	grey sediment	EM	0.52	0.10	4.22	n/a	5.31	6.25	2.06	0.57	0.04	n/a	n/a	17.10	0.37	0.13	0.82	0.01
63/69	Ub917	136.65	0.05	grey sediment	IV	0.51	0.10	5.25	n/a	6.01	6.25	2.30	0.71	n/a	n/a	0.02	19.75	0.24	0.11	0.86	0.03
63/69	Ub918	136.70	0.05	grey sediment --> **removed mud**	IV	0.51	0.10	4.97	0.31	5.76	6.47	2.11	0.71	0.06	0.05	0.03	19.29	0.44	0.13	0.78	0.00
63/69	Ub919	136.75	0.05	grey sediment	IV	0.47	0.10	5.17	n/a	7.27	6.40	2.31	0.76	n/a	n/a	n/a	20.29	0.33	0.13	0.83	0.02
63/69	Ub920	136.80	0.05	grey/ cream --> **removed mud**	IV	0.51	0.10	5.43	n/a	7.40	6.66	2.26	0.72	0.06	0.08	0.01	19.69	0.38	0.14	0.92	0.02
63/69	Ub921	136.85	0.05	pale grey/ cream sed --> **removed mud**	IV	0.51	0.10	5.52	n/a	7.90	6.74	2.27	0.90	n/a	0.08	n/a	19.74	0.58	0.13	0.93	0.01
63/69	Ub922	136.90	0.1	grey/ cream sediment	EM	0.50	0.10	4.35	n/a	5.51	6.91	2.01	0.68	0.04	n/a	n/a	16.76	0.91	0.11	0.86	0.01
63/69	Ub923	137.00	0.05	grey/ cream sediment --> **removed mud**	IV	0.50	0.10	4.78	0.19	6.59	6.70	2.11	0.74	n/a	n/a	n/a	17.70	0.39	0.14	0.88	n/a
63/69	Ub924	137.05	0.05	grey/ cream sediment	IV	n/a	n/a	n/a	n/a	n/a	n/a	n/a	n/a	n/a	n/a	n/a	n/a	n/a	n/a	n/a	n/a
63/69	Ub925	137.10	0.04	grey/cream sediment	EM	n/a	n/a	n/a	n/a	n/a	n/a	n/a	n/a	n/a	n/a	n/a	n/a	n/a	n/a	n/a	n/a
64/69	Ub926	137.14	0.05	pale grey/ cream sediment	EM	n/a	n/a	n/a	n/a	n/a	n/a	n/a	n/a	n/a	n/a	n/a	n/a	n/a	n/a	n/a	n/a
64/69	Ub927	137.19	0.05	pale grey/ cream sediment	EM	n/a	n/a	n/a	n/a	n/a	n/a	n/a	n/a	n/a	n/a	n/a	n/a	n/a	n/a	n/a	n/a
64/69	Ub928	137.24	0.05	pale grey/ cream sediment	EM	0.51	0.11	4.82	0.26	4.63	6.50	2.20	0.64	0.05	n/a	n/a	17.41	0.39	0.10	0.88	0.02
64/69	Ub929	137.29	0.05	grey/ cream sediment	EM	0.51	0.10	4.54	n/a	7.69	6.15	2.04	0.70	n/a	0.05	n/a	16.85	0.41	0.13	0.90	0.02
64/69	Ub930	137.34	0.05	pale grey/ cream sediment	EM	0.48	0.10	4.50	0.26	7.62	6.52	2.13	0.69	n/a	0.07	0.03	17.97	0.29	0.15	0.88	0.01
64/69	Ub931	137.39	0.05	pale grey/ cream sediment	EM	0.50	0.10	4.63	n/a	6.47	6.42	2.33	0.68	0.04	n/a	0.02	18.63	0.41	0.13	0.95	0.01
64/69	Ub932	137.44	0.05	pale grey/ cream --> **drilling mud removed**	EM	n/a	n/a	n/a	n/a	n/a	n/a	n/a	n/a	n/a	n/a	n/a	n/a	n/a	n/a	n/a	n/a

64/69	Ub933	137.49	0.05	grey/cream sediment	EM	n/a	n/a	n/a	n/a	n/a	n/a	n/a	n/a	n/a	n/a	n/a	n/a	n/a	n/a	n/a
64/69	Ub934	137.54	0.05	pale grey/ cream sediment	EM	0.54	0.10	4.48	0.29	6.50	6.58	2.03	0.68	0.04	n/a	0.02	17.93	0.40	0.14	0.88	0.02
64/69	Ub935	137.59	0.1	pale grey/ white sediment	EM	0.46	0.12	4.59	0.20	7.89	6.15	2.26	0.66	0.05	n/a	0.03	16.84	0.45	0.15	0.93	0.00
64/69	Ub936	137.69	0.05	pale grey/ cream sediment	EM	0.50	0.10	4.41	n/a	6.48	6.31	2.06	0.67	0.06	n/a	n/a	17.36	0.35	0.14	0.83	n/a
64/69	Ub937	137.74	0.05	pale grey/ white --> **removed red band**	EM	0.54	0.14	4.74	n/a	6.93	6.49	2.17	0.67	n/a	0.06	n/a	18.26	0.43	0.13	0.80	0.00
64/69	Ub938	137.79	0.05	grey/cream sediment	EM	n/a	n/a	n/a	n/a	n/a	n/a	n/a	n/a	n/a	n/a	n/a	n/a	n/a	n/a	n/a	n/a
64/69	Ub939	137.84	0.1	pale grey/ cream sediment	EM	0.48	0.11	3.75	0.26	6.62	5.74	1.83	0.56	n/a	n/a	n/a	15.43	0.20	0.14	0.80	n/a
64/69	Ub940	137.94	0.05	pale grey/ cream sediment	EM	n/a	n/a	n/a	n/a	n/a	n/a	n/a	n/a	n/a	n/a	n/a	n/a	n/a	n/a	n/a	n/a
64/69	Ub941	137.99	5.75	pale grey/ cream - thin **red band**	EM	0.46	0.12	3.97	b/a	5.88	6.43	2.02	0.58	0.05	0.09	0.02	16.06	0.53	0.12	0.86	0.01
65/69	Ub942	143.74	0.05	pale grey/ white sediment	IV	n/a	n/a	n/a	n/a	n/a	n/a	n/a	n/a	n/a	n/a	n/a	n/a	n/a	n/a	n/a	n/a
65/69	Ub943	143.79	0.05	pale grey/ white sediment	IV	n/a	n/a	n/a	n/a	n/a	n/a	n/a	n/a	n/a	n/a	n/a	n/a	n/a	n/a	n/a	n/a
65/69	Ub944	143.84	0.05	pale grey/ white sediment	IV	0.51	0.10	2.90	n/a	13.11	4.17	2.19	0.77	0.14	0.08	n/a	22.77	1.13	0.06	0-.34	0.02
65/69	Ub945	143.89	0.05	pale grey/ white sediment - **mud removed**	IV	n/a	n/a	n/a	n/a	n/a	n/a	n/a	n/a	n/a	n/a	n/a	n/a	n/a	n/a	n/a	n/a
65/69	Ub946	143.94	0.05	pale grey/white sediment - **bioturbation**	IV	0.50	0.10	3.08	n/a	15.97	4.59	2.10	0.58	0.10	0.07	n/a	17.06	0.39	0.17	0.52	0.00
65/69	Ub947	143.99	0.05	pale grey/ white sediment	IV	n/a	n/a	n/a	n/a	n/a	n/a	n/a	n/a	n/a	n/a	n/a	n/a	n/a	n/a	n/a	n/a
65/69	Ub948	144.04	0.05	pale grey/ white sediment	IV	n/a	n/a	n/a	n/a	n/a	n/a	n/a	n/a	n/a	n/a	n/a	n/a	n/a	n/a	n/a	n/a
65/69	Ub949	144.09	0.05	pale grey/ white sediment	IV	0.51	0.10	3.32	n/a	15.92	4.17	2.18	0.52	0.13	n/a	n/a	17.39	0.06	0.14	0.35	n/a
65/69	Ub950	144.14	0.05	pale grey/ white sediment	IV	n/a	n/a	n/a	n/a	n/a	n/a	n/a	n/a	n/a	n/a	n/a	n/a	n/a	n/a	n/a	n/a

65/69	Ub951	144.19	0.01	pale grey/ white sediment	IV	0.51	0.20	2.97	n/a	12.37	4.91	1.81	0.57	0.11	n/a	0.02	12.93	0.14	0.17	0.41	n/a
66/69	Ub952	144.20	0.05	pale grey/ white sediment	IV	n/a	n/a	n/a	n/a	n/a	n/a	n/a	n/a	n/a	n/a	n/a	n/a	n/a	n/a	n/a	n/a
66/69	Ub953	144.25	0.05	pale grey/ White --> **removed mud**	IV	0.51	0.10	2.73	n/a	10.65	5.69	1.20	0.51	0.07	n/a	n/a	12.04	0.14	0.18	0.52	n/a
66/69	Ub954	144.30	0.05	pale grey/ white sediment	IV	0.52	0.10	3.61	0.27	10.50	6.97	1.26	0.69	0.06	n/a	n/a	14.35	0.41	0.12	0.45	0.03
66/69	Ub955	144.35	0.05	pale grey sediment	IV	0.53	0.11	3.66	0.38	10.63	6.54	1.32	0.70	0.07	n/a	n/a	13.49	0.20	0.14	0.51	0.00
66/69	Ub956	144.40	0.05	pale grey	IV	0.52	0.12	3.46	n/a	11.39	6.76	1.30	0.68	0.07	n/a	n/a	12.78	0.48	0.17	0.45	n/a
66/69	Ub957	144.45	0.05	pale grey/ cream	IV	n/a	n/a	n/a	n/a	n/a	n/a	n/a	n/a	n/a	n/a	n/a	n/a	n/a	n/a	n/a	n/a
66/69	Ub958	144.50	0.05	pale grey/ cream	IV	0.52	0.10	3.62	0.33	12.33	6.30	1.95	0.77	0.06	0.10	n/a	15.69	0.31	0.16	0.53	n/a
66/69	Ub959	144.55	0.05	pale grey sediment - **burrow red**	IV	n/a	n/a	n/a	n/a	n/a	n/a	n/a	n/a	n/a	n/a	n/a	n/a	n/a	n/a	n/a	n/a
66/69	Ub960	144.60	0.05	pale grey sediment --> **removed mud**	IV	0.51	0.10	3.54	0.38	9.19	6.28	1.70	0.63	0.04	0.05	0.02	14.99	0.21	0.15	0.42	n/a
66/69	Ub961	144.65	0.05	pale grey sediment	IV	0.49	0.10	3.93	n/a	9.39	6.72	1.90	0.72	n/a	n/a	n/a	17.13	0.30	0.14	0.51	0.00
66/69	Ub962	144.70	0.05	pale grey --> **removed mud**	IV	n/a	n/a	n/a	n/a	n/a	n/a	n/a	n/a	n/a	n/a	n/a	n/a	n/a	n/a	n/a	n/a
66/69	Ub963	144.75	0.05	pale grey/ white sediment	IV	n/a	n/a	n/a	n/a	n/a	n/a	n/a	n/a	n/a	n/a	n/a	n/a	n/a	n/a	n/a	n/a
66/69	Ub964	144.80	0.05	pale grey sediment	IV	0.55	0.10	3.70	0.35	12.33	6.92	1.82	0.79	0.08	0.07	n/a	15.23	n/a	0.17	0.54	n/a
66/69	Ub965	144.85	0.05	pale grey sediment	IV	n/a	n/a	n/a	n/a	n/a	n/a	n/a	n/a	n/a	n/a	n/a	n/a	n/a	n/a	n/a	n/a
66/69	Ub966	144.90	0.05	pale grey/white sediment	IV	n/a	n/a	n/a	n/a	n/a	n/a	n/a	n/a	n/a	n/a	n/a	n/a	n/a	n/a	n/a	n/a
66/69	Ub967	144.95	0.05	pale grey sediment	IV	0.48	0.10	2.98	n/a	16.92	4.37	2.01	0.59	0.09	0.53	n/a	14.74	0.40	0.21	0.49	n/a
66/69	Ub968	145.00	0.09	pale grey	IV	0.53	0.10	3.22	0.30	15.60	4.33	2.10	0.63	0.10	n/a	0.01	17.39	n/a	0.18	0.42	0.00
66/69	Ub969	145.09	0.2	pale grey	IV	0.50	0.10	3.77	n/a	12.75	6.60	1.62	0.80	0.08	n/a	n/a	16.26	0.24	0.05	0.44	0.05
67/69	Ub970	145.29	0.05	pale grey	IV	0.53	0.10	3.08	0.10	14.80	4.87	2.07	0.69	0.08	n/a	0.01	18.08	0.12	0.12	0.52	0.01
67/69	Ub971	145.34	0.05	pale grey sediment	IV	n/a	n/a	n/a	n/a	n/a	n/a	n/a	n/a	n/a	n/a	n/a	n/a	n/a	n/a	n/a	n/a

67/69	Ub972	145.39	0.15	grey/ cream sediment	IV	0.49	0.10	1.76	n/a	16.67	3.12	1.46	0.32	0.09	n/a	n/a	16.93	0.11	0.12	0.26	n/a
67/69	Ub973	145.54	0.05	grey/ green sediment	IV	n/a	n/a	n/a	n/a	n/a	n/a	n/a	n/a	n/a	n/a	n/a	n/a	n/a	n/a	n/a	n/a
67/69	Ub974	145.59	0.1	grey/ cream sediment	IV	n/a	n/a	n/a	n/a	n/a	n/a	n/a	n/a	n/a	n/a	n/a	n/a	n/a	n/a	n/a	n/a
67/69	Ub975	145.69	0.05	grey/ cream sediment	IV	0.47	0.11	2.96	0.18	16.15	5.10	1.96	0.55	0.09	n/a	n/a	15.42	0.08	0.14	0.45	n/a
67/69	Ub976	145.74	0.05	pale grey sediment	IV	0.49	0.10	3.19	n/a	15.90	5.17	1.79	0.60	0.06	n/a	n/a	13.81	0.14	0.18	0.53	n/a
67/69	Ub977	145.79	0.1	pale grey sediment	IV	0.49	0.10	1.50	n/a	33.45	1.87	1.06	0.40	0.14	0.12	n/a	13.39	0.15	0.06	0.30	0.03
67/69	Ub978	145.89	0.05	pale grey sediment	IV	0.47	0.10	1.78	n/a	35.17	2.15	1.47	0.58	0.14	0.16	n/a	11.40	n/a	0.07	0.40	0.02
67/69	Ub979	145.94	0.05	pale grey/white	IV	0.47	0.10	2.00	0.17	29.49	2.67	1.33	0.46	0.09	0.21	n/a	13.12	0.08	0.07	0.22	0.03
67/69	Ub980	145.99		pale grey/white	IV	n/a	n/a	n/a	n/a	n/a	n/a	n/a	n/a	n/a	n/a	n/a	n/a	n/a	n/a	n/a	n/a

Appendix 2 - Core pictures of Site 16/28 - sb01

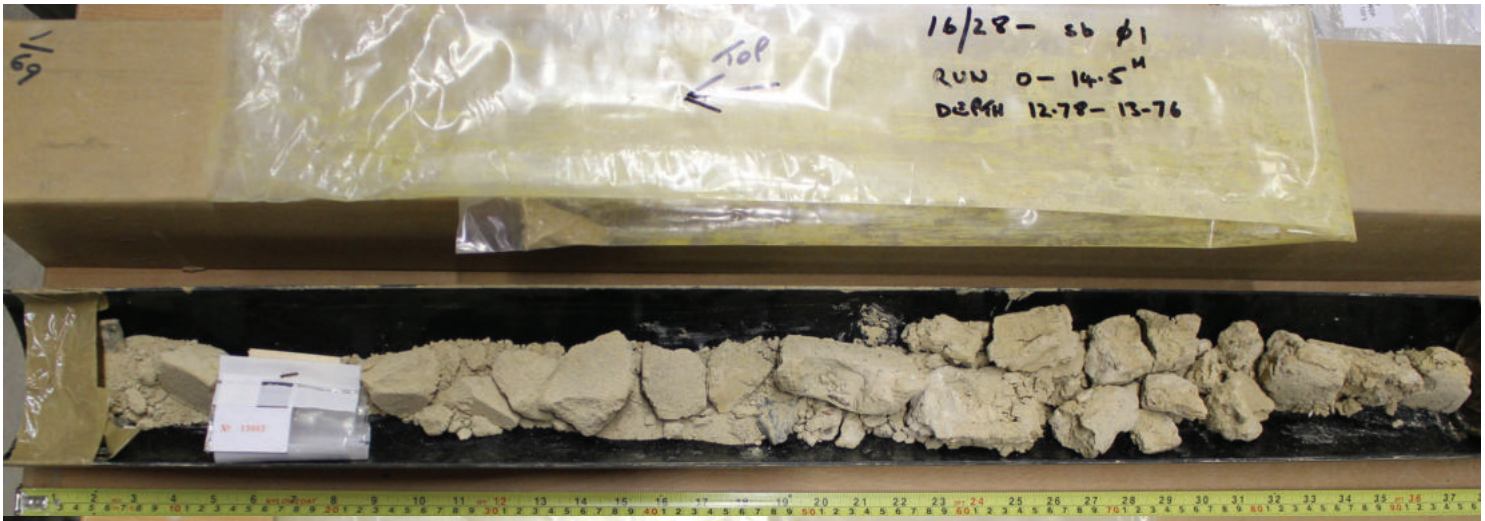

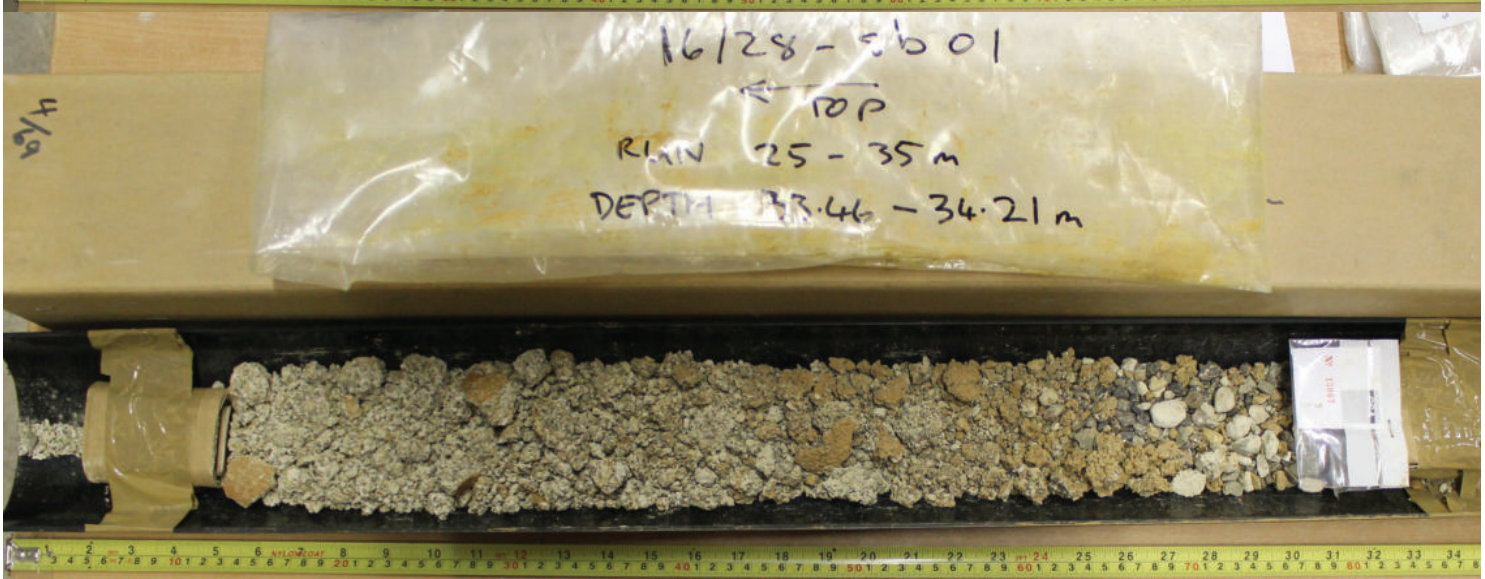


TOP
16/28-SB01
RUN 25-35.0m
DEPTH 36.21 - 35.0m
5/6
16/28-SB01
TOP
RUN 35.0 - 44.0m
DEPTH 40.77 - 41.59m
6/6
16/28-SB01
TOP
RUN 35.0 - 44.0m
DEPTH 41.59 - 42.42m
7/6


16/28-sb01
TOP
RUN 35.0 - 44.0m
DEPTH 42.62 - 43.26m
69/8
16/28-sb01
TOP
RUN 35.0 - 44.0m
DEPTH 43.26 - 44.0m
69/9
16/28-sb01
TOP
RUN 44.0 - 54.0m
DEPTH 52.44 - 53.30m
69/10

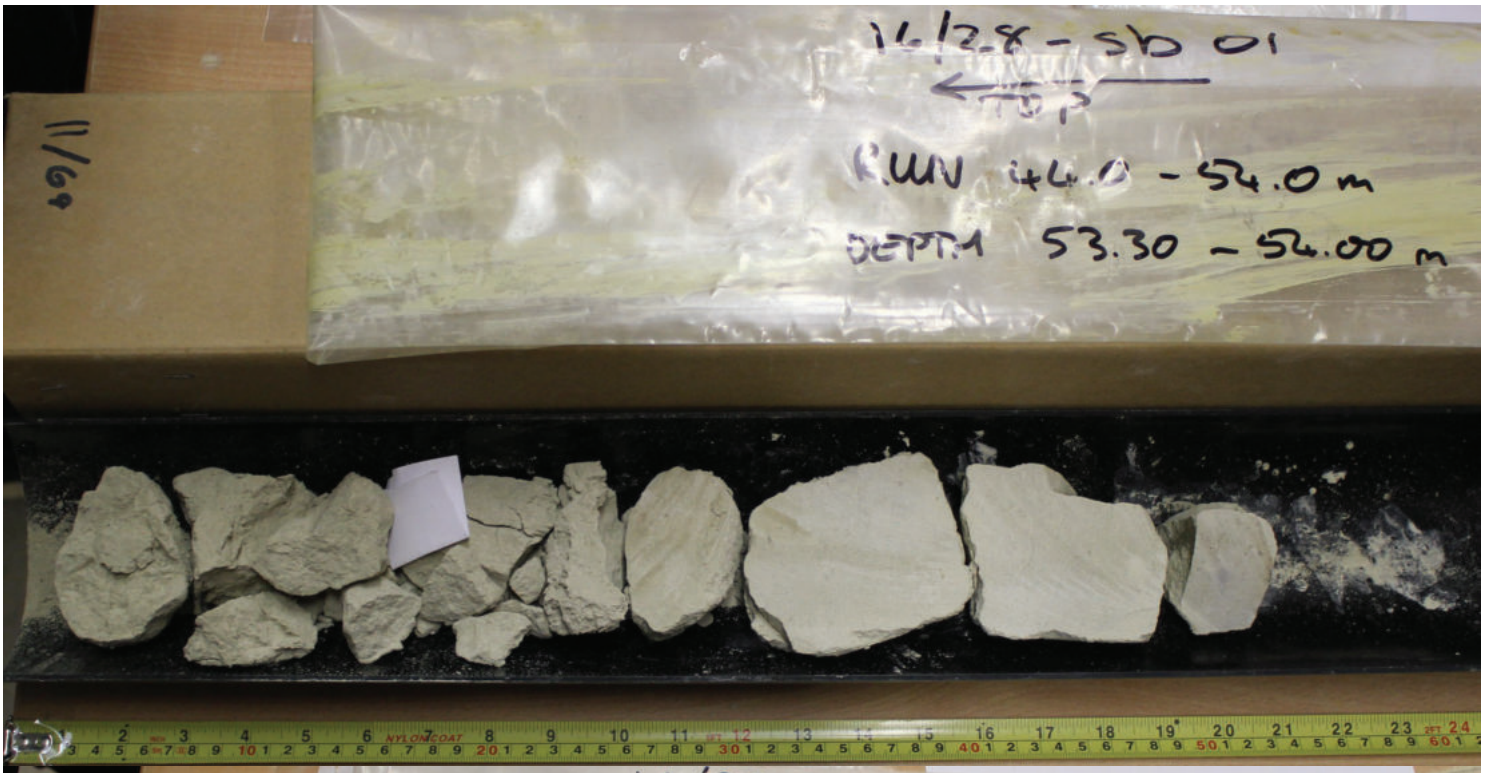
16/28 - SB 01
TOP
RUN 44.0 - 54.0 m
DEPTH 53.30 - 54.00 m
11/69


16/28 - SB01
TOP
RUN: 54 - 60.8m
Depths: 60.52 - 60.80m
TOP
RUN: 60.8 → 71m.
Depths: 66.21 - 66.62m
GAP HERE?
7.3.16
BIRMINGHAM
12/69

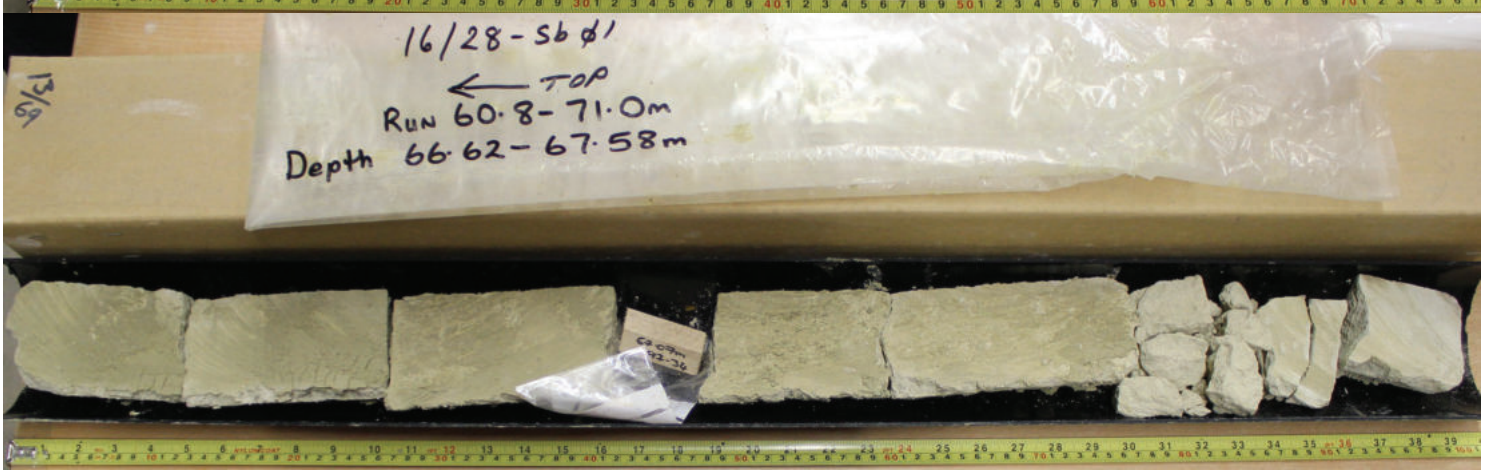
16/28 - SB 01
TOP
RUN 60.8 - 71.0m
Depth 66.62 - 67.58m
13/69

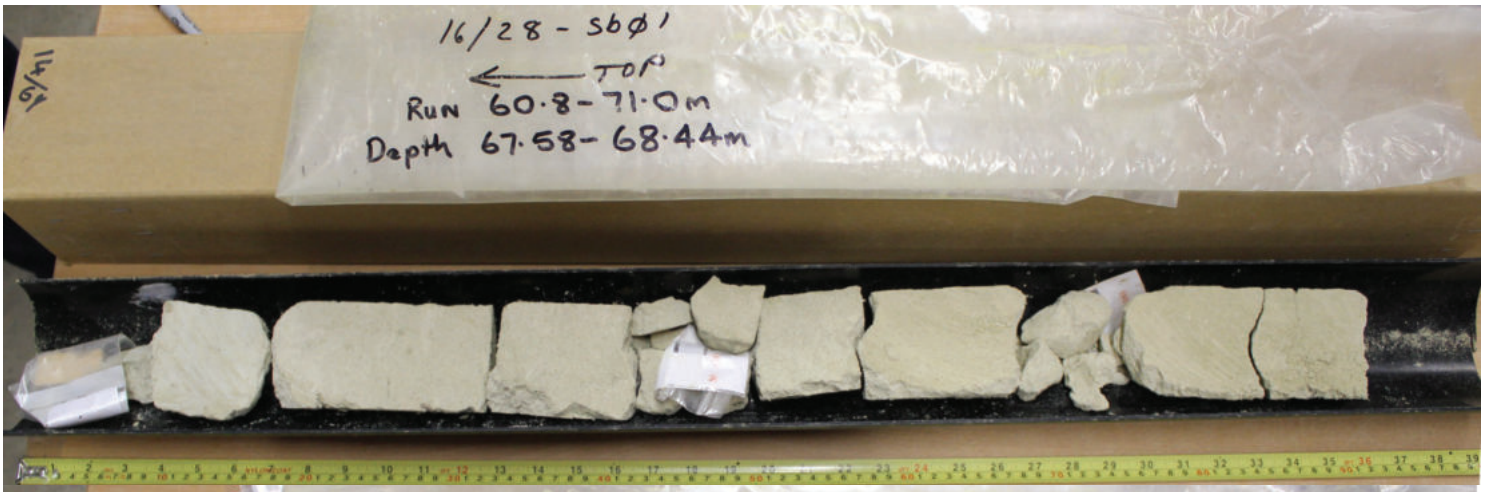
16/28 - SBØ1
TOP
RUN 60.8 - 71.0m
Depth 67.58 - 68.44m

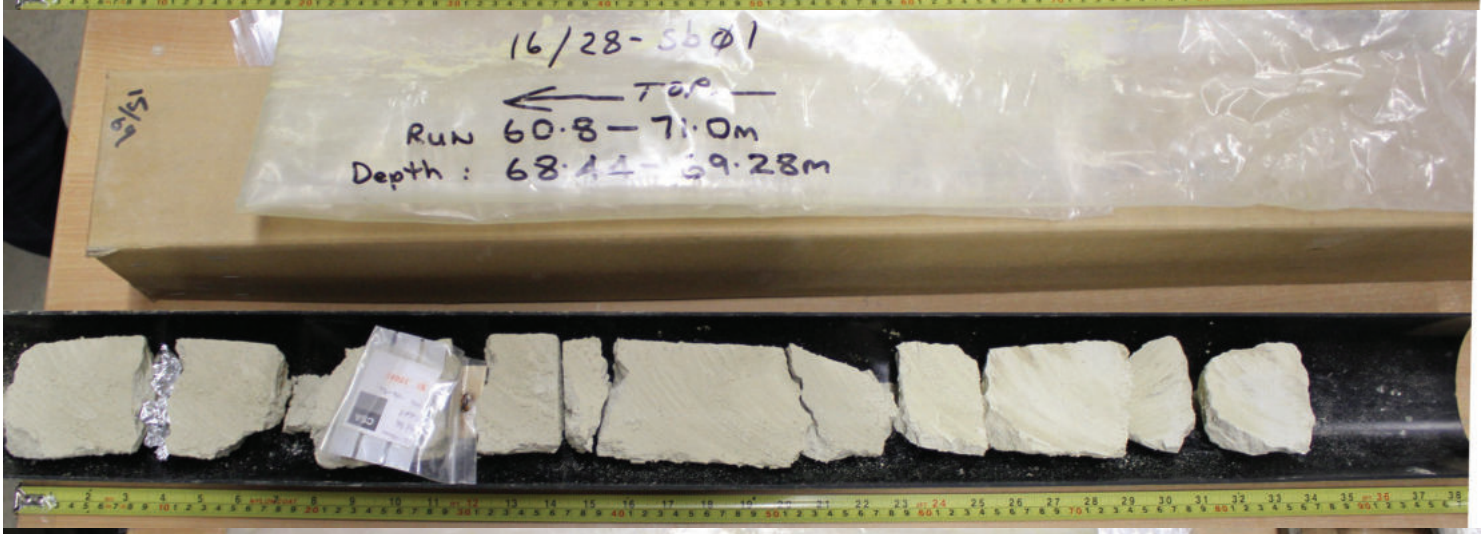
16/28 - SBØ1
TOP
RUN 60.8 - 71.0m
Depth : 68.44 - 69.28m

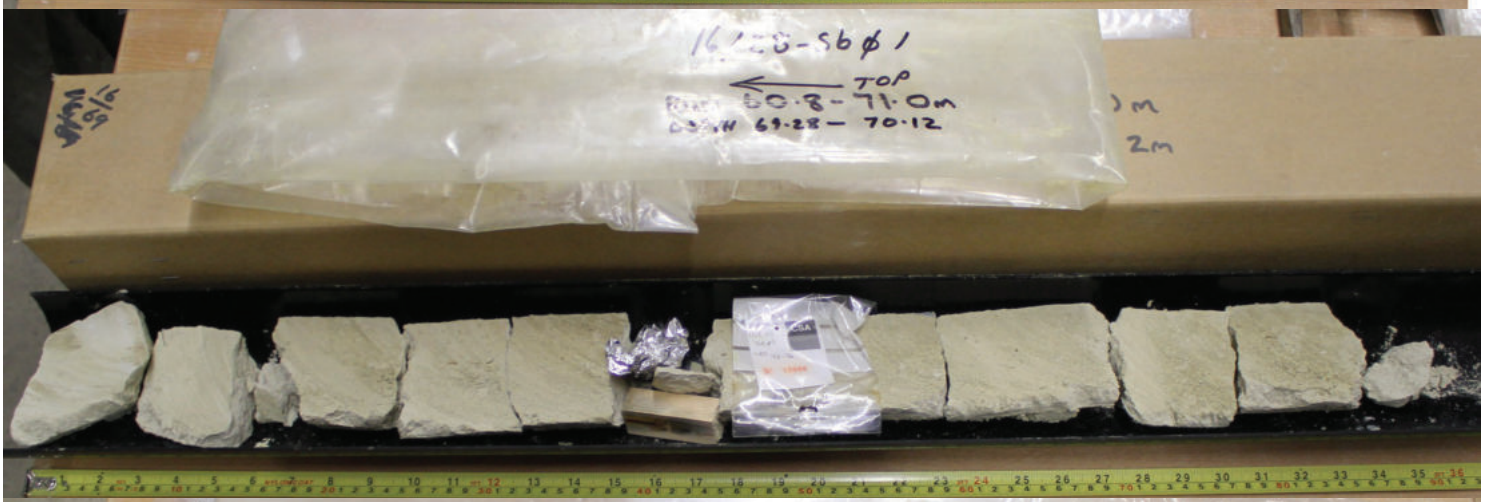
16/28-SBØ1
TOP
60.8 - 71.0m
69.28 - 70.12

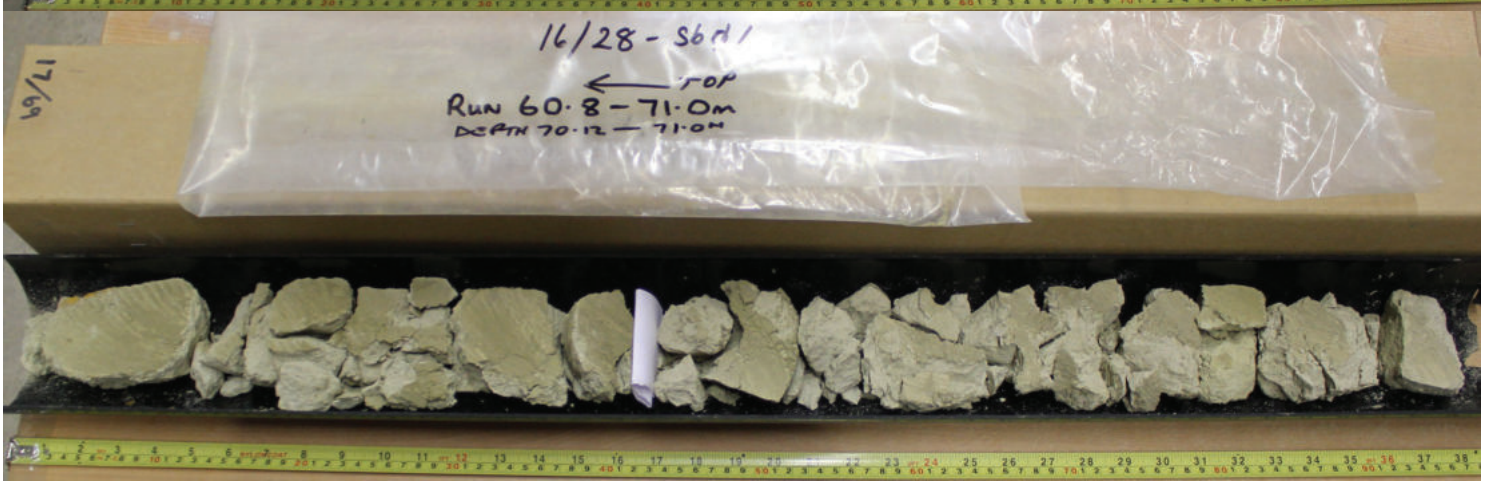
16/28 - SBØ1
TOP
RUN 60.8 - 71.0m
DEPTH 70.12 - 71.0M

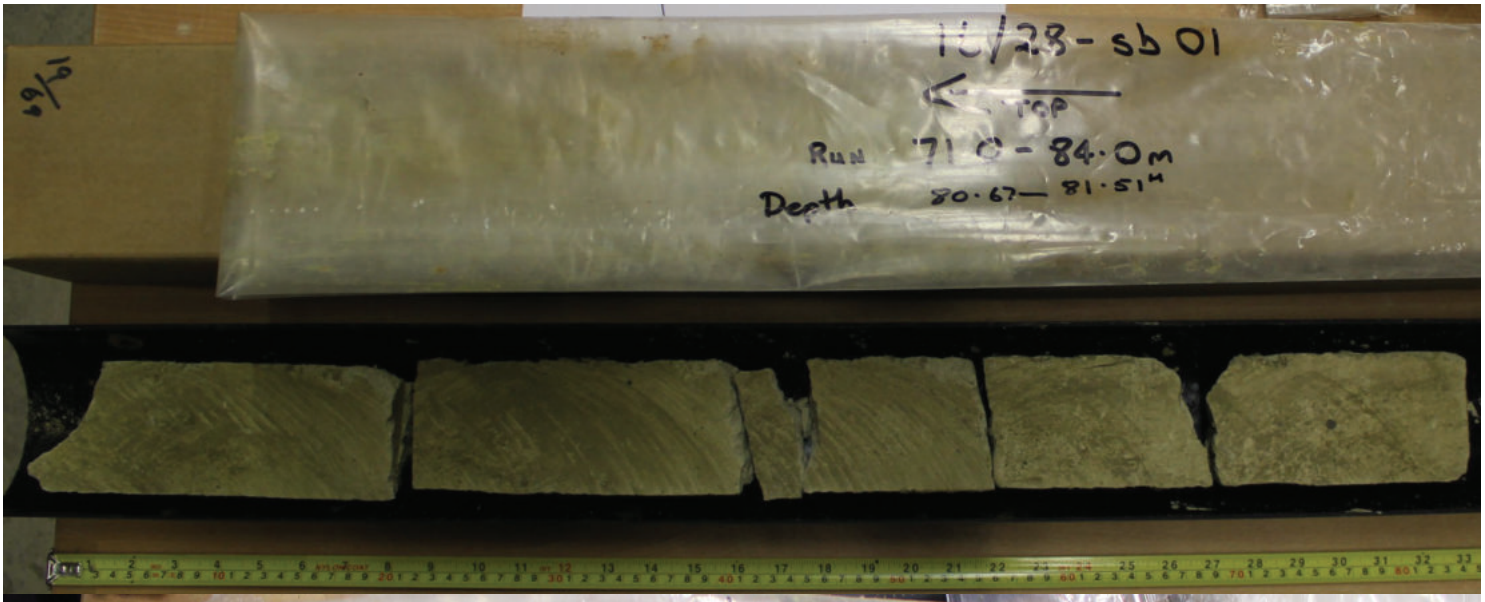
16/28-sb01
TOP
Run 71.0 - 84.0m
Depth 80.67 — 81.51m

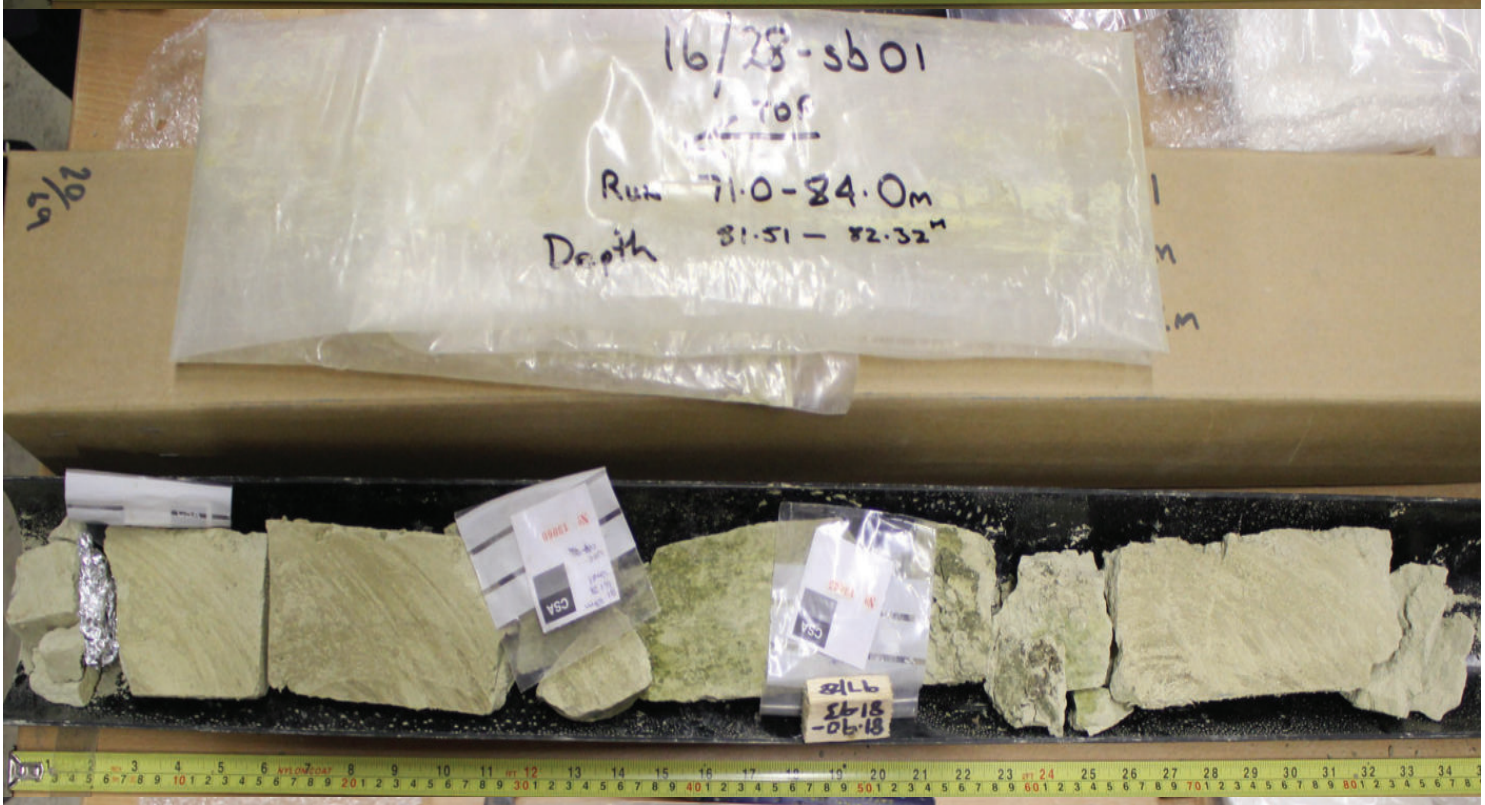
16/28-sb01
TOP
Run 71.0-84.0m
Depth 81.51 — 82.32m

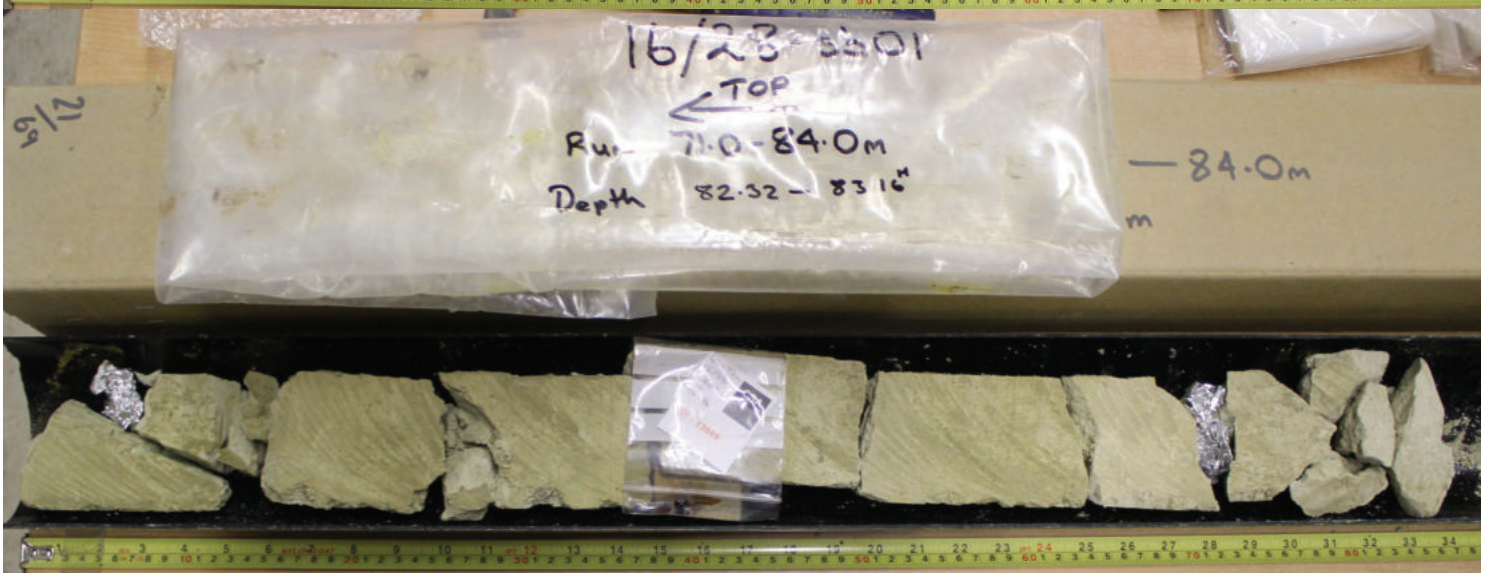
16/28-sb01
TOP
Run 71.0-84.0m
Depth 82.32 — 83.16m


16/28-sb01


TOP
RUN 71.0 - 84.0m
Depth 83.16 - 84.0m
sb01
Box 84.0m
84.0m


16/28 - sb01
TOP
Box 23 of 69
RUN 84.0 - 92.0m
DEPTH 87.50 - 88.38m

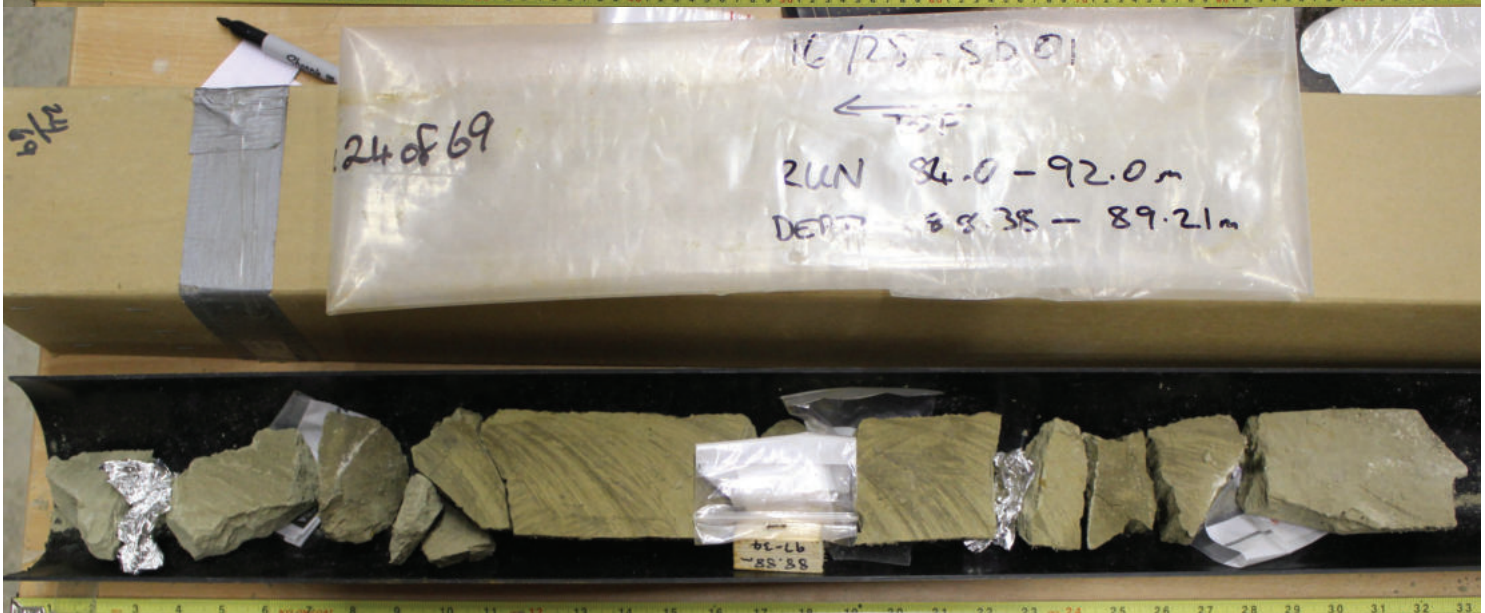
16/28 - sb01
TOP
24 of 69
RUN 84.0 - 92.0m
DEPTH 88.38 - 89.21m

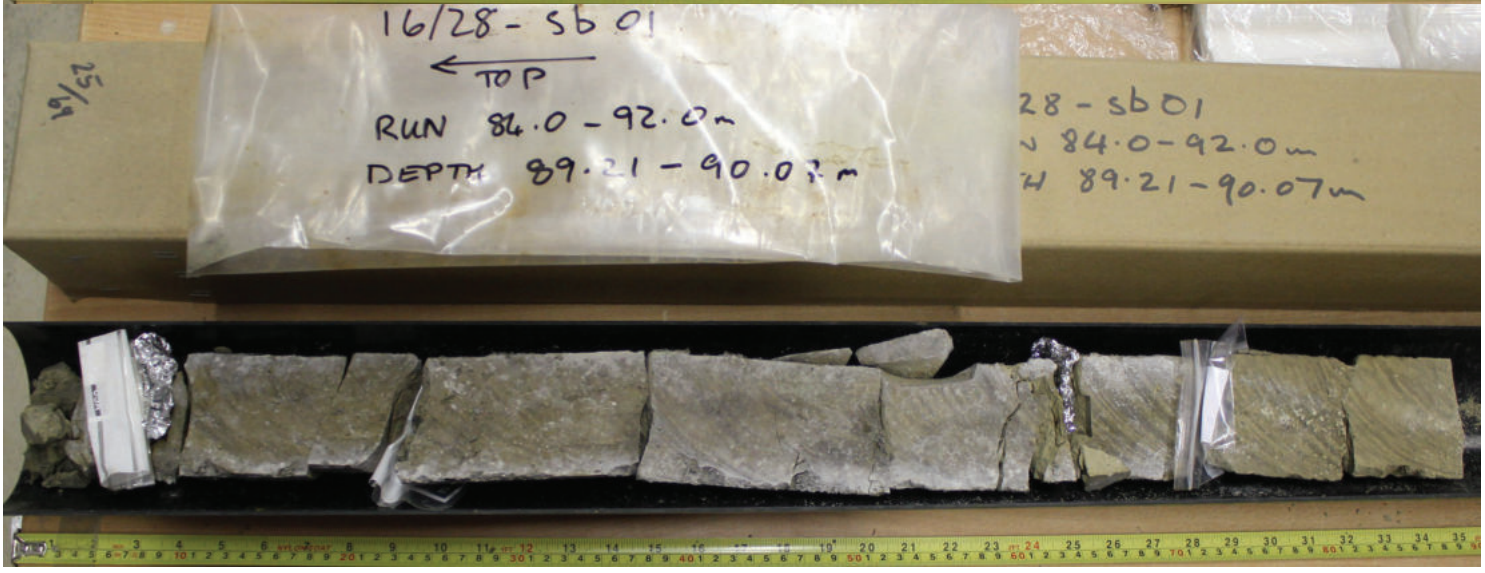
16/28 - sb01
TOP
RUN 84.0 - 92.0m
DEPTH 89.21 - 90.07m
28 - sb01
84.0 - 92.0m
89.21 - 90.07m

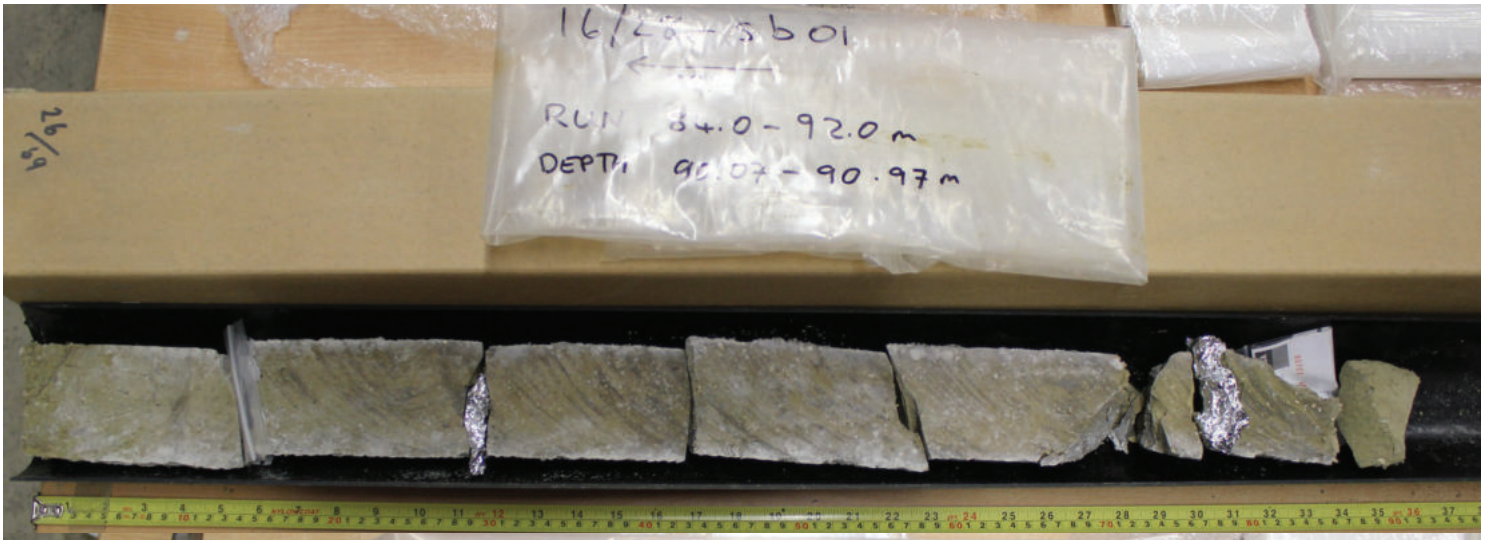
16/28 - sb01
RUN 84.0 - 92.0 m
DEPTH 90.07 - 90.97 m
26/69

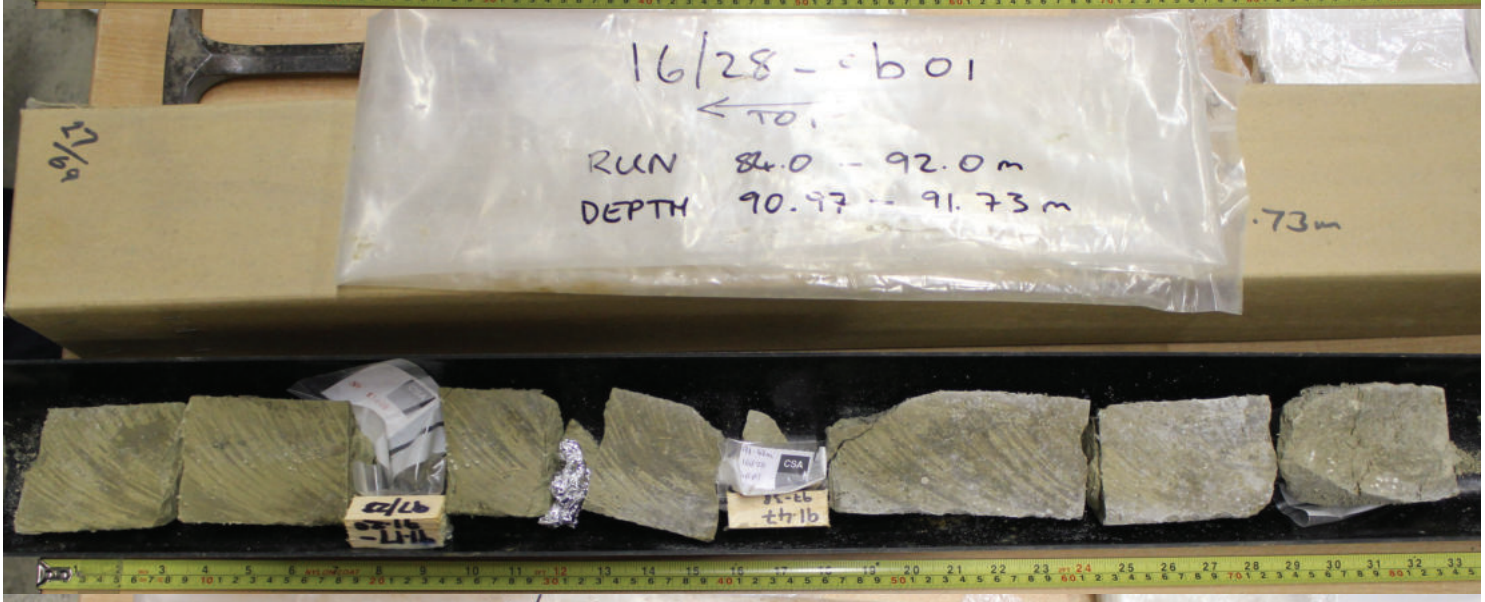
16/28 - sb01
TOP
RUN 84.0 - 92.0 m
DEPTH 90.97 - 91.73 m
27/69

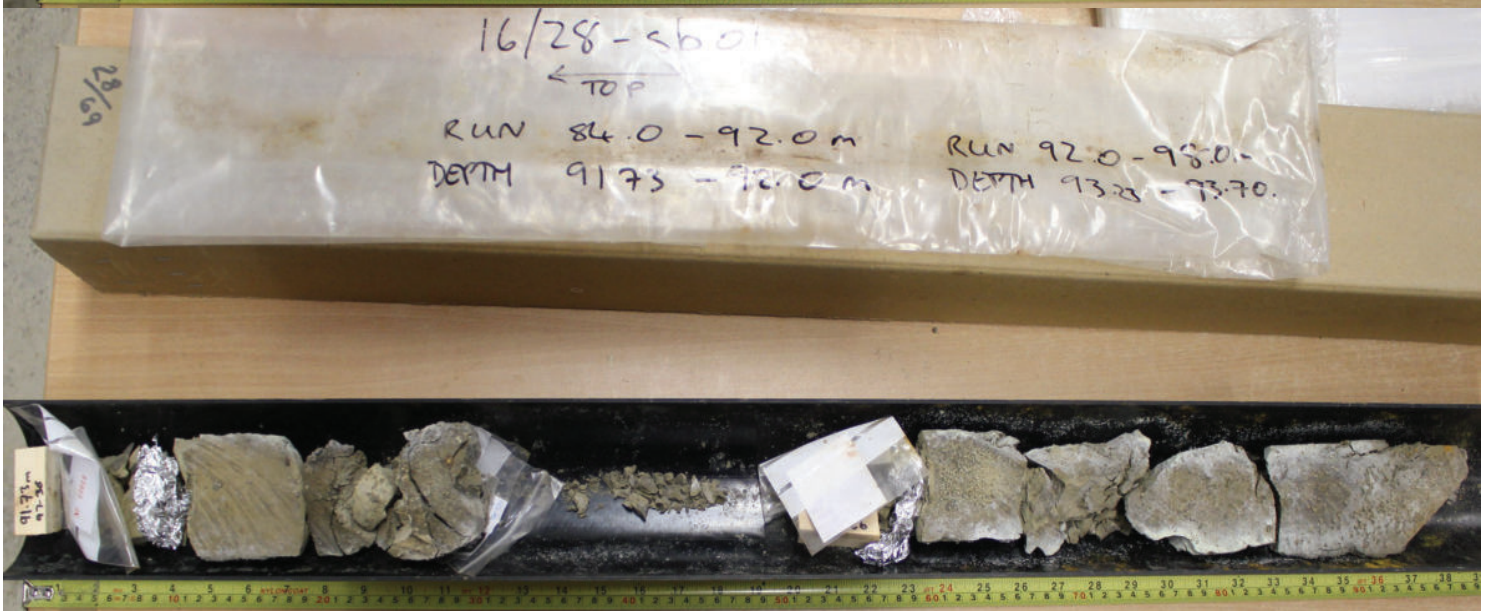
16/28 - sb01
TOP
RUN 84.0 - 92.0 m
DEPTH 91.73 - 92.0 m
RUN 92.0 - 98.0 m
DEPTH 93.29 - 93.70
28/69


16/28 - sb01

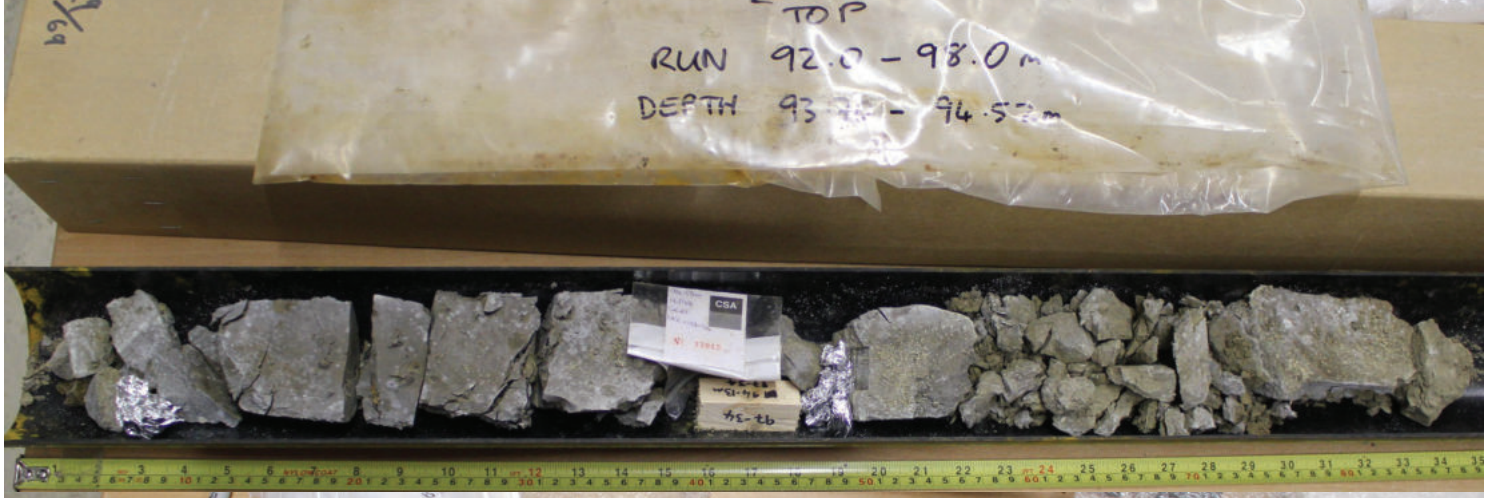
TOP
RUN 92.0 - 98.0m
DEPTH 93 - 94.5

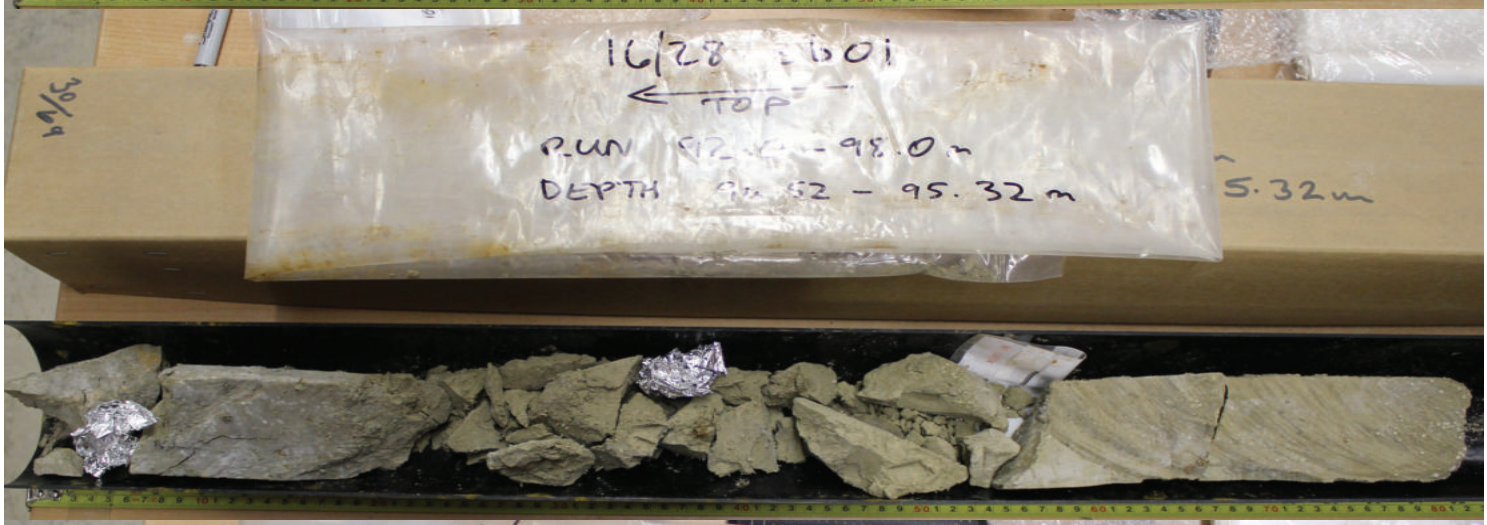
16/28 - sb01
TOP
RUN 92.0 - 98.0m
DEPTH 95.32 - 95.32m


16/28 - sb01
TOP
RUN 92.0 - 98.0m
DEPTH 95.32 - 96.14m
16/28-sb01
RUN 92.0-98.0m
DEPTH 95.32-96.14m

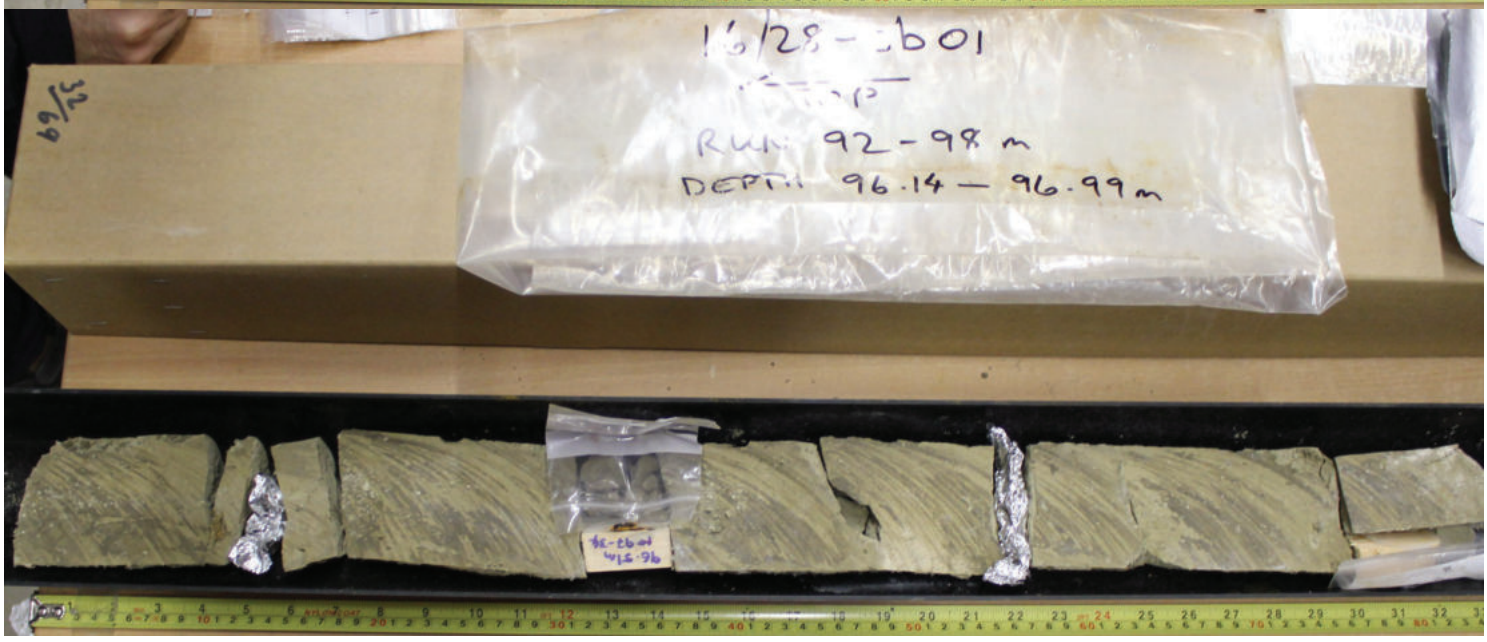
16/28 - sb01
RUN 92 - 98 m
DEPTH 96.14 - 96.99m


16/28 - sb01
TOP
RUN 92-98m
DEPTH 96.99 - 97.77m
8.0
97.77m
16/28 - sb 01
TOP
RUN 92-98m
DEPTH 97.77 -
16/28 - sb01
TOP
RUN 102-110m
Depth 105.23 - 105.69


16/28-sb01
TOP
Run 102-110m
Depth 105.69 - 106.5m
16/28-sb01
TOP
Run 102-110m
Depth 106.5 - 107.43
16/28-sb01
TOP
Run 102-110m
Depth 107.43 -

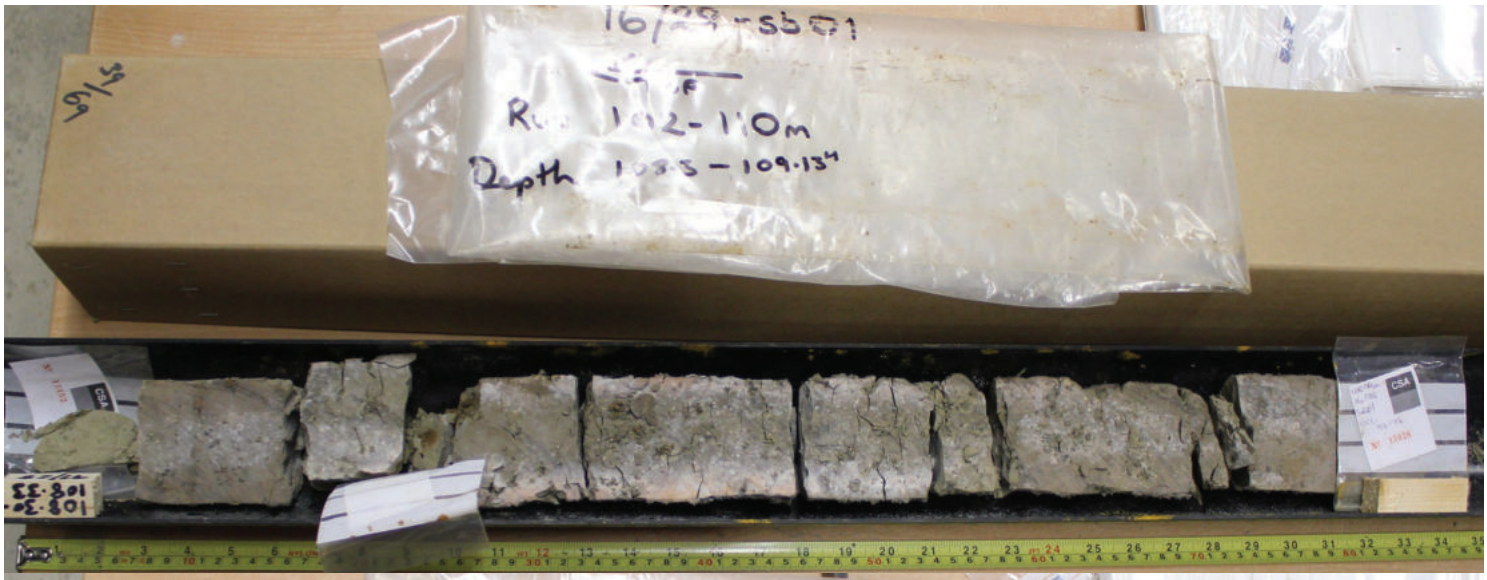
16/29-SS01
TOP
Run 102-110m
Depth 108.33-109.13m


16/28-SS01
TOP
102-110m
109.13-110.04m

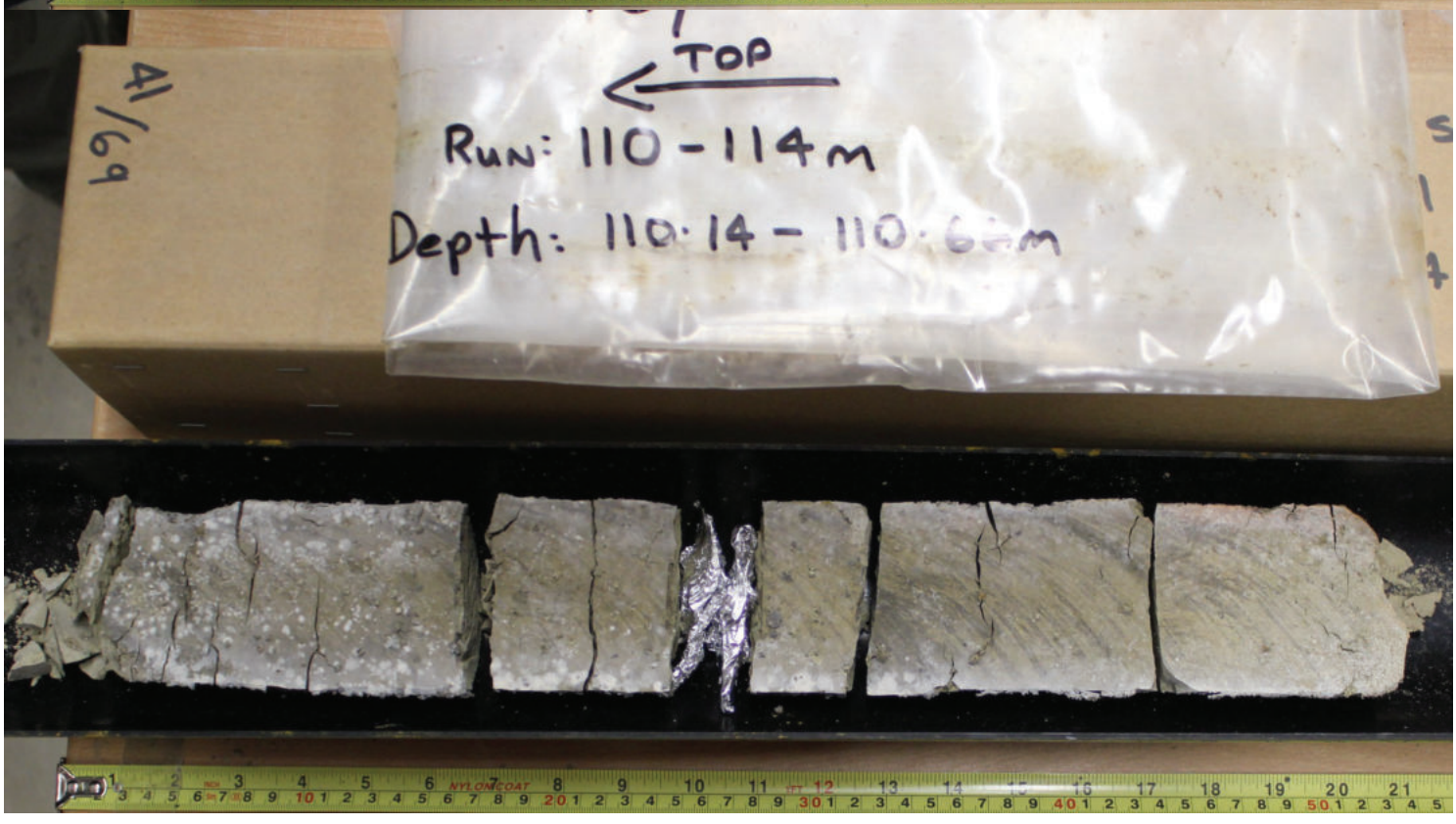
TOP
Run: 110-114m
Depth: 110.14-110.63m

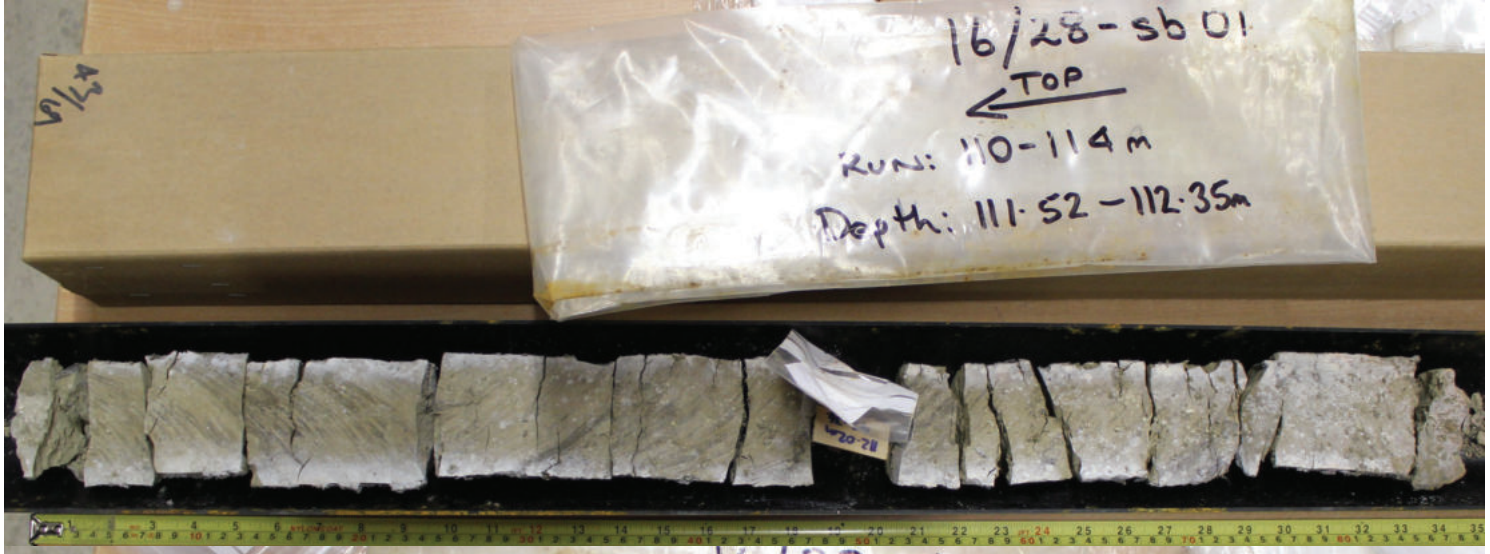
16/28-sb01
TOP
RUN: 110-114m
Depth: 111.52-112.35m

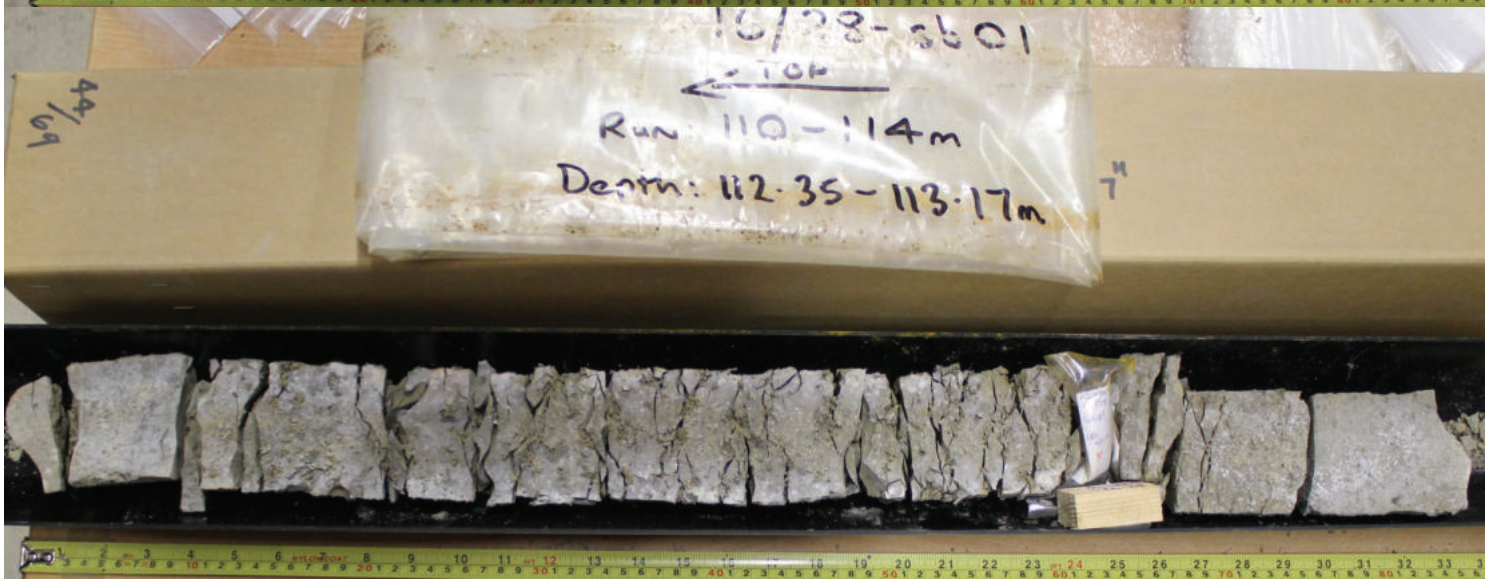
16/28-sb01
TOP
Run 110-114m
Depth: 112.35-113.17m


16/28-sb01
TOP
RUN: 110-114m
Depth: 113.17-

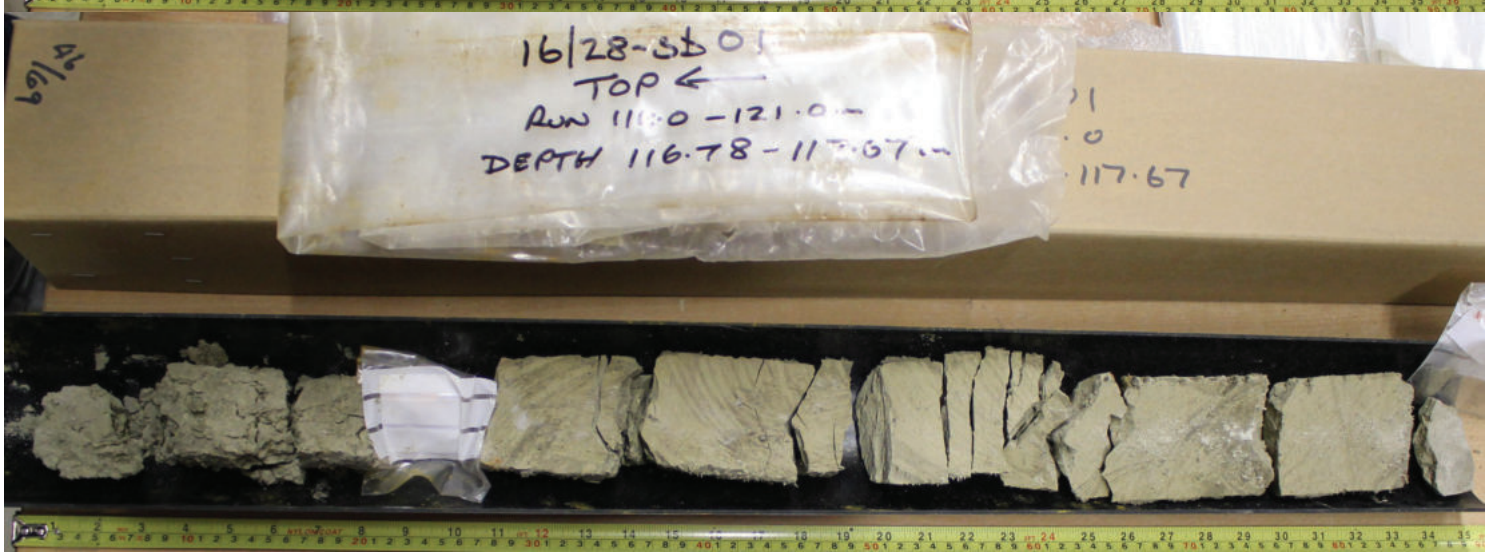
16/28-sb01
TOP
RUN 110.0-121.0
DEPTH 116.78-117.67
117.67

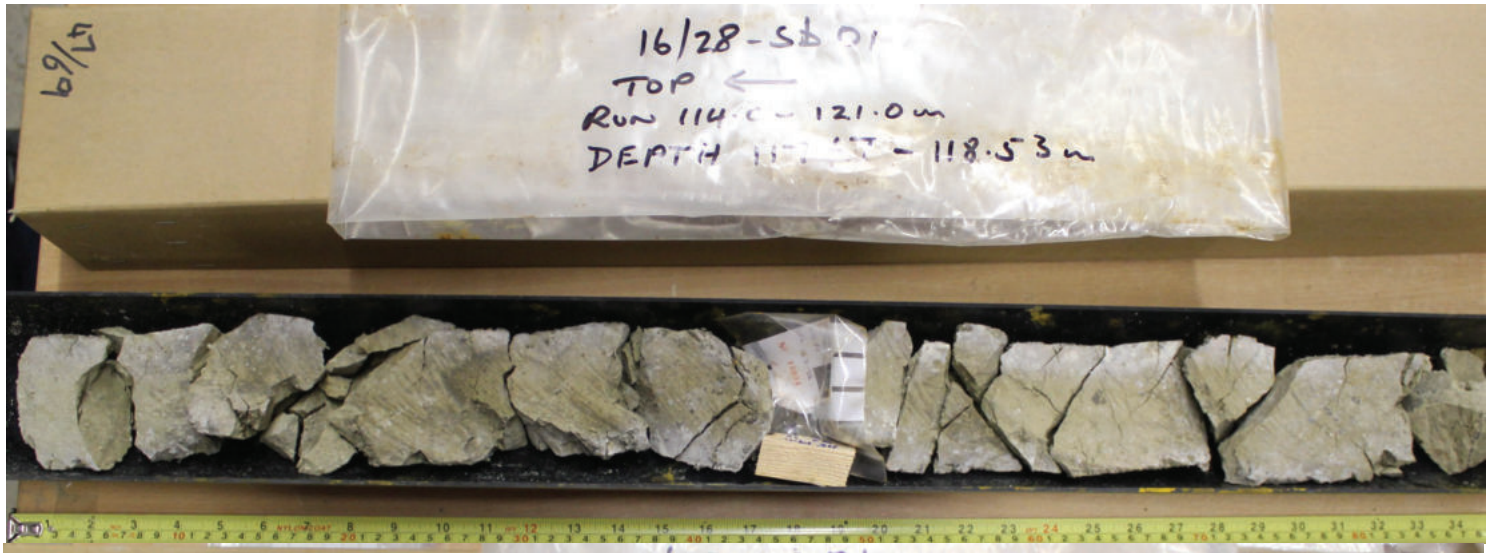
16/28-SB01
TOP
RUN 114.0 - 121.0m
DEPTH 118.53 - 118.53m

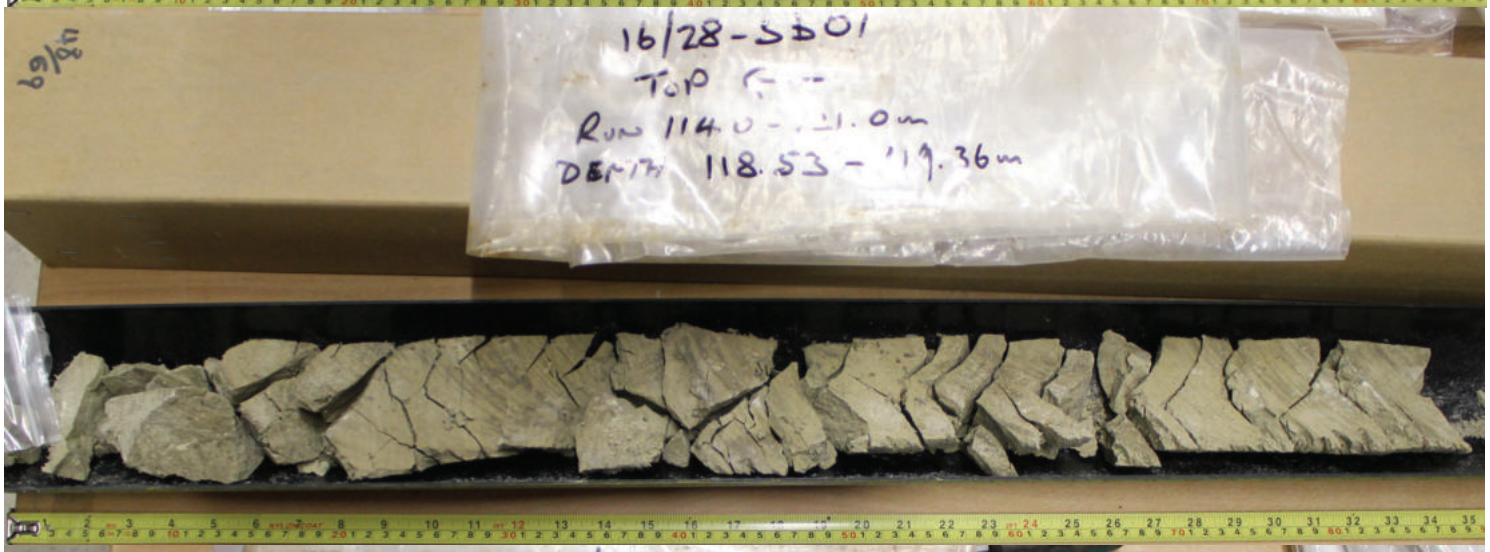
16/28-SB01
TOP
RUN 114.0 - 121.0m
DEPTH 118.53 - 119.36m

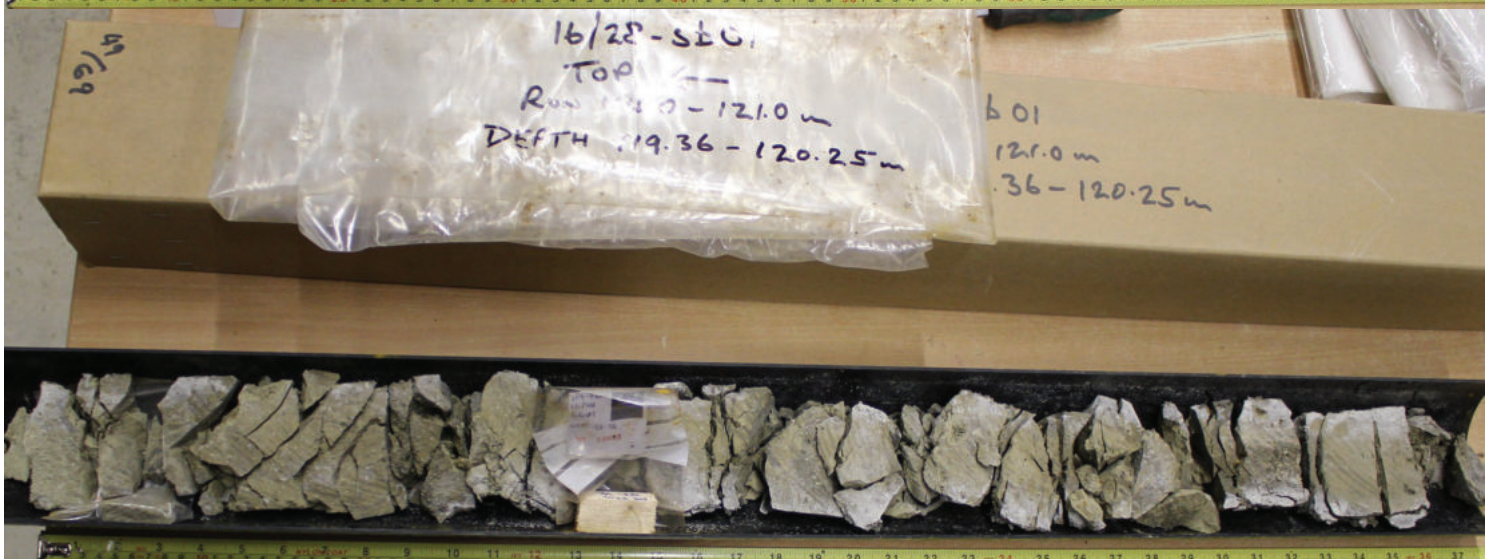
16/28-SB01
TOP
DEPTH 119.36 - 120.25m


16/28-SB01
DEPTH 120.25 - 121.00m
CSA


16/28-sb01
TOP
RUN 121 - 127m
DEPTH 122.28 - 123.16m


16/28-sb2
TOP
RUN 121 - 127m
DEPTH 123.16 - 123.98m


16/28-sb01
TOP
RUN 121 - 127
DEPTH 123.98 - 124.80m

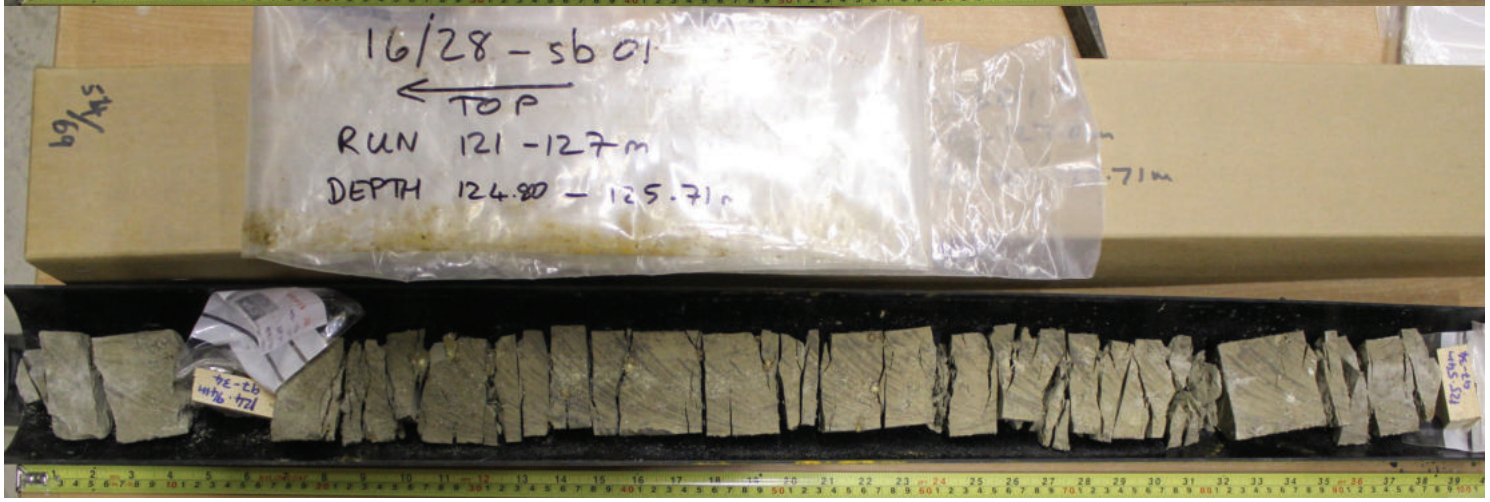
16/28-sb01
TOP
RUN 121 - 127m
DEPTH 124.80 - 125.71m


16/28 sb01
TOP
RUN 121 - 127 m
DEPTH: 125.71 — 126.59 m
RUN 12
DEPTH
16/28-sb01
TOP
Run: 127 - 131m
Depth: 127.55 - 128.44m


16/28-sb 01
TOP
RUN: 127 - 131m
DEPTH 128.44 - 129.20m
16/28-sb 01
TOP
RUN 127 - 131m
16/28-sb 01
TOP
RUN: 131 - 138m
Depth: 134.95 - 135.56m
16/28-sb01
TOP
Depth: 135.56m - 136.35m

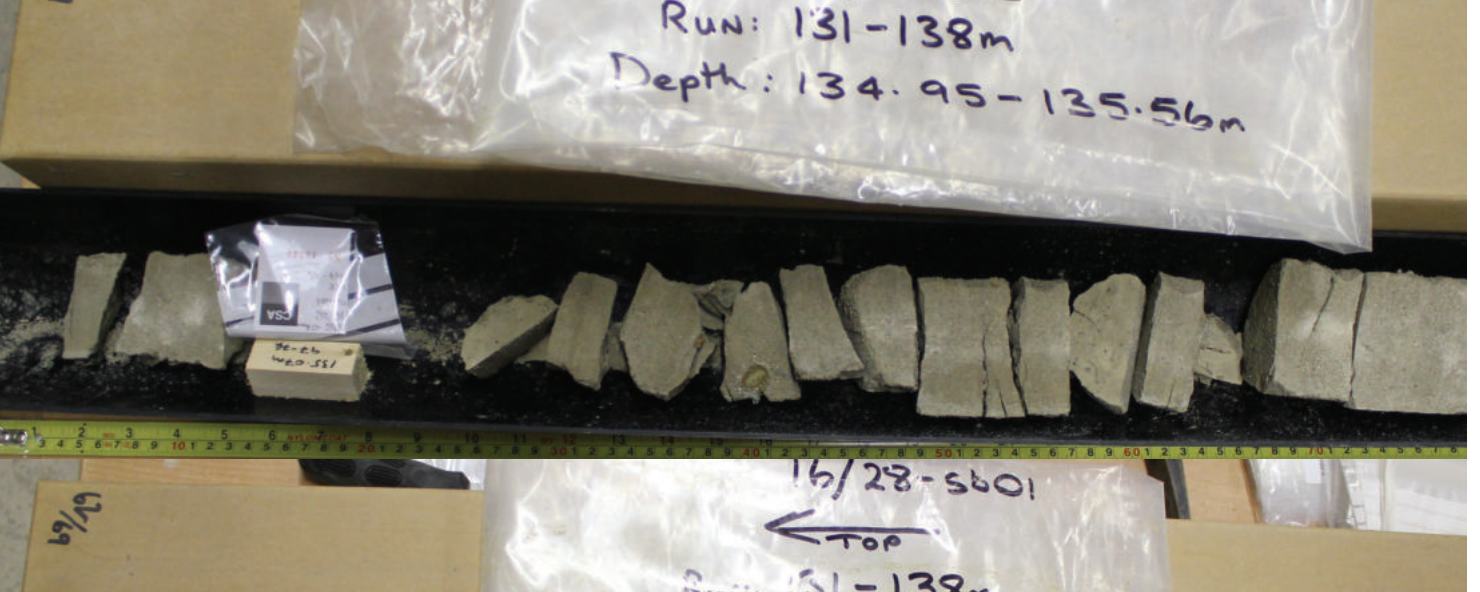
Run: 131-138m
Depth: 134.95-135.56m
16/28-5601
TOP


16/28-SB01
TOP
RUN: 131 - 138m
Depth: 136.35 - 137.14m

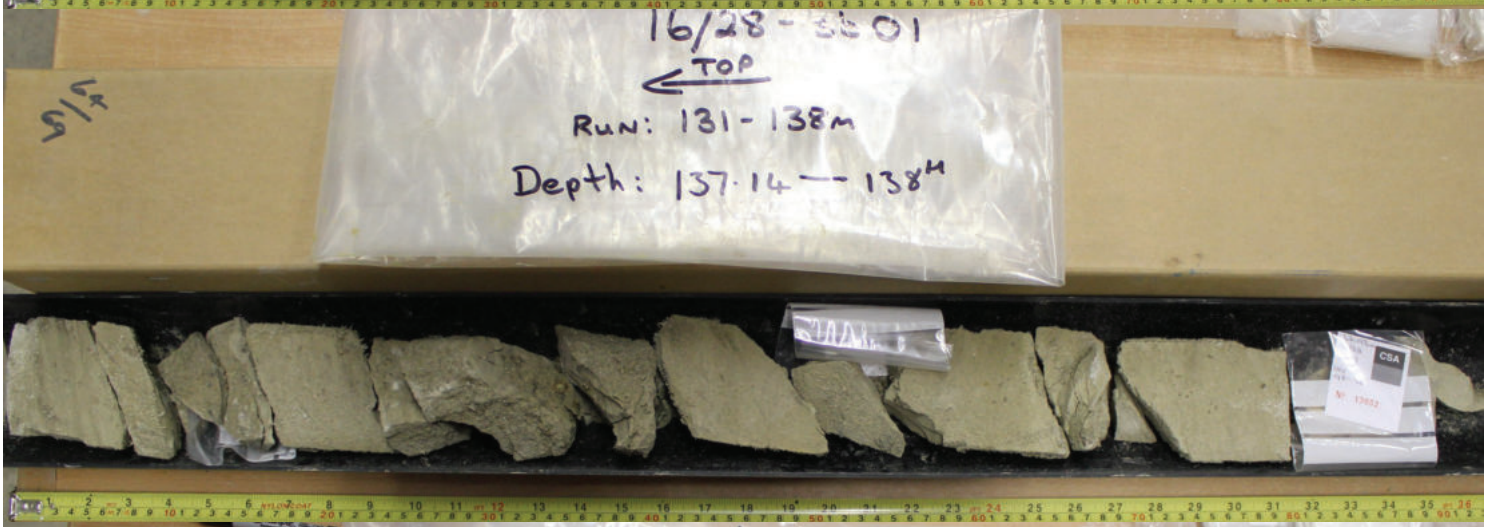
16/28-SB01
TOP
RUN: 131 - 138m
Depth: 137.14 — 138m

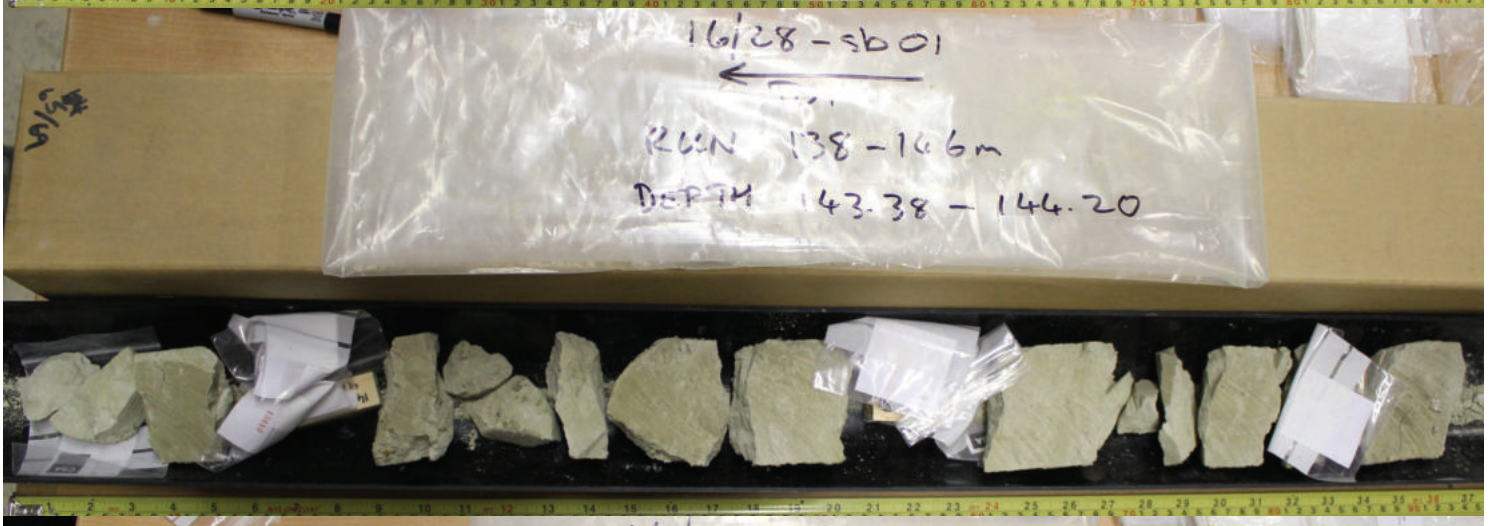
16/28-SB01
RUN 138 - 146m
DEPTH 143.38 - 144.20

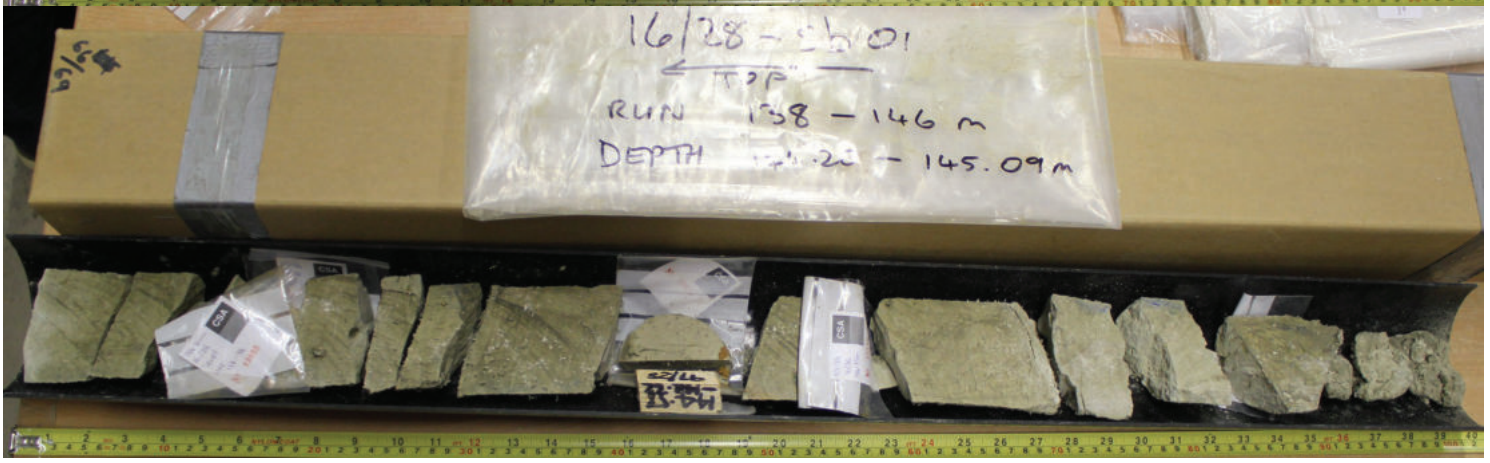
16/28-SB01
TOP
RUN 138 - 146 m
DEPTH 144.20 - 145.09m


16/28 - SB 01
TOP
Box 67 of 69
RUN 138 - 146 m
DEPTH. 145.09 - 146.00 m
67/69
16/28 - SB01
TOP
RUN 146 - 148.25
DEPTH 147.06 - 147.76
Box 68 of 69
Box 68 of 69
16/28 - SB 01
TOP
RUN 146 - 148.25 m
DEPTH 147.06 - 147.76 m
147.76 m
69/69
16/28 - SB01
RUN 146.0 - 148.25m
DEPTH 147.76 - 148.25m
TOP
TOP
16/28 - SB01
RUN 146 - 148.25
DEPTH 147.76 - 148.25

Appendix 3 – Bulk carbon and oxygen isotope data

Table 1 Displays the final results for the high-resolution bulk stable isotope stratigraphy, reruns are not shown, the table below shows which run has been used and if there was an average used see last three columns. In a second table below this one two samples are tested to see the inter sample variability all four reruns are shown for each of these two samples. In the last table a comparison of bulk isotope measurements on the whole sediment against the < 20 µm fraction of the sediment is shown.

Sample	depth	Carbonate inferred from bulk isotopes [wt %]	$CaCO_3$ infered from XRF [wt.%]	$\delta^{13}C$	stdev	$\delta^{18}O$	stdev	Peak	weight [µg]	cell	first run	second run	third run
UBA001	40.82	32.48	54.15	1.01	0.05	0.44	0.03	2.05	197	8	UB17-1		
UBA002	40.87	33.33	50.85	1.07	0.07	0.44	0.15	1.74	166	9	UB17-1		
UBA003	40.92	34.18	54.13	0.97	0.08	0.28	0.2	2.46	221	11	UB17-1		
UBA004	40.97	31.48	79.48	0.8	0.14	-0.09	0.13	1.22	129	12	UB17-1		
UBA005	41.02	51.62		1.09	0.04	0.55	0.18	3.02	184	13	UB17-1		
UBA006	41.07	52.07	84.03	0.93	0.04	0.57	0.12	3.33	199	14	UB17-1		
UBA007	41.12	47.38		1.03	0.05	0.27	0.14	3.54	229	16	UB17-1		
UBA008	41.17	50.71	71.78	0.9	0.12	0.11	0.11	4.16	249	17	UB17-1		
UBA009	41.22	47.91	71.78	0.83	0.02	0.23	0.35	2.96	193	18	UB17-1		
UBA010	41.27	41.57	68.38	1.05	0.15	0.04	0.16	3.12	230	19	UB17-1		
UBA011	41.32	50.19	70.83	1.02	0.01	0.25	0.01	3.63	222	21	UB17-1		
UBA012	41.37	46	73	0.91	0.02	-0.02	0.04	3.06	206	22	UB17-1		
UBA013	41.42	43.74	77.18	0.91	0.02	0.46	0.03	2.23	163	23	UB17-1		
UBA014	41.47	51.19	78.75	0.88	0.09	0.01	0.11	2.39	151	24	UB17-1		
UBA015	41.52	66.31	81.63	0.9	0.01	0.01	0.06	4.05	191	27	UB17-1		
UBA016	41.57	53.75	81.75	0.81	0.06	-0.12	0.08	3.11	182	28	UB17-1		
UBA017	41.58	54.74	77.13	0.94	0	0.13	0.14	2.97	172	29	UB17-1		
UBA018	41.59	43.84	79.4	0.92	0.12	0.1	0.26	3.22	225	31	UB17-1		
UBA019	41.64	55.27	84.38	0.91	0.12	0.16	0.05	2.3	137	32	UB17-1		
UBA020	41.69	53.4	81.18	0.94	0	0	0.06	2.2	136	33	UB17-1		
UBA021	41.74	54.36	84.1	1.12	0.02	0.35	0.01	4.32	242	34	UB17-1		
UBA022	41.79	57.38		1.06	0.04	0.45	0.09	3.98	214	36	UB17-1		
UBA023	41.84	57.67	84	1.02	0.11	0.35	0.05	4.19	223	37	UB17-1		
UBA024	41.89	55.56	81.33	1.01	0.07	0.38	0.08	3.71	207	38	UB17-1		
UBA025	41.94	56.52	82.18	1.1	0.04	0.45	0.04	4.17	226	39	UB17-1		
UBA026	41.99	65.14	83.55	0.97	0.07	0.48	0.08	2.92	146	41	UB17-1		
UBA027	42.04	64.39	90.8	1.08	0.03	0.46	0.3	3.21	160	42	UB17-1		
UBA028	42.09	56.4		1.02	0.04	0.47	0.01	4.1	223	43	UB17-1		
UBA028.5	42.14	50.94	76.95	1.04	0.07	0.24	0.02	4.12	246	44	UB17-1		
UBA029	42.19	54.88	80.58	1.11	0.02	0.38	0.09	4.42	245	46	UB17-1		
UBA030	42.24	48.32	84.45	1.01	0	0.14	0.33	2.85	185	47	UB17-1		
UBA031	42.29	66.27	90.6	0.93	0.04	0.29	0.03	2.92	144	48	UB17-1		
UBA032	42.42	40.81	59.33	0.95	0.01	0.49	0.1	3.21	240	49	UB17-1		
UBA033	42.47	52.85	78.5	0.97	0.14	0.28	0.02	2.5	153	51	UB17-1		
UBA034	42.52	49.09	84.58	1.17	0.13	0.39	0.08	3.9	242	52	UB17-1		

UBA035	42.57	52.19	88.88	0.98	0.04	0.3	0.05	3.49	207	53	UB17-1	
UBA036	42.62	60.16	82.83	1.06	0.07	0.3	0.26	2.22	124	54	UB17-1	
UBA037	42.67	58.12	88.65	1.02	0.01	0.52	0.09	3.78	202	56	UB17-1	
UBA038	42.72	54.86	81.33	0.95	0.02	0.13	0.13	2.7	158	57	UB17-1	
UBA039	42.77	55.56	78.13	1.09	0.07	0.48	0.31	2.01	122	58	UB17-1	
UBA040	42.82	55.09	79.73	1.03	0.04	0.46	0.26	3.6	203	59	UB17-1	
UBA041	42.87	52.87	81.85	0.89	0.02	0.36	0.11	3.34	197	8	UB17-2	
UBA042	42.92	58.33	76.45	0.9	0.02	0.17	0.06	2.72	151	9	UB17-2	
UBA043	42.97	41.1	61.18	1	0.05	-0.21	0.16	3.07	229	11	UB17-2	
UBA044	43.02	54.06	79.8	1	0.05	0.35	0.09	4.34	244	12	UB17-2	
UBA045	43.15	40.17	55.9	1.06	0.07	0.13	0.03	2.47	192	13	UB17-2	
UBA046	43.25	52.35		0.95	0.21	0.13	0.38	2.93	177	14	UB17-2	
UBA047	43.26	51.79	82.45	0.99	0.06	0.05	0.05	3.14	190	16	UB17-2	
UBA048	43.31	53.52	79.45	0.98	0.01	0.25	0	4.31	245	17	UB17-2	
UBA049	43.36	55.2	80.45	0.92	0.06	0.15	0.31	3.09	177	18	UB17-2	
UBA050	43.41	52.66	73.7	0.88	0.07	0.26	0.24	2.53	155	19	UB17-2	
UBA051	43.46	41.75	62.95	1.02	0.05	0.4	0.13	3.42	249	21	UB17-2	
UBA052	43.51	45.99	71.3	0.88	0.1	0.34	0.04	3.51	233	22	UB17-2	
UBA053	43.56	54.79	82.05	0.99	0.02	0.15	0.06	4.16	232	23	UB17-2	
UBA054	43.61	49.4	76.53	0.91	0.05	0.34	0.04	3.95	243	24	UB17-2	
UBA055	43.66	55.83	77.63	1.02	0.06	0.34	0.25	4.02	221	27	UB17-2	
UBA056	43.76	33.23	52.73	1.04	0.07	0.39	0.2	2.39	221	28	UB17-2	
UBA057	43.86	40.31	61.25	0.96	0.01	0.56	0.06	3.26	246	29	UB17-2	
UBA058	43.91	47.02	61.9	0.94	0.11	0.37	0.04	2.7	181	31	UB17-2	
UBA059	44	44.25		0.87	0.07	0.28	0.01	2.13	155	32	UB17-2	
UBA060	52.44	57.49	74.43	0.82	0.1	-0.03	0.04	2.16	126	33	UB17-2	
UBA061	52.49	56.22		0.87	0.06	0	0.08	2.42	141	34	UB17-2	
UBA062	52.54	53.33	77.43	0.94	0.03	0.02	0.08	2.74	164	36	UB17-2	
UBA063	52.59	60.5	73.68	1.03	0.09	-0.06	0.15	2.28	126	37	UB17-2	
UBA064	52.64	49.38	68.85	1.07	0.07	-0.16	0.02	2.8	179	38	UB17-2	
UBA065	52.69	54.94	70.63	0.91	0.06	-0.04	0.1	2.62	154	39	UB17-2	
UBA066	52.74	53.27		1.07	0.01	0.13	0.17	3.39	198	41	UB17-2	
UBA067	52.79	42.62	70.55	0.98	0.08	0.1	0.15	2.96	214	42	UB17-2	
UBA068	52.84	51.75		0.93	0.01	0.35	0	3.03	184	43	UB17-2	
UBA069	52.89	50.15		0.89	0.11	0.47	0.18	2.77	175	44	UB17-2	
UBA070	52.94	41.61	62.8	1.02	0.13	0.01	0.05	1.75	138	46	UB17-2	
UBA071	52.99	50.17	69.7	0.96	0.07	0.17	0.13	3.14	195	47	UB17-2	
UBA072	53.04	51.9	71.28	0.87	0.01	0.19	0.04	3.84	227	48	UB17-2	
UBA073	53.09	44.94	67.1	0.89	0.06	0.13	0.06	2.94	203	49	UB17-2	
UBA074	53.14	43.23	62	0.99	0.05	0.14	0.12	3.23	229	51	UB17-2	
UBA74.5	53.19	46.21	63.1	1.05	0.15	0.23	0.02	1.67	122	52	UB17-2	
UBA075	53.24	45.72	61.63	1.12	0.08	-0.09	0.08	3.11	210	53	UB17-2	
UBA076	53.28	37.43	68.08	0.93	0.01	0.5	0.06	13.94	1053	8	failed	UB17-25

UBA077	53.3	36.2	58.48	0.96	0.07	-0.21	0.12	2.76	233	56	UB17-2	
UBA078	53.35	36.37	59.85	1.04	0.18	-0.42	0.03	1.42	130	57	UB17-2	
UBA079	53.4	37.8	57.5	1.26	0.03	-0.22	0.03	2.43	200	58	UB17-2	
UBA080	53.45	40.84	64.18	1.16	0.07	-0.36	0.13	2.2	171	59	UB17-2	
UBA081	53.5	49.73	73.53	0.93	0.01	0.68	0.03	3.85	236	8	UB17-3	
UBA082	53.55	49.07		1.05	0.07	0.72	0.01	3.67	229	9	UB17-3	
UBA083	53.6	44.6	70.6	0.84	0.06	0.52	0.18	2.95	205	11	UB17-3	
UBA084	53.7	47.47	67.28	0.88	0.03	0.69	0.14	3.62	233	12	UB17-3	
UBA085	53.75	36.72		0.84	0.02	0.2	0.2	1.57	140	13	UB17-3	
UBA086	60.61	43.72	75.7	1.08	0.17	0.22	0.03	3.25	228	14	UB17-3	
UBA087	60.66	50.57	71	1.06	0.05	0.29	0.03	3.58	218	16	UB17-3	
UBA088	60.75	62.61	79.23	0.92		0.41		3.26			average used of two runs	
UBA089	60.8	35.72	77.63	0.94	0.08	0.32	0.15	2.54	219	18	UB17-3	
UBA090	66.21	56.21	81.23	0.92	0.01	0.38	0.09	3.64	201	19	UB17-3	
UBA091	66.26	48.74	75.5	0.95	0	0.34	0.15	3.86	241	21	UB17-3	
UBA092	66.31	142.85	78.5	1	0.01	0.32	0.06	10.99	783	22	failed due to peak height	UB18-26
UBA093	66.36	51.29		1.12	0.06	0.39	0.18	2.65	165	23	UB17-3	
UBA094	66.41	49.89	83.28	1.06	0.04	0.18	0.15	2.85	180	24	UB17-3	
UBA095	66.46	52.47	85	1.07	0.02	0.4	0.03	4.13	240	27	UB17-3	
UBA096	66.51	54.86		1.05	0.07	0.33	0.03	4.42	245	28	UB17-3	
UBA097	66.62	48.63	82.38	1.03	0.06	0.15	0.02	2.67	174	29	UB17-3	
UBA098	66.67	58.85		0.89	0.05	0.3	0.13	2.47	138	31	UB17-3	
UBA099	66.72	52.34	80.33	0.93	0.02	0.04	0.07	3.65	215	32	UB17-3	
UBA100	66.77	54.51	88.43	0.93	0.1	0.06	0.01	3.74	212	33	UB17-3	
UBA101	66.82	62.26	90.58	0.99	0.04	0.31	0.14	4.5	222	34	UB17-3	
UBA102	66.87	58.36	87.75	0.86	0.01	-0.11	0.13	3.31	179	36	UB17-3	
UBA103	66.92	65.02	91.35	0.84	0.04	0.28	0.09	3.29	162	37	UB17-3	
UBA104	66.97	67.78	88.33	0.97	0.03	0.23	0.01	2.97	143	38	UB17-3	
UBA105	67.02	67.65	89.88	0.92	0.01	0.18	0.02	2.64	130	39	UB17-3	
UBA106	67.12	54.38	86.2	0.85	0	0.28	0.07	4.42	247	41	UB17-3	
UBA107	67.17	59.42	92.5	0.93	0.05	0.39	0.05	3.41	181	42	UB17-3	
UBA108	67.22	62.55	88.4	0.95	0.01	0.47	0.19	3.21	164	43	UB17-3	
UBA109	67.27	51.71	86.53	0.93	0.03	0.29	0.09	3.51	210	44	UB17-3	
UBA110	67.32	59.06	83.28	0.95	0.05	0.2	0	3.29	176	46	UB17-3	
UBA111	67.37	58.43	80.03	0.94	0.04	0.14	0.22	2.98	163	47	UB17-3	
UBA112	67.42	56.09	80.93	1.16	0.03	0.3	0.23	2.78	159	48	UB17-3	
UBA113	67.47	54.26	75.5	1.04	0.01	0.44	0.15	3.94	223	49	UB17-3	
UBA114	67.52	42.38	64.88	1.16	0.01	0.13	0.12	2.88	210	51	UB17-3	
UBA115	67.57	43.77		1.19	0.08	0.1	0.29	2.25	164	52	UB17-3	
UBA116	67.63	37.76		1.1	0	-0.14	0.05	3	242	53	UB17-3	
UBA117	67.68	42.1	57.15	1.14	0.02	-0.03	0.09	3.45	249	54	UB17-3	
UBA118	67.73	35.86	54.58	0.99	0	-0.11	0	2.44	210	56	UB17-3	
UBA119	67.78	56.29		0.92	0.1	0	0.12	3.11	175	57	UB17-3	

UBA120	67.83	49.15	74.85	0.81	0.14	-0.05	0.1	2.88	184	58	UB17-3
UBA121	67.88	49.87	74.98	1.02	0.02	-0.01	0.13	3.75	230	59	UB17-3
UBA122	67.93	46.63		0.87	0.06	0.16	0.15	3.47	228	8	UB17-4
UBA123	67.98	44.2	67.8	1.03	0.07	0.05	0.02	2.46	176	9	UB17-4
UBA124	68.03	42.76	74.9	0.96	0.01	0.29	0.21	3.12	224	11	UB17-4
UBA125	68.08	42.5	73.65	0.9	0.06	0.02	0.19	3.07	222	12	UB17-4
UBA126	68.13	36.23	73.15	0.97	0.13	0.17	0.04	1.68	150	13	UB17-4
UBA127	68.18	41.35		0.91	0.13	-0.02	0.39	1.93	151	14	UB17-4
UBA128	68.23	44.79	69.45	0.94	0.01	0.36	0.08	3.48	237	16	UB17-4
UBA129	68.28	63.31		0.83	0.04	-0.09	0.09	2.31	123	17	UB17-4
UBA130	68.33	35.21	69.4	0.85	0.05	-0.04	0.1	2.56	223	18	UB17-4
UBA131	68.38	38.42	68.38	0.74	0.02	0.17	0.01	2.94	234	19	UB17-4
UBA132/982/983	68.43	35.1	67.25	0.7	0.02	-0.23	0.16	3.11	267.5		average used; sample used to evaluate homogeneity of dataset
UBA133	68.44	44.26		0.7	0.11	-0.33	0.12	3.41	235	22	UB17-4
UBA134	68.49	48.73	74	0.79	0.01	-0.4	0.32	2.57	168	23	UB17-4
UBA135	68.54	49.97	80.98	0.76	0.01	-0.06	0	4.06	247	24	UB17-4
UBA136	68.64	49.61	79.65	0.84	0.09	0.01	0.01	3.23	202	27	UB17-4
UBA137	68.69	50.58	81.93	0.85	0.17	-0.33	0.12	2.89	180	28	UB17-4
UBA138	68.74	48.39		0.75	0.1	-0.24	0.01	3.1	199	29	UB17-4
UBA139	68.79	55.55	83.18	0.68	0.09	-0.12	0.18	3.65	204	31	UB17-4
UBA140	68.84	54.44	86.93	0.59	0.02	-0.08	0.12	3.95	223	32	UB17-4
UBA141	68.89	52.33	82.55	0.76	0.01	-0.01	0.06	3.08	185	33	UB17-4
UBA142	68.94	52.77		0.75	0.1	-0.1	0.02	3.01	180	34	UB17-4
UBA143	68.99	45.19	77.88	0.77	0.06	-0.23	0.06	2.01	145	36	UB17-4
UBA144	69.04	55.29	83.15	0.79	0.11	0	0.09	2.5	147	37	UB17-4
UBA145	69.09	45.74	72.93	0.99	0.04	0	0.12	3.34	224	38	UB17-4
UBA146	69.14	36.42		0.93	0.01	-0.26	0.01	1.54	139	39	UB17-4
UBA147	69.24	49.47	73.25	1.02	0.02	-0.13	0	2.84	181	41	UB17-4
UBA148	69.28	47.74	70.35	0.95	0.04	-0.09	0.01	3.73	238	42	UB17-4
UBA149	69.38	42.13	59.78	0.8	0.12	0.03	0.04	2.12	161	43	UB17-4
UBA150	69.43	40.4		0.85	0.06	-0.1	0.02	2.99	227	44	UB17-4
UBA151	69.48	47.43		0.69	0.05	-0.04	0.05	2.95	194	46	UB17-4
UBA152	69.53	52.3	80.23	0.91	0.04	0.05	0.06	2.91	176	47	UB17-4
UBA153	69.58	56.35	65.28	0.68	0.06	0.22	0.03	2.67	153	48	UB17-4
UBA154	69.63	50.93		0.82	0.12	0.03	0.01	2.23	143	49	UB17-4
UBA155	69.68	49.55	76.98	0.75	0.1	-0.3	0.19	2.92	185	51	UB17-4
UBA156	69.73	56.51	76.7	0.67	0	0.02	0.04	3.51	194	52	UB17-4
UBA157	69.78	42.89		0.64	0.03	-0.06	0.03	3.3	235	53	UB17-4
UBA158	69.83	45.38	72.85	0.84	0	-0.19	0.14	2.18	155	54	UB17-4
UBA159	69.88	42.85	64.43	0.78	0.03	0.04	0.02	2.79	202	56	UB17-4
UBA160	69.93	39.36	64.5	0.69	0.07	-0.14	0.18	1.84	151	57	UB17-4

UBA161	69.98	41.97	62.6	0.95	0.08	0.04	0.09	2.94	216	58	UB17-4	
UBA162	70.03	38.08	63.23	0.8	0.03	-0.28	0.04	2.28	188	59	UB17-4	
UBA163	70.08	15.72		0.81	0.13	-0.73	0.59	1.22	236	8	UB17-5	
UBA164	70.12	29.87	61.95	0.77	0.17	-0.3	0.19	2.01	208	9	UB17-5	
UBA165	70.17	32.42	58.38	0.61	0.07	-0.01	0.1	2.35	223	11	UB17-5	
UBA166	70.22	36.28	68.05	0.85	0.1	-0.23	0.08	2.33	200	12	UB17-5	
UBA167	70.27	37.62		0.68	0.03	-0.09	0.05	2.46	203	13	UB17-5	
UBA168	70.32	43.18	65.75	0.87	0.03	0	0.31	2.87	206	14	UB17-5	
UBA169	70.37	35.06	70.03	0.82	0.13	0.02	0.2	1.85	168	16	UB17-5	
UBA170	70.42	41.66	74.33	0.75	0	0.26	0.2	1.87	146	17	UB17-5	
UBA171	70.47	30.63	56.15	0.73	0.1	-0.62	0.33	1.83	187	18	UB17-5	
UBA172	70.52	21.33	58.18	0.81	0.16	-0.56	0.24	1.26	185	19	UB17-5	
UBA173	70.57	36.83		0.58	0.01	-0.38	0.07	1.73	152	21	UB17-5	
UBA174	70.62	34.88	66.4	0.44	0.05	-0.34	0.22	2.12	190	22	UB17-5	
UBA175	70.67	25.42	56.85	0.54	0.11	-0.91	0.1	1.51	186	23	UB17-5	
UBA176	70.72	32.03		0.59	0.13	-0.47	0.13	2.15	208	24	UB17-5	
UBA177	70.77	33.46	61.05	0.59	0	-0.42	0.03	2.65	241	27	UB17-5	
UBA178	70.82	30.21	54.1	0.55	0.02	-0.65	0.14	1.64	172	28	UB17-5	
UBA179	70.87	37.3	63.15	0.6	0.08	-0.65	0.01	2.79	229	29	UB17-5	
UBA180	70.92	55.73		0.95		-0.03		2.4			average used	UB18-26
UBA181	70.97	33.58	53.55	0.56	0.07	-0.83	0.07	2.17	201	32	UB17-5	
UBA182	79.86	39.27	62.35	0.76	0.27	-0.52	0.2	1.72	143	33	UB17-5	
UBA183	79.91	39.01	49.25	0.69	0	-0.14	0.18	1.62	137	34	UB17-5	
UBA184	79.96	43.12	63	0.81	0.08	0	0.12	2.96	212	36	UB17-5	
UBA185	80.01	34.41		0.55	0.04	-0.31	0.04	1.93	177	37	UB17-5	
UBA186	80.06	32.86	57.95	0.72	0.14	-0.37	0.21	2.32	217	38	UB17-5	
UBA187	80.16	39.22		0.73	0	-0.54	0.04	1.39	120	39	UB17-5	
UBA188	80.21	36.17	59.7	0.64	0.04	-0.37	0.02	2.38	204	41	UB17-5	
UBA189	80.26	40.96	55.5	0.78		-0.93		1.79	265	24	average used	UB18-26
UBA190	80.31	33.61		0.84	0	-0.65	0.16	1.53	148	43	UB17-5	
UBA191	80.36	34.85	55.33	0.6	0.07	-0.6	0.13	2.2	197	44	UB17-5	
UBA192	80.41	32.86	44.6	0.76	0.17	-0.44	0.29	2.01	191	46	UB17-5	
UBA193	80.46	39.6	52.1	0.92	0	-0.36	0	2.76	215	47	UB17-5	
UBA194	80.51	41.94		1.01	0.03	-0.22	0.24	2.68	199	48	UB17-5	
UBA195	80.56	35.85	53.88	0.89	0.07	-0.29	0.05	2.53	217	49	UB17-5	
UBA196	80.61	39.1	34.45	1.05	0.24	0.05	0.32	1.94	159	51	UB17-5	
UBA197	80.66	23.89	53.23	1.01	0	-0.56	0.26	1.71	220	52	UB17-5	
UBA198	80.67	30.07	51.15	0.84	0.14	-0.72	0.23	2.39	242	53	UB17-5	
UBA199	80.72	34.84	54.53	0.91	0.03	-0.82	0.15	1.78	163	54	UB17-5	
UBA200	80.77	63.91	60.05	0.99		-0.52		3.28			rerun due to carbon value; average used	Ub18-26
UBA201	80.82	31.2	55.43	0.71	0.02	-0.75	0.09	1.89	190	57	UB17-5	
UBA202	80.87	37.61	64.73	0.66	0.01	-0.78	0.04	1.7	147	58	UB17-5	

UBA203	80.92	39.66	46.58	0.95	0.05	-0.48	0.19	2.67	208	59	UB17-5
UBA204	80.97	41.64	67.85	0.82	0.06	-0.4	0.02	4.87	346	26	UB17-6
UBA205	81.02	48.9	74.25	0.88	0.05	-0.15	0.03	5.76	348	27	UB17-6
UBA206	81.07	45.97	71.85	0.81	0.03	-0.15	0.06	5.71	366	28	UB17-6
UBA207	81.12	52.43	46.7	0.94	0.03	0.13	0.04	6.42	361	29	UB17-6
UBA208	81.17	47.4	71.95	1.03	0.12	0.18	0.13	5.27	330	31	UB17-6
UBA209	81.22	52.68		0.98	0.09	0.28	0.07	6.74	376	32	UB17-6
UBA210	81.27	37.26	68.13	0.69	0.12	-0.11	0.01	4.24	337	33	UB17-6
UBA211	81.32	50.96	38.13	0.85	0.04	0.22	0.08	6.41	370	34	UB17-6
UBA212	81.37	61.77	81.15	0.97	0.01	0.12	0.03	6.98	335	36	UB17-6
UBA213	81.42	51.71	55.13	0.97	0.08	0.03	0.05	6.13	350	37	UB17-6
UBA214	81.47	49.89	77.43	0.81	0.02	-0.03	0.04	5.8	344	38	UB17-6
UBA215	81.5	49.08	55.55	1	0.05	0.13	0.04	5.8	349	39	UB17-6
UBA216	81.51	55.5	81.75	0.94	0.07	0.28	0.02	6.68	355	41	UB17-6
UBA217	81.56	54.78	82.98	0.92	0.11	0.33	0.09	6.87	369	42	UB17-6
UBA218	81.61	54.44	87.98	0.85	0.01	0.17	0.03	6.67	361	43	UB17-6
UBA219	81.66	55.57	89.25	0.95	0.04	0.32	0.13	6.78	360	44	UB17-6
UBA220	81.71	47.32	81.95	0.89	0.04	0.11	0.01	5.73	357	46	UB17-6
UBA221	81.76	57.96	85.28	0.9	0.03	0.46	0	6.97	355	47	UB17-6
UBA222	81.81	53.74	82.55	0.94	0.01	0.45	0.06	6.19	341	48	UB17-6
UBA223	81.86	45.28	83.68	0.83	0.07	0.02	0.11	5.54	361	49	UB17-6
UBA224	81.91	51.02	84.7	0.91	0.06	0.14	0.11	5.97	346	51	UB17-6
UBA225	81.96	60.55	90.68	0.97	0.01	0.23	0.06	7.09	346	52	UB17-6
UBA226	82.01	45.5	71.85	0.98	0.02	0.1	0.05	5.74	371	53	UB17-6
UBA227	82.06	44.53	69.98	0.83	0.01	0.15	0.06	5.24	348	54	UB17-6
UBA228	82.11	54.89	85.48	0.94	0.03	0.25	0.04	6.46	348	56	UB17-6
UBA229	82.16	45.31	71.63	0.85	0.08	-0.22	0.05	5.47	356	57	UB17-6
UBA230	82.21	45.36	67.8	0.95	0.03	-0.24	0.14	5.24	342	58	UB17-6
UBA231	82.26	49.9	71.03	0.87	0.05	-0.21	0.08	6.31	372	59	UB17-6
UBA232	82.31	45.65	73.3	0.91	0.02	-0.12	0.09	5.46	353	8	UB17-7
UBA233	82.32	40.32	73.18	0.81	0.01	-0.02	0.08	5.05	369	9	UB17-7
UBA234	82.37	49.13	72.75	0.85	0.05	0.06	0.05	6.18	370	11	UB17-7
UBA235	82.42	47.78	77.28	0.79	0.03	0.31	0.12	6.06	373	12	UB17-7
UBA236	82.47	40.16	77.28	0.62	0	0.07	0.01	4.96	364	13	UB17-7
UBA237	82.52	45.1	73.95	0.75	0.03	-0.07	0.06	5.33	349	14	UB17-7
UBA238	82.57	44.66	72.5	0.73	0.06	-0.06	0.08	5.26	348	16	UB17-7
UBA239	82.62	51	84.8	0.77	0.06	-0.1	0.07	6.28	363	17	UB17-7
UBA240	82.67	51.94	81.8	0.8	0.01	0.03	0.04	6.3	358	18	UB17-7
UBA241	82.72	48.73	78.45	0.85	0	-0.25	0.02	5.55	337	19	UB17-7
UBA242	82.77	47.9	78.15	0.79	0.03	-0.06	0	5.74	354	21	UB17-7
UBA243	82.82	48.58	79.25	0.93	0.04	-0.29	0.04	5.79	352	22	UB17-7
UBA244	82.87	43.36	84.5	0.83	0.02	0.02	0.01	5.18	353	23	UB17-7
UBA245	82.92	47.6	79.5	0.75	0.01	-0.02	0.09	5.6	348	24	UB17-7

UBA246	82.97	44.03	82.9	0.82	0.07	0.08	0.07	4.93	332	8	UB17-8		
UBA247	83.05	46.13	79.95	0.72	0.04	0.22	0.03	5.65	361	9	UB17-8		
UBA248	83.1	45.41	77.48	0.87	0.07	0.2	0.08	5.49	357	11	UB17-8		
UBA249	83.15	50.12	73.83	0.91	0.12	0.07	0.06	6.28	369	12	UB17-8		
UBA250	83.16	44.58	71.08	0.91	0.02	-0.23	0.12	5.33	353	13	UB17-8		
UBA251	83.21	45.7	67.83	0.85	0.02	-0.05	0	5.71	368	14	UB17-8		
UBA252	83.26	44.21	74.7	0.86	0.19	0.01	0.01	5.32	355	16	UB17-8		
UBA253	83.31	49.33	72.48	0.84	0.03	-0.23	0	5.86	351	17	UB17-8		
UBA254	83.36	46.77	68.3	0.75	0.05	-0.08	0.01	5.22	331	18	UB17-8		
UBA255	83.41	49.31	71.5	0.67	0.01	-0.04	0.1	5.65	339	19	UB17-8		
UBA256	83.46	32.24	76.1	0.7	0	-0.03	0.07	3.91	358	21	UB17-8		
UBA257	83.51	53.36	76	0.86	0.05	0.39	0	6.67	368	22	UB17-8		
UBA258	83.56	51.57	76.23	0.72	0.01	0.54	0.08	6.41	366	23	UB17-8		
UBA259	83.61	49.39	79.15	0.89	0.08	0.33	0.04	6.23	371	24	UB17-8		
UBA260	83.66	44.92	72.85	0.61	0.01	0.47	0.12	5.31	349	26	UB17-7		
UBA261	83.71	45.38	70.93	0.6	0.02	0.82	0.19	5.36	349	27	UB17-7		
UBA262	83.76	39.05	73.98	0.64	0.09	0.61	0.01	4.68	354	28	UB17-7		
UBA263	83.81	39.27	63.38	0.47	0.01	0.17	0.05	4.53	341	29	UB17-7		
UBA264	83.86	41.55	73.08	0.42	0.08	0.26	0.05	5.16	366	31	UB17-7		
UBA265	83.91	34.98	62.8	0.46	0.01	0.07	0.02	4.42	372	32	UB17-7		
UBA266	83.96	30.31	47.03	0.53	0.03	-0.5	0.09	3.8	369	33	UB17-7		
UBA267	87.5	3.33	6.2	1.12	0.08	-2.91	0.1	2.63	2216	9	failed	UB17-25	
UBA268	87.55	2.57	5.78	1.17	0.07	-3.07	0.03	2.99	3244	11	failed	UB17-25	
UBA269	87.6	3.09	6.35	1.12	0.12	-3.06	0.16	2.89	2611	12	failed	UB17-25	
UBA270	87.65	4.09	8.35	1.05	0.02	-3.15	0.12	2.8	1918	13	failed	UB17-25 rerun due to carbon value, average used	UB18-26
UBA271	87.7	2.69	5.63	0.97		-3.03		3.53			failed	UB17-8	
UBA272	87.75	4.58	7.15	1.4	0.04	-2.98	0.02	3.81	2326	44	failed	UB17-8	
UBA273	87.8	4.04	7.28	1.27	0.06	-3.12	0.17	3.55	2456	46	failed	UB17-8	
UBA274	87.85	3.79	6.4	1.39	0.11	-2.97	0.2	4.83	3555	47	failed	UB17-8	
UBA275	87.9	3.94	6.43	1.28	0.07	-3.28	0.15	3.33	2366	48	failed	UB17-8	
UBA276	87.95	4.07	6.8	1.35	0.05	-3.31	0.05	3.25	2238	49	failed	UB17-8	
UBA277	88	3.02	5.38	1.44	0.09	-3.09	0.06	3.65	3370	51	failed	UB17-8	
UBA278	88.05	2.83	6.2	1.26	0.05	-3.15	0.12	2.79	2756	14	failed	UB17-25	
UBA279	88.15	5.52	14.03	1.28	0.07	-1.73	0.16	2.61	1330	16	failed	UB17-25	
UBA280	88.2	4.45	12.68	1.08	0.1	-1.47	0.07	2.42	1532	17	failed	UB17-25	
UBA281	88.25	4.55	9.38	0.98	0.12	-1.44	0.1	2.97	1829	18	failed	UB17-25	
UBA282	88.3	3.65	7.75	1.08	0.16	-1.08	0.03	2.53	1941	19	failed	UB17-25	
UBA283	88.35	3.46	9.13	0.88	0.06	-1.4	0.07	3.04	2460	21	failed	UB17-25	
UBA284	88.38	3.07	8.18	1.04	0.06	-1.74	0.04	2.27	2072	22	failed	UB17-25	
UBA285	88.48	4.04	11.4	1.12	0.07	-1.49	0.03	2.51	1744	23	failed	UB17-25	
UBA286	88.53	4.22	9.98	1.05	0.1	-1.51	0.1	2.87	1901	24	failed	UB17-25	

UBA287	88.58	4.58	10.5	0.97	0.16	-1.55	0.04	2.62	1604	26	failed	UB17-25
UBA288	88.63	2.76	4.4	1.58	0.11	-2.29	0.11	1.75	1779	52	UB17-8	
UBA289	88.68	2.57	4.38	1.63	0.02	-2.57	0.04	1.68	1836	53	UB17-8	
UBA290	88.73	3.55	5.8	1.61	0.13	-2.4	0.15	2.22	1757	54	UB17-8	
UBA291	88.78	1.65	3.63	1.26	0.12	-2.94	0.02	2.81	4756	29	failed	UB17-25
UBA292	88.83	5.49	8.2	1.65	0.04	-2.24	0	3.65	1867	57	UB17-8	
UBA293	88.88	4.86	7.65	1.66	0	-2.46	0.17	3.15	1818	58	UB17-8	
UBA294	88.93	4.55	4.7	1.7	0.22	-2.61	0.1	3.01	1856	59	UB17-8	
UBA295	88.98	1.58	3.38	1.25	0.09	-2.63	0.08	3.61	6354	31	failed	UB17-25
UBA296	89.03	3.35	6.7	1.67	0	-2.42	0	2.82	2350	9	UB17-09	
UBA297	89.08	2.62	4.65	1.42	0	-2.57	0	2.2	2353	11	UB17-09	
UBA298	89.13	3.84	6.9	1.63	0	-2.76	0	3.28	2390	12	UB17-09	
UBA299	89.18	2.76	5.33	1.57	0.02	-2.78	0.02	2.36	2585	28	rerun due to oxygen value	UB18-26
UBA300	89.21	3.86	6.98	1.6	0	-2.64	0	3.3	2387	14	UB17-09	
UBA301	89.26	4.36	8.4	1.35	0	-2.51	0	3.66	2347	16	UB17-09	
UBA302	89.31	3.91	6.63	1.53	0	-2.32	0	3.3	2358	17	UB17-09	
UBA303	89.36	4.36	9	1.5	0	-2.27	0	3.66	2344	18	UB17-09	
UBA304	89.41	3.82	6.43	1.35	0	-2.56	0	3.21	2349	19	UB17-09	
UBA305	89.46	3.6	7.48	1.62	0	-2.53	0	3.03	2349	21	UB17-09	
UBA306	89.51	4.74	6.93	1.59	0	-2.15	0	4	2361	22	UB17-09	
UBA307	89.56	4.36	7.93	1.64	0	-2.36	0	3.59	2303	23	UB17-09	
UBA308	89.61	5.88	9.78	1.61	0	-2.11	0	4.94	2348	24	UB17-09	
UBA309	89.66	4.5	7.68	1.62	0	-2.35	0	3.86	2397	26	UB17-09	
UBA310	89.71	4.66	8.25	1.68	0	-2.49	0	3.91	2345	27	UB17-09	
UBA311	89.76	4.6	7.78	1.67	0	-2.62	0	3.83	2326	28	UB17-09	
UBA312	89.81	5.54	8.63	1.48	0	-2.34	0	4.66	2355	29	UB17-09	
UBA313	89.86	5.46	8.88	1.51	0	-2.38	0	4.58	2346	31	UB17-09	
UBA314	89.91	5.6	9.95	1.71	0	-2.42	0	4.78	2388	32	UB17-09	
UBA315	89.96	5.92	10.18	1.68	0	-2.47	0	4.93	2326	33	UB17-09	
UBA316	90.01	5.87	10.9	1.61	0	-2.46	0	4.95	2357	34	UB17-09	
UBA317	90.06	6.68	9.85	1.65	0	-2.33	0	5.6	2345	36	UB17-09	
UBA318	90.07	3.88	6.93	1.74	0	-2.48	0	3.27	2356	37	UB17-09	
UBA319	90.12	5.84	8.73	1.87	0	-2.2	0	4.97	2378	38	UB17-09	
UBA320	90.17	3.25	11.48	1.65	0.18	-2.53	0.17	2.73	1363	29	rerun due to oxygen value	UB18-26
UBA321	90.22	6.64	10.23	1.65	0	-2.45	0	5.63	2372	41	UB17-09	
UBA322	90.27	5.13	7.38	1.56	0	-2.41	0	4.24	2311	42	UB17-09	
UBA323	90.32	4.58	8.93	1.47	0	-2.81	0	3.85	2355	43	UB17-09	
UBA324	90.37	5.7	9.98	1.62	0	-2.43	0	4.8	2357	44	UB17-09	
UBA325	90.42	5.74	9.08	1.34	0	-2.6	0	4.75	2313	46	UB17-09	
UBA326	90.47	6.32	9.43	1.29	0	-2.67	0	5.39	2385	47	UB17-09	
UBA327	90.52	5.54	8.48	1.13	0	-2.74	0	4.69	2366	48	UB17-09	
UBA328	90.57	7.12	10.35	1.36	0	-2.66	0	5.91	2322	49	UB17-09	
UBA329	90.62	6.3	9.78	1.41	0	-2.57	0	5.23	2323	51	UB17-09	

UBA330	90.67	5.82	9.63	0.8	0	-2.84	0	4.93	2365	52	UB17-09		
UBA331	90.72	3.16	9.03	1.45	0.06	-2.87	0.23	2.62	1870	31	rerun due to carbon value	UB18-26	
UBA332	90.77	5.37	8.13	1.41	0	-2.77	0	4.47	2325	54	UB17-09		
UBA333	90.82	6.54	9.23	0.92	0	-2.87	0	5.53	2362	56	UB17-09		
UBA334	90.87	5.57	8.23	0.97	0	-2.22	0	4.75	2384	57	UB17-09		
UBA335	90.92	4.99	9.03	0.93	0	-2.28	0	4.12	2307	58	UB17-09		
UBA336	90.96	4.78	7.58	1.61	0	-2.17	0	4.08	2382	59	UB17-09		
UBA337	90.97	5.1	8.35	1.65	0	-2.21	0	4.36	2394	8	UB17-10		
UBA338	91.01	5.63	9.1	1.65	0	-2.36	0	4.64	2303	9	UB17-10		
UBA339	91.05	5.73	9.45	1.59	0	-2.13	0	4.76	2321	11	UB17-10		
UBA340	91.09	5.57	9.33	1.57	0	-2.24	0	4.68	2350	12	UB17-10		
UBA341	91.13	5.22	7.98	1.73	0	-2.23	0	4.38	2344	13	UB17-10		
UBA342	91.18	4.42	7.93	1.78	0	-2.4	0	3.79	2398	14	UB17-10		
UBA343	91.22	6.4	9.2	1.58	0	-2.05	0	5.39	2354	16	UB17-10		
UBA344	91.26	3.99	6.63	1.85	0	-2.13	0	3.39	2377	17	UB17-10		
UBA345	91.3	3.17	6.15	1.71	0	-2.31	0	2.69	2374	18	UB17-10		
UBA346	91.34	4.38	7.7	1.63	0	-2.06	0	3.73	2381	19	UB17-10		
UBA347	91.39	4.29	5.73	1.64	0	-2.41	0	3.68	2394	21	UB17-10		
UBA348	91.43	3.19	5.25	1.7	0	-2.75	0	2.66	2334	22	UB17-10		
UBA349	91.47	4.14	7.6	1.69	0.01	-2.67	0.22	2	1361	26	UB17-8		
UBA350	91.51	4.39	7.55	1.71	0.12	-2.44	0.19	2.06	1320	27	UB17-8		
UBA351	91.55	4.4	7.78	1.7	0.31	-2.64	0.24	2.08	1334	28	UB17-8		
UBA352	91.6	2.66	4.9	1.83	0.01	-2.72	0.21	1.95	2059	29	UB17-8		
UBA353	91.64	3.25	5.25	1.66	0.01	-2.76	0.06	2.29	1975	31	UB17-8		
UBA354	91.68	3.11	5.53	1.75	0	-2.41	0.21	2.05	1847	32	UB17-8		
UBA355	91.72	2.82	5	1.62	0.03	-2.88	0	2.05	2040	33	UB17-8		
UBA356	91.75	2.14	6.48	1.53	0.03	-2.73	0.06	3.07	4008	32	failed	UB17-25	
UBA357	91.8	2.74	5.73	1.46	0.06	-3.1	0.17	1.73	1766	36	UB17-8		
UBA358	91.85	2.87	5.45	1.56	0.1	-2.84	0.17	1.89	1845	37	UB17-8		
UBA359	91.9	2.16	4.48	1.39	0.12	-2.83	0.09	1.78	2300	38	UB17-8		
UBA360	91.95	5	48.68	-2.45		-1.24		3.22	2440	32	failed	rerun due to carbon value	averaged but very weird might be able to exclude it due to inconsistency in-between data points
UBA361	92	2.7	5.45	1.39	0.05	-3.1	0.04	1.84	1907	41	UB17-8		
UBA362	93.27	2.17	6.18	1.24	0	-2.67	0.12	3.88	4968	55	failed	UB17-25	
UBA363	93.32	4.35	7.55	1.24	0	-2.91	0	4.19	2693	23	UB17-10		
UBA364	93.37	2.61	5.28	1.3	0	-2.94	0	3.62	3864	24	UB17-10		
UBA365	93.42	2.82	4.68	1.27	0	-2.57	0	4.32	4269	26	UB17-10		
UBA366	93.47	3.12	5.88	1.13	0	-2.64	0	3.81	3406	27	UB17-10		
UBA367	93.52	3.82	6.45	1.25	0	-2.84	0	4.26	3114	28	UB17-10		
UBA368	93.57	3.01	5.13	1.3	0	-2.8	0	4.26	3946	29	UB17-10		

UBA369	93.62	3.2	6.68	1.28	0	-3.04	0	3.53	3076	31	UB17-10	
UBA370	93.67	3.53	5.35	1.36	0	-2.76	0	4.78	3777	32	UB17-10	
UBA371	93.7	2.49	4.9	1.29	0	-2.71	0	3.69	4128	33	UB17-10	
UBA372	93.75	3.62	6.18	1.35	0	-2.7	0	4.26	3278	34	UB17-10	
UBA373	93.8	3.61	5.88	1.25	0	-2.88	0	4.41	3406	36	UB17-10	
UBA374	93.85	3.51	6.35	1.39	0	-2.88	0	4.01	3186	37	UB17-10	
UBA375	93.9	4.14	6.2	1.31	0	-2.69	0	4.8	3232	38	UB17-10	
UBA376	93.95	3.44	5.73	1.27	0	-2.61	0	4.38	3551	39	UB17-10	
UBA377	94	1.11	3.08	1.08	0.04	-2.32	0.13	2.64	10037	33	rerun due to carbon value average?	UB18-26
UBA378	94.05	2.17	4.05	1.2	0	-2.81	0	3.9	4996	42	UB17-10	
UBA379	94.1	2.66	4.85	1.27	0	-2.45	0	4.01	4206	43	UB17-10	
UBA380	94.15	2.94	4.95	1.32	0	-2.49	0	4.27	4042	44	UB17-10	
UBA381	94.2	1.94	3.68	1.25	0	-2.55	0	3.84	5505	46	UB17-10	
UBA382	94.25	2.71	4.63	1.28	0	-2.44	0	4.29	4407	47	UB17-10	
UBA383	94.3	4.1	7.4	1.26	0	-2.43	0	4	2721	48	UB17-10	
UBA384	94.35	4.09	6.28	1.41	0	-2.2	0	4.74	3233	49	UB17-10	
UBA385	94.4	2.26	4.6	1.19		-3.01		3.54			rerun due to oxygen value	average used
UBA386	94.45	2.79	5.1	1.31	0	-2.41	0	3.97	3961	52	UB17-10	
UBA387	94.5	4.73	7.5	1.44	0	-2.41	0	4.52	2669	53	UB17-10	
UBA388	94.52	5.2	8.75	1.27	0	-2.54	0	4.37	2353	54	UB17-10	
UBA389	94.57	4.24	6.4	1.27	0	-2.57	0	4.84	3179	56	UB17-10	
UBA390	94.62	4.01	6.33	1.35	0	-2.55	0	4.63	3224	57	UB17-10	
UBA391	94.67	4.85	7.8	1.28	0	-2.47	0	4.5	2592	58	UB17-10	
UBA392	94.72	3.85	6.28	1.33	0	-2.62	0	4.45	3219	59	UB17-10	
UBA393	94.77	3.29	8.5	1.24	0	-2.71	0	2.82	2395	8	UB17-11	
UBA394	94.82	4.45	8.65	1.32	0	-2.38	0	3.69	2315	9	UB17-11	
UBA395	94.87	5.65	9.23	1.48	0	-2	0	4.48	2220	11	UB17-11	
UBA396	94.92	5.63	9.2	1.58	0	-2.18	0	4.37	2171	12	UB17-11	
UBA397	94.97	5.81	9.93	1.58	0	-2.33	0	4.22	2030	13	UB17-11	
UBA398	95.02	6.06	10.23	1.51	0	-2.19	0	4.32	1997	14	UB17-11	
UBA399	95.07	5.08	8.18	1.59	0	-2.22	0	4.52	2483	16	UB17-11	
UBA400	95.12	5.62	9.33	1.59	0	-2.23	0	4.38	2184	17	UB17-11	
UBA401	95.17	7.25	11.58	1.54	0	-2.32	0	4.51	1746	18	UB17-11	
UBA402	95.22	6.26	9.4	1.58	0	-2.21	0	4.84	2165	19	UB17-11	
UBA403	95.27	5.55	9.05	1.57	0	-2.26	0	4.55	2290	21	UB17-11	
UBA404	95.3	4.35	7.38	1.7	0	-2.17	0	4.23	2719	22	UB17-11	
UBA405	95.32	5.31	8.15	1.74	0	-2.29	0	4.8	2527	23	UB17-11	
UBA406	95.37	4.74	8.3	1.77	0	-2.38	0	4.11	2422	24	UB17-11	
UBA407	95.42	3.15	5.38	1.78	0	-2.38	0	4.26	3766	26	UB17-11	
UBA408	95.47	4.36	6.48	1.72	0	-2.38	0	4.89	3132	27	UB17-11	
UBA409	95.52	3.14		1.76	0	-2.4	0	3.51	3123	28	UB17-11	
UBA410	95.57	4.08	6.43	1.74	0	-2.43	0	4.56	3120	29	UB17-11	

UBA411	95.62	4.18	8.75	1.72	0	-2.27	0	3.52	2354	31	UB17-11	
UBA412	95.67	5.37	8.08	1.68	0	-2.37	0	4.91	2555	32	UB17-11	
UBA413	95.72	4.82		1.72	0	-2.4	0	4.95	2861	33	UB17-11	
UBA414	95.77	3.56	6.2	1.72	0	-2.54	0	4.15	3252	34	UB17-11	
UBA415	95.82	4.07	5.45	1.73	0	-2.31	0	5.41	3707	36	UB17-11	
UBA416	95.87	3.28	9.05	1.69	0.01	-2.5	0.11	2.66	2270	33	failed	UB17-25
UBA417	95.92	5.3	8.58	1.89	0	-2.26	0	4.49	2367	38	UB17-11	
UBA418	95.97	5.02	7.6	1.82	0	-2.21	0	4.82	2684	39	UB17-11	
UBA419	96.02	5.36	8.85	1.6	0	-2.38	0	4.34	2267	41	UB17-11	
UBA420	96.07	2.58	6.13	1.31	0	-2.44	0	3.06	3310	42	UB17-11	
UBA421	96.12	5.79		1.62	0	-2.38	0	5.38	2596	43	UB17-11	
UBA422	96.14	6.49	11.03	1.68	0	-2.43	0	4.32	1865	44	UB17-11	
UBA423	96.19	7.19	13.18	1.64	0	-2.19	0	3.92	1532	46	UB17-11	
UBA424	96.24	7.49	11.6	1.58	0	-2.36	0	4.64	1739	47	UB17-11	
UBA425	96.29	6.16	12.5	1.45	0	-2.44	0	3.55	1617	48	UB17-11	
UBA426	96.34	6.99		1.58	0	-2.34	0	4.38	1760	49	UB17-11	
UBA427	96.39	7.34	11.43	1.59	0	-2.24	0	4.7	1794	51	UB17-11	
UBA428	96.44	8.25		1.39	0	-2.26	0	4.75	1618	52	UB17-11	
UBA429	96.49	7.83	14.13	1.43	0	-2.32	0	4.03	1450	53	UB17-11	
UBA430	96.54	7.81	14	1.51	0	-2.44	0	4.01	1442	54	UB17-11	
UBA431	96.59	7.86	14.25	1.08	0	-2.16	0	4.09	1462	56	UB17-11	
UBA432	96.64	8.96	62.13	-2.67	0.01	-1.08	0.13	3.3	1041	34	failed	UB17-25
UBA433	96.69	7.87		0.56		-2.15		2.98			rerun due to carbon value	average used
UBA434	96.74	6.24	11.23	1.36	0	-2.36	0	4.02	1803	59	UB17-11	
UBA435	96.79	6.43	11.98	1.24	0	-2.42	0	4	1747	8	UB17-12	
UBA436	96.84	5.69		1.26	0	-2.36	0	3.9	1918	9	UB17-12	
UBA437	96.89	6.12	9.68	1.15	0	-2.55	0	4.56	2087	11	UB17-12	
UBA438	96.94	6.21		1.19	0	-2.52	0	5.57	2506	12	UB17-12	
UBA439	96.99	3.92	7.1	1.26	0	-2.5	0	4.06	2888	13	UB17-12	
UBA440	97	5.23	8.8	1.31	0	-2.68	0	4.27	2287	14	UB17-12	
UBA441	97.04	5.23	9.03	1.44	0	-2.63	0	4.27	2282	16	UB17-12	
UBA442	97.09	4.64	8.23	1.31	0	-2.64	0	4.11	2472	17	UB17-12	
UBA443	97.14	4.53	7.6	1.18	0	-2.69	0	4.37	2694	18	UB17-12	
UBA444	97.19	4.23	8.15	1.31	0	-2.8	0	3.85	2540	29	UB17-12	
UBA445	97.24	4.94		1.18	0	-2.78	0	4.52	2558	21	UB17-12	
UBA446	97.29	3.77	7.63	1.36	0	-2.82	0	3.65	2704	22	UB17-12	
UBA447	97.34	4.18	7.2	1.31	0	-2.54	0	4.19	2796	23	UB17-12	
UBA448	97.39	4.47	8.03	1.29	0	-2.64	0	3.97	2482	24	UB17-12	
UBA449	97.44	6.3	9.93	1.21	0	-2.68	0	4.62	2054	26	UB17-12	
UBA450	97.49	4.32	7.95	1.27	0	-2.66	0	3.95	2557	27	UB17-12	
UBA451	97.54	5.96	9.25	1.3	0	-2.93	0	4.7	2205	28	UB17-12	
UBA452	97.59	6.38	10.38	1.27	0	-2.72	0	4.5	1975	29	UB17-12	
UBA453	97.64	4.9	7.98	1.21	0	-2.71	0	4.5	2565	31	UB17-12	

UBA454	97.69	5.15	8.65	1.39	0	-2.86	0	4.36	2365	32	UB17-12	
UBA455	97.74	5.18	8.18	1.25	0	-2.9	0	4.61	2490	33	UB17-12	
UBA456	97.77	4.51	7.5	1.29	0	-2.75	0	4.42	2734	34	UB17-12	
UBA457	97.82	4.22	7.4	1.11	0	-2.92	0	4.13	2733	36	UB17-12	
UBA458	97.87	4.71	7.85	1.36	0	-2.53	0	4.36	2589	37	UB17-12	
UBA459	97.92	3.74	7.53	1.26		-3.04		3.61			rerun due to oxygen value	average used
UBA460	97.97	4.93	7.53	1.34	0	-2.66	0	4.73	2683	39	UB17-12	
UBA461	101.63	6.27	11.5	1.51	0	-2.72	0	4	1791	41	UB17-12	
UBA462	101.67	6.5		1.53	0	-2.72	0	4.01	1729	42	UB17-12	
UBA463	101.73	7.81	12.6	1.23	0	-2.67	0	4.59	1652	43	UB17-12	
UBA464	101.78	6.16	10.23	1.46	0	-2.49	0	4.31	1957	44	UB17-12	
UBA465	101.83	6.33	10.85	1.58	0	-2.64	0	4.36	1928	46	UB17-12	
UBA466	101.88	5.88	9.6	1.38	0	-2.63	0	4.49	2136	47	UB17-12	
UBA467	101.93	5.79	9.48	1.66	0	-2.66	0	4.36	2109	48	UB17-12	
UBA468	101.98	5.78	10.38	1.53	0	-2.7	0	3.97	1926	49	UB17-12	
UBA469	105.23	5.39	8.88	1.66	0	-2.7	0	4.63	2401	51	UB17-12	
UBA470	105.3	5.2	8.5	1.56	0	-2.71	0	4.38	2353	52	UB17-12	
UBA471	105.41	4.54	8.3	1.67	0	-2.98	0	4.01	2470	53	UB17-12	
UBA472	105.56	4.56	7.4	1.52	0	-3.05	0	4.51	2762	54	UB17-12	
UBA473	105.61	4.35	7.8	1.36	0	-2.93	0	4.06	2609	56	UB17-12	
UBA474	105.66	3.18	6.35	1.67	0	-3.07	0	3.59	3151	57	UB17-12	
UBA475	105.69	3.9	7.08	1.6	0	-2.94	0	4.01	2867	58	UB17-12	
UBA476	105.79	3.89	6.78	1.53	0	-3.18	0	4.13	2963	59	UB17-12	
UBA477	105.84	3.47	6.38	1.38	0.01	-3.04	0.06	3.92	3157	8	UB17-13	
UBA478	105.89	3.68	7.53	1.46	0.02	-2.89	0.43	3.53	2677	9	UB17-13	
UBA479	105.94	2.82	4.68	1.47	0.01	-2.9	0.02	4.34	4293	11	UB17-13	
UBA480	105.99	3.65	6.1	1.39	0.02	-2.81	0.08	4.35	3321	12	UB17-13	
UBA481	106.04	2.33	5.85	1.4	0.01	-3.2	0.07	2.87	3439	13	UB17-13	
UBA482	106.09	2.95		1.47	0.05	-2.86	0.11	3.53	3338	14	UB17-13	
UBA483	106.14	3.17	6.25	1.46	0.03	-2.66	0.02	3.68	3234	16	UB17-13	
UBA484	106.19	3.01	6.7	1.39	0.05	-2.74	0.03	3.23	2987	17	UB17-13	
UBA485	106.24	3.04	5.75	1.37	0.16	-2.79	0.16	3.81	3493	18	UB17-13	
UBA486	106.29	2.71	5.58	1.44	0.09	-2.78	0.12	3.53	3630	29	UB17-13	
UBA487	106.34	2.96	5.18	1.58	0.08	-2.97	0.1	4.15	3901	21	UB17-13	
UBA488	106.39	3.96	7.6	1.29	0.13	-3.08	0.08	3.79	2669	22	UB17-13	
UBA489	106.44	2.75	6.45	1.34	0.14	-3.13	0.03	3.06	3113	23	UB17-13	
UBA490	106.49	3.87	7.55	1.2	0.05	-3.31	0.11	3.77	2719	24	UB17-13	
UBA491	106.54	7.62	14.08	1.51	0.03	-2.69	0.12	3.89	1438	26	UB17-13	
UBA492	106.59	8.24	14.18	1.38	0.02	-2.45	0.03	4.29	1466	27	UB17-13	
UBA493	106.64	7.13	14.6	1.52	0.02	-2.42	0.01	3.59	1416	28	UB17-13	
UBA494	106.69	10.72	18	1.24	0.09	-2.47	0.03	4.2	1107	29	UB17-13	
UBA495	106.74	8.59	14.6	1.34	0.01	-2.49	0.05	4.42	1448	31	UB17-13	
UBA496	106.79	4.89	8	1.2	0.06	-2.75	0.01	4.43	2532	32	UB17-13	

UBA497	106.84	4.39	8.15	1.18	0.01	-3.12	0.11	3.87	2466	33	UB17-13	
UBA498	106.89	4.57	8.08	1.2	0	-2.91	0.08	4.11	2517	34	UB17-13	
UBA499	106.94	6.93	11.25	1.25	0.06	-2.53	0.12	4.4	1781	36	UB17-13	
UBA500	106.99	8.67	15.68	1.08	0.1	-2.8	0.08	4.03	1309	37	UB17-13	
UBA501	107.04	9.43	14.65	1.3	0.06	-2.56	0.08	4.74	1415	38	UB17-13	
UBA502	107.09	8.31	13.7	1.55	0.06	-2.36	0.09	4.42	1495	39	UB17-13	
UBA503	107.14	9.07	16.33	1.22	0	-2.29	0.02	3.95	1229	41	UB17-13	
UBA504	107.19	8.94	15.1	1.21	0.05	-2.49	0.11	4.3	1354	42	UB17-13	
UBA505	107.24	9.47	16.25	1.15	0.02	-2.36	0.05	4.28	1273	43	UB17-13	
UBA506	107.29	8.13	14.55	1.13	0.04	-2.33	0.02	4.05	1402	44	UB17-13	
UBA507	107.34	9.19	16.58	1.08	0	-2.33	0.11	4.18	1281	46	UB17-13	
UBA508	107.39	8.8	15.23	1	0.09	-2.44	0.09	4.16	1331	47	UB17-13	
UBA509	107.43	8.56	20.98	0.6		-2.07		3.04			rerun due to carbon value	average used
UBA510	107.48	5.95	17.1	0.59		-1.89		2.54			rerun due to oxygen value	average used
UBA511	107.53	8.75	16.1	0.82	0.02	-2.4	0.04	3.93	1265	51	UB17-13	
UBA512	107.58	7.7	17.15	0.89	0.02	-2.65	0.06	3.23	1184	52	UB17-13	
UBA513	107.63	8.1	13.05	1.03	0.06	-2.65	0.02	4.45	1542	53	UB17-13	
UBA514	107.68	8.86	13.7	1.09	0.07	-2.61	0.15	4.88	1548	54	UB17-13	
UBA515	107.73	7.8	13.3	1.09	0.02	-2.71	0.11	4.17	1503	56	UB17-13	
UBA516	107.78	6.47	12.35	1.14	0.08	-2.81	0.04	3.9	1690	57	UB17-13	
UBA517	107.83	7.67	13.13	1.11	0.03	-2.76	0.1	4.4	1612	58	UB17-13	
UBA518	107.88	8.53	13.78	1.1	0.09	-2.68	0.08	4.55	1501	59	UB17-13	
UBA519	107.93	6.51	11.15	1.15	0.01	-3	0.01	4.26	1835	8	UB17-14	
UBA520	107.98	6.1	10.58	1.19	0.03	-2.85	0.08	4.28	1967	9	UB17-14	
UBA521	108.03	5.21	9.83	1.24	0.04	-2.99	0	3.81	2046	11	UB17-14	
UBA522	108.08	4.25	9.4	1.26	0	-2.83	0.14	3.28	2159	12	UB17-14	
UBA523	108.13	5.59	10.33	1.13	0.03	-3.01	0.07	3.97	1989	13	UB17-14	
UBA524	108.18	4.22	8.38	1.28	0.07	-2.86	0	3.71	2462	14	UB17-14	
UBA525	108.23	5.05	8.65	1.19	0.01	-2.99	0.16	4.25	2356	16	UB17-14	
UBA526	108.28	3.73	8.08	1.23	0.09	-2.93	0.1	3.34	2504	17	UB17-14	
UBA527	108.35	4.18	7.43	1.28	0.01	-2.77	0	4.03	2692	18	UB17-14	
UBA528	108.4	3.26	6.43	1.28	0.04	-2.83	0.02	3.69	3161	29	UB17-14	
UBA529	108.45	4.56	8.1	1.2	0.04	-2.99	0.09	4.06	2493	21	UB17-14	
UBA530	108.5	3.15	6.9	1.47	0.2	-2.96	0	3.3	2930	22	UB17-14	
UBA531	108.55	3.85	7.1	1.33	0.06	-2.84	0.11	3.89	2827	23	UB17-14	
UBA532	108.6	3.57	6.8	1.41	0.01	-3.07	0.14	3.83	2999	24	UB17-14	
UBA533	108.65	4.99	9.88	1.31	0.08	-3.02	0.12	3.68	2063	26	UB17-14	
UBA534	108.7	3.87	7.75	1.43	0.05	-2.93	0.06	3.6	2599	27	UB17-14	
UBA535	108.75	4.41	7.08	1.38	0.06	-2.86	0.1	4.5	2846	28	UB17-14	
UBA536	108.8	3.38	5.98	1.43	0.03	-2.89	0.06	4.1	3387	29	UB17-14	
UBA537	108.85	4.25	7.03	1.33	0.02	-2.96	0.18	4.47	2932	31	UB17-14	
UBA538	108.9	5.71	8.88	1.27	0.03	-2.99	0.14	4.66	2285	32	UB17-14	
UBA539	108.95	3.76	6.83	1.45	0.08	-2.91	0.02	3.98	2954	33	UB17-14	

UBA540	109	3.35	6.35	1.39	0.02	-3.08	0.08	3.88	3227	34	UB17-14	
UBA541	109.05	3.32	5.85	1.39	0.08	-3.04	0.04	4.11	3445	36	UB17-14	
UBA542	109.1	3.93	7.4	1.41	0.05	-2.88	0.01	3.81	2710	37	UB17-14	
UBA543	109.13	4.36	8.18	1.33	0.09	-3.07	0.02	3.92	2510	38	UB17-14	
UBA544	109.18	4.27	6.78	1.34	0	-3.1	0	4.55	2973	39	UB17-14	
UBA545	109.23	2.87	4.9	1.44	0.03	-2.78	0.13	4.21	4089	41	UB17-14	
UBA546	109.28	4.38	7.1	1.37	0.02	-3.05	0.01	4.5	2868	42	UB17-14	
UBA547	109.33	3.79	6.73	1.44	0.07	-2.94	0.05	4.13	3038	43	UB17-14	
UBA548	109.38	7.16	12.98	1.59	0.11	-2.62	0.07	3.93	1540	44	UB17-14	
UBA549	109.43	6.71	11.93	1.75	0.04	-2.37	0.12	4.22	1763	46	UB17-14	
UBA550	109.48	7.71	12.8	1.73	0.06	-2.49	0.11	4.3	1567	47	UB17-14	
UBA551	109.53	7.11	11.68	1.71	0.09	-2.55	0.09	4.42	1742	48	UB17-14	
UBA552	109.58	8.42	14.15	1.65	0.07	-2.5	0.06	4.32	1444	49	UB17-14	
UBA553	109.63	7.18	11.5	1.76	0.03	-2.42	0.05	4.48	1750	51	UB17-14	
UBA554	109.68	8.82	14.93	1.54	0.01	-2.32	0.12	4.44	1417	52	UB17-14	
UBA555	109.73	9.15	21.23	0.74		-1.99		3.05	1031	41	Looks a little odd	average used
UBA556	109.78	8.31	13.35	1.92	0.03	-2.24	0.11	4.49	1519	54	UB17-14	
UBA557	109.83	9.1	13.73	1.86	0.01	-2.32	0.12	4.94	1524	56	UB17-14	
UBA558	109.88	6.46	11.25	1.88	0.06	-2.47	0.12	4.2	1823	57	UB17-14	
UBA559	109.93	5.38	8.58	1.82	0.05	-2.39	0.02	4.5	2337	58	UB17-14	
UBA560	109.98	4.83	8.48	1.87	0.02	-2.44	0.01	4.16	2411	59	UB17-14	
UBA561	110	5.85	10.95	0.81	0	-2.47	0.01	3.97	1904	8	UB17-15	
UBA562	110.14	4.78	8.9	0.71	0.12	-3.01	0.03	3.93	2299	9	UB17-15	
UBA563	110.19	6.5	11.13	0.86	0.07	-2.89	0.07	4.25	1834	11	UB17-15	
UBA564	110.24	5.33	9.48	0.91	0.06	-2.78	0.03	4.05	2128	12	UB17-15	
UBA565	110.29	6.05	10.9	0.77	0.04	-2.8	0.17	4.12	1907	13	UB17-15	
UBA566	110.34	5.89	10.3	0.88	0.02	-2.65	0.11	4.23	2012	14	UB17-15	
UBA567	110.39	7.71	12.8	0.99	0.05	-2.54	0.01	4.44	1617	16	UB17-15	
UBA568	110.44	6.61	11.73	1.07	0.01	-2.69	0.08	4.14	1757	17	UB17-15	
UBA569	110.49	5.63	12.23	1.06	0.01	-2.61	0.1	3.45	1719	18	UB17-15	
UBA570	110.54	7.28	12.85	1.07	0.07	-2.67	0.11	4.04	1561	29	UB17-15	
UBA571	110.59	7.58	15.28	0.53		-2.5		3.62			rerun due to carbon value	average used
UBA572	110.64	10.2	16.18	0.81	0.06	-2.52	0.11	4.47	1235	22	UB17-15	
UBA573	110.72	11	18.55	0.83	0.01	-2.17	0	4.28	1100	23	UB17-15	
UBA574	110.77	11.17	19.28	0.81	0.08	-2.16	0.03	4.28	1082	24	UB17-15	
UBA575	110.82	10.85		1.09	0.1	-2.04	0.2	4.79	1244	26	UB17-15	
UBA576	110.87	9.52	15.45	1.1	0.01	-2.32	0.1	4.51	1335	27	UB17-15	
UBA577	110.92	8.78	14.05	1.21	0.04	-2.06	0.05	4.66	1492	28	UB17-15	
UBA578	110.97	8.53	13.98	1.29	0.06	-2.18	0.2	4.56	1502	29	UB17-15	
UBA579	111.02	9.37	17	1.19	0.06	-2.17	0.07	4	1205	31	UB17-15	
UBA580	111.07	9.62	16.68	1.34	0.02	-2.13	0.18	4.33	1270	32	UB17-15	
UBA581	111.12	9.91	15.95	1.29	0.08	-2.29	0.09	4.72	1341	33	UB17-15	
UBA582	111.17	11.27	18.63	1.25	0.01	-2.38	0.04	4.62	1158	34	UB17-15	

UBA583	111.22	9.5	14	1.43	0.06	-2.1	0.11	5.08	1504	36	UB17-15
UBA584	111.27	10.84	18.65	1.24	0.05	-2.33	0.04	4.3	1120	37	UB17-15
UBA585	111.32	11.42	19.03	1.34	0.01	-2.12	0.11	4.35	1077	38	UB17-15
UBA586	111.37	11.76	18.18	1.47	0.04	-2.2	0.04	4.94	1185	39	UB17-15
UBA587	111.42	10.86	16.38	1.39	0.01	-2.04	0.06	4.97	1289	41	UB17-15
UBA588	111.47	10.55	17	1.32	0.07	-2.16	0.01	4.47	1196	42	UB17-15
UBA589	111.52	8.86	14.7	1.5	0.1	-2.45	0.03	4.43	1407	43	UB17-15
UBA590	111.54	11.24	17.73	1.71	0.05	-2.42	0.14	4.83	1211	44	UB17-15
UBA591	111.59	10.31	15.85	1.61	0.05	-2.37	0.09	4.8	1311	46	UB17-15
UBA592	111.64	9.24	14.43	1.58	0.01	-2.33	0.11	4.71	1432	47	UB17-15
UBA593	111.69	8.25	16.4	1.67	0.02	-2.5	0.2	3.69	1259	48	UB17-15
UBA594	111.74	9.48	14.43	1.38	0.07	-2.5	0.27	4.79	1422	49	UB17-15
UBA595	111.79	10.45	16.28	1.69	0.01	-2.26	0.15	4.81	1296	51	UB17-15
UBA596	111.84	7.59	14.53	1.59	0.03	-2.43	0.1	3.95	1463	52	UB17-15
UBA597	111.89	6.7	12.48	1.59	0.04	-2.38	0.02	3.98	1669	53	UB17-15
UBA598	111.94	9.81	15.63	1.58	0.03	-2.43	0.08	4.5	1292	54	UB17-15
UBA599	111.99	7.34	12.55	1.44	0.03	-2.5	0.11	4.22	1616	56	UB17-15
UBA600	112.04	8.59	12.83	1.53	0.03	-2.58	0.12	4.76	1556	57	UB17-15
UBA601	112.09	8.77	17.38	1.47	0.01	-2.58	0.06	3.72	1197	58	UB17-15
UBA602	112.14	9.3	14.55	1.54	0	-2.4	0.19	4.67	1412	59	UB17-15
UBA603	112.19	6.66	13.4	1.93		-2.26		3.6			rerun due to carbon value
UBA604	112.24	6.65	13.15	1.69	0.08	-1.85	0.03	3.65	1543	9	UB17-16
UBA605	112.29	8.49	13.85	1.49	0.05	-2.39	0.08	4.39	1454	11	UB17-16
UBA606	112.34	7.15	13.35	1.41	0.05	-2.41	0.1	3.91	1539	12	UB17-16
UBA607	112.4	7.58	11.85	1.47	0.11	-2.44	0.08	4.65	1720	13	UB17-16
UBA608	112.45	7.37	11.48	1.51	0	-2.54	0.16	4.74	1803	14	UB17-16
UBA609	112.5	7.66	13.65	1.33	0.05	-2.4	0.05	4.18	1532	16	UB17-16
UBA610	112.55	6.34	10.4	1.59	0.07	-2.4	0.14	4.43	1955	17	UB17-16
UBA611	112.6	6.68	11.1	1.5	0.08	-2.49	0.08	4.45	1866	18	UB17-16
UBA612	112.65	6.08	10.73	1.57	0.03	-2.64	0.17	4.17	1920	29	UB17-16
UBA613	112.7	5.97	9.68	1.59	0.02	-2.55	0.16	4.59	2150	21	UB17-16
UBA614	112.75	4.75	10.1	1.54	0.04	-2.63	0.04	3.43	2025	22	UB17-16
UBA615	112.8	5.99	10.63	1.57	0.03	-2.4	0.17	4.12	1925	23	UB17-16
UBA616	112.85	5.22	8.8	1.52	0	-2.55	0.06	4.29	2297	24	UB17-16
UBA617	112.9	5.12	8.73	1.63	0.01	-2.62	0.05	4.3	2349	26	UB17-16
UBA618	112.95	5.76	9.53	1.58	0.05	-2.65	0.05	4.45	2161	27	UB17-16
UBA619	113	6.11	11.45	1.51	0.03	-2.51	0.1	3.88	1783	28	UB17-16
UBA620	113.05	6.38	11	1.53	0.04	-2.57	0.05	4.28	1882	29	UB17-16
UBA621	113.1	6.65	10.28	1.42	0.06	-2.57	0.06	4.64	1957	31	UB17-16
UBA622	113.15	7.71	11.83	1.36	0.07	-2.49	0.08	4.77	1736	32	UB17-16
UBA623	113.23	5.97	10.55	1.93	0.01	-2.47	0.08	4.07	1911	33	UB17-16

average used

UBA624/984/985	113.28	6.09	11.7	1.67	0.04	-2.23	0.07	3.8	1753		average used; sample used to evaluate homogeneity of dataset	
UBA625	113.33	6.72	11.93	1.61	0.08	-2.34	0.08	4.02	1680	36	UB17-16	
UBA626	113.38	6.62	11.45	1.51	0.04	-2.36	0.21	4.32	1830	37	UB17-16	
UBA627	113.43	7.33	13.95	1.58	0.09	-2.56	0.38	3.76	1443	38	UB17-16	
UBA628	113.48	6.89	12.4	1.7	0.02	-2.15	0.06	4.08	1663	39	UB17-16	
UBA629	113.53	8.41	13.78	1.68	0.04	-2.09	0.13	4.58	1530	41	UB17-16	
UBA630	113.58	7.21	11.9	1.56	0.04	-2.43	0.08	4.38	1704	42	UB17-16	
UBA631	113.63	6.65	11.93	1.62	0.02	-2.5	0.03	3.98	1679	43	UB17-16	
UBA632	113.68	7.12	12.25	1.7	0.04	-2.48	0.15	4.14	1632	44	UB17-16	
UBA633	113.73	8.98	14.9	1.66	0.02	-2.22	0.06	4.29	1345	46	UB17-16	
UBA981	113.78	6.92	13.68	1.68	0.04	-2.09	0.09	3.76	1526	28	UB17-25	
UBA634	113.83	7.43	12.33	1.7	0.01	-2.19	0.08	4.39	1660	47	UB17-16	
UBA635	113.88	8.03	12.85	1.74	0.13	-2.36	0.08	4.65	1627	48	UB17-16	
UBA636	113.93	7.15	11.63	1.66	0.02	-2.25	0.08	4.41	1728	49	UB17-16	
UBA637	113.98	10.83	17.78	1.67	0.02	-2.08	0.03	4.46	1164	51	UB17-16	
UBA638	116.78	12.05	19.65	1.69	0.03	-2	0.05	4.43	1039	52	UB17-16	
UBA639	116.83	8.78	13.85	1.73	0.06	-2.24	0.12	4.54	1454	53	UB17-16	
UBA640	116.88	7.36	14.33	1.86		-2.25		3.77			rerun due to oxygen value	average used
UBA641	116.93	6.52	19.2	1.75	0.17	-2.13	0.05	2.48	782	46	rerun due to oxygen value	UB18-26
UBA642	116.98	11.46	19.55	1.66	0.05	-2.04	0.03	4.32	1065	57	UB17-16	
UBA643	117.03	12.66	20.18	1.61	0.03	-2.12	0.05	4.71	1051	58	UB17-16	
UBA644	117.08	11.56	19.23	1.66	0.02	-2.23	0.06	4.27	1046	59	UB17-16	
UBA645	117.13	9.85	18.05	0.97	0.05	-2.62	0.15	3.86	1108	8	UB17-17	
UBA646	117.18	10.91		0.94	0.02	-2.58	0.1	4.1	1064	9	UB17-17	
UBA647	117.23	13.68	22.43	1.13	0.01	-2.61	0.1	4.59	952	11	UB17-17	
UBA648	117.28	11.73	18	1.18	0.04	-2.61	0.03	4.65	1119	12	UB17-17	
UBA649	117.33	11.94	21.6	0.92	0.04	-2.57	0.08	4.22	1002	13	UB17-17	
UBA650	117.38	11.75	18.28	1.1	0	-2.34	0.36	4.71	1133	14	UB17-17	
UBA651	117.43	9.42	17.58	0.99	0.01	-2.6	0.04	3.9	1167	16	UB17-17	
UBA652	117.48	9.52	18.45	1.15		-2.55		3.71			rerun due to carbon value	average used
UBA653	117.53	9.61	17.33	0.96	0.05	-2.54	0.07	4.1	1204	18	UB17-17	
UBA654	117.58	5.43	14.13	1.64	0.03	-2.31	0.01	2.75	1075	48	rerun due to carbon value	UB18-26
UBA655	117.63	8.11	14.73	1.4	0.05	-2.58	0.32	3.95	1370	21	UB17-17	
UBA656	117.67	11.74	19.38	1.58	0.06	-2.38	0.1	4.31	1038	22	UB17-17	
UBA657	117.72	11.78	19.15	1.55	0.06	-2.26	0	4.4	1056	23	UB17-17	
UBA658	117.77	11.21	20.9	1.46	0.01	-2.29	0	3.77	953	24	UB17-17	
UBA659	117.82	11.34	20.3	1.58	0.01	-2.1	0.02	4.18	1044	26	UB17-17	
UBA660	117.87	12.79	21.15	1.34	0.01	-2.32	0.07	4.31	955	27	UB17-17	
UBA661	117.92	12.83	22.35	1.39	0.09	-2.24	0.06	4.42	976	28	UB17-17	
UBA662	117.97	11.83	20.45	1.48	0.03	-2.14	0.11	4.18	1000	29	UB17-17	

UBA663	118.02	11.29	20.4	1.59	0.02	-2.16	0.07	4.03	1012	31	UB17-17
UBA664	118.32	9.77	15.95	1.61	0.01	-2.26	0.01	4.33	1250	32	UB17-17
UBA665	118.07	9.76	15.05	1.69	0	-2.34	0.01	4.82	1390	33	UB17-17
UBA666	118.12	7.61	14.43	1.76	0.01	-2.22	0.13	3.91	1444	34	UB17-17
UBA667	118.17	7.43	12.58	1.67	0.02	-2.48	0.06	4.25	1608	36	UB17-17
UBA668	118.22	10.36	16.25	1.6	0.01	-2.29	0	4.69	1275	37	UB17-17
UBA669	118.27	11.3	18.93	1.65	0.05	-2.08	0.14	4.41	1102	38	UB17-17
UBA670	118.37	8.7	15.55	1.36	0.02	-2.29	0.04	4.13	1337	39	UB17-17
UBA671	118.42	7.67	13.68	1.31	0	-2.44	0.07	4.13	1512	41	UB17-17
UBA672	118.47	9.25	14.5	1.23	0.01	-2.6	0.03	4.8	1458	42	UB17-17
UBA673	118.52	8.76	14.35	1.34	0.07	-2.38	0	4.34	1395	43	UB17-17
UBA674	118.53	9	15.18	1.6	0.05	-2.52	0.09	4.48	1402	44	UB17-17
UBA675	118.58	8.9	15.65	1.52	0.13	-2.39	0.02	4.22	1336	46	UB17-17
UBA676	118.63	8.2	13.63	1.53	0.08	-2.65	0.09	4.32	1480	47	UB17-17
UBA677	118.68	7.03	13.05	1.43	0.16	-2.37	0.18	3.85	1539	48	UB17-17
UBA678	118.73	8.67	14.3	1.48	0.06	-2.41	0.09	4.45	1445	49	UB17-17
UBA679	118.78	7.29	12.83	1.4	0.02	-2.42	0.06	4.03	1554	51	UB17-17
UBA680	118.83	9.45	13.88	1.2	0.02	-2.32	0.17	4.87	1450	52	UB17-17
UBA681	118.88	8.66	13.35	1.4	0.06	-2.24	0.2	4.81	1562	53	UB17-17
UBA682	118.93	7.93	11.93	1.46	0.04	-2.58	0.06	4.76	1684	54	UB17-17
UBA683	118.98	7.88	12.78	1.51	0.04	-2.25	0.01	4.57	1629	56	UB17-17
UBA684	119.03	10.04	15.88	1.4	0	-2.29	0	4.67	1310	57	UB17-17
UBA685	119.08	9.42	15.13	1.39	0.03	-2.35	0.05	4.48	1339	58	UB17-17
UBA686	119.13	6.5	10.23	1.61	0.02	-2.19	0.08	4.54	1957	59	UB17-17
UBA687	119.18	4.99	12.48	1.74	0.09	-2.32	0.11	2.84	1598	8	UB17-18
UBA688	119.23	8.97	15.85	1.72	0.08	-2.07	0.04	4.13	1299	9	UB17-18
UBA689	119.28	9.66		1.72	0.05	-2.23	0.19	4.38	1277	11	UB17-18
UBA690	119.33	10.5	17.7	1.56	0.07	-2.14	0.12	4.22	1134	12	UB17-18
UBA691	119.36	10.38	17.75	1.8	0.02	-2.13	0.04	4.13	1125	13	UB17-18
UBA692	119.4	8.76	18.95	1.6	0.03	-2.12	0.24	3.42	1103	14	UB17-18
UBA693	119.45	9.98	18.4	1.66	0.02	-2.31	0.03	3.95	1118	16	UB17-18
UBA694	119.5	9.57	17.25	1.81	0.04	-2.36	0.01	4.21	1240	17	UB17-18
UBA695	119.55	10.49	18.05	1.51	0.01	-2.44	0.13	4.32	1164	18	UB17-18
UBA696	119.6	10.23	17.38	1.74	0.07	-2.12	0.13	4.46	1228	29	UB17-18
UBA697	119.65	10.76	18	1.55	0.03	-2.12	0.01	4.39	1151	21	UB17-18
UBA698	119.7	8.25	15.28	1.92	0.06	-2.21	0.03	3.9	1330	22	UB17-18
UBA699	119.75	9.29	17.2	1.83	0.11	-2.24	0	3.81	1158	23	UB17-18
UBA700	119.8	9.24	15.93	1.9	0.01	-2.27	0.05	4.31	1315	24	UB17-18
UBA701	119.85	7.39		1.89	0.19	-2.31	0.02	3.21	1225	26	UB17-18
UBA702	119.9	9.53	17.45	1.86	0.02	-2.06	0.17	3.93	1164	27	UB17-18
UBA703	119.95	9.85	17.98	1.81	0.02	-2.14	0.07	4.1	1176	28	UB17-18
UBA704	120	7.63	15.1	1.91	0.03	-2.24	0.14	3.79	1397	29	UB17-18
UBA705	120.05	10.01	18.38	1.7	0.01	-2.26	0.13	4.02	1135	31	UB17-18

UBA706	120.1	6.23	15.05	1.78	0.02	-2.01	0.18	3.04	1146	49	rerun due to oxygen value	UB18-26
UBA707	120.15	7.89	15.5	1.9	0.01	-2.13	0.08	3.8	1355	33	UB17-18	
UBA708	120.2	9.8	16.93	1.84	0.06	-2.26	0.04	4.25	1224	34	UB17-18	
UBA709	120.25	7.43		1.75	0	-2.42	0.12	3.78	1433	36	UB17-18	
UBA710	120.3	7.24		1.76	0	-2.62	0.02	1.86	732	37	UB17-18	
UBA711	120.35	6.25	12	1.92	0.05	-2.47	0.09	3.87	1735	38	UB17-18	
UBA712	120.4	7.4	12.53	1.7	0.04	-2.44	0.03	4.23	1605	39	UB17-18	
UBA713	120.45	5.67	12.03	1.7	0.02	-2.58	0.06	3.39	1681	41	UB17-18	
UBA714	120.5	8.16	12.73	1.76	0	-2.71	0.03	4.76	1638	42	UB17-18	
UBA715	120.55	7.75	13.33	1.79	0.04	-2.54	0.1	4.23	1533	43	UB17-18	
UBA716	120.6	7.45	12.43	1.71	0.03	-2.65	0.01	4.34	1637	44	UB17-18	
UBA717	120.65	9.11	15.83	1.4	0.03	-2.52	0.02	4.09	1265	46	UB17-18	
UBA718	120.7	6.23	12.38	1.58	0.09	-2.58	0.03	3.69	1660	47	UB17-18	
UBA719	120.75	7.16	13.18	1.71	0.12	-2.52	0.09	3.89	1525	48	UB17-18	
UBA720	120.8	8.46		1.49	0.07	-2.47	0.08	5.09	1688	49	UB17-18	
UBA721	120.85	6.87	11.75	1.73	0.01	-2.52	0.09	4.34	1770	51	UB17-18	
UBA722	120.9	7.33	13.7	1.68	0.07	-2.75	0	4.01	1536	52	UB17-18	
UBA723	120.95	8.28		1.65	0	-2.67	0.03	4.23	1439	53	UB17-18	
UBA724	121	8.68	15.18	1.65	0.05	-2.71	0.1	4.28	1388	54	UB17-18	
UBA725	122.28	5.99		1.68	0.03	-3.17	0	3.53	1655	56	UB17-18	
UBA726	122.33	6.23	10.58	1.56	0.04	-2.98	0.05	4.28	1922	57	UB17-18	
UBA727	122.38	6.27	10.4	1.63	0	-2.96	0.08	4.39	1961	58	UB17-18	
UBA728	122.43	6.54	10.95	1.67	0.02	-2.96	0.01	4.28	1834	59	UB17-18	
UBA729	122.48	6.09	12.25	1.42	0.05	-2.91	0.18	3.54	1633	8	UB17-19	
UBA730	122.53	5.76	10.8	1.32	0	-2.74	0.12	3.9	1898	9	UB17-19	
UBA731	122.58	6.1	11.33	1.44	0.02	-2.85	0.12	3.9	1792	11	UB17-19	
UBA732	122.63	3.17	8.18	1.76	0.01	-2.86	0.16	2.84	2503	12	UB17-19	
UBA733	122.68	5.37	10.25	1.53	0.02	-2.57	0.15	3.83	1994	13	UB17-19	
UBA734	122.73	1.73	5.45	1.63	0.08	-3.08	0.13	2.29	3684	14	UB17-19	
UBA735	122.78	2.75		1.5	0.05	-2.98	0.01	4.05	4092	16	UB17-19	
UBA736	122.83	2.35	4.6	1.55	0	-3.18	0.05	3.7	4376	17	UB17-19	
UBA737	122.88	5.53		1.28	0.07	-2.93	0.17	6.76	3411	18	UB17-19	
UBA738	122.93	3.92		1.43	0.01	-3.02	0.06	4.85	3450	29	UB17-19	
UBA739	122.98	3.49	8.4	1.49	0.07	-2.95	0.08	2.96	2371	21	UB17-19	
UBA740	123.03	4.04	8.78	1.34	0.01	-3.13	0.01	3.3	2283	22	UB17-19	
UBA741	123.08	3.21	7.23	1.31	0.1	-3.15	0.17	3.27	2844	23	UB17-19	
UBA742	123.13	5.31		1.29	0.01	-2.94	0.09	4.83	2541	24	UB17-19	
UBA743	123.16	4.4		1.41	0.02	-3.2	0.13	2.08	1329	26	UB17-19	
UBA744	123.21	5.34		1.32	0.09	-3.38	0.1	2.42	1276	27	UB17-19	
UBA745	123.26	3.99		1.46	0.13	-3.31	0.06	1.8	1272	28	UB17-19	
UBA746	123.31	4.42	8.73	1.25	0.02	-2.9	0.01	3.71	2348	29	UB17-19	
UBA747	123.36	5.67	10.98	1.29	0.03	-3.07	0.04	3.67	1816	31	UB17-19	
UBA748	123.41	4.75	9.65	1.47	0.09	-2.75	0.08	3.57	2103	32	UB17-19	

UBA749	123.46	3.59		1.34	0.05	-3.03	0.09	2.66	2073	33	UB17-19	
UBA750	123.51	3.72	10.03	1.25	0.06	-3.21	0.07	2.72	2050	34	UB17-19	
UBA751	123.56	5.83		1.31	0.05	-2.95	0.05	4.64	2228	36	UB17-19	
UBA752	123.61	6.18		1.33	0.01	-3.3	0.08	2.32	1063	37	UB17-19	
UBA753	123.66	6.62		1.14	0.03	-3.28	0.14	2.63	1122	38	UB17-19	
UBA754	123.71	4.36	8.73	1.45	0	-2.63	0.06	3.66	2346	39	UB17-19	
UBA755	123.76	4.24	8.58	1.22	0.05	-2.91	0.03	3.56	2351	41	UB17-19	
UBA756	123.81	4.1	8.03	1.34	0.12	-2.84	0.05	3.65	2487	42	UB17-19	
UBA757	123.86	3.47		1.2	0.01	-3.09	0.05	2.78	2235	43	UB17-19	
UBA758	123.91	4.68		1.19	0.07	-3.05	0.15	1.77	1070	44	UB17-19	
UBA759	123.96	5.24	10.65	1.08	0.03	-2.91	0.03	3.54	1894	46	UB17-19	
UBA760	123.98	4.55	8.83	1.02	0.06	-3.04	0.11	3.73	2293	47	UB17-19	
UBA761	124.03	4.43	9.5	1.21	0.14	-2.96	0.02	3.44	2175	48	UB17-19	
UBA762	124.08	4.86		1.09	0.12	-2.89	0.04	3.66	2110	49	UB17-19	
UBA763	124.13	5.01	9.78	1.02	0.03	-2.77	0.04	3.82	2131	51	UB17-19	
UBA764	124.18	4.51	7.83	1.11	0	-3.06	0.09	4.24	2623	52	UB17-19	
UBA765	124.23	4.01	7.75	0.89	0.05	-2.93	0.03	3.82	2658	53	UB17-19	
UBA766	124.28	3.47		1.06	0.08	-3	0.03	3.03	2442	54	UB17-19	
UBA767	124.33	8.33		0.88	0.04	-3.1	0.06	3.67	2185	51	rerun due to carbon value	UB18-26
UBA768	124.38	4.57		1.11	0.01	-3.27	0	1.97	1218	57	UB17-19	
UBA769	124.43	4.17	8.88	0.94	0	-3.06	0.1	3.45	2311	58	UB17-19	
UBA770	124.48	4.79	8.8	0.99	0.08	-3.03	0.26	4	2335	59	UB17-19	
UBA771	124.53	3.7	7.83	0.87	0	-3.05	0.11	3.49	2634	8	UB17-20	
UBA772	124.58	3.43	9.28	0.87	0.1	-3.12	0.19	2.74	2235	9	UB17-20	
UBA773	124.63	3.3	7.65	0.97	0.07	-3.04	0.18	3.09	2613	11	UB17-20	
UBA774	124.68	2.98	6.23	1.09	0.09	-3.03	0.03	3.53	3302	12	UB17-20	
UBA775	124.73	2.91		0.9	0.05	-3.22	0.01	3.17	3045	13	UB17-20	
UBA776	124.78	3.23	7.18	1	0.03	-3.11	0.11	3.26	2820	14	UB17-20	
UBA777	124.8	2.93		0.95	0.04	-3.4	0.04	3.37	3207	16	UB17-20	
UBA778	124.86	2.41		1	0.06	-3.59	0.07	1.37	1589	17	UB17-20	
UBA779	124.91	2.6	5.58	1.13	0.07	-3.18	0.13	3.37	3607	18	UB17-20	
UBA780	124.96	3.18		0.97	0.03	-3.02	0.35	3.55	3113	29	UB17-20	
UBA781	125.01	3.5	7.68	0.95	0.03	-3.25	0.1	3.32	2649	21	UB17-20	
UBA782	125.06	2.69	5.63	0.89	0.03	-3.3	0.09	3.47	3595	22	UB17-20	
UBA783	125.11	2.6	5.38	1.04	0	-3.26	0.04	3.5	3750	23	UB17-20	
UBA784	125.16	2.62		0.91	0.05	-3.21	0.12	2.99	3179	24	UB17-20	
UBA785	125.21	1.61	7.85	0.71	0.05	-3.5	0.17	1.46	2542	26	UB17-20	
UBA786	125.3	2.51		1.01	0.07	-3.43	0.05	2.45	2722	27	UB17-20	
UBA787	125.35	2.93	7.15	0.89	0.15	-3.36	0.01	3.01	2861	28	UB17-20	
UBA788	125.4	2.96	6.2	0.8	0.01	-3.39	0.07	3.47	3270	29	UB17-20	
UBA789	125.45	4.17	8.13	0.76	0.04	-3.01	0.15	3.77	2521	31	UB17-20	
UBA790	125.5	3.39	6.63	1.03	0.04	-3.21	0.05	3.7	3045	32	UB17-20	
UBA791	125.55	3.25	6.83	0.88	0.04	-3.35	0.03	3.46	2970	33	UB17-20	

UBA792	125.6	3.95		0.85	0.06	-3.36	0.01	3.98	2812	34	UB17-20	
UBA793	125.65	3.46	7.6	0.74	0.11	-3.39	0.02	3.33	2682	36	UB17-20	
UBA794	125.71	3.56		0.91	0.03	-3.28	0.03	3.58	2810	37	UB17-20	
UBA795	125.72	3.06	7.05	0.76	0.11	-3.28	0.14	3.21	2923	38	UB17-20	
UBA796	125.76	3.55	10.7	0.54	0	-3.35	0.05	2.38	1878	39	UB17-20	
UBA797	125.81	4.12		0.56	0.03	-3.27	0.29	2.74	1861	41	UB17-20	
UBA798	125.86	11.19		0.64	0.07	-3.52	0.02	3.89	2772	52	rerun due to oxygen value	UB18-26
UBA799	125.91	2.59	10.8	0.81	0.09	-3.61	0.18	1.71	1858	43	UB17-20	
UBA800	125.96	3.92	8.2	0.71	0.02	-3.43	0.04	3.46	2466	44	UB17-20	
UBA801	126.01	4.29	9.68	0.65	0.01	-3.33	0.24	3.26	2127	46	UB17-20	
UBA802	126.06	3.72	7.63	0.75	0.07	-3.5	0.05	3.53	2650	47	UB17-20	
UBA803	126.11	3.88	5.13	0.82	0.03	-3.3	0.09	5.54	6991	53	rerun due to oxygen value	UB18-26
UBA804	126.16	2.4	6.43	0.74	0.07	-3.45	0.04	2.76	3199	49	UB17-20	
UBA805	126.21	3.58		0.6	0.05	-3.28	0.07	3.53	2759	51	UB17-20	
UBA806	126.26	4	8.85	0.55	0.07	-3.2	0.09	3.26	2280	52	UB17-20	
UBA807	126.31	5.33	12.23	0.42	0.02	-3.54	0.06	3.26	6315	54	rerun due to carbon value	UB18-26
UBA808	126.36	4.4		0.52	0.06	-3.48	0.1	3.05	1946	54	UB17-20	
UBA809	126.41	4.46	9.45	0.8	0.13	-3.19	0.11	3.44	2158	56	UB17-20	
UBA810	126.54	3.65		0.57	0.06	-3.44	0	3.29	2520	57	UB17-20	
UBA811	126.59	2.83	7.03	0.6	0.09	-3.52	0.2	2.91	2872	58	UB17-20	
UBA812	126.64	4.02	8.25	0.81	0.06	-3.26	0.07	3.55	2468	59	UB17-20	
UBA813	126.69	2.75	7	0.61	0.1	-2.98	0.14	2.85	2888	8	UB17-21	
UBA814	126.74	3.73	8.43	0.71	0.11	-3.08	0	3.2	2395	9	UB17-21	
UBA815	126.78	3.21		0.68	0.06	-3.15	0.09	2.65	2305	11	UB17-21	
UBA816	126.85	4.28	9.55	0.68	0.01	-3.11	0.13	3.22	2104	12	UB17-21	
UBA817	126.89	6.23	12.48	1.24		-2.65		3.7			rerun due to carbon value	average used
UBA818	126.92	5.35		1.12	0	-2.98	0.03	2.86	1501	14	UB17-21	
UBA819	126.97	5.94		1.23	0.22	-2.96	0.23	1.58	758	16	UB17-21	
UBA820	127.4	4.37	14.55	0.89	0.16	-3.24	0.01	2.22	1432	17	UB17-21	
UBA821	127.55	5.68	12.8	1.3	0.11	-2.49	0.1	3.25	1608	18	UB17-21	
UBA822	127.6	6.1		1.18	0.14	-2.55	0.18	3.36	1548	29	UB17-21	
UBA823	127.65	6		1.06	0.06	-2.63	0.12	1.61	767	21	UB17-21	
UBA824	127.7	6.06	12.9	1.32	0.11	-2.75	0.1	3.49	1619	22	UB17-21	
UBA825	127.75	5.94	13.83	1.26	0.06	-2.88	0.12	3.09	1463	23	UB17-21	
UBA826	127.8	4.93	10.03	1.34	0.06	-2.83	0	3.52	1998	24	UB17-21	
UBA827	127.85	5.35	11.53	1.12	0.05	-2.72	0.28	3.4	1785	26	UB17-21	
UBA828	127.9	5.39	12.35	1.25	0.09	-2.81	0.16	3.21	1671	27	UB17-21	
UBA829	127.95	4.48	10.75	1.13	0.05	-2.76	0	2.98	1865	28	UB17-21	
UBA830	128	4.73	12.05	1.13	0	-2.6	0.18	2.82	1673	29	UB17-21	
UBA831	128.05	5.69	13	1	0.04	-2.58	0.14	3.25	1604	31	UB17-21	
UBA832	128.1	6.05	11.93	1.06	0.01	-2.69	0.16	3.62	1681	32	UB17-21	
UBA833	128.15	5.27	11.4	0.89	0.01	-2.83	0.13	3.46	1839	33	UB17-21	

UBA834	128.2	6.78	14.68	0.84	0.01	-2.94	0.02	3.36	1393	34	UB17-21
UBA835	128.25	5.64	11.83	0.98	0.02	-2.82	0.06	3.4	1692	36	UB17-21
UBA836	128.3	5.65	12.2	1.01	0.08	-2.79	0.03	3.33	1653	37	UB17-21
UBA837	128.35	5.09	11.73	0.95	0.1	-2.82	0.08	3.1	1712	38	UB17-21
UBA838	128.46	5.47	12.4	0.99	0.09	-2.85	0.08	3.25	1665	39	UB17-21
UBA839	128.51	8.33	15.48	1.07	0.03	-2.44	0.05	3.95	1336	41	UB17-21
UBA840	128.56	8.32	16.2	1.15	0.03	-2.65	0.1	3.67	1244	42	UB17-21
UBA841	128.61	5.75	11	1	0.09	-2.41	0.23	3.8	1854	43	UB17-21
UBA842	128.66	7.79	16.88	0.81	0.08	-2.52	0.11	3.47	1257	44	UB17-21
UBA843	128.71	7.82	14.65	0.86	0.08	-2.42	0.18	3.84	1383	46	UB17-21
UBA844	128.76	6.6	12.08	0.8	0.07	-2.44	0.13	4.04	1717	47	UB17-21
UBA845	128.81	6.14	12.88	0.87	0.02	-2.61	0.14	3.44	1573	48	UB17-21
UBA846	128.86	6.56	11.15	0.92	0.03	-2.39	0.13	4.25	1816	49	UB17-21
UBA847	128.91	7.12	14.4	1.01	0.02	-2.68	0.02	3.61	1426	51	UB17-21
UBA848	128.96	6.86	13.75	1.1	0.1	-2.57	0.31	3.59	1470	52	UB17-21
UBA849	129.01	6.23	13.45	1.04	0.12	-2.56	0.15	3.46	1560	53	UB17-21
UBA850	129.06	6.91	13.73	1.03	0	-2.59	0.14	3.61	1468	54	UB17-21
UBA851	129.11	6.48	14.4	1.06	0.06	-2.53	0.04	3.23	1403	56	UB17-21
UBA852	129.16	5.75	12.35	1.12	0.03	-2.39	0.12	3.4	1662	57	UB17-21
UBA853	129.21	5.99	11.6	1.28	0.02	-2.42	0.05	3.82	1787	58	UB17-21
UBA854	129.26	5.97	13.93	1.1	0.01	-2.47	0.02	3.24	1525	59	UB17-21
UBA855	129.34	3.42	7.8	1.41	0.19	-2.85	0.07	3.21	2622	8	UB17-22
UBA856	129.39	3.33	9.38	1.67	0.04	-2.96	0.18	2.57	2162	9	UB17-22
UBA857	129.44	4.91	11.15	1.52	0.07	-2.81	0.12	3.19	1820	11	UB17-22
UBA858	129.49	2.88	6.78	1.69	0.09	-2.92	0	3.11	3009	12	UB17-22
UBA859	129.54	6.04	12.1	1.52	0.12	-2.75	0.15	3.7	1718	13	UB17-22
UBA860	129.59	6.38		1.28	0.09	-2.73	0.14	3.65	1606	14	UB17-22
UBA861	129.64	5.95	13.05	1.15	0.02	-2.67	0.15	3.41	1610	16	UB17-22
UBA862	129.69	7.08		0.84	0.01	-2.71	0.03	3.86	1532	17	UB17-22
UBA863	129.74	7.39	14.63	0.86	0.14	-2.7	0.03	3.62	1378	18	UB17-22
UBA864	129.79	7.02	15.88	1.08	0.01	-2.86	0.12	3.21	1287	29	UB17-22
UBA865	129.84	6.14	13.15	1.19	0.02	-2.93	0.13	3.42	1566	21	UB17-22
UBA866	129.89	6.78	13.83	1.05	0.01	-2.73	0.11	3.59	1488	22	UB17-22
UBA867	129.94	7.31	16	0.97	0.09	-2.62	0.11	3.3	1273	23	UB17-22
UBA868	129.99	7.41	15.68	1.19	0.09	-2.71	0.07	3.36	1277	24	UB17-22
UBA869	130.04	7.72	15.58	1.01	0.02	-2.84	0.05	3.63	1324	26	UB17-22
UBA870	130.09	7.58	14.6	1.07	0.05	-2.79	0.19	3.9	1446	27	UB17-22
UBA871	130.22	4.74	10.85	1.57	0.17	-3	0.11	3.14	1856	28	UB17-22
UBA872	130.27	4.43		1.53	0.02	-2.82	0.21	3.18	2012	29	UB17-22
UBA873	130.32	4.98	9.1	1.57	0.05	-2.78	0.01	4.04	2268	31	UB17-22
UBA874	130.37	3.59	8.48	1.6	0.06	-2.7	0	3.13	2437	32	UB17-22
UBA875	130.42	5.68	9.85	1.78	0.09	-2.74	0.05	4.22	2081	33	UB17-22
UBA876	130.47	4.49	8.75	1.61	0.01	-2.93	0.03	3.75	2333	34	UB17-22

UBA877	130.52	4.69	9.38	1.74	0.01	-2.54	0.03	3.61	2153	36	UB17-22	
UBA878	130.57	4.59	8.53	1.8	0.07	-2.62	0.18	3.91	2382	37	UB17-22	
UBA879	130.62	5.98	11.73	1.71	0.07	-2.59	0.02	3.7	1734	38	UB17-22	
UBA880	130.67	5.1	9.98	1.67	0.22	-2.81	0.11	3.67	2018	39	UB17-22	
UBA881	130.72	6.38	12.68	1.62	0.05	-2.75	0.07	3.74	1644	41	UB17-22	
UBA882	130.77	6.25	11.05	1.64	0.08	-2.54	0.07	4.06	1821	42	UB17-22	
UBA883	130.82	4.83	9.9	1.75	0.11	-2.68	0.05	3.57	2070	43	UB17-22	
UBA884	130.87	4.15	7.83	1.52	0.06	-2.77	0.07	3.87	2601	44	UB17-22	
UBA885	130.92	6.02	10.35	1.66	0.03	-2.61	0.07	4.24	1972	46	UB17-22	
UBA886	134.95	5.21	10	1.49	0.05	-2.49	0.12	3.77	2024	47	UB17-22	
UBA887	135	4.61	9.7	1.4	0.15	-2.78	0.01	3.39	2060	48	UB17-22	
UBA888	135.1	5.66	11.43	1.21	0.08	-2.73	0.06	3.62	1794	49	UB17-22	
UBA889	135.15	4.52		1.37	0.04	-2.64	0.22	3.37	1543	57	rerun due to carbon value	UB18-26
UBA890	135.2	3.93	8.2	1.34	0.09	-2.61	0.11	3.55	2525	52	UB17-22	
UBA891	135.25	5.45	11.2	1.35	0.02	-2.87	0.11	3.5	1799	53	UB17-22	
UBA892	135.3	5.21	11.3	1.24	0.01	-2.87	0.11	3.33	1788	54	UB17-22	
UBA893	135.35	4.34	9.08	1.17	0.03	-2.88	0.05	3.46	2231	56	UB17-22	
UBA894	135.4	5.57		1.27	0.08	-2.66	0.06	4.18	2100	57	UB17-22	
UBA895	135.45	4.59	10.25	1.21	0.03	-2.76	0.14	3.22	1966	58	UB17-22	
UBA896	135.5	6.18	12.53	1.07	0.06	-2.76	0.13	3.63	1648	59	UB17-22	
UBA897	135.62	3.81		0.87	0.09	-2.87	0.14	2.62	1931	8	UB17-23	
UBA898	135.67	3.84		1.17	0.06	-3.39	0.3	1.27	940	9	UB17-23	
UBA899	135.72	4.62	9.15	1.2	0.01	-2.84	0.05	3.67	2226	11	UB17-23	
UBA900	135.77	3.73		1.22	0.05	-3.18	0.05	3.15	2360	12	UB17-23	
UBA901	135.82	3.65	7.88	1.16	0.15	-3.09	0.06	3.4	2607	13	UB17-23	
UBA902	135.87	2.04		1.26	0.02	-3.04	0.04	1.77	2426	14	UB17-23	
UBA903	135.92	8.9		1.09	0.08	-3.3	0.24	3.84	3964	58	rerun due to carbon value average?	
UBA904	135.97	4.24	9.1	0.99	0.09	-2.81	0.18	3.37	2223	17	UB17-23	
UBA905	136.02	3.13		0.9	0.08	-3.39	0.04	2.33	2087	18	UB17-23	
UBA906	136.07	5.56	10.88	1.35	0.06	-2.8	0.12	3.77	1898	29	UB17-23	
UBA907	136.12	5.29		1.14	0	-3.18	0.12	2.94	1560	21	UB17-23	
UBA908	136.22	4.64		1.39	0.15	-3.35	0.04	1.27	778	22	UB17-23	
UBA909	136.27	8.45	16.63	1.41	0.07	-2.55	0.03	3.86	1286	23	UB17-23	
UBA910	136.32	8.93	19.8	1.24	0.04	-2.59	0.1	3.29	1042	24	UB17-23	
UBA911	136.35	8.9		1.26	0.07	-2.29	0.15	3.7	1174	26	UB17-23	
UBA912	136.4	7.56		1.53	0.01	-2.87	0.05	1.57	598	27	UB17-23	
UBA913	136.45	8.75	16.7	1.56	0.14	-2.3	0.02	3.71	1198	28	UB17-23	
UBA914	136.5	6.06	12.43	1.8		-2.49		3.6			rerun due to both oxygen and carbon	average used
UBA915	136.55	8.11	14.08	1.4	0.05	-2.38	0.01	4.2	1455	31	UB17-23	
UBA916	136.6	7.33	13.28	1.4	0.02	-2.42	0.01	4.13	1581	32	UB17-23	
UBA917	136.65	7.66	15.03	1.48	0.08	-2.55	0.07	3.78	1387	33	UB17-23	

UBA918	136.7	6.44	14.4	1.37	0.02	-2.66	0.05	3.22	1406	34	UB17-23
UBA919	136.75	8.49	18.18	1.47	0.04	-2.64	0.1	3.51	1169	36	UB17-23
UBA920	136.8	9.42	18.5	1.56	0.04	-2.48	0.06	3.7	1110	37	UB17-23
UBA921	136.85	9.09	19.75	1.63	0.05	-2.6	0.12	3.51	1091	38	UB17-23
UBA922	136.9	7.05	13.78	1.55	0.07	-2.39	0.07	3.77	1505	39	UB17-23
UBA923	137	8.98	16.48	1.57	0.03	-2.41	0.03	4.02	1263	41	UB17-23
UBA924	137.05	10.92		1.57	0.07	-2.31	0.05	5.77	1486	42	UB17-23
UBA925	137.1	8.63		1.55	0.08	-2.53	0	2.3	761	43	UB17-23
UBA926	137.14	8.12		1.44	0	-2.86	0.42	2.22	781	44	UB17-23
UBA927	137.19	9.37		1.47	0.07	-2.87	0.04	2.44	743	46	UB17-23
UBA928	137.24	6.14	11.58	1.53	0	-2.57	0.09	3.96	1807	47	UB17-23
UBA929	137.29	10.29	19.23	1.5	0.06	-2.42	0.06	3.96	1087	48	UB17-23
UBA930	137.34	11.05	19.05	1.45	0.01	-2.48	0.07	4.15	1063	49	UB17-23
UBA931	137.39	8.67	16.18	1.53	0.07	-2.37	0.09	3.96	1286	51	UB17-23
UBA932	137.44	8.5		1.55	0.03	-2.7	0.08	3.75	1243	52	UB17-23
UBA933	137.49	10.02		1.47	0.07	-2.73	0.22	2.3	659	53	UB17-23
UBA934	137.54	8.99	16.25	1.46	0.04	-2.66	0.06	3.98	1247	54	UB17-23
UBA935	137.59	10.79	19.73	1.32	0.03	-2.55	0.05	3.99	1046	56	UB17-23
UBA936	137.69	9	16.2	1.29	0.13	-2.54	0.09	4.19	1313	57	UB17-23
UBA937	137.74	8.76	17.33	1.38	0.07	-2.75	0.08	3.62	1166	58	UB17-23
UBA938	137.79	9.86		1.3	0.11	-2.3	0.11	4.22	1206	59	UB17-23
UBA939	137.84	7.61	16.55	1.36	0.07	-2.53	0.04	3.26	1209	8	UB17-24
UBA940	137.94	9.46		1.33	0.11	-2.22	0.03	4.57	1361	9	UB17-24
UBA941	137.99	7.64	14.7	1.32	0.1	-2.36	0.04	3.85	1417	11	UB17-24
UBA942	143.74	23.17		-0.52	0.04	-1.16	0.08	8.47	1035	12	UB17-24
UBA943	143.79	19.96		-0.45	0.02	-1.43	0.12	3.65	529	13	UB17-24
UBA944	143.84	18.01	32.78	-0.4	0.05	-1.34	0	4.06	647	14	UB17-24
UBA945	143.89	23.49		-0.51	0.04	-1.22	0.1	5.09	622	16	UB17-24
UBA946	143.94	21.6	39.93	-0.47	0.06	-1.36	0.03	3.96	530	17	UB17-24
UBA947	143.99	19.47		-0.3	0.02	-1.66	0.03	3.72	551	18	UB17-24
UBA948	144.04	17.69		-0.19	0.01	-1.57	0.11	3.04	498	29	UB17-24
UBA949	144.09	22.2	39.8	-0.37	0.02	-1.55	0.07	3.79	495	21	UB17-24
UBA950	144.14	16.5		-0.22	0.14	-1.45	0	3.57	622	22	UB17-24
UBA951	144.19	19.34	30.93	-0.28	0.09	-1.66	0.02	4.92	726	23	UB17-24
UBA952	144.2	16.65		-0.32	0.03	-2.01	0.15	4.34	744	24	UB17-24
UBA953	144.25	16.86	26.63	-0.3	0.02	-1.72	0.08	4.77	806	26	UB17-24
UBA954	144.3	10.6	26.25	-0.37	0.02	-2.22	0.06	2.91	781	27	UB17-24
UBA955	144.35	15.34	26.58	-0.31	0.02	-1.79	0.07	4.01	746	28	UB17-24
UBA956	144.4	14.6	28.48	-0.36	0.06	-1.82	0.21	3.85	752	29	UB17-24
UBA957	144.45	16.12		-0.15	0	-2.22	0.1	4.2	743	31	UB17-24
UBA958	144.5	16.75	30.83	-0.13	0.02	-2.17	0.01	4.29	732	32	UB17-24
UBA959	144.55	14.1		-0.03	0	-2.17	0.01	3.89	786	33	UB17-24
UBA960	144.6	11.92	22.98	-0.08	0.03	-2.17	0.1	3.82	910	34	UB17-24

UBA961	144.65	13.38	23.48	-0.08	0.03	-2.25	0.01	3.99	848	36	UB17-24
UBA962	144.7	13.63		-0.03	0.01	-2.13	0.04	3.9	815	37	UB17-24
UBA963	144.75	16.09		-0.09	0	-2.13	0.01	4.55	805	38	UB17-24
UBA964	144.8	17.97	30.83	-0.05	0.05	-1.97	0.02	4.2	669	39	UB17-24
UBA965	144.85	19.3		-0.09	0.01	-2.05	0.11	4.13	615	41	UB17-24
UBA966	144.9	19.88		-0.06	0.12	-1.5	0.01	4.38	632	42	UB17-24
UBA967	144.95	20.44	42.3	-0.25	0.03	-1.64	0	3.79	536	43	UB17-24
UBA968	145	23.09	39	-0.18	0.03	-1.42	0.07	4.64	579	44	UB17-24
UBA969	145.09	15.64	31.88	-0.3	0.1	-1.42	0.22	3.81	697	46	UB17-24
UBA970	145.29	19.91	37	-0.07	0.1	-1.47	0.1	4.11	594	47	UB17-24
UBA971	145.34	20.26		-0.07	0.1	-1.42	0.01	3.74	533	48	UB17-24
UBA972	145.39	22.46	41.68	0.2	0.02	-1.16	0.01	3.88	500	49	UB17-24
UBA973	145.54	21.45		-0.19	0.03	-1.62	0.08	4.16	559	51	UB17-24
UBA974	145.59	19.58		-0.16	0.01	-1.63	0.01	3.49	515	52	UB17-24
UBA975	145.69	22.18	40.38	-0.03	0.14	-1.33	0.05	4.45	578	53	UB17-24
UBA976	145.74	20.93	39.75	-0.01	0.07	-1.69	0.09	4.25	585	54	UB17-24
UBA977	145.79	54.56	83.63	0.43	0.08	-0.21	0.22	5.03	277	56	UB17-24
UBA978	145.89	55.28	87.93	0.39	0.08	-0.33	0.04	4.57	251	57	UB17-24
UBA979	145.94	38.39	73.73	0.39	0.01	-0.55	0.03	4.67	359	58	UB17-24
UBA980	145.99	57.28		0.59	0.02	-0.06	0.05	8.4	428	59	UB17-24

Table 2 Two samples are tested for their homogeneity, to see their inter sample variability all four reruns are shown for each of these two samples.

Sample	depth	Carbonate infered from bulk isotopes	CaCO3 infered from XRF	$\delta^{13}C$	st.dev.	$\delta^{18}O$	st.dev.	peak	weight [µg]	cell	first run
UBA132/982/983	68.43	35.10366637	67.25	0.69751	0.0211	-0.23022	0.1553	3.114	267.5		average used; sample used to evaluate homogeneity of dataset
UBA132	68.43			0.66	0.04	-0.29	0.29	2.06	185	21	UB17-4
UBA132-2	68.43			0.70	0.04	-0.11	0.04	3.73	334	36	UB17-25
UBA982	68.43			0.68	0.00	-0.18	0.14	3.56	281	37	UB17-25
UBA983	68.43			0.75	0.00	-0.33	0.15	3.10	270	38	UB17-25
UBA624/984/985	113.28	6.086434417	11.7	1.67034	0.0414	-2.23088	0.0666	3.803	1753		average used; sample used to evaluate homogeneity of dataset
UBA624				1.68	0.01	-2.22	0.17	4.50	1760	34	UB17-16
UBA624				1.64	0.09	-2.15	0.06	3.63	1759	39	UB17-25
UBA984				1.64	0.02	-2.38	0.04	3.22	1708	41	UB17-25
UBA985				1.72	0.04	-2.17	0.00	3.86	1783	42	UB17-25

Table 3 A comparison of bulk isotope measurements on the whole bulk sediment against the < 20 µm fraction of the sediment is shown.

Sample	depth	d13C	stdev	d18O	stdev	peak	weight [µg]	cell	run	comment
UB986	43.52	1.00829	0.0722	0.05941	0.0251	3.083	249	43	UB17-25	bulk sediment weight in
UB996	43.52	0.88397	0.0453	0.08287	0.1039	3.146	242	8	UB 17-26	< 20 µm fraction weight in
UB987	52.51	0.85931	0.0168	-0.09978	0.0339	3.527	232	44	UB17-25	bulk sediment weight in
UB997	52.51	0.9107	0.0659	-0.01822	0.0186	2.708	214	9	UB 17-26	< 20 µm fraction weight in
UB988	80.05	0.60297	0.0433	-0.31955	0.1196	2.915	338	46	UB17-25	bulk sediment weight in
UB998	80.05	0.61238	0.1484	-0.52173	0.0292	3.8	346	11	UB 17-26	< 20 µm fraction weight in
UB989	82.39	0.77297	0.0062	0.00192	0.1543	3.61	246	47	UB17-25	bulk sediment weight in
UB999	82.39	0.71214	0.104	0.02254	0.142	2.953	207	12	UB 17-26	< 20 µm fraction weight in
UB990	83.39	0.74568	0.012	-0.10007	0.2255	3.578	253	48	UB17-25	bulk sediment weight in
UB1000	83.39	0.78525	0.0738	-0.514	0.1471	2.414	208	13	UB 17-26	< 20 µm fraction weight in
UB991	91.28	1.67706	0.0438	-2.04377	0.0158	5.04	2894	49	UB17-25	bulk sediment weight in
UB1001	91.28	1.74388	0.0328	-2.97391	0.0212	3.663	2833	14	UB 17-26	< 20 µm fraction weight in
UB992	111.08	1.51674	0.0746	-2.15605	0.1287	3.661	1230	51	UB17-25	bulk sediment weight in
UB1002	111.08	1.56794	0.0051	-2.57973	0.0006	3.257	1245	16	UB 17-26	< 20 µm fraction weight in
UB993	120.2	1.65928	0.0782	-1.29892	0.153	3.792	1358	52	UB17-25	bulk sediment weight in
UB1003	120.2	1.5029	0.0987	-3.67117	0.1254	1.769	1328	17	UB 17-26	< 20 µm fraction weight in
UB994	128.44	0.88929	0.0087	-3.11291	0.0698	3.757	1722	53	UB17-25	bulk sediment weight in
UB1004	128.44	1.02904	0.0801	-4.14287	0.0932	2.516	1655	18	UB 17-26	< 20 µm fraction weight in
UB995	136.4	1.57619	0.0953	-2.36353	0.1915	2.212	930	54	UB17-25	bulk sediment weight in
UB1005	136.4	1.44877	0.0477	-3.32649	0.3195	2.04	882	19	UB 17-26	< 20 µm fraction weight in

Appendix 5: Foraminiferal samples and dry weights

Table 1: Gives the sample labels for the foraminiferal samples, BMC numbers are used for the TEX_{86} analysis, it is a Birmingham in-house lab labelling system of the working group of James Bendle. Additionally, their age according to the new age model developed in this thesis, the sample weight before processing, dry weight before and after processing and sample depth is given.

BMC number	Sample Id Consisting of Site Sample depth [m] Core section [x of a total of 69]	Top Depth [m]	Bottom Depth [m]	Age [Ma]	weight before adding to the drying oven [g]	dry weight before processing [g]	Dry weight after Calgon coarse fraction >63 µm [g]
1474	16/28-sb01 013.00 - .02 1/69	13.00	13.02		18.19	17.60	14.72
1475	16/28-sb01 013.58 - .61 1/69	13.58	13.61		30.85	29.51	19.21
1476	16/28-sb01 014.33 - .37 2/69	14.33	14.37		37.96	36.72	26.36
1478	16/28-sb01 033.08 - .11 3b/69	33.08	33.11		10.23	10.08	2.06
1479	16/28-sb01 033.38 - .40 3b/69	33.38	33.40		22.50	21.52	7.08
208	16/28 Sbo1 041.00 -.02 6/69	41.00	41.02	44.8795		8.88	2.09
1482	16/28-sb01 041.27 - .30 6/69	41.27	41.30	44.8891	68.35	64.58	11.97
1483	16/28-sb01 041.56 - .59 6/69	41.56	41.59	44.8995	84.81	80.12	26.52
1484	16/28-sb01 041.85 - .87 7/69	41.85	41.87	44.9098	38.28	42.70	13.81
1485	16/28-sb01 042.06 - .08 7/69	42.06	42.08	44.9174	18.25	9.25	3.82
1486	16/28-sb01 042.49 - .51 8/69	42.49	42.51	44.9327	21.37	20.46	6.74
902	16/28 Sbo1 042.50 -.52 8/69	42.50	42.52	44.9331		8.56	3.5
1487	16/28-sb01 042.70 - .72 8/69	42.70	42.72	44.9402	41.75	39.60	13.59
1488	16/28-sb01 042.90 - .92 8/69	42.90	42.92	44.9474	49.61	45.19	
1489	16/28-sb01 043.41 - .43 9/69	43.41	43.43	44.9656	31.05	30.61	21.99
903	16/28 Sbo1 043.50 -.52 9/69	43.50	43.52	44.9688		14.11	3.96
1490	16/28-sb01 043.52 - .54 9/69	43.52	43.54	44.9696	30.05	29.17	9.24
214	16/28 Sbo1 052.50 -.52 10/69	52.50	52.52	45.2906		8.28	1.58
1491	16/28-sb01 52.51 - .53 10/69	52.51	52.53	45.2910	69.57	66.79	18.22
1492	16/28-sb01 52.60 - .62 10/69	52.60	52.62	45.2942	81.18	77.24	32.64
1493	16/28-sb01 53.28 - .30 10/69	53.28	53.30	45.3185	38.48	36.32	10.25
1494	16/28-sb01 53.42 - .44 11/69	53.42	53.44	45.3235	27.63	26.30	8.72
904	16/28 Sbo1 053.50 -.52 11/69	53.5	53.52	45.3263		12.71	4.81
1495	16/28-sb01 053.53 - .55 11/69	53.53	53.55	45.3274	30.10	29.04	12.40
1496	16/28-sb01 053.97 - 54.00 11/69	53.97	54.00	45.3431	6.73	6.52	4.59
905	16/28 Sbo1 060.60 -.62 12/69	60.60	60.62	45.5802		15.62	15.24
1497	16/28-sb01 060.78 - .80 12a/69	60.78	60.80	45.5866	90.07	86.33	36.63
1498	16/28-sb01 066.59 - .62 12b/69	66.59	66.62	45.7943	42.47	40.59	26.81
1499	16/28-sb01 066.87 - .89 13/69	66.87	66.89	45.8043	26.83	24.25	12.95
1500	16/28-sb01 066.89 - .91 13/69	66.89	66.91	45.8050	22.02	19.86	8.41
1501	16/28-sb01 067.48 - .50 13/69	67.48	67.50	45.8261	36.52	34.76	31.37

211	16/28 Sbo1	067.50 -.52 13/69	67.50	67.52	45.8269		5.54	5.25
1502	16/28-sb01	067.88 - .90 14/69	67.88	67.90	45.8404	30.57	29.35	14.55
1503	16/28-sb01	068.15 -.17 14/69	68.15	68.17	45.8501	28.13	27.09	12.91
1504	16/28-sb01	068.40 - .44 14/69	68.40	68.44	45.8590	53.86	51.02	17.62
1505	16/28-sb01	068.48 - .50 15/69	68.48	68.50	45.8619	38.57	36.68	8.18
906	16/28 Sbo1	068.50 -.52 15/69	68.50	68.52	45.8626		9.51	2.01
1506	16/28-sb01	068.52 - .54 15/69	68.52	68.54	45.8633	24.96	23.75	4.66
1507	16/28-sb01	069.05-.07 15/69	69.05	69.07	45.8823	45.50	43.70	35.68
1508	16/28-sb01	069.42 -.44 16/69	69.42	69.44	45.8955	25.19	24.25	9.35
1509	16/28-sb01	069.45-.47 16/69	69.45	69.47	45.8966	30.67	29.37	9.95
907	16/28 Sbo1	069.50 -.52 16/69	69.50	69.52	45.8984		9.90	3.56
1510	16/28-sb01	070.08-.12 16/69	70.08	70.12	45.9191	52.46	50.17	18.47
908	16/28 Sbo1	070.50 -.52 17/69	70.5	70.52	45.9341		19.64	3.68
1511	16/28-sb01	070.52 - .54 17/69	70.52	70.54	45.9348	25.24	23.20	5.08
1512	16/28-sb01	070.56 - .58 17/69	70.56	70.58	45.9363	32.74	29.33	3.27
1513	16/28-sb01	070.96 - 71.00 17/69	70.96	71.00	45.9506	113.79	101.73	20.13
909	16/28 Sbo1	080.00 -.02 18/69	80.00	80.02	46.2565		12.45	2.61
1514	16/28-sb01	080.05 - .07 18/69	80.05	80.07	46.2581	40.16	38.30	7.03
1515	16/28-sb01	080.07 - .09 18/69	80.07	80.09	46.2587	38.06	36.26	6.62
1516	16/28-sb01	080.64 - .67 18/69	80.64	80.67	46.2770	32.14	30.44	5.62
1517	16/28-sb01	080.94 - .96 19/69	80.94	80.96	46.2865	35.22	32.09	8.03
910	16/28 Sbo1	081.00 -.02 19/69	81.00	81.02	46.2885		15.86	6.75
1518	16/28-sb01	081.05 - .07 19/69	81.05	81.07	46.2901	33.68	31.57	14.73
1519	16/28-sb01	81.49 - .51 19/69	81.49	81.51	46.3041	48.32	45.46	22.45
911	16/28 Sbo1	081.60 -.62 20/69	81.60	81.62	46.3077		8.73	4.19
1520	16/28-sb01	081.67 - .70 20/69	81.67	81.70	46.3099	57.04	54.79	27.02
912	16/28 Sbo1	081.90 -.92 20/69	81.90	81.92	46.3173		13.26	2.17
1521	16/28-sb01	081.97 -.82.00 20/69	81.97	82.00	46.3195	52.59	49.72	9.96
1522	16/28-sb01	082.30 - 32 20/69	82.30	82.32	46.3300	41.99	39.96	16.90
1523	16/28-sb01	082.39 - .44 21/69	82.39	82.44	46.3329	46.29	43.65	15.39
913	16/28 Sbo1	082.40 -.42 21/69	82.4	82.42	46.3332		10.33	5.36
1524	16/28-sb01	082.47 -.50 21/69	82.47	82.50	46.3355	72.00	62.62	15.64
914	16/28 Sbo1	082.90 -.92 21/69	82.90	82.92	46.3492		16.34	3.53
1525	16/28-sb01	082.98 - .99 21/69	82.98	82.99	46.3518	53.49	48.56	12.04
1526	16/28-sb01	083.04 - .06 21/69	83.04	83.06	46.3537	27.85	25.83	5.19
1527	16/28-sb01	083.13 - .16 21/69	83.13	83.16	46.3566	44.41	40.64	8.04
1528	16/28-sb01	083.34 - .37 22/69	83.34	83.37	46.3633	52.43	50.05	11.13
1529	16/28-sb01	083.39 - .40 22/69	83.39	83.40	46.3649	24.19	23.06	6.77
915	16/28 Sbo1	083.40 -.42 22/69	83.40	83.42	46.3652		15.29	4.03
1530	16/28-sb01	083.77 - .80 22/69	83.77	83.80	46.3771	41.53	39.75	9.42
1531	16/28-sb01	083.86 - .88 22/69	83.86	83.88	46.3799	56.95	54.67	14.70
916	16/28 Sbo1	083.90 -.92 22/69	83.90	83.92	46.3812		29.23	7.79
920	16/28 Sbo1	087.52 -.54 23/69	87.52	87.54	46.4970		10.28	0.02

1532	16/28-sb01	087.56 - .58 23/69	87.56	87.58	49.2351	56.71	50.64	0.22
1533	16/28-sb01	87.65 - .66 23/69	87.65	87.66	49.2388	34.91	31.08	0.16
217	16/28 Sbo1	087.90 -.92 23/69	87.90	87.92	49.2489			0.95
1534	16/28-sb01	088.07 - .08 23/69	88.07	88.08	49.2558	38.23	32.53	2.97
1535	16/28-sb01	088.10 - .13 23/69	88.10	88.13	49.2570	83.02	77.29	10.93
1536	16/28-sb01	088.35 - .38 23/69	88.35	88.38	49.2672	91.07	86.67	25.71
917	16/28 Sbo1	088.40 -.42 24/69	88.40	88.42	49.2692		18.16	4.44
1537	16/28-sb01	088.43 - .45 24/69	88.43	88.45	49.2704	71.43	67.65	17.69
1538	16/28-sb01	088.48 - .50 24/69	88.48	88.50	49.2725	74.89	70.88	21.68
918	16/28 Sbo1	088.80 -.82 24/69	88.80	88.82	49.2855		18.79	0.04
1539	16/28-sb01	088.90 - .92 24/69	88.90	88.92	49.2895	47.53	44.29	0.09
1540	16/28-sb01	088.94 - .96 24/69	88.94	88.96	49.2911	43.03	44.65	0.10
1541	16/28-sb01	089.18 - .21 24/69	89.18	89.21	49.3009	98.12	90.40	0.17
919	16/28 Sbo1	089.25 -.27 25/69	89.25	89.27	49.3037		11.02	0.07
1542	16/28-sb01	089.31 - .34 25/69	89.31	89.34	49.3062	94.52	81.69	0.51
921	16/28 Sbo1	089.70 -.72 25/69	89.70	89.72	49.3220		20.64	0.09
1543	16/28-sb01	089.81 - .83 25/69	89.81	89.83	49.3265	80.22	68.64	0.33
1544	16/28-sb01	089.85 - .87 25/69	89.85	89.87	49.3281	48.64	42.61	0.18
1545	16/28-sb01	090.03 - .06 25/69	90.03	90.06	49.3354	67.32	61.83	0.52
922	16/28 Sbo1	090.20 -.22 26/69	90.20	90.22	49.3423		14.23	0.06
1546	16/28-sb01	090.34 - 36 26/69	90.34	90.36	49.3480	55.20	51.25	0.23
1547	16/28-sb01	090.38 -.40 26/69	90.38	90.40	49.3496	56.33	51.00	0.20
923	16/28 Sbo1	090.80 -.82 26/69	90.80	90.82	49.3667		11.54	0.13
1548	16/28-sb01	090.81 - .83 26/69	90.81	90.83	49.3671	68.71	58.37	0.39
1549	16/28-sb01	090.83 - .86 26/69	90.83	90.86	49.3679	94.74	86.08	0.71
1550	16/28-sb01	091.25 -.27 27/69	91.25	91.27	49.3875	62.05	57.67	0.44
1551	16/28-sb01	091.28 - .30 27/69	91.28	91.30	49.3889	61.02	57.64	0.50
924	16/28 Sbo1	091.30 -.32 27/69	91.30	91.32	49.3899		15.44	0.13
1552	16/28-sb01	091.67 - .70 27/69	91.67	91.70	49.4076	76.83	71.36	0.24
925	16/28 Sbo1	091.80 -.82 28a/69	91.80	91.82	49.4138		13.01	0.03
1553	16/28-sb01	091.83 - .86 28a/69	91.83	91.86	49.4152	94.29	84.06	0.25
1073	16/28 Sbo1	093.40 -.42 28b/69	93.40	93.42	49.4902			1.13
1554	16/28-sb01	093.51 - .53 28b/69	93.51	93.53	49.4954	72.08	68.71	0.45
1555	16/28-sb01	093.90 - .92 29/69	93.54	93.60	49.4968	77.91	70.01	0.39
926	16/28 Sbo1	093.70 -.72 29/69	93.70	93.72	49.5045		10.77	0.06
1556	16/28-sb01	093.82 - .84 29/69	93.82	93.84	49.5102	40.94	35.10	0.14
1557	16/28-sb01	093.90 - .92 29/69	93.90	93.92	49.5140	71.67	59.47	0.29
927	16/28 Sbo1	094.00 -.02 29/69	94.00	94.02	49.5188		13.52	0.09
1558	16/28-sb01	094.19 - .23 29/69	94.19	94.23	49.5258	93.95	81.63	0.26
1559	16/28-sb01	094.47 - .49 29/69	94.47	94.49	49.5359	61.84	54.38	0.23
928	16/28 Sbo1	094.55 --.57 30/69	94.55	94.57	49.5388		22.27	0.06
1560	16/28-sb01	094.62 - .65 30/69	94.62	94.65	49.5414	153.10	139.99	0.50
929	16/28 Sbo1	094.80 -.82 30/69	94.80	94.82	49.5479		27.82	0.15

1561	16/28-sb01 94.85 - .88 30/69	94.85	94.88	49.5497	126.97	114.94	0.56
1562	16/28 SB 01 94.98 - .95.02 30/69	94.98	95.02	49.5544	115.34	105.07	1.29
1563	16/28-sb01 095.29 - .32 30/69	95.29	95.32	49.5657	90.35	84.77	0.46
930	16/28 Sbo1 095.35 -.37 31/69	95.35	95.37	49.5679		17.47	0.11
1564	16/28-sb01 095.36 - .38 31/69	95.36	95.38	49.5682	58.99	54.10	0.30
1565	16/28-sb01 095.40 - .42 31/69	95.40	95.42	49.5697	61.93	56.14	0.24
931	16/28 Sbo1 095.70 -.72 31/69	95.70	95.72	49.5806		21.56	0.09
1566	16/28-sb01 095.92 - .93 31/69	95.92	95.93	49.5885	45.16	41.00	0.19
1567	16/28-sb01 095.96 - .99 31/69	95.96	95.99	49.5900	94.72	87.18	0.31
1568	16/28-sb01 096.11 - .14 31/69	96.11	96.14	49.5954	66.75	61.90	0.28
1569	16/28-sb01 096.25 - .26 32/69	96.25	96.26	49.6005	37.75	34.20	0.98
1570	16/28-sb01 096.28 - .30 32/69	96.28	96.30	49.6016	76.57	69.05	0.24
213	16/28 Sbo1 096.30 -.32 32/69	96.30	96.32	49.6023		9.63	0.06
1571	16/28-sb01 096.67 - .69 32/69	96.67	96.69	49.6158	51.37	47.90	0.42
1572	16/28-sb01 096.71 - .73 32/69	96.71	96.73	49.6172	38.94	36.16	0.27
932	16/28 Sbo1 096.80 -.82 32/69	96.80	96.82	49.6205		12.52	0.10
1573	16/28-sb01 096.87 - .90 32/69	96.87	96.90	49.6230	93.14	86.17	0.40
1574	16/28-sb01 097.14 - .18 33/69	97.14	97.18	49.6328	111.42	99.33	0.19
933	16/28 Sbo1 097.40 -.42 33/69	97.40	97.42	49.6423		21.70	0.07
1575	16/28-sb01 097.71 - .73 33/69	97.71	97.73	49.6535	60.45	55.54	0.26
934	16/28 Sbo1 097.80 -.82 34a/69	97.80	97.82	49.6568		15.51	0.07
1576	16/28-sb01 097.90 - .94 34a/69	97.90	97.94	49.6604	119.93	109.84	0.33
1577	16/28-sb01 101.76 - .80 34b/69	101.76	101.80	49.8005	115.81	106.66	0.14
1074	16/28 Sbo1 101.80 -.82 34/69	101.80	101.82	49.8019			
935	16/28 Sbo1 105.30 -.32 35/69	105.30	105.32	49.9289		12.35	0.08
1578	16/28-sb01 105.49 - .43 35/69	105.49	105.53	49.9358	61.57	57.95	0.49
936	16/28 Sbo1 105.70 -.72 36/69	105.70	105.72	49.9435		9.86	0.05
1579	16/28-sb01 105.74 - .77 36/69	105.74	105.77	49.9449	73.08	68.72	0.22
937	16/28 Sbo1 106.00 -.02 36/69	106.00	106.02	49.9543		11.87	0.08
1580	16/28-sb01 106.02 - .04 36/69	106.02	106.04	49.9551	52.35	49.02	0.16
1581	16/28-sb01 106.09 - .11 36/69	106.09	106.11	49.9576	48.88	45.70	0.12
1582	16/28-sb01 106.39 - .41 36/69	106.39	106.41	49.9685	43.16	40.36	0.11
938	16/28 Sbo1 106.51 -.53 37/69	106.51	106.53	49.9729		13.93	0.03
1583	16/28-sb01 106.53 - .56 37/69	106.53	106.56	49.9736	59.35	53.69	0.16
215	16/28 Sbo1 107.00 -.02 37/69	107.00	107.02	49.9906		7.08	0.03
1584	16/28-sb01 107.02 - .03 37/69	107.02	107.03	49.9914	24.47	21.30	0.10
1585	16/28-sb01 107.19 - .22 37/69	107.19	107.22	49.9975	52.42	45.97	0.99
1586	16/28-sb01 107.37 - .40 37/69	107.37	107.40	50.0041	79.06	75.77	3.76
939	16/28 Sbo1 107.45 -.47 38/69	107.45	107.47	50.0076		31.17	4.15
1587	16/28-sb01 107.47 - .50 38/69	107.47	107.50	50.0089	81.37	78.97	10.79
1588	16/28-sb01 107.86 - .88 38/69	107.86	107.88	50.0340	49.27	44.70	0.15
940	16/28 Sbo1 107.88 -.89 38/69	107.88	107.89	50.0353		15.48	0.10
1589	16/28-sb01 107.89 - .90 38/69	107.89	107.90	50.0360	35.18	32.10	0.14

1590	16/28-sb01 108.18 - .21 38/69	108.18	108.21	50.0547	48.68	45.11	0.14
941	16/28 Sbo1 108.32 -.34 39/69	108.32	108.34	50.0637		20.29	0.08
1591	16/28-sb01 108.40 - .43 39/69	108.4	108.43	50.0689	59.03	53.33	0.22
1592	16/28-sb01 108.48 - .50 39/69	108.48	108.50	50.0741	45.79	40.61	0.09
942	16/28 Sbo1 108.70 -.72 39/69	108.70	108.72	50.0883		23.06	0.06
1593	16/28-sb01 108.73 - .75 39/69	108.73	108.75	50.0902	40.62	35.75	0.16
1594	16/28-sb01 108.80 - .82 39/69	108.80	108.82	50.0947	66.06	56.69	0.33
1595	16/28-sb01 109.01 - .03 39/69	109.01	109.03	50.1083	80.03	69.51	0.43
943	16/28 Sbo1 109.20 -.22 40/69	109.20	109.22	50.1206		17.57	0.08
1596	16/28-sb01 109.21 - 23 40/69	109.21	109.23	50.1212	74.65	66.67	0.24
1597	16/28-sb01 109.25 - .28 40/69	109.25	109.28	50.1238	49.01	43.65	0.17
1598	16/28-sb01 109.56 - .58 40/69	109.56	109.58	50.1438	60.31	50.62	0.19
944	16/28 Sbo1 109.60 -.62 40/69	109.60	109.62	50.1464		17.02	0.11
1599	16/28 Sb 01 109.63 -.65 40/69	109.63	109.65	50.1483	49.67	41.59	0.83
1600	16/28-sb01 109.98 - 110.00 40/69	109.98	110.00	50.1709	77.79	51.69	0.62
945	16/28 Sbo1 110.20 -.22 41/69	110.20	110.22	50.1851		23.10	0.15
1601	16/28-sb01 110.35 - .39 41/69	110.36	110.39	50.1955	93.04	83.2	0.68
1602	16/28-sb01 110.44 - .46 41/69	110.44	110.46	50.2006	62.35	56.09	0.33
1603	16/28-sb01 110.57 - .60 41/69	110.57	110.60	50.2090	75.81	68.61	0.46
1604	16/28-sb01 110.66 - 68 42/69	110.66	110.68	50.2126	29.74	27.37	0.16
946	16/28 Sbo1 110.68 -.70 42/69	110.68	110.70	50.2132		12.17	0.07
1605	16/28-sb01 110.72 - .75 42/69	110.72	110.75	50.2146	87.53	79.94	0.46
1606	16/28-sb01 111.08 - .10 42/69	111.08	111.10	50.2270	74.47	65.61	0.37
947	16/28 Sbo1 111.10 -.12 42/69	111.10	111.12	50.2277		26.45	0.17
1607	16/28-sb01 111.12 - .14 42/69	111.12	111.14	50.2284	37.58	33.29	0.28
1608	16/28-sb01 111.36 - .39 42/69	111.36	111.39	50.2367	72.08	64.09	0.47
1609	16/28-sb01 111.52 - .54 43/69	111.52	111.54	50.2422	53.50	48.37	0.23
948	16/28 Sbo1 111.55 -.57 43/69	111.55	111.57	50.2432		13.04	0.06
949	16/28 Sbo1 111.90 -.92 43/69	111.90	111.92	50.2553		19.14	0.10
1610	16/28-sb01 111.94 - .96 43/69	111.94	111.96	50.2567	47.10	41.77	0.37
1611	16/28-sb01 111.99 - 112.01 43/69	111.99	112.01	50.2584	50.76	44.43	0.26
1612	16/28-sb01 112.30 - .33 43/69	112.30	112.33	50.2691	73.86	65.37	0.35
1613	16/28-sb01 112.33 - .35 43/69	112.33	112.35	50.2701	49.03	43.82	0.19
1614	16/28-sb01 112.35 - 36 44/69	112.35	112.36	50.2708	40.31	36.25	0.14
950	16/28 Sbo1 112.36 -.37 44/69	112.36	112.37	50.2712		16.68	0.11
1615	16/28-sb01 112.39 - 41 44/69	112.39	112.41	50.2722	68.21	58.75	0.27
951	16/28 Sbo1 112.80 -.82 44/69	112.80	112.82	50.2863		20.71	0.13
1616	16/28-sb01 112.82 - .84 44/69	112.82	112.84	50.2870	48.13	42.41	0.21
1617	16/28-sb01 112.84 - 86 44/69	112.84	112.86	50.2877	41.67	36.77	0.19
1618	16/28-sb01 113.14 - .17 44/69	113.14	113.17	50.2981	72.04	65.19	0.22
952	16/28 Sbo1 113.30 -.32 45/69	113.30	113.32	50.3036		26.45	0.22
1619	16/28-sb01 113.33 - .35 45/69	113.33	113.35	50.3046	100.96	85.10	0.55
1620	16/28-sb01 113.37 - .39 45/69	113.37	113.39	50.3060	40.93	34.53	0.21

1621	16/28-sb01 113.87 - .89 45/69	113.87	113.89	50.3232	85.00	73.92	0.42	
1622	16/28-sb01 113.94 - .96 45/69	113.94	113.96	50.3257	59.52	52.12	0.23	
953	16/28 Sbo1 113.97 -.99 45/69	113.97	113.99	50.3267		19.81	0.09	
1623	16/28-sb01 116.78 - .81 46/69	116.78	116.81	50.4236	56.16	52.78	0.30	
954	16/28 Sbo1 116.80 -.82 46/69	116.80	116.82	50.4243		27.47	0.19	
1624	16/28-sb01 116.88 - .90 46/69	116.88	116.90	50.4270	66.85	61.99	0.56	
218	16/28 Sbo1 117.20 -.22 46/69	117.20	117.22	50.4381				
1625	16/28-sb01 117.24 - .26 46/69	117.24	117.26	50.4394	53.60	48.57	0.42	
1626	16/28-sb01 117.34 - 36 46/69	117.34	117.36	50.4429	52.01	47.15	0.88	
1627	16/28-sb01 117.65 - .67 46/69	117.65	117.67	50.4502	62.25	57.02	0.27	
1628	16/28-sb01 117.68 - .70 47/69	117.68	117.70	50.4509	69.29	63.54	0.29	
1075	16/28 Sbo1 117.70 -.72 47/69	117.70	117.72	50.4514				
1629	16/28-sb01 117.75 - .77 47/69	117.75	117.77	50.4525	58.81	51.87	0.25	
1630	16/28-sb01 118.02 - .04 47/69	118.02	118.04	50.4586	57.58	53.93	0.26	
1631	16/28-sb01 118.05 - .07 47/69	118.05	118.07	50.4593	55.77	51.66	0.35	
955	16/28 Sbo1 118.10 -.12 47/69	118.10	118.12	50.4605		26.40	0.16	
1632	16/28-sb01 118.50 - .53 47/69	118.50	118.53	50.4696	80.94	73.49	0.36	
1633	16/28-sb01 118.55 - .57 48/69	118.55	118.57	50.4707	68.70	63.40	0.26	
956	16/28 Sbo1 118.60 -.62 48/69	118.6	118.62	50.4719		15.95	0.09	
1634	16/28-sb01 118.78 - .81 48/69	118.78	118.81	50.4760	104.07	96.00	0.45	
1635	16/28-sb01 118.95 - .97 48/69	118.95	118.97	50.4798	75.28	68.74	0.75	
957	16/28 Sbo1 119.00 -.02 48/69	119.00	119.02	50.4810		21.5	0.14	
1636	16/28-sb01 119.05 - .07 48/69	119.05	119.07	50.4821	85.26	77.78	0.51	
1637	16/28-sb01 119.34 - .36 48/69	119.34	119.36	50.4887	64.39	59.55	0.35	
958	16/28 Sbo1 119.38 -.40 49/69	119.38	119.40	50.4896		23.95	0.17	
1638	16/28-sb01 119.40 - .42 49/69	119.40	119.42	50.4901	58.02	53.81	0.30	
1639	16/28-sb01 119.46 - .50 49/69	119.46	119.50	50.4915	68.21	62.69	0.36	
1640	16/28-sb01 119.75 - .78 49/69	119.75	119.78	50.4981	74.26	65.42	0.42	
959	16/28 Sbo1 119.80 -.82 49/69	119.80	119.82	50.4992		23.64	0.18	
1641	16/28-sb01 119.82 - .85 49/69	119.82	119.85	50.4997	97.32	82.65	0.49	
1642	16/28-sb01 120.20 - .23 49/69	120.20	120.23	50.5083	63.85	59.91	0.28	
960	16/28 Sbo1 120.30 -.32 50/69	120.30	120.32	50.5106		18.2	0.12	
1643	16/28-sb01 120.43 - .46 50/69	120.43	120.46	50.5136	77.8	74.77	0.38	
1644	16/28 Sbo1 120.85 - .88 50/69	120.85	120.88	50.5231	96.79	87.49	1.09	
212	16/28 Sbo1 120.88 -.90 50/69	120.88	120.90	50.5238		15.22	0.09	
1645	16/28-sb01 120.90 - .92 50/69	120.90	120.92	50.5243	48.04	44.61	0.36	
961	16/28 Sbo1 122.30 -.32 51/69	122.30	122.32	50.5562		21.30	0.11	
1646	16/28-sb01 122.32 - .34 51/69	122.32	122.34	50.5566	46.18	43.64	0.17	
1647	16/28-sb01 122.38 - .40 51/69	122.38	122.40	50.5580	49.67	47.06	0.17	
1648	16/28-sb01 122.65 - .67 51/69	122.65	122.67	50.5641	51.22	48.52	0.14	
962	16/28 Sbo1 122.70 -.72 51/69	122.70	122.72	50.5653		19.78	0.05	
1649	16/28-sb01 122.78 - .80 51/69	122.78	122.80	50.5671	35.04	33.46	0.09	
1650	16/28-sb01 123.14 - .16 51/69	123.14	123.16	50.5753	64.98	61.74	0.14	

963	16/28 Sbo1 123.18 -.20 52/69	123.18	123.20	50.5762		13.06	0.05
1651	16/28-sb01 123.20 - .23 52/69	123.20	123.23	50.5767	83.27	78.55	0.24
964	16/28 Sbo1 123.60 -.62 52/69	123.60	123.62	50.5858		18.69	0.06
1652	16/28-sb01 123.62 - .66 52/69	123.62	123.66	50.5862	56.39	53.43	0.20
1653	16/28-sb01 123.94 - .98 52/69	123.94	123.98	50.5935	102.72	102.25	0.39
965	16/28 Sbo1 124.00 -.02 53/69	124.00	124.02	50.5949		14.29	0.04
1654	16/28-sb01 124.09 - .11 53/69	124.09	124.11	50.5969	50.01	47.39	0.13
1655	16/28-sb01 124.16 - .18 53/69	124.16	124.18	50.5985	45.84	43.55	0.12
966	16/28 Sbo1 124.40 -.42 53/69	124.40	124.42	50.6040		11.42	0.07
1656	16/28-sb01 124.42 - .44 53/69	124.42	124.44	50.6045	71.14	67.69	0.24
1657	16/28-sb01 124.50 - .52 53/69	124.50	124.52	50.6063	50.47	47.75	0.17
1658	16/28-sb01 124.76 - 80 53/69	124.76	124.80	50.6122	84.64	78.96	0.19
967	16/28 Sbo1 124.81 -.83 54/69	124.81	124.83	50.6133		16.72	0.04
1659	16/28-sb01 124.83 - .86 54/69	124.83	124.86	50.6138	78.34	72.34	0.19
216	16/28 Sbo1 125.20 -.22 54/69	125.20	125.22	50.6222		12.74	0.09
1660	16/28-sb01 125.25 - .29 54/69	125.25	125.29	50.6234	110.65	97	1.37
1661	16/28-sb01 125.65 - .68 54/69	125.65	125.68	50.6325	77.08	71.77	0.16
968	16/28 Sbo1 125.71 -.72 55/69	125.71	125.73	50.6338		18.24	0.06
1662	16/28-sb01 125.74 - .77 55/69	125.74	125.77	50.6345	99.12	93.28	0.24
1663	16/28-sb01 126.06 - .08 55/69	126.06	126.08	50.6418	60.21	56.7	0.18
969	16/28 Sbo1 126.10 -.12 55/69	126.10	126.12	50.6427		14.8	0.06
1664	16/28-sb01 126.14 - .16 55/69	126.14	126.16	50.6436	67.21	65.53	0.14
1665	16/28-sb01 126.56 - .59 55/69	126.56	126.59	50.6532	70.8232	65.22	0.15
1666	16/28-sb01 126.59 - .60 56a/69	126.59	126.60	50.6539	19.9	18.81	0.06
970	16/28 Sbo1 126.60 -.62 56a/69	126.60	126.62	50.6541		12.75	0.08
1667	16/28-sb01 126.64 - .66 56a/69	126.64	126.66	50.6550	53.87	50.66	0.13
1668	16/28-sb01 126.86 - .88 56a/69	126.86	126.88	50.6601	61.95	60.34	0.23
1669	16/28-sb01 126.89 - .91 56a/69	126.89	126.91	50.6607	49.59	46.52	0.13
1670	16/28-sb01 126.95 - .98 56a/69	126.95	126.98	50.6621	102.73	96.4	0.52
971	16/28 Sbo1 126.98 -127.00 56/69	126.98	127.00	50.6628		18.64	0.3
972	16/28 Sbo1 127.60 -.62 57/69	127.60	127.62	50.6769		13.66	0.07
1671	16/28-sb01 127.65 - .67 57/69	127.65	127.67	50.6780	36.16	33.69	0.12
1672	16/28-sb01 127.67 - .69 57/69	127.67	127.69	50.6785	59.88	55.67	0.19
973	16/28 Sbo1 128.00 -.02 57/69	128.00	128.02	50.6860		14.79	0.06
1673	16/28-sb01 128.02 - .04 57/69	128.02	128.04	50.6865	56.02	52.1	0.14
1674	16/28-sb01 128.05 - .07 57/69	128.05	128.07	50.6872	56.68	52.48	0.11
1675	16/28 Sbo1 128.35 - 38 57/69	128.35	128.38	50.6940	64.86	57.35	0.4
974	16/28 Sbo1 128.40 -.42 58/69	128.40	128.42	50.6951		14.89	0.06
1676	16/28-sb01 128.44 - .46 58/69	128.44	128.46	50.6960	47.20	41.31	0.18
975	16/28 Sbo1 128.90 -.92 58/69	128.90	128.92	50.7065		18.20	0.11
1677	16/28-sb01 128.92 - .94 58/69	128.92	128.94	50.7070	55.37	51.07	0.17
1678	16/28-sb01 129.12 - .14 58/69	129.12	129.14	50.7115	62.28	58.81	0.22
1679	16/28-sb01 129.21 - .23 58/69	129.21	129.23	50.7136	46.76	42.81	0.16

1680	16/28-sb01 129.28 - .30 59/69	129.28	129.30	50.7152	46.58	42.92	0.15
976	16/28 Sbo1 129.30 -.32 59/69	129.30	129.32	50.7156		19.83	0.12
1681	16/28-sb01 129.32 - .34 59/69	129.32	129.34	50.7161	39.69	36.93	0.25
1682	16/28-sb01 129.83 - .85 59/69	129.83	129.85	50.7277	53.66	47.93	0.28
977	16/28 Sbo1 129.85 -.87 59/69	129.85	129.87	50.7282		21.62	0.1
1683	16/28-sb01 129.88 - .90 59/69	129.88	129.90	50.7289	63.11	56.28	0.44
1684	16/28-sb01 130.16 - .18 59/69	130.16	130.18	50.7337	60.74	56.07	0.23
1685	16/28-sb01 120.18 - .20 60/69	130.18	130.20	50.7339	51.38	48.09	0.28
978	16/28 Sbo1 130.20 -.22 60/69	130.20	130.22	50.7341		13.04	0.05
1686	16/28-sb01 130.78 - .80 60/69	130.78	130.80	50.7410	57.86	54.03	0.24
1076	16/28 Sbo1 130.80 -.82 60/69	130.80	130.82	50.7413			
1687	16/28-sb01 130.82 - .84 60/69	130.82	130.84	50.7415	37.81	35.92	0.18
1688	16/28-sb01 130.97 - .131.00 60/69	130.97	131.00	50.7433	60.12	56.03	0.69
1689	16/28-sb01 135.24 - .26 61/69	135.24	135.26	50.7941	48.98	44.80	1.27
209	16/28 Sbo1 135.35 -.37 61/69	135.35	135.37	50.7954		8.84	0.04
1690	16/28-sb01 135.40 - .42 61/69	135.40	135.42	50.7960	67.78	61.72	0.29
1691	16/28-sb01 135.53 - .56 61/69	135.53	135.56	50.7975	119.08	108.38	0.46
1692	16/28-sb01 135.79 - .81 62/69	135.79	135.81	50.8006	66.89	62.19	0.29
979	16/28 Sbo1 135.85 -.87 62/69	135.85	135.87	50.8013		21.89	0.6
1693	16/28-sb01 135.98 - 136.00 62/69	135.98	136.00	50.8029	77.15	70.77	0.7
1694	16/28-sb01 136.26 - .28 62/69	136.26	136.28	50.8057	65.43	60.9	0.44
1695	16/28-sb01 136.28 - .31 62/69	136.28	136.31	50.8059	51.23	47.37	0.38
980	16/28 Sbo1 136.35 -.37 63/69	136.35	136.37	50.8067		10.32	0.36
1696	16/28-sb01 136.40 - .42 63/69	136.40	136.42	50.8072	34.24	32.12	0.26
1697	16/28-sb01 136.81 - .83 63/69	136.81	136.83	50.8113	41.88	38.95	0.51
981	16/28 Sbo1 136.85 -.87 63/69	136.85	136.87	50.8118		10.65	0.31
1698	16/28-sb01 136.91 - .93 63/69	136.91	136.93	50.8124	56.4	52.57	0.59
1699	16/28-sb01 137.12 - .14 63/69	137.12	137.14	50.8145	79.27	73.37	0.78
982	16/28 Sbo1 137.20 -.22 64/69	137.20	137.22	50.8153		16.51	0.51
1700	16/28-sb01 137.23 - .25 64/69	137.23	137.25	50.8156	76.80	69.07	0.68
1701	16/28-sb01 137.30 - .32 64/69	137.30	137.32	50.8163	51.08	45.59	3.03
1702	16/28-sb01 137.64 - .66 64/69	137.64	137.66	50.8198	66.21	61.19	0.53
1703	16/28-sb01 137.69 - .71 64/69	137.69	137.71	50.8203	53.28	49.40	0.41
983	16/28 Sbo1 137.70 -.72 64/69	137.70	137.72	50.8204		18.19	0.61
1704	16/28-sb01 137.91 - .93 64/69	137.91	137.93	50.8226	77.03	70.89	0.59
1705	16/28-sb01 143.88 - .90 65/69	143.88	143.9	52.6450	65.09	61.06	16.51
1078	16/28 Sbo1 143.90 -.92 65/69	143.90	143.92	52.6457			
1706	16/28-sb01 143.98 - 144.00 65/69	143.98	144.00	52.6486	45.18	43.16	12.54
1707	16/28-sb01 144.17 - .20 65/69	144.17	144.20	52.6554	110.37	103.59	9.55
984	16/28 Sbo1 144.20 -.22 66/69	144.20	144.22	52.6565		12.43	0.16
210	16/28 Sbo1 144.70 -.72 66/69	144.70	144.72	52.6745			
1708	16/28-sb01 144.73 - .75 66/69	144.73	144.75	52.6755	60.95	54.15	2.66
1709	16/28-sb01 144.78 - .80 66/69	144.78	144.80	52.6773	49.93	44.04	1.95

1710	16/28-sb01	145.00 - .04	66/69	145.00	145.04	52.6852	118.89	110.91	7.49
1077	16/28 Sbo1	145.20 -.22	67/69	145.20	145.22	52.6924			
1711	16/28-sb01	145.39 - .40	67/69	145.39	145.40	52.6992	57.38	53.52	7.94
1712	16/28-sb01	145.42 - .45	67/69	145.42	145.45	52.7003	118.14	109.69	4.20
1713	16/28-sb01	145.81 - .83	67/69	145.81	145.83	52.7143	74.85	68.90	12.68

Appendix 6: Absolute foraminiferal abundances, preservation, palaeowaterdepth calculations, "cenospherioid" radiolarian absent or present, and coarse and fine fraction percentages

BMC	Label Id	Top Depth (m)	Bottom Depth (m)	Age model this thesis [Ma]	Dry weight whole sample, before processing [g]	Dry weight after calgon/ coarse fraction > 63µm dry weight [g]	Percent coarse fraction >63µm after calgon	Percent fine fraction <63µm after calgon	Visual preservation glassy [g] or frosty [f]	preservation - good [g]- moderate [m] - poor [p]	cenospherioid radiolaria influx no [n]; yes [y]	abundance "cenospheroid" radiolaria none[n]; vr[very rare]; medium [m]; high [h]; very high [vh]	in size fraction >150 µm									
													per g sediment *Globoturborotalita* spp.	per g sediment *Subbotina* spp.	per g sediment *Acarinina* spp.	per g *Morozovella* spp.	per g *Pseudohastigerina* spp.	planktonic foraminifera per g sediment	benthic foraminifera per g sediment	All foraminifera per gram sediment	% P	Van Zwaan (1990) water depth estimation
208	16/28 Sbo1 041.00 -.02 6/69	41.00	41.02	44.8795	8.88	2.09	24	76										42.6	2.9	45.5	93.6	986.1
902	16/28 Sbo1 042.50 -.52 8/69	42.50	42.52	44.9331	8.56	3.5	41	59														
903	16/28 Sbo1 043.50 -.52 9/69	43.50	43.52	44.9688	14.11	3.96	28	72														
214	16/28 Sbo1 052.50 -.52 10/69	52.50	52.52	45.2906	8.28	1.58	19	81														
904	16/28 Sbo1 053.50 -.52 11/69	53.50	53.52	45.3263	12.71	4.81	38	62														
905	16/28 Sbo1 060.60 -.62 12/69	60.60	60.62	45.5802	15.62	15.24	98	2														

211	16/28 Sbo1 067.50 -.52 13/69	67.50	67.52	45.8269	5.54	5.25	95	5																
906	16/28 Sbo1 068.50 -.52 15/69	68.50	68.52	45.8626	9.51	2.01	21	79																
907	16/28 Sbo1 069.50 -.52 16/69	69.50	69.52	45.8984	9.90	3.56	36	64																
908	16/28 Sbo1 070.50 -.52 17/69	70.50	70.52	45.9341	19.64	3.68	19	81																
909	16/28 Sbo1 080.00 -.02 18/69	80.00	80.02	46.2565	12.45	2.61	21	79																
910	16/28 Sbo1 081.00 -.02 19/69	81.00	81.02	46.2885	15.86	6.75	43	57																
911	16/28 Sbo1 081.60 -.62 20/69	81.60	81.62	46.3077	8.73	4.19	48	52																
912	16/28 Sbo1 081.90 -.92 20/69	81.90	81.92	46.3173	13.26	2.17	16	84																
913	16/28 Sbo1 082.40 -.42 21/69	82.40	82.42	46.3332	10.33	5.36	52	48																
914	16/28 Sbo1 082.90 -.92 21/69	82.90	82.92	46.3492	16.34	3.53	22	78																
915	16/28 Sbo1 083.40 -.42 22/69	83.40	83.42	46.3652	15.29	4.03	26	74																
916	16/28 Sbo1 083.90 -.92 22/69	83.90	83.92	46.3812	29.23	7.79	27	73															85.8	6.2	92.0	93.3	977.0
920	16/28 Sbo1 087.52 -.54 23/69	87.52	87.54	46.4970	10.28	0.02	0	100															11.9	1.8	13.7	86.5	768.9
217	16/28 Sbo1 087.90 -.92 23/69	87.90	87.92	49.2489		0.9499																				
917	16/28 Sbo1 088.40 -.42 24/69	88.40	88.42	49.2692	18.16	4.44	24	76	g	g	n	n	21.4	20.7	3.5	0.8	49.3	8.0	57.4	86.0	754.5			

918	16/28 Sbo1 088.80 -.82 24/69	88.80	88.82	49.2855	18.79	0.04	0	100	g-f	g	n	n		3.5	0.3			3.8	1.1	4.9	77.2	552.5
919	16/28 Sbo1 089.25 -.27 25/69	89.25	89.27	49.3037	11.02	0.07	1	99	f-g	m	n	n	0.1	4.1	0.5		0.3	5.1	2.4	7.4	68.3	403.7
921	16/28 Sbo1 089.70 -.72 25/69	89.70	89.72	49.3220	20.64	0.09	0	100	f	m	y	vvvr		0.5	0.8		0.1	1.4	2.0	3.4	40.8	153.0
922	16/28 Sbo1 090.20 -.22 26/69	90.20	90.22	49.3423	14.23	0.06	0	100	g-f	m	y	vvvvr	0.1	5.7	1.9		0.2	7.9	3.3	11.2	70.4	435.5
923	16/28 Sbo1 090.80 -.82 26/69	90.80	90.82	49.3667	11.54	0.13	1	99	g-f	p	n	n		0.6				0.6	1.2	1.8	33.3	117.4
924	16/28 Sbo1 091.30 -.32 27/69	91.30	91.32	49.3899	15.44	0.13	1	99	f	p	n	n		4.6	0.1	0.2		5.1	4.9	10.0	50.6	216.4
925	16/28 Sbo1 091.80 -.82 28a/69	91.80	91.82	49.4138	13.01	0.03	0	100	g	g	n	n		0.2				0.2	1.0	1.2	18.8	70.1
926	16/28 Sbo1 093.70 -.72 29/69	93.70	93.72	49.5045	10.77	0.06	1	99	g	g	n	n		1.6				1.6	1.7	3.2	48.6	201.1
927	16/28 Sbo1 094.00 -.02 29/69	94.00	94.02	49.5188	13.52	0.09	1	99	g	m	n	n		0.1				0.1	0.6	0.7	20.0	73.3
928	16/28 Sbo1 094.55 --.57 30/69	94.55	94.57	49.5388	22.27	0.06	0	100	g-f	g	n	n		0.9				1.0	1.3	2.3	43.1	165.9
929	16/28 Sbo1 094.80 -.82 30/69	94.80	94.82	49.5479	27.82	0.15	1	99	g	m	n	n	0.3	7.1	1.8		0.4	9.6	2.1	11.7	82.2	660.1
1562	16/28 SB 01 94.98 - . 95.02 30/69	94.98	95.02	49.5544	105.07	1.29	1	99	g-f	g	n	n		3.9	1.0	0.04	0.2	5.1	1.7	6.9	74.7	505.4
930	16/28 Sbo1 095.35 -.37 31/69	95.35	95.37	49.5679	17.47	0.11	1	99	g-f	g	n	n		1.9	0.2		0.5	2.7	0.9	3.5	75.8	526.5
931	16/28 Sbo1 095.70 -.72 31/69	95.70	95.72	49.5806	21.56	0.09	0	100	g-f	m	n	n		1.0	0.05		0.05	1.2	1.0	2.2	53.2	236.7
213	16/28 Sbo1 096.30 -.32 32/69	96.30	96.32	49.6023	9.63	0.06	1	99	g-f	m	n	n		6.1			0.6	7.0	1.1	8.1	85.9	752.0

932	16/28 Sbo1 096.80 -.82 32/69	96.80	96.82	49.6205	12.52	0.1	1	99	g	p	n	n		3.4			0.2	3.9	3.0	6.9	57.0	270.6
933	16/28 Sbo1 097.40 -.42 33/69	97.40	97.42	49.6423	21.70	0.07	0	100	g	m	n	n		0.7	0.05			0.8	1.0	1.8	43.6	168.6
934	16/28 Sbo1 097.80 -.82 34a/69	97.80	97.82	49.6568	15.51	0.07	0	100	g	m	y	vvvvr		0.4				0.4	0.4	0.8	50.0	211.5
935	16/28 Sbo1 105.30 -.32 35/69	105.30	105.32	49.9289	12.35	0.08	1	99	g	g	n	n		3.2			0.6	4.0	1.1	5.1	79.4	597.0
936	16/28 Sbo1 105.70 -.72 36/69	105.70	105.72	49.9435	9.86	0.05	1	99	g	g	n	n		0.5				0.5	0.8	1.3	38.5	140.7
937	16/28 Sbo1 106.00 -.02 36/69	106.00	106.02	49.9543	11.87	0.08	1	99	g-f	m	n	n		1.5	0.3			1.9	0.8	2.7	68.8	410.3
938	16/28 Sbo1 106.51 -.53 37/69	106.51	106.53	49.9729	13.93	0.03	0	100	g	p	n	n		0.2	0.1			0.3	1.2	1.5	19.0	70.8
215	16/28 Sbo1 107.00 -.02 37/69	107.00	107.02	49.9906	7.08	0.03	0	100	g-f	p	n	n			0.6			0.6	2.4	3.0	19.0	70.8
939	16/28 Sbo1 107.45 -.47 38/69	107.45	107.47	50.0076	31.17	4.15	13	87	g-f	p	n	n		0.2	0.2			0.4	0.4	0.8	50.0	211.5
940	16/28 Sbo1 107.88 -.89 38/69	107.88	107.89	50.0353	15.48	0.1	1	99	g-f	m-p	n	n		1.5	0.5			2.0	1.9	3.9	51.7	224.3
941	16/28 Sbo1 108.32 -.34 39/69	108.32	108.34	50.0637	20.29	0.08	0	100	g-f	p	y	vvvvr		0.8			0.05	0.8	1.6	2.5	34.0	120.1
942	16/28 Sbo1 108.70 -.72 39/69	108.70	108.72	50.0883	23.06	0.06	0	100	g-f	p	n	n		0.2				0.2	0.5	0.7	31.3	109.0
943	16/28 Sbo1 109.20 -.22 40/69	109.20	109.22	50.1206	17.57	0.08	0	100	g-f	m	n	n	0.1	0.8				0.9	1.4	2.3	40.0	148.5
944	16/28 Sbo1 109.60 -.62 40/69	109.60	109.62	50.1464	17.02	0.11	1	99	f-g	m	n	n	0.1	1.3	1.5			3.1	2.5	5.6	54.7	250.0
1599	16/28 Sb 01 109.63 -.65 40/69	109.63	109.65	50.1483	41.59	0.83	2	98	g-f	m	n	n		1.6	0.4	0.05	0.6	2.6	2.8	5.4	48.9	203.3

945	16/28 Sbo1 110.20 -.22 41/69	110.20	110.22	50.1851	23.10	0.15	1	99	f-g	m	n	n	0.1	0.4	0.6			1.1	1.5	2.6	41.7	157.5
946	16/28 Sbo1 110.68 -.70 42/69	110.68	110.70	50.2132	12.17	0.07	1	99	g	p	n	n		0.6	0.1	0.1		0.7	0.9	1.6	45.0	177.2
947	16/28 Sbo1 111.10 -.12 42/69	111.10	111.12	50.2277	26.45	0.17	1	99	g-f	m	n	n	0.4	1.9	0.2	0.04		2.6	2.2	4.8	54.8	250.3
948	16/28 Sbo1 111.55 -.57 43/69	111.55	111.57	50.2432	13.04	0.06	0	100	g	p	n	n	0.1	1.1	0.3		0.1	1.7				
949	16/28 Sbo1 111.90 -.92 43/69	111.90	111.92	50.2553	19.14	0.1	1	99	g-f	m	n	n		0.2	1.7			1.9	0.9	2.9	67.3	389.4
950	16/28 Sbo1 112.36 -.37 44/69	112.36	112.37	50.2712	16.68	0.11	1	99	g-f	g	n	n	0.2	3.4	1.3		0.30	5.2				
951	16/28 Sbo1 112.80 -.82 44/69	112.80	112.82	50.2863	20.71	0.13	1	99	g-f	m	n	n		1.4				1.4	1.5	2.9	46.7	188.0
952	16/28 Sbo1 113.30 -.32 45/69	113.30	113.32	50.3036	26.45	0.22	1	99	g-f	m	n	n		0.1	0.04			0.1	0.5	0.6	18.8	70.1
953	16/28 Sbo1 113.97 -.99 45/69	113.97	113.99	50.3267	19.81	0.09	0	100	g	p	n	n		0.1				0.1	0.5	0.6	16.7	65.1
954	16/28 Sbo1 116.80 -.82 46/69	116.80	116.82	50.4243	27.47	0.19	1	99	g-f	g	n	n		5.5		0.1	0.3	5.7	1.8	7.5	75.8	527.2
218	16/28 Sbo1 117.20 -.22 46/69	117.20	117.22	50.4381					g	g	?some rads there	n						5.1	1.0	6.1	83.3	686.9
955	16/28 Sbo1 118.10 -.12 47/69	118.10	118.12	50.4605	26.40	0.16	1	99	g-f	p	n	n		1.4	0.6	0.04		2.0	1.1	3.1	65.9	370.3
956	16/28 Sbo1 118.60 -.62 48/69	118.60	118.62	50.4719	15.95	0.09	1	99	g	p	n	n		4.5	1.9	0.1		6.5	1.3	7.8	83.1	680.4
957	16/28 Sbo1 119.00 -.02 48/69	119.00	119.02	50.4810	21.50	0.14	1	99	g	p	n	n	0.6	2.5	0.6	0.05	0.05	3.8	1.3	5.1	73.6	487.6
958	16/28 Sbo1 119.38 -.40 49/69	119.38	119.40	50.4896	23.95	0.17	1	99	f-g	m	n	n	0.1	7.2	0.8	0.2		8.3	1.6	9.9	83.9	700.7

959	16/28 Sbo1 119.80 -.82 49/69	119.80	119.82	50.4992	23.64	0.18	1	99	g-f	p	n	n	0.1	1.8	1.7	0.2		3.8	1.6	5.4	70.1	430.0
960	16/28 Sbo1 120.30 -.32 50/69	120.30	120.32	50.5106	18.20	0.12	1	99	g	p	n	n		0.1	0.1			0.2	0.8	1.0	22.2	79.2
1644	16/28 Sbo1 120.85 - .88 50/69	120.85	120.88	50.5231	87.49	1.09	1	99						0.2	0.03	0.03		0.2	0.3	0.5	42.6	162.6
212	16/28 Sbo1 120.88 -.90 50/69	120.88	120.90	50.5238	15.22	0.09	1	99	g-f	m	n	n	0.3	7.6	0.1		0.1	8.1	1.4	9.5	84.8	724.1
961	16/28 Sbo1 122.30 -.32 51/69	122.30	122.32	50.5562	21.30	0.11	1	99	g-f	m	n	n		2.0	0.05			2.0	0.7	2.7	75.4	519.7
962	16/28 Sbo1 122.70 -.72 51/69	122.70	122.72	50.5653	19.78	0.05	0	100	g	p	n	n		0.1				0.1	1.4	1.5	6.9	46.1
963	16/28 Sbo1 123.18 -.20 52/69	123.18	123.20	50.5762	13.06	0.05	0	100	f-g	p	n	n	0.2	0.8				1.5	0.8	2.3	66.7	381.1
964	16/28 Sbo1 123.60 -.62 52/69	123.60	123.62	50.5858	18.69	0.06	0	100	g	p	n	n		0.3				0.3	0.4	0.7	38.5	140.7
965	16/28 Sbo1 124.00 -.02 53/69	124.00	124.02	50.5949	14.29	0.04	0	100	g	?	n	n		0.1				0.1	0.6	0.7	10.0	51.4
966	16/28 Sbo1 124.40 -.42 53/69	124.40	124.42	50.6040	11.42	0.07	1	99	g	p	n	n		0.1				0.1	0.8	0.9	10.0	51.4
967	16/28 Sbo1 124.81 -.83 54/69	124.81	124.83	50.6133	16.72	0.04	0	100	f	p	n	n		0.1				0.1	0.7	0.7	8.3	48.5
216	16/28 Sbo1 125.20 -.22 54/69	125.20	125.22	50.6222	12.74	0.09	1	99	f-g	m	y	vvvr	0.1	0.9				1.0	0.9	2.0	52.0	227.0
968	16/28 Sbo1 125.71 -.72 55/69	125.71	125.73	50.6338	18.24	0.06	0	100	f	p	y	vvvr							0.8	0.8		
969	16/28 Sbo1 126.10 -.12 55/69	126.10	126.12	50.6427	14.80	0.06	0	100	f-g	p	y	vvr		0.3				0.3	0.8	1.1	29.4	102.2
970	16/28 Sbo1 126.60 -.62 56a/69	126.60	126.62	50.6541	12.75	0.08	1	99	f-g	p	y	vvr		0.4				0.4	0.6	1.0	38.5	140.7

971	16/28 Sbo1 126.98 - 127.00 56/69	126.98	127.00	50.6628	18.64	0.3	2	98	f-g	p	y	vr		0.6			0.1	0.6	1.7	2.3	27.9	96.9
972	16/28 Sbo1 127.60 -.62 57/69	127.60	127.62	50.6769	13.66	0.07	1	99	f	p	y	r		0.6				0.6	1.2	1.8	33.3	117.4
973	16/28 Sbo1 128.00 -.02 57/69	128.00	128.02	50.6860	14.79	0.06	0	100	g	p	y	r		1.0				1.0	1.5	2.5	40.5	151.4
1675	16/28 Sbo1 128.35 - 38 57/69	128.35	128.38	50.6940	57.35	0.4	1	99	f	p	y	m		2.5	0.4	0.1	0.1	3.0	2.5	5.5	54.3	245.8
974	16/28 Sbo1 128.40 -.42 58/69	128.40	128.42	50.6951	14.89	0.06	0	100	g	m	y	vr		3.6	2.2			5.8				
975	16/28 Sbo1 128.90 -.92 58/69	128.90	128.92	50.7065	18.20	0.11	1	99	f	p	y	r		2.8	2.0		0.1	5.1				
976	16/28 Sbo1 129.30 -.32 59/69	129.30	129.32	50.7156	19.83	0.12	1	99	f	m	y	m		2.8	2.4			5.2	1.4	6.6	79.4	597.5
977	16/28 Sbo1 129.85 -.87 59/69	129.85	129.87	50.7282	21.62	0.1	0	100	g-f	m	y	m		1.6	2.2		0.05	3.9				
978	16/28 Sbo1 130.20 -.22 60/69	130.20	130.22	50.7341	13.04	0.05	0	100	g-f	m	y	m-r		0.1	0.9			1.0				
209	16/28 Sbo1 135.35 -.37 61/69	135.35	135.37	50.7954	8.84	0.04	0	100	f	m	y	r		1.1	1.8			3.1	0.3	3.4	90.0	869.4
979	16/28 Sbo1 135.85 -.87 62/69	135.85	135.87	50.8013	21.89	0.6	3	97	f-g	p	y	m	0.05	0.4	0.4			1.0	0.5	1.4	67.7	395.9
980	16/28 Sbo1 136.35 -.37 63/69	136.35	136.37	50.8067	10.32	0.36	3	97	f	p	y	h		0.9	0.8			1.6	0.2	1.8	89.5	853.4
981	16/28 Sbo1 136.85 -.87 63/69	136.85	136.87	50.8118	10.65	0.31	3	97	g	g	y	m		3.3	1.9	0.1		5.3				
982	16/28 Sbo1 137.20 -.22 64/69	137.20	137.22	50.8153	16.51	0.51	3	97	g-f	p	y	h		0.8	1.5	0.1		2.4	1.2	3.6	66.1	373.6
983	16/28 Sbo1 137.70 -.72 64/69	137.70	137.72	50.8204	18.19	0.61	3	97	f	m-p	y	m		6.9	0.4		0.1	7.5	2.5	10.1	74.9	509.2

	16/28 Sbo1 143.90 -.92 65/69	143.9	143.92	52.6457					f mor	p	y	vh				18.2			
984	16/28 Sbo1 144.20 -.22 66/69	144.20	144.22	52.6565	12.43	0.16	1	99	f than g		y	vr	0.1	0.1		0.1	0.3	0.4	20.0
210	16/28 Sbo1 144.70 -.72 66/69	144.70	144.72	52.6745					f	m-p	y	vh							

Appendix 7: All carbon and oxygen isotopes of all measured foraminiferal species, the size fraction measured, their weight, the cleaning procedure used and their preservation

Vial label unique ID for species specific isotope samples	Sample depth	Species	Size fraction	Numbers of individuals taken from sample including broken ones by processing and lost ones by moving samples to weighing tray	Number of individuals given to BGS and measured	Number of glassy foraminifera	Number of glassy to frosty	weight [µg] aim 50-70 µg	Cleaning yes no; yb = with DI-water and paintbrush; uson= ultrasonication	Average weight per individual specimen [µg]	$\delta^{13}C$ [‰ VPDB]	$\delta^{18}O$ [‰ VPDB]	Comment
U1	83.90 -92 m	*A. punctocarinata*	> 355 µm	4	4		4	136	yb, uson	34.00	2.91	-1.70	
U2	83.90 -92 m	*M. crater*	> 355 µm	3	3	2	2	86	yb, uson	28.67	2.92	-1.52	
U3	83.90 -92 m	*G. nuttali*	> 355 µm	4	4	4		129	yb, uson	32.25	0.65	-0.44	
U4	83.90 -92 m	*C. unicavus*	> 355 µm	2	2		2	64	yb, uson	32.00	0.89	-0.99	
U5	83.90 -92 m	*S. patagonica*	> 355 µm	2	2	2		45	yb, uson	22.50	0.92	-1.35	
U6	83.90 -92 m	*S. lineaperta*	> 355 µm	2	2	2		57	yb, uson	28.50	0.84	-1.13	
U7	83.90 -92 m	*S. yeguaensis*	> 355 µm	3	3	1	2	93	yb, uson	31.00			failed, too small
U8	83.90 -92 m	*S. hagni*	> 355 µm	1	1	1		26	yb, uson	26.00	0.39	-1.18	
U9	83.90 -92 m	*S. corpulenta*	> 355 µm	3	3	1	2	90	yb, uson	30.00	0.72	-0.67	
U10	83.90 -92 m	*S. eocena*	> 355 µm	4	4	4		85	yb, uson	21.25	0.79	-1.17	
U11	83.90 -92 m	*A. cuneicamerata*	300-355 µm	2	2		2	42	yb, uson	21.00	1.10	-0.84	
U12	83.90 -92 m	*A. pentacamerata*	300-355 µm	4	2		2	20	yb, uson	10.00	1.81	-1.81	
U13	83.90 -92 m	*A. praetopilensis*	300-355 µm	2	2	1	1	30	yb, uson	15.00	3.42	-2.52	
U14	83.90 -92 m	*A. bullbrooki*	300-355 µm	4	4		4	91	yb, uson	22.75	1.96	-1.18	
U15	83.90 -92 m	*A. boudreauxi*	300-355 µm	2	2	1	1	33	yb, uson	16.50	2.07	-1.52	
U16	83.90 -92 m	*A. punctocarinata/ M. crater*	300-355 µm	4	4		4	103	yb, uson	25.75	2.38	-1.51	

U17	83.90 -92 m	*S. patagonica*	300-355 µm	4	4	2	2	59	yb, uson	14.75	0.92	-1.35
U18	83.90 -92 m	*S. yeguaensis*	300-355 µm	2	2	1	1	23	yb, uson	11.50	0.35	-0.78
U19	83.90 -92 m	*S. corpulenta*	300-355 µm	3	3		3	61	yb, uson	20.33	0.64	-0.73
U20	83.90 -92 m	*S. eocena*	300-355 µm	4	4	1	3	75	yb, uson	18.75	0.88	-1.30
U21	83.90 -92 m	*A. pentacamerata*	250-300 µm	5	5	2	3	39	yb, uson	7.80	3.53	-1.89
U22	83.90 -92 m	*A. bullbrooki*	250-300 µm	7	7	4	3	98	yb, uson	14.00	1.30	-1.00
U23	83.90 -92 m	*A. boudreauxi*	250-300 µm	6	6		6	85	yb, uson	14.17	1.84	-1.44
U24	83.90 -92 m	*G. bassriverensis*	250-300 µm	3	3	2	1	28	yb, uson	9.33	0.47	-0.65
U25	83.90 -92 m	*C. unicavus*	250-300 µm	6	6	3	3	57	yb, uson	9.50	0.37	-0.62
U26	83.90 -92 m	*S. patagonica*	250-300 µm	7	7	7		101	yb, uson	14.43	0.61	-1.11
U27	83.90 -92 m	*S. lineaperta*	250-300 µm	7	7	5	2	80	yb, uson	11.43	0.82	-1.23
U28	83.90 -92 m	*S. yeguaensis*	250-300 µm	6	6	2	4	62	yb, uson	10.33	0.47	-0.64
U29	83.90 -92 m	*S. corpulenta*	250-300 µm	7	7	4	3	73	yb, uson	10.43	0.46	-0.67
U30	83.90 -92 m	*S. eocena*	250-300 µm	6	6	5	2	64	yb, uson	10.67	0.69	-0.96
U31	83.90 -92 m	*S. senni*	250-300 µm	4	4	2	2	53	yb, uson	13.25	1.38	-1.32
U32	83.90 -92 m	*S. roesnaensis*	250-300 µm	6	6	1	5	76	yb, uson	12.67	0.56	-0.79
U33	83.90 -92 m	*A. pentacamerata* flat spiral side	212 - 250 µm	14	14	8	6	76	yb	5.43	2.82	-1.52
U34	83.90 -92 m	*A. pentacamerata* high spiral side	212 - 250 µm	14	13	6	7	89	yb	6.85	2.92	-1.71
U35	83.90 -92 m	*A. bullbrooki*	212 - 250 µm	15	15	3	12	137	yb	9.13	0.96	-0.85
U36	83.90 -92 m	*A. boudreauxi*	212 - 250 µm	14	14	6	8	142	yb	10.14	0.93	-0.86
U37	83.90 -92 m	*Pseudohastigerina spp.*	212 - 250 µm	6	6	3	3	19	yb	3.17	-0.37	-0.91
U38	83.90 -92 m	*S. patagonica*	212 - 250 µm	16	16	9	7	148	yb	9.25	0.74	-1.11
U39	83.90 -92 m	*S. lineaperta*	212 - 250 µm	10	10	7	3	66	yb	6.60	0.71	-1.05
U40	83.90 -92 m	*S. yeguaensis*	212 - 250 µm	14	14	6	8	83	yb	5.93	0.37	-0.78
U41	83.90 -92 m	*S. corpulenta*	212 - 250 µm	14	14	11	3	113	yb	8.07	0.52	-0.67
U42	83.90 -92 m	*S. eocena*	212 - 250 µm	11	11	5	6	94	yb	8.55	0.62	-0.85
U43	83.90 -92 m	*A. cuneicamerata*	180 - 212 µm	14	14	6	8	62	yb	4.43	1.75	-1.14

U44	83.90 -92 m	*A. pentacamerata*	180 - 212 µm	19	19	11	8	68	yb	3.58	2.07	-1.28
U45	83.90 -92 m	*A. collactea*	180 - 212 µm	19	18	11	7	66	yb	3.67	2.45	-1.60
U46	83.90 -92 m	*A. bullbrooki*	180 - 212 µm	17	17	13	4	79	yb	4.65	1.57	-1.38
U47	83.90 -92 m	*A. boudreauxi*	180 - 212 µm	20	20	8	12	123	yb	6.15	0.81	-0.94
U48	83.90 -92 m	*P. micra?*	180 - 212 µm	19	18	8	10	57	yb	3.17	0.09	-0.96
U49	83.90 -92 m	*C. unicavus*	180 - 212 µm	20	20	9	11	99	yb	4.95	0.38	-0.55
U50	83.90 -92 m	*S. patagonica*	180 - 212 µm	21	21	10	11	124	yb	5.90	0.45	-0.81
U51	83.90 -92 m	*S. yeguaensis*	180 - 212 µm	20	20	10	10	87	yb	4.35	0.33	-0.67
U52	83.90 -92 m	*S. eocena*	180 - 212 µm	20	19	10	9	74	yb	3.89	0.48	-0.97
U53	83.90 -92 m	*A. cuneicamerata*	150 - 180 µm	19	19	17	2	53	yb	2.79	1.73	-1.28
U54	83.90 -92 m	*A. pentacamerata*	150 - 180 µm	19	19	15	4	38	yb	2.00	1.88	-1.41
U55	83.90 -92 m	*A. collactea*	150 - 180 µm	19	19	12	7	45	yb	2.37	1.63	-1.50
U56	83.90 -92 m	*A. boudreauxi*	150 - 180 µm	20	18	16	2	74	yb	4.11	0.62	-1.04
U57	83.90 -92 m	*A. punctocarinata / M. crater*	150 - 180 µm	9	9	6	3	33	yb	3.67	2.01	-2.12
U58	83.90 -92 m	*P. micra ?*	150 - 180 µm	21	21	12	9	53	yb	2.52	0.16	-1.06
U59	83.90 -92 m	*S. patagonica*	150 - 180 µm	12	12		12	39	yb	3.25	0.21	-0.97
U60	83.90 -92 m	*S. hagni*	150 - 180 µm	19	17	12	5	48	yb	2.82	0.10	-1.05
U61	83.90 -92 m	*S. eocena*	150 - 180 µm	20	20	9	11	68	yb	3.40	0.28	-0.96
U62	83.90 -92 m	*P. micra ?*	125 - 150 µm	36	35	22	13	49	yb	1.40	0.21	-0.98

Vial label unique ID for species specific isotope samples	Sample depth	Species	Size fraction	Numbers of individuals taken from sample including broken ones by processing and lost ones by moving samples to weighing tray	Lost	Number of individuals given to BGS	Number of glassy foraminfiera	Number of glassy to frosty foraminifera	Preservation comment: pyrite present =p; infilled with pyrite = ip; brownish yellow bits on top = b	Weight [µg] aim 50-70 µg	Cleaning yes no; yesb = cleaning with DI-water and paintbrush	Average weight per individual specimen er sample [µg]	Number of foraminifera found at the BGS by retransfer (were sent by post and needed finding)	Number of lost foraminifera (due to the postage of samples)	$\delta^{13}C$ [VPDB ‰]	$\delta^{18}O$ [VPDB ‰]
U63	119.80 - 82 m	*A. bullbrooki*	300 - 355 µm	5		5		4	1 ip; b	44	yb	8.8	4	1	3.27	-2.39
U64	119.38 - .40 m	*A. cuneicamerata*	250 - 300 µm	3		3		3	1 ip; p	14	yb	4.7	3	0	3.91	-2.95
U65	119.38 - .40 m	*A. bullbrooki*	300 - 355 µm	2		2		2	p	18	yb	9	2	0	4.20	-2.80
U66	119.38 - .40 m	*A. boudreauxi*	250 - 300 µm	2		2		2		6	yb	3	2	0	4.35	-3.06
U67	119.38 - .40 m	*A. boudreauxi*	212 - 250 µm	4	2	2		4		6	yb	3	2	0	DIDN'T RUN	
U68	119.38 - .40 m	*M. subbotinae ?*	300 - 355 µm	2		2		2	1ip	17	yb	8.5	2	0	3.34	-2.10
U69	119.38 - .40 m	*N. trumpyi*	212 - 250 µm	1		1		1		18	yb	18	1	0	0.42	-0.73
U70	119.80 - 82 m	*A. bullbrooki*	250 - 300 µm	4		4		3	p; b	20	yb	5	4	0	3.26	-2.31
U71	119.80 - 82 m	*A. boudreauxi*	250 - 300 µm	4		4		4	p, b	24	yb	6	3	1	3.51	-2.63
U72	119.80 - 82 m	*A. boudreauxi*	212 - 250 µm	8	1	7				14	yb	1.8	5	2	3.28	-2.37
U73	119.80 - 82 m	*A. boudreauxi*	180 - 212 µm	13	2	11		13		27	yb	2.5	9	2	2.70	-2.56
U74	119.80 - 82 m	*Morozovella spp.*	> 355 µm	1.5		1.5		1.5		22	yb	14.7	1.5	0	4.38	-2.38
U75	83.90 - .92 m	*N. trumpyi*	212 -250 µm	2		2		2		44	yb	22	2	0	0.35	-0.19

U76	119.38 - .40 m	*S. corpulenta*	300 - 355 µm	4	4	4		ip	34	yb	8.5	4	0	1.52	-1.17
U77	119.38 - .40 m	*S. corpulenta*	250 - 300 µm	5	4	4		p	18	yb	4.5	4	0	2.39	-1.30
U78	119.38 - .40 m	*S. eocaena*	300 - 355 µm	2	2		2		15	yb	7.5	2	0	2.56	-1.63
U79	119.38 - .40 m	*S. eocaena*	250 - 300 µm	16	9	8	1		27	yb	3	9	0	1.77	-1.37
U80	119.38 - .40 m	*S. eocaena*	212 - 250 µm	15	10	7	3		26	yb	2.6	9	1	1.82	-1.42

Vial lable unique ID for species specific isotopes	Top depth [m]	Bottom depth [m]	Species	Size fraction	Numbers of individuals taken from foraminiferal sample	Lost during ultrasonication [uson.]	Number recovered after uson.	Lost during weighing	Number giving to BGS for measuring	Number of glassy before uson.	Number of glassy to frosty before uson.	Number of frosty before uson.	Number of glassy after uson.	Number of glassy to frosty after uson.	Number of frosty after uson.	Preservation comment: pyrite present =p; infilled with pyrite = ip; brownish yellow bits on top = b	Weight [µg] aim 50-70 µg	Cleaning yes no; yesb = with DI water and paintbrush; uson=ultrasonication	Notes	Weight per individual specimen [µg]	δ13C [VPDB ‰]	δ18O [VPDB ‰]
U81	43.5	43.52	*A. bullbrooki*	250-300 µm	3	0	3	0	3	3	0	0	3	0	0		17	yesb; uson	one broke during ultra sonication	6	2.88	-1.46
U82	43.5	43.52	*S. eocaena*	250-300 µm	17	1.5	15.5	0	15.5	0	17	0	15	0	0	some carbonate particels inside and grown on top - where possible removed	221	yesb; uson	1.5 lost due to breakage whilest ultrasonication	14	0.94	-0.94
U83	52.5	52.52	*S. eocaena*	250-300 µm	9	0.5	8.5	0	8.5	0	9	0	4	5	0	some carbonate particels inside and grown on top - where possible removed	168	yesb; uson	0.5 lost due to ultrasonication	20	0.74	-1.02

U84	52.5	52.52	*A. bullbrooki*	250-300 µm	11	0	11	0	11	3	8	0	8	3	0	some carbonate particles inside and grown on top - where possible removed	172	yesb; uson		16	2.78	-1.45
U85	82.4	82.42	*A. bullbrooki*	250-300 µm	11	0	11	0	11	10	1	0	7	4	0	some carbonate particles inside and grown on top - where possible removed	163	yesb; uson		15	2.17	-0.89
U86	83.4	83.42	*A. bullbrooki*	250-300 µm	8	0	8	0	8	4	4	0	7	1	0	some carbonate particles inside and grown on top - where possible removed	107	yesb; uson		13	1.98	-1.18
U87	91.3	91.32	*S. eocaena*	250-300 µm	19	6.5	12.5	0	12.5	13	6	0	8	5	0	p	54	yesb; uson	some dissolution signs holes in a couple of tests - might not withstand ultrasonication; 7 broken due to ultrasonication	4	1.39	-1.45
U88	94.85	94.88	*S. eocaena*	250-300 µm	15	1	14	1	13	15	0	0	10	4	0	p	46	yesb; uson	lots of small ones; lost 1 due to uson	4	1.23	-1.50
U89	96.3	96.32	*S. eocaena*	250-300 µm	5	1	4	0	4	4	1	0	3	1	0	p	15	yesb; uson	1 lost due to uson	4	1.56	-1.84
U90	96.8	96.82	*S. eocaena*	250-300 µm	7	0	7	1	6	4	3	0	4	3	0	1pi;	18	yesb; uson		3	1.68	-1.41

U91	105.3	105.32	*S. eocaena*	250-300 µm	4	1.5	2.5	0	2.5	3	1	0	2	0.5	0	b	19	yesb; uson	2 broken open due to uson; some fragments recovered	8	1.51	-2.03
U92	107.88	107.89	*S. eocaena*	250-300 µm	8	1.5	6.5	1	5.5	6	2	0	5	1	0	p;1pi	24	yesb; uson	1.5 lost due to uson	4	1.28	-2.01
U93	111.1	111.12	*S. eocaena*	250-300 µm	8	0	8	0	8	8	0	0	6	2	0		25	yesb; uson		3	1.47	-1.60
U94	118.1	118.12	*S. eocaena*	250-300 µm	5	2	3	0	3	3	2	0	2	1	0	1pi;	12	yesb; uson		4	2.02	-1.03
U95	118.6	118.62	*A. bullbrooki*	250-300 µm	4	0	4	0	4	4	0	0	4	0	0	2pi;	21	yesb; uson		5	3.70	-2.77
U96	118.6	118.62	*S. eocaena*	250-300 µm	12	4	8	0	8	11	1	0	7	1	0	p;	20	yesb; uson		3	1.79	-1.42
U97	119.8	119.82	*S. eocaena*	250-300 µm	12	1	11	1	10	7	5	0	8	3	0	2pi; p	30	yesb; uson	1 lost due to uson	3	1.61	-1.47
U98	119.82	119.82	*A. bullbrooki*	250-300 µm	7	0	7	0	7	5	2	0	5	2	0	p	61	yesb; uson		9	3.39	-2.72
U99	119.82	119.85	*S. eocaena*	250-300 µm	9	0	9	0	9	7	2	0	7	2	0	p but almost none	71	yesb; uson		8	1.66	-1.38
	123.18	123.2	*S. eocaena*	250-300 µm	3	3	0			0	3	0	0	3	0	p		yesb; uson	2 slightly broken; all lost during uson --> all broke			
U100	122.3	122.32	*S. eocaena*	250-300 µm	7	1.5	5.5	0	5.5				3	2.5	0	p	20	yesb; uson		4	1.93	-1.60
U101	128	128.02	*S. eocaena*	250-300 µm	4	0	4	0	4	0	4	0	0	4	0	4 pi;	32	yesb; uson	might need breaking for weighing - all four infilled with pyrite; 2 broke during uson	8	0.86	-1.89
U102	128.4	128.42	*A. bullbrooki*	250-300 µm	10	1.5	8.5	0	8.5	3	7	0	3	5	0	p	76	yesb; uson	one broken excluded so minimized to 10 --> one broke by trying to remove additional carbonate --> might need breaking they are full of	9	2.41	-3.34

																			carbonate crystals - might need breaking to clean out			
U103	128.4	128.42	*S. eocaena*	250-300 µm	5	0	5	0.5	4.5	4	1	0	4	1	0	p almost none	22	yesb; uson		5	0.76	-1.77
U104	128.9	128.92	*A. bullbrooki*	250-300 µm	6	3.5	2.5	0	2.5	0	0	6	0	0	2.5	1pi	27	yesb; uson		11	2.65	-3.53
U105	128.9	128.92	*S. eocaena*	250-300 µm	6	4.5	1.5	0	1.5	4	2	0	0	1.5	0	p; 2pi; 1b	12	yesb; uson		8	Didn't run	
U106	129.85	129.87	*A. bullbrooki*	250-300 µm	5	1.5	3.5	0	3.5	2	3	0	1.5	2	0	p	19	yesb; uson		5	3.02	-2.68
U107	129.85	129.87	*S. eocaena*	250-300 µm	3	0.5	2.5	0	2.5	2	1	0	2.5	0	0	p	14	yesb; uson		6	1.68	-1.49
U108	135.24	135.26	*A. bullbrooki*	250-300 µm	10	1	9	0	9	0	0	10	0	0	9	2pi;p	133	yesb; uson	very poor preservation!	15	4.21	-3.85
U109	135.85	135.87	*A. bullbrooki*	250-300 µm	3	0	3	0	3	0	3	0	0	3	0	p	30	yesb; uson	might be more *A. spp* two Acarinina not sure to be *A. bullbrooki*	10	2.74	-2.86
U110	136.35	136.37	*A. bullbrooki*	250-300 µm	3	0	3	0	3	0	0	3	0	0	3	p; 1pi	20	yesb; uson		7	4.01	-3.25
U111	136.35	136.37	*S. eocaena*	250-300 µm	4	0.5	3.5	0	3.5	2	0	2	0	0	3.5		22	yesb; uson	infilled 2 with carbonate --> dissolved test--> might be not enough material to measure	6	Didn't run	
U112	137.12	137.14	*A. bullbrooki*	250-300 µm	10	0	10	0	10	2	8	0	2	8	0	1pi	131	yesb; uson		13	3.37	-2.91
U113	137.12	137.14	*S. eocaena*	250-300 µm	7	0	7	0	7	4	3	0	4	3	0	3pi	131	yesb; uson		19	1.72	-1.36
U114	144.17	144.2	*A. bullbrooki*	250-300 µm	10	0	10	0	10	4	6	0	4	6	0		175	yesb; uson		18	2.96	-3.26
U115	144.73	144.75	*S. eocaena*	250-300 µm	7	0	7	0	7	5	2	0	5	2	0	p	131	yesb; uson		19	0.18	-2.02

U116	145	145.04	*A. bullbrooki*	250-300 µm	5	0	5	0	5	5	0	0	5	0	0	52	yesb; uson		10	2.87	-3.61
U117	42.5	42.52	*S. eocaena*	250-300 µm	7	0	7	0	7	5	2	0	5	2	0	120	yesb; uson		17	0.96	-0.39
U118	80	80.02	*A. bullbrooki*	250-300 µm	12	0	12	0	12	12	0	0	12	0	0	203	yesb; uson		17	1.82	-1.39
U119	80	80.02	*S. eocaena*	250-300 µm	15	0	15	0	15	15	0	0	15	0	0	278	yesb; uson		19	0.92	-0.99
U120	82.4	82.42	*S. eocaena*	250-300 µm	15	0	15	0	15	15	0	0	15	0	0	210	yesb; uson	2 broken during uson	14	1.23	-0.72
U121	83.4	83.42	*S. eocaena*	250-300 µm	15	0	15	0	15	15	0	0	15	0	0	234	yesb; uson		16	1.16	-0.88
U122	87.52	87.54	*S. eocaena*	250-300 µm	9	0	9	0	9	6	3	0	6	3	0	30	yesb; uson	1 broke during uson	3	1.21	-1.89
U123	90.2	90.22	*S. eocaena*	250-300 µm	13	2.5	10.5	1	9.5	5	8	0	8	3	0	47	yesb; uson	1 broke during uson	5	1.24	-1.68
U124	116.8	116.82	*S. eocaena*	250-300 µm	14	0	14	2	12	0	4	10	8	6	0	50	yesb; uson		4	1.61	-1.20
U125	117.2	117.22	*S. eocaena*	250-300 µm	11	0	11	0	11	6	5	0	8	3	0	45	yesb; uson		4	Didn't run	
U126	120.88	120.9	*S. eocaena*	250-300 µm	13	1.5	11.5	0	11.5	5	8	0	8	5	0	51	yesb; uson		4	1.56	-1.55
U127	129.3	129.32	*S. eocaena*	250-300 µm	9	1	8	0	8	0	9	0	3	5	0	61	yesb; uson	1 broke during uson	8	1.20	-1.86
U128	135.4	135.42	*A. bullbrooki*	250-300 µm	5	0.5	4.5	0	4.5	0	5	0	0	5	0	59	yesb; uson	2 broke during uson	13	4.36	-3.86
U129	135.53	135.56	*A. bullbrooki*	250-300 µm	13	0	13	1	12	4	9	0	4	9	0	140	yesb; uson	some broken during uson	12	4.36	-3.89
U130	136.4	136.42	*A. bullbrooki*	250-300 µm	6	0	6	0	6	2	4	0	2	4	0	79	yesb; uson		13	Didn't run	
U131	136.4	136.42	*S. eocaena*	250-300 µm	6	0	6	0	6	3	3	0	3	3	0	59	yesb; uson		10	1.52	-1.13
U132	137.91	137.93	*S. eocaena*	250-300 µm	7	0	7	0	7	3	4	0	3	4	0	92	yesb; uson		13	1.08	-1.44
U133	144.17	144.2	*S. eocaena*	250-300 µm	15	1	14	0	4	15	0	0	14	0	0	305	yesb; uson		76	0.03	-1.52
U134	144.7	144.72	*S. eocaena*	250-300 µm	7	0	7	0	7	3	4	0	4	3	0	133	yesb; uson		19	0.18	-1.75
U135	145	145.04	*S. eocaena*	250-300 µm	16	0	16	1	15	16	0	0	16	0	0	211	yesb; uson		14	0.29	-1.55
U136	145.39	145.4	*S. eocaena*	250-300 µm	15	0	15	0	15	15	0	0	15	0	0	237	yesb; uson		16	0.33	-1.57
U137	145.42	145.45	*S. eocaena*	250-300 µm	14	0	14	0	14	14	0	0	14	0	0	229	yesb; uson	yesb; uson	16	0.30	-1.60

U138	89.25	89.27	*S. eocaena*	250-300 µm	3	0	3	0	3	1	2	0		10	yesb; uson		3	1.86	-1.48
U139	90.8	90.82	*S. eocaena*	250-300 µm	3	2	1	0	1	1	0	0		5	yesb; uson		5	Didn't run	
U140	93.7	93.72	*S. eocaena*	250-300 µm	3	0	3	0	3	3	0	0		9	yesb; uson		3	1.60	-2.28
U141	95.7	95.72	*S. eocaena*	250-300 µm	4	0.5	3.5	0	3.5	2	1.5	0	p dots	15	yesb; uson		4	1.82	-2.00
U142	108.32	108.34	*S. eocaena*	250-300 µm	4	1	3	0	3	2	1	0	p dots	9	yesb; uson		3	1.61	-2.01
U143	111.55	111.57	*S. eocaena*	250-300 µm	4	0	4	0	4	4	0	0	1 partly ip	15	yesb; uson		4	1.78	-1.55
U144	119.75	119.78	*S. eocaena*	250-300 µm	4	0.5	3.5	0	3.5	3.5	0	0		18	yesb; uson	average weight A. bullbrooki	5	1.87	-1.33
U145	119.75	119.78	*A. bullbrooki*	250-300 µm	4	0	4	0	4	2	2	0	p dots	47	yesb; uson	average weight S. eoceana	12	3.96	-2.97
U146	126.95	126.98	*S. eocaena*	250-300 µm	4	0	4	0	4	3	1	0		42	yesb; uson		11	1.24	-1.89
U147	127.65	127.67	*S. eocaena*	250-300 µm	6	1.5	4.5	0	4.5	0	4.5	0	some infill	71	yesb; uson		16	1.29	-1.69
U148	129.83	129.85	*S. eocaena*	250-300 µm	3	0	3	0	3	2	1	0		28	yesb; uson		9	1.59	-1.99
U149	129.83	129.85	*A. bullbrooki*	250-300 µm	3	0	3	0	3	0	3	0	p dots; infill	32	yesb; uson		11	3.73	-3.73
U150	129.88	129.9	*S. eocaena*	250-300 µm	3	0	3	0	3	1	2	0	some infill	27	yesb; uson		9	Didn't run	
U151	129.88	129.9	*A. bullbrooki*	250-300 µm	4	2	2	0	2	0	2	0	pi	29	yesb; uson		15	3.52	-3.66
U152	135.35	135.37	*A. bullbrooki*	250-300 µm	4	1.5	2.5	0	2.5	0	0	2.5	p dots	12	yesb; uson		5	3.68	-3.40
U153	135.4	135.42	*S. eocaena*	250-300 µm	3	0.5	2.5	0	2.5	1	1.5	0	1 pi	36	yesb; uson		14	1.56	-1.47
U154	135.53	135.56	*S. eocaena*	250-300 µm	3	0.5	2.5	0	2.5	2	0.5	0		42	yesb; uson		17	1.33	-1.59
U155	137.2	137.22	*S. eocaena*	250-300 µm	5	0.5	4.5	1.5	3	1	3.5	0	some infill	34	yesb; uson		11	1.67	-1.78
U156	137.23	137.25	*S. eocaena*	250-300 µm	3	0.5	2.5	0	2.5	2	0.5	0	1 ip	43	yesb; uson		17	1.67	-1.45
U157	137.23	137.25	*A. bullbrooki*	250-300 µm	4	0	4	0	4	2	2	0	1 ip; p dots	56	yesb; uson		14	4.03	-3.48
U158	137.3	137.32	*A. bullbrooki*	250-300 µm	4	0	4	0	4	0	4	0	2 ip;p dots	60	yesb; uson		15	3.87	-3.39
U159	137.69	137.71	*S. eocaena*	250-300 µm	3	0	3	0	3	0	3	0	2 ip	57	yesb; uson		19	1.72	-1.24

U160	137.7	137.72	*S. eocaena*	250-300 µm	4	0	4	0	4		0	4	0	1 ip	29	yesb; uson		7	1.11	-1.48
U161	144.78	144.8	*S. eocaena*	250-300 µm	3	0	3	0	3		3	0	0	some infill	65	yesb; uson		22	-0.01	-1.76
U162	145.42	145.45	*A. bullbrooki*	250-300 µm	3	0	3	0	3		3	0	0		43	yesb; uson		14	1.67	-2.42

Appendix 8 – GDGT peak integration raw data

Table 1 The raw data and peak integration for the isoprenoid GDGTs against core depth and age [Ma] is given. From the 11 fine fraction extracted samples six could achieve interpretable peaks, samples from which the fine fractions were extracted are: 129.83-.85 m, 129.88-.90 m, 135.24-.26 m,.135.40-.42 m, 135.53-.56 m, 136.28-.31 m, 137.23 - .25m, 137.30-.32 m, 144.73-.75m, 144.78-.80 m and 145.82-.83 m.

			Isoprenoid GDGTs					
Top depth [m]	Bottom depth [m]	Age [Ma]	GDGT-0	GDGT-1	GDGT-2	GDGT-3	Crenarchaeol (Cren.)	Cren. isomer
42.5	42.52	44.933	125431.37	28039.11	44155.18	14735.88	375145.13	57458.54
43.5	43.52	44.969	22608.42	7630.98	5127.14	906.03	47109.25	6713.00
60.6	60.62	45.580	20872.19	1540.93	2995.17	0.00	15896.56	689.75
80	80.02	46.256	248865.92	54073.00	62686.45	21423.73	385842.69	39784.84
82.4	82.42	46.333	1022511.72	146743.60	199700.09	37364.96	476757.35	40601.92
82.9	82.92	46.349	158179.35	0.00	14396.65	0.00	84461.59	7742.52
83.4	83.42	46.365	60709.46	14674.37	19221.14	3855.07	141075.07	11091.76
87.52	87.54	49.233	22937657.04	4049311.91	4790455.61	1106553.93	16418403.35	2163531.24
88.4	88.42	49.269	2843950.77	1099078.48	1317534.73	503673.79	6670182.10	958228.30
89.25	89.27	49.304	21859989.51	4558342.92	2651799.13	1413516.76	22465235.52	3257493.35
89.7	89.72	49.322	16573207.32	3455770.48	4773395.88	1086927.54	18543156.38	2611737.23
90.2	90.22	49.342	456762.97	99551.24	149969.08	19808.05	948898.52	112699.59
90.8	90.82	49.367	3739000.09	569829.79	656682.93	204380.83	3669777.65	573105.28
91.3	91.32	49.390	3033920.13	745224.76	986932.66	210573.41	5207247.68	662385.17
91.8	91.82	49.414	3739427.72	875834.71	1100059.08	269113.94	5576435.76	742304.86
93.7	93.72	49.504	14908710.23	3910707.52	5087004.92	887172.95	21576937.60	2894438.20
94.55	94.57	49.539	2079844.20	376500.71	692380.28	207928.54	2366007.74	347397.81
94.8	94.82	49.548	11302669.34	2260431.23	3182554.72	829852.63	11962470.19	2235578.47
95.7	95.72	49.581	798462.28	173726.17	173726.17	33555.29	1336641.08	157333.12
96.8	96.82	49.620	16611278.16	3803687.80	5280166.94	1301176.86	20321597.00	3671981.52
97.4	97.42	49.642	4817210.28	1232508.49	1863060.54	421777.06	7243093.03	1257342.59
97.8	97.82	49.657	1617070.33	443826.84	624928.31	125501.01	2848560.84	359556.41
105.3	105.3	49.929	19425326.55	4657426.98	6476108.45	1872074.03	24598666.53	3078967.56
105.7	105.7	49.943	817497.60	188790.61	254750.74	68670.64	1415474.92	182272.72
106	106	49.954	9101119.20	1930801.60	2902599.21	744148.68	12384105.56	1586253.79
106.5	106.5	49.973	4823532.64	1380744.38	1746052.76	533111.67	9671175.26	1257405.53
107.5	107.5	50.008	15882169.32	4667069.56	7249946.17	1694773.87	21098425.49	3991983.56
107.9	107.9	50.035	694029.12	175270.90	256786.43	67660.71	1189038.69	209605.19
108.3	108.3	50.064	17688512.47	4459950.19	6503208.65	1878621.12	22604610.80	4069821.57
108.7	108.7	50.088	24572120.48	5756934.35	8316402.42	2038639.69	21343098.01	4088479.52
109.2	109.2	50.121	10155385.42	792868.74	1256907.88	348672.50	5316940.18	737823.86
109.6	109.6	50.146	1968488.41	371996.12	449373.23	106286.78	1877375.47	347659.54
110.2	110.2	50.185	15630795.16	4011270.66	5035242.22	1359750.73	15149956.40	2933970.98
110.7	110.7	50.213	7909076.49	2152906.67	3095767.86	719605.85	10565514.78	1249323.04
111.1	111.1	50.228	15383033.41	3875436.82	4258124.08	1428965.30	18868999.73	3085346.76
111.6	111.6	50.243	12520151.93	3111651.90	3150779.75	977944.01	14087807.63	1815212.38
112.4	112.4	50.271	20245216.50	4777049.54	5957461.11	1438802.93	24084765.68	3204078.57
112.8	112.8	50.286	18771561.34	4818005.89	6201040.74	1547734.26	19144836.55	2813377.90
113.3	113.3	50.304	11868149.32	2923319.95	3492519.01	1138984.49	16497717.46	2587711.57
114	114	50.327	1538146.74	380735.62	418885.73	118888.72	2043228.77	240583.40
116.8	116.8	50.424	10783420.60	2459988.87	3541085.47	916295.50	13924684.51	2384858.16
118.1	118.1	50.460	10535110.03	2317903.36	2620472.17	618798.84	12305127.04	1446127.74
118.6	118.6	50.472	715887.92	151059.52	208205.03	43757.57	1247348.71	141165.99
119	119	50.481	3801417.92	978040.92	1281571.23	348013.24	7604523.69	926654.99
119.4	119.4	50.490	2069380.05	487229.90	604853.35	156754.89	3308595.14	429088.00
119.8	119.8	50.499	7729201.31	1322543.94	2198100.15	483141.39	7788092.81	781140.10
120.3	120.3	50.511	6341602.90	1485424.00	1843193.74	557387.96	8899621.19	984693.34
122.3	122.3	50.556	11383332.73	2902207.45	3900600.28	1030337.51	13509402.00	2370713.24
122.7	122.7	50.565	1059918.89	300472.17	360141.37	92236.63	1709380.08	271863.99

123.2	123.2	50.576	16300773.36	3471053.62	5084943.65	1590023.09	16940578.00	3454664.69
123.6	123.6	50.586	11686411.88	2450452.08	3284475.65	1047506.22	14953310.19	1950430.08
124	124	50.595	15322812.53	4462015.79	5917507.65	1742765.82	23640536.15	3634300.83
124.4	124.4	50.604	641218.19	150797.08	231380.83	70758.50	944912.73	159494.41
124.8	124.8	50.613	24205891.06	6122765.56	7245845.32	2167908.85	34058563.86	4440437.02
124.8	124.8	50.613	24174698.33	5830397.21	7786136.83	2324408.83	33368359.28	4694981.19
125.7	125.7	50.634	14610820.20	3609253.45	5344581.36	1561629.83	18498295.35	3662237.82
126.1	126.1	50.643	20318040.28	6170589.49	8569523.40	2353948.37	32967077.63	5696515.91
126.6	126.6	50.654	17383664.98	4356250.47	5550150.85	1704384.77	29254156.85	5282239.17
127	127	50.663	8530226.56	2455425.96	3830085.04	905037.27	13640223.76	2366585.92
127.6	127.6	50.677	15425125.97	4222930.04	5251087.24	1436096.49	22619753.94	4364801.34
128	128	50.686	7716644.71	3707542.73	5724868.93	1614906.92	21391631.73	4154396.75
128.4	128.4	50.695	12078986.73	3192108.97	5173421.44	1444955.72	18046667.38	2789841.18
128.9	128.9	50.707	6078809.35	1657812.08	2097620.29	597245.46	8966162.22	1723414.75
129.3	129.3	50.716	2814016.64	815565.27	1174516.61	361334.70	5550043.62	1032101.59
129.8	129.9	50.728	3242596.39	791114.50	1309028.54	399578.02	6012518.97	1009085.98
129.9	129.9	50.728	21837741.21	5543939.23	7027679.44	2265912.78	24213190.27	4657477.53
129.9	129.9	50.729	5780830.01	1386624.16	2222745.28	498276.45	9016827.59	1562326.45
130.2	130.2	50.734	16881534.26	5496509.62	7306225.23	2081943.82	24843501.21	3981361.76
135.2	135.3	50.794	1061099.24	354497.94	407958.79	139961.77	1969552.17	308859.58
135.9	135.9	50.801	16647500.17	4518359.96	5398338.19	1594415.21	20117608.59	3000170.82
136.4	136.4	50.807	3479490.88	909443.93	1298745.47	353034.50	6815472.58	924009.87
136.9	136.9	50.812	11826.93	1616.72	3588.46	633.60	29072.14	4140.47
137.2	137.2	50.815	3120501.61	778646.26	1242884.35	377438.50	5147141.12	751921.42
137.7	137.7	50.820	727654.10	164531.75	248237.35	68266.11	1491286.84	188594.56
137.2	137.3	50.816	4108652.99	1030992.53	1462492.44	386163.50	7213698.54	1197569.20
137.3	137.3	50.816	1340081.49	298030.28	356857.44	100106.92	1612720.59	242951.71
144.2	144.2	52.657	793874.65	81430.43	113556.67	24846.69	478203.41	56789.40
144.7	144.8	52.676	3717670.17	1165946.39	1931234.51	613584.61	7118589.92	1395123.21

Table 2: The raw data for the integrated peaks for the branched GDGTs is presented below

			Branched GDGTs														
Top depth [m]	Bottom depth [m]	Age [Ma]	bGDGT-1a	bGDGT-1b	bGDGT-1c	bGDGT-2a	bGDGT-2a'	bGDGT-2b	bGDGT-2b'	bGDGT-2c	bGDGT-2c'	bGDGT-3a	bGDGT-3a'	bGDGT-3b	bGDGT-3b'	bGDGT-3c	bGDGT-3c'
42.5	42.52	44.933															
43.5	43.52	44.969															
60.6	60.62	45.580															
80	80.02	46.256															
82.4	82.42	46.333															
82.9	82.92	46.349															
83.4	83.42	46.365															
87.52	87.54	49.233	11697416.47	984687.14	519687.88	1058733.74	1842265.29	351997.32	475044.97	123336.43	82023.14						
88.4	88.42	49.269	1146299.04	189090.61	82765.97	82973.37	100898.90	22366.37	62775.71			50628.16	48404.76				
89.25	89.27	49.304	9340574.26	981807.00	427969.15	721616.24	899583.88	295464.21	386266.10	121852.66	81956.44	351763.15	505767.46	45691.93	88535.27		
89.7	89.72	49.322	6761268.43	876479.24	337030.31	435397.72	640869.56	239711.21	314483.57	132881.17	72442.52	220108.30	322277.38				
90.2	90.22	49.342	164355.19	19049.91	7647.12	9248.85	12523.48	2648.58	5380.76								
90.8	90.82	49.367	1608895.06	235987.32	154405.07	117955.44	178162.01	150654.97	103558.48	35893.79	32008.04	57912.17	106878.80				
91.3	91.32	49.390	1327606.19	194934.53	82555.33	132371.76	102060.89	54615.54	64592.43	18487.75	18387.79	67348.57	77981.66				
91.8	91.82	49.414	2232072.44	298898.71	112705.78	217245.92	238617.31	76117.18	92893.81	65372.90	27330.75	103957.54	128777.25				
93.7	93.72	49.504	6493849.22	1117789.63	435164.60	517108.41	1079807.93	280827.03	351349.58	210941.53	104219.64	464108.87	494821.75				
94.55	94.57	49.539	1144328.00			53304.38	85996.37										
94.8	94.82	49.548	5400328.73	720950.87	338769.64	417707.30	571283.42	155505.38	231086.86	78065.88	67513.29	218484.75	217468.62				
95.7	95.72	49.581	312505.84	44093.44	15422.80	26032.90	24426.20										
96.8	96.82	49.620	7813457.30	986430.23	483187.00	715473.84	1068570.63	177025.60	295948.82	92194.45	111824.09	423055.43	452333.11				
97.4	97.42	49.642	2836141.10	427053.34	155335.72	159001.64	276561.94	102176.82	120383.43	102176.82	120383.43	123813.36	146181.53				
97.8	97.82	49.657	1444313.31	178280.66	66467.36	120090.68	160714.36	63272.46	40177.55	28673.15	19891.77						
105.3	105.3	49.929	17290238.00	2142112.62	790393.17	1344202.48	1771724.63	397179.50	541956.86	308251.83	170145.49	530691.12	717370.39				
105.7	105.7	49.943	487897.05	54541.94	14357.63	37632.40	40096.94	15387.19	14190.98	13113.53	3409.10	20989.85	17923.73				
106	106	49.954	6824173.16	1050060.57	392434.27	644112.32	714743.14	267960.33	278763.75	210973.20	96264.31	354426.84	420878.98				
106.5	106.5	49.973	2876905.60	440223.21	176853.74	238242.07	458417.34	93187.08	113169.83	82109.08	21097.45	133482.84	141663.08				
107.5	107.5	50.008	8107309.66	1230793.45	503518.30	474461.12	976563.71	311011.38	377730.27	157901.82	115523.28	299716.08	271107.23				
107.9	107.9	50.035	238147.03	33804.39	13669.60	21786.20	21537.71	7148.28	10769.28	5817.36	2912.14	9521.74	9605.74				
108.3	108.3	50.064	9543871.59	1452296.48	592587.32	660084.40	1257320.97	375744.12	491280.24	313440.05	142152.38	383543.08	573891.59				
108.7	108.7	50.088	15303014.11	2448557.44	901480.08	1242149.37	1393946.25	606533.14	594366.63	405397.68	253467.14	738955.57	913510.03				
109.2	109.2	50.121	2663421.73	426742.71	157097.49	199263.83	301211.26	103443.10	89233.23	65979.43	37586.23	128255.24	152342.71				
109.6	109.6	50.146	17670814.65	1511787.00	820399.46	925464.98	1438764.04	396917.09	524586.14	150373.50	170111.04						

110.2	110.2	50.185	7920997.26	1206566.27	492560.15	794626.76	854890.34	329374.29	304089.89	183283.55	95340.50	379114.44	607344.89	
110.7	110.7	50.213	4954846.77	699764.64	289964.30	328789.89	607949.95	200733.48	188730.83	147534.73	60404.14	219417.24	284106.13	
111.1	111.1	50.228	4609775.38	880797.97	356957.12	459008.30	641160.19	198677.99	317930.75	101409.46	116355.42	287810.47	481901.44	
111.6	111.6	50.243	6234904.77	905852.70	277567.55	499925.27	556362.30	247007.90	283281.82	144981.34	79503.26	288554.85	453436.45	
112.4	112.4	50.271	14106535.78	1588197.31	718494.28	1508285.41	1399260.74	541007.51	431658.08	293555.75	143117.72	787389.92	911209.71	
112.8	112.8	50.286	11455385.49	1804015.45	656381.83	966179.47	1683771.16	430773.66	398098.78	306013.51	192286.33	647553.35	741129.49	
113.3	113.3	50.304	8585704.69	1198794.38	434430.00	710403.19	939571.16	328636.13	346053.29	231756.14	125824.51	408702.83	611344.27	
114	114	50.327	972523.49	120562.67	52858.39	60156.40	86405.65	34720.53	40651.16	25731.81	8678.58			
116.8	116.8	50.424	4567077.22	686178.86	307317.61	500712.87	565933.80	173218.61	181167.83	74375.50	91912.58	238664.33	345839.17	
118.1	118.1	50.460	4854456.85	663006.41	238254.12	464989.35	500516.62	182730.24	211215.38	151277.41	57002.62	263430.93	267699.89	
118.6	118.6	50.472	231700.58	39984.95	14402.59	25413.10	19943.78	12458.06	9658.53					
119	119	50.481	4462671.79	211290.93	136860.60	172174.61	127348.16	70686.34	58433.86	38653.17	17317.33	73257.83	77105.22	
119.4	119.4	50.490	1444312.65	194178.20	70843.88	115626.94	165678.17	59469.90	66011.11	28729.00	17131.96	58171.73	78879.27	
119.8	119.8	50.499	3479225.17	505877.80	195724.35	337188.03	349649.60	116261.76	143761.25			143593.50	198599.32	
120.3	120.3	50.511	5353661.60	747655.29	278827.37	360937.01	624516.76	140139.80	238879.65	116696.50	35085.65	198424.25	243500.89	
122.3	122.3	50.556	9789712.03	1343484.84	715080.13	869403.04	1126339.72	304005.46	448468.67	396922.46	139936.48	424981.31	571796.38	541415.25
122.7	122.7	50.565	525758.08	89688.50	34563.83	38842.50	77270.77	14828.81	19556.68	12824.11	5676.55	20203.40	28934.70	
123.2	123.2	50.576	11589825.31	1717134.79	642661.28	1020197.94	1278660.00	372241.16	397877.24	195025.01	129765.77	542839.91	488004.26	363932.87
123.6	123.6	50.586	6108931.67	1105940.80	412212.28	517628.07	812840.60	221173.11	208485.93	160615.75	88246.52	362988.03	370400.56	300128.76
124	124	50.595	10780472.06	1627377.95	648428.79	923091.34	1199458.84	406112.21	272261.01	252273.89	85828.28	515231.57	525468.31	
124.4	124.4	50.604	401177.72	56058.51	22035.16	21571.99	54819.71	9215.67	16860.91	7185.26	3924.04	9483.38	16106.29	
124.8	124.8	50.613	20395164.95	3168678.20	913325.61	1889886.63	2220311.17	712756.34	528970.91	342541.76	149623.15	1121124.61	829558.20	
124.8	124.8	50.613	19930821.51	3055037.03	855582.55	1967780.29	2560545.83	665447.88	742823.04	364241.33	198777.76	1136960.15	1065399.24	
125.7	125.7	50.634	10435856.19	1588747.13	526255.17	1023812.39	1281580.43	413032.50	319455.71	244364.32	96291.05	454836.82	645681.97	443915.75
126.1	126.1	50.643	15566405.18	2646577.55	954955.19	1273545.41	2495470.52	606464.12	686772.60	561879.46	234880.23	1063909.55	846059.19	854102.00
126.6	126.6	50.654	16162664.62	2225149.09	866477.46	1124330.60	1987855.84	472721.79	510532.55	294814.98	119219.09	639413.78	701840.99	617469.59
127	127	50.663	6272539.80	916674.73	438722.57	395505.65	760931.32	198574.97	191224.41	134520.34	53725.57	308505.66	286645.19	
127.6	127.6	50.677	14584689.56	2054099.09	793815.52	869734.98	1747258.47	558929.41	408782.82	449735.53	208233.93	753644.12	812016.51	892702.95
128	128	50.686	11950753.88	1797788.98	842968.63	670689.65	1175196.17	403946.28	406682.04	375365.15	120561.76	463503.99	523588.52	530118.64
128.4	128.4	50.695	11145580.06	1611661.33	670283.09	744166.37	844732.13	317851.24	305966.35	223313.11	79498.67	358000.76	419973.38	372713.89
128.9	128.9	50.707	2724219.49	432875.63	194065.28	140393.28	336865.74	83847.56	128332.56	69882.47	29511.57	127243.77	131345.68	109345.00
129.3	129.3	50.716	1474901.51	245611.01	119397.01	110489.39	132402.02	66087.55	51228.11	53226.27	25654.65	53226.27	25654.65	80342.16
129.8	129.9	50.728	1604312.85	253954.38	103655.13	145322.42	191314.32	77979.51	63140.38	60910.14	23226.15	94646.87	107029.04	
129.9	129.9	50.728	16794577.80	2961305.77	1084416.43	1176305.94	1871478.15	659444.64	566771.16	353853.39	362332.77	753061.92	853584.40	
129.9	129.9	50.729	2184232.07	394490.91	159017.13	261186.31	270523.72	101707.54	64447.61	104883.56	41505.04	209692.02	207355.98	
130.2	130.2	50.734	17594410.42	2652484.39	1034726.05	1729660.93	2192638.75	564445.18	448465.17	383106.65	161311.99	920746.24	1198340.24	635966.91
135.2	135.3	50.794	879236.78	128572.17	25635.43	86217.86	126168.68	26743.76	32480.77	14241.58	7225.37	33909.56	28975.08	34024.15
135.9	135.9	50.801	14991112.93	2175810.12	807053.44	1498532.64	1917724.42	454850.73	452591.18	250537.43	136382.55	522085.84		522085.84
136.4	136.4	50.807	1894336.27	286339.44	111309.24	164391.42	251070.25	81914.99	32535.14	56702.09	34681.41	77211.31	114937.25	
136.9	136.9	50.812												
137.2	137.2	50.815	2058608.89	250072.28	101612.40	150431.77	180496.70	80184.04	48203.98	36941.54	16740.05	119803.55	104577.02	

137.7	137.7	50.820	12657.76	72339.86	32458.40	35960.08	60852.99	12657.76	18221.69					
137.2	137.3	50.816	2608869.50	311540.93	102150.01	258103.74	321692.18	102050.85	113262.58	41148.45	25726.13	154035.74	178709.68	105820.01
137.3	137.3	50.816	595678.40	98711.04	51124.65	52817.17	86367.28					23347.40	34855.34	
144.2	144.2	52.657	78069.16	10463.28	6189.61	5363.39	5308.12	4253.10	4019.21					
144.7	144.8	52.676	1087789.76	150766.70	98206.85	103674.91	143641.72	49679.23	65428.87			82248.56	36995.46	

Table 3 The sediment dry weight [g] and the total lipid extract (TLE) weight [g] is given within this table.

Top depth [m]	Bottom depth [m]	Age [Ma]	Dry Weight (g) for organic geochemical analysis	TLE weight (g)
42.5	42.52	44.933	12.6	0.0051
43.5	43.52	44.969	15.9	0.0083
60.6	60.62	45.58	10.16	0.0089
80	80.02	46.256	9.2	0.0052
82.4	82.42	46.333	11.14	0.0059
82.9	82.92	46.349	14.39	0.0021
83.4	83.42	46.365	9.26	0.006
87.52	87.54	49.233		
88.40	88.42	49.269	11.89	0.006
89.25	89.27	49.304	10.11	0.0045
89.70	89.72	49.322	9.25	0.0061
90.20	90.22	49.342	6.95	0.0071
90.80	90.82	49.367	7.13	0.0054
91.30	91.32	49.39	6.49	0.0045
91.80	91.82	49.414	7.14	0.0063
93.70	93.72	49.504	6.61	0.0071
94.55	94.57	49.539	7.13	0.0071
94.80	94.82	49.548	9.23	0.0081
95.70	95.72	49.581	7.91	0.008
96.80	96.82	49.62	10.19	0.0031
97.40	97.42	49.642	10.54	0.0074
97.80	97.82	49.657	8.73	0.0063
105.30	105.32	49.929	8.1	0.0034
105.70	105.72	49.943	7.57	0.0095
106.00	106.02	49.954	8.65	0.0087
106.51	106.53	49.973	8.01	0.006
107.45	107.47	50.008	11.64	0.0076
107.88	107.89	50.035	9.81	0.0076
108.32	108.34	50.064	10.44	0.0076
108.70	108.72	50.088	9.93	0.0056
109.20	109.22	50.121	10.38	0.0026
109.60	109.62	50.146	12.47	0.007
110.20	110.22	50.185	8.08	0.0024
110.68	110.7	50.213	6.89	0.0062
111.10	111.12	50.228	10.83	0.006
111.55	111.57	50.243	9.91	0.0169
112.36	112.37	50.271	6.45	0.0061
112.80	112.82	50.286	6.76	0.0052
113.30	113.32	50.304	9.19	0.0059
113.97	113.99	50.327		
116.80	116.82	50.424	9.94	0.0065
118.10	118.12	50.46	10.97	0.0057

118.60	118.62	50.472	7.1	0.0083
119.00	119.02	50.481	11.8	0.0126
119.38	119.4	50.49	10.09	0.0048
119.80	119.82	50.499	10.89	0.0025
120.30	120.32	50.511	7.2	0.0061
122.30	122.32	50.556	7.97	0.0125
122.70	122.72	50.565	10.27	0.0091
123.18	123.2	50.576	10.23	0.0051
123.60	123.62	50.586	7.01	0.0065
124.00	124.02	50.595	10.5	0.0087
124.40	124.42	50.604	6.94	0.0071
124.81	124.83	50.613	7.94	0.013
124.81	124.83	50.613	7.94	0.013
125.71	125.72	50.634	6.06	0.0092
126.10	126.12	50.643	6.89	0.0046
126.60	126.62	50.654	8.91	0.105
126.98	127	50.663	8.76	0.0105
127.60	127.62	50.677	9.48	0.0064
128.00	128.02	50.686	7.93	0.0092
128.40	128.42	50.695	6.12	0.0056
128.90	128.92	50.707	6.19	0.0051
129.30	129.32	50.716	9.87	0.0079
129.83	129.85	50.728	5.16	0.0101
129.85	129.87	50.728	8.43	0.0085
129.88	129.9	50.729	5.47	0.0102
130.20	130.22	50.734		
135.24	135.26	50.794	10.05	0.0149
135.85	135.87	50.801	7.8	0.0038
136.35	136.37	50.807	10.55	0.0049
136.85	136.87	50.812	6.29	0.0024
137.20	137.22	50.815	9.87	0.003
137.70	137.72	50.82	7.84	0.0014
137.23	137.25	50.816	9.12	0.0104
137.30	137.32	50.816	7.26	0.012
144.20	144.22	52.657		
144.73	144.75	52.676	6.6	0.0083

Table 4 The calculated TEX86 and SST are given for SST-H and TEX^{H}_{86} (Kim et al., 2010), 1/TEX86 gives the SST reconstructed after (Liu et al., 2009) and for the BAYSPAR calibration the 5th, 50th and 95th percentile is given, where the 50th is used in Figures of this thesis. Values used for quality control are given as well as the BIT, MI (Zhang et al., 2011) and %GDGT-RS (Inglis et al., 2015).

							BAYSPAR					
top depth [m]	bottom depth [m]	Age [Ma]	TEX86	TEX-86-H	SST-H	BIT	5th	50th	95th	1/TEX86	MI	%GDGT-RS
42.5	42.52	44.93	0.80581	-0.09	32.18625		28.86	34.71	42.46	30.21	0.17	31.42
43.5	43.52	44.97	0.62551	-0.20	24.66256		17.64	23.46	28.97	24.37	0.20	22.89
60.6	60.62	45.58	0.70513	-0.15	28.22177		22.88	28.42	34.68	27.31	0.21	3.20
80	80.02	46.26	0.69616	-0.16	27.84149		22.30	27.85	34.02	27.02	0.25	13.78
82.4	82.42	46.33	0.65424	-0.18	25.99648		19.50	25.23	30.89	25.51	0.43	3.82
83.4	83.42	46.37	0.69956	-0.16	27.98587		22.49	28.05	34.22	27.13	0.20	15.45
87.52	87.54	49.23	0.66562	-0.18	26.50861		20.24	25.95	31.80	25.94	0.35	8.62
88.40	88.42	49.27	0.71662	-0.14	28.70192	0.17646	23.50	29.13	35.52	27.68	0.28	25.20
89.25	89.27	49.30	0.61634	-0.21	24.22363	0.34474	16.94	22.87	28.32	23.98	0.25	12.97
89.70	89.72	49.32	0.71028	-0.15	28.43765	0.31125	23.20	28.78	35.05	27.48	0.31	13.61
90.20	90.22	49.34	0.73941	-0.13	29.63191		24.99	30.58	37.28	28.39	0.20	19.79
90.80	90.82	49.37	0.71565	-0.15	28.66168	0.36062	23.52	29.10	35.50	27.65	0.25	13.29
91.30	91.32	49.39	0.71394	-0.15	28.59038	0.24692	23.29	28.93	35.37	27.60	0.25	17.92
91.80	91.82	49.41	0.70682	-0.15	28.29252	0.34373	22.96	28.51	34.71	27.37	0.26	16.56
93.70	93.72	49.50	0.69398	-0.16	27.7482	0.29548	22.11	27.75	33.80	26.94	0.29	16.26
94.55	94.57	49.54	0.76819	-0.11	30.76622		26.64	32.31	39.43	29.21	0.32	14.31
94.80	94.82	49.55	0.73433	-0.13	29.42696	0.36328	24.69	30.29	36.86	28.23	0.31	16.51
95.70	95.72	49.58	0.67729	-0.17	27.02513		21.02	26.67	32.65	26.36	0.20	16.46
96.80	96.82	49.62	0.72941	-0.14	29.22726	0.34009	24.38	29.95	36.55	28.08	0.30	18.10
97.40	97.42	49.64	0.74187	-0.13	29.73027	0.3284	25.10	30.72	37.47	28.46	0.29	20.70
97.80	97.82	49.66	0.71436	-0.15	28.60804		23.41	29.02	35.34	27.61	0.27	18.19
105.30	105.32	49.93	0.71044	-0.15	28.44453	0.46817	23.22	28.75	35.06	27.49	0.32	13.68
105.70	105.72	49.94	0.72816	-0.14	29.1762	0.29928	24.24	29.84	36.42	28.05	0.24	18.23
106.00	106.02	49.95	0.73048	-0.14	29.27073	0.41974	24.48	30.00	36.56	28.12	0.29	14.84

106.51	106.53	49.97	0.71921	-0.14	28.80883	0.28467	23.68	29.32	35.77	27.77	0.25	20.68
107.45	107.47	50.01	0.73488	-0.13	29.4493	0.32437	24.74	30.27	36.89	28.25	0.35	20.09
107.88	107.89	50.04	0.7529	-0.12	30.16899	0.20179	25.77	31.40	38.24	28.78	0.26	23.20
108.32	108.34	50.06	0.73628	-0.13	29.50569	0.35458	24.75	30.35	37.04	28.29	0.32	18.70
108.70	108.72	50.09	0.71501	-0.15	28.63494	0.47861	23.42	29.05	35.48	27.63	0.39	14.27
109.20	109.22	50.12	0.74719	-0.13	29.94284	0.39314	25.48	31.06	37.90	28.62	0.28	6.77
109.60	109.62	50.15	0.70831	-0.15	28.3553		22.98	28.62	35.00	27.42	0.29	15.01
110.20	110.22	50.19	0.69931	-0.16	27.97542	0.41067	22.44	28.04	34.23	27.12	0.37	15.80
110.68	110.7	50.21	0.70171	-0.15	28.07737	0.37706	22.64	28.19	34.41	27.20	0.34	13.64
111.10	111.12	50.23	0.69359	-0.16	27.73143	0.25562	22.10	27.70	33.83	26.93	0.30	16.71
111.55	111.57	50.24	0.65638	-0.18	26.09357	0.36315	19.64	25.38	31.12	25.59	0.31	12.66
112.36	112.37	50.27	0.68935	-0.16	27.54911	0.43724	21.81	27.45	33.52	26.78	0.31	13.66
112.80	112.82	50.29	0.68674	-0.16	27.43655	0.4473	21.61	27.28	33.28	26.69	0.36	13.03
113.30	113.32	50.30	0.71178	-0.15	28.50029	0.40556	23.31	28.83	35.22	27.53	0.28	17.90
113.97	113.99	50.33	0.67152	-0.17	26.77096		20.65	26.35	32.14	26.15	0.29	13.53
116.80	116.82	50.42	0.73555	-0.13	29.47621	0.30871	24.74	30.30	36.98	28.27	0.30	18.11
118.10	118.12	50.46	0.66903	-0.17	26.66035	0.34043	20.46	26.17	32.04	26.06	0.29	12.07
118.60	118.62	50.47	0.72241	-0.14	28.94093		23.88	29.50	35.99	27.87	0.22	16.47
119.00	119.02	50.48	0.72327	-0.14	28.97616	0.39247	23.93	29.56	36.03	27.89	0.23	19.60
119.38	119.4	50.49	0.70962	-0.15	28.41032	0.3602	23.18	28.71	34.97	27.46	0.25	17.17
119.80	119.82	50.50	0.7236	-0.14	28.98978	0.36663	23.98	29.56	36.03	27.90	0.32	9.18
120.30	120.32	50.51	0.69503	-0.16	27.79298	0.43245	22.16	27.81	33.94	26.98	0.28	13.44
122.30	122.32	50.56	0.71558	-0.15	28.65851	0.48617	23.51	29.08	35.50	27.65	0.33	17.24
122.70	122.72	50.57	0.70677	-0.15	28.29082	0.28787	22.94	28.49	34.80	27.37	0.28	20.41
123.18	123.2	50.58	0.74479	-0.13	29.84705	0.46828	25.29	30.90	37.66	28.55	0.33	17.49
123.60	123.62	50.59	0.7194	-0.14	28.81673	0.3534	23.76	29.29	35.72	27.77	0.29	14.30
124.00	124.02	50.59	0.71682	-0.14	28.70988	0.371	23.59	29.20	35.54	27.69	0.31	19.17
124.40	124.42	50.60	0.75377	-0.12	30.20325	0.34747	25.85	31.48	38.40	28.81	0.29	19.92
124.81	124.83	50.61	0.71746	-0.14	28.73672	0.44414	23.53	29.18	35.59	27.71	0.30	16.26
125.71	125.72	50.63	0.74543	-0.13	29.87253	0.42801	25.35	30.95	37.76	28.57	0.32	20.04

126.10	126.12	50.64	0.72925	-0.14	29.22068	0.39189	24.33	29.92	36.45	28.08	0.31	21.90
126.60	126.62	50.65	0.74213	-0.13	29.74072	0.41339	25.15	30.73	37.48	28.47	0.25	23.30
126.98	127	50.66	0.74308	-0.13	29.7788	0.37038	25.22	30.78	37.56	28.50	0.31	21.72
127.60	127.62	50.68	0.72354	-0.14	28.98717	0.45346	24.01	29.57	36.03	27.90	0.29	22.06
128.00	128.02	50.69	0.75611	-0.12	30.29522	0.40867	25.93	31.59	38.67	28.87	0.30	35.00
128.40	128.42	50.70	0.74666	-0.13	29.92179	0.42816	25.40	31.01	37.80	28.60	0.32	18.76
128.90	128.92	50.71	0.72716	-0.14	29.13542	0.27845	24.21	29.79	36.34	28.01	0.29	22.09
129.30	129.32	50.72	0.75896	-0.12	30.40695	0.24455	26.15	31.80	38.80	28.96	0.26	26.83
129.83	129.85	50.73	0.77453	-0.11	31.01039	0.26273	27.02	32.77	39.98	29.39	0.26	23.73
129.85	129.87	50.73	0.71562	-0.15	28.66039	0.46973	23.48	29.08	35.40	27.65	0.34	17.58
129.88	129.9	50.73	0.75544	-0.12	30.26905	0.25786	25.91	31.55	38.44	28.86	0.28	21.28
130.20	130.22	50.73	0.70866	-0.15	28.36978	0.48754	23.09	28.65	34.99	27.43	0.34	19.08
135.24	135.26	50.79	0.70734	-0.15	28.31439	0.36955	22.95	28.58	34.85	27.39	0.28	22.55
135.85	135.87	50.80	0.68863	-0.16	27.51829		21.78	27.38	33.47	26.76	0.33	15.27
136.35	136.37	50.81	0.73906	-0.13	29.61761	0.26852	24.97	30.53	37.23	28.38	0.25	20.98
136.85	136.87	50.81	0.83799	-0.08	33.34961		30.69	36.79	44.90	30.99	0.15	25.93
137.20	137.22	50.82	0.75288	-0.12	30.16806	0.3368	25.82	31.40	38.27	28.78	0.29	19.42
137.70	137.72	50.82	0.75429	-0.12	30.2238		25.85	31.48	38.48	28.82	0.22	20.58
137.23	137.25	50.82	0.74713	-0.13	29.94043	0.32803	25.48	31.07	37.84	28.62	0.26	22.57
137.30	137.32	50.82	0.70136	-0.15	28.06221	0.32965	22.60	28.20	34.34	27.19	0.29	15.35
144.20	144.22	52.66	0.70563	-0.15	28.24254		22.93	28.45	34.71	27.33	0.29124	6.68
144.73	144.75	52.68	0.77165	-0.11	30.89943	0.16964	26.87	32.56	39.76	29.31	0.30	27.29